frontiers | Research Topics

Understanding mitochondrial dynamics and metabolic plasticity in cancer stem cells: Recent advances in cancer treatment and potential therapeutic approaches

Edited by
Pramod Darvin and Varun Sasidharan Nair

Published in
Frontiers in Oncology

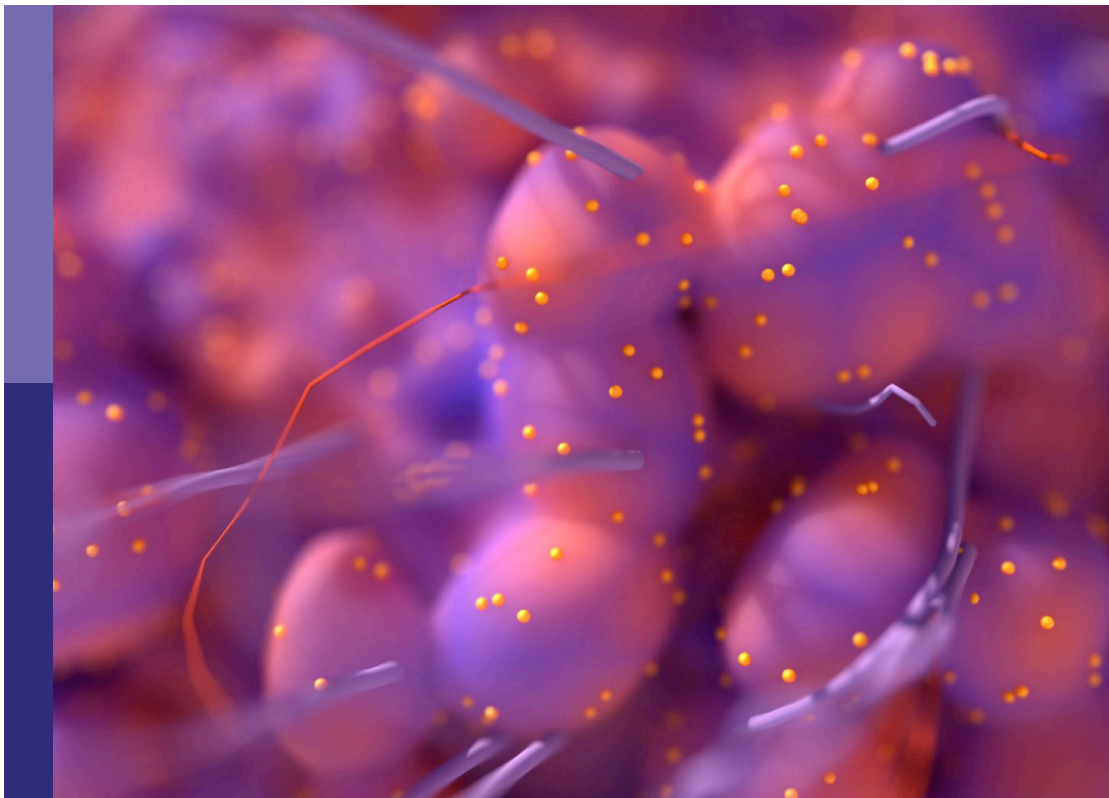

ISSN 1664-8714
ISBN 978-2-8325-2504-3
DOI 10.3389/978-2-8325-2504-3

About Frontiers

Frontiers is more than just an open access publisher of scholarly articles: it is a pioneering approach to the world of academia, radically improving the way scholarly research is managed. The grand vision of Frontiers is a world where all people have an equal opportunity to seek, share and generate knowledge. Frontiers provides immediate and permanent online open access to all its publications, but this alone is not enough to realize our grand goals.

Frontiers journal series

The Frontiers journal series is a multi-tier and interdisciplinary set of open-access, online journals, promising a paradigm shift from the current review, selection and dissemination processes in academic publishing. All Frontiers journals are driven by researchers for researchers; therefore, they constitute a service to the scholarly community. At the same time, the *Frontiers journal series* operates on a revolutionary invention, the tiered publishing system, initially addressing specific communities of scholars, and gradually climbing up to broader public understanding, thus serving the interests of the lay society, too.

Dedication to quality

Each Frontiers article is a landmark of the highest quality, thanks to genuinely collaborative interactions between authors and review editors, who include some of the world's best academicians. Research must be certified by peers before entering a stream of knowledge that may eventually reach the public - and shape society; therefore, Frontiers only applies the most rigorous and unbiased reviews. Frontiers revolutionizes research publishing by freely delivering the most outstanding research, evaluated with no bias from both the academic and social point of view. By applying the most advanced information technologies, Frontiers is catapulting scholarly publishing into a new generation.

What are Frontiers Research Topics?

Frontiers Research Topics are very popular trademarks of the *Frontiers journals series*: they are collections of at least ten articles, all centered on a particular subject. With their unique mix of varied contributions from Original Research to Review Articles, Frontiers Research Topics unify the most influential researchers, the latest key findings and historical advances in a hot research area.

Find out more on how to host your own Frontiers Research Topic or contribute to one as an author by contacting the Frontiers editorial office: frontiersin.org/about/contact

Understanding mitochondrial dynamics and metabolic plasticity in cancer stem cells: Recent advances in cancer treatment and potential therapeutic approaches

Topic editors

Pramod Darvin — Queen Mary University of London, United Kingdom

Varun Sasidharan Nair — Helmholtz Center for Infection Research, Helmholtz Association of German Research Centers (HZ), Germany

Citation

Darvin, P., Nair, V. S., eds. (2023). *Understanding mitochondrial dynamics and metabolic plasticity in cancer stem cells: Recent advances in cancer treatment and potential therapeutic approaches*. Lausanne: Frontiers Media SA.

doi: 10.3389/978-2-8325-2504-3

Table of contents

frontiers | Frontiers in Oncology

TYPE Editorial
PUBLISHED 14 March 2023
DOI 10.3389/fonc.2023.1155774

OPEN ACCESS

EDITED AND REVIEWED BY
Ubaldo Emilio Martinez-Outschoorn,
Thomas Jefferson University, United States

*CORRESPONDENCE
Pramod Darvin
pramoddarvin@rgcb.res.in
Varun Sasidharan Nair
varunsasidharan.nair@helmholtz-hzi.de

SPECIALTY SECTION
This article was submitted to Cancer Metabolism, a section of the journal Frontiers in Oncology

RECEIVED 31 January 2023
ACCEPTED 07 March 2023
PUBLISHED 14 March 2023

CITATION
Darvin P and Sasidharan Nair V (2023) Editorial: Understanding mitochondrial dynamics and metabolic plasticity in cancer stem cells: Recent advances in cancer treatment and potential therapeutic approaches. *Front. Oncol.* 13:1155774. doi: 10.3389/fonc.2023.1155774

Editorial: Understanding mitochondrial dynamics and metabolic plasticity in cancer stem cells: Recent advances in cancer treatment and potential therapeutic approaches

Pramod Darvin[1]* and Varun Sasidharan Nair[2]*

[1]Cancer Research Division, Rajiv Gandhi Centre for Biotechnology, Trivandrum, India, [2]Department Experimental Immunology, Helmholtz Centre for Infection Research, Braunschweig, Germany

KEYWORDS

mitochondrial dynamics, mitophagy, mitochondrial immune evasion, cancer stem cell (CSC), hypoxic microenvironment

Editorial on the Research Topic
Understanding mitochondrial dynamics and metabolic plasticity in cancer stem cells: Recent advances in cancer treatment and potential therapeutic approaches

Mitochondria and mitochondrial homeostasis have been shown to play critical roles in the pathology of various chronic medical conditions including cancer. In cancer, mitochondria are associated with most of the basic cellular mechanisms and signaling events. Being the powerhouse of the cell, mitochondria control cellular energy metabolism and the generation of ATP through oxidative phosphorylation and reactive oxygen species (ROS). Mitochondria are also responsible for the maintenance of cellular homeostasis through controlled cell death. Several factors contribute to the vulnerability of mitochondrial genes to mutation, including the lack of proof-reading mechanism in the replication process, high ROS levels, and the absence of histone proteins (1, 2). This results in a high degree of acquired heterogeneity in tumor microenvironments during disease progression. Due to the direct involvement of mitochondria in cellular events, mitochondrial genes and mitochondrial proteins have immense potential as therapeutic targets and biomarkers for early detection and prognosis.

The mitochondrial DNA (mtDNA) copy number is a direct indication of mitochondrial activity and is known to be associated with cancer by influencing numerous cellular mechanisms. It is also interesting that both increases and decreases in mtDNA copy number alterations are responsible for cancer initiation and progression (3). In adult gliomas, the mtDNA copy number has been evaluated as an age-related predictive marker (4), and, in colon cancer (CRC), it has been reported as a predictor for poor prognosis (5). Moreover, mtDNA copy number variation has been found to be associated with poor prognosis of various other cancers such as cervical cancer, breast cancer, esophageal squamous carcinoma, and chronic lymphocytic leukemia (6–9). Apart from the

CNVs, mitochondrial protein expressions were also reported as prognostic biomarkers. Ubiquinol cytochrome *c* reductase binding protein (UQCRB), the protein responsible for the stabilization of mitochondrial ETC complex-III, was reported as a biomarker for CRC. The overall expression and CNV have been reported to be highly associated with CRC progression (10). In a case-control study of 260 renal cell carcinoma patients and 280 matched control individuals, a decreased mtDNA copy number was reported as a heritable predictive marker for higher cancer incidence (11).

In response to cell demands and environmental conditions, mitochondria can divide (mitochondrial fission) and fuse (mitochondrial fusion) (12). These dynamics have important roles in the pathology of cancer. The balance between fission and fusion is crucial in the maintenance of cellular processes such as energy metabolism, calcium signaling, oxygen sensing, and ROS generation. Most genes regulating mitochondrial fission and fusion are encoded by nuclear genes (13). In solid tumours, mitochondrial fission induces a reduction in the expression of MHC-I, causing immune escape (14) and making it a target to prevent immune evasion. Similarly, in triple negative breast cancer (TNBC) samples, significantly increased mitochondrial fission is associated with poorer survival (15). It is also observed that the survival of TNBC cells increased with a positive feedback loop to mitochondrial fission, by enhancing the Notch- and surviving-mediated pathways (15). On the other hand, Humphries et al. reported that TNBC with increased mitochondrial fission showed reduced metastatic potential (16).

Mitophagy, the elimination of defective mitochondria through autophagy, is considered to be a quality control mechanism, and any defects in mitophagy lead to impairment of mitochondrial functions, creating pathological alterations (17). Dysfunction of mitophagy leads to tumorigenesis (18) and the role of mitophagy varies with tumour progression. In a study using mitochondrial depletion, Yu-Seoun et al., demonstrated that mitochondrial dysfunction can lead to cancer cells acquiring stem cell-like properties (19). Furthermore, the mitochondrial density decreases as a result of increased mitophagy, which results in low reactive oxygen levels and low energy levels in the cells. Consequently, cells that possess stem cell-like quiescence properties survive in hypoxic conditions, resulting in residual cells and relapses of cancer. The majority of chemotherapies target rapidly dividing cells and ROS-producing cells, both of which become ineffective against quiescent cells, resulting in chemo resistance (20).

Metabolic reprogramming is an extremely prevalent feature of cancer cells and is directly linked to mitochondria. Mitochondria are indispensable to cancer cells because of their ability to generate ATP. In breast cancer cells, Lu et al., reported that the overexpression of mitochondrial fission regulator protein (MTFR2) alters the metabolism of glucose. MTFR2 changes oxidative phosphorylation (*OXPHOS*) into glycolysis in a HIF1α- and HIF2α-dependent manner (21). In hypoxic conditions, cancer cells also switch from *OXPHOS* to glycolysis. During this switching, anaerobic glycolysis generates lactate as the end product, which assists the cells in reducing ROS levels by utilizing metabolic intermediates such as pyruvate (22). In addition, it has been reported that glycolytic enzymes are upregulated during hypoxia; therefore, inhibiting these enzymes could be a promising way to eradicate residual cells and cancer stem cells (23–25). In addition to switching to glycolysis, the hypoxic microenvironment activates the pentose phosphate pathway (PPP). PPP activation produces NADPH and facilitates cancer cell survival in hypoxic environments by maintaining ROS homeostasis (26, 27).

Notably, mitochondria are the major source of intracellular ROS for a cell. By the oxidation of nucleotides, increased intracellular ROS directly damages nuclear and mitochondrial DNA. Similarly, reduced ROS levels cause cancer cells to enter a quiescent state, preventing them from being damaged by oxidative stress (28). Low levels of ROS are reported in cancer stem cells and metabolically inactive drug resistance cells (1). It has been shown that mitochondria-targeted photodynamic therapies (PDT) are effective in eliminating quiescent cancer stem cells and chemo-resistant cancers that are in a low-energy state (29). Integrated PDT uses the cancer cell's ROS and metabolic state to convert prodrugs into active photosensitizers or to specifically target photosensitizers to mitochondria, resulting in effective photosensitizer accumulation (30). Upon exposure to irradiation, mitochondria suffer irreversible damage, resulting in cell death.

In the tumor microenvironment (TME) hypoxia induces acidification with low pH through the accumulation of lactic acid from glycolysis. The low pH alters the expression of multiple genes that promote cancer cell invasion and metastasis, and inhibits immune cell infiltration into the TME (31). Mitochondria-mediated upregulation of carbonic anhydrase enzyme, responsible for cancer cell survival in acidic environments, is a target for inhibiting cancer progression and metastasis (van Gisbergen et al.). Moreover, at an acidic pH, the immune cells lose their ability to counteract cancer cells. According to a recent study by Yi-Ru et al., decreased mitophagy in T cells leads to the accumulation of depolarized mitochondria and terminal exhaustion of T cells. Notably, T cells treated with nicotinamide riboside recovered mitochondrial fitness and became responsive to PD-1 inhibitors, confirming the role of mitochondrial dynamics in T-cell exhaustion (32). In addition, MDSCs infiltrate tumors by secreting chemokines that are regulated by mitochondria through HIF-1α (28). An immune responsive TME results from targeting mitochondria to impede chemokine production, thereby affecting the recruitment of MDSCs and Tregs.

The transfer of mitochondria between cells of the TME is yet another mechanism for cell survival and immune evasion. Saha et al., with the help of advanced technologies, depicted the nanotube-mediated transfer of mitochondria between cancer cells and immune cells. The cancer cells benefit from this exchange by generating more energy and increasing their cell division, whereas the immune cells become inactive and exhausted from this exchange. A promising strategy to target the TME for cancer treatment is to inhibit nanotube formation to enhance immune therapies (33).

Mitochondria provide resistance against chemotherapeutic agents through a number of different ways. As discussed previously, the most important way is ROS homeostasis. Additionally, ATP-dependent efflux pathways for multidrug resistance (MDR) (34), as well as TME acidifications, are reported

to have a mechanistic impact on chemoresistance (35). Besides chemoresistance, the ROS scavenging ability protects cancer cells against radiotherapy (27).

Another therapeutic target is mitochondrial biogenesis in cancer cells. In a bioinformatics-based analysis of lung cancer patients, the key gene for mitochondrial biogenesis, HSPD1, was confirmed as a predictive biomarker (36). Additionally, pharmacological induction of Mfn-2 with Leflunomide increased mitochondrial fusion, with decreased ATP production and tumor growth in pancreatic ductal adenocarcinoma (37). Anti-mitochondrial therapy is a potential approach to target caner progression and metastasis. By inhibiting cancer cell mitochondria, numerous precancerous changes can be targeted. As well as preventing therapy resistance, targeting mitochondria can enhance chemotherapy, radiotherapy, and immunotherapy.

In this Research Topic, we discuss the critical function of mitochondria in cancer cells and TMEs. The mitochondria provide a connection between the cells of the TME and support the survival and progression of cancer cells. By modifying ROS homeostasis, mitochondria control the glycolytic flux and the induction of genes involved in progression and metastasis. Mitochondria in acidic TMEs inhibit immune infiltration, cause immune cell exhaustion, and induce cancer cell immune evasion. In cancer cells, mitochondria provide resistance to chemotherapy, radiotherapy, and immunotherapy. Taken together, mitochondria are crucial targets for drug therapies, and changes in mitochondrial copy number variations and gene expressions function as predictive and prognostic biomarkers.

Author contributions

PD and VSN equally contributed writing, editing, and proof reading. All authors contributed to the article and approved the submitted version.

Conflict of interest

The authors declare that the research was conducted in the absence of any commercial or financial relationships that could be construed as a potential conflict of interest.

Publisher's note

References

1. Fulda S, Galluzzi L, Kroemer G. Targeting mitochondria for cancer therapy. *Nat Rev Drug Discov* (2010) 9(6):447–64. doi: 10.1038/nrd3137

2. Bianchi NO, Bianchi MS, Richard SM. Mitochondrial genome instability in human cancers. *Mutat Res* (2001) 488(1):9–23. doi: 10.1016/S1383-5742(00)00063-6

3. Abd Radzak SM, Mohd Khair SZN, Ahmad F, Patar A, Idris Z, Mohamed Yusoff AA. Insights regarding mitochondrial DNA copy number alterations in human cancer (Review). *Int J Mol Med* (2022) 50(2):104. doi: 10.3892/ijmm.2022.5160

4. Sourty B, Dardaud L-M, Bris C, Desquiret-Dumas V, Boisselier B, Basset L, et al. Mitochondrial DNA copy number as a prognostic marker is age-dependent in adult glioblastoma. *Neurooncol Adv* (2022) 4(1):vdab191. doi: 10.1093/noajnl/vdab191

5. van Osch FHM, Voets AM, Schouten LJ, Gottschalk RWH, Simons CCJM, van Engeland M, et al. Mitochondrial DNA copy number in colorectal cancer: Between tissue comparisons, clinicopathological characteristics and survival. *Carcinogenesis* (2015) 36(12):1502–10. doi: 10.1093/carcin/bgv151

6. Campa D, Barrdahl M, Santoro A, Severi G, Baglietto L, Omichessan H, et al. Mitochondrial DNA copy number variation, leukocyte telomere length, and breast cancer risk in the European prospective investigation into cancer and nutrition (EPIC) study. *Breast Cancer Res* (2018) 20(1):29. doi: 10.1186/s13058-018-0955-5

7. Li H, Tian Z, Zhang Y, Yang Q, Shi B, Hou P, et al. Increased copy number of mitochondrial DNA predicts poor prognosis of esophageal squamous cell carcinoma. *Oncol Lett* (2018) 15(1):1014–20. doi: 10.3892/ol.2017.7416

8. Lan Q, Lim U, Liu C-S, Weinstein SJ, Chanock S, Bonner MR, et al. A prospective study of mitochondrial DNA copy number and risk of non-Hodgkin lymphoma. *Blood* (2008) 112(10):4247–9. doi: 10.1182/blood-2008-05-157974

9. Warowicka A, Kwasniewska A, Gozdzicka-Jozefiak A. Alterations in mtDNA: A qualitative and quantitative study associated with cervical cancer development. *Gynecol Oncol* (2013) 129(1):193–8. doi: 10.1016/j.ygyno.2013.01.001

10. Kim H-C, Chang J, Lee HS, Jeong Kwon H. Mitochondrial UQCRB as a new molecular prognostic biomarker of human colorectal cancer. *Exp Mol Med* (2017) 49 (11):e391–1. doi: 10.1038/emm.2017.152

11. Xing J, Chen M, Wood CG, Lin J, Spitz MR, Ma J, et al. Mitochondrial DNA content: Its genetic heritability and association with renal cell carcinoma. *JNCI: J Natl Cancer Institute* (2008) 100(15):1104–12. doi: 10.1093/jnci/djn213

12. Archer SL. Mitochondrial dynamics — mitochondrial fission and fusion in human diseases. *New Engl J Med* (2013) 369(23):2236–51. doi: 10.1056/NEJMra1215233

13. Koopman WJH, Willems PHGM, Smeitink JAM. Monogenic mitochondrial disorders. *New Engl J Med* (2012) 366(12):1132–41. doi: 10.1056/NEJMra1012478

14. Lei X, Lin H, Wang J, Ou Z, Ruan Y, Sadagopan A, et al. Mitochondrial fission induces immunoescape in solid tumors through decreasing MHC-I surface expression. *Nat Commun* (2022) 13(1):3882. doi: 10.1038/s41467-022-31417-x

15. Chen L, Zhang J, Lyu Z, Chen Y, Ji X, Cao H, et al. Positive feedback loop between mitochondrial fission and notch signaling promotes survivin-mediated survival of TNBC cells. *Cell Death Dis* (2018) 9(11):1050. doi: 10.1038/s41419-017-0127-z

16. Humphries BA, Cutter AC, Buschhaus JM, Chen Y-C, Qyli T, Palagama DSW, et al. Enhanced mitochondrial fission suppresses signaling and metastasis in triple-negative breast cancer. *Breast Cancer Res* (2020) 22(1):60. doi: 10.1186/s13058-020-01301-x

17. Youle RJ, van der Bliek AM. Mitochondrial fission, fusion, and stress. *Science* (2012) 337(6098):1062–5. doi: 10.1126/science.1219855

18. Chang JY, Yi H-S, Kim H-W, Shong M. Dysregulation of mitophagy in carcinogenesis and tumor progression. *Biochim Biophys Acta (BBA) - Bioenergetics* (2017) 1858(8):633–40. doi: 10.1016/j.bbabio.2016.12.008

19. Han Y-S, Yi E-Y, Jegal M-E, Kim Y-J. Cancer stem-like phenotype of mitochondria dysfunctional Hep3B hepatocellular carcinoma cell line. *Cells* (2021) 10(7). doi: 10.3390/cells10071608

20. Blagosklonny MV. Carcinogenesis, cancer therapy and chemoprevention. *Cell Death Differ* (2005) 12(6):592–602. doi: 10.1038/sj.cdd.4401610

21. Lu G, Yuanhui L, Wang T, Lin W, Lu J, Ma Y, et al. Mitochondrial fission regulator 2 (MTFR2) promotes growth, migration, invasion and tumour progression in breast cancer cells. *Aging* (2019) 11(22):10203–19. doi: 10.18632/aging.102442

22. Vaupel P, Multhoff G. Revisiting the warburg effect: historical dogma versus current understanding. *J Physiol* (2021) 599(6):1745–57. doi: 10.1113/JP278810

23. Chang C-W, Lo J-F, Wang XW. Roles of mitochondria in liver cancer stem cells. *Differentiation* (2019) 107:35–41. doi: 10.1016/j.diff.2019.04.001

24. Song K, Kwon H, Han C, Zhang J, Dash S, Lim K, et al. Active glycolytic metabolism in CD133(+) hepatocellular cancer stem cells: regulation by MIR-122. *Oncotarget* (2015) 6(38). doi: 10.18632/oncotarget.5812

25. Hur W, Ryu JY, Kim HU, Hong SW, Lee EB, Lee SY, et al. Systems approach to characterize the metabolism of liver cancer stem cells expressing CD133. *Sci Rep* (2017) 7(1):45557. doi: 10.1038/srep45557

26. Paredes F, Williams HC, San Martin A. Metabolic adaptation in hypoxia and cancer. *Cancer Lett* (2021) 502:133–42. doi: 10.1016/j.canlet.2020.12.020

27. Li P, Zhang D, Shen L, Dong K, Wu M, Ou Z, et al. Redox homeostasis protects mitochondria through accelerating ROS conversion to enhance hypoxia resistance in cancer cells. *Sci Rep* (2016) 6(1):22831. doi: 10.1038/srep22831

28. Chiu DK-C, Xu IM-J, Lai RK-H, Tse AP-W, Wei LL, Koh H-Y, et al. Hypoxia induces myeloid-derived suppressor cell recruitment to hepatocellular carcinoma through chemokine (C-c motif) ligand 26. *Hepatology* (2016) 64(3):797–813. doi: 10.1002/hep.28655

29. Darvin P, Aneesh C, Shankara NV, Chandrasekhar L, Thomas Maliakkal R, John SSM, et al. Mitochondria targeted redox GFP reveals time and dose dependent onset and progression of mitochondrial oxidation with diverging cell death decisions during photodynamic therapy. *Photodiagnosis Photodyn Ther* (2020) 31:101921. doi: 10.1016/j.pdpdt.2020.101921

30. Zhang ZJ, Wang K-P, Mo J-G, Xiong L, Wen Y. Photodynamic therapy regulates fate of cancer stem cells through reactive oxygen species. *World J Stem Cells* (2020) 12 (7):562–84. doi: 10.4252/wjsc.v12.i7.562

31. White KA, Grillo-Hill BK, Barber DL. Cancer cell behaviors mediated by dysregulated pH dynamics at a glance. *J Cell Sci* (2017) 130(4):663–9. doi: 10.1242/jcs.195297

32. Yu Y-R, Imrichova H, Wang H, Chao T, Xiao Z, Gao M, et al. Disturbed mitochondrial dynamics in CD8+ TILs reinforce T cell exhaustion. *Nat Immunol* (2020) 21(12):1540–51. doi: 10.1038/s41590-020-0793-3

33. Saha T, Dash C, Jayabalan R, Khiste S, Kulkarni A, Kurmi K, et al. Intercellular nanotubes mediate mitochondrial trafficking between cancer and immune cells. *Nat Nanotech* (2022) 17(1):98–106. doi: 10.1038/s41565-021-01000-4

34. Ji L, Li H, Gao P, Shang G, Zhang DD, Zhang N, et al. Nrf2 pathway regulates multidrug-Resistance-Associated protein 1 in small cell lung cancer. *PloS One* (2013) 8 (5):e63404. doi: 10.1371/journal.pone.0063404

35. Bohloli M, Atashi A, Soleimani M, Kaviani S, Anbarlou A. Investigating effects of acidic pH on proliferation, invasion and drug-induced apoptosis in lymphoblastic leukemia. *Cancer Microenviron* (2016) 9(2):119–26. doi: 10.1007/s12307-016-0187-0

36. Sotgia F, Lisanti MP. Mitochondrial markers predict survival and progression in non-small cell lung cancer (NSCLC) patients: Use as companion diagnostics. *Oncotarget* (2017) 8(40). doi: 10.18632/oncotarget.19677

37. Yu M, Nguyen ND, Huang Y, Lin D, Fujimoto TN, Molkentine JM, et al. Mitochondrial fusion exploits a therapeutic vulnerability of pancreatic cancer. *JCI Insight* (2019) 4(16). doi: 10.1172/jci.insight.126915

frontiers in Oncology

ORIGINAL RESEARCH
published: 15 September 2020
doi: 10.3389/fonc.2020.546110

Clinical and Prognostic Relevance of B7-H3 and Indicators of Glucose Metabolism in Colorectal Cancer

Ting Zhang[1], Yufen Jin[2], Xin Jiang[2], Longhai Li[2], Xiaowei Qi[2,3], Yong Mao[2,4]* and Dong Hua[1,2,4]**

[1] Institue of Cancer, Affiliated Hospital of Jiangnan University, Wuxi, China, [2] Wuxi School of Medicine, Jiangnan University, Wuxi, China, [3] Department of Pathology, Affiliated Hospital of Jiangnan University, Wuxi, China, [4] Department of Oncology, Affiliated Hospital of Jiangnan University, Wuxi, China

OPEN ACCESS

Edited by:
Joseph Curry,
Thomas Jefferson University,
United States

Reviewed by:
Christos K. Kontos,
National and Kapodistrian University of Athens, Greece
Amilcare Barca,
University of Salento, Italy

***Correspondence:**
Ting Zhang
ztcathy_05@163.com
Yong Mao
mydoctor@aliyun.com
Dong Hua
wx89211@163.com

Specialty section:
This article was submitted to Cancer Metabolism, a section of the journal Frontiers in Oncology

Received: 29 April 2020
Accepted: 20 August 2020
Published: 15 September 2020

Citation:
Zhang T, Jin Y, Jiang X, Li L, Qi X, Mao Y and Hua D (2020) Clinical and Prognostic Relevance of B7-H3 and Indicators of Glucose Metabolism in Colorectal Cancer. Front. Oncol. 10:546110. doi: 10.3389/fonc.2020.546110

Objective: This study aimed to investigate the clinical and prognostic relevance of B7-H3 expression and indicators of glucose metabolism in patients with colorectal cancer (CRC).

Methods: Using immunohistochemistry, the expression of B7-H3 was detected in a total of 213 formalin-fixed paraffin-embedded CRC tissue specimens. Furthermore, levels of fasting blood glucose (FBG), lactic dehydrogenase (LDH), and fructosamine (FMN) as indicators of glucose metabolism were analyzed in CRC patients and stratified into high or low expression sub-groups based on Youden Index. The relationship between B7-H3, FBG, LDH, FMN expression, and clinicopathological characteristics were also evaluated to establish their prognostic significance in patients with CRC.

Results: B7-H3 was highly expressed in CRC tissue. The positive rates of B7-H3 expression was 63.8% (136/213). We found a linear correlation between B7-H3 and FBG in depth of tumor invasion (T3/4) ($p = 0.037$, $r = 0.259$), lymph node metastasis (N0) ($p = 0.004$, $r = 0.259$), and TNM stage (I/II) ($p = 0.009$, $r = 0.242$). High expression of FBG, LDH, FMN [hazard ratio (HR) = 1.916, 95% CI: 1.223–3.00, $p = 0.005$; HR = 1.801, 95% CI: 1.153–2.813, $p = 0.010$; HR = 2.154, 95% CI: 1.336–3.472, $p = 0.002$], respectively, was identified as a significant independent predictor of poor overall survival (OS). Although B7-H3 expression did not affect OS, CRC patients expressing both high B7-H3 and high FMN contributed to a significant decrease in OS (HR = 1.881, 95%CI: 1.059–3.339, $p = 0.031$). Moreover, with low expression of B7-H3, high expression of FBG, LDH and FMN were also recognized as predictors of inferior OS (HR = 3.393, 95% CI: 1.493-7.709, $p = 0.004$; HR = 7.107, 95% CI: 2.785–18.138, $p = 0.000$; HR = 2.800, 95% CI: 1.184–6.625, $p = 0.019$).

Conclusion: B7-H3 combined with FBG, LDH, or FMN, could reflect the clinical outcomes of patients with CRC.

Keywords: B7-H3, glucose metabolism, colorectal cancer, correlation, prognosis

INTRODUCTION

Colorectal cancer (CRC) remains the third most frequently diagnosed gastrointestinal tract malignancy in men and second in women, globally. Although the mortality rate of CRC has been declining progressively, it still represents the third leading cause of cancer-associated mortality for both men and women (1). In contrast to these declines, CRC remains the most rapidly increasing cancer in China over the past few decades. This rise in CRC incidence has become one of the major public health concerns causing a substantial health burden to families and also contributing to overburdened healthcare systems (2). Recently, Gu et al. summarized tobacco smoking, alcohol abuse, obesity, low physical activity, low fruit and fiber consumption, and high intake of red and processed meat as the significant attributable causes of CRC in China (3). Moreover, these risk factors were also associated with poor prognosis of CRC, particularly in CRC patients with diabetes mellitus (DM).

In the past three decades, the prevalence of DM and associated health complications has substantially increased in the world, and DM represented the ninth leading cause of death (4). Notably, China has rapidly emerged as a region with DM global epidemic, owing to an unhealthy diet and a sedentary lifestyle as critical drivers (5). Moreover, accumulating epidemiological studies have indicated a positive association of DM with the risk of CRC (6). Several similar risk factors, including western lifestyle, have been reported between DM and CRC. Furthermore, fasting blood glucose (FBG), as an indicator of DM, was also found to be significantly related to the risk of CRC (7). Also, aerobic glycolysis is the most common energy metabolism characteristic of cancer cells. Previously, Graziano et al. analyzed mRNA expression of the key enzymes including GLUT1, LDHA, HK1, PKM2, and VDAC1 mRNA involved in glycolysis in CRC patients and revealed that expression levels were significantly higher in primary tumor tissues compared with normal mucosa (8). Besides, altered expression of genes involved in glucose uptake and glycolysis was also reported in CRC tissues (9, 10).

Immune checkpoint protein B7 homolog 3 (B7-H3 or CD276), a type I transmembrane glycoprotein, belongs to the B7 and CD28 superfamilies. While limited-expression has been observed in normal healthy tissues, overexpression of B7-H3 has been reported in a variety of malignancy and plays a crucial role in tumor progression (11). Clinically, B7-H3 overexpression in tumors has been associated with poor clinical outcomes (12). Moreover, increasing studies have indicated that the aberrant expression of B7-H3 is a consistent characteristic of CRC. Thus, B7-H3 detection might be an effective means to predict the prognosis in patients with CRC. Besides, Fang et al. demonstrated an increased level of soluble B7-H3 in type 1 diabetes patients compared with healthy controls (13), implying that B7-H3 might be a promising biomarker in the pathogenesis of diabetes. Furthermore, by inducing expression of the key glycolytic enzyme, hexokinase 2 (HK2), overexpression of B7-H3 has been documented to increase the rate of glucose consumption and lactate production (14). These findings indicated that B7-H3 might be a novel regulator of glucose metabolism in CRC cells and a promising therapeutic target for CRC. Moreover, in hypoxic conditions, lactic dehydrogenase (LDH) has been known to convert pyruvate to lactic acid to support tumor cells, and elevated serum LDH has been reported to express in cancer and considered to be an independent prognostic predictor (15, 16). Besides, fructosamine (FMN) predominantly represents a measure of glycated albumin, which is the most abundant of the serum proteins. As the half-life of albumin is shorter than that of hemoglobin A1c (HbA1c), FMN reflects a shorter duration of glycemic control over the past 2–3 weeks period. This evidence indicates that FMN could be used as a short-term marker of glucose control. Moreover, elevated FMN levels have been associated with an increased risk of colorectal adenoma, a precursor of CRC (17).

Despite these pieces of evidence, only limited studies have been focused on B7-H3 and the indicators of glucose metabolism (FBG, LDH, and FMN) in CRC patients. Therefore, the present study was initiated to investigate the clinical and prognostic significance of B7-H3, FBG, LDH, and FMN in patients CRC.

MATERIALS AND METHODS

Patients and Samples Collection

The medical records of patients who received a histopathological diagnosis and underwent surgical resection for CRC at the Affiliated Hospital of Jiangnan University between June 2008 and December 2011 were included. A total of 213 formalin-fixed paraffin-embedded CRC tissue samples were included in this study. For this study, only histopathologically confirmed cases were included. Besides, patients who received chemo- or radiotherapy before surgery and cases with incomplete clinical data were excluded from the study. For all patients, pathological stages were defined according to the seventh edition American Joint Committee on Cancer (AJCC) cancer staging manual using available clinical and pathologic tumor, node, and metastasis data. Patient demographic data, including age and gender and clinicopathologic characteristics, such as tumor size and histologic grade and FBG, LDH, and FMN from clinical laboratory investigation, were also collected. This study was approved by the Medical Ethics Committee of the Affiliated Hospital of Jiangnan University (No. LS2019027), and written informed consent was obtained from all patients. All the patients were followed-up over telephone up to October 31, 2017, in order to analyze patient survival. The median follow-up was 80 months (range; 8–115 months).

Tissue Microarray Construction and Immunohistochemistry Staining

Two experienced pathologists examined the section stained with hematoxylin and eosin (HE) and marked the carcinoma sites in the corresponding paraffin block. The detailed tissue microarray (TMA) construction protocol followed was as described previously (18). Briefly, the TMAs were constructed by obtaining a tissue cylinder of 1.0-mm in diameter core tissue

biopsies from representative paraffin-embedded sections of each donor tissue block and implanted into the hole of the premade recipient paraffin block. The tissue paraffin blocks were serially sectioned into 4 μm thick sections, deparaffinized in xylene, and hydrated in an ethanol gradient. Antigen retrieval was performed by heating the tissue sections at 100°C in sodium citrate buffer for 30 min. Moreover, endogenous peroxidase was blocked by incubation in 3% hydrogen peroxide for 10 min. Subsequently, the sections were incubated in 5% bovine serum albumin (BSA) at room temperature (RT) for 30 min. Primary antibody, mouse anti-human B7-H3 monoclonal antibody (1:200, Santa Cruz, CA, United States) added dropwise followed by overnight incubation at 4°C. Following incubation, the slides were washed and incubated with a horseradish peroxidase-conjugated secondary antibody for 30 min. The immunostaining was carried out by staining with 3, 3'-diaminobenzidine chromogen (DAB) (GTVisionII Immunohistochemistry Detection Kit for Rabbit/Mouse, GeneTech, China) and counter-stained with hematoxylin, dehydrated, and mounted and the sections were examined under a microscope. Two independent pathologists evaluated the percentage of positive cells (score of 0: ≤5%; score of 1: 6–25%; score of 2: 26–50%; score of 3: 51–75%; score of 4: >76%) and the intensity [0 for negative staining (no coloration); 1 for weakly positive (faint yellow); 2 for moderately positive (yellowish brown); 3 for strongly positive (brown)] of all samples. The two scores were multiplied to generate the final score for each specimen range from 0 to 12.

Verification of the Cut-Off Value

We analyzed the receiver operating characteristics (ROC) curve of B7-H3, FBG, LDH, and FMN through SPSS 23.0 software (IBM, United States). Then, the Youden Index was calculated according to the formula sensitivity + specificity − 1. The maximum Youden Index representing the expression value of the target was considered as the cut-off value. Based on values, patients with less than cut-off value was defined as low expression group and those with a value equal or greater than cut-off value as described as high expression group.

Statistical Analysis

The relationship between clinicopathological parameters and B7-H3, FBG, LDH, or FMN was analyzed using the Chi-square test. The Mann–Whitney test was used to analyze the difference of the expression of B7-H3, FBG, LDH, and FMN for each clinical characteristic. The non-parametric Spearman test evaluated the correlation of B7-H3 and FBG, LDH, or FMN expression in CRC patients. Overall survival (OS) was plotted using the Kaplan–Meier method and compared using the log-rank test. The Cox proportional hazard model was used to perform multivariate survival analysis. The R software version 3.6.1 and the RMS package (R Foundation for Statistical Computing) were used to perform the nomogram analysis and calibration plot. All data were analyzed using the SPSS package (version 23.0, IBM, Chicago, IL, United States). All figures were generated with GraphPad Prism 6.0 (GraphPad Software Inc., United States). A P-value of <0.05 was considered statistically significant.

RESULTS

Clinicopathological Parameters of Patients

The clinicopathological parameters of 213 CRC patients were summarized in **Table 1**. The study comprised 118 males (55.4%) and 95 females (44.6%). The age at initial diagnosis was classified into <60 years (37.6%) or ≥60 years (62.4%), and the median age of the patients was 62 (range, 27–87 years old). 38.5% of tumors were located or distributed in the colon (n = 82) and 61.5% of tumors were located in the rectum (n = 131). Lymph node metastasis (N1–N2) was noted in 43.7% of cases. There were 115 (54.0%) cases with stage I-II disease and 98 (46.0%) cases with stage III–IV disease.

Expression of B7-H3, FBG, LDH, and FMN in CRC Patients

Using immunochemistry, we detected the expression of B7-H3 in CRC tissue. According to the cut-off value of 2.5, scores of 0–2 were defined as the low expression group, and scores of 3–12 were considered as the high expression group. Similar to previous studies, B7-H3 was highly expressed in CRC tissue. The positive rates of B7-H3 expression were 63.8% (136/213). Furthermore, positive staining of B7-H3 was predominantly localized in the cytoplasm and membrane of tumor cells. The representative images were presented in **Figure 1**. Similarly, based on the value of FBG, LDH, and FMN from the clinical laboratory and survival outcome of patients, we calculated the cut-off value using the Youden Index. Thus, patients were defined as either low expression of FBG with the value <5.425 or high expression of FBG with the value ≥5.425. We found that 32.9% of cases exhibited high expression of FBG (70/213). Also, the cut-off value of LDH and FMN were defined as 169.5 and 202.5, respectively, and the corresponding positive rates of LDH and FMN expression in patients with CRC were 35.7% (76/213) and 21.1% (45/213).

Correlation Between B7-H3, FBG, LDH, and FMN and Clinicopathological Characteristics of Patients With CRC

A significant difference between the expression of B7-H3 and the gender of patients with CRC was found (p = 0.028). Notably, positive expression of LDH was significantly associated with tumor location (p = 0.048) and distant metastasis (p = 0.009). Furthermore, the FMN expression was significantly related to the lymph node metastasis (p = 0.013) and the TNM stage (p = 0.014). However, the expression of FBG exhibited no significant association with any clinicopathological characteristics (**Table 1**). Using the Mann–Whitney test, we confirmed the marked differences between B7-H3 and gender (p = 0.046), LDH, and distant metastasis (p = 0.009). Notably, the expression of FMN was significantly associated with tumor location (p = 0.016), colon cancer site (p = 0.009), depth of tumor invasion (p = 0.032), lymph node metastasis (p = 0.046), and TNM stage (p = 0.033) (**Figure 2**).

TABLE 1 | Association of B7-H3, FBG, LDH, and FMN expression in CRC patients with clinicopathological parameters.

Clinical parameter	Case (*n*)	B7-H3 expression		*p* value	FBG expression		*p* value	LDH expression		*p* value	FMN expression		*p* value
		Low	High		Low	High		Low	High		Low	High	
Gender				**0.028**			0.216			0.545			0.718
Male	118	35	83		75	43		78	40		92	26	
Female	95	42	53		68	27		59	36		76	19	
Age (years)				0.572			0.831			0.872			0.467
<60	80	27	53		53	27		52	28		61	19	
≥60	133	50	83		90	43		85	48		107	26	
Tumor location				0.098			0.237			**0.048**			0.252
Colon	82	24	58		59	23		46	36		68	14	
Rectum	131	53	78		84	47		91	40		100	31	
Colon cancer site				0.371			0.655			0.763			0.212
Left-sided	176	66	110		117	59		114	62		136	40	
Right-sided	37	11	26		26	11		23	14		32	5	
Depth of tumor invasion				0.130			0.335			0.231			0.588
T1/2	64	28	36		46	18		45	19		49	15	
T3/4	149	49	100		97	52		92	57		119	30	
Lymph node metastasis				0.494			0.192			0.600			**0.013**
N0	120	41	79		85	35		79	41		102	18	
N1/2	93	36	57		58	35		58	35		66	27	
Distant metastasis				0.428			0.968			**0.009**			0.063
Yes	15	4	11		10	5		5	10		9	6	
No	198	73	125		133	65		132	66		159	39	
TNM stage				0.870			0.161			0.384			**0.014**
I/II	115	41	74		82	33		77	38		98	17	
III/IV	98	36	62		61	37		60	38		70	28	
Neural invasion				0.685			0.288			0.479			0.917
Yes	39	13	26		29	10		27	12		31	8	
No	174	64	110		114	60		110	64		137	37	
Vascular invasion				0.307			0.554			0.337			0.278
Yes	35	10	25		25	10		25	10		30	5	
No	178	67	111		118	60		112	66		138	40	
Mucinous adenocarcinoma				0.707			0.831			0.124			0.897
Yes	20	8	12		13	7		16	4		16	4	
No	193	69	124		130	63		121	72		152	41	
Differentiation				0.461			0.538			0.739			0.284
Well	76	25	51		49	27		50	26		63	13	
Moderate/Poor	137	52	85		94	43		87	50		105	32	

LDH, lactic dehydrogenase; FMN, fructosamine; FBG, fasting blood glucose; OS, overall survival. Bold values mean significant p value which is < 0.05.

Correlation Between B7-H3 and FBG, LDH, or FMN Expression in CRC

To determine whether B7-H3 expression associated with FBG, LDH, or FMN expression in CRC, correlations analysis was conducted. However, there was no significant linear relationship between the expression of B7-H3 and FBG, LDH or FMN in all CRC tissue. Further, we analyzed the correlation between B7-H3 and FBG, LDH or FMN in different stages. We found a linear correlation between B7-H3 and FBG with depth of tumor invasion (T3/4) (p = 0.037, r = 0.259), lymph node metastasis (N0) (p = 0.004, r = 0.259) and TNM stage (I/II) (p = 0.009, r = 0.242) (**Figure 3**). These findings indicated a significant correlation between the expression of B7-H3 and FBG in the early stage of CRC.

Prognostic Value of B7-H3, FBG, LDH, and FMN Expression

OS was computed from the date of surgery until the patient's death. The 5-year survival rate was 63.4% (135/213) for patients with CRC in this study. We respectively analyzed the associations between OS and the expression of B7-H3, FBG, LDH, or FMN. Although the expression of B7-H3 did not affect the OS of patients (p = 0.195) (**Figure 4A**), notably, patients with the high expression of FBG, LDH, or FMN exhibited a significantly worse OS compared to patients with low expression (p = 0.004,

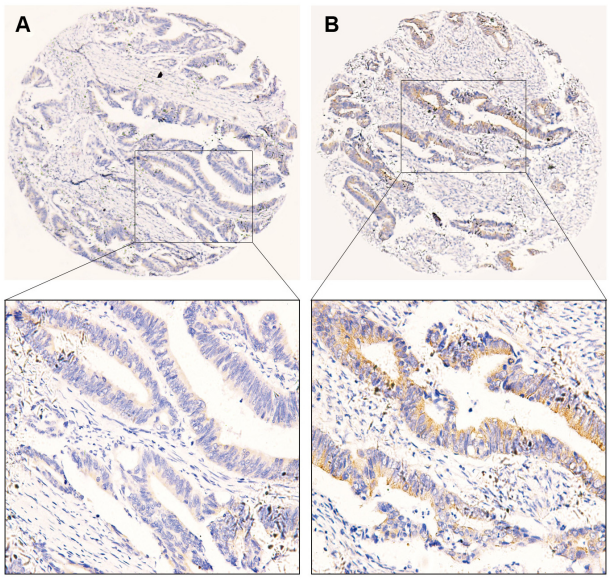

FIGURE 1 | Representative images of immunohistochemical staining of B7-H3 expression in colorectal cancer tissue. **(A)** Low expression of B7-H3 (40×). **(B)** High expression of B7-H3 (40×). The images below show the magnification of each zone (200×). Scale bar = 50μm.

$p = 0.009$, and $p = 0.001$) (**Figures 4B–D**). Furthermore, we also evaluated the correlation between OS and FBG, LDH, or FMN in the subgroup with different expression of B7-H3. Interestingly, in the subgroup with high B7-H3 expression, the only subgroup with high FMN expression exhibited significantly worse OS compared to the subgroup with high FBG or LDH expression ($p = 0.028$) (**Figures 4E,G,I**). However, a subgroup of patients with low expression of B7-H3 and high FBG, or high LDH, or high FMN exhibited significantly worse prognosis as compared to patients with low expression of FBG, LDH or FMN ($p = 0.002$, $p < 0.0001$, and $p = 0.014$) (**Figures 4F,H,J**).

Furthermore, to evaluate the risk factors associated with the prognosis of patients with CRC, univariate Cox proportional hazard model analysis was performed. As represented in **Table 2**, depth of tumor invasion (T3/4), lymph node metastasis (N1/2), distant metastasis, TNM stage (III/IV), neural invasion, high expression of FBG, high expression of LDH, high expression of FMN, high expression of both B7-H3 and FMN, low expression of B7-H3 and high expression of FBG, low expression of B7-H3 and high expression of LDH, low expression of B7-H3 and high expression of FMN were highly correlated with the OS of patients with CRC. Besides, the multivariate analysis revealed that distant metastasis and high expression of FBG were significant independent prognostic factors for OS of patients with CRC (**Table 2**).

Development and Validation of Nomograms for Predicting Prognosis

To envisage the prognostic significance of B7-H3, FBG, LDH, and FMN expression, we generated nomograms for OS based on the expression of B7-H3, FBG, LDH, and FMN, and other clinicopathological characteristics (**Figure 5A**). Using nomogram construction, we could identify the score on the point-scale corresponding to significant factors of each subtype. Then, the total points of each patient were calculated by adding up the score of independent variables altogether. Lastly, by analyzing the complete point scale, we were able to estimate the probability of survival at different time points. The findings indicated that distant metastasis was a significant determinant of prognosis, followed by the FBG expression, depth of tumor invasion, and TNM stage. Overall, it implied that, the larger the score, the higher the survival rate, and *vice versa*. Subsequently, we were able to predict the prognosis based on nomogram analysis. **Figures 5B,C** showed the 3-year and 5-year calibration of the nomogram for OS, establishing a pronounced prediction accuracy of this nomogram, indicating that calibration curves for nomogram revealed no deviations from the reference line.

DISCUSSION

Colorectal cancer remains one of the most frequently diagnosed malignancies worldwide. Increasing pieces of evidence support that the majority of CRC are sporadic, which are predominantly attributable to the constellation of modifiable risk factors characterizing westernization as the significant risk factor (19). These risk factors have also been consistently related to the occurrence of DM (20). In addition, the risk of developing CRC was estimated to be 27% higher in patients with type 2 DM compared to non-diabetic controls (21). Recently, a meta-analysis by Zhu et al. suggested that diabetes had a negative effect on CRC in OS (22). DM was a chronic disease mainly characterized by disturbances in glucose metabolism (23). Besides, altered energy metabolism is one of the biochemical fingerprints of cancer cells, representing it as one of the hallmarks of cancer, including CRC. Colorectal cancer has also been characterized by altered glucose metabolism mediated by glycolytic pathways (24). Although conceptual advances have significantly improved the understanding on the clinical significance of tumor metabolism, only limited studies have been focused on B7-H3 as indicators of glucose metabolism in CRC patients. Therefore, this study investigated the survival outcome of patients with CRC by the indicators of glucose metabolism.

In the present study, three clinical indicators most frequently used in our hospital were selected, including FBG, LDH, and FMN. FBG was measured as the major criterion of DM, indicating the level of glucose in the blood. LDH is a key enzyme of glycolysis, which catalyzes the inter-conversion of pyruvate and lactate, and it also converts pyruvate, the final product of glycolysis, to lactate in the absence of oxygen. The high expression of LDH can reveal abnormal glucose metabolism. Fructosamine is formed through glycosylation of serum protein, such as albumin. The concentration of FMN in serum directly reflects blood glucose concentration precisely than HbA1c.

Furthermore, a deregulated or altered energy metabolism has been predominantly recognized as the "hallmarks of cancer." Recently, studies have implicated different roles of lactate

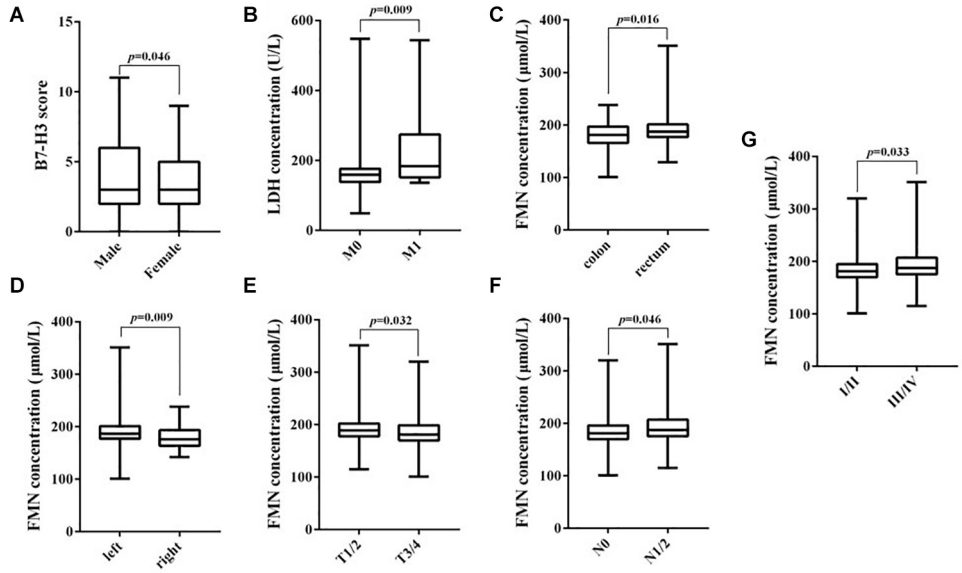

FIGURE 2 | Correlation between B7-H3, LDH, and FMN expression and clinicopathological parameters. **(A)** B7-H3 and gender; **(B)** LDH and distant metastasis; **(C)** FMN and tumor location; **(D)** FMN and colon cancer site; **(E)** FMN and depth of tumor invasion; **(F)** FMN and lymph node metastasis; **(G)** FMN and TNM stage.

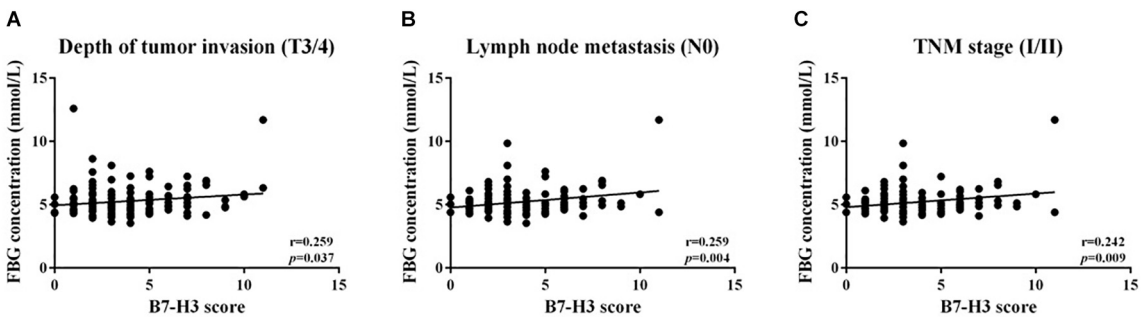

FIGURE 3 | Positive linear relationship between B7-H3 and FBG. **(A)** Depth of tumor invasion (T3/4); **(B)** lymph node metastasis (N0); **(C)** TNM stage (I/II).

export/import contributing to the survival and growth of cancer. In this study, the expression of LDH was significantly correlated with tumor location and distant metastasis, the expression of FMN was notably associated with lymph node metastasis and TNM stage; however, no significant relationship between the expression of FBG and clinicopathological characteristics were recorded. Next, a significant correlation between LDH expression and distant metastasis, also between FMN expression and tumor location, colon cancer site, depth of tumor invasion, lymph node metastasis, and TNM stage was demonstrated with Mann Whitney test. In contrast, FBG expression had no relation with pathological features. These findings suggested the respective expression of LDH or FMN had a closer relationship with the parameters of CRC patients than FBG expression in this study. Moreover, high expression of FBG, LDH, or FMN all indicated poor OS of CRC patients eloquently. Conceivably, FBG, LDH, and FMN could predict the prognosis of patients with CRC as an independent prognostic factor. Clinically, the value of FBG, LDH, and FMN could be controlled to perceive the progression in patients with CRC.

Treatment with immune checkpoint inhibitors has emerged as a frontline treatment for patients with CRC, mainly targeting cytotoxic T-lymphocyte antigen 4 (CTLA-4) and programed death-1 receptor (PD1) and its ligand PD-L1 (25). B7-H3, as one of the crucial immune checkpoint proteins, plays a critical role in the occurrence and development of CRC. Clinically, the expression of B7-H3 was associated with unfavorable outcomes in CRC patients (12, 26). However, there was no relationship between B7-H3 expression and OS in this study, which might be attributed to low sample size or the uncertainty of repeated experiments. Nevertheless, over 1000 cases were included in other investigations in order to predict the prognosis of patients. It is noteworthy that the overexpression of B7-H3 has been suggested as a predictor of poor OS in our previous study with more than 200 patients. Thus, the prognostic significance of B7-H3 warrants further validation in future investigation.

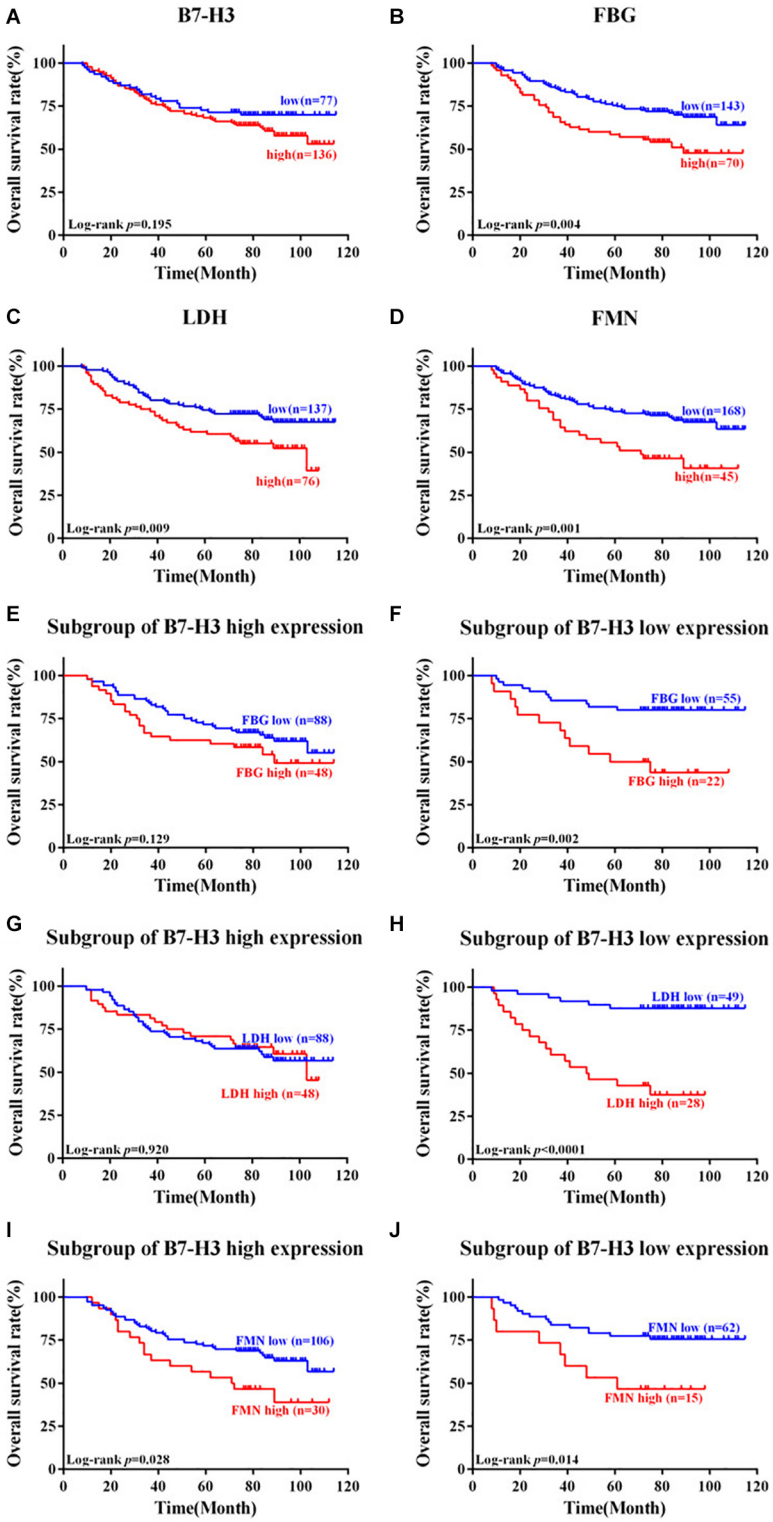

FIGURE 4 | Kaplan-Meier survival curves of patients with colorectal cancer expressing B7-H3, FBG, LDH, and FMN. **(A)** Patients with low expression of B7-H3 vs. high expression of B7-H3. **(B)** Patients with low expression of FBG vs. high expression of FBG. **(C)** Patients with low expression of LDH vs. high expression of LDH. **(D)** Patients with low expression of FMN vs. high expression of FMN. **(E)** Subgroup of patients with high expression of B7-H3 and low expression of FBG vs. high expression of FBG. **(F)** Subgroup of patients with low expression of B7-H3 and low expression of FBG vs. high expression of FBG. **(G)** Subgroup of patients with high expression of B7-H3 and low expression of LDH vs. high expression of LDH. **(H)** Subgroup of patients with low expression of B7-H3 and low expression of LDH vs. high expression of LDH. **(I)** Subgroup of patients with high expression of B7-H3 and low expression of FMN vs. high expression of FMN. **(J)** Subgroup of patients with low expression of B7-H3 and low expression of FMN vs. high expression of FMN.

TABLE 2 | Univariate and multivariate analyses of clinical parameters associated with OS in CRC patients.

Clinical parameter	Univariate analysis		Multivariate analysis	
	HR (95%CI)	*p* value	HR (95%CI)	*p* value
Gender (male vs. female)	0.876 (0.559–1.373)	0.563		
Age (≥60 vs. <60)	1.201 (0.753–1.916)	0.441		
Tumor location (colon vs. rectum)	0.770 (0.492–1.206)	0.254		
Colon cancer site (right-sided vs. left-sided)	1.112 (0.624–1.983)	0.719		
Depth of tumor invasion (T3/4 vs. T1/2)	2.481 (1.367–4.503)	**0.003**	1.812 (0.972–3.372)	0.061
Lymph node metastasis (N1/2 vs. N0)	2.445 (1.547–3.865)	**0.000**	0.597(0.177–2.015)	0.406
Distant metastasis (yes vs. no)	11.646 (6.364–21.312)	**0.000**	5.949 (2.788–12.697)	**0.000**
TNM stage (III/IV vs. I/II)	3.001 (1.871–4.814)	**0.000**	3.349 (0.911–12.307)	0.069
Neural invasion (yes vs. no)	1.726 (1.037–2.871)	**0.036**	1.219 (0.699–2.126)	0.484
Vascular invasion (yes vs. no)	1.565 (0.914–2.681)	0.103		
Mucinous adenocarcinoma (no vs. yes)	0.792 (0.344–1.824)	0.584		
Differentiation (well vs. moderate/poor)	0.786 (0.500–1.236)	0.297		
B7-H3 (high vs. low)	1.377 (0.846–2.240)	0.198		
FBG (high vs. low)	1.916 (1.223–3.000)	**0.005**	1.733 (1.050–2.861)	**0.032**
LDH (high vs. low)	1.801 (1.153–2.813)	**0.010**	1.430 (0.902–2.266)	0.128
FMN (high vs. low)	2.154 (1.336–3.472)	**0.002**	1.377 (0.807–2.352)	0.241
B7-H3 high (FBG high vs. low)	1.444 (0.841–2.479)	0.183		
B7-H3 high (LDH high vs. low)	0.972 (0.557–1.695)	0.920		
B7-H3 high (FMN high vs. low)	1.881 (1.059–3.339)	**0.031**		
B7-H3 low (FBG high vs. low)	3.393 (1.493–7.709)	**0.004**		
B7-H3 low (LDH high vs. low)	7.107 (2.785–18.138)	**0.000**		
B7-H3 low (FMN high vs. low)	2.800 (1.184–6.625)	**0.019**		

Bold values mean significant p value which is < 0.05.

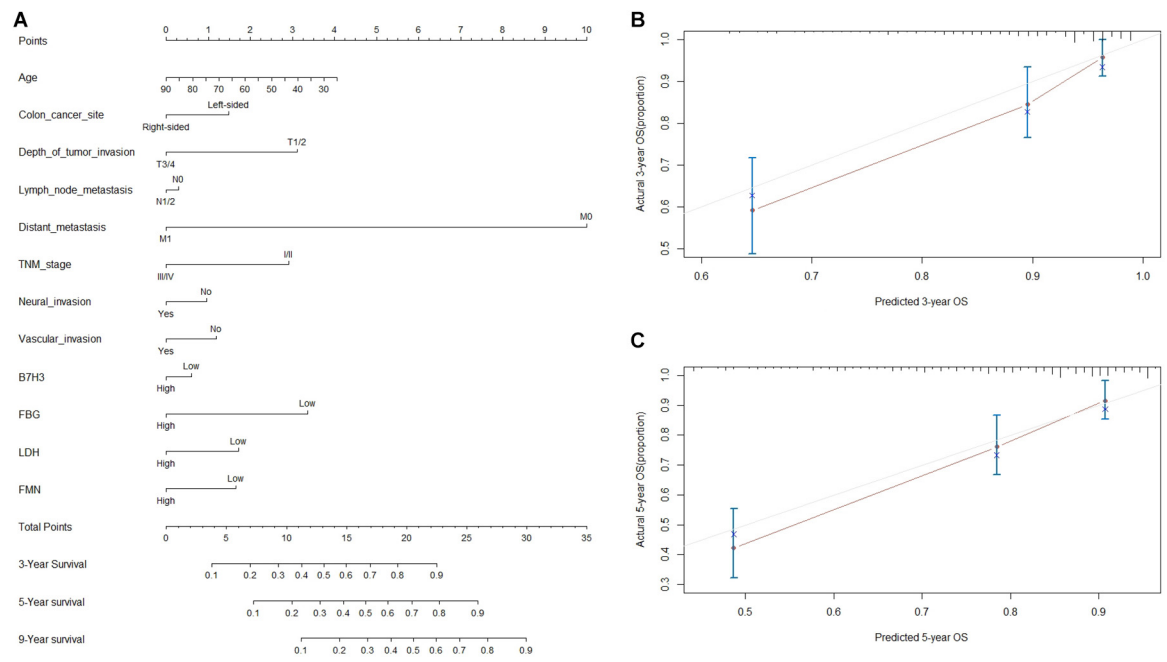

FIGURE 5 | Nomogram based prediction of prognosis. **(A)** Nomogram for OS based on B7-H3, FBG, LDH, FMN, and other clinicopathological characteristics. **(B)** The calibration of the nomogram for OS of 3 years. **(C)** The calibration of nomogram for OS of 5-year.

Therefore, B7-H3 was still a feasible and effective marker to predict the prognosis in patients with CRC. Besides, recently, B7-H3 antibodies had been reported to be safely used in humans in early phase clinical trials (27, 28). Therefore, B7-H3 might serve as a reliable biomarker and therapeutic target for CRC.

Previously, our team has analyzed the non-immunological role of B7-H3 in CRC tumorigenesis, which mainly focused on anti-apoptosis (29), pro-metastasis (30, 31), 5-Fu resistance (32, 33), and lipid metabolism (34); however, the relationship between B7-H3 and glucose metabolism was not investigated. Recently, Shi et al. suggested that B7-H3 might be a novel regulator of glucose metabolism via regulating HK2 expression in CRC cells (14). It motivated us to explore the clinical and prognostic significance of B7-H3 expression as indicators of glucose metabolism in patients with CRC. Thus, we evaluated the clinical correlation and performed survival analysis in patients with CRC for the combined expression of B7-H3 with FBG, LDH, and FMN. We found a linear relationship between B7-H3 and FBG with the depth of tumor invasion (T3/4), lymph node metastasis (N0), and TNM stage (I/II). However, there were no significant linear relationships between the expression of B7-H3 and FBG, LDH, or FMN in all CRC tissue, and also between B7-H3 and LDH or FMN among different subgroups. These results indicated a positive correlation between the expression of B7-H3 and FBG in the early stage of CRC tissue. Furthermore, we considered analyzing the risk of CRC by investigating the aberrant expression of B7-H3 and FBG. In the future, we anticipate detecting B7-H3 and FBG in biopsy tissue specimens and serum of patients with CRC. However, it would possibly be beneficial if the expression of B7-H3 could also be determined in the serum of patients. Further, a subgroup of B7-H3 high expression revealed that only patients with high FMN expression exhibited significantly worse OS compared with FBG and LDH expression. However, a subgroup of patients with low expression of B7-H3 and high FBG, or high LDH, or high FMN exhibited significantly worse prognosis as compared to patients with low expression of FBG, LDH, or FMN. These shreds of evidence implied that FMN is a crucial factor for OS prediction in CRC patients irrespective of high or low expression of B7-H3. Besides, high expression FBG or LDH could warn poor survival outcomes when B7-H3 expression was low. Possibly, in the subgroup of patients with low expression of B7-H3, indicators of glucose metabolism (FBG, LDH, and FMN) should be monitored continually for improved evaluation of prognosis in these patients. Moreover, Cox regression analysis and nomogram manifested the contribution of different clinicopathological characteristics to OS. Conceivably, the survival status and rate of CRC patients could be estimated to stratify the patients for clinical treatment appropriately.

The present study revealed the clinical and prognostic significance of B7-H3 and the clinical indicators of glucose metabolism (FBG, LDH, and FMN) in patients with CRC. Collectively, the findings of this study presented B7-H3 as a hub molecular biomarker, which, combined with indicators like FBG, LDH, or FMN, could possibly reflect the clinical outcomes of patients with CRC. B7-H3 intervention and control of glucose metabolic level appeared to be a promising antitumor strategy with possible benefits in clinical translation. In conclusion, this study provided new insight into the relationship of B7-H3 and glucose metabolism in patients with CRC.

DATA AVAILABILITY STATEMENT

All datasets presented in this study are included in the article/supplementary material.

ETHICS STATEMENT

The studies involving human participants were reviewed and approved by Medical Ethics Committee of the Affiliated Hospital of Jiangnan University. The patients/participants provided their written informed consent to participate in this study. Written informed consent was obtained from the individual(s) for the publication of any potentially identifiable images or data included in this article.

AUTHOR CONTRIBUTIONS

TZ, XQ, YM, and DH designed the research. TZ, YJ, XJ, and LL performed the research. TZ and LL analyzed the data. TZ, YJ, XJ, and LL wrote the manuscript. XQ, YM, and DH revised the manuscript. All authors contributed to the article and approved the submitted version.

ACKNOWLEDGMENTS

We gratefully acknowledge the financial support from the National Natural Science Foundation Youth Project of China (81902492), the Youth Project of Wuxi Health Committee (Q201822), and Natural Science Foundation of Jiangsu Province (BK20171150).

REFERENCES

1. Siegel RL, Miller KD, Jemal A. Cancer statistics, 2019. *CA Cancer J Clin*. (2019) 69:7–34.
2. Chen W, Zheng R, Baade PD, Zhang S, Zeng H, Bray F, et al. Cancer statistics in China, 2015. *CA Cancer J Clin*. (2016) 66:115–32. doi: 10.3322/caac.21338
3. Gu MJ, Huang QC, Bao CZ, Li YJ, Li XQ, Ye D, et al. Attributable causes of colorectal cancer in China. *BMC Cancer*. (2018) 18:38. doi: 10.1186/s12885-017-3968-z
4. Hu C, Jia W. Therapeutic medications against diabetes: what we have and what we expect. *Adv Drug Deliv Rev*. (2019) 139:3–15. doi: 10.1016/j.addr.2018.11.008
5. Zheng Y, Ley SH, Hu FB. Global aetiology and epidemiology of type 2 diabetes mellitus and its complications. *Nat Rev Endocrinol*. (2018) 14:88–98. doi: 10.1038/nrendo.2017.151
6. Tsilidis KK, Kasimis JC, Lopez DS, Ntzani EE, Ioannidis JP. Type 2 diabetes and cancer: umbrella review of meta-analyses of observational studies. *BMJ*. (2015) 350:g7607. doi: 10.1136/bmj.g7607

7. Park H, Cho S, Woo H, Park SK, Shin HR, Chang SH, et al. Fasting glucose and risk of colorectal cancer in the Korean Multi-center Cancer Cohort. *PLoS One*. (2017) 12:e0188465. doi: 10.1371/journal.pone.0188465
8. Graziano F, Ruzzo A, Giacomini E, Ricciardi T, Aprile G, Loupakis F, et al. Glycolysis gene expression analysis and selective metabolic advantage in the clinical progression of colorectal cancer. *Pharmacogenomics J*. (2017) 17:258–64. doi: 10.1038/tpj.2016.13
9. Wang Y, Lu JH, Wu QN, Jin Y, Wang DS, Chen YX, et al. LncRNA LINRIS stabilizes IGF2BP2 and promotes the aerobic glycolysis in colorectal cancer. *Mol Cancer*. (2019) 18:174.
10. Deng F, Zhou R, Lin C, Yang S, Wang H, Li W, et al. Tumor-secreted dickkopf2 accelerates aerobic glycolysis and promotes angiogenesis in colorectal cancer. *Theranostics*. (2019) 9:1001–14. doi: 10.7150/thno.30056
11. Castellanos JR, Purvis IJ, Labak CM, Guda MR, Tsung AJ, Velpula KK, et al. B7-H3 role in the immune landscape of cancer. *Am J Clin Exp Immunol*. (2017) 6:66–75.
12. Tang J, Jiang W, Liu D, Luo J, Wu X, Pan Z, et al. The comprehensive molecular landscape of the immunologic co-stimulator B7 and TNFR ligand receptor families in colorectal cancer: immunotherapeutic implications with microsatellite instability. *Oncoimmunology*. (2018) 7:e1488566. doi: 10.1080/2162402x.2018.1488566
13. Fang C, Li S, Xu R, Guo H, Jiang R, Ding S, et al. Soluble B7-H3 (sB7-H3) is over-expressed in the serum of type 1 diabetes patients. *Diabetes Res Clin Pract*. (2018) 143:332–6. doi: 10.1016/j.diabres.2018.08.004
14. Shi T, Ma Y, Cao L, Zhan S, Xu Y, Fu F, et al. B7-H3 promotes aerobic glycolysis and chemoresistance in colorectal cancer cells by regulating HK2. *Cell Death Dis*. (2019) 10:308.
15. Wei Y, Xu H, Dai J, Peng J, Wang W, Xia L, et al. Prognostic significance of serum lactic acid, lactate dehydrogenase, and albumin levels in patients with metastatic colorectal cancer. *BioMed Res Int*. (2018) 2018:1804086.
16. Zhao Z, Han F, Yang S, Hua L, Wu J, Zhan W. The clinicopathologic importance of serum lactic dehydrogenase in patients with gastric cancer. *Dis Markers*. (2014) 2014:140913.
17. Misciagna G, De Michele G, Guerra V, Cisternino AM, Di Leo A, Freudenheim JL, et al. Serum fructosamine and colorectal adenomas. *Eur J Epidemiol*. (2004) 19:425–32. doi: 10.1023/b:ejep.0000027359.95727.24
18. Zhang T, Wang F, Wu JY, Qiu ZC, Wang Y, Liu F, et al. Clinical correlation of B7-H3 and B3GALT4 with the prognosis of colorectal cancer. *World J Gastroenterol*. (2018) 24:3538–46. doi: 10.3748/wjg.v24.i31.3538
19. Keum N, Giovannucci E. Global burden of colorectal cancer: emerging trends, risk factors and prevention strategies. *Nat Rev Gastroenterol Hepatol*. (2019) 16:713–32. doi: 10.1038/s41575-019-0189-8
20. Volaco A, Cavalcanti AM, Filho RP, Precoma DB. Socioeconomic status: the missing link between obesity and diabetes mellitus? *Curr Diabetes Rev*. (2018) 14:321–6. doi: 10.2174/1573399813666170621123227
21. Gonzalez N, Prieto I, Del Puerto-Nevado L, Portal-Nunez S, Ardura JA, Corton M, et al. 2017 update on the relationship between diabetes and colorectal cancer: epidemiology, potential molecular mechanisms and therapeutic implications. *Oncotarget*. (2017) 8:18456–85. doi: 10.18632/oncotarget.14472
22. Zhu B, Wu X, Wu B, Pei D, Zhang L, Wei L. The relationship between diabetes and colorectal cancer prognosis: a meta-analysis based on the cohort studies. *PLoS One*. (2017) 12:e0176068. doi: 10.1371/journal.pone.0176068
23. Wu H, Deng X, Shi Y, Su Y, Wei J, Duan H. PGC-1alpha, glucose metabolism and type 2 diabetes mellitus. *J Endocrinol*. (2016) 229:R99–115.
24. Wang G, Wang JJ, Yin PH, Xu K, Wang YZ, Shi F, et al. New strategies for targeting glucose metabolism-mediated acidosis for colorectal cancer therapy. *J Cell Physiol*. (2018) 234:348–68. doi: 10.1002/jcp.26917
25. Ciardiello D, Vitiello PP, Cardone C, Martini G, Troiani T, Martinelli E, et al. Immunotherapy of colorectal cancer: challenges for therapeutic efficacy. *Cancer Treat Rev*. (2019) 76:22–32. doi: 10.1016/j.ctrv.2019.04.003
26. Fan H, Zhu JH, Yao XQ. Prognostic significance of B7-H3 expression in patients with colorectal cancer: a meta-analysis. *Pak J Med Sci*. (2016) 32:1568–73.
27. Majzner RG, Theruvath JL, Nellan A, Heitzeneder S, Cui Y, Mount CW, et al. CAR T cells targeting B7-H3, a pan-cancer antigen, demonstrate potent preclinical activity against pediatric solid tumors and brain tumors. *Clin Cancer Res*. (2019) 25:2560–74. doi: 10.1158/1078-0432.ccr-18-0432
28. Flem-Karlsen K, Fodstad O, Tan M, Nunes-Xavier CE. B7-H3 in cancer – beyond immune regulation. *Trends Cancer*. (2018) 4:401–4. doi: 10.1016/j.trecan.2018.03.010
29. Zhang T, Jiang B, Zou ST, Liu F, Hua D. Overexpression of B7-H3 augments anti-apoptosis of colorectal cancer cells by Jak2-STAT3. *World J Gastroenterol*. (2015) 21:1804–13. doi: 10.3748/wjg.v21.i6.1804
30. Jiang B, Zhang T, Liu F, Sun Z, Shi H, Hua D, et al. The co-stimulatory molecule B7-H3 promotes the epithelial-mesenchymal transition in colorectal cancer. *Oncotarget*. (2016) 7:31755–71. doi: 10.18632/oncotarget.9035
31. Liu F, Zhang T, Zou S, Jiang B, Hua D. B7H3 promotes cell migration and invasion through the Jak2/Stat3/MMP9 signaling pathway in colorectal cancer. *Mol Med Rep*. (2015) 12:5455–60. doi: 10.3892/mmr.2015.4050
32. Jiang B, Liu F, Liu Z, Zhang T, Hua D. B7-H3 increases thymidylate synthase expression via the PI3k-Akt pathway. *Tumour Biol*. (2016) 37:9465–72. doi: 10.1007/s13277-015-4740-0
33. Sun ZZ, Zhang T, Ning K, Zhu R, Liu F, Tang SC, et al. B7-H3 upregulates BRCC3 expression, antagonizing DNA damage caused by 5-Fu. *Oncol Rep*. (2016) 36:231–8. doi: 10.3892/or.2016.4808
34. Wu J, Wang F, Liu X, Zhang T, Liu F, Ge X, et al. Correlation of IDH1 and B7H3 expression with prognosis of CRC patients. *Eur J Surg Oncol*. (2018) 44:1254–60. doi: 10.1016/j.ejso.2018.05.005

Conflict of Interest: The authors declare that the research was conducted in the absence of any commercial or financial relationships that could be construed as a potential conflict of interest.

frontiers in Oncology

ORIGINAL RESEARCH
published: 03 November 2021
doi: 10.3389/fonc.2021.781720

Pivotal Role of Iron Homeostasis in the Induction of Mitochondrial Apoptosis by 6-Gingerol Through PTEN Regulated PD-L1 Expression in Embryonic Cancer Cells

Nipin Sp[1†], Dong Young Kang[1†], Eun Seong Jo[2], Jin-Moo Lee[2,3], Se Won Bae[4] and Kyoung-Jin Jang[1*]*

[1] Department of Pathology, School of Medicine, Institute of Biomedical Science and Technology, Konkuk University, Chungju, South Korea, [2] Pharmacological Research Division, National Institute of Food and Drug Safety Evaluation, Osong Health Technology Administration Complex, Cheongju-si, South Korea, [3] SK Bioscience, Seongnam-si, South Korea, [4] Department of Chemistry and Cosmetics, Jeju National University, Jeju, South Korea

OPEN ACCESS

Edited by:
Varun Sasidharan Nair,
Helmholtz Association of German Research Centers (HZ), Germany

Reviewed by:
Salman M. Toor,
Hamad bin Khalifa University, Qatar
Bijinu Balakrishnan,
Ohio University, United States
Reem Saleh,
Peter MacCallum Cancer Centre, Australia

***Correspondence:**
Se Won Bae
swbae@jejunu.ac.kr
Kyoung-Jin Jang
jangkj@konkuk.ac.kr

[†]These authors have contributed equally to this work and share first authorship

Specialty section:
This article was submitted to Cancer Metabolism, a section of the journal Frontiers in Oncology

Received: 23 September 2021
Accepted: 15 October 2021
Published: 03 November 2021

Citation:
Sp N, Kang DY, Jo ES, Lee J-M, Bae SW and Jang K-J (2021) Pivotal Role of Iron Homeostasis in the Induction of Mitochondrial Apoptosis by 6-Gingerol Through PTEN Regulated PD-L1 Expression in Embryonic Cancer Cells. Front. Oncol. 11:781720. doi: 10.3389/fonc.2021.781720

Embryonic cancer stem cells (CSCs) can differentiate into any cancer type. Targeting CSCs with natural compounds is a promising approach as it suppresses cancer recurrence with fewer adverse effects. 6-Gingerol is an active component of ginger, which exhibits well-known anti-cancer activities. This study determined the mechanistic aspects of cell death induction by 6-gingerol. To analyze cellular processes, we used Western blot and real-time qPCR for molecular signaling studies and conducted flow cytometry. Our results suggested an inhibition of CSC marker expression and Wnt/β-catenin signaling by 6-gingerol in NCCIT and NTERA-2 cells. 6-Gingerol induced reactive oxygen species generation, the DNA damage response, cell cycle arrest, and the intrinsic pathway of apoptosis in embryonic CSCs. Furthermore, 6-gingerol inhibited iron metabolism and induced PTEN, which both played vital roles in the induction of cell death. The activation of PTEN resulted in the inhibition of PD-L1 expression through PI3K/AKT/p53 signaling. The induction of PTEN also mediated the downregulation of microRNAs miR-20b, miR-21, and miR-130b to result in PD-L1 suppression by 6-gingerol. Hence, 6-gingerol may be a promising candidate to target CSCs by regulating PTEN-mediated PD-L1 expression.

Keywords: embryonic CSC, 6-gingerol, iron metabolism, PTEN, PI3K/AKT signaling, p53, PD-L1, miR-20b/miR-21/miR-130b

INTRODUCTION

Stem cells differentiate into any kind of tissue, and embryonic stem (ES) cells can differentiate into embryonic germ layer derivatives that could generate any kind of tissue present in the human body. Embryonic cancer stem cells (CSCs), however, exhibit these properties in addition to non-restricted proliferation, which makes them more hazardous than other cancer cell types (1, 2). Embryonic CSCs may be able to differentiate into various cancers, such as those of the colon, breast, and lung (3). The sex-

determining region Y (SRY)-box 2 (SOX2), octamer-binding transcription factor 4 (OCT4), and homeobox protein NANOG are CSC markers overexpressed in CSC that help initiate tumorigenesis and maintain their pluripotent nature (4, 5). Many additional signaling pathways exist that can promote the self-renewal ability and pluripotency of CSC, among them is the Wnt/β-catenin pathway, which plays a vital role in tumor progression (6, 7). In canonical Wnt signaling, secreted glycoprotein Wnt family proteins and β-catenin, a transcriptional activator for the Wnt family, promote homeostasis and embryonic development (8). The activation of β-catenin is regulated by casein kinase 1α and glycogen synthase kinase 3β (GSK-3β) for proteasomal degradation or ubiquitination, respectively. Activation allows β-catenin to bind a transcription factor (TCF)-binding element of the TCF/lymphoid enhancer-binding factor in the nucleus to initiate transcription (9). Hence, Wnt/β-catenin signaling plays a key role in developing CSCs, which makes Wnt/β-catenin signaling and CSC markers potential targets for effective CSC treatments and possibly other cancer cells (10, 11).

The tumor suppressor phosphatase and tensin homologue (PTEN) is a tumor suppressor with a crucial rule in tumorigenesis of negatively regulating phosphoinositide 3-kinase (PI3K) and protein kinase B (AKT) signaling, which is a key pathway for cancer cell proliferation and survival (12, 13). Loss of PTEN function is considered a major reason for tumorigenesis and has been associated with most cancer types; PTEN mutation causes a disease known as Cowden syndrome (14). During the tumorigenesis stage, a loss of PTEN inhibits p53 signaling through the activation of PI3K/AKT, which then promotes the upregulation of CSC markers such as SOX2 and OCT4, and it activates programmed death-ligand 1 (PD-L1) (15, 16). PD-L1 is overexpressed in many cancer types, and it facilitates immune escape by binding its ligand, PD-1, which is present on the surface of lymphocytes, myeloid cells, T-cells, and B-cells (17–19). Hence, anti-cancer treatments that target PTEN could also lead to the suppression of PD-L1 expression and prevent immunosuppression.

Iron plays a central role in cellular metabolism and is a necessary cofactor in enzymes that mediate cell growth and cell death. Iron-containing proteins regulate mitochondrial functions, DNA synthesis, damage response, and oxygen transport (20). Biomolecule oxidation can generate reactive oxygen species (ROS) that make iron toxic (21). Hence, iron homeostasis must balance the presence of iron with the help of iron channels to prevent excessive ROS. Furthermore, in cancer, iron levels may regulate epigenetic alterations and maintain genomic stability as well as mediate tumor metastasis and the tumor microenvironment (TME) (22). The possibility that iron homeostasis possesses the dual role of cancer cell death and tumor proliferation depends on its specific role in cellular functions (23). Generally, transferrin-iron complexes (Fe3+) enter the cytoplasm *via* the transferrin receptor. Then, the iron is converted into Fe2+ with the help of several enzymes such as six-transmembrane epithelial antigen of prostate 3 (STEAP3) and divalent metal transporter 1 (DMT1), prior to taking part in cellular metabolism and heme biosynthesis (24). Next, this shows the significance of iron metabolism in the body, as their variation may result in inflammation and tumorigenesis.

Patients suffering from cancer also struggle with the adverse effects of chemotherapeutic drugs (25, 26). Cancer treatments that use natural compounds are good alternatives, due to the possibility of a multi-targeted treatment with fewer side effects compared to chemotherapeutics (27, 28). Ginger is a very popular spice commonly used in Asian countries, and 6-gingerol is a bioactive phenolic compound and primary pharmacological component of ginger (29). It exhibits antioxidant, anti-platelet, anti-inflammatory, anti-proliferative, and anti-cancer activities (30–33). 6-Gingerol has been reported to induce anti-tumor activity against breast (28), colorectal (34), gastric (35), and pancreatic cancers (36). However, the mechanism of cell death by 6-gingerol in CSCs is unknown.

This study demonstrates the ability of 6-gingerol to induce apoptosis in NCCIT and NTERA-2 embryonic CSCs and a role for iron metabolism in PTEN-mediated PD-L1 under these conditions. Also, we analyzed the molecular mechanism behind the induction of apoptosis by 6-gingerol in CSCs.

MATERIALS AND METHODS

Antibodies and Cell Culture Reagents

Roswell Park Memorial Institute-1640 (RPMI-1640) medium, penicillin-streptomycin solution, and trypsin-EDTA (0.05%) were purchased from Gibco (Thermo Fisher Scientific, Inc., Waltham, MA, USA). Dulbecco's modified Eagle's Media (DMEM; LM001-51) was purchased from Welgene Biotech (Taipei City, Taipei, Taiwan). 6-Gingerol (cat no. 23513-14-6) was purchased from TCI (Tokyo Chemical Industry Co., Tokyo, Japan). Fetal bovine serum (FBS; 12003C) and primary antibodies specific for SOX2 (MAB4423), OCT4 (MABD76), NANOG (MABD24), SF1670 (SML0684), and iron (II) sulfate heptahydrate (F8633) were purchased from Sigma-Aldrich (Merck KGaA, St. Louis, MO, USA). Antibodies specific for β-actin (sc-47778), Wnt5A (sc-365370), BCL-2 (sc-7382), p21 (sc-756), cyclin E (sc-481), and CDK4 (sc-260) and secondary antibodies [anti-mouse (sc-516102) and anti-rabbit (sc-2357)] were obtained from Santa Cruz Biotechnology, Inc. (Dallas, TX, USA). Next, the Wnt8A (H00007478-B01P) antibody was obtained from Abnova (Taipei City, Taiwan). β-Catenin (#9582), GSK-3β (#9315), BAX (#2772), BCL-xL (#2764), cytochrome C (#11940), p27 Kip1 (#3686), p53 (#9282), pATM (#5883), pATR (#2853), pCHK1 (#2348), pCHK2 (#2197), pBRCA1 (#9009), TCF3/TCF7L1 (#2883), Casp9 (#9502), C-Casp9 (#9505), PTEN (#9188), pAKT (#4060), AKT (#4691), pPI3K (#4228), PI3K (#4257), COX IV (#4850), and GAPDH (#2118) antibodies were purchased from Cell Signaling Technology, Inc. (Beverly, MA, USA). TFR1 (ab84036), STEAP3 (ab151566), DMT1 (ab55735), and cyclin D1 (ab6152) antibodies were purchased from Abcam (Cambridge, MA, USA). FPN1 (NBP1-21502) and iNOS (NB300-650) antibodies were obtained from Novus Biologicals (Littleton, CO, USA). Finally, the antibody

specific for PD-L1 (R30949) was obtained from NSJ Bioreagents (San Diego, CA, USA).

Cell Culture and Treatment

NCCIT (CRL-2073) and NTERA-2 (CRL-1973) cell lines were purchased from the American Type Culture Collection (ATCC; Manassas, VA, USA). Next, NCCIT cells were cultured and maintained in RPMI-1640 media, and NTERA-2 cells were cultured and maintained in DMEM media plus 10% FBS and 1% penicillin at 37°C in 5% CO2. The medium was changed three times a week after cells reached up to 80% confluence and treated with 6-gingerol. Lastly, the treated cells were incubated at 37°C for 48 h.

Cell Viability Assay

Cell viability was measured using a 3-(4,5-dimethylthiazol-2-yl)-2,5-diphenyltetrazolium bromide (MTT) assay. Then, NCCIT or NTERA-2 cells were maintained in culture media in 96-well culture plates at 3×10^3 per well (density) for 24 h. Next, cells were incubated in fresh medium containing dimethyl sulfoxide (DMSO) as the vehicle control and treated with 6-gingerol (50–400 μM) for 48 h. Subsequently, MTT (5 mg/mL) was added and incubated for 4 h at 37°C. The resulting formazan product was dissolved in DMSO, and an Ultra Multifunctional Microplate Reader (Tecan, Durham, NC, USA) was used to measure the absorbance at a wavelength of 590 nm. All measurements and experiments were conducted in triplicate.

Western Blotting

Protein samples were isolated from untreated (control) or 6-gingerol-treated NCCIT or NTERA-2 cells using radioimmunoprecipitation (RIPA) lysis buffer (20–188; EMD Millipore), which contained protease and phosphatase inhibitors. First, the concentration of proteins was measured using Bradford's method (Thermo Fisher Scientific). Next, 100 μg of protein from each sample were resolved with sodium dodecyl sulfate-polyacrylamide gel (10%–15%) electrophoresis. Then, the separated proteins were transferred onto nitrocellulose membranes, followed by blocking with 5% skim milk (BD Biosciences, San Jose, CA, USA) in TBS-T buffer [20-μM Tris-HCl (Sigma-Aldrich; Merck KGa A), pH 7.6, 137-μM NaCl (Formedium, Norfolk, UK; NAC03), and 0.1× Tween20 (Scientific Sales, Inc. OakRidge, TN, USA)] for 1 h. Next, the membranes were incubated overnight at 4°C in a shaker with specific primary antibodies diluted in 5% bovine serum albumin (EMDMillipore). Then, the membranes were washed with TBS-T and incubated with HRP-conjugated secondary antibodies for 1 h at room temperature. Finally, the detection was performed using a Femto Clean Enhanced Chemiluminescence Solution Kit (77449; GenDEPOT, Katy, TX, USA) in a LAS-4000 imaging device (Fujifilm, Tokyo, Japan). Quantifications were conducted using ImageJ software (v.1.8.0_172; National Institutes of Health).

Quantitative Real-Time Polymerase Chain Reaction (qPCR)

Total RNA was isolated using the RNeasy Mini Kit (Qiagen GmbH, Hilden, Germany) and then quantified using a spectrophotometer at 260 nm. A thermal cycler (C1000 Thermal Cycler; Bio-Rad, Hercules, CA, USA) was used to make cDNA from the total RNA using a first-strand cDNA synthesis kit (Bioneer, Daejeon, Korea) and oligo (dT) primers. PD-L1, p53, and GAPDH cDNA (2-5 μg) were amplified using an RT-PCR Premix Kit (Bioneer) with primers synthesized by Bioneer. The Light Cycler 480II (Roche) was used for qPCR as follows: 2 μL of diluted cDNA was mixed with 10 μL of TB Green Advantage Premix (Takara Bio, Japan) and 1 μL each of the forward and reverse primers. The cycling conditions were as follows: 95°C for 5 min for the initial denaturation, which was followed by 40 cycles of 95°C for 40 s, 58°C for 40 s, 72°C for 40 s, and a final extension of 5 min at 72°C. All reactions were conducted three times and normalized to GAPDH; quantifications were conducted using the obtained Cp values.

FACS Analysis for Mitochondrial Membrane Potential and ROS

The cultured cells were washed with pre-warmed culturing medium supplemented with 10% FBS (staining buffer), and 1×10^6 cells were re-suspended in 1 mL of staining buffer containing MitoTracker Deep Red (40 nM; Invitrogen, Carlsbad, CA, USA: M22426) to measure mitochondrial membrane potential, MitoSOX (5 μM; M36008; Invitrogen) to measure mROS, or CM-H2DCFDA (5 μM; Invitrogen, C6827) to measure cellular ROS. Then, the cells were incubated in a CO2 incubator at 37°C for 30 min, and the stained cells were washed with 1 mL of pre-warmed staining buffer prior to fluorescence-activated cell sorting (FACS). The analysis was performed using FlowJo software.

Cell Cycle Analysis

The DNA content of 6-gingerol-treated and non-treated cells was determined using a BD Cycletest Plus DNA Reagent Kit (BD Biosciences, San Jose, CA, USA) according to the manufacturer's protocol. Approximately 5×10^5 cells, incubated with or without 6-gingerol for 48 h, were washed with PBS and permeabilized with trypsin. RNA interactions with propidium iodide (PI) were neutralized by treating the cells with RNase buffer and trypsin inhibitor. Then, the samples were stained with PI and incubated for 30 min in the dark at room temperature prior to analysis with a FACSCalibur flow cytometer (BD Biosciences, San Jose, CA, USA).

Comet Assay

The comet assay kit (Abcam, Cambridge, MA, USA) was used to measure cellular DNA damage. This assay is a single-cell gel electrophoresis method for the simple evaluation of cellular DNA damage. First, a base layer of comet agarose was created on a slide, followed by a layer of cells, agarose, and lysis. Next, electrophoresis was performed under neutral conditions, and the cells were stained with DNA dye. Finally, cell morphology was observed by fluorescence microscopy (Olympus IX71/DP72).

Apoptosis Analysis

Fluorescein-conjugated annexin V (annexin V-FITC) was used to measure apoptosis in NCCIT and NTERA-2 cells. First, the 6-gingerol-treated or untreated cells were washed with PBS and re-

suspended in a binding buffer at a concentration of 1×10^6 cells. Then, the cells were stained with annexin V-FITC and PI for 10 min in a dark room at room temperature. Finally, the percentage of apoptotic cells was measured by flow cytometry *via* FACSCalibur, and the analysis was performed using FlowJo software.

Isolation of Mitochondria/ Cytosol Fractions

Mitochondria/cytosol fractions from 6-gingerol-treated and non-treated NCCIT and NTERA-2 cells were extracted using a mitochondria/cytosol fractionation kit (Abcam). A 1X cytosol extraction buffer containing DTT and protease inhibitors was added to the cells (5×10^7), which were then incubated on ice for 10 min. After incubation, samples were centrifuged at 700 x g for 10 min at 4°C to collect the supernatant, which was centrifuged again at 10,000 x g for 30 min at 4°C. The supernatant was removed and saved as the cytosol fraction, while the pellet was re-suspended in PBS to obtain the mitochondrial fraction. Next, western blotting of cytochrome c was carried out as described above.

ATP Determination Assay

The ATP Determination Kit (Molecular Probes, Eugene, OR, USA) was used to measure ATP. Briefly, NCCIT or NTERA-2 cells were treated with 6-gingerol, and an equal number of cells was collected for the ATP determination assay. The standard reaction solution was made using reaction buffer, DTT, D-luciferin, and firefly luciferase as provided in the kit; then, cells were added along with the standard reaction solution. Luminescence readings were taken immediately using a plate-reading luminometer, and calculations were performed according to the assay protocol.

Iron Estimation Assay

Iron estimation was performed using an iron assay kit (MAK025) purchased from Sigma-Aldrich (Merck KGaA, St. Louis, MO). Briefly, NCCIT or NTERA-2 cells (2×10^6) treated with or without 6-gingerol were homogenized in an iron assay buffer and collected by centrifugation at 16,000 × g for 10 min at 4°C. Then, the cells were mixed with an iron assay buffer, added to a 96-well plate along with an iron reducer, and incubated in a horizontal shaker for 30 min at 25°C. Then, 100 µL of the iron probe was added to each well and incubated for 1 h at 25°C. Absorbance was measured at 593 nm, and controls were set to 100% for comparison.

FACS Analysis for Ferrous Iron (Fe^{2+})

After cultured cells (NCCIT or NTERA-2) were washed with culturing medium, 2 mL of staining solution containing FerroFarRed (5 µM; GC903-01; GORYO Chemical) was added prior to incubation in a CO2 incubator at 37°C for 30–40 min. After staining, cells were washed with 1 mL of pre-warmed serum-free culture medium and used for FACS analysis.

Statistical Analyses

All experiments were performed in triplicate. The results were expressed as the mean ± standard error of the mean. Statistical analyses were conducted *via* the one-way analysis of variance (ANOVA) or Student's t-test. Additionally, the one-way ANOVA was performed using Tukey's *post hoc* test. The analyses were performed using SAS 9.3 software (SAS Institute, Inc., Cary, NC, USA). A p-value < 0.05 (*) was considered statistically significant.

RESULTS

6-Gingerol In hibits CSC Markers and Wnt/ β-catenin Signaling in Embryonic CSCs

To begin our study, first, we analyzed the proliferation inhibition of 6-gingerol on embryonic CSC viability by the MTT assay. Increasing concentrations of 6-gingerol in NCCIT and NTERA-2 (**Supplementary Figure 1A**) resulted in a concentration-dependent inhibition of cell viability. From these results, we calculated 200 µM 6-gingerol to be the IC_{50} dosage and selected 100 or 200 µM of 6-gingerol for concentration-dependent studies. We also evaluated the cell morphology of embryonic CSCs after treatment with 6-gingerol using DAPI staining. We observed a decrease in cell number upon 6-gingerol treatment (**Supplementary Figure 1B**). Next, we determined whether 6-gingerol could suppress CSC markers in embryonic CSCs. Evaluation of the CSC markers SOX2, OCT4, and NANOG in embryonic CSCs with 6-gingerol treatment showed a downregulation in the expression patterns of these CSC markers (**Figure 1A**). Then, we confirmed their downregulation in NCCIT and NTERA-2 cells at the mRNA level using real-time qPCR analysis (**Figure 1B**). These results also suggested the ability of 6-gingerol to inhibit CSC proliferation.

Next, we analyzed the expression patterns of Wnt/β-catenin signaling in embryonic CSCs following 6-gingerol treatment. The results showed a downregulation in the expression of Wnt5A, Wnt8A, GSK-3β, β-catenin, and TCF proteins by 6-gingerol treatment in NCCIT and NTERA-2 cells (**Figure 1C**). Then, we confirmed the inhibition of Wnt/β-catenin signaling at the mRNA level (**Figure 1D**). These results suggested the capability of 6-gingerol against embryonic CSCs. We also analyzed the ability of 6-gingerol to inhibit tumor invasion in embryonic CSC using the Matrigel invasion assay. Results indicated a successful inhibition of tumor invasion in NCCIT and NTERA-2 cells by 6-gingerol treatment (**Supplementary Figure 1C**). These results suggested the overall cytotoxic activity of 6-gingerol against embryonic cancer stem cells.

6-Gingerol Induces ROS and DNA Damage Response in Embryonic CSCs

We hypothesized that the anti-tumor activity of 6-gingerol might begin by generating ROS. To analyze this, we measured iNOS expression following 6-gingerol treatment. Our results showed that increasing concentrations of 6-gingerol upregulated iNOS expression in NCCIT and NTERA-2 cells (**Figure 2A**). We confirmed this by measuring the expression of *iNOS* mRNA level in embryonic CSCs after treatment with 6-gingerol with similar results (**Figure 2B**). The induction of iNOS suggested

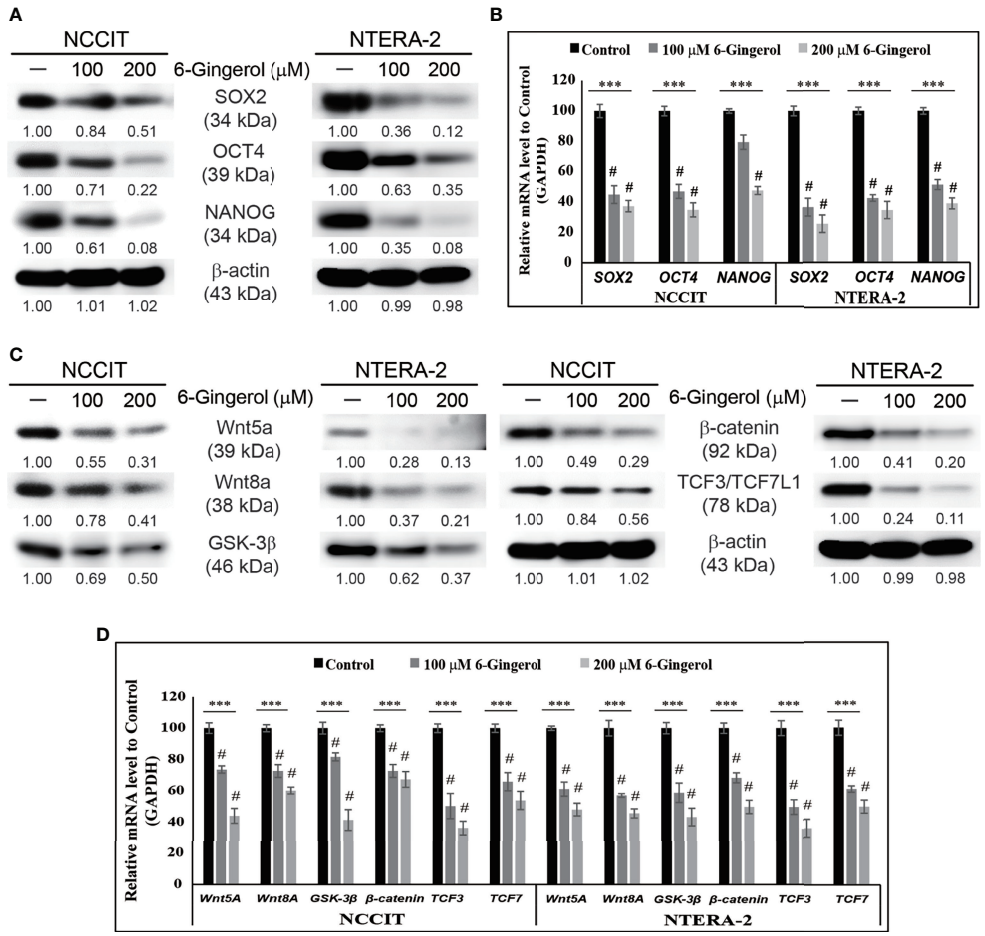

FIGURE 1 | Inhibition of CSC markers and Wnt/β-catenin signaling by 6-gingerol. **(A)** Western blot analysis of SOX2, OCT4, and NANOG in NCCIT and NTERA-2 cells after treatment with 100 or 200 μM 6-gingerol for 48 h. Expression levels of proteins were estimated by densitometry and normalized to β-actin. Data were obtained in triplicate. **(B)** Real-time qPCR showing illus-trative expression of *SOX2*, *OCT4*, and *NANOG* genes in embryonic CSCs. The obtained Cp values were normalized to *GAPDH* mRNA. Controls were set at 100. ***$p < 0.001$ (ANOVA). $^{\#}p < 0.001$ *vs*. control. **(C)** Western blot of Wnt5a, Wnt8A, GSK-3β, β-catenin, and TCF3/TCF7L1 in NCCIT and NTERA-2 cells after treatment with 100 or 200 μM 6-gingerol for 48 h. Expression levels were normalized to β-actin. Experiments were conducted three times for confirmation. **(D)** Real-time qPCR showing illustrative expression of *Wnt5a*, *Wnt8A*, *GSK-3β*, *β-catenin*, *TCF3*, and *TCF7* genes in NCCIT and NTERA-2 cells. Cp values were normalized to *GAPDH* mRNA. Controls were set at 100. ***$p < 0.001$ (ANOVA). $^{\#}p < 0.001$ *vs*. control.

that 6-gingerol may cause ROS generation in embryonic CSCs. As we expected, we found that 6-gingerol treatment successfully induced cellular (**Figure 2C**) and mitochondrial (**Figure 2D**) ROS, which suggested ROS as the reason for the anti-tumor activity of 6-gingerol.

Then, we verified the ability of 6-gingerol to induce the DNA damage response (DDR) in NCCIT and NTERA-2 cells. To analyze this, we used a comet assay to determine DNA double-strand breaks, which showed that 6-gingerol induced DNA double-strand breaks in NCCIT and NTERA-2 cells (**Supplementary Figure 2A**). Moreover, we observed a significant increase in the comet length and number of comet-positive cells in 6-gingerol-treated cells compared with non-treated control cells (**Supplementary Figure 2B**). These results hinted at the DDR induction of 6-gingerol in embryonic CSCs. To confirm this, we evaluated the expression levels of proteins involved in the DDR and found an increase in the expression of phosphorylated histone, ATM, ATR, CHK1, CHK2, and BRCA1 following 6-gingerol treatment in NCCIT and NTERA-2 cells (**Supplementary Figure 2C**). These results suggested that either ATM or ATR may act as a key regulator of DDR induction by 6-gingerol.

6-Gingerol Induces Cell Cycle Arrest and Intrinsic Apoptosis in Embryonic CSCs

Based on previous results, we showed that 6-gingerol induces ROS and the DDR in embryonic CSCs. Therefore, we analyzed the impact of 6-gingerol on the cell cycle and apoptosis induction. Flow cytometry of embryonic CSCs treated with 6-gingerol showed an arrest in the G0/G1 phase of the cell cycle (**Supplementary Figure 3A**). These results indicated that DDR induction leads to prolonged cell cycle arrest, and to confirm this, we analyzed cell cycle checkpoint protein levels by Western blot.

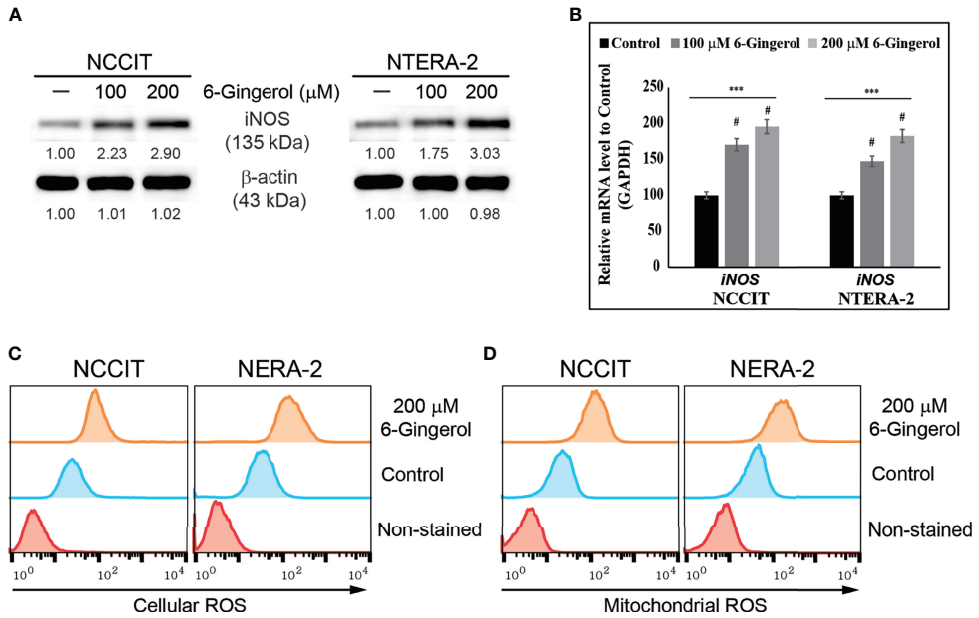

FIGURE 2 | 6-Gingerol induced ROS formation in embryonic CSCs. **(A)** Western blot of iNOS protein expression in NCCIT and NTERA-2 cells incubated with 100 or 200 μM 6-gingerol for 48 h. Expression levels were estimated by densitometry and normalized to β-actin. Data were obtained in triplicate. **(B)** Real-time qPCR analysis showing illustrative expression of iNOS in NCCIT and NTERA-2 cells. Next, the obtained Cp values were normalized to *GAPDH* mRNA. Controls were set at 100. $^{***}p < 0.001$ (ANOVA). $^{\#}p < 0.001$ *vs*. control. **(C)** Flow cytometry of cellular ROS in NCCIT and NTERA-2 cells incubated with 200 μM of 6-gingerol for 48 h. The graphical representation shows cells with ROS induction. **(D)** Flow cytometry of mitochondrial ROS following 200 μM 6-gingerol treatment of NCCIT and NTERA-2 cells for 48 h. The graphical representation shows cells with mitochondrial ROS.

These results showed an elevation in the expression of tumor suppressor proteins p21 and p27 as well as a decrease in the expression of cyclin D1, cyclin E, and CDK4 proteins (**Supplementary Figure 3B**). Then, we confirmed these results by measuring the transcriptional expression of *CCND1*, *CCNE1*, *CDK4*, *CDKN1A*, and *CDKN1B* genes (**Supplementary Figure 3C**), which confirmed the induction of a cell cycle arrest. These results indicated that 6-gingerol causes cell cycle arrest in embryonic CSCs and may also induce apoptosis.

Next, we evaluated apoptosis induction by 6-gingerol in embryonic CSCs using flow cytometry. The results showed that 6-gingerol induced apoptosis in NCCIT and NTERA-2 cells (**Figure 3A**). Then, we investigated the apoptosis pathway by measuring protein levels of the key apoptosis regulators BCL2 associated X (BAX), B-cell lymphoma 2 (BCL-2), B-cell lymphoma-extra-large (BCL-xL), cleaved caspase 9, and cytochrome c (**Figure 3B**). These results showed a downregulation in the expression levels of BCL-2 and BCL-xL while BAX, cleaved caspase 9, and cytochrome c were upregulated upon 6-gingerol treatment. These data suggested a possible induction of the intrinsic apoptosis pathway. As intrinsic apoptosis depends heavily on the BAX/BCL-2 ratio, we confirmed the expression of *BAX*, *BCL-2*, and *CASPASE 9* mRNA following 6-gingerol treatment in embryonic CSCs (**Figure 3C**). These results suggested a possible release of cytochrome c from the mitochondria into the cytosol, which was confirmed by comparing cytochrome c levels in the cytosol and mitochondria (**Figure 3D**). These results showed a decrease in the amount of cytochrome c in mitochondria and a corresponding increase in the cytosol. Also, we analyzed the ATP concentration of embryonic CSCs after treatment with 6-gingerol (**Figure 3E**); the results indicated a decrease in ATP production, which corresponds with a 6-gingerol induction of the intrinsic apoptosis pathway.

6-Gingerol Regulates PTEN-Mediated PD-L1 Expression in Embryonic CSCs

Taken together, these data indicate the induction of intrinsic apoptosis by 6-gingerol in embryonic CSCs. To identify the molecular signaling responsible for this mechanism, we analyzed the expression of tumor suppressor protein PTEN and its downstream targets PI3K, AKT, and p53. We found elevated expression of PTEN and p53 while phosphorylated PI3K and AKT were downregulated by 6-gingerol treatment of NCCIT and NTERA-2 cells (**Figure 4A**). Also, we analyzed the expression of PD-L1, as PI3K/AKT/p53 signaling may regulate its expression. Our results suggested the same, as 6-gingerol suppressed the expression levels of PD-L1 in embryonic CSCs. This result hinted at the role of PTEN/PI3K/AKT/p53 signaling in PD-L1 inhibition by 6-gingerol. To confirm this signaling and its effect on PD-L1 expression, we repeated our experiment with a specific inhibitor of PTEN (SF1670). We found increased phospho-PI3K/AKT and PD-L1 expression upon SF1670 treatment, and 6-gingerol successfully inhibited the expression

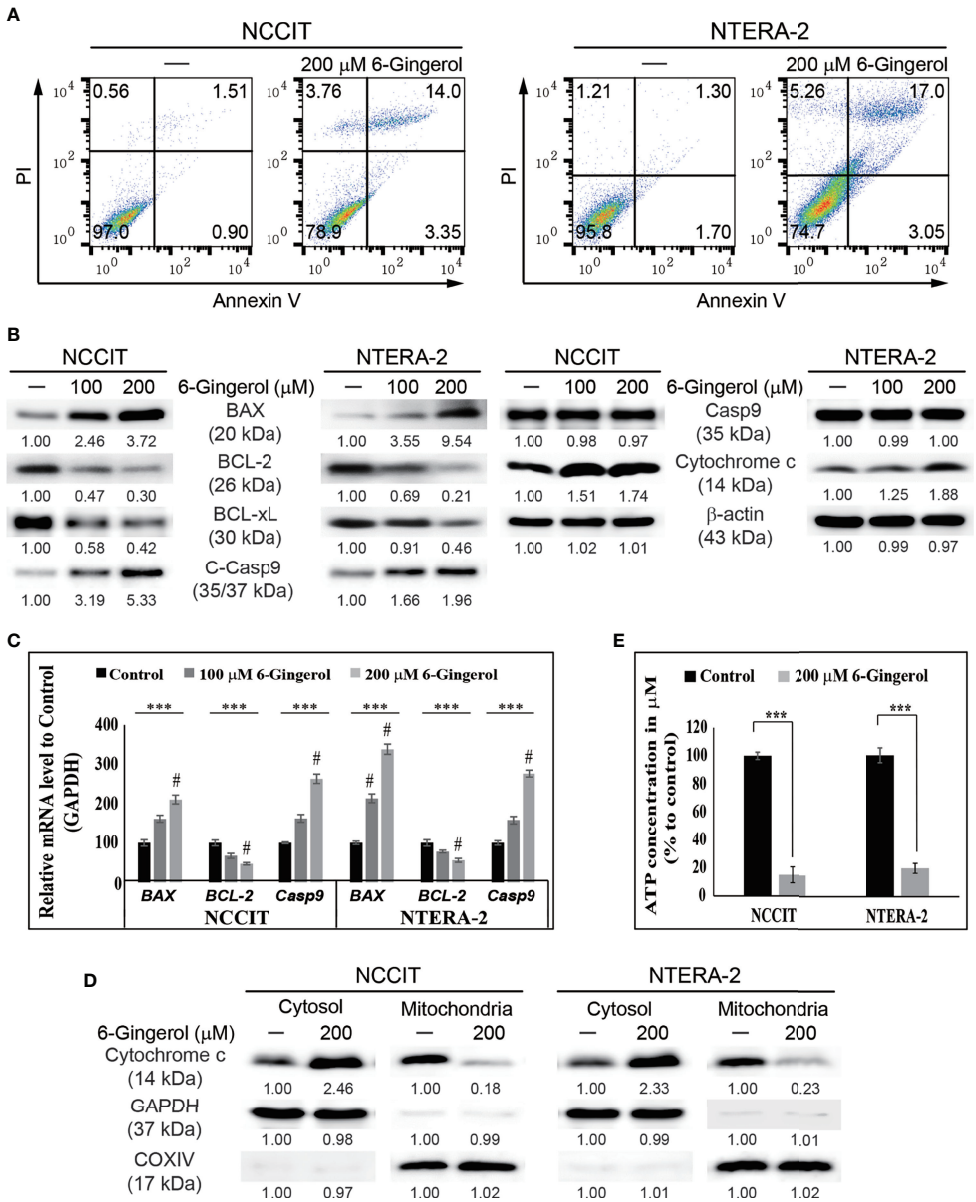

FIGURE 3 | 6-Gingerol induced intrinsic apoptosis pathway. **(A)** Fluorescein-conjugated annex-in V (annexin V-FITC) *vs*. propidium iodide (PI) staining analysis in NCCIT and NTERA-2 cells following incubation with 200 μM 6-gingerol for 48 h. **(B)** Western blot of BAX, BCL-2, BCL-xL, C-Casp9, Casp9, and cytochrome c in NCCIT and NTERA-2 cells with 100 or 200 μM 6-gingerol for 48 h. Expression levels were estimated by densitometry and normalized to β-actin. Data were obtained in triplicate. **(C)** Real-time qPCR analysis showing illustrative expression of *BAX*, *BCL-2*, and *caspase 9* genes in NCCIT and NTERA-2 cells incubated with 100 or 200 μM 6-gingerol for 48 h. Next, the obtained Cp values were normalized to *GAPDH* mRNA. Controls were set at 100. ***$p < 0.001$ (ANOVA test). $^{\#}p < 0.001$ *vs*. control. **(D)** Western blot of cyto-chrome c in cytosolic and mitochondrial fractions isolated from NCCIT and NTERA-2 cells after 48 h treatment with 200 μM of 6-gingerol. *GAPDH* and COXIV were the controls for cyto-solic and mitochondrial fractions, respectively. **(E)** A plot of the ATP concentration following treatment with 200 μM of 6-gingerol in NCCIT and NTERA-2 cells. Controls were set at 100. ***$p < 0.001$ (Student's t-test).

of these proteins (**Figure 4B**). The expression of p53 was suppressed with PTEN inhibitor treatment and rescued by the addition of 6-gingerol in embryonic CSCs, which suggested the ability of 6-gingerol to induce PTEN and p53 expression and thereby inhibit PD-L1 expression. It also suggested a role for PTEN in the regulation of PD-L1 during 6-gingerol treatment.

6-Gingerol Induces Iron Release and Inhibits Iron Metabolism in Embryonic CSCs

We found that 6-gingerol can induce intrinsic apoptosis in embryonic CSCs. Next, we analyzed the mechanism of these activities and hypothesized that iron homeostasis might play a

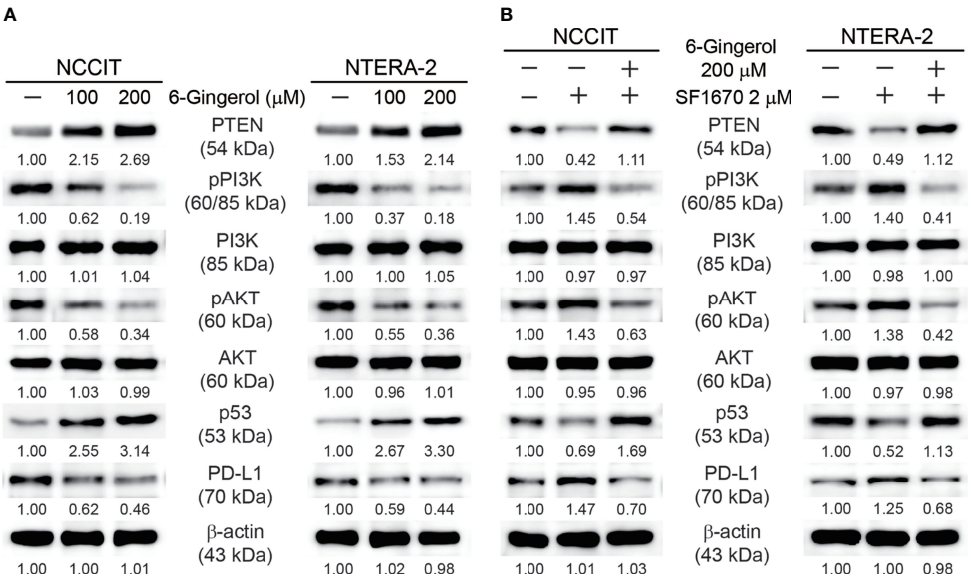

FIGURE 4 | 6-Gingerol regulated PTEN/PD-L1 expression. **(A)** Western blot of PTEN, phos-pho-PI3K, PI3K, phospho-AKT, AKT, p53, and PD-L1 in NCCIT and NTERA-2 cells incubated with 100 or 200 μM 6-gingerol for 48 h. Expression levels were estimated by densitometry and normalized to β-actin. Data were obtained in triplicate. **(B)** Western blot of PTEN, phos-pho-PI3K, PI3K, phospho-AKT, AKT, p53, and PD-L1 in NCCIT and NTERA-2 cells incubated with 2 μM SF1670 or 200 μM 6-gingerol for 48 h. Expression levels were estimated by densi-tometry and normalized to β-actin. Data were obtained in triplicate.

role. First, we estimated the total iron concentration in NCCIT and NTERA-2 cells and media with or without 6-gingerol treatment using an iron assay kit (**Figure 5A**). The results showed an increase in the total iron concentration in the medium following 6-gingerol treatment. However, the concentration of iron in 6-gingerol-treated cells was significantly reduced. This suggested an enhanced iron release into the medium. We confirmed this by using flow cytometry to estimate the ferrous ion (Fe2+) concentration in NCCIT and NTERA-2 cells after treatment with 6-gingerol; results suggested a significant decrease in the Fe2+ ion concentration following 6-gingerol treatment (**Figure 5B**). These results indicated an upregulation in iron transport by the conversion of Fe2+ to Fe3+, which highlighted the conversion of total iron for iron metabolism.

To confirm this, we analyzed the expression levels of proteins responsible for iron transport, and the results showed downregulated expression of TFR1 and ferroportin (FPN1), which transports iron (**Figure 5C**). Also, we found that 6-gingerol suppressed the expression of DMT1 and STEAP3, helping iron conversion. These results suggested a role of iron metabolism in the anti-cancer activity of 6-gingerol against embryonic CSCs. Next, we analyzed the role of iron metabolism in PTEN induction and p53/PD-L1 signaling. For this, we added iron sulfate ($FeSO_4$) to NCCIT and NTERA-2 cells with or without 6-gingerol treatment. Supplementation with $FeSO_4$ resulted in suppressed PTEN and p53 expression, which was accompanied by an elevation in PD-L1 expression (**Figure 5D**). The addition of 6-gingerol reversed these expression patterns, which suggested a role for iron metabolism in PTEN-mediated p53 and PD-L1 expressions following 6-gingerol treatment in embryonic CSCs.

6-Gingerol Downregulates miR-20b, miR-21, and miR-130b

We found that iron metabolism and PTEN/p53/PD-L1 signaling may play a role in the induction of apoptosis by 6-gingerol in embryonic CSCs. Here, we analyzed the potential role of microRNA in the apoptotic activity of 6-gingerol and the role of iron metabolism in microRNA expression in the presence of 6-gingerol. First, we measured the expression levels of miR-20b, miR-21, and miR-130b, which play key roles in PTEN-mediated PD-L1 expression. The mRNA analysis showed a downregulation of miR-20b, miR-21, and miR-130b following 6-gingerol treatment in NCCIT and NTERA-2 cells (**Figure 6A**). These data indicated a potential role for these microRNAs in apoptosis induction by 6-gingerol. To confirm this activity, we used the PTEN inhibitor SF1670 and analyzed the expression of these microRNAs in the presence of 6-gingerol (**Figure 6B**). The results showed elevated expression of miR-20b, miR-21, and miR-130b with PTEN inhibitor treatment, which was downregulated by 6-gingerol treatment. These results suggested a role for PTEN in regulating these microRNAs.

Next, we verified the role of iron metabolism in the expression of miR-20b, miR-21, and miR-130b by supplementing $FeSO_4$ with or without 6-gingerol. These results also showed an increase in the expression of miR-20b, miR-21, and miR-130b following $FeSO_4$ treatment, which were reversed by the addition of 6-gingerol in both NCCIT and NTERA-2 cells (**Figure 6C**). These results contributed to evidence that iron metabolism plays a role

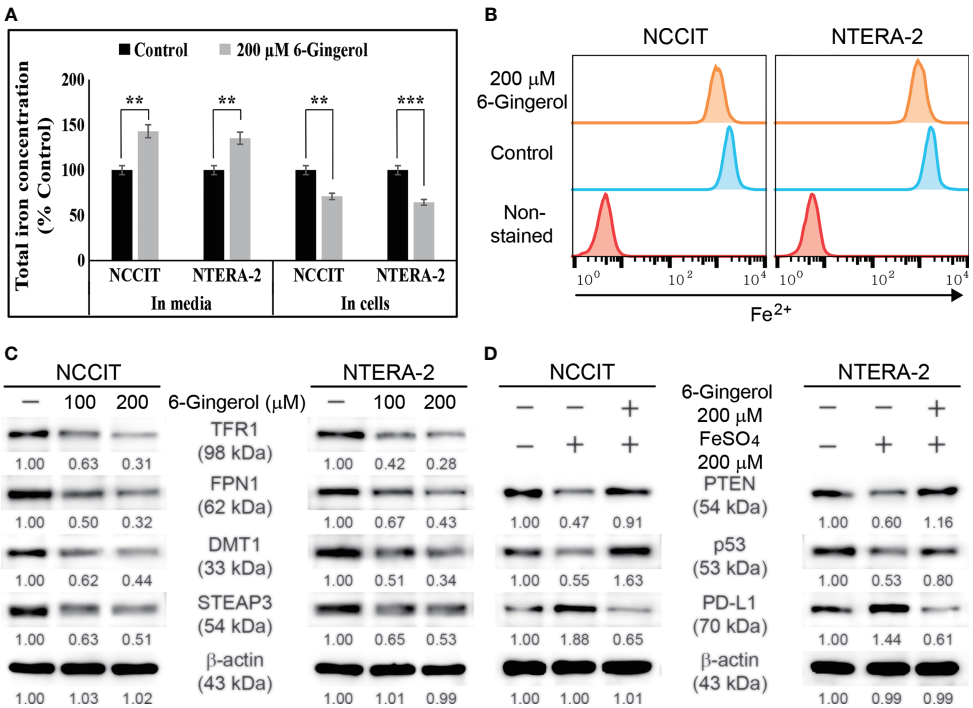

FIGURE 5 | 6-Gingerol inhibited iron metabolism. **(A)** Iron assay of the total iron concentration in NCCIT and NTERA-2 cells treated with 200 μM 6-gingerol for 48 h. Data were obtained in triplicate. Controls were set at 100. $^{**}p < 0.01$ and $^{***}p < 0.001$ (control *vs.* 6-gingerol; Student's t-test). **(B)** Flow cytometry of Fe^{2+} in NCCIT and NTERA-2 cells after treatment with 200 μM of 6-gingerol for 48 h. The graphical representation shows cells with intracellular Fe2+ level. **(C)** Western blot of TFR1, DMT1, STEAP3, and FPN1 in NCCIT and NTERA-2 cells after in-cubation with 100 or 200 μM of 6-gingerol for 48 h. Expression levels were estimated by densi-tometry and normalized to β-actin. Data were obtained in triplicate. **(D)** Western blot of PTEN, p53, and PD-L1 in NCCIT and NTERA-2 cells incubated with 200 μM $FeSO_4$ or 200 μM 6-gingerol for 48 h. Expression levels were estimated by densitometry and normalized to β-actin. Data were obtained in triplicate.

in the induction of cell death by regulating microRNA expression following 6-gingerol treatment.

DISCUSSION

Anti-cancer activity partially depends on how a drug impacts cancer cells and prevent cancer recurrence by targeting CSCs. Cancer recurrence is one of the major challenges for many chemotherapeutic drugs, as they successfully suppress tumor progression but may not have targeted CSCs (37). The use of natural compounds as cancer therapeutics is promising for long-term use as they may reduce side effects and target both cancer cells and CSCs. 6-Gingerol successfully suppressed the expression of CSC markers and Wnt/β-catenin signaling in NCCIT and NTERA-2 cells, suggesting that 6-gingerol might target cancer cells as well as CSCs.

A natural compound that can induce DDR, thereby inducing cell cycle arrest and apoptosis in cancer cells, should be considered as a candidate for further studies. Previous studies showed that 6-gingerol can induce cell cycle arrest and apoptosis against several cancer types (28, 34, 38). The anti-cancer activity of a natural compound also depends on its capability to induce ROS generation (39). We found that 6-gingerol elevated the expression of iNOS at the transcriptional and translational levels so that iNOS induction leads to ROS generation (28). As a result, treatment with 6-gingerol significantly elevated cellular and mitochondrial ROS, which may hint for anti-cancer activity of 6-gingerol. We demonstrated 6-gingerol induction of DDR by introducing DNA double-strand breaks. ATM or ATR kinases sense DNA damage and are central regulators in the response to DNA damage (40). Next, our results also showed an elevation in the expression levels of these kinases, which then activated p53 expression to proceed to cell cycle arrest and apoptosis. This leads to the phosphorylation of other substrates such as BRCA1, CHK1, or CHK2 (41, 42). Prolonged DNA damage results in cell cycle arrest, and p53 is a key factor in this mechanism (43). We showed that 6-gingerol successfully induced DDR, G0/G1 cell cycle arrest, and p53 expression in NCCIT and NTERA-2 cells. These results suggested a possible apoptosis induction in embryonic CSCs following 6-gingerol treatment.

The apoptosis pathway is divided into intrinsic and extrinsic pathways. Mitochondria play a central role in the intrinsic pathway through the p53-dependent upregulation of BAX and downregulation of BCL-2, which promotes the release of cytochrome c from mitochondria to the cytosol. The presence of cytochrome c in the cytosol activates caspase proteins to induce apoptosis (44, 45). Flow cytometry results suggested 6-gingerol induction of apoptosis in NCCIT and NTERA-2 cells.

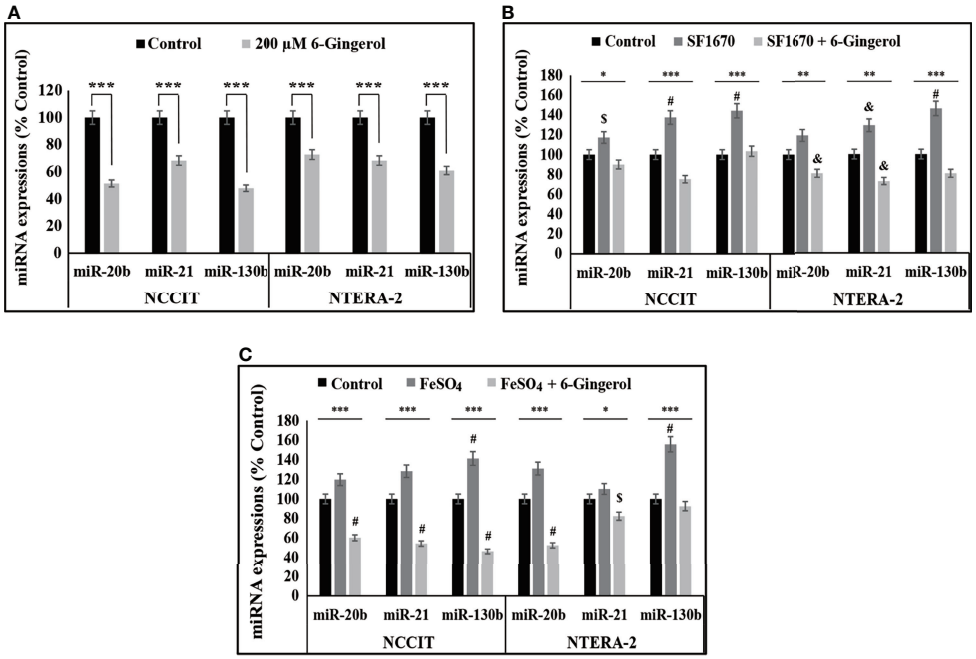

FIGURE 6 | 6-Gingerol regulated expression of miR-20b, miR-21, and miR-130b. **(A)** Repre-sentative real-time qPCR analysis of miR-20b, miR-21, and miR-130b transcripts following treatment with 200 µM 6-gingerol for 48 h in embryonic CSCs. Then, Cp values were normalized to U6 mRNA. Controls were set at 100. ***$p < 0.001$. (Student's t-test). **(B)** Representative real-time qPCR of miR-20b, miR-21, and miR-130b transcripts following treatment with 2 µM SF1670 with or without 200 µM 6-gingerol for 48 h in NCCIT and NTERA-2 cells. Cp values were normalized to *U6* mRNA. Controls were set at 100. *$p < 0.05$, **$p < 0.01$, and ***$p < 0.001$. (ANOVA test), $^{\$}p < 0.05$ vs. control, $^{\&}p < 0.01$ *vs*. control, and $^{\#}p < 0.001$ *vs*. control. **(C)** Representative real-time qPCR of miR-20b, miR-21, and miR-130b in NCCIT and NTERA-2 cells treated with 200 µM 6-gingerol for 48 h, followed by 200 µM $FeSO_4$ for an additional 48 h. Cp values were normalized to *U6* mRNA. Controls were set at 100. *$p < 0.05$ and ***$p < 0.001$ (ANOVA test). $^{\$}p < 0.05$ *vs*. control. $^{\#}p < 0.001$ *vs*. control.

An analysis of the apoptosis induction pathway following 6-gingerol treatment matched the expectations of intrinsic pathway activation; we observed an upregulation of BAX, cleaved caspase 9, and cytochrome c expression as well as downregulated expression of BCL-2 and BCL-xL. These results provide evidence that 6-gingerol induces mitochondrial apoptosis.

Iron metabolism can induce ROS generation that might lead to the DDR, thereby causing cell cycle arrest and apoptosis. Iron metabolism also plays a crucial role in tumor progression; control of iron homeostasis could be a key target in anti-cancer activity (46). Adding 6-gingerol to NCCIT and NTERA-2 cells showed a decrease in the amount of cellular Fe2+ and a release of total iron into spent medium, suggesting the inhibition of iron transport in NCCIT and NTERA-2 cells by 6-gingerol. Molecular analysis of the proteins responsible for iron homeostasis provided additional proof for our hypothesis of iron metabolism inhibition by 6-gingerol. Hence, ROS generation and an inhibition of iron metabolism might contribute to apoptosis induction by 6-gingerol. The role of iron metabolism was also confirmed by the activity of $FeSO_4$ on the expression of the tumor suppressor protein PTEN. PTEN exhibits an essential role in embryonic development, and it may regulate the renewal and differentiation of stem cells by mediating GSK3-β expression, a key factor in Wnt/β-catenin signaling (47). A loss of PTEN upregulates PD-L1 expression through the activation of the PI3K/AKT pathway (48, 49). The suppression of p53 also involves the regulation of PD-L1 expression through PI3K/AKT signaling (50). Our results demonstrated an increase in the expression patterns of PTEN and p53, with a decrease in PI3K/AKT signaling and PD-L1 expression following 6-gingerol treatment of NCCIT and NTERA-2 embryonic CSCs. We also confirmed the role of PTEN in PD-L1 expression in both cell types using a specific PTEN inhibitor and demonstrated the ability of 6-gingerol to regulate these signaling pathway by reversing the effect of the PTEN inhibitor.

The suppression of PD-L1 depends on the regulation of microRNAs (miRNAs). miRNAs are a family of small noncoding RNAs that play vital roles in cancer by regulating other signaling pathways, inhibiting mRNA translation, and promoting mRNA degradation, all of which result in the post-transcriptional modification of gene expression (51). Many microRNAs such as miR-34a, miR-197, and miR-200 are involved in the expression of PD-L1 (51). Among others, miR-20, miR-21, and miR-130 mediate PD-L1 expression by regulating PTEN expression (52). Treatment of NCCIT and NTERA-2 cells with 6-gingerol showed a downregulation of miR-20b, miR-21, and miR-130b expression. Next, the regulation of these miRNAs was confirmed using a PTEN inhibitor and 6-gingerol treatment. To analyze the role of iron metabolism in these miRNAs' expression, we used $FeSO_4$ to treat NCCIT and NTERA-2 cells with and without 6-gingerol. The expression of miR-20b, miR-21, and miR-130b were increased

with $FeSO_4$ supplementation, which was successfully reversed by 6-gingerol treatment. It is evident that the inhibition of iron metabolism contributes to the ability of these microRNAs to elevate PTEN expression, which thereby inhibits PD-L1 expression to promote the intrinsic apoptosis pathway.

This study demonstrated that a natural sulfur-containing compound, 6-gingerol, targets embryonic CSCs by inhibiting CSC markers and Wnt/β-catenin signaling in NCCIT and NTERA-2 cells. Furthermore, 6-gingerol induced the intrinsic pathway of apoptosis in these embryonic CSCs through the induction of PTEN, thereby inhibiting PD-L1 expression. Iron metabolism plays a vital role in the elevation of PTEN expression through ROS generation, thereby regulating PI3K/AKT/p53 signaling to inhibit PD-L1 expression and suppress the expression of miR-20b, miR-21, and miR-130b. Altogether, 6-gingerol is a candidate for adjuvant chemotherapy, as it may suppress cancer recurrence by targeting CSCs.

DATA AVAILABILITY STATEMENT

The original contributions presented in the study are included in the article/**Supplementary Material**. Further inquiries can be directed to the corresponding authors.

AUTHOR CONTRIBUTIONS

K-JJ and SWB designed the experiments. NS, DYK, and ESJ performed all the experiments. J-ML served as scientific advisors and participated in technical editing of the manuscript. NS and K-JJ wrote the manuscript. NS, DYK, SWB, and K-JJ analyzed the data. All authors helped in revising the manuscript and approved the final version for publication. All authors read and agreed to the published version of the manuscript.

FUNDING

This work was supported by the research grant of Jeju National University in 2021.

SUPPLEMENTARY MATERIAL

The Supplementary Material for this article can be found online at: https://www.frontiersin.org/articles/10.3389/fonc.2021.781720/full#supplementary-material

REFERENCES

1. Andrews PW, Damjanov I, Berends J, Kumpf S, Zappavigna V, Mavilio F, et al. Inhibition of Proliferation and Induction of Differentiation of Pluripotent Human Embryonal Carcinoma Cells by Osteogenic Protein-1 (or Bone Morphogenetic Protein-7). *Lab Invest* (1994) 71(2):243–51.
2. Donovan PJ, Gearhart J. The End of the Beginning for Pluripotent Stem Cells. *Nature* (2001) 414(6859):92–7. doi: 10.1038/35102154
3. Sp N, Kang DY, Jo ES, Rugamba A, Kim WS, Park YM, et al. Tannic Acid Promotes TRAIL-Induced Extrinsic Apoptosis by Regulating Mitochondrial ROS in Human Embryonic Carcinoma Cells. *Cells* (2020) 9(2):282. doi: 10.3390/cells9020282
4. Sp N, Kang DY, Kim DH, Park JH, Lee HG, Kim HJ, et al. Nobiletin Inhibits CD36-Dependent Tumor Angiogenesis, Migration, Invasion, and Sphere Formation Through the Cd36/Stat3/Nf-Kappab Signaling Axis. *Nutrients* (2018) 10(6):772. doi: 10.3390/nu10060772
5. Eini R, Stoop H, Gillis AJ, Biermann K, Dorssers LC, Looijenga LH. Role of SOX2 in the Etiology of Embryonal Carcinoma, Based on Analysis of the NCCIT and NT2 Cell Lines. *PloS One* (2014) 9(1):e83585. doi: 10.1371/journal.pone.0083585
6. de Sousa EMF, Vermeulen L. Wnt Signaling in Cancer Stem Cell Biology. *Cancers (Basel)* (2016) 8(7):60. doi: 10.3390/cancers8070060
7. Mavila N, Thundimadathil J. The Emerging Roles of Cancer Stem Cells and Wnt/Beta-Catenin Signaling in Hepatoblastoma. *Cancers (Basel)* (2019) 11 (10):1406. doi: 10.3390/cancers11101406
8. MacDonald BT, Tamai K, He X. Wnt/beta-Catenin Signaling: Components, Mechanisms, and Diseases. *Dev Cell* (2009) 17(1):9–26. doi: 10.1016/j.devcel.2009.06.016
9. Aberle H, Bauer A, Stappert J, Kispert A, Kemler R. Beta-Catenin Is a Target for the Ubiquitin-Proteasome Pathway. *EMBO J* (1997) 16(13):3797–804. doi: 10.1093/emboj/16.13.3797
10. Jang GB, Kim JY, Cho SD, Park KS, Jung JY, Lee HY, et al. Blockade of Wnt/beta-Catenin Signaling Suppresses Breast Cancer Metastasis by Inhibiting CSC-Like Phenotype. *Sci Rep* (2015) 5:12465. doi: 10.1038/srep12465
11. Chen Y, Shi L, Zhang L, Li R, Liang J, Yu W, et al. The Molecular Mechanism Governing the Oncogenic Potential of SOX2 in Breast Cancer. *J Biol Chem* (2008) 283(26):17969–78. doi: 10.1074/jbc.M802917200
12. Kim DH, Suh J, Surh YJ, Na HK. Regulation of the Tumor Suppressor PTEN by Natural Anticancer Compounds. *Ann N Y Acad Sci* (2017) 1401(1):136–49. doi: 10.1111/nyas.13422
13. Franke TF. PI3K/Akt: Getting It Right Matters. *Oncogene* (2008) 27(50):6473–88. doi: 10.1038/onc.2008.313
14. Tan MH, Mester JL, Ngeow J, Rybicki LA, Orloff MS, Eng C. Lifetime Cancer Risks in Individuals With Germline PTEN Mutations. *Clin Cancer Res* (2012) 18(2):400–7. doi: 10.1158/1078-0432.CCR-11-2283
15. Dong P, Xiong Y, Yue J, Hanley SJB, Watari H. Tumor-Intrinsic PD-L1 Signaling in Cancer Initiation, Development and Treatment: Beyond Immune Evasion. *Front Oncol* (2018) 8:386. doi: 10.3389/fonc.2018.00386
16. Chen J, Jiang CC, Jin L, Zhang XD. Regulation of PD-L1: A Novel Role of Pro-Survival Signalling in Cancer. *Ann Oncol* (2016) 27(3):409–16. doi: 10.1093/annonc/mdv615
17. Havel JJ, Chowell D, Chan TA. The Evolving Landscape of Biomarkers for Checkpoint Inhibitor Immunotherapy. *Nat Rev Cancer* (2019) 19(3):133–50. doi: 10.1038/s41568-019-0116-x
18. Baitsch L, Baumgaertner P, Devevre E, Raghav SK, Legat A, Barba L, et al. Exhaustion of Tumor-Specific CD8(+) T Cells in Metastases From Melanoma Patients. *J Clin Invest* (2011) 121(6):2350–60. doi: 10.1172/JCI46102
19. Sharma P, Allison JP. The Future of Immune Checkpoint Therapy. *Science* (2015) 348(6230):56–61. doi: 10.1126/science.aaa8172
20. Muckenthaler MU, Rivella S, Hentze MW, Galy B. A Red Carpet for Iron Metabolism. *Cell* (2017) 168(3):344–61. doi: 10.1016/j.cell.2016.12.034
21. Cornelissen A, Guo L, Sakamoto A, Virmani R, Finn AV. New Insights Into the Role of Iron in Inflammation and Atherosclerosis. *EBioMedicine* (2019) 47:598–606. doi: 10.1016/j.ebiom.2019.08.014
22. Wang Y, Yu L, Ding J, Chen Y. Iron Metabolism in Cancer. *Int J Mol Sci* (2018) 20(1):95. doi: 10.3390/ijms20010095
23. Chen Y, Fan Z, Yang Y, Gu C. Iron Metabolism and Its Contribution to Cancer (Review). *Int J Oncol* (2019) 54(4):1143–54. doi: 10.3892/ijo.2019.4720
24. Ponka P. Tissue-Specific Regulation of Iron Metabolism and Heme Synthesis: Distinct Control Mechanisms in Erythroid Cells. *Blood* (1997) 89(1):1–25.
25. Plaimee P, Weerapreeyakul N, Barusrux S, Johns NP. Melatonin Potentiates Cisplatin-Induced Apoptosis and Cell Cycle Arrest in Human Lung Adenocarcinoma Cells. *Cell Prolif* (2015) 48(1):67–77. doi: 10.1111/cpr.12158

26. Lissoni P, Chilelli M, Villa S, Cerizza L, Tancini G. Five Years Survival in Metastatic non-Small Cell Lung Cancer Patients Treated With Chemotherapy Alone or Chemotherapy and Melatonin: A Randomized Trial. *J Pineal Res* (2003) 35(1):12–5. doi: 10.1034/j.1600-079x.2003.00032.x
27. Sp N, Kang DY, Joung YH, Park JH, Kim WS, Lee HK, et al. Nobiletin Inhibits Angiogenesis by Regulating Src/FAK/STAT3-Mediated Signaling Through PXN in ER(+) Breast Cancer Cells. *Int J Mol Sci* (2017) 18(5):935. doi: 10.3390/ijms18050935
28. Sp N, Kang DY, Lee JM, Bae SW, Jang KJ. Potential Antitumor Effects of 6-Gingerol in P53-Dependent Mitochondrial Apoptosis and Inhibition of Tumor Sphere Formation in Breast Cancer Cells. *Int J Mol Sci* (2021) 22 (9):4660. doi: 10.3390/ijms22094660
29. Mao QQ, Xu XY, Cao SY, Gan RY, Corke H, Beta T, et al. Bioactive Compounds and Bioactivities of Ginger (Zingiber Officinale Roscoe). *Foods* (2019) 8(6):185. doi: 10.3390/foods8060185
30. Young HY, Luo YL, Cheng HY, Hsieh WC, Liao JC, Peng WH. Analgesic and Anti-Inflammatory Activities of [6]-Gingerol. *J Ethnopharmacol* (2005) 96(1-2):207–10. doi: 10.1016/j.jep.2004.09.009
31. Shukla Y, Singh M. Cancer Preventive Properties of Ginger: A Brief Review. *Food Chem Toxicol* (2007) 45(5):683–90. doi: 10.1016/j.fct.2006.11.002
32. Rahmani AH, Shabrmi FM, Aly SM. Active Ingredients of Ginger as Potential Candidates in the Prevention and Treatment of Diseases *via* Modulation of Biological Activities. *Int J Physiol Pathophysiol Pharmacol* (2014) 6(2):125–36.
33. Zhang M, Viennois E, Prasad M, Zhang Y, Wang L, Zhang Z, et al. Edible Ginger-Derived Nanoparticles: A Novel Therapeutic Approach for the Prevention and Treatment of Inflammatory Bowel Disease and Colitis-Associated Cancer. *Biomaterials* (2016) 101:321–40. doi: 10.1016/j.biomaterials.2016.06.018
34. Lee SH, Cekanova M, Baek SJ. Multiple Mechanisms Are Involved in 6-Gingerol-Induced Cell Growth Arrest and Apoptosis in Human Colorectal Cancer Cells. *Mol Carcinog* (2008) 47(3):197–208. doi: 10.1002/mc.20374
35. Ishiguro K, Ando T, Maeda O, Ohmiya N, Niwa Y, Kadomatsu K, et al. Ginger Ingredients Reduce Viability of Gastric Cancer Cells *via* Distinct Mechanisms. *Biochem Biophys Res Commun* (2007) 362(1):218–23. doi: 10.1016/j.bbrc.2007.08.012
36. Park YJ, Wen J, Bang S, Park SW, Song SY. [6]-Gingerol Induces Cell Cycle Arrest and Cell Death of Mutant P53-Expressing Pancreatic Cancer Cells. *Yonsei Med J* (2006) 47(5):688–97. doi: 10.3349/ymj.2006.47.5.688
37. Dawood S, Austin L, Cristofanilli M. Cancer Stem Cells: Implications for Cancer Therapy. *Oncol (Williston Park)* (2014) 28(12):1101–7.
38. Kapoor V, Aggarwal S, Das SN. 6-Gingerol Mediates its Anti Tumor Activities in Human Oral and Cervical Cancer Cell Lines Through Apoptosis and Cell Cycle Arrest. *Phytother Res* (2016) 30(4):588–95. doi: 10.1002/ptr.5561
39. Rugamba A, Kang DY, Sp N, Jo ES, Lee JM, Bae SW, et al. Silibinin Regulates Tumor Progression and Tumorsphere Formation by Suppressing PD-L1 Expression in Non-Small Cell Lung Cancer (NSCLC) Cells. *Cells* (2021) 10 (7):1632. doi: 10.3390/cells10071632
40. Marechal A, Zou L. DNA Damage Sensing by the ATM and ATR Kinases. *Cold Spring Harb Perspect Biol* (2013) 5(9):a012716. doi: 10.1101/cshperspect.a012716
41. Shiloh Y. ATM and Related Protein Kinases: Safeguarding Genome Integrity. *Nat Rev Cancer* (2003) 3(3):155–68. doi: 10.1038/nrc1011
42. Lavin MF. Ataxia-Telangiectasia: From a Rare Disorder to a Paradigm for Cell Signalling and Cancer. *Nat Rev Mol Cell Biol* (2008) 9(10):759–69. doi: 10.1038/nrm2514
43. Pellegata NS, Antoniono RJ, Redpath JL, Stanbridge EJ. DNA Damage and P53-Mediated Cell Cycle Arrest: A Reevaluation. *Proc Natl Acad Sci USA* (1996) 93(26):15209–14. doi: 10.1073/pnas.93.26.15209
44. Pawlowski J, Kraft AS. Bax-Induced Apoptotic Cell Death. *Proc Natl Acad Sci U.S.A.* (2000) 97(2):529–31. doi: 10.1073/pnas.97.2.529
45. Sp N, Kang DY, Kim DH, Yoo JS, Jo ES, Rugamba A, et al. Tannic Acid Inhibits Non-Small Cell Lung Cancer (NSCLC) Stemness by Inducing G0/G1 Cell Cycle Arrest and Intrinsic Apoptosis. *Anticancer Res* (2020) 40(6):3209–20. doi: 10.21873/anticanres.14302
46. Forciniti S, Greco L, Grizzi F, Malesci A, Laghi L. Iron Metabolism in Cancer Progression. *Int J Mol Sci* (2020) 21(6):2257. doi: 10.3390/ijms21062257
47. Wang W, Lu G, Su X, Tang C, Li H, Xiong Z, et al. Pten-Mediated Gsk3beta Modulates the Naive Pluripotency Maintenance in Embryonic Stem Cells. *Cell Death Dis* (2020) 11(2):107. doi: 10.1038/s41419-020-2271-0
48. Parsa AT, Waldron JS, Panner A, Crane CA, Parney IF, Barry JJ, et al. Loss of Tumor Suppressor PTEN Function Increases B7-H1 Expression and Immunoresistance in Glioma. *Nat Med* (2007) 13(1):84–8. doi: 10.1038/nm1517
49. Crane CA, Panner A, Murray JC, Wilson SP, Xu H, Chen L, et al. PI(3) Kinase Is Associated With a Mechanism of Immunoresistance in Breast and Prostate Cancer. *Oncogene* (2009) 28(2):306–12. doi: 10.1038/onc.2008.384
50. Kang DY, Sp N, Jo ES, Rugamba A, Hong DY, Lee HG, et al. The Inhibitory Mechanisms of Tumor PD-L1 Expression by Natural Bioactive Gallic Acid in Non-Small-Cell Lung Cancer (NSCLC) Cells. *Cancers (Basel)* (2020) 12 (3):727. doi: 10.3390/cancers12030727
51. Wu KL, Tsai YM, Lien CT, Kuo PL, Hung AJ. The Roles of MicroRNA in Lung Cancer. *Int J Mol Sci* (2019) 20(7):1611. doi: 10.3390/ijms20071611
52. Zhu J, Chen L, Zou L, Yang P, Wu R, Mao Y, et al. MiR-20b, -21, and -130b Inhibit PTEN Expression Resulting in B7-H1 Over-Expression in Advanced Colorectal Cancer. *Hum Immunol* (2014) 75(4):348–53. doi: 10.1016/j.humimm.2014.01.006

Conflict of Interest: Author J-ML was employed by company SK Bioscience.

The remaining authors declare that the research was conducted in the absence of any commercial or financial relationships that could be construed as a potential conflict of interest.

Publisher's Note: All claims expressed in this article are solely those of the authors and do not necessarily represent those of their affiliated organizations, or those of the publisher, the editors and the reviewers. Any product that may be evaluated in this article, or claim that may be made by its manufacturer, is not guaranteed or endorsed by the publisher.

frontiers in Oncology

REVIEW
published: 10 February 2022
doi: 10.3389/fonc.2022.807266

OPEN ACCESS

Edited by:
Pramod Darvin,
Rajiv Gandhi Centre for Biotechnology, India

Reviewed by:
Daniela Cilloni,
University of Turin, Italy
Eleni Ladikou,
Brighton and Sussex Medical School, United Kingdom
Naeem Khan,
University of Birmingham, United Kingdom

***Correspondence:**
Patrick Connerty
Pconnerty@ccia.org.au

†ORCID:
Yashar Mesbahi
orcid.org/0000-0002-1730-9309

‡These authors have contributed equally to this work and share senior authorship

Specialty section:
This article was submitted to Cancer Metabolism, a section of the journal Frontiers in Oncology

Received: *01 November 2021*
Accepted: *18 January 2022*
Published: *10 February 2022*

Citation:
Mesbahi Y, Trahair TN, Lock RB and Connerty P (2022) Exploring the Metabolic Landscape of AML: From Haematopoietic Stem Cells to Myeloblasts and Leukaemic Stem Cells. Front. Oncol. 12:807266. doi: 10.3389/fonc.2022.807266

Exploring the Metabolic Landscape of AML: From Haematopoietic Stem Cells to Myeloblasts and Leukaemic Stem Cells

Yashar Mesbahi[1,2,3†], Toby N. Trahair[1,2,4], Richard B. Lock[1,2,3‡] and Patrick Connerty[1,2,3‡]*

[1] Children's Cancer Institute, Lowy Cancer Centre, University of New South Wales (UNSW) Sydney, Kensington, NSW, Australia, [2] School of Women's and Children's Health, University of New South Wales (UNSW) Sydney, Kensington, NSW, Australia, [3] University of New South Wales Centre for Childhood Cancer Research, University of New South Wales (UNSW) Sydney, Kensington, NSW, Australia, [4] Kids Cancer Centre, Sydney Children's Hospital, Randwick, NSW, Australia

Despite intensive chemotherapy regimens, up to 60% of adults with acute myeloid leukaemia (AML) will relapse and eventually succumb to their disease. Recent studies suggest that leukaemic stem cells (LSCs) drive AML relapse by residing in the bone marrow niche and adapting their metabolic profile. Metabolic adaptation and LSC plasticity are novel hallmarks of leukemogenesis that provide important biological processes required for tumour initiation, progression and therapeutic responses. These findings highlight the importance of targeting metabolic pathways in leukaemia biology which might serve as the Achilles' heel for the treatment of AML relapse. In this review, we highlight the metabolic differences between normal haematopoietic cells, bulk AML cells and LSCs. Specifically, we focus on four major metabolic pathways dysregulated in AML; (i) glycolysis; (ii) mitochondrial metabolism; (iii) amino acid metabolism; and (iv) lipid metabolism. We then outline established and emerging drug interventions that exploit metabolic dependencies of leukaemic cells in the treatment of AML. The metabolic signature of AML cells alters during different biological conditions such as chemotherapy and quiescence. Therefore, targeting the metabolic vulnerabilities of these cells might selectively eradicate them and improve the overall survival of patients with AML.

Keywords: acute myeloid leukaemia, metabolic plasticity, leukaemic stem cells, cancer metabolism, metabolic targeting

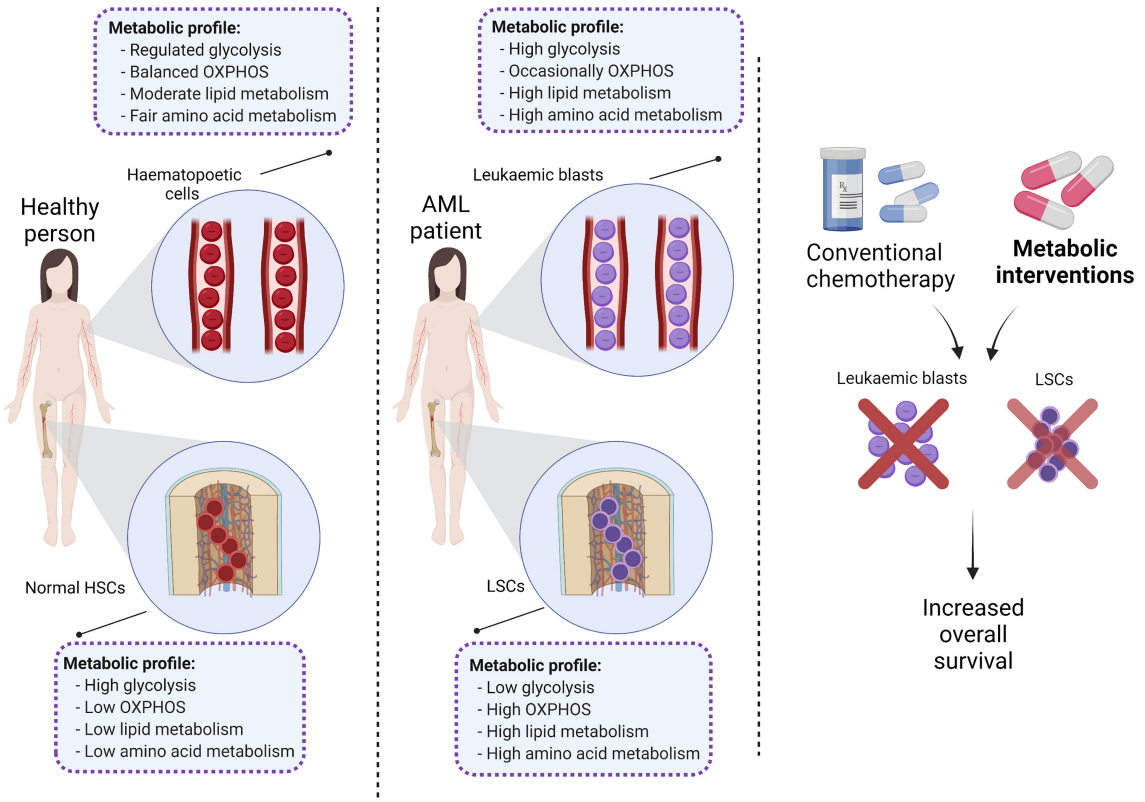

GRAPHICAL ABSTRACT |

INTRODUCTION

Acute myeloid leukaemia (AML) is the most common acute leukaemia in adults (1, 2). It is characterised by abnormal proliferation of undifferentiated haematopoietic cells called leukaemic blasts (3). The incidence of AML follows an age-dependent pattern, accounting for around 23% of leukaemias in adults (1). Several treatment strategies have been proposed to improve clinical outcomes in patients with AML including allogeneic stem cell transplantation, monoclonal antibodies, and small-molecule inhibitors targeting key leukemogenic drivers. However, combination chemotherapy remains the mainstay of disease treatment (4). Historically, AML treatment has been divided into induction and consolidation phases. The backbone of induction therapy consists of the "7+3" regimen, comprising cytarabine (Ara-C) for 7 days with 3 days of anthracyclines including daunorubicin, doxorubicin or idarubicin (4, 5).

Despite intensive treatment regimens, the median survival rate remains disappointingly low in adults and the majority of patients will eventually succumb to complications of drug treatment or disease relapse. Treatment outcome is significantly better in younger patients with a complete remission rate of ≥80%, however, due to relapse and refractory disease, there is still a 5-year overall survival rate of ~40% (4). Therefore, targeting AML is challenging and requires in-depth knowledge of the underlying cellular and molecular mechanisms which drive the disease.

Metabolism is defined as a series of dynamic processes that allow energy production according to cellular demands. Metabolism is therefore dependent on a cell's state of proliferation, differentiation, and quiescence (6). For instance, normal cells employ a well-organised network of metabolic programs and a balanced turnover between supply and demand (6). Normal haematopoietic stem cells (HSCs) are characteristically quiescent and adapt their metabolic profiles at a low demand status to maintain their survival and produce multipotent progenitors in the bone marrow (BM) niche (7, 8). In contrast, the bulk AML population is comprised of rapidly proliferating cells that require additional sources of energy for growth and survival (9).

During normal haematopoiesis, HSCs produce multipotent progenitors that, over multiple cycles of proliferation and differentiation, will produce the entire repertoire of haematopoietic cells (**Figure 1**) (10). However, occasionally these myeloid stem/progenitor cells acquire genetic aberrations, transform into malignant leukaemic stem cells (LSCs), and overproduce immature $CD34^+/CD38^+$ blast cells which do not undergo differentiation (3, 11). As well as metabolic differences (12), HSCs, LSCs and AML blasts are genetically and phenotypically distinct and have high levels of heterogeneity within each cell population (13, 14). Pioneering studies functionally characterised LSCs as a rare subset of the immature

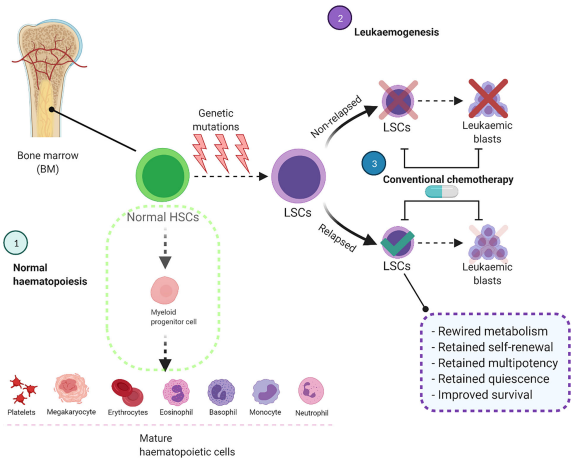

FIGURE 1 | Conventional chemotherapy is ineffective to target and eliminate LSCs, leading to AML relapse. In the normal haematopoietic system, HSCs differentiate into myeloid progenitor cells and eventually produce mature haematopoietic cells. In AML these HSCs acquire genetic mutations which impair the differentiation process and convert them to LSCs. These cells acquire self-renewal ability and produce leukaemic blasts in the bone marrow and other organs. Although the current treatment strategies eliminate leukaemic blasts, they are unable to destroy LSCs completely which will cause AML relapse. BM, Bone marrow; HSCs, Haematopoietic stem cells; LSCs, Leukaemic stem cells.

$CD34^+/CD38^-$ population which is capable of initiating leukaemia in immunodeficient mice (11, 15). In contrast, more mature $CD34^+/CD38^+$ AML blasts failed to propagate the disease under the same conditions (15). However, as LSCs and normal HSCs share similar $CD34^+/CD38^-$ surface immunophenotype, more research has been done to identify unique membrane markers for LSCs including CD32, CD44, CD47, CD123, TIM3, CD45RA and CD96 (14, 16, 17).

Genome and metabolome heterogeneity is also prevalent within sub-populations of unique haematopoietic cell types. For example, recent studies indicated that within certain immunophenotypic fractions such as $CD34^+/CD38^-$, other factors such as reactive oxygen species content are able to identify which cells are functional LSCs (18, 19). Furthermore, mathematical modelling studies of leukaemogenesis have indicated that mature myeloid cells can often have the same genotype as leukaemic blasts, highlighting that differentiation of leukaemic blasts is not completely blocked in the disease (20). A comprehensive single-cell sequencing study by Bernstein et al. has indicated intra-tumoural heterogeneity of malignant AML cells and uncovered that some undefined phenotypic markers may be expressed by both malignant and normal cells (21). This further reinforces the fact that identification of immunophenotypes might not be powerful enough to detect the origin of leukaemogenesis and investigating other molecular markers such as metabolites and metabolic pathways would help determine disease initiating populations in AML (22).

Like normal HSCs, LSCs reside in the BM niche of AML patients (23) which supports their survival and protects them against chemotherapeutic drug treatment (24–26). In addition, hypoxic conditions in the bone marrow microenvironment (BMME) result in lower reactive oxygen species (ROS) content which not only distinguishes LSCs from AML blasts, but also contributes to maintaining a quiescent cellular status, promotes anaerobic metabolism, and sustains stemness (27, 28); all of which protect LSCs from chemotherapy (29, 30). Unlike quiescent LSCs, circulating AML blasts have higher levels of ROS (18, 31) and upregulate multiple metabolic pathways to supply the required energy for proliferation (19).

Previous studies have extensively focused on the metabolic profile of AML and the rationale for targeting deregulated metabolic pathways in leukaemic blasts (9, 32–35). However, the metabolic landscape of different haematopoietic cells remains unclear and needs further elucidation. Therefore, this review will focus on the differences between the metabolic profiles of normal haematopoietic and AML cells. It will then focus on the metabolic differences between normal HSCs, LSCs, and AML blasts as a means to rationally develop novel treatment approaches to eliminate cells responsible for AML.

METABOLIC DIFFERENCES BETWEEN HSCs, LSCs AND LEUKAEMIC BLASTS

Previous reports have indicated that normal HSCs, LSCs and AML blasts have distinct and unique metabolic profiles. Compared to the low energy demands of normal HSCs (36), leukaemic blasts require higher production of ATP to support their increased cellular division (37). Leukaemic blasts upregulate metabolic pathways such as glycolysis (37) and the pentose-phosphate pathway (38) to produce the building blocks of macromolecules including amino acids, nucleotides, fatty acids (FAs) and electron carriers that are necessary for maintaining the leukaemic state (33, 39). In contrast, LSCs depend more on mitochondrial metabolism to maintain their quiescence and self-renewal ability (18, 40). Notable reprogrammed metabolic pathways in AML include glycolysis, oxidative phosphorylation (OXPHOS), amino acid synthesis, and lipid synthesis (**Figure 2**).

GLUCOSE METABOLISM

Nearly a century ago, Dr Otto Warburg discovered that even in the presence of oxygen, tumour cells prefer to ferment glucose to convert pyruvate into lactate rather than allowing it to enter the tri-carboxylic acid (TCA) cycle. This provides cancer cells with a high rate of ATP production to fuel rapid cell division (41). Besides its role in bioenergetics, glucose metabolism involves other pathways including the pentose-phosphate pathway which generates pentose phosphate for ribonucleotide synthesis, serine biosynthesis which generates amino acids and one-carbon metabolism which generates NADPH as the universal electron carrier (42). Therefore, glycolysis not only generates energy but also serves as a platform to produce molecular building blocks for cancer (42).

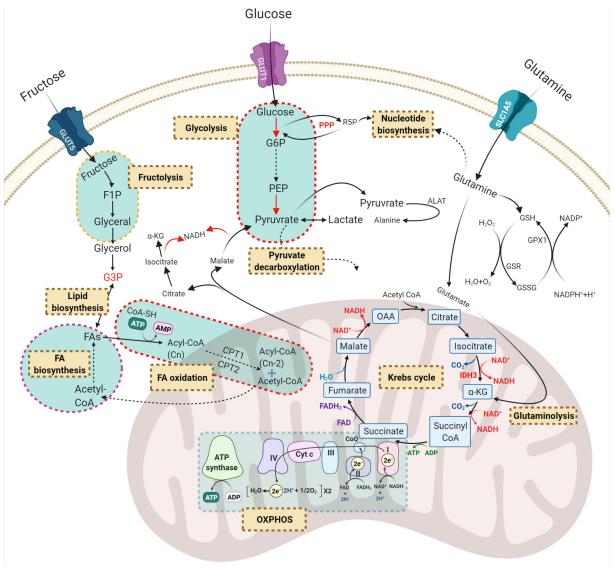

FIGURE 2 | Principal dysregulated metabolic pathways in AML. Carbohydrates and amino acids are two main sources of energy for AML cells which can be used in other metabolic pathways. *Red*, *green*, and *purple* texts are critical compounds in the relevant pathways. *Brown-cream rectangles*, indicating the crucial metabolic processes required for cell survival and proliferation. GLUT, glucose transporter; G6P, glucose-6-phosphate; R5P, ribose-5-phosphate; F1P, fructose-1-phosphate; PEP, phosphoenolpyruvate; G3P, glycerol-3-phosphate; OAA, oxaloacetate; α-KG, α-ketoglutarate; PPP, pentose phosphate pathway; ALAT, alanine transferase; GSH, glutathione; GSR, glutathione-disulfide reductase; GPX1, glutathione peroxidase 1; FA, fatty acid; GLS, glutaminolysis; OXPHOS, oxidative phosphorylation.

To initiate glycolysis, AML cells take up glucose by special membrane transporters called GLUTs encoded by the solute carrier family 2A gene. Higher glucose content in both AML cell lines and blasts derived from patient samples correlated with the overexpression of GLUT1 and lactate dehydrogenase leading to drug resistance and tumour cell survival (43). Similarly, higher amounts of pyruvate and lactate were observed in the serum of AML patients at diagnosis compared to healthy controls and were associated with poor survival (37). Pyruvate and lactate are two crucial compounds of glycolysis that are produced in the final glycolytic reactions catalysed by PKM2 and LDHA respectively. Interestingly, deleterious mutations of *PKM2* impaired progenitor cell function without perturbing HSCs, while *LDHA* deletion significantly blocked the function of both HSCs and progenitors during haematopoiesis, demonstrating a key metabolic difference among distinct haematopoietic cells (44).

Glycolysis is controlled through a network of signalling molecules including AMPK and PI3K/Akt/mTOR (45, 46). This network interrelates with all other metabolic pathways such as OXPHOS, the pentose phosphate pathway, and nucleotide biosynthesis which are necessary for normal haematopoiesis. In the case of AML, many pathways are dysregulated, thereby allowing blast cells to proliferate faster and drive leukaemia. For example, it has been shown that loss-of-function mutations of AMPK suppressed leukemogenesis by perturbing the glucose flux *via* downregulation of the GLUT1 transporter (47). Similarly, mTORC1 is highly expressed in LSCs compared to HSCs and inhibition of mTOR complex 1 (mTORC1) was shown to suppress leukemogenesis (38). mTORC1 plays a crucial role in several cellular processes including glycolysis and the pentose phosphate pathway. Moreover, mTORC1 induces glucose addiction and its inhibition enforces AML cells to generate their ATP from OXPHOS instead of glycolysis, which eventually leads to oxidative stress and DNA damage (38). Therefore, although leukaemic blasts prefer glycolytic metabolism to survive and proliferate, they can rewire their metabolic profile and rely on OXPHOS to resist chemotherapy.

mTORC1 is induced by the PI3K/Akt pathway which is constitutively active in 50-80% of AML cases and is associated with decreased overall survival (48). A comprehensive protein array profiling showed that >60% of primary AML cells are characterised by high PI3K/Akt phosphorylation and activity (48). Moreover, the PI3K/Akt axis plays an essential role in normal haematopoiesis and leukemogenesis by regulating glucose uptake and glycolytic flux (49, 50). The PI3K/Akt pathway is essential for the functionality of normal HSCs while its dysregulation depleted the normal HSC cell population and induced myeloproliferative disease and AML in mouse models with constitutive activation of PI3K/Akt (49). Another study by Xu et al. demonstrated that the PI3K/Akt/mTOR pathway is constitutively active in primary AML blasts and is required for their survival while normal HSCs don't rely on mTOR for long- or short-term survival (51). In the same study, inhibition of the PI3K/Akt/mTOR pathway with rapamycin re-sensitised LSCs to the topoisomerase II inhibitor etoposide without toxicity against normal HSCs, which highlights the role of this pathway in LSC population maintenance (51).

Furthermore, in AML cells harbouring an Fms-like tyrosine kinase-3 internal tandem duplication (*FLT3-ITD*), a common leukaemic mutation that confers a poor prognosis in AML patients, glycolysis is associated with the pentose phosphate pathway to sustain a high flux of glucose for cell survival (52). In a separate study, glucose-6-phosphate dehydrogenase was identified as a crucial regulator of the pentose phosphate pathway and its overexpression correlated with an adverse prognosis (38). Suppression of glucose-6-phosphate dehydrogenase and pharmacological inhibition of FLT3 with lestaurtinib induced a significant anti-leukaemic effect in AML cells with *FLT3-ITD* and was identified as a potential therapeutic strategy (53). In contrast to AML blasts, the role of the pentose-phosphate pathway has not been thoroughly investigated in normal HSCs and malignant LSCs and further *in vivo* and *in vitro* studies are needed in these cells.

An important regulator of carbohydrate consumption and glycolysis is the BMME. HSCs and ROS-low LSCs are both dependent on the BMME to survive. HSCs supply their energy mainly through glycolysis, whereas ROS-low LSCs achieve energy metabolism through mitochondrial respiration (19, 54). In contrast, rapidly dividing leukaemic blasts can take up much higher amounts of glucose and fructose in the peripheral blood. In line with this, suppressed fructose uptake has been found to

reduce leukemogenesis and intensify the cytotoxicity of Ara-C in fast-proliferative cells in the BMME. This suggests that rapidly proliferating AML cells in the BMME rely on carbohydrate metabolism to confer resistance to Ara-C (55).

Collectively, compared to LSCs, normal HSCs and rapidly proliferating AML blasts have higher glucose content and glycolytic activity (**Figure 3**) (37, 56) which highlights the role of glucose metabolism in leukemogenesis.

MITOCHONDRIAL METABOLISM

Mitochondria are classically considered as the powerhouse of cancer cells, where multiple metabolic pathways that feed on carbohydrates, amino acids and fatty acids converge into the TCA cycle (57). In addition to bioenergetics functions, the mitochondria environment supports and coordinates main metabolic processes including the TCA cycle, glutaminolysis, OXPHOS and fatty acid oxidation (FAO) (58). Some of these mitochondrial pathways are significantly altered in AML cells and are vital for AML cell survival and function.

The TCA or Krebs Cycle

The TCA cycle serves as a central metabolic hub that collects high-energy electron carriers, such as NADH and $FADH_2$, from glycolysis and delivers them to the electron transport chain (ETC) in the mitochondria (59). Normal HSCs have a well-organised metabolic profile in which the TCA cycle is triggered by the glycolysis end-stage product, pyruvate (**Figure 2**). However, AML blasts with a dysregulated metabolic signature disconnect the association of glycolysis and the TCA cycle by enforcing cells to convert pyruvate to lactate. This uncoupling assists AML cells to utilise other carbon sources such as glutamate to fulfil their energy demands. Therefore, targeting glutamine metabolism could potentially serve as an effective therapy for AML (60).

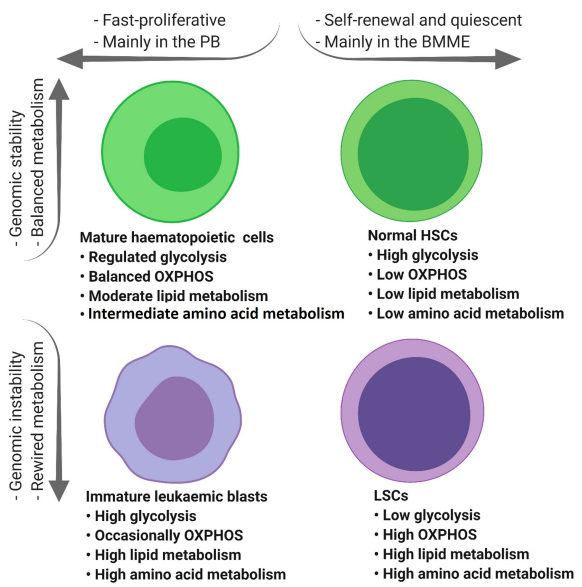

FIGURE 3 | The tumour microenvironment alters the metabolic profile of different types of haematopoietic cells. Mature haematopoietic cells and normal HSCs maintain their genome integrity and therefore regulate their metabolic profile in a balanced manner (green cells). In contrast, immature leukaemic blasts and LSCs with an unstable genome display dysregulated metabolic profiles (purple cells). PB, peripheral blood; BMME, bone marrow microenvironment; OXPHOS, oxidative phosphorylation; TCA, tricarboxylic acid cycle; ETC, electron transfer chain; HSCs, haematopoietic stem cells; FAO, fatty acid oxidation; AAs, amino acids; LSCs, leukaemic stem cells.

In contrast, cancer cells convert glutamate to α-ketoglutarate (α-KG) by glutamate dehydrogenase as an auxiliary reaction to replenish TCA intermediates (61). In line with this notion, CRISPR/Cas9 knockout screens indicate that AML cell lines enrich for glutamine transporters (SLC1A5, SLC38A1, and SLC38A2) and glutaminase (GLS) to supply α-KG for the TCA cycle, which has been shown to protect them against the anti-proliferative effects of the BCL-2 inhibitor ABT-199 (venetoclax) (62). These results frame a classic concept that cancer cells shunt carbon from glutamine into citrate which then can be fed into the TCA cycle (63). TCA cycle activity is also upregulated in ROS-low LSCs but not in ROS-high AML blasts. ROS-low LSCs showed significant $^{13}C_{16}$ palmitate uptake which was incorporated into the TCA cycle intermediates citrate and malate (18). In contrast to LSCs and rapidly dividing AML cells, metabolomic profiling of quiescent long-term HSCs showed low levels of TCA metabolites (2-oxoglutarate, acetyl-CoA and succinyl-CoA) which are regulated by HIF-1α; a transcription factor responsive to cellular hypoxia. HSCs harbouring HIF-1α loss-of-function mutations exhibited decreased dependence on glycolysis and impaired quiescence (64).

In the TCA cycle, α-KG is produced from isocitrate which is catalysed by isocitrate dehydrogenase (IDH). However, it has been shown that somatic mutations in the active site of IDH1/2 in AML cells lead to the overproduction of the oncometabolite 2-D-hydroxyglutarate, which blocks differentiation and contributes to AML progression (65). Moreover, $IDH2^{R140Q}$ mutations *in vivo* drive aberrant self-renewal activity and block differentiation in normal HSCs. Furthermore, co-mutant *in vivo* models of $IDH2^{R140Q}$ and FLT3-ITD induced acute leukaemia and were essential for leukaemia maintenance (66). Mutations of IDH1/2 have been shown to promote self-renewal and suppress differentiation of normal HSCs, leading to the clonal expansion of stem/progenitor cells, known as pre-LSCs (67). These mutations persisted in the pre-LSC population in AML patients with long-term complete remission following induction therapy (68). In addition, IDH1 mutations have been shown to be conserved during disease evolution. Matched paired analysis of AML patients revealed identical IDH1 mutations in diagnosis versus relapse samples demonstrating the conservation of IDH1 mutations in LSCs which drive disease relapse (69). In a similar study, Shlush et al. examined the existence of a pre-leukaemic cell population in AML patients with IDH1/2 mutations and indicated that 2 out of 6 samples acquired IDH2 mutations in some progenitor and mature populations (70).

Oxidative Phosphorylation

It was originally assumed that mitochondrial respiration was impaired in cancer cells as they mainly rely on glycolysis for survival (41). However, it is now understood that tumour cells utilise oxygen in OXPHOS to generate high levels of ATP by transferring electrons to the TCA cycle for cell survival (71). In addition to providing energy, OXPHOS also regulates mitochondrial membrane permeabilisation, controlling the balance between apoptosis and proliferation and playing an important role in redox biology (71).

Normal HSCs maintain their quiescent state by reducing their mitochondrial respiration rate and relying on glycolysis (72). In line with this, Škrtić et al. have shown that AML blasts have higher mitochondrial biogenesis and basal oxygen consumption compared to normal HSCs (73). However, it has also been shown that quiescent HSCs and not AML blasts can maximise their energy production with higher glycolytic activity and electron flux, known as the spare reserve capacity while coping with oxidative stress (46, 72). This implies that normal HSCs can compensate for energy loss by upregulating glycolysis while AML blasts are vulnerable to mitochondrial oxidative stress.

Similar to quiescent HSCs, LSCs also have characteristically low levels of oxygen consumption and OXPHOS, but they still rely on this metabolic pathway for their survival (19). A recent study by Cole et al. found that mitochondrial ATP-dependent Clp protease (ClpP) is overexpressed in the $CD34^+$ $CD38^-$ LSC population of primary AML samples (74). Therefore, increased ClpP expression might serve as a biomarker of elevated OXPHOS in AML patients. In line with this, metabolomics and gene expression analyses by Jones et al. indicated that LSC-enriched subsets are metabolically dormant populations and, unlike HSCs, preferably depend on amino acid metabolism for OXPHOS-related energy production (18).

Mitochondrial metabolism, the TCA cycle and OXPHOS are critical pathways to produce ATP molecules in LSCs and, under certain conditions, AML blasts. Thus, targeting OXPHOS alone or in combination with other metabolic pathways could be an attractive therapeutic strategy to re-sensitise LSCs and AML blasts to conventional chemotherapeutic agents and improve AML patient outcomes.

AMINO ACID METABOLISM

The 20 standard amino acids are required for a diverse set of cellular processes crucial for tumour cell proliferation, including the biosynthesis of proteins, nucleotides, lipids, and glutathione (GSH) (75). In addition to their role in metabolism, amino acids are fundamental in mediating epigenetic regulation and post-transcriptional modification (75).

Among all amino acids, glutamine is the most important for AML survival and proliferation. Along with glucose, glutamine plays a critical role in tumour progression not only to provide α-KG for the TCA cycle but also for the importation of leucine into AML cells, leading to the activation of mTORC1-mediated protein synthesis (60). Glutamine is imported into the AML cells by the SLC1A5 transporter where it is converted into glutamate and α-KG in a process known as glutaminolysis (76). Compared to normal HSCs, leukaemic blasts import relatively more glutamine for their survival and growth (**Figure 3**). In an *in vivo* study, normal HSCs from healthy donors were resistant to apoptosis induction following glutamine removal. In contrast, depletion of glutamine by shRNA knockdown of SLC1A5, induced apoptosis in eight primary AML samples (77), suggesting a reliance on glutamine metabolism in leukaemic blasts compared to normal HSCs. Furthermore, low-glutamine containing cells showed a significant reduction in their oxygen consumption rate compared to high-glutamine cells, suggesting that OXPHOS inhibition is caused by glutamine deprivation (60, 78).

ROS-low LSCs derived from AML patients at diagnosis mainly rely on amino acid metabolism to fuel OXPHOS for survival (18). In contrast, LSCs from relapsed AML escaped amino acid loss by enhancing FA metabolism; mainly by inducing palmitate uptake. Palmitate can be metabolised to TCA cycle intermediates to provide NADH and $FADH_2$ for OXPHOS (18). Therefore, to target and eliminate ROS-low LSCs derived from patients with relapsed AML, it is necessary to inhibit subsidiary pathways that provide oxidative-related energy such as the inhibition of fatty acid metabolism in the mitochondria (79). Likewise, a comprehensive proteomic analysis of leukaemic cells revealed a high level of branched-chain amino acid transaminase 1 (BCAT1) in $CD34^+CD38^-$ LSCs compared to the non-LSC AML population. BCAT1 is a negative regulator of α-KG which is a crucial intermediate of the TCA cycle. Besides its role in the TCA cycle, α-KG acts as a co-factor for DNA demethylases such as the Egl-9 family hypoxia-inducible factor 1 and the ten-eleven translocation family. Therefore, the $CD34^+CD38^-$ LSC population with increased levels of BCAT1 shows a hyper-methylated phenotype similar to cases with mutant IDH1/2, in which DNA demethylases are blocked by the oncometabolite D-2-hydroxyglutarate (80). This hypermethylation causes the inhibition of key tumour suppressor genes which lead to LSC development. Accordingly, knockdown of BCAT1 in leukaemia cells caused αKG accumulation leading to demethylases protein degradation and abrogated leukaemia-initiating potential (80).

Aside from glutamine metabolism, AML cells rely on other amino acids for survival such as arginine. Arginine is crucial to provide amine groups and aspartate for the production of nucleotides. Unlike normal HSCs, AML cells with arginosuccinate synthetase-1 mutations are unable to generate arginine from citrulline and aspartate and are dependent on importing extracellular arginine (81). Arginine catabolism is a key player in blocking the immune response to antigens on AML blasts and therefore measurement of plasma arginine could be an important addition to immunotherapy of AML patients (82). Overall, amino acid content and metabolism are more prominent in LSCs compared to AML blasts and present an opportunity to selectively target the LSC population (18, 19, 83).

LIPID METABOLISM

After glucose and glutamine, lipids are the third source of fuel for cancer cells proliferation and survival (84). Lipids are highly

complex biomolecules that not only function as an energy source but also provide building blocks for functional fatty acids that are required for cell membrane biogenesis and signalling pathways regulation (85).

Lipid metabolism is often deregulated in AML blasts compared to normal haematopoietic cells (**Figure 3**) implying the potential of targeting lipid synthesis for therapeutic benefit in patients with AML (86, 87). Comprehensive lipidomic profiling of plasma from AML patients at diagnosis and healthy blood donors showed an increase in certain free fatty acids such as arachidonic acid and depletion of total fatty acids and cholesterol which was probably driven by enhanced FAO (86). FAO itself feeds the TCA cycle with acetyl-CoA intermediate, leading to citrate increment which is the starting point of *de novo* fatty acid synthesis (88).

FA synthase (FASN) is a multi-enzyme protein that catalyses FA synthesis. It is required for AML cell proliferation and was shown to be low in normal HSCs derived from healthy donors and highly overexpressed in AML patients. Inhibition of FASN with RNAi or epigallocatechin-3-gallate accelerated granulocytic differentiation in acute promyelocytic leukaemia cells and re-sensitised them to ATRA treatment (89). This process was suggested to be mediated through lysosomal biogenesis and autophagy (89).

Fatty acid oxidation (FAO) is another deregulated pathway in AML, playing an important role in promoting leukaemic cell survival and quiescence (90). FAO generates acetyl-CoA from the oxidation of FAs which is the reverse pathway of FA synthesis (**Figure 2**). In addition to FAO, glycolysis and amino acid catabolism also provide more acetyl-CoA molecules which then will be fed into the TCA cycle to produce ATP (91). Therefore, understanding the molecular mechanisms of one pathway would shed light on others that can be exploited therapeutically. Several enzymes and transporters involved in the process of FAO, including carnitine palmitoyltransferase 1A and carnitine transporter CT2, are overexpressed in AML cells compared to normal HSCs (32, 92, 93). Quiescent HSCs maintain FAO rates at a basal level to preserve their dormancy (94). HSC fate depends on whether they undergo symmetric or asymmetric cell division when they leave quiescence (95). The asymmetric division generates two daughter cells; one will acquire self-renewal ability and remain quiescent and the other will differentiate and enter the circulatory system. However, the symmetric division will generate two daughter cells only capable of undergoing cell proliferation and differentiation (95). FAO metabolism supports asymmetric division and thus preserves the self-renewal ability of HSCs (94).

Similar to HSCs, FAO is important for LSC maintenance and plays a key role in venetoclax resistance (79). Transcriptional profiling of resistant ROS-low LSCs with RAS pathways mutations showed enrichment in FAO and increased CD36 expression (79). CD36 is an important fatty acid transporter that facilitates lipid uptake in the $CD36^+$ LSC population. These $CD36^+CD34^+$ cells are significantly enriched in gonadal adipose tissues of the BM which protects them from destructive effects of venetoclax and allows them to utilise FAO required for their maintenance (87). In line with this, it has been shown that the interaction of AML blasts and BM adipocyte cells induces lipolysis, releases FAs from adipocytes to AML and supports AML cell survival, and proliferation *in vivo* (96).

In addition to FAs and related metabolic pathways, sphingolipids also play a critical role in leukemogenesis by regulating the balance between cell proliferation and cell death (97, 98). The formation and functionality of sphingolipids rely on oncogenic proteins including sphingosine kinases and acid ceramidases in AML cells. Sphingosine-1-phosphate is a bioactive lipid that is generated by sphingosine kinase 1 and regulates AML cell survival and death in a constitutively active manner (99). A recent study has demonstrated that S1PR3, a receptor for sphingosine-1-phosphate, is upregulated in AML blasts and $CD34^+CD38^-$ LSCs compared to normal HSCs. S1PR3 regulates myeloid differentiation and activates inflammatory pathways in AML blasts and $CD34^+CD38^-$ LSCs. S1PR3 activation in primitive AML samples promoted LSC differentiation leading to the elimination of these cells (100).

Based on these observations, the metabolism of HSCs, LSCs and AML blasts each rely on distinct pathways for energy production. Therefore, targeting metabolic pathways with selective inhibitors could be a promising strategy to target specific cellular populations in AML.

THE METABOLIC PROFILE OF LSCs DRIVES DRUG RESISTANCE

AML is a clonal disorder of haematopoiesis in which normal HSCs or multipotent progenitors acquire genetic mutations that result in dysregulated self-renewal ability (13, 101). These cells are known as "pre-leukaemic HSCs", representing the evolutionary ancestors of leukaemia (101). In normal haematopoiesis, HSCs eventually differentiate into mature blood cells, but specific genetic mutations interrupt differentiation resulting in LSCs with acquired clonogenic and leukaemia initiating potential (3, 13, 101, 102). These LSCs produce AML blasts and the accumulation of blast cells in the BM defines the disease (**Figure 1**).

The LSC population represent a minor fraction of the disease which is resistant to chemotherapy (103, 104) and are generated by evolutionary processes before the initiation of treatment (104). Following treatment and subsequent remission in patients, relapse of the disease is driven by this drug-resistant $CD34^+CD38^-$ LSC fraction which has unlimited self-renewal capabilities (102). Current treatment regimens are effective against the majority of rapidly dividing bulk AML cells but less successful at eliminating the LSC population due to homing in the BMME which supports their quiescence and self-renewal capacity (**Figure 1**) (105, 106). The BMME is critical for the maintenance and retention of quiescent LSCs and provides crosstalk between LSCs and stromal cells, which significantly influences leukaemia initiation, progression, and response to therapy (106). Furthermore, the gene expression profiles of HSCs and LSCs are profoundly influenced by the BMME cellular architecture and these cells express a dynamic and

heterogenous molecular landscape compared to leukaemic blasts (23).

A recent study by van Gils et al. comprehensively categorised six major processes involved in therapy resistance of LSCs; altered epigenetic pathways, cellular plasticity, the tumour microenvironment, integrated stress responses, cellular signalling and metabolic dysregulation (107). Among these processes, the role of metabolic dysregulation in chemotherapy resistance of LSCs has gained favourable attention (24, 108). As a well-known example, the upregulation of ABC transporters in LSCs allows these cells to pump small molecule inhibitors and cytotoxic drugs out of the cell (109). Moreover, much like HSCs, LSCs rarely divide and are maintained in a state of long-term dormancy called quiescence with a low level of oxidative stress and ROS contents (15, 19). AML cells with low ROS levels, defined as ROS-low LSCs, decrease their ATP or oxygen requirements and mainly rely on low energy metabolic pathways to survive and promote leukemogenesis (19). This is a major reason that conventional chemotherapeutics such as Ara-C are unable to eliminate LSCs, as these drugs are more effective against rapidly dividing AML blasts (**Figure 1**) (110). It should be noted that studies have identified a fraction of blast cells with retained mitochondrial activity and a high proliferation rate are less sensitive against Ara-C, implying that different types of haematopoietic cells exhibit varied metabolic profiles which can be exploited for targeting (111).

METABOLIC TARGETING IN AML

Metabolic targeting is considered a promising therapeutic strategy that is gaining ground in various human cancers including AML. Previous studies have emphasised that metabolic pathways are complex in AML cells and therefore in-depth investigations are required to further shed light on the molecular mechanism of these pathways. Extensive research has been conducted to identify and develop new drugs targeting metabolism in AML. These drugs mainly target glucose metabolism, mitochondrial metabolism, amino acid, and lipid metabolism. Although metabolic interventions have been effective at eliminating leukaemic cells, more comprehensive preclinical studies are needed to increase treatment outcomes and confirm that these drug modulations do not target normal haematopoietic cells. **Table 1** lists information on common metabolic inhibitors that have been tested against AML either in preclinical *in vitro* and *in vivo* studies or clinical trials.

TABLE 1 | Modulators of metabolic pathways, preclinical studies, and clinical trials in AML.

Compound	Metabolic target or process	Metabolic pathway	Reference	Study type	Findings
2-DG	Glucose	Glycolysis	(37, 112, 113)	*In vitro* & *in vivo*	Decreased AML cell proliferation, sensitivity to Ara-C
A2-32-01	ATP-dependent Clp protease	OXPHOS	(74)	*In vitro* & *in vivo*	Antileukaemic effects in PDXs & cell lines
Brequinar sodium	DHODH	Nucleotides & OXPHOS	(114, 115)	*In vitro, in vivo* & phase I/II	Reduced leukaemic burden, improved survival & induced differentiation
Rapamycin, 2-DG & 6-AN	mTORC1, glucose & G6PD	Glycolysis & PPP	(38)	Phase I/II	Reduced AML cell viability
Venetoclax	Mitochondrial antiapoptotic BCL-2	OXPHOS & pyrimidine biosynthesis	(18, 19, 116–119)	Phase I/II/III	Selective elimination of LSCs & reduced relapse
Tigecycline	Cox-1 & Cox-2	Mitochondrial protein translation	(73, 120)	*In vitro, in vivo* & Phase I	Antileukaemic activity in PDXs
ddC	mtDNA polymerase	mtDNA replication	(121)	*In vitro* & *in vivo*	Selective elimination of LSCs & induced tumour regression
Enasidenib AG-221	IDH2 mutant enzyme	2-HG production	(122–124)	Phase I/III	Reduced relapse & increased overall survival
ADI-PEG 20	Arginine	Amino acid metabolism	(81)	*In vitro* & *in vivo*	Induced sensitivity to Ara-C & apoptosis
BCT-100	Arginine	Amino acid metabolism	NCT03455140	Phase I/II	Well tolerated without toxicity
L-asparaginase & high-dose Ara-C	Asparagine glutamine availability	Amino acid metabolism	(125–127)	Phase I/II	Increased median survival in relapsed patients
CB-839	Glutaminase	Glutaminolysis	(78, 128)	Phase I	Inhibited AML growth in PDXs & prolonged survival in patients
Avocatin B	CPT1a	Fatty acid oxidation	(129)	*In vitro*	Induced apoptosis
CPI613	PDH	Fatty acid synthesis	(130)	*In vitro* & *in vivo*	Increased sensitivity to doxorubicin
Etomoxir	CPT1a	Fatty acid oxidation	(131)	*In vitro*	Increased sensitivity to ATO & apoptosis
LCL204	Acid ceramidase	Sphingolipids	(132)	*In vivo*	Increased overall survival of PDXs & decreased leukaemic burden
Statins: lovastatin, pravastatin	HMG-CoA reductase	Mevalonate biosynthesis	(133)	Phase I/II	Increased sensitivity to Venetoclax
ST1326	CPT1a	Fatty acid oxidation	(134)	*In vitro* & *in vivo*	Growth arrest & induced apoptosis

6-AN, 6-aminonicotinamide; 2-DG, 2-deoxy-D-glucose; 2-D-HG, 2-D-hydroxyglutarate; Bap, a combination of lipid-regulating bezafibrate (BEZ) and the sex hormone medroxyprogesterone acetate; CKMT1, creatine kinase mitochondrial 1; CPT1A, carnitine palmitoyltransferase 1A; DHODH, dihydroorotate dehydrogenase; ETC, electron transport chain; IDH1, isocitrate dehydrogenase 1; mTOR, mechanistic target of rapamycin kinase; HMG, hydroxy methylglutaryl; OXPHOS, oxidative phosphorylation; PPP, pentose phosphate pathway.

Targeting Glucose Metabolism

As outlined above, the reliance of AML blasts on glucose metabolism makes it an attractive target for AML therapy. Unsurprisingly, inhibition of glycolytic enzymes has been shown to suppress glycolysis, leading to significant energy loss and leukaemia cell death (38). Overexpression of GLUT1 is associated with poor chemotherapy response in patients with AML and inhibition of GLUT1 is considered to be a promising treatment strategy (43). Inhibition of the glycolysis rate-limiting enzyme hexokinase-2 with 2-Deoxy-D-glucose (2-DG) significantly improved the cytotoxicity of Ara-C in primary AML blasts and cell lines (37). 2-DG is a synthetic glucose analogue that not only perturbs glucose metabolism, but also interferes with OXPHOS, depleting cellular energy, N-linked glycosylation, and autophagy induction (135). AML primary blasts and cell lines harbouring c-KIT and FLT3-ITD mutations showed sensitivity to 2-DG treatment, compared with normal haematopoietic cells (112).

Direct inhibition of hexokinase-2 with 3-bromopyruvate is also considered as another treatment strategy in AML cells with high glycolytic activity, such as HL-60 cells (43). Also, AML cells with FLT3-ITD showed resistance to sorafenib treatment, a kinase inhibitor for the treatment of FLT-ITD+ cells, but were sensitive to hexokinase-2 inhibitors including 2-DG and 3-bromopyruvic acid (113). Inhibiting glycolysis is mainly investigated in AML patients at diagnosis or in the bulk of the AML population and further investigations in relapsed AML and LSCs are needed.

Targeting Mitochondria-Related Pathways

Inhibition of different mitochondrial metabolic processes such as OXPHOS and aerobic respiration are emerging treatment strategies in patients with AML. An ongoing phase I clinical trial is using a selective and potent OXPHOS inhibitor, IACS-010759, in treating patients with relapsed/refractory AML (ClinicalTrials.gov Identifier NCT02882321). The anti-leukaemic activity of IACS-010759 is mediated by the AMPK pathway in OXPHOS-dependent primary AML blasts and cell lines (136). In sensitive primary AML blasts with high levels of AMPK, IACS-010759 induced AMPK activation leading to mTOR suppression and reduced cell growth. In contrast, resistant primary AML blasts with low AMPK expression were less responsive to the treatment (136). mTORC1 suppression enforces primary AML blasts to reprogram from glycolysis to OXPHOS by promoting the TCA cycle and this has led to the use of mTORC1 inhibitor (rapamycin) and OXPHOS inhibitor (metformin) in targeting resistant blast cells (38). Another drug that targets the ETC is Brequinar sodium which suppresses the inner mitochondrial membrane protein dihydroorotate dehydrogenase, playing an important role in pyrimidine biosynthesis (137). Inhibition of dihydroorotate dehydrogenase with Brequinar induced myeloid differentiation and apoptosis of primary AML blasts (114, 115).

The pyruvate dehydrogenase complex is responsible for catalysing the carboxylation of pyruvate to acetyl-CoA. The pyruvate dehydrogenase complex acts as a central hub between three different metabolic pathways including glycolysis, the TCA cycle, and OXPHOS (138). Hampering the pyruvate dehydrogenase complex with a selective inhibitor dichloroacetate has led to increased OXPHOS, ROS content, and activated antioxidant response which activates DNA repair genes (138). Therefore, applying dichloroacetate in combination with genotoxic drugs including doxorubicin and Ara-C induced ROS generation, DNA damage and apoptosis in AML cells (139, 140). A study by Emadi et al. found that sequential administration of dichloroacetate in combination with arsenic trioxide exerted synergistic anti-leukaemic effects in primary blasts from AML patients and AML cell lines with FLT3-ITD (139).

Another mitochondrial-related treatment approach is the exposure of AML cells to BCL-2 inhibitors. Venetoclax is a potent BCL-2 inhibitor that has shown activity in haematologic malignancies including both as a single agent or in combination with chemotherapeutics agents (116, 141). Treatment of 32 relapsed/refractory AML patients with venetoclax led to a favourable response in 19% of patients while another 19% of patients showed a modest anti-leukaemic response (116). Likewise, in a small-scale study of seven patients with secondary AML, two patients achieved complete remission with venetoclax monotherapy (142). However, combination therapy of venetoclax has been demonstrated to be much more efficient than single-agent treatment (117, 118). The combination treatment of elderly patients with venetoclax and azacitidine led to 36.7% of patients achieving complete remission compared to 17.9% of patients in the control group (118). In a similar study, venetoclax combined with the FLT3 inhibitor quizartinib showed synergistic anti-leukaemic activity in cell lines and primary patient samples, and prolonged the survival of FLT-ITD+ AML mice, compared to the modest effects of single-agent treatments (119).

Venetoclax in combination with statins has also been proven to induce synergistic anti-leukaemic effects. It was reported that statins increased venetoclax efficacy in AML which is mediated by protein geranyl-geranylation, BCL-2 modulation, and upregulation of pro-apoptotic genes such as PUMA (133). Moreover, the FAO inhibitor etomoxir was shown to increase the therapeutic efficacy of another BCL-2 inhibitor ABT-737 *in vivo* (143). On the other hand, a recent genome-wide CRISPR/Cas9 screen and metabolomics study revealed heme biosynthesis as a key regulator of drug sensitivity. AML cells treated with venetoclax have upregulated heme biosynthesis which is an important regulator of mitochondrial-related apoptosis through ETC and OXPHOS (62). In line with these studies, Jones et al. indicated that both depleting amino acid in the culture media and inhibition of BCL-2 with venetoclax significantly reduced OXPHOS and selectively reduced the viability of ROS-low LSCs *ex vivo* and sensitised them to azacitidine treatment (18).

As discussed above, AML cells with IDH1/2 mutations have a higher amount of 2-D-hydroxyglutarate, which blocks differentiation. Targeting AML cells with mutant IDH1/2 profiles has resulted in promising anti-leukaemic effects in patients and cell

lines. Single-agent treatment of relapsed/refractory AML patients with enasidenib, a selective IDH2 inhibitor, had an overall response rate of 40.3% (122). Co-occurring mutations in NRAS and MAPK pathways were observed in nonresponding patients which were consistent with the role of RAS signalling in primary therapeutic resistance (123). Moreover, treatment of mutant IDH2 cells with enasidenib suppressed 2-D-hydroxyglutarate production and induced cellular differentiation in primary AML cells and xenograft models (124). Enasidenib also increased survival rates in IDH2-mutant AML xenografts which supported the initiation of clinical trials of enasidenib in patients with haematologic malignancies with IDH2 mutations (ClinicalTrials.gov Identifier: NCT01915498).

Aside from suppression of mitochondria-related pathways, direct perturbation of mitochondrial components has also been shown to be another attractive therapeutic strategy and its significance is increasingly being recognised in hematologic malignancies including AML. For example, blockade of translation with tigecycline has led to a significant antileukaemic effect against primary AML cells. Tigecycline is a glycylcycline class antibiotic that binds to the 30S ribosomal subunit and perturbs mitochondrial translation. It selectively destroyed primary bulk AML cells and $CD34^{+}CD38^{-}$ LSCs without affecting normal haematopoietic cells (73). Inhibition of a mitochondrial caseinolytic protein protease with A2-32-01 has led to promising results in AML (74). A2-32-01 is an anti-virulence drug that specifically inhibited ClpP and eliminated both AML cell lines and primary samples with elevated ClpP expression without killing normal haematopoietic cells (74). Suppression of mtDNA replication with 2',3'-dideoxy-cytidine is also effective in the treatment of AML patients with high mtDNA polymerase activity. 2',3'-dideoxy-cytidine is a nucleoside analogue that selectively inhibits mtDNA polymerase, perturbs OXPHOS and induces cytotoxicity in AML cell lines and primary samples while sparing normal haematopoietic cells (121). 2',3'-dideoxy-cytidine also decreases mtDNA, ETC proteins and induces tumour regression without toxicity *in vivo* and selectively targeted LSCs with leukaemia initiating potential in secondary xenografts (121). Overall, these observations emphasise the potential of targeting mitochondrial related pathways to improve AML treatment outcomes.

Targeting Amino Acid Metabolism

Significant glutamine uptake is a common metabolic feature of AML cells (60, 62) and unsurprisingly inhibition of glutamine uptake or function is a potent strategy to treat AML. GLS1 is an important enzyme to increase glutamine levels and its overexpression is reported to be involved in the drug resistance of AML cells. Depletion of glutamine in the culture media or inhibition of glutamine biosynthesis by GLS1 knockdown has been shown to suppress the growth of primary AML cells and cell lines (144). Moreover, inhibition of glutamine metabolism by a GLS1 inhibitor (CB-839) perturbs GSH production in AML cell lines, leading to the elevation of ROS and apoptotic cell death (145). Moreover, GLS1 inhibition made AML cells susceptible to chemotherapeutic drugs such as arsenic trioxide (ATO) that synergistically perturbed mitochondrial redox state and induced apoptosis in AML cell lines, primary samples and *in vivo* models (145). Suppression of GLS1 with CB-839 activated mitochondrial apoptosis and depleted glutamine in the culture of AML cell lines which synergises with the anti-leukaemic effects of venetoclax (78). A CRISPR/Cas9 screen of MOLM-13 AML cells treated with FLT3 inhibitors revealed that GLS1 mediates resistance to tyrosine kinase inhibitors (76). Concomitant exposure of FLT3-ITD AML cell lines to quizartinib (FLT3 inhibitor) and CB-839 potently decreased viability and enhanced the overall survival of immune-deficient mice engrafted with AML patient-derived xenografts implying the dependence of AML cells on glutamine metabolism for drug resistance (146).

Recent studies have highlighted the association of amino acid metabolism with OXPHOS in AML cells. Pharmacological inhibition of amino acid metabolism with venetoclax reduced OXPHOS and induced cell death in *de novo* ROS-low LSCs (18). In the same study, it was shown that ROS-low LSCs derived from patients with relapsed AML were able to resist venetoclax as they are not reliant on amino acid metabolism and supply their energy through fatty acid metabolism (18). Moreover, comprehensive metabolomics analysis of relapsed ROS-low LSCs indicated high levels of nicotinamide and NAD+, which play an important role in sustaining OXPHOS. Therefore, perturbation of nicotinamide metabolism selectively targeted and eliminated relapsed ROS-low LSCs, highlighting the value of targeting amino acid metabolism (147). Another study has indicated that ROS-low LSCs metabolise exogenous cysteine to GSH which, in turn, activates succinate dehydrogenase a key component of mitochondrial ETC complex II. The same study showed that cysteine depletion impaired GSH synthesis disrupted ETC, which eventually inhibited OXPHOS and ATP production leading to ROS-low LSC death (148).

Asparagine is another important amino acid in AML metabolism which is generated by glutamine and aspartate (149). L-asparaginase converts asparagine to aspartic acid and has shown potent anti-leukaemic activity and has been used for the treatment of patients with *de novo* and relapsed AML (125, 126). The combination of L-asparaginase with high-dose Ara-C and mitoxantrone has resulted in positive outcomes in AML patients with an aberrant asparagine metabolism (125, 150). These results have led to the initiation of a randomised phase 2b trial which evaluates the efficacy of ERY001, L-asparaginase encapsulated in red blood cells, in elderly AML patients who are unfit for intensive chemotherapy (127).

Lastly, inhibition of arginine has resulted in promising results in AML treatment. A study by Miraki-Moud et al. demonstrated that AML blasts obtained from patients at diagnosis relied on arginine to survive and proliferate (81). Decreased arginosuccinate synthetase-I activity with a pegylated arginine deiminase called ADI-PEG 20 showed anti-leukaemic activity *in vitro* and *in vivo* with minor toxicity on normal haematopoietic cells (81). Depletion of arginine with another pegylated recombinant arginase, BCT-100, suppressed AML blast cell proliferation and reduced leukaemia engraftment *in vivo* (151). In addition, single-agent BCT-100 caused significant cell death in adult AML blasts and synergised

with cytarabine activity (151). Likewise, an ongoing study is further testing the safety and efficacy of BCT-100 in younger patients with relapsed/refractory leukaemia (ClinicalTrials.gov Identifier NCT03455140). Together these studies demonstrate that the targeting of amino acid metabolism, much like glycolysis and mitochondrial metabolism, is a promising strategy for the treatment of AML.

Targeting Lipid Metabolism

Increased FA synthesis and FAO are two deregulated metabolic pathways that support leukemogenesis. Unsurprisingly FA synthesis and FAO are therefore attractive targets for inhibition (84, 152). Inhibition of FA synthesis with CPI-613 synergised with the anti-leukaemic effects of doxorubicin in cell line-derived AML xenografts and extended the median survival from 12 days with doxorubicin alone to 16 days with the combination of both (130).

Likewise, FAO suppression has been shown to inhibit AML. Suppressing FAO by a specific CPT1A inhibitor, ST1326, reduced cell growth, induced apoptosis, and had favourable interaction with the cytotoxic effects of Ara-C in AML cell lines (134). In a similar study, inhibition of CPT1A with etomoxir synergised with arsenic trioxide and caused anti-leukaemic activity in AML cell lines. Etomoxir inhibits carnitine palmitoyl transferase 1 activity thus, hindering fatty acid transport into mitochondria and β-oxidation (131). Moreover, blockade of CPT1A with avocatin B selectively targeted AML blasts while preserving normal HSCs through decreased NADPH levels and increased DNA damage-related cell death (129). More interestingly, concomitant treatment of LSCs from patients at relapse with azacitidine and venetoclax resulted in only a minor reduction of viability due to increased FAO as a resistance mechanism (18). Suppression of FA uptake by a CD36 inhibitor, sorbitan sesquioleate, re-sensitised ROS-low LSCs from patients at relapse to azacitidine (18). Another study has suggested that LSCs residing in the BMME are enriched in adipose tissue and are protected by lipolysis or FAO. $CD36^+CD34^+$ LSCs have a higher FAO rate compared to differentiated leukaemia cells or normal HSCs. Therefore, targeting FAO might selectively target and eliminate the $CD36^+CD34^+$ LSC population (87).

Targeting sphingolipids has recently been suggested as a novel avenue for AML therapy (99, 100). Acid ceramidase catalyses a reaction that generates sphingolipids, contributing to AML blast survival *via* upregulation of the anti-apoptotic protein MCL-1. The acid ceramidase inhibitor LCL204 reduced the leukaemic burden in NSG mice engrafted with primary AML cells (132). Consistent with this finding, inhibition of ceramide in AML cells harbouring FLT3-ITD sensitised them to FLT3 inhibitors, which provides an opportunity to target resistant primary AML cells with FLT3 mutations (153). Treatment of AML cell lines, primary blasts and $CD34^+CD38^-CD123^+$ LSCs with MP-A08, a selective sphingosine kinase inhibitor, significantly induced apoptosis, with negligible effects on normal HSCs from healthy samples (99). Furthermore, exposure of AML patient-derived xenografts to MP-A08 reduced tumour burden and prolonged mouse survival without affecting normal murine haematopoiesis (99).

Compared to glycolytic, mitochondrial, and amino acid metabolism, the role of FAO and FA biosynthesis is more important in normal HSCs and LSCs than in the bulk of leukaemic cells. These findings suggest that AML progenitor cells utilise lipid metabolism to survive and that targeting these pathways is a viable future therapeutic strategy for the elimination of these cells.

CONCLUSION

In the past decade, extensive efforts have been made to uncover the main metabolic features of tumour cells compared to their normal counterparts (6, 9). These investigations have suggested that some cancers, such as leukaemia, are driven by metabolic alterations and thus appropriate metabolic-based treatment strategies are needed (32, 33, 154). Moreover, the unique metabolic signature of leukaemic cells could be used for monitoring disease progression and prognosis.

The majority of previous research on AML metabolism has suggested that leukaemic blasts can compensate for energy shortage and adapt to new metabolic programs during disease progression and chemotherapy. However, perturbing metabolic pathways in leukaemic blasts alone is not efficient enough to improve clinical outcomes and reduce the relapse rate in patients. This stems from the fact that previous studies mainly focused on leukaemic blasts and not LSCs, and the latter are the main mediators of AML relapse (3).

A major limitation is the lack of clinically relevant *in vivo* models to study AML metabolism (155). Clinically relevant mouse models are required to improve the efficacy and correlation between *in vitro* and *in vivo* experiments (155). For example, discrepancy of *in vitro* and *in vivo* models is evident in the growth of AML cells in human plasma-like medium (HPLM). HPLM contains biologically relevant levels of uric acid which inhibits *de novo* pyrimidine synthesis. Uric acid levels are higher in human blood than in mice serum and therefore can inhibit uridine monophosphate synthase, a crucial enzyme for pyrimidine synthesis. This has been shown to reduce the sensitivity of AML cells to chemotherapeutic drugs such as 5-fluorouracil and highlights the importance of the tumour microenvironment on cell metabolism and the efficacy of drugs (156).

Another limiting issue is the lack of efficient culture media to accurately represent the tumour environment in patients (155). Extensive research has been done to supplement culture media with nutrients that are crucial in human serum and this has led to the use of enriched mediums such as HPLM and Plasmax to better represent the biological conditions of patients (156, 157). Furthermore, cell co-cultures and 3D cultures provide a tumour microenvironment which is an important regulator of drug response and metabolic reprogramming *in vitro* and therefore these cultures better represent the cellular environment of patients. As we mentioned in this review, adipose tissues and adipocytes can modulate drug response in AML and provide compensatory nutrients for leukaemic cells to resist chemotherapy. Therefore, it is unsurprising that co-culturing AML cells with bone marrow adipocytes noticeably induced resistance against CPT1a inhibitors and increased FAO (143, 158). Treatment of AML cells with CPT1a

inhibitor significantly increased free FAs and glucose uptake specifically in the co-cultures with bone marrow adipocytes; underlining the vital role of the microenvironment in regulating energy demands and chemotherapy response (158). Therefore, the lack of plasma and blood metabolites in cell culture could impair the efficacy of metabolic inhibitors and question the clinical translatability of many *in vitro* approaches.

Patient and cellular heterogeneity is another level of complexity in investigating AML metabolism and identifying effective treatment strategies. Previous research has shown that AML cells evade chemotherapy by altering their gene expression pattern which leads to rewired metabolism (22, 120). In fact, AML patients treated with Ara-C and metabolic inhibitors showed altered metabolic and transcriptional regulation. It has also been shown that the antiproliferative effect of metabolic inhibitors differs across patients and the AML cells derived from different patients are metabolically heterogenic, likely due to genomic heterogeneity (22). In another study, the comparison of the gene expression profile of chemotherapy responders and non-responders showed a significant level of genome heterogeneity which was linked to altered cellular pathways including metabolism (120). This level of genome and metabolome heterogeneity reinforces the notion that a "one-size-fits-all" strategy would not be effective for AML therapy and therefore, personalised medicine is required to tailor treatments to achieve the best outcome for individual patients (159). Nevertheless, targeting metabolic pathways in AML is a promising therapeutic approach and a rapidly emerging field that requires significant attention. Therefore, further *in vivo* studies distinguishing metabolic requirements of normal HSCs, AML blasts, and LSCs are necessary to design efficient treatment regimens for patients with AML at different stages of the disease including diagnosis, relapse and remission.

In this review, we provide a timely update on the latest findings of dysregulated metabolic pathways in HSCs, LSCs and AML blasts and how these pathways can be targeted for better treatment outcomes. Previous literature has shown that AML is mainly driven by LSCs and targeting these cells would be an effective treatment strategy for AML. Residing in the BMME allows LSCs to adapt their metabolic profile, evade chemotherapy and drive disease relapse. Conventional chemotherapy fails to selectively eliminate LSCs, is almost ineffective to perturb metabolic pathways, and is toxic to normal HSCs. Therefore, targeting metabolic pathways can re-sensitise AML blasts and LSCs to conventional chemotherapy while sparing healthy haematopoietic cells and normal HSCs. Finally, AML is genetically, and metabolically heterogeneous and *in vitro* experiments do not reflect what might occur *in vivo* and in patients. Therefore, further studies are required to effectively increase survival and enhance treatment outcomes in patients.

AUTHOR CONTRIBUTIONS

YM, RL and PC were primarily responsible for the manuscript. All authors contributed to editing and reviewing content for the manuscript and approved the final version.

FUNDING

This work was supported by Tour de Cure Pioneering Grant (Tour De Cure, Australia) [Grant #: RSP-00122-19/20] to PC and National Health and Medical Research Council of Australia [NHMRC Fellowships APP1059804 and APP1157871] to RBL. We acknowledge the Research Training Program Scholarship (RTP) awarded to YM for study towards a PhD in the Faculty of Medicine. Figures were created with BioRender.com.

REFERENCES

1. Dong Y, Shi O, Zeng Q, Lu X, Wang W, Li Y, et al. Leukemia Incidence Trends at the Global, Regional, and National Level Between 1990 and 2017. *Exp Hematol Oncol* (2020) 9(1):14. doi: 10.1186/s40164-020-00170-6
2. Short NJ, Rytting ME, Cortes JE. Acute Myeloid Leukaemia. *Lancet* (2018) 392(10147):593–606. doi: 10.1016/S0140-6736(18)31041-9
3. Thomas D, Majeti R. Biology and Relevance of Human Acute Myeloid Leukemia Stem Cells. *Blood* (2017) 129(12):1577–85. doi: 10.1182/blood-2016-10-696054
4. Dombret H, Gardin C. An Update of Current Treatments for Adult Acute Myeloid Leukemia. *Blood* (2016) 127(1):53–61. doi: 10.1182/blood-2015-08-604520
5. Rashidi A, Walter RB, Tallman MS, Appelbaum FR, DiPersio JF. Maintenance Therapy in Acute Myeloid Leukemia: An Evidence-Based Review of Randomized Trials. *Blood* (2016) 128(6):763–73. doi: 10.1182/blood-2016-03-674127
6. Lehuede C, Dupuy F, Rabinovitch R, Jones RG, Siegel PM. Metabolic Plasticity as a Determinant of Tumor Growth and Metastasis. *Cancer Res* (2016) 76(18):5201–8. doi: 10.1158/0008-5472.CAN-16-0266
7. Du W, Amarachintha S, Wilson AF, Pang Q. SCO2 Mediates Oxidative Stress-Induced Glycolysis to Oxidative Phosphorylation Switch in Hematopoietic Stem Cells. *Stem Cells* (2016) 34(4):960–71. doi: 10.1002/stem.2260
8. Ito K, Bonora M, Ito K. Metabolism as Master of Hematopoietic Stem Cell Fate. *Int J Hematol* (2019) 109(1):18–27. doi: 10.1007/s12185-018-2534-z
9. Kreitz J, Schonfeld C, Seibert M, Stolp V, Alshamleh I, Oellerich T, et al. Metabolic Plasticity of Acute Myeloid Leukemia. *Cells* (2019) 8(8):805. doi: 10.3390/cells8080805
10. Velten L, Haas SF, Raffel S, Blaszkiewicz S, Islam S, Hennig BP, et al. Human Haematopoietic Stem Cell Lineage Commitment is a Continuous Process. *Nat Cell Biol* (2017) 19(4):271–81. doi: 10.1038/ncb3493
11. Lapidot T, Sirard C, Vormoor J, Murdoch B, Hoang T, Caceres-Cortes J, et al. A Cell Initiating Human Acute Myeloid Leukaemia After Transplantation Into SCID Mice. *Nature* (1994) 367(6464):645–8. doi: 10.1038/367645a0
12. Ye H, Adane B, Khan N, Sullivan T, Minhajuddin M, Gasparetto M, et al. Leukemic Stem Cells Evade Chemotherapy by Metabolic Adaptation to an Adipose Tissue Niche. *Cell Stem Cell* (2016) 19(1):23–37. doi: 10.1016/j.stem.2016.06.001
13. Velten L, Story BA, Hernandez-Malmierca P, Raffel S, Leonce DR, Milbank J, et al. Identification of Leukemic and Pre-Leukemic Stem Cells by Clonal Tracking From Single-Cell Transcriptomics. *Nat Commun* (2021) 12 (1):1366. doi: 10.1038/s41467-021-21650-1
14. Herrmann H, Sadovnik I, Eisenwort G, Rulicke T, Blatt K, Herndlhofer S, et al. Delineation of Target Expression Profiles in CD34+/CD38- and CD34 +/CD38+ Stem and Progenitor Cells in AML and CML. *Blood Adv* (2020) 4 (20):5118–32. doi: 10.1182/bloodadvances.2020001742

15. Hope KJ, Jin L, Dick JE. Acute Myeloid Leukemia Originates From a Hierarchy of Leukemic Stem Cell Classes That Differ in Self-Renewal Capacity. *Nat Immunol* (2004) 5(7):738–43. doi: 10.1038/ni1080
16. Chopra M, Bohlander SK. The Cell of Origin and the Leukemia Stem Cell in Acute Myeloid Leukemia. *Genes Chromosomes Cancer* (2019) 58(12):850–8. doi: 10.1002/gcc.22805
17. Zhou J, Chng WJ. Identification and Targeting Leukemia Stem Cells: The Path to the Cure for Acute Myeloid Leukemia. *World J Stem Cells* (2014) 6 (4):473–84. doi: 10.4252/wjsc.v6.i4.473
18. Jones CL, Stevens BM, D'Alessandro A, Reisz JA, Culp-Hill R, Nemkov T, et al. Inhibition of Amino Acid Metabolism Selectively Targets Human Leukemia Stem Cells. *Cancer Cell* (2018) 34(5):724–40.e4. doi: 10.1016/j.ccell.2018.10.005
19. Lagadinou ED, Sach A, Callahan K, Rossi RM, Neering SJ, Minhajuddin M, et al. BCL-2 Inhibition Targets Oxidative Phosphorylation and Selectively Eradicates Quiescent Human Leukemia Stem Cells. *Cell Stem Cell* (2013) 12 (3):329–41. doi: 10.1016/j.stem.2012.12.013
20. Agarwal A, Bolosky WJ, Wilson DB, Eide CA, Olson SB, Fan G, et al. Differentiation of Leukemic Blasts is Not Completely Blocked in Acute Myeloid Leukemia. *Proc Natl Acad Sci USA* (2019) 116(49):24593–9. doi: 10.1073/pnas.1904091116
21. van Galen P, Hovestadt V, Wadsworth Ii MH, Hughes TK, Griffin GK, Battaglia S, et al. Single-Cell RNA-Seq Reveals AML Hierarchies Relevant to Disease Progression and Immunity. *Cell* (2019) 176(6):1265–81.e24. doi: 10.1016/j.cell.2019.01.031
22. Gronningsaeter IS, Reikvam H, Aasebo E, Bartaula-Brevik S, Tvedt TH, Bruserud O, et al. Targeting Cellular Metabolism in Acute Myeloid Leukemia and The Role of Patient Heterogeneity. *Cells* (2020) 9(5):1155. doi: 10.3390/cells9051155
23. Zhou HS, Carter BZ, Andreeff M. Bone Marrow Niche-Mediated Survival of Leukemia Stem Cells in Acute Myeloid Leukemia: Yin and Yang. *Cancer Biol Med* (2016) 13(2):248–59. doi: 10.20892/j.issn.2095-3941.2016.0023
24. Wang A, Zhong H. Roles of the Bone Marrow Niche in Hematopoiesis, Leukemogenesis, and Chemotherapy Resistance in Acute Myeloid Leukemia. *Hematology* (2018) 23(10):729–39. doi: 10.1080/10245332.2018.1486064
25. Haltalli MLR, Lo Celso C. Targeting Adhesion to the Vascular Niche to Improve Therapy for Acute Myeloid Leukemia. *Nat Commun* (2020) 11 (1):3691. doi: 10.1038/s41467-020-17594-7
26. Tabe Y, Konopleva M. Role of Microenvironment in Resistance to Therapy in AML. *Curr Hematol Malig Rep* (2015) 10(2):96–103. doi: 10.1007/s11899-015-0253-6
27. Ito K, Suda T. Metabolic Requirements for the Maintenance of Self-Renewing Stem Cells. *Nat Rev Mol Cell Biol* (2014) 15(4):243–56. doi: 10.1038/nrm3772
28. Jang YY, Sharkis SJ. A Low Level of Reactive Oxygen Species Selects for Primitive Hematopoietic Stem Cells That may Reside in the Low-Oxygenic Niche. *Blood* (2007) 110(8):3056–63. doi: 10.1182/blood-2007-05-087759
29. Ishikawa F, Yoshida S, Saito Y, Hijikata A, Kitamura H, Tanaka S, et al. Chemotherapy-Resistant Human AML Stem Cells Home to and Engraft Within the Bone-Marrow Endosteal Region. *Nat Biotechnol* (2007) 25 (11):1315–21. doi: 10.1038/nbt1350
30. Forte D, Garcia-Fernandez M, Sanchez-Aguilera A, Stavropoulou V, Fielding C, Martin-Perez D, et al. Bone Marrow Mesenchymal Stem Cells Support Acute Myeloid Leukemia Bioenergetics and Enhance Antioxidant Defense and Escape From Chemotherapy. *Cell Metab* (2020) 32(5):829–43 e9. doi: 10.1016/j.cmet.2020.09.001
31. Hole PS, Zabkiewicz J, Munje C, Newton Z, Pearn L, White P, et al. Overproduction of NOX-Derived ROS in AML Promotes Proliferation and is Associated With Defective Oxidative Stress Signaling. *Blood* (2013) 122(19):3322–30. doi: 10.1182/blood-2013-04-491944
32. Chapuis N, Poulain L, Birsen R, Tamburini J, Bouscary D. Rationale for Targeting Deregulated Metabolic Pathways as a Therapeutic Strategy in Acute Myeloid Leukemia. *Front Oncol* (2019) 9:405. doi: 10.3389/fonc.2019.00405
33. Stuani L, Sabatier M, Sarry JE. Exploiting Metabolic Vulnerabilities for Personalized Therapy in Acute Myeloid Leukemia. *BMC Biol* (2019) 17 (1):57. doi: 10.1186/s12915-019-0670-4
34. Castro I, Sampaio-Marques B, Ludovico P. Targeting Metabolic Reprogramming in Acute Myeloid Leukemia. *Cells* (2019) 8(9):976. doi: 10.3390/cells8090967
35. Mistry JJ, Hellmich C, Moore JA, Marlein CR, Pillinger G, Collins A, et al. Daratumumab Inhibits AML Metabolic Capacity and Tumor Growth Through Inhibition of CD38 Mediated Mitochondrial Transfer From Bone Marrow Stromal Cells to Blasts in the Leukemic Microenvironment. *Blood* (2019) 134(Supplement_1):1385. doi: 10.1182/blood-2019-128592
36. Simsek T, Kocabas F, Zheng J, Deberardinis RJ, Mahmoud AI, Olson EN, et al. The Distinct Metabolic Profile of Hematopoietic Stem Cells Reflects Their Location in a Hypoxic Niche. *Cell Stem Cell* (2010) 7(3):380–90. doi: 10.1016/j.stem.2010.07.011
37. Chen WL, Wang JH, Zhao AH, Xu X, Wang YH, Chen TL, et al. A Distinct Glucose Metabolism Signature of Acute Myeloid Leukemia With Prognostic Value. *Blood* (2014) 124(10):1645–54. doi: 10.1182/blood-2014-02-554204
38. Poulain L, Sujobert P, Zylbersztejn F, Barreau S, Stuani L, Lambert M, et al. High Mtorc1 Activity Drives Glycolysis Addiction and Sensitivity to G6PD Inhibition in Acute Myeloid Leukemia Cells. *Leukemia* (2017) 31(11):2326–35. doi: 10.1038/leu.2017.81
39. Ye H, Adane B, Khan N, Alexeev E, Nusbacher N, Minhajuddin M, et al. Subversion of Systemic Glucose Metabolism as a Mechanism to Support the Growth of Leukemia Cells. *Cancer Cell* (2018) 34(4):659–73 e6. doi: 10.1016/j.ccell.2018.08.016
40. Panuzzo C, Jovanovski A, Pergolizzi B, Pironi L, Stanga S, Fava C, et al. Mitochondria: A Galaxy in the Hematopoietic and Leukemic Stem Cell Universe. *Int J Mol Sci* (2020) 21(11):3928. doi: 10.3390/ijms21113928
41. Liberti MV, Locasale JW. The Warburg Effect: How Does it Benefit Cancer Cells? *Trends Biochem Sci* (2016) 41(3):211–8. doi: 10.1016/j.tibs.2015.12.001
42. Hay N. Reprogramming Glucose Metabolism in Cancer: Can it be Exploited for Cancer Therapy? *Nat Rev Cancer* (2016) 16(10):635–49. doi: 10.1038/nrc.2016.77
43. Song K, Li M, Xu X, Xuan LI, Huang G, Liu Q. Resistance to Chemotherapy is Associated With Altered Glucose Metabolism in Acute Myeloid Leukemia. *Oncol Lett* (2016) 12(1):334–42. doi: 10.3892/ol.2016.4600
44. Wang YH, Israelsen WJ, Lee D, Yu VWC, Jeanson NT, Clish CB, et al. Cell-State-Specific Metabolic Dependency in Hematopoiesis and Leukemogenesis. *Cell* (2014) 158(6):1309–23. doi: 10.1016/j.cell.2014.07.048
45. Mirabilii S, Ricciardi MR, Piedimonte M, Gianfelici V, Bianchi MP, Tafuri A. Biological Aspects of mTOR in Leukemia. *Int J Mol Sci* (2018) 19(8):2396. doi: 10.3390/ijms19082396
46. Jones CL, Inguva A, Jordan CT. Targeting Energy Metabolism in Cancer Stem Cells: Progress and Challenges in Leukemia and Solid Tumors. *Cell Stem Cell* (2021) 28(3):378–93. doi: 10.1016/j.stem.2021.02.013
47. Saito Y, Chapple RH, Lin A, Kitano A, Nakada D. AMPK Protects Leukemia-Initiating Cells in Myeloid Leukemias From Metabolic Stress in the Bone Marrow. *Cell Stem Cell* (2015) 17(5):585–96. doi: 10.1016/j.stem.2015.08.019
48. Bertacchini J, Guida M, Accordi B, Mediani L, Martelli AM, Barozzi P, et al. Feedbacks and Adaptive Capabilities of the PI3K/Akt/mTOR Axis in Acute Myeloid Leukemia Revealed by Pathway Selective Inhibition and Phosphoproteome Analysis. *Leukemia* (2014) 28(11):2197–205. doi: 10.1038/leu.2014.123
49. Kharas MG, Okabe R, Ganis JJ, Gozo M, Khandan T, Paktinat M, et al. Constitutively Active AKT Depletes Hematopoietic Stem Cells and Induces Leukemia in Mice. *Blood* (2010) 115(7):1406–15. doi: 10.1182/blood-2009-06-229443
50. Allegretti M, Ricciardi MR, Licchetta R, Mirabilii S, Orecchioni S, Reggiani F, et al. The Pan-Class I Phosphatidyl-Inositol-3 Kinase Inhibitor NVP-BKM120 Demonstrates Anti-Leukemic Activity in Acute Myeloid Leukemia. *Sci Rep* (2015) 5:18137. doi: 10.1038/srep18137
51. Xu Q, Thompson JE, Carroll M. mTOR Regulates Cell Survival After Etoposide Treatment in Primary AML Cells. *Blood* (2005) 106(13):4261–8. doi: 10.1182/blood-2004-11-4468
52. Daver N, Schlenk RF, Russell NH, Levis MJ. Targeting FLT3 Mutations in AML: Review of Current Knowledge and Evidence. *Leukemia* (2019) 33 (2):299–312. doi: 10.1038/s41375-018-0357-9
53. Gregory MA, D'Alessandro A, Alvarez-Calderon F, Kim J, Nemkov T, Adane B, et al. ATM/G6PD-Driven Redox Metabolism Promotes FLT3 Inhibitor Resistance in Acute Myeloid Leukemia. *Proc Natl Acad Sci USA* (2016) 113(43):E6669–E78. doi: 10.1073/pnas.1603876113

54. Testa U, Labbaye C, Castelli G, Pelosi E. Oxidative Stress and Hypoxia in Normal and Leukemic Stem Cells. *Exp Hematol* (2016) 44(7):540–60. doi: 10.1016/j.exphem.2016.04.012
55. Chen WL, Wang YY, Zhao A, Xia L, Xie G, Su M, et al. Enhanced Fructose Utilization Mediated by SLC2A5 Is a Unique Metabolic Feature of Acute Myeloid Leukemia With Therapeutic Potential. *Cancer Cell* (2016) 30 (5):779–91. doi: 10.1016/j.ccell.2016.09.006
56. Herst PM, Howman RA, Neeson PJ, Berridge MV, Ritchie DS. The Level of Glycolytic Metabolism in Acute Myeloid Leukemia Blasts at Diagnosis is Prognostic for Clinical Outcome. *J Leukoc Biol* (2011) 89(1):51–5. doi: 10.1189/jlb.0710417
57. Spinelli JB, Haigis MC. The Multifaceted Contributions of Mitochondria to Cellular Metabolism. *Nat Cell Biol* (2018) 20(7):745–54. doi: 10.1038/s41556-018-0124-1
58. Oliveira GL, Coelho AR, Marques R, Oliveira PJ. Cancer Cell Metabolism: Rewiring the Mitochondrial Hub. *Biochim Biophys Acta Mol Basis Dis* (2021) 1867(2):166016. doi: 10.1016/j.bbadis.2020.166016
59. Anderson NM, Mucka P, Kern JG, Feng H. The Emerging Role and Targetability of the TCA Cycle in Cancer Metabolism. *Protein Cell* (2018) 9(2):216–37. doi: 10.1007/s13238-017-0451-1
60. Willems L, Jacque N, Jacquel A, Neveux N, Maciel TT, Lambert M, et al. Inhibiting Glutamine Uptake Represents an Attractive New Strategy for Treating Acute Myeloid Leukemia. *Blood* (2013) 122(20):3521–32. doi: 10.1182/blood-2013-03-493163
61. Cluntun AA, Lukey MJ, Cerione RA, Locasale JW. Glutamine Metabolism in Cancer: Understanding the Heterogeneity. *Trends Cancer* (2017) 3(3):169–80. doi: 10.1016/j.trecan.2017.01.005
62. Lin KH, Xie A, Rutter JC, Ahn YR, Lloyd-Cowden JM, Nichols AG, et al. Systematic Dissection of the Metabolic-Apoptotic Interface in AML Reveals Heme Biosynthesis to Be a Regulator of Drug Sensitivity. *Cell Metab* (2019) 29(5):1217–31 e7. doi: 10.1016/j.cmet.2019.01.011
63. Yang C, Ko B, Hensley CT, Jiang L, Wasti AT, Kim J, et al. Glutamine Oxidation Maintains the TCA Cycle and Cell Survival During Impaired Mitochondrial Pyruvate Transport. *Mol Cell* (2014) 56(3):414–24. doi: 10.1016/j.molcel.2014.09.025
64. Takubo K, Nagamatsu G, Kobayashi CI, Nakamura-Ishizu A, Kobayashi H, Ikeda E, et al. Regulation of Glycolysis by Pdk Functions as a Metabolic Checkpoint for Cell Cycle Quiescence in Hematopoietic Stem Cells. *Cell Stem Cell* (2013) 12(1):49–61. doi: 10.1016/j.stem.2012.10.011
65. Ward PS, Patel J, Wise DR, Abdel-Wahab O, Bennett BD, Coller HA, et al. The Common Feature of Leukemia-Associated IDH1 and IDH2 Mutations is a Neomorphic Enzyme Activity Converting Alpha-Ketoglutarate to 2-Hydroxyglutarate. *Cancer Cell* (2010) 17(3):225–34. doi: 10.1016/j.ccr.2010.01.020
66. Kats LM, Reschke M, Taulli R, Pozdnyakova O, Burgess K, Bhargava P, et al. Proto-Oncogenic Role of Mutant IDH2 in Leukemia Initiation and Maintenance. *Cell Stem Cell* (2014) 14(3):329–41. doi: 10.1016/j.stem.2013.12.016
67. Jan M, Snyder TM, Corces-Zimmerman MR, Vyas P, Weissman IL, Quake SR, et al. Clonal Evolution of Preleukemic Hematopoietic Stem Cells Precedes Human Acute Myeloid Leukemia. *Sci Transl Med* (2012) 4 (149):149ra18. doi: 10.1126/scitranslmed.3004315
68. Chou WC, Peng KY, Lei WC, Ko BS, Tsay W, Kuo CH, et al. Persistence of Mutant Isocitrate Dehydrogenase in Patients With Acute Myeloid Leukemia in Remission. *Leukemia* (2012) 26(3):527–9. doi: 10.1038/leu.2011.215
69. Chou WC, Hou HA, Chen CY, Tang JL, Yao M, Tsay W, et al. Distinct Clinical and Biologic Characteristics in Adult Acute Myeloid Leukemia Bearing the Isocitrate Dehydrogenase 1 Mutation. *Blood* (2010) 115 (14):2749–54. doi: 10.1182/blood-2009-11-253070
70. Shlush LI, Zandi S, Mitchell A, Chen WC, Brandwein JM, Gupta V, et al. Identification of Pre-Leukaemic Haematopoietic Stem Cells in Acute Leukaemia. *Nature* (2014) 506(7488):328–33. doi: 10.1038/nature13038
71. Ashton TM, McKenna WG, Kunz-Schughart LA, Higgins GS. Oxidative Phosphorylation as an Emerging Target in Cancer Therapy. *Clin Cancer Res* (2018) 24(11):2482–90. doi: 10.1158/1078-0432.CCR-17-3070
72. Sriskanthadevan S, Jeyaraju DV, Chung TE, Prabha S, Xu W, Skrtic M, et al. AML Cells Have Low Spare Reserve Capacity in Their Respiratory Chain That Renders Them Susceptible to Oxidative Metabolic Stress. *Blood* (2015) 125(13):2120–30. doi: 10.1182/blood-2014-08-594408
73. Skrtic M, Sriskanthadevan S, Jhas B, Gebbia M, Wang X, Wang Z, et al. Inhibition of Mitochondrial Translation as a Therapeutic Strategy for Human Acute Myeloid Leukemia. *Cancer Cell* (2011) 20(5):674–88. doi: 10.1016/j.ccr.2011.10.015
74. Cole A, Wang Z, Coyaud E, Voisin V, Gronda M, Jitkova Y, et al. Inhibition of the Mitochondrial Protease ClpP as a Therapeutic Strategy for Human Acute Myeloid Leukemia. *Cancer Cell* (2015) 27(6):864–76. doi: 10.1016/j.ccell.2015.05.004
75. Lieu EL, Nguyen T, Rhyne S, Kim J. Amino Acids in Cancer. *Exp Mol Med* (2020) 52(1):15–30. doi: 10.1038/s12276-020-0375-3
76. Gallipoli P, Giotopoulos G, Tzelepis K, Costa ASH, Vohra S, Medina-Perez P, et al. Glutaminolysis is a Metabolic Dependency in FLT3(ITD) Acute Myeloid Leukemia Unmasked by FLT3 Tyrosine Kinase Inhibition. *Blood* (2018) 131(15):1639–53. doi: 10.1182/blood-2017-12-820035
77. Cormerais Y, Massard PA, Vucetic M, Giuliano S, Tambutte E, Durivault J, et al. The Glutamine Transporter ASCT2 (SLC1A5) Promotes Tumor Growth Independently of the Amino Acid Transporter LAT1 (Slc7a5). *J Biol Chem* (2018) 293(8):2877–87. doi: 10.1074/jbc.RA117.001342
78. Jacque N, Ronchetti AM, Larrue C, Meunier G, Birsen R, Willems L, et al. Targeting Glutaminolysis has Antileukemic Activity in Acute Myeloid Leukemia and Synergizes With BCL-2 Inhibition. *Blood* (2015) 126 (11):1346–56. doi: 10.1182/blood-2015-01-621870
79. Stevens BM, Jones CL, Pollyea DA, Culp-Hill R, D'Alessandro A, Winters A, et al. Fatty Acid Metabolism Underlies Venetoclax Resistance in Acute Myeloid Leukemia Stem Cells. *Nat Cancer* (2020) 1(12):1176–87. doi: 10.1038/s43018-020-00126-z
80. Raffel S, Falcone M, Kneisel N, Hansson J, Wang W, Lutz C, et al. BCAT1 Restricts alphaKG Levels in AML Stem Cells Leading to IDHmut-Like DNA Hypermethylation. *Nature* (2017) 551(7680):384–8. doi: 10.1038/nature24294
81. Miraki-Moud F, Ghazaly E, Ariza-McNaughton L, Hodby KA, Clear A, Anjos-Afonso F, et al. Arginine Deprivation Using Pegylated Arginine Deiminase has Activity Against Primary Acute Myeloid Leukemia Cells In Vivo. *Blood* (2015) 125(26):4060–8. doi: 10.1182/blood-2014-10-608133
82. Mussai F, Wheat R, Sarrou E, Booth S, Stavrou V, Fultang L, et al. Targeting the Arginine Metabolic Brake Enhances Immunotherapy for Leukaemia. *Int J Cancer* (2019) 145(8):2201–8. doi: 10.1002/ijc.32028
83. Raffel S, Hansson J, Falcone M, Lutz C, Bischel O, Ho AD, et al. Characteristic Amino Acid and Energy Metabolism in AML Stem Cells As Revealed By Quantitative Multiplex Proteomics. *Blood* (2018) 132 (Supplement 1):2780–. doi: 10.1182/blood-2018-99-117046
84. Maher M, Diesch J, Casquero R, Buschbeck M. Epigenetic-Transcriptional Regulation of Fatty Acid Metabolism and Its Alterations in Leukaemia. *Front Genet* (2018) 9:405. doi: 10.3389/fgene.2018.00405
85. Snaebjornsson MT, Janaki-Raman S, Schulze A. Greasing the Wheels of the Cancer Machine: The Role of Lipid Metabolism in Cancer. *Cell Metab* (2020) 31(1):62–76. doi: 10.1016/j.cmet.2019.11.010
86. Pabst T, Kortz L, Fiedler GM, Ceglarek U, Idle JR, Beyoglu D. The Plasma Lipidome in Acute Myeloid Leukemia at Diagnosis in Relation to Clinical Disease Features. *BBA Clin* (2017) 7:105–14. doi: 10.1016/j.bbacli.2017.03.002
87. Balko JM, Schwarz LJ, Luo N, Estrada MV, Giltnane JM, Davila-Gonzalez D, et al. Triple-Negative Breast Cancers With Amplification of JAK2 at the 9p24 Locus Demonstrate JAK2-Specific Dependence. *Sci Transl Med* (2016) 8(334):334ra53. doi: 10.1126/scitranslmed.aad3001
88. Samudio I, Konopleva M. Targeting Leukemia's "Fatty Tooth". *Blood* (2015) 126(16):1874–5. doi: 10.1182/blood-2015-08-665125
89. Humbert M, Seiler K, Mosimann S, Rentsch V, Sharma K, Pandey AV, et al. Reducing FASN Expression Sensitizes Acute Myeloid Leukemia Cells to Differentiation Therapy. *Cell Death Differ* (2021) 28(8):2465–81. doi: 10.1101/2020.01.29.924555
90. Tabe Y, Konopleva M, Andreeff M. Fatty Acid Metabolism, Bone Marrow Adipocytes, and AML. *Front Oncol* (2020) 10:155. doi: 10.3389/fonc.2020.00155
91. Pietrocola F, Galluzzi L, Bravo-San Pedro JM, Madeo F, Kroemer G. Acetyl Coenzyme A: A Central Metabolite and Second Messenger. *Cell Metab* (2015) 21(6):805–21. doi: 10.1016/j.cmet.2015.05.014
92. Shi J, Fu H, Jia Z, He K, Fu L, Wang W. High Expression of CPT1A Predicts Adverse Outcomes: A Potential Therapeutic Target for Acute Myeloid Leukemia. *EBioMedicine* (2016) 14:55–64. doi: 10.1016/j.ebiom.2016.11.025

93. Wu Y, Hurren R, MacLean N, Gronda M, Jitkova Y, Sukhai MA, et al. Carnitine Transporter CT2 (SLC22A16) is Over-Expressed in Acute Myeloid Leukemia (AML) and Target Knockdown Reduces Growth and Viability of AML Cells. *Apoptosis* (2015) 20(8):1099–108. doi: 10.1007/s10495-015-1137-x
94. Ito K, Carracedo A, Weiss D, Arai F, Ala U, Avigan DE, et al. A PML-PPAR-Delta Pathway for Fatty Acid Oxidation Regulates Hematopoietic Stem Cell Maintenance. *Nat Med* (2012) 18(9):1350–8. doi: 10.1038/nm.2882
95. Loeffler D, Schroeder T. Symmetric and Asymmetric Activation of Hematopoietic Stem Cells. *Curr Opin Hematol* (2021) 28(4):262–8. doi: 10.1097/MOH.0000000000000644
96. Shafat MS, Oellerich T, Mohr S, Robinson SD, Edwards DR, Marlein CR, et al. Leukemic Blasts Program Bone Marrow Adipocytes to Generate a Protumoral Microenvironment. *Blood* (2017) 129(10):1320–32. doi: 10.1182/blood-2016-08-734798
97. Powell JA, Wallington-Beddoe CT, Pitson SM. Targeting Sphingosine Kinase 1 in Acute Myeloid Leukemia: Translation to Clinic. *Int J Hematol Oncol* (2017) 6(2):31–4. doi: 10.2217/ijh-2017-0011
98. Ghazaly EA, Miraki-Moud F, Smith P, Gnanaranjan C, Koniali L, Oke A, et al. Repression of Sphingosine Kinase (SK)-Interacting Protein (SKIP) in Acute Myeloid Leukemia Diminishes SK Activity and its Re-Expression Restores SK Function. *J Biol Chem* (2020) 295(16):5496–508. doi: 10.1074/jbc.RA119.010467
99. Powell JA, Lewis AC, Zhu W, Toubia J, Pitman MR, Wallington-Beddoe CT, et al. Targeting Sphingosine Kinase 1 Induces MCL1-Dependent Cell Death in Acute Myeloid Leukemia. *Blood* (2017) 129(6):771–82. doi: 10.1182/blood-2016-06-720433
100. Xie SZ, Kaufmann KB, Wang W, Chan-Seng-Yue M, Gan OI, Laurenti E, et al. Sphingosine-1-Phosphate Receptor 3 Potentiates Inflammatory Programs in Normal and Leukemia Stem Cells to Promote Differentiation. *Blood Cancer Discov* (2021) 2(1):32–53. doi: 10.1158/2643-3230.BCD-20-0155
101. Corces MR, Chang HY, Majeti R. Preleukemic Hematopoietic Stem Cells in Human Acute Myeloid Leukemia. *Front Oncol* (2017) 7:263. doi: 10.3389/fonc.2017.00263
102. Shlush LI, Mitchell A, Heisler L, Abelson S, Ng SWK, Trotman-Grant A, et al. Tracing the Origins of Relapse in Acute Myeloid Leukaemia to Stem Cells. *Nature* (2017) 547(7661):104–8. doi: 10.1038/nature22993
103. Garg M, Nagata Y, Kanojia D, Mayakonda A, Yoshida K, Haridas Keloth S, et al. Profiling of Somatic Mutations in Acute Myeloid Leukemia With FLT3-ITD at Diagnosis and Relapse. *Blood* (2015) 126(22):2491–501. doi: 10.1182/blood-2015-05-646240
104. Ding L, Ley TJ, Larson DE, Miller CA, Koboldt DC, Welch JS, et al. Clonal Evolution in Relapsed Acute Myeloid Leukaemia Revealed by Whole-Genome Sequencing. *Nature* (2012) 481(7382):506–10. doi: 10.1038/nature10738
105. Vu LP, Kharas MG. Targeting the Residual Leukemia Cells After Chemotherapy. *Cancer Cell* (2018) 34(3):353–5. doi: 10.1016/j.ccell.2018.08.012
106. Hira VVV, Van Noorden CJF, Carraway HE, Maciejewski JP, Molenaar RJ. Novel Therapeutic Strategies to Target Leukemic Cells That Hijack Compartmentalized Continuous Hematopoietic Stem Cell Niches. *Biochim Biophys Acta Rev Cancer* (2017) 1868(1):183–98. doi: 10.1016/j.bbcan.2017.03.010
107. van Gils N, Denkers F, Smit L. Escape From Treatment; the Different Faces of Leukemic Stem Cells and Therapy Resistance in Acute Myeloid Leukemia. *Front Oncol* (2021) 11:659253. doi: 10.3389/fonc.2021.659253
108. Vidal RS, Quarti J, Rodrigues MF, Rumjanek FD, Rumjanek VM. Metabolic Reprogramming During Multidrug Resistance in Leukemias. *Front Oncol* (2018) 8:90. doi: 10.3389/fonc.2018.00090
109. Salvia AM, Cuviello F, Coluzzi S, Nuccorini R, Attolico I, Pascale SP, et al. Expression of Some ATP-Binding Cassette Transporters in Acute Myeloid Leukemia. *Hematol Rep* (2017) 9(4):7406–. doi: 10.4081/hr.2017.7406
110. Saito Y, Uchida N, Tanaka S, Suzuki N, Tomizawa-Murasawa M, Sone A, et al. Induction of Cell Cycle Entry Eliminates Human Leukemia Stem Cells in a Mouse Model of AML. *Nat Biotechnol* (2010) 28(3):275–80. doi: 10.1038/nbt.1607
111. Farge T, Saland E, de Toni F, Aroua N, Hosseini M, Perry R, et al. Chemotherapy-Resistant Human Acute Myeloid Leukemia Cells Are Not Enriched for Leukemic Stem Cells But Require Oxidative Metabolism. *Cancer Discov* (2017) 7(7):716–35. doi: 10.1158/2159-8290.CD-16-0441
112. Larrue C, Saland E, Vergez F, Serhan N, Delabesse E, Mansat-De Mas V, et al. Antileukemic Activity of 2-Deoxy-D-Glucose Through Inhibition of N-Linked Glycosylation in Acute Myeloid Leukemia With FLT3-ITD or C-KIT Mutations. *Mol Cancer Ther* (2015) 14(10):2364–73. doi: 10.1158/1535-7163.MCT-15-0163
113. Huang A, Ju HQ, Liu K, Zhan G, Liu D, Wen S, et al. Metabolic Alterations and Drug Sensitivity of Tyrosine Kinase Inhibitor Resistant Leukemia Cells With a FLT3/ITD Mutation. *Cancer Lett* (2016) 377(2):149–57. doi: 10.1016/j.canlet.2016.04.040
114. Sykes DB, Kfoury YS, Mercier FE, Wawer MJ, Law JM, Haynes MK, et al. Inhibition of Dihydroorotate Dehydrogenase Overcomes Differentiation Blockade in Acute Myeloid Leukemia. *Cell* (2016) 167(1):171–86.e15. doi: 10.1016/j.cell.2016.08.057
115. Wu D, Wang W, Chen W, Lian F, Lang L, Huang Y, et al. Pharmacological Inhibition of Dihydroorotate Dehydrogenase Induces Apoptosis and Differentiation in Acute Myeloid Leukemia Cells. *Haematologica* (2018) 103(9):1472–83. doi: 10.3324/haematol.2018.188185
116. Konopleva M, Pollyea DA, Potluri J, Chyla B, Hogdal L, Busman T, et al. Efficacy and Biological Correlates of Response in a Phase II Study of Venetoclax Monotherapy in Patients With Acute Myelogenous Leukemia. *Cancer Discov* (2016) 6(10):1106–17. doi: 10.1158/2159-8290.CD-16-0313
117. Pollyea DA, Stevens BM, Jones CL, Winters A, Pei S, Minhajuddin M, et al. Venetoclax With Azacitidine Disrupts Energy Metabolism and Targets Leukemia Stem Cells in Patients With Acute Myeloid Leukemia. *Nat Med* (2018) 24(12):1859–66. doi: 10.1038/s41591-018-0233-1
118. DiNardo CD, Pratz KW, Letai A, Jonas BA, Wei AH, Thirman M, et al. Safety and Preliminary Efficacy of Venetoclax With Decitabine or Azacitidine in Elderly Patients With Previously Untreated Acute Myeloid Leukaemia: A non-Randomised, Open-Label, Phase 1b Study. *Lancet Oncol* (2018) 19(2):216–28. doi: 10.1016/S1470-2045(18)30010-X
119. Mali RS, Zhang Q, DeFilippis R, Cavazos A, Kuruvilla VM, Raman J, et al. Venetoclax Combines Synergistically With FLT3 Inhibition to Effectively Target Leukemic Cells in FLT3-ITD+ Acute Myeloid Leukemia Models. *Haematologica* (2020) 106(4):1034–46. doi: 10.3324/haematol.2019.244020
120. Reed GA, Schiller GJ, Kambhampati S, Tallman MS, Douer D, Minden MD, et al. A Phase 1 Study of Intravenous Infusions of Tigecycline in Patients With Acute Myeloid Leukemia. *Cancer Med* (2016) 5(11):3031–40. doi: 10.1002/cam4.845
121. Liyanage SU, Hurren R, Voisin V, Bridon G, Wang X, Xu C, et al. Leveraging Increased Cytoplasmic Nucleoside Kinase Activity to Target mtDNA and Oxidative Phosphorylation in AML. *Blood* (2017) 129(19):2657–66. doi: 10.1182/blood-2016-10-741207
122. Stein EM, DiNardo CD, Pollyea DA, Fathi AT, Roboz GJ, Altman JK, et al. Enasidenib in Mutant IDH2 Relapsed or Refractory Acute Myeloid Leukemia. *Blood* (2017) 130(6):722–31. doi: 10.1182/blood-2017-04-779405
123. Amatangelo MD, Quek L, Shih A, Stein EM, Roshal M, David MD, et al. Enasidenib Induces Acute Myeloid Leukemia Cell Differentiation to Promote Clinical Response. *Blood* (2017) 130(6):732–41. doi: 10.1182/blood-2017-04-779447
124. Yen K, Travins J, Wang F, David MD, Artin E, Straley K, et al. AG-221, a First-In-Class Therapy Targeting Acute Myeloid Leukemia Harboring Oncogenic IDH2 Mutations. *Cancer Discov* (2017) 7(5):478–93. doi: 10.1158/2159-8290.CD-16-1034
125. Ahmed T, Holwerda S, Klepin HD, Isom S, Ellis LR, Lyerly S, et al. High Dose Cytarabine, Mitoxantrone and L-Asparaginase (HAMA) Salvage for Relapsed or Refractory Acute Myeloid Leukemia (AML) in the Elderly. *Leuk Res* (2015) 39(9):945–9. doi: 10.1016/j.leukres.2015.05.010
126. Michelozzi IM, Granata V, De Ponti G, Alberti G, Tomasoni C, Antolini L, et al. Acute Myeloid Leukaemia Niche Regulates Response to L-Asparaginase. *Br J Haematol* (2019) 186(3):420–30. doi: 10.1111/bjh.15920
127. Thomas XG, Tardy ET, Guieze R, Chevallier P, Marolleau JP, Orsini F, et al. GRASPA-AML 2012-01 Study (NCT01810705): A Multicenter, Open, Randomized Phase 2b Trial Evaluating ERY001 (L-Asparaginase Encapsulated in Red Blood Cells) Plus Low-Dose Cytarabine vs Low-Dose Cytarabine Alone, in Treatment of Newly Diagnosed Acute Myeloid Leukemia (AML) Elderly Patients, Unfit for Intensive Chemotherapy. *Am*

J Clin Oncol (2015) 33(15_suppl):TPS7099–TPS. doi: 10.1200/jco.2015.33.15_suppl.tps7099
128. Wang ES, Frankfurt O, Orford KW, Bennett M, Flinn IW, Maris M, et al. Phase 1 Study of CB-839, a First-In-Class, Orally Administered Small Molecule Inhibitor of Glutaminase in Patients With Relapsed/Refractory Leukemia. *Blood* (2015) 126(23):2566–. doi: 10.1182/blood.V126.23.2566.2566
129. Lee EA, Angka L, Rota SG, Hanlon T, Mitchell A, Hurren R, et al. Targeting Mitochondria With Avocatin B Induces Selective Leukemia Cell Death. *Cancer Res* (2015) 75(12):2478–88. doi: 10.1158/0008-5472.CAN-14-2676
130. Pardee T, DeFord-Watts LM, Peronto E, Levitan DA, Hurd DD, Kridel S. Altered Lipid and Mitochondrial Metabolism Are Viable Targets in Acute Leukemia. *Blood* (2011) 118(21):3618–. doi: 10.1182/blood.V118.21.3618.3618
131. Estan MC, Calvino E, Calvo S, Guillen-Guio B, Boyano-Adanez Mdel C, de Blas E, et al. Apoptotic Efficacy of Etomoxir in Human Acute Myeloid Leukemia Cells. Cooperation With Arsenic Trioxide and Glycolytic Inhibitors, and Regulation by Oxidative Stress and Protein Kinase Activities. *PloS One* (2014) 9(12):e115250. doi: 10.1371/journal.pone.0115250
132. Tan SF, Liu X, Fox TE, Barth BM, Sharma A, Turner SD, et al. Acid Ceramidase is Upregulated in AML and Represents a Novel Therapeutic Target. *Oncotarget* (2016) 7(50):83208–22. doi: 10.18632/oncotarget.13079
133. Lee JS, Roberts A, Juarez D, Vo TT, Bhatt S, Herzog LO, et al. Statins Enhance Efficacy of Venetoclax in Blood Cancers. *Sci Transl Med* (2018) 10 (445):1240. doi: 10.1126/scitranslmed.aaq1240
134. Ricciardi MR, Mirabilii S, Allegretti M, Licchetta R, Calarco A, Torrisi MR, et al. Targeting the Leukemia Cell Metabolism by the CPT1a Inhibition: Functional Preclinical Effects in Leukemias. *Blood* (2015) 126(16):1925–9. doi: 10.1182/blood-2014-12-617498
135. Giammarioli AM, Gambardella L, Barbati C, Pietraforte D, Tinari A, Alberton M, et al. Differential Effects of the Glycolysis Inhibitor 2-Deoxy-D-Glucose on the Activity of Pro-Apoptotic Agents in Metastatic Melanoma Cells, and Induction of a Cytoprotective Autophagic Response. *Int J Cancer* (2012) 131(4):E337–47. doi: 10.1002/ijc.26420
136. Yang H, Tabe Y, Sekihara K, Saito K, Ma H, Ruvolo V, et al. Novel Oxidative Phosphorylation Inhibitor IACS-010759 Induces AMPK-Dependent Apoptosis of AML Cells. *Blood* (2017) 130(Supplement 1):1245–. doi: 10.1182/blood.V130.Suppl_1.1245.1245
137. Sykes DB. The Emergence of Dihydroorotate Dehydrogenase (DHODH) as a Therapeutic Target in Acute Myeloid Leukemia. *Expert Opin Ther Targets* (2018) 22(11):893–8. doi: 10.1080/14728222.2018.1536748
138. Stacpoole PW. Therapeutic Targeting of the Pyruvate Dehydrogenase Complex/Pyruvate Dehydrogenase Kinase (PDC/PDK) Axis in Cancer. *J Natl Cancer Inst* (2017) 109(11). doi: 10.1093/jnci/djx071
139. Emadi A, Carter-Cooper B, Sadowska M, Wonodi O, Lapidus RG, Levis M, et al. Synergistic Antileukemic Effect Of Sequential Administration Of Dichloroacetate (DCA) Combined With Arsenic Trioxide (ATO) In Primary Blasts From Patients With Acute Myeloid Leukemia (AML) and FLT3-ITD AML Cell Lines. *Blood* (2013) 122(21):3955–. doi: 10.1182/blood.V122.21.3955.3955
140. Khan AUH, Rathore MG, Allende-Vega N, Vo DN, Belkhala S, Orecchioni S, et al. Human Leukemic Cells Performing Oxidative Phosphorylation (OXPHOS) Generate an Antioxidant Response Independently of Reactive Oxygen Species (ROS) Production. *EBioMedicine* (2016) 3:43–53. doi: 10.1016/j.ebiom.2015.11.045
141. DiNardo CD, Jonas BA, Pullarkat V, Thirman MJ, Garcia JS, Wei AH, et al. Azacitidine and Venetoclax in Previously Untreated Acute Myeloid Leukemia. *N Engl J Med* (2020) 383(7):617–29. doi: 10.1056/NEJMoa2012971
142. Huemer F, Melchardt T, Jansko B, Wahida A, Jilg S, Jost PJ, et al. Durable Remissions With Venetoclax Monotherapy in Secondary AML Refractory to Hypomethylating Agents and High Expression of BCL-2 and/or BIM. *Eur J Haematol* (2019) 102(5):437–41. doi: 10.1111/ejh.13218
143. Samudio I, Harmancey R, Fiegl M, Kantarjian H, Konopleva M, Korchin B, et al. Pharmacologic Inhibition of Fatty Acid Oxidation Sensitizes Human Leukemia Cells to Apoptosis Induction. *J Clin Invest* (2010) 120(1):142–56. doi: 10.1172/JCI38942
144. Matre P, Velez J, Jacamo R, Qi Y, Su X, Cai T, et al. Inhibiting Glutaminase in Acute Myeloid Leukemia: Metabolic Dependency of Selected AML Subtypes. *Oncotarget* (2016) 7(48):79722–35. doi: 10.18632/oncotarget.12944
145. Gregory MA, Nemkov T, Park HJ, Zaberezhnyy V, Gehrke S, Adane B, et al. Targeting Glutamine Metabolism and Redox State for Leukemia Therapy. *Clin Cancer Res* (2019) 25(13):4079–90. doi: 10.1158/1078-0432.CCR-18-3223
146. Gregory MA, Nemkov T, Reisz JA, Zaberezhnyy V, Hansen KC, D'Alessandro A, et al. Glutaminase Inhibition Improves FLT3 Inhibitor Therapy for Acute Myeloid Leukemia. *Exp Hematol* (2018) 58:52–8. doi: 10.1016/j.exphem.2017.09.007
147. Jones CL, Stevens BM, Pollyea DA, Culp-Hill R, Reisz JA, Nemkov T, et al. Nicotinamide Metabolism Mediates Resistance to Venetoclax in Relapsed Acute Myeloid Leukemia Stem Cells. *Cell Stem Cell* (2020) 27(5):748–64.e4. doi: 10.1016/j.stem.2020.07.021
148. Jones CL, Stevens BM, D'Alessandro A, Culp-Hill R, Reisz JA, Pei S, et al. Cysteine Depletion Targets Leukemia Stem Cells Through Inhibition of Electron Transport Complex II. *Blood* (2019) 134(4):389–94. doi: 10.1182/blood.2019898114
149. Luo M, Brooks M, Wicha MS. Asparagine and Glutamine: Co-Conspirators Fueling Metastasis. *Cell Metab* (2018) 27(5):947–9. doi: 10.1016/j.cmet.2018.04.012
150. Patzke CL, Duffy AP, Duong VH, El Chaer F, Trovato JA, Baer MR, et al. Comparison of High-Dose Cytarabine, Mitoxantrone, and Pegaspargase (HAM-Pega) to High-Dose Cytarabine, Mitoxantrone, Cladribine, and Filgrastim (CLAG-M) as First-Line Salvage Cytotoxic Chemotherapy for Relapsed/Refractory Acute Myeloid Leukemia. *J Clin Med* (2020) 9(2):536. doi: 10.3390/jcm9020536
151. Mussai F, Egan S, Higginbotham-Jones J, Perry T, Beggs A, Odintsova E, et al. Arginine Dependence of Acute Myeloid Leukemia Blast Proliferation: A Novel Therapeutic Target. *Blood* (2015) 125(15):2386–96. doi: 10.1182/blood-2014-09-600643
152. Stuani L, Riols F, Millard P, Sabatier M, Batut A, Saland E, et al. Stable Isotope Labeling Highlights Enhanced Fatty Acid and Lipid Metabolism in Human Acute Myeloid Leukemia. *Int J Mol Sci* (2018) 19(11):3325. doi: 10.3390/ijms19113325
153. Dany M, Gencer S, Nganga R, Thomas RJ, Oleinik N, Baron KD, et al. Targeting FLT3-ITD Signaling Mediates Ceramide-Dependent Mitophagy and Attenuates Drug Resistance in AML. *Blood* (2016) 128(15):1944–58. doi: 10.1182/blood-2016-04-708750
154. Leni Z, Parakkal G, Arcaro A. Emerging Metabolic Targets in the Therapy of Hematological Malignancies. *BioMed Res Int* (2013) 2013:946206. doi: 10.1155/2013/946206
155. Ghaffari P, Mardinoglu A, Nielsen J. Cancer Metabolism: A Modeling Perspective. *Front Physiol* (2015) 6:382. doi: 10.3389/fphys.2015.00382
156. Cantor JR, Abu-Remaileh M, Kanarek N, Freinkman E, Gao X, Louissaint A Jr, et al. Physiologic Medium Rewires Cellular Metabolism and Reveals Uric Acid as an Endogenous Inhibitor of UMP Synthase. *Cell* (2017) 169(2):258–72.e17. doi: 10.1016/j.cell.2017.03.023
157. Vande Voorde J, Ackermann T, Pfetzer N, Sumpton D, Mackay G, Kalna G, et al. Improving the Metabolic Fidelity of Cancer Models With a Physiological Cell Culture Medium. *Sci Adv* (2019) 5(1):eaau7314. doi: 10.1126/sciadv.aau7314
158. Tabe Y, Saitoh K, Yang H, Sekihara K, Yamatani K, Ruvolo V, et al. Inhibition of FAO in AML Co-Cultured With BM Adipocytes: Mechanisms of Survival and Chemosensitization to Cytarabine. *Sci Rep* (2018) 8(1):16837. doi: 10.1038/s41598-018-35198-6
159. Horibata S, Gui G, Lack J, DeStefano CB, Gottesman MM, Hourigan CS. Heterogeneity in Refractory Acute Myeloid Leukemia. *Proc Natl Acad Sci USA* (2019) 116(21):10494–503. doi: 10.1073/pnas.1902375116

Conflict of Interest: The authors declare that the research was conducted in the absence of any commercial or financial relationships that could be construed as a potential conflict of interest.

GLOSSARY

6-AN	6-aminonicotinamide
2-DG	2-Deoxy-D-glucose
2-D-HG	2-D-hydroxyglutarate
α-KG	α-ketoglutarate
AAs	Amino acids
ABT-199	Venetoclax
ABC	ATP-Binding Cassette
Akt	Protein kinase B
ALAT	Alanine transferase
AML	Acute myeloid leukaemia
AMPK	AMP-activated protein kinase
Bap	A combination of lipid-regulating bezafibrate (BEZ) and the sex hormone medroxyprogesterone acetate
BCAT1	branched-chain amino acid transaminase 1
BMME	Bone marrow microenvironment
Cas9	CRISPR-associated protein 9
CD	Cluster of differentiation
c-KIT	Cluster of differentiation 117
CKMT1	Creatine kinase mitochondrial 1
ClpP	ATP-dependent Clp protease
CoA	Coenzyme A
CPT1A	Carnitine palmitoyltransferase 1A
CRISPR	Clustered regularly interspaced short palindromic repeats
Cytarabine	Ara-C
DHODH	Dihydroorotate dehydrogenase
ETC	Electron transport chain
F1P	Fructose-1-phosphate
FADH2	Flavin adenine dinucleotide
FLT3-ITD	Fms-like tyrosine kinase-3 internal tandem duplication
G3P	Glycerol-3-phosphate
G6P	Glucose-6-phosphate
GLS	Glutaminase
GLUTs	Glucose transporters
GPX1	Glutathione peroxidase 1
GSH	Glutathione
GSR	Glutathione-disulfide reductase
HIF-1α	Hypoxia-inducible factor 1-alpha
HMG	Hydroxy methylglutaryl
HPLM	Human plasma-like medium
HSCs	Haematopoietic stem cells
IDH	Isocitrate dehydrogenase
LDHA	Lactate dehydrogenase
LSCs	Leukaemic stem cells
MCL-1	Myeloid Cell Leukaemia 1
mtDNA	Mitochondrial DNA
mTOR	Mechanistic target of rapamycin
NAD	Nicotinamide adenine dinucleotide
NADPH	Nicotinamide adenine dinucleotide phosphate
NSG	NOD scid gamma mouse
OAA	Oxaloacetate
OXPHOS	Oxidative phosphorylation
PEP	Phosphoenolpyruvate
PI3K	Phosphoinositide 3-kinase
PKM2	Pyruvate kinase M2
PPP	Pentose phosphate pathway
PUMA	p53 upregulated modulator of apoptosis
R5P	Ribose-5-phosphate
ROS	Reactive oxygen species
shRNA	Short or small hairpin RNA
SLCs	Solute carriers
TCA	Tricarboxylic acid

frontiers | Frontiers in Oncology

ORIGINAL RESEARCH
published: 18 May 2022
doi: 10.3389/fonc.2022.874900

Solasonine Causes Redox Imbalance and Mitochondrial Oxidative Stress of Ferroptosis in Lung Adenocarcinoma

Yao-Ying Zeng[1†], Ying-Bin Luo[1†], Xu-Dong Ju[2†], Bo Zhang[1], Ya-Jing Cui[1], Yan-Bin Pan[1], Jian-Hui Tian[1], Wen-Jing Teng[1], Jianchun Wu[1] and Yan Li[1*]*

[1] Department of Oncology, Shanghai Municipal Hospital of Traditional Chinese Medicine, Shanghai University of Traditional Chinese Medicine, Shanghai, China, [2] Department of Respiratory Medicine, Shanghai Municipal Hospital of Traditional Chinese Medicine, Shanghai University of Traditional Chinese Medicine, Shanghai, China

OPEN ACCESS

Edited by:
Kaiyuan Ni, Massachusetts Institute of Technology, United States

Reviewed by:
Tong Wu, The University of Chicago, United States
Jaroslav Truksa, Institute of Biotechnology (ASCR), Czechia

***Correspondence:**
Jianchun Wu
eq219@126.com
Yan Li
yan.xiaotian@shutcm.edu.cn

†These authors have contributed equally to this work

Specialty section:
This article was submitted to Pharmacology of Anti-Cancer Drugs, a section of the journal Frontiers in Oncology

Received: *13 February 2022*
Accepted: *24 March 2022*
Published: *18 May 2022*

Citation:
Zeng Y-Y, Luo Y-B, Ju X-D, Zhang B, Cui Y-J, Pan Y-B, Tian J-H, Teng W-J, Wu J and Li Y (2022) Solasonine Causes Redox Imbalance and Mitochondrial Oxidative Stress of Ferroptosis in Lung Adenocarcinoma. Front. Oncol. 12:874900. doi: 10.3389/fonc.2022.874900

Ferroptosis, a type of iron-dependent oxidative cell death caused by excessive lipid peroxidation, is emerging as a promising cancer therapeutic strategy. Solasonine has been reported as a potential compound in tumor suppression, which is closely linked to ferroptosis. However, ferroptosis caused by solasonine is insufficiently identified and elaborated in lung adenocarcinoma, a fatal disease with high morbidity and mortality rates. First, the biochemical and morphological changes in Calu-1 and A549 cells exposed to solasonine are observed using a cell death assay and a microscope. The cell viability assay is performed after determining the executive concentration of solasonine to assess the effects of solasonine on tumor growth in Calu-1 and A549 cells. The ferroptosis is then identified by using ferroptosis-related reagents on CCK-8, lipid peroxidation assessment, Fe^{2+}, and ROS detection. Furthermore, the antioxidant system, which includes GSH, Cys, GPx4, SLC7A11, and mitochondrial function, is measured to identify the potential pathways. According to the results, solasonine precisely exerts antitumor ability in lung adenocarcinoma cells. Ferroptosis is involved in the solasonine-induced cell death, as well as the accumulation of lipid peroxide, Fe^{2+}, and ROS. Moreover, the failures of antioxidant defense and mitochondrial damage are considered to make a significant contribution to the occurrence of ferroptosis caused by solasonine. The study describes the potential process of ferroptosis caused by solasonine when dealing with lung adenocarcinoma. This encouraging evidence suggests that solasonine may be useful in the treatment of lung cancer.

Keywords: solasonine, ferroptosis, lung adenocarcinoma, oxidation, mitochondrial dysfunction

INTRODUCTION

It is common knowledge that when a cell proliferates at an uncontrollable rate with an abnormal shape and malfunctions, trouble is on the way. Cancer is a multistage disease that is driven by genetic factors, immunological problems, adaptive metabolism, and other mutations. When a process occurs in the lungs, it may indicate that lung cancer, a lethal tumor with the highest morbidity and fatality rates in the world, is posing a threat to your life. According to statistics, lung adenocarcinoma (LUAD), the most common subtype of lung cancer, accounts for approximately 40% of all lung cancer occurrences (1). Despite a slew of obstacles, researchers continue to push

forward in oncology research. Regulated cell death (RCD) has recently become a primary focus of researchers because of its possible therapeutic value in cancer. Ferroptosis, a new type of cell death with specific features, could be an adaptive mechanism that plays a key part in the eradication of cancerous cells (2).

Ferroptosis, formally proposed in 2012, was characterized by iron overload and lipid reactive oxygen species accumulation in the biochemical process (3). Other distinctive traits included cytological abnormalities in mitochondria, which manifested as smaller mitochondria with no cristae, a high density of mitochondrial membrane, and even rupture of the outer mitochondrial membrane (4). Iron toxicity, antioxidant defense failure, free radical production, and mitochondrial fatty-acid metabolism were identified as pathways in the process of ferroptosis, and those factors required for ferroptosis were integrated into attenuating the selective permeability of the plasma membrane, definitively causing cell termination (5). Ferroptosis was discovered to have benefits in cancer treatment by reversing drug resistance, sensitizing radiation, and synergizing immunotherapy, along with related basic research rapidly developing (6). According to emerging investigations, many natural compounds with anti-tumor potential have been discovered by inducing ferroptosis.

Solasonine (SS), a natural glycoalkaloid compound, may be a promising candidate for cancer treatment development and advancement. SS has been demonstrated to be toxic to a variety of cancer cell lines, including hepatocellular carcinoma cells (7), lung cancer cells (8), acute monocytic leukemic cell lines (9), glioma cells (10), and gastric cancer cells (11). Besides apoptosis (7–9), cell cycle arrest (9) and anti-inflammatory (10), ferroptosis (12) was discovered to contribute to the pharmacological advantages of SS. However, the pharmacological mechanisms by which SS causes ferroptosis in LUAD have yet to be identified and interpreted.

We investigated the toxicity of SS on Calu-1 and A549 cells in this study. Afterward, the induction of ferroptosis in response to SS was confirmed by combining the detection of lipid ROS, Fe^{2+}, and ROS with the application of multiple ferroptosis-related reagents. In addition to redox imbalance, mitochondrial oxidative stress was observed in cells exposed to SS in the following investigation. The findings of this study are intended to supplement the knowledge of SS in the application of cancer treatment.

MATERIALS AND METHODS

Cell Culture and Treatment

Calu-1 and A549 cancer cells were obtained from the National Collection of Authenticated Cell Cultures (NCACC) and cultured in DMED medium supplemented with 10% fetal bovine serum (FBS) (Gibco) and 1% antibiotic in a humidified incubator at 37˚C and 5% CO_2. Cells with a density of 70% to 80% were deemed ready to adopt measures for subsequent detection. To enhance the effect of the inhibitors used in this study, they were intentionally added to cells 2 h before SS.

Reagents

The reagents included solasonine (HY-N0070, MCE), Z-VAD-FMK (S7023, Selleck), DCFH-DA (S0033S, Beyotime), Cell Counting Kit-8 (40203ES76, YEASEN), SYTOX green (S7020, Invitrogen), Trolox (C3183, APExBIO), DFO (HY-B0988, MCE), Mito-TEMPO (HY-112879, MCE), Necrostatin-1(HY-15760, MCE), Hoechst 3342 (23491-52-3, Solarbio), Ferrostatin-1 (HY-100579, MCE), RSL3 (HY-100218A, MCE), Bafilomycin A1 (HY-100558, MCE), C11-BODIPY581/591 (D3861, Invitrogen), Erastin (HY-15763,MCE), GSH assay kit (A006-2-1, Nanjing Jiancheng), Cysteine assay kit (BC185, Solarbio), FerroOrange probes (M489, Dojindo), MitoPeDPP (M466-5,Dojindo), and JC-1 (MT09-1, Dojindo).The following antibody purchased from Cell Signaling Technology was GAPDH (5174, CST), the others purchased from BOSTER included GPX4 (BM5231, BOSTER) and SLCA711 (BM5318, BOSTER). According to the manufacturer's instructions, the drugs were initially dissolved in dimethylsulfoxide (DMSO) at a stock solution.

Cell Viability Assay

Approximately 5000 Calu-1 cells and 10,000 A549 cells were seeded into the 96-well plates in triplicate and cultured in the appropriate conditions for 24 h. Incidentally, the objective drugs and reagents involving various inducers and inhibitors were applied based on the manufacturer's protocol. Specifically, the inhibitors including Z-VAD-FMK (Z-V), Necrostatin-1 (Nec), Ferrostatin-1 (Fer-1), Bafilomycin A1 (Baf-A1), Deferoxamine mesylate (DFO), Mito TEMPO, Trolox, and RSL3 were added to the cells for 2 h prior to SS for pretreatment. The medium was then supplemented with the Cell Counting Kit 8 (CCK8) reagent, and the cells were incubated for 2 h. Finally, the absorbance at 450 nm was measured using a microplate reader (Bio Tek, United States).

Cell Death Assessment

The SYTOX Green staining solution was used to visualize cancer cell death. Calu-1 and A549 cells were seeded into 24-well plates at a density of approximately 5*104 cells/well and 1*105 cells/well, respectively, and cultured at 37°C in an incubator. Calu-1 cells were exposed to SS (10 μM, 15 μM, 20 μM) after 24 h, while A549 cells were exposed to SS (20 μM, 25 μM, 30 μM). Meanwhile, the cells were stained with 100 nM SYTOX Green and cultured in the dark before being observed under a fluorescence microscope (Leica, Germany).

Cellular Iron Detection

The levels of intracellular Fe^{2+} were assessed using FerroOrange probes (Dojindo) according to the manufacturer's protocol. Cells were drug-treated for the time indicated before being stained with a final concentration of 1 mol/L of FerroOrange for 30 min at 37°C. The signal from the samples was collected using a flow cytometer and analyzed using the GraphPad Prism software.

Measurement of Cytosolic Reactive Oxygen Species (ROS) Generation

In the study, DCFH-DA, a cell-permeable probe, was used to measure the levels of cytosolic ROS using flow cytometry and a

fluorescence microscope. In brief, cells were drug-treated before being cultured with DCFH-DA for 30 min at 37°C. The level of ROS was measured using the flow cytometer and fluorescence microscope mentioned above after the samples were washed twice with PBS.

Lipid Peroxidation Assessed by C11-BODIPY581/591

C11-BODIPY581/591 was performed on cells by incubating them in PBS containing 5% FBS and 10 μM C11-BODIPY581/591 for 1 h at 37°C in the dark after being treated as indicated. The cells were then rinsed twice with PBS and examined under a fluorescence microscope. The labeled cells were distinguished by a shift in the fluorescence emission peak from 590 nm to -510 nm, which was proportional to lipid ROS generation and would be measured using a flow cytometer.

Determination of GSH Activity

The glutathione (GSH) concentration was determined using a glutathione assay kit purchased from Jiancheng Bioengineering institute and carried out according to the manufacturer s instructions. The treated cells were harvested and homogenized in PBS on ice, the detected result was read by a microplate reader, and the glutathione in the cell lysate was calculated using the formula provided by the GSH assay kit's product protocol.

Measurement of Intracellular Cysteine

Intracellular cysteine (Cys) levels were determined in the lysates of cells exposed to drugs using a Cys assay kit (BC185, Solarbio) according to the manufacturer's instructions. The final data obtained from a microplate reader at an absorbance of 600 nm was calculated using the formula provided by the Cys assay kit's product protocol.

Mitochondrial Injury Assessment

The change in mitochondrial membrane potential was measured using JC-1 (Dojindo) staining as directed by the manufacturer. The ratio of red fluorescence to green fluorescence was used to describe each group.

Mitochondrial Lipid Peroxidation

The MitoPeDPP (Dojindo), a cell-membrane-permeable probe that specifically localizes in mitochondria due to the triphenylphosphonium moiety, will be used to assess lipid peroxidation in mitochondria. Cells were treated as indicated, then washed twice with PBS and stained with 1 μM MitoPeDPP and 10 μM Hoechst nuclear stain in certain experiments. Following that, images of cells were captured at random by a fluorescence microscope with 100 m scale bars.

Western Blot Assays

Total proteins were isolated using a cell lysis buffer supplemented with protease and phosphatase inhibitors (Beyotime, Shanghai, China). Protein concentrations were measured using a BCA protein assay kit (Beyotime). After boiling in the 1% SDS loading buffer, the protein samples were separated by SDS/PAGE and transferred to polyvinylidene fluoride (PVDF) membranes (Millipore, Billerica, MA). The samples were then incubated with the primary antibodies (GAPDH, SLC7A11, GPX4) overnight before being incubated with the secondary antibody anti-rabbit IgG (925-32211, LICOR) with the membranes. Finally, protein brand images were obtained using an infrared laser two-color image analysis system (Odyssey LICOR, United States). Image J was used to calculate and normalize the objective protein expression level.

Data Analysis

In the study, all results obtained from experiments were independently repeated three times and tested for normality. The continuous variables of normal distribution or nearly normal distribution were displayed as average value ± standard deviation. After homogeneity of variance test, one-way ANOVA and LSD *post hoc* comparisons were used for those meeting data requirements in SPSS 25 or GraphPad Prism 8.0. $P < 0.05$ was considered significantly different.

RESULTS

Solasonine Promoted Cell Death in LUAD Cells

Previous studies have demonstrated that SS has anti-proliferative properties. The Calu-1 and A549 cells, which belong to the LUAD cell lines, were used in this study for cytotoxicity experiments and subsequent examinations. The cells were subjected to the treatments described above, and the IC50 values of SS for Calu-1 or A549 cells were determined to be 15.08 or 21.59 μM, respectively (**Figure 1A**). Based on the findings, Calu-1 cells were found to be more sensitive to SS than A549 cells, so we tailored the appropriate drug concentrations for follow-up work. In addition, the cell morphology changed, with the cells becoming shriveled and even broken as the administration concentration increased (**Figure 1B**). Likewise, the fluorescent images indicated by the SYTOX Green confirmed that SS elicited cell death in a dose-dependent manner (**Figure 1C**).

Ferroptosis Contributed to Solasonine-Induced Growth Inhibition in LUAD Cells

What types of cell death contributed to the solasonine-induced growth inhibition in LUAD cells? This question prompted us to conduct additional research into the work. In the CCK8 assay, the descent was rescued by Z-V, Nec, Fer-1, and Baf-A1, indicating that apoptosis, necroptosis, ferroptosis, and autophagy may play a part in solasonine-induced cell death (**Figure 2A**). Several ferroptosis-related reagents, including inhibitor DFO and inducer RSL3, were used for extra validation to assess the involvement of ferroptosis. Fer-1, a lipid peroxidation inhibitor, and DFO, an iron chelator, are both commonly used ferroptosis inhibitors and are widely used in ferroptosis reports (13). In addition, since their discovery, RSL3 and erastin have been well known for their ferroptosis-induced property (14). The data indicated that Fer-1 and DFO protected both cells from solasonine-induced destruction, however, the toxicity was amplified by the combination of

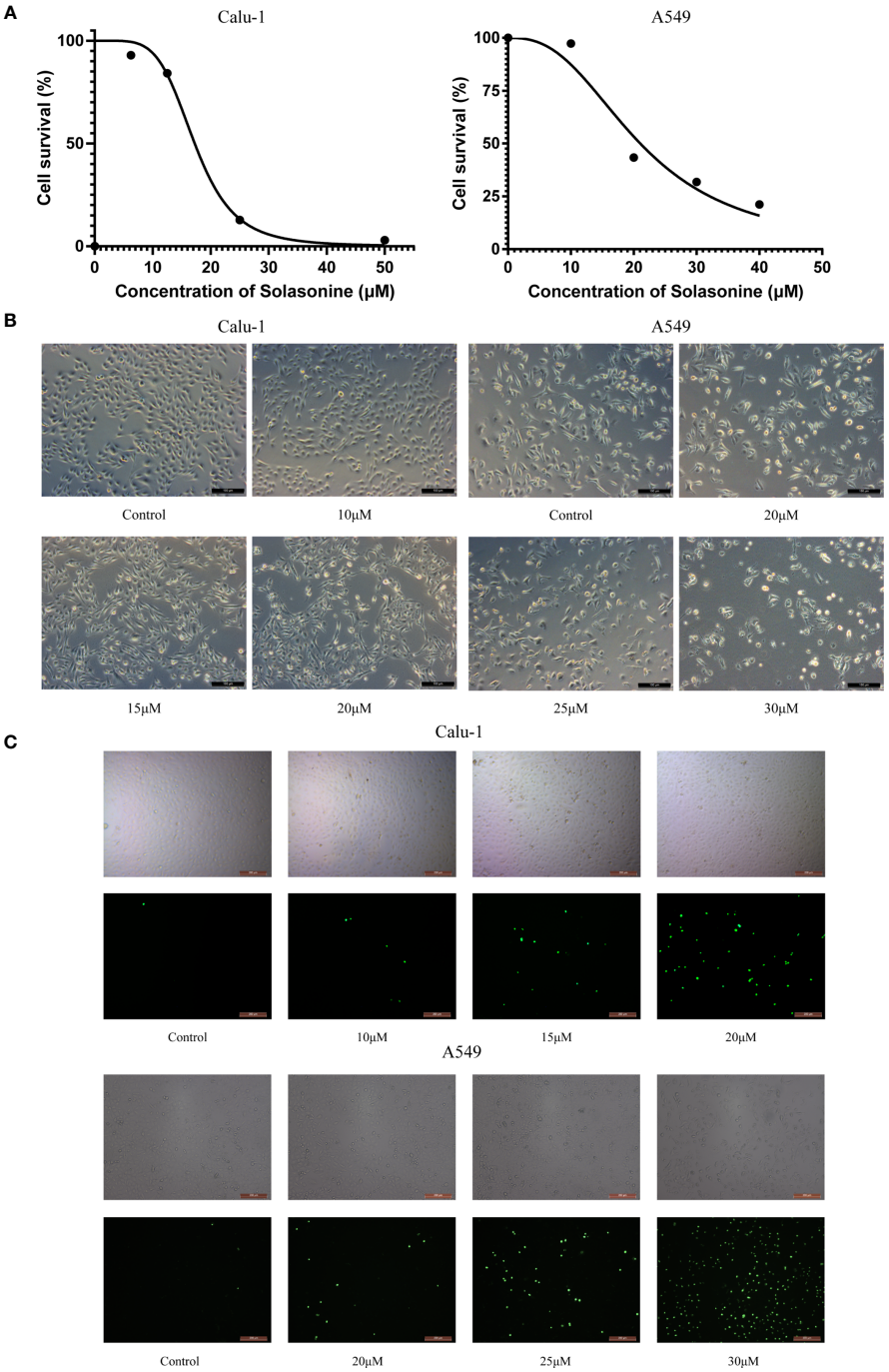

FIGURE 1 | The cytotoxicity of solasonine in LUAD cells. **(A)** The cell viability of Calu-1 and A549 cells was measured using the CCK-8 assay after SS treatment for 24 h. **(B)** Microscope observation of Calu-1 or A549 cells treated with 10, 15, 20 μM or 20, 25, 30 μM of SS for 24 h, respectively. Scale bars: 100 μm. **(C)** Cells were exposed to different concentrations of SS and 100 nM of SYTOX Green for 24 h. The signal was captured and examined through the FITC channel of fluorescence microscopy. Scale bars: 200 μm.

RSL3 and SS (**Figure 2B**). The fluorescent indicator C11-BODIPY581/591 was used to directly observe lipid peroxidation, which is located in the membrane and shifts the fluorescence from red to green when oxidization occurred (15). As expected, solasonine-treated Calu-1 and A549 cells exhibited high fluorescence in green and low fluorescence in red, referring to the accumulation of lipid peroxidation, whereas the Fer-1 restricted this process (**Figures 2C, D**).

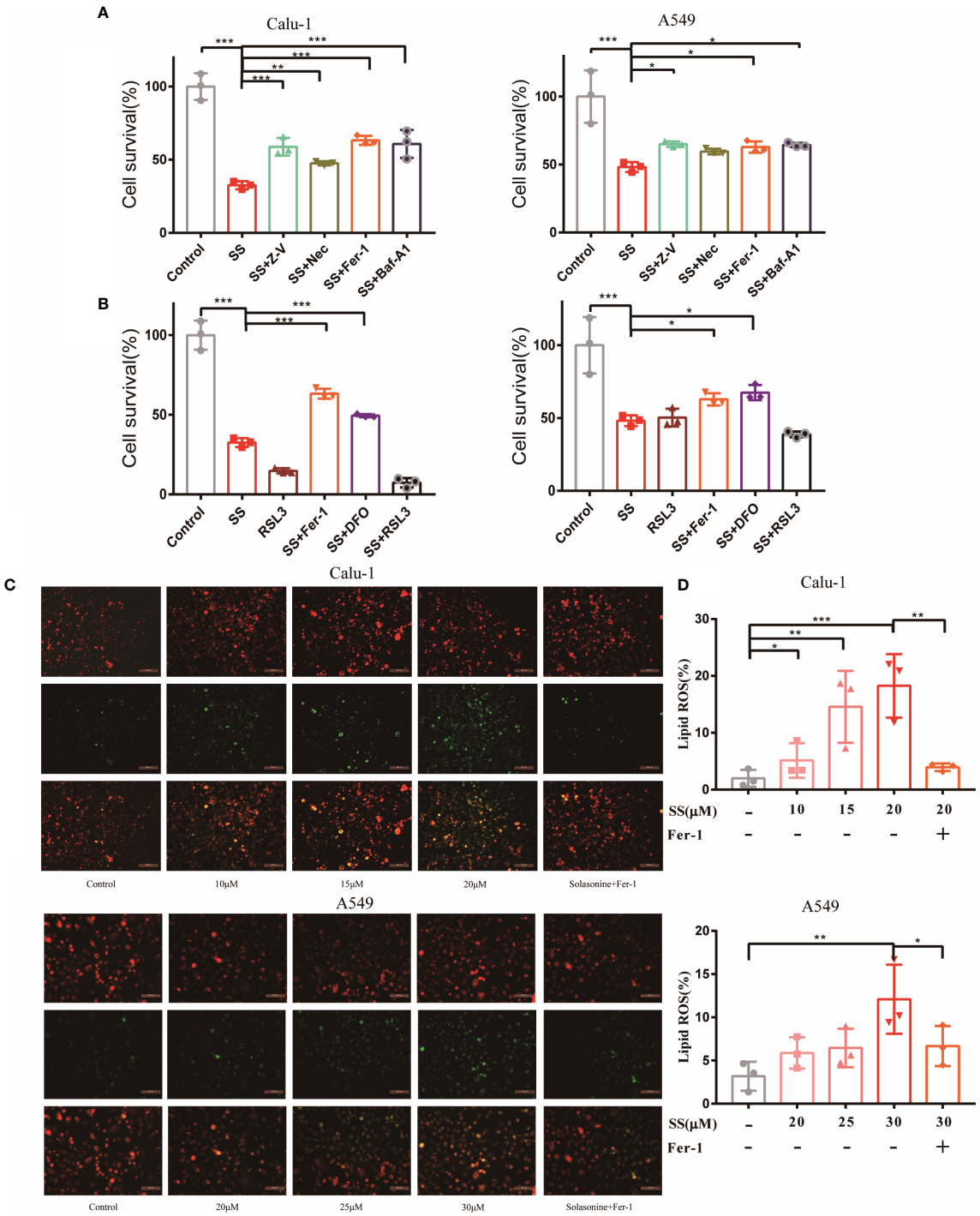

FIGURE 2 | Ferroptosis contributed to solasonine-induced cell death in LUAD cells. **(A, B)** CCK8 assay was used to determine the cell viability of Calu-1 or A549 cells treated with 20 μM or 30 μM SS, respectively, with or without pretreatment of Z-V (20 μM), Nec (30 μM), Fer-1 (1μM), Baf-A1 (100 nM), RSL3 (0.5 μM), and DFO (80 μM). **(C)** Fluorescence microscopy was used to detect the lipid ROS in Calu-1 or A549 cells, which were respectively treated with 10, 15, 20 μM or 20, 25, 30 μM SS for 6 h and pretreated with or without Fer-1(1 μM). Scale bars: 100μm. **(D)** Flow cytometry was used to detect the double signals of C11-BODIPY581/591, which were then digitized and analyzed using histogram statistics. (*P < 0.05, **P < 0.01, ***P < 0.001).

Solasonine Caused Iron Overload and Redox Imbalance in LUAD Cells

Since ferroptosis has been identified, the critical events of the process, which include Fe2+overload and intracellular ROS accumulation, will be investigated and validated in the next step. It should be noted that the occurrence of ferroptosis is dependent on the level of iron content rather than any other metallic element, so measuring the content of Fe2+ is required. Fortunately, Fe2+ was discovered to be required for SS action, as evidenced by the experimental results shown in **Figure 3A**. The levels of Fe2+ increased as drug concentrations increased. However, a high dose of SS had a remarkable effect, which was completely reversed by DFO. On the other hand, intracellular ROS, while not as specific as lipid ROS in ferroptosis, is a major character that runs throughout the entire process. The images demonstrated that the intracellular ROS marked with DCFH-DA probes was excessively generated when SS was administered (**Figure 3B**). Besides the fluorescent images, the detailed information about the integral fluorescent intensity was presented in the histogram (**Figure 3C**).

The Destruction of the Glutathione Redox System Caused by Solasonine Contributed to Ferroptosis in LUAD Cells

When discussing ferroptosis, the glutathione redox system is a popular point of penetration. Intracellular antioxidant enzyme glutathione peroxidase 4 (GPX4), cystine/glutamate transporter SLC7A11, substrate GSH, and Cys all contribute to the antioxidant machinery's response to redox imbalance. The statistical graph displayed that the GSH and Cys decreased significantly when compared to the control group (**Figures 4A, B**).

Furthermore, the Western blot results revealed that the protein expression of GPX4 and SLC7A11 was altered on the sensitive cell line Calu-1 between SS treated cells and the control (**Figure 4C**), and the gray value was transformed into quantitative data displayed by the bar graph (**Figure 4D**). It is suggested that the inhibition of the expression of protein GPX4 and SLC7A11 by SS had parallels with the effect of the positive control group (**Figures 4E, F**). Incidentally, Fer-1 successfully counteracted the effect of SS on these four redox components to some extent. All the evidence pointed to SS paralyzing the antioxidant defense, collapsing the redox balance, and causing ferroptosis.

Mitochondrial Injury Contributed to the Solasonine-Induced Ferroptosis in LUAD Cells

It is well known that the mitochondria are the cell's energy centers, responding to various stimuli and conducting oxidative metabolism in some biological activities. Thus far, studies have shown that mitochondria, a major site for ROS production, play a critical role in ferroptosis (16). Therefore, the relationship between mitochondria and solasonine-induced ferroptosis on Calu-1 cells needs to be revealed.

To begin with, the viability of the cells was determined using the antioxidants Trolox and MitoTEMPO. Trolox, in addition to protecting cells from oxidation, prevents membrane damage for cell integrity, and MitoTEMPO targets superoxide and alkyl radicals found in mitochondria. With the assistance of Trolox and MitoTEMPO, the solasonine-treated cells rejuvenated to a great extent (**Figure 5A**).

According to these findings, mitochondria were found to play a role in solasonine-induced ferroptosis. To gain more insights, mitochondrial functional assessments such as mitochondrial injury and mitochondrial lipid peroxidation assays were launched. According to the diagram, the solasonine-treated group with a low fluorescent ratio showed high mitochondrial membrane potential depolarization paralleled to the positive control. However, this alternation could be reversed after using Fer-1, Trolox, and MitoTEMPO (**Figures 5D, E**). Moreover, the level of mitochondrial ROS production was evaluated using MitoPeDPP dye, a selective probe that targets peroxide in the mitochondrial inner membrane (17). The enhancement of a green, fluorescent signal indicated that erastin or SS action increased mitochondrial ROS production. In addition to Fer-1, Trolox, and MitoTEMPO, they were also capable of reversing excessive mitochondrial ROS production (**Figure 5F**). The data showed that the SS may obstruct mitochondrial function directly and exacerbate the redox imbalance when ferroptosis occurs on LUAC cells.

DISCUSSION

In addition to surgery, chemotherapy, and radiotherapy, common cancer treatment options include innovative targeted therapies that are aimed at selectively eliminating malignant cells to the greatest extent feasible, hopefully without damaging normal cells.

Because the RCD process involves several deadly subroutines that can intervene in tumor formation and progression, it has enabled breakthroughs in cancer treatment (18). To take advantage of this, ongoing research on apoptosis, necroptosis, pyroptosis, and ferroptosis in response to various malignancies is being conducted (19). With a better understanding of the specific molecular mechanism, ferroptosis is looking like a viable option.

Ferroptosis, in particular, is a critical impediment to LUAD development. The high ventilation and active gaseous metabolism of the lungs shape a unique condition in the tumor setting when compared to other tissues. Carcinogenic cells evolve sophisticated mechanisms to adapt to high-oxygen tension under high oxidative stress, indicating that these carcinogenic cells are sensitive to ferroptosis (20). Erastin was the first to trigger LUAD cell ferroptosis in K-ras mutant A549 cells (21). According to the following article, the combination of erastin and cisplatin had a synergistic impact in suppressing LUAD cells in a ferroptosis-like way by depleting GSH and inactivating GPXs (22).

The main character in the current study was the natural compound solasonine, which had an excellent tumor-suppression performance in LUAD, as shown in **Figure 1**. Zhang previously discovered that SS induced apoptosis and cell cycle arrest in acute monocytic leukemia through upregulating

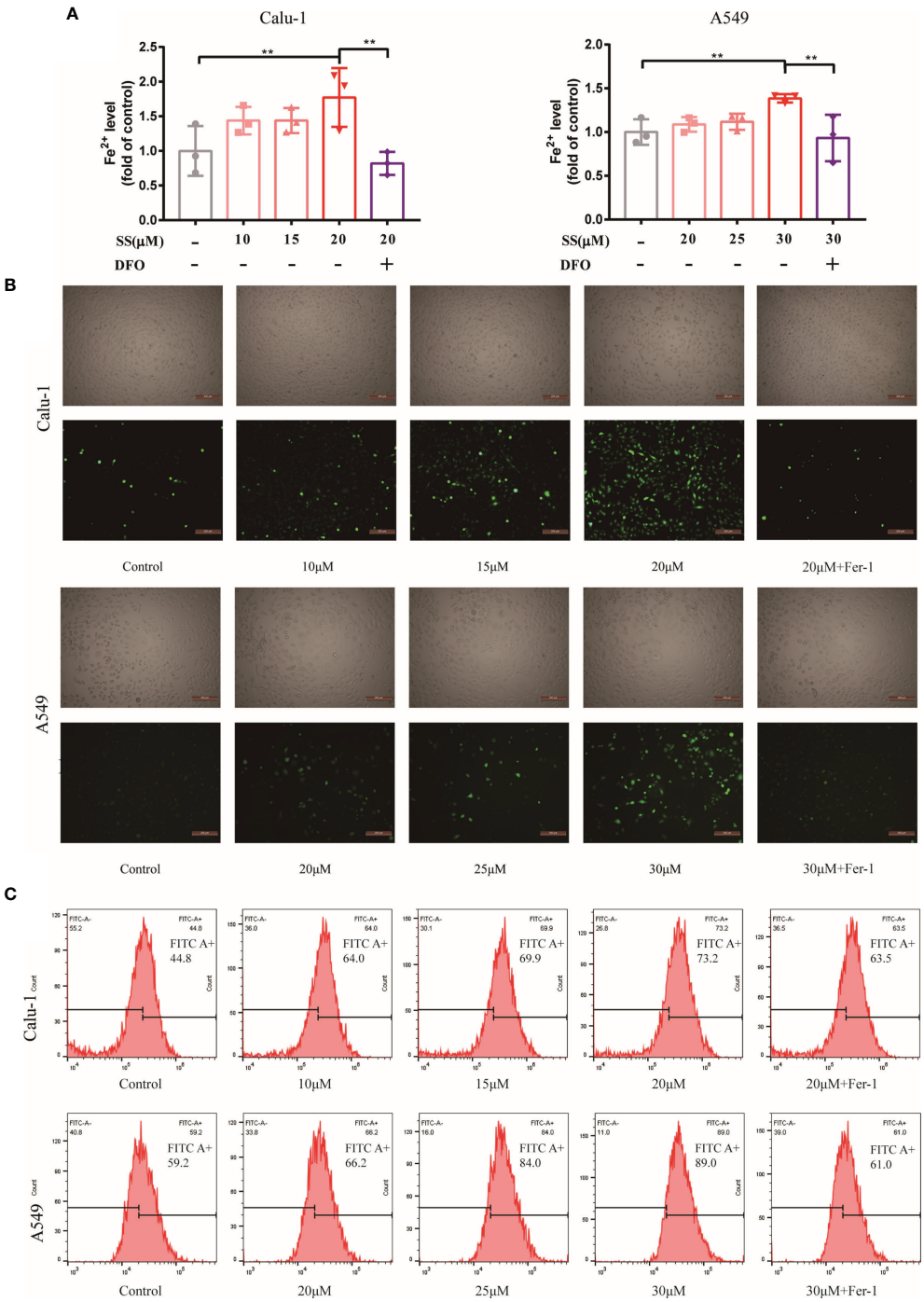

FIGURE 3 | SS caused Fe^{2+} overload and ROS accumulation in LUAD cells. **(A)** Flow cytometry was used to detect the Fe^{2+} level in Calu-1 or A549 cells, which were respectively treated with 10, 15, 20 μM or 20, 25, 30 μM of SS for 6 h and pretreated with or without DFO (80 μM), the data statistic was shown in a histogram. (**P < 0.01). **(B, C)** Fluorescence microscopy and flow cytometry were used to detect ROS production in Calu-1 or A549 cells treated for 6 h with 10, 15, 20 μM or 20, 25, 30 μM SS and pretreated with or without Fer-1 (1 μM), scale bars: 200 μm.

the AMPK/FOXO3A pathway (9). Wang claimed that SS inhibited glioma growth by modulating MAPK signaling *via* p-p38 and p-JNK in the inflammatory signaling pathway (10). Furthermore, SS was found to be effective against gastric cancer through modifying the miR-486-5p/PI3KR1 axis (11). What counts is that SS has been linked to tumor cell ferroptosis, which provides the potential that it may contribute to LUAD cell death *via* ferroptosis. Fortunately, observations of

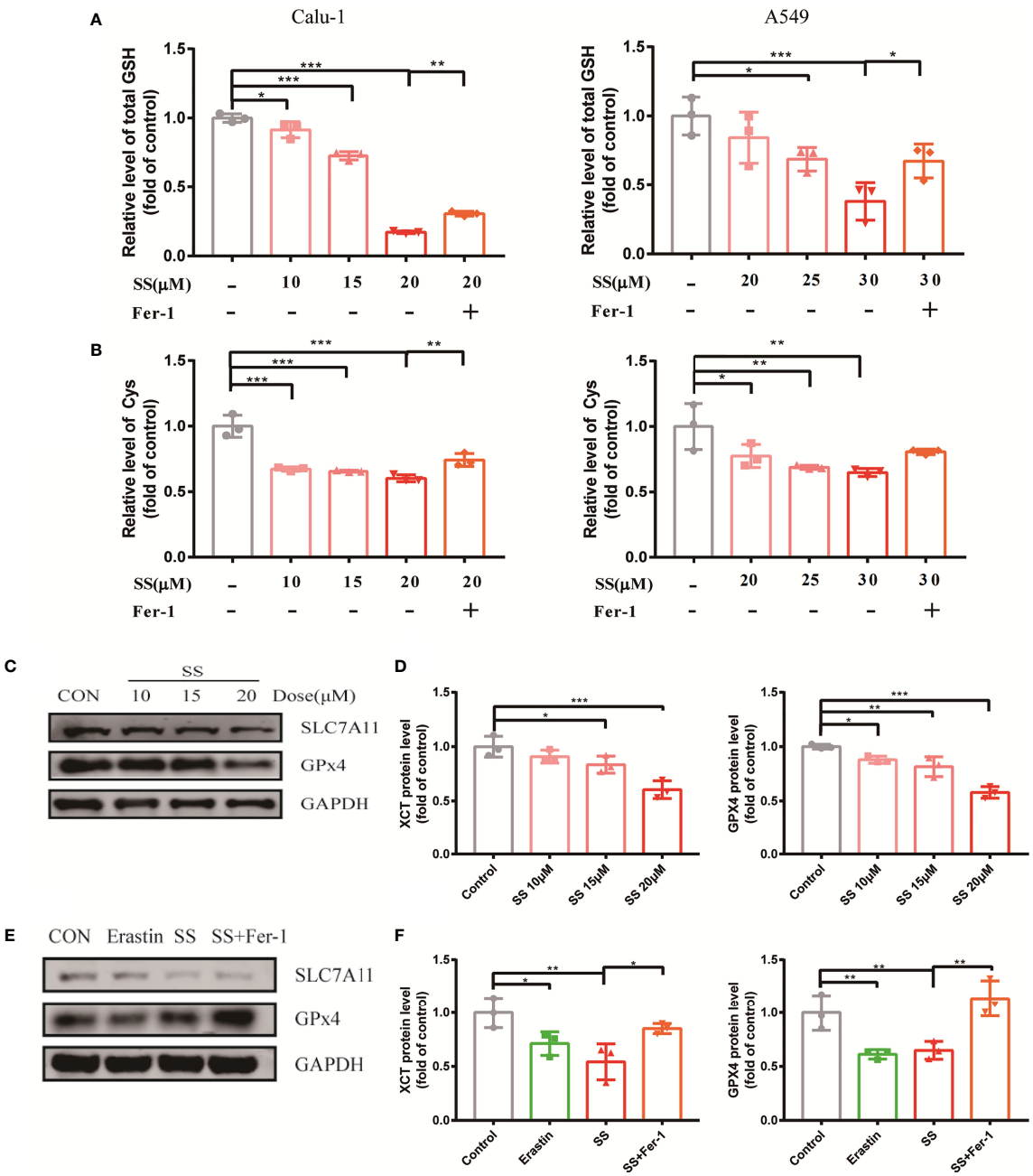

FIGURE 4 | SS attenuated the oxidation resistance of LUAD cells. **(A, B)** GSH or Cys was detected in Calu-1 or A549 cells, which were respectively treated with 10, 15, 20 μM or 20, 25, 30 μM SS for 6 h, and pretreated with or without Fer-1 (1 μM), the data statistic was shown in a histogram (*P < 0.05, **P < 0.01, ***P < 0.001). **(C)** Western blot analysis was used to detect the expressions of SLC7A11 and GPX4 in Calu-1 cells, which were treated with 10, 15, 20 μM SS for 6 h. **(D)** Quantitative analysis of gray value of the SLC7A11 and GPX4 blots. **(E)** Western blotting analysis was used to detect the expressions of SLC7A11 and GPX4 in Calu-1 cells, which were treated with 20 μM SS or 4 μM erastin, with or without Fer-1 (1 μM) for 6 h. **(F)** Quantitative analysis of gray value of the SLC7A11 and GPX4 blots.

ferroptosis-related products and cell viability corroborated the theory.

Since the SS was shown to reduce cell viability, the cell-rescue would be observed by using numerous cell death inhibitors to determine the potential role of various cell death mechanisms. As shown in **Figure 2A**, ferroptosis is partially responsible for cell death. The effect of Fer-1 was similar to that of Z-V, Nec, and Baf-A1, suggesting that solasonine-induced cell death may be a synergistic result. This basic experiment provides a valuable reference in the preliminary stage of the study. Although ferroptosis appears to be independent of other known cell death mechanisms, there are some crossovers between

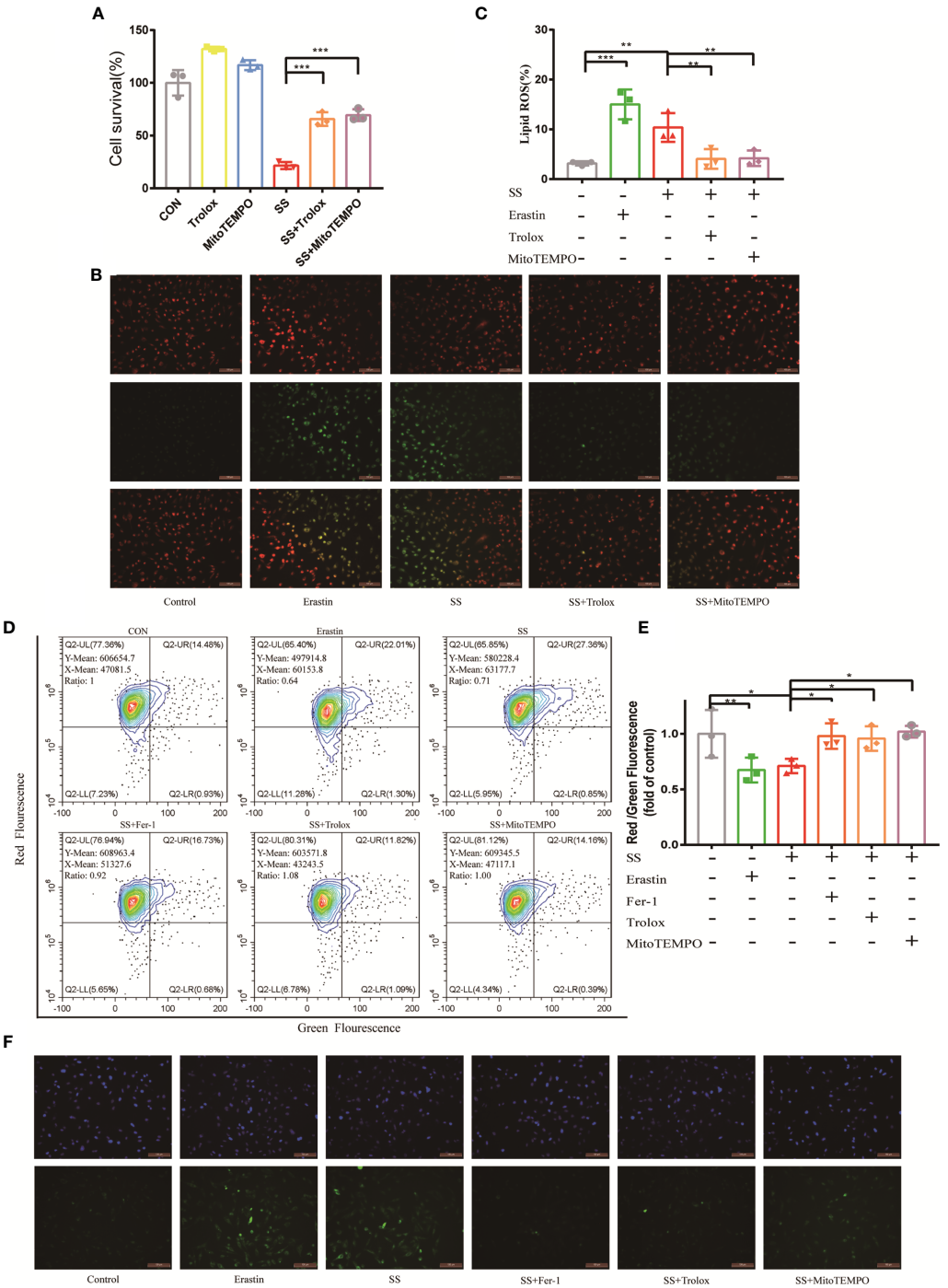

FIGURE 5 | The dysfunction of mitochondria contributed to solasonine-induced ferroptosis in LUAD cells. **(A)** CCK8 assay was used to determine the cell viability of Calu-1,which were treated with 20 μM SS, and pretreated with or without Trolox (100 μM) or Mito TEMPO (10 μM). **(B)** Fluorescence microscopy was used to detect the lipid ROS production in Calu-1cells, which were treated with 20 μM SS for 6 h and pretreated with or without Trolox (100 μM) or Mito TEMPO (10 μM). Scale bars: 100 μm. **(C)** Flow cytometry was used to detect the double signals of C11-BODIPY581/591, which were then digitized and analyzed using histogram statistics (*P < 0.05, **P < 0.01, ***P < 0.001). **(D)** JC-1 staining was used to detect the mitochondrial transmembrane potential (Δψmt) in Calu-1 cells, which were treated with 20 μM SS or erastin (4 μM) for 6 h and pretreated with or without Fer-1 (1 μM), Trolox (100 μM), or Mito TEMPO (10 μM). **(E)** Quantitative analysis of red/green fluorescence ratio of cells. **(F)** Fluorescence microscopy was used to detect the lipid ROS of mitochondria in Calu-1cells, which were treated with 20 μM SS or erastin for 6 h and pretreated with or without Fer-1 (1 μM), Trolox (100 μM), or Mito TEMPO (10 μM). Scale bars: 100 μm. Nuclei were stained with Hoechst 3342. Scale bars: 100 μm.

ferroptosis and other cell death pathways. According to new data, ferroptosis is an autophagic cell death process that is aided by autophagy's hyperactive lysosome activity, which regulates iron homeostasis and ferroptosis-associated ROS production (23, 24). In addition, P53, a canonical tumor suppressor protein, has been found to induce ferroptosis in certain conditions, suggesting molecular interaction between ferroptosis and apoptosis (25). Necroptosis and ferroptosis can be triggered by erastin simultaneously (3). The ferroptosis may affect or be influenced by other RCDs, specific efforts should be made in the future to demonstrate the relationship.

The findings illustrated that SS increased iron accumulation and lipid peroxidation, which could be limited by Fer-1, which is thought to cause ferroptosis in LUAD cells. Essentially, glutathione-dependent antioxidant defenses were the primary focus of research into the mechanism of ferroptosis. Inhibiting the cystine-glutamate antiporter (system Xc–) and the downstream enzyme glutathione peroxidase 4 (GPX4) appears to have depleted glutathione (GSH), a major cellular antioxidant whose synthesis requires Cys, resulting in antioxidant defense failure in ferroptosis (26, 27). SLC7A11 is a subunit of system Xc–, which was identified early on to be one of the most vital regulators in ferroptosis.

Because SLC7A11 is a recognized target in ferroptosis, blocking it will directly rein in the uptake of Cys, which can be utilized for GSH synthesis in the antioxidant process (28). Moreover, SLC7A11 has been found to be highly expressed in non-small cell lung cancer (NSCLC) with a poor prognosis (29). After that, the presence of GSH is required for the other canonical biomarker of ferroptosis, GPX4, to detoxify lipid hydroperoxides (30). It follows that these widely reported biomarkers of ferroptosis were actually affected by SS. Taken together, our findings (**Figure 4**) suggest that suppression of SLC711 and GPx4 expression was likely to be responsible for GSH and Cys depletion in SS therapy.

As our understanding of the mechanism of ferroptosis has progressed, mitochondria have been found to be associated with ferroptosis. Inhibiting the mitochondrial TCA cycle or the electron transfer chain (ETC) reduced hyperpolarization of the mitochondrial membrane potential, lipid peroxide accumulation, and ferroptosis (16, 31). The reaction between ROS and polyunsaturated fatty acids of lipid membranes can enhance lipid peroxidation that depended on the particular lipid precursor afforded by mitochondrial fatty-acid metabolism (32). Moreover, the previous research elaborated that peroxidized lipids were preferentially transferred to mitochondria by the mitochondrial membrane lipid transport protein and intercepting this process would mitigate the effect of ferroptosis (33). Nevertheless, the concrete contribution of mitochondria to ferroptosis may be context-dependent; to determine unambiguously whether mitochondria play a role in solasonine-induced ferroptosis, we set a succession of examinations with mitochondria.

Intriguingly, the cells exposed to SS showed the amplification of mitochondrial lipid ROS, suggesting the potential involvement of mitochondria in solasonine-induced ferroptosis (**Figure 5F**). A sequence of metabolic activities occurs across the mitochondrial membrane, and hyperpolarization of the mitochondrial membrane potential (MMP) has been observed in ferroptosis, which reflects the subsequent formation of lipid ROS (16). The JC-1 was used in this case to signify MMP in the process of accomplishing these tentative efforts. As shown in the image, MMP hyperpolarization was discovered, which was attributed to SS (**Figures 5D, E**). The high cell mortality, lipid ROS production, MMP hyperpolarization, and oxidative lipid in mitochondria were significantly alleviated with the antioxidant Trolox and mitochondrial ROS scavenger MitoTEMPO, highlighting the role of mitochondrial ROS in the SS treatment (**Figure 5**).

CONCLUSIONS

To determine the medical properties of solasonine, this research used LUAD cells that were exposed to the compound, with the results indicating that the compound was able to inhibit LUAD cells and cause ferroptosis. As a result, it was concluded that redox imbalance and mitochondrial malfunction were the essential factors in solasonine ferroptosis. From an objective point of view, there were some unaddressed issues in this study, such as the precise targets and causative link of mitochondrial injury. It is obvious that the research will continue because the next stage will involve more in-depth studies. Incidentally, the findings of this study support previous research and serve as a benchmark for future research into solasonine-induced ferroptosis in the treatment of LUAD.

DATA AVAILABILITY STATEMENT

The raw data supporting the conclusions of this article will be made available by the authors, without undue reservation.

AUTHOR CONTRIBUTIONS

YL and J-CW contributed conception and design of the study. Y-YZ performed the experimental practices and wrote the original draft. Y-BL conducted the analytic process. BZ and Y-BP generated the figures. W-JT and Y-JC contributed to data sorting and literature search. J-HT performed the statistical analysis and analysis outcome. X-DJ reviewed and edited the manuscript. All authors contributed to the article and approved the submitted version.

FUNDING

This research was funded by National Natural Science Foundation of China (81973795), National Natural Science Foundation of China (82174183), Shanghai Pujiang Program (2020PJD057) and Clinical Research Plan of SHDC (SHDC2020CR4052).

REFERENCES

1. Denisenko TV, Budkevich IN, Zhivotovsky B. Cell Death-Based Treatment of Lung Adenocarcinoma. *Cell Death Dis* (2018) 9(2):11. doi: 10.1038/s41419-017-0063-y
2. Dixon SJ, Lemberg KM, Lamprecht MR, Skouta R, Zaitsev EM, Gleason CE, et al. Ferroptosis: An Iron-Dependent Form of Nonapoptotic Cell Death[J]. *Cell* (2012) 149(5):1060–72. doi: 10.1016/j.cell.2012.03.042
3. Xie Y, Hou W, Song X, Yu Y, Huang J, Sun X, et al. Ferroptosis: Process and Function. *Cell Death Differ* (2016) 23(3):369–79. doi: 10.1038/cdd.2015.158
4. Yang WS, Stockwell BR. Synthetic Lethal Screening Identifies Compounds Activating Iron-Dependent, Nonapoptotic Cell Death in Oncogenic-RAS-Harboring Cancer Cells. *Chem Biol* (2008) 15:234–45. doi: 10.1016/j.chembiol.2008.02.010
5. Stockwell BR, Friedmann Angeli JP, Bayir H. Ferroptosis: A Regulated Cell Death Nexus Linking Metabolism, Redox Biology, and Disease. *Cell* (2017) 171(2):273–85. doi: 10.1016/j.cell.2017.09.021
6. Xu T, Ding W, Ji X, Ao X, Liu Y, Yu W, et al. Molecular Mechanisms of Ferroptosis and its Role in Cancer Therapy. *J Cell Mol Med* (2019) 23(8):4900–12. doi: 10.1111/jcmm.14511
7. Pham MQ, Tran THV, Pham QL, Gairin JE. In Silico Analysis of the Binding Properties of Solasonine to Mortalin and P53, and *In Vitro* Pharmacological Studies of its Apoptotic and Cytotoxic Effects on Human HepG2 and Hep3b Hepatocellular Carcinoma Cells. *Fundam Clin Pharmacol* (2019) 33(4):385–96. doi: 10.1111/fcp.12447
8. Huang W, Wang Y, Zhu H, Wu Y, Xie X, Wang D. Solasonine-Induced Apoptosis in Lung Cancer Cell Line H446 and Its Mechanism. *Zhongguo Fei Ai Za Zhi* (2015) 18(7):416–21. doi: 10.3779/j.issn.1009-3419.2015.07.05
9. Zhang H, Tian F, Jiang P, Qian S, Dai X, Ma B, et al. Solasonine Suppresses the Proliferation of Acute Monocytic Leukemia Through the Activation of the AMPK/FOXO3A Axis. *Front Oncol* (2021) 10:614067. doi: 10.3389/fonc.2020.614067
10. Wang X, Zou S, Lan YL, Xing JS, Lan XQ, Zhang B. Solasonine Inhibits Glioma Growth Through Anti-Inflammatory Pathways. *Am J Transl Res* (2017) 9 (9):3977–89.
11. Zhang Y, Han G, Cao Y, Zhang Y, Zhang X, Gong H. Solasonine Inhibits Gastric Cancer Proliferation and Enhances Chemosensitivity Through microRNA-486-5p. *Am J Transl Res* (2020) 12(7):3522–30.
12. Jin M, Shi C, Li T, Wu Y, Hu C, Huang G. Solasonine Promotes Ferroptosis of Hepatoma Carcinoma Cells *via* Glutathione Peroxidase 4-Induced Destruction of the Glutathione Redox System. *BioMed Pharmacother* (2020) 129:110282. doi: 10.1016/j.biopha.2020.110282
13. Liang C, Zhang X, Yang M, Dong X. *Adv Mater (Deerfield Beach Fla)* (2019) 31 (51):e1904197. doi: 10.1002/adma.201904197
14. Sui X, Zhang R, Liu S, Duan T, Zhai L, Zhang M, et al. RSL3 Drives Ferroptosis Through GPX4 Inactivation and ROS Production in Colorectal Cancer. *Front Pharmacol* (2018) 9:1371. doi: 10.3389/fphar.2018.01371
15. Drummen GP, van Liebergen LC, Op den Kamp JA, Post JA. C11-BODIPY (581/591), an Oxidation-Sensitive Fluorescent Lipid Peroxidation Probe: (Micro) Spectroscopic Characterization and Validation of Methodology. *Free Radic Biol Med* (2002) 33(4):473–90. doi: 10.1016/s0891-5849(02)00848-1
16. Gao M, Yi J, Zhu J, Minikes AM, Monian P, Thompson CB, et al. Role of Mitochondria in Ferroptosis. *Mol Cell* (2019) 73(2):354–363.e3. doi: 10.1016/j.molcel.2018.10.042
17. Shioji K, Oyama Y, Okuma K, Nakagawa H. Synthesis and Properties of Fluorescence Probe for Detection of Peroxides in Mitochondria. *Bioorg Med Chem Lett* (2010) 20(13):3911–5. doi: 10.1016/j.bmcl.2010.05.017
18. Chen X, Kang R, Kroemer G, Tang D. Broadening Horizons: The Role of Ferroptosis in Cancer. *Nat Rev Clin Oncol* (2021) 18(5):280–96. doi: 10.1038/s41571-020-00462-0
19. T ang D, Kang R, Berghe TV, Vandenabeele P, Kroemer G. The Molecular Machinery of Regulated Cell Death. *Cell Res* (2019) 29:347–64. doi: 10.1038/s41422-019-0164-5
20. Zhang W, Sun Y, Bai L, Zhi L, Yang Y, Zhao Q, et al. RBMS1 Regulates Lung Cancer Ferroptosis Through Translational Control of SLC7A11. *J Clin Invest* (2021) 131(22):e152067. doi: 10.1172/JCI152067
21. Wu S, Zhu C, Tang D, Dou QP, Shen J, Chen X. The Role of Ferroptosis in Lung Cancer. *biomark Res* (2021) 9(1):82. doi: 10.1186/s40364-021-00338-0
22. Guo J, Xu B, Han Q, Zhou H, Xia Y, Gong C, et al. Ferroptosis: A Novel Anti-Tumor Action for Cisplatin. *Cancer Res Treat* (2018) 50(2):445–60. doi: 10.4143/crt.2016.572
23. Gao M, Monian P, Pan Q, Zhang W, Xiang J, Jiang X. Ferroptosis is an Autophagic Cell Death Process. *Cell Res* (2016) 26(9):1021–32. doi: 10.1038/cr.2016.95
24. Zhou B, Liu J, Kang R, Klionsky DJ, Kroemer G, Tang D. Ferroptosis is a Type of Autophagy-Dependent Cell Death. *Semin Cancer Biol* (2020) 66:89–100. doi: 10.1016/j.semcancer.2019.03.002
25. Mou Y, Wang J, Wu J, He D, Zhang C, Duan C, et al. Ferroptosis, a New Form of Cell Death: Opportunities and Challenges in Cancer. *J Hematol Oncol* (2019) 12(1):34. doi: 10.1186/s13045-019-0720-y
26. Friedmann Angeli JP, Schneider M, Proneth B, Tyurina YY, Tyurin VA, Hammond VJ. Inactivation of the Ferroptosis Regulator Gpx4 Triggers Acute Renal Failure in Mice. *Nat Cell Biol* 16:1180–91. doi: 10.1038/ncb3064
27. Yang WS, SriRamaratnam R, Welsch ME, Shimada K, Skouta R, Viswanathan VS, et al. Regulation of Ferroptotic Cancer Cell Death by GPX4. *Cell* (2014) 156(1-2):317–31. doi: 10.1016/j.cell.2013.12.010
28. Lin W, Wang C, Liu G, Bi C, Wang X, Zhou Q, et al. SLC7A11/xCT in Cancer: Biological Functions and Therapeutic Implications. *Am J Cancer Res* (2020) 10 (10):3106–26.
29. Ji X, Qian J, Rahman SMJ, Siska PJ, Zou Y, Harris BK, et al. xCT (SLC7A11)-Mediated Metabolic Reprogramming Promotes non-Small Cell Lung Cancer Progression. *Oncogene* (2018) 37(36):5007–19. doi: 10.1038/s41388-018-0307-z
30. Friedmann Angeli JP, Krysko DV, Conrad M. Ferroptosis at the Crossroads of Cancer-Acquired Drug Resistance and Immune Evasion. *Nat Rev Cancer* (2019) 19:405–14. doi: 10.1038/s41568-019-0149-1
31. Martínez-Reyes I, Chandel NS. Mitochondrial TCA Cycle Metabolites Control Physiology and Disease. *Nat Commun* (2020) 11(1):102. doi: 10.1038/s41467-019-13668-3
32. Wang H, Liu C, Zhao Y, Gao G. Mitochondria Regulation in Ferroptosis. *Eur J Cell Biol* (2020) 99(1):151058. doi: 10.1016/j.ejcb.2019.151058
33. \Kerins MJ, Milligan J, Wohlschlegel JA, Ooi A. Fumarate Hydratase Inactivation in Hereditary Leiomyomatosis and Renal Cell Cancer is Synthetic Lethal With Ferroptosis Induction. *Cancer Sci* (2018) 109(9):2757–66. doi: 10.1111/cas.13701

Conflict of Interest: The authors declare that the research was conducted in the absence of any commercial or financial relationships that could be construed as a potential conflict of interest.

frontiers | Frontiers in Oncology

REVIEW
published: 26 May 2022
doi: 10.3389/fonc.2022.835549

Potential of Mitochondrial Ribosomal Genes as Cancer Biomarkers Demonstrated by Bioinformatics Results

*Shunchao Bao[1], Xinyu Wang[2], Mo Li[1], Zhao Gao[3], Dongdong Zheng[4], Dihan Shen[5] and Linlin Liu[1]**

[1] Department of Radiotherapy, Second Hospital of Jilin University, Changchun, China, [2] Department of Breast Surgery, Second Hospital of Jilin University, Changchun, China, [3] Nuclear Medicine Department, Second Hospital of Jilin University, Changchun, China, [4] Department of Cardiovascular Surgery, Second Hospital of Jilin University, Changchun, China, [5] Medical Research Center, Second Hospital of Jilin University, Changchun, China

Next-generation sequencing and bioinformatics analyses have clearly revealed the roles of mitochondrial ribosomal genes in cancer development. Mitochondrial ribosomes are composed of three RNA components encoded by mitochondrial DNA and 82 specific protein components encoded by nuclear DNA. They synthesize mitochondrial inner membrane oxidative phosphorylation (OXPHOS)-related proteins and participate in various biological activities *via* the regulation of energy metabolism and apoptosis. Mitochondrial ribosomal genes are strongly associated with clinical features such as prognosis and foci metastasis in patients with cancer. Accordingly, mitochondrial ribosomes have become an important focus of cancer research. We review recent advances in bioinformatics research that have explored the link between mitochondrial ribosomes and cancer, with a focus on the potential of mitochondrial ribosomal genes as biomarkers in cancer.

Keywords: mitochondrial ribosome, bioinformatics, cancer, biomarker, apoptosis, energy metabolism

OPEN ACCESS

Edited by:
Matiullah Khan, AIMST University, Malaysia

Reviewed by:
Sven Dennerlein, University Medical Center Göttingen, Germany
Halina Abramczyk, Lodz University of Technology, Poland

****Correspondence:***
Linlin Liu
1299935176@qq.com

Specialty section:
This article was submitted to Cancer Molecular Targets and Therapeutics, a section of the journal Frontiers in Oncology

Received: *14 December 2021*
Accepted: *27 April 2022*
Published: *26 May 2022*

Citation:
Bao S, Wang X, Li M, Gao Z, Zheng D, Shen D and Liu L (2022) Potential of Mitochondrial Ribosomal Genes as Cancer Biomarkers Demonstrated by Bioinformatics Results. Front. Oncol. 12:835549. doi: 10.3389/fonc.2022.835549

1 INTRODUCTION

In human cells, the vast majority of mitochondria-associated proteins are encoded by nuclear genes and synthesized by cytoplasmic ribosomes. Mitochondria, as endosymbiotic organelles, retain the characteristics of the original genomic DNA of their bacterial ancestors and possess relatively independent gene expression mechanisms (1). Human mitochondrial DNA (mtDNA) encodes two ribosomal RNAs (rRNAs) and a group of transfer RNAs (tRNAs) as well as oxidative phosphorylation (OXPHOS)-related proteins. These mitochondrially encoded proteins are

Abbreviations: mtDNA, mitochondrial DNA; rRNA, ribosomal RNA; tRNA, transfer RNA; LSU, Large Subunit; SSU, Small Subunit; MRPs, Mitochondrial Ribosomal Proteins; OXPHOS, Oxidative Phosphorylation; DAP3, Death-Associated Protein 3; GEO, Gene Expression Omnibus; TCGA, The Cancer Genome Atlas; WGCNA, Weighted Gene Co-Expression Network Analysis; RNAseq, RNA sequencing; ceRNAs, competing endogenous RNAs; DNAseq, DNA sequencing; HCC, Hepatocellular Carcinoma; CRC, Colorectal Cancer; OC, Ovarian Cancer; BLCA, Bladder Cancer; SNP, Single Nucleotide Polymorphisms.

located within the inner mitochondrial membrane and are synthesized by mitochondrial ribosomes (2). The mitochondrial ribosome differs from bacterial and cytoplasmic mitochondria with respect to complexity, structure, and mechanisms of action. It is composed of three RNA components encoded by mitochondrial DNA and 82 specific protein components encoded by nuclear DNA (3, 4). Over the past decade, the roles of mitochondrial ribosomal proteins in apoptosis and cellular energetics have been revealed (5, 6). Importantly, the inhibition of cell death, proliferative signaling, and deregulation of cellular energetics are hallmarks of cancer (7).

Margaret Dayhoff (1925–1983), an American physical chemist known as "the father of bioinformatics", was the first to apply computational methods to the biological realm (8). Relying on advances in both molecular biology and computer science, bioinformatics has been evolving over several decades. The application of microarray technology, next-generation sequencing, and big data analysis techniques has revealed the important roles of mitochondrial ribosomal proteins in cancer biology.

This review examines the link between mitochondrial ribosomes and cancer. In particular, the composition, structure, and function of the mitochondrial ribosome are described. Bioinformatics tools, including relevant databases and methods for sequencing and analysis, are described with a focus on their application to the mining of candidate mitochondrial ribosomal protein biomarkers for malignancy. This review adds a bioinformatics perspective to research on mitochondrial ribosomes in relation to malignancies.

2 MITOCHONDRIAL RIBOSOMES

2.1 Components and Structure

In all organisms, the mature mitochondrial ribosome is composed of a large subunit (LSU) responsible for catalyzing peptidyl transferase reactions and a small subunit (SSU) providing a platform for mRNA binding and decoding (**Figure 1**). The 28S mt-SSU of the mammalian mitochondrial ribosome consists of one 12S rRNA and 29 mitochondrial ribosomal proteins (MRPs), whereas the 39S mt-LSU consists of one 16S rRNA, 48 MRPs, and one structural tRNA (9, 10). Using deep RNA sequencing, Alan Brown identified this structural tRNA as mt-tRNA ^{Val}, a molecule whose position resembles that occupied by 5S rRNA in the cytoplasmic ribosome (11). In addition, 16 mt-SSU proteins and 28 mt-LSU proteins are homologous to their counterparts in *Escherichia coli*, and the rest are mitochondria-specific proteins (12, 13). These nuclear-encoded subunit proteins are synthesized within the cytosol and enter mitochondria for subsequent assembly, mediated by chaperones and the transmembrane transport complex including Translocase of the Outer mitochondrial Membrane (TOM) and Translocase of the Inner Membrane (TIM) (14, 15). Unlike cytoplasmic ribosomes, the majority of mitochondrial ribosomes are permanently anchored to the inner mitochondrial membrane by mL45 (*MRPL45*) of the large subunit (4). The large and small subunits are connected by three protein–protein and six protein–RNA inter-subunit bridges, whereas bridges in bacterial and eukaryotic cytoplasmic ribosomes mainly consist of conserved RNA–RNA interactions (16). In addition, mitochondrial ribosomes differ from cytoplasmic and bacterial ribosomes by a high RNA-to-protein ratio (17). Finally, two relevant publications are cited that provide the nomenclature of mitochondrial ribosomal proteins for readers to consult (18, 19).

2.2 MRPs and Energy Metabolism

Mitochondrial ribosomes are responsible for the translation of 13 subunit proteins of OXPHOS complex I, III, IV and V, which are encoded by the mitochondrial DNA. These proteins located in the inner mitochondrial membrane include seven subunits of complex I (NADH: ubiquinone oxidoreductase), one subunit of complex III (ubiquinone: cytochrome c oxidoreductase), three subunits of complex IV (cytochrome C: oxidoreductase), and two subunits of complex V (ATP synthase) (**Figure 2**) (2, 11, 20). Single-stranded mRNAs formed after mtDNA transcription are enriched at the SSU neck, where the pentatricopeptide repeat protein *MRPS39* (mS39) recognizes and binds to the 5′ end of the mRNA and activates the translation machinery (21, 22).

In mammalian cells under normal conditions, more than 80% of cellular ATP requirements are met by ATP generated by oxidative phosphorylation (OXPHOS). The OXPHOS metabolic pathway generates ATP by transporting electrons along a series of transmembrane protein complexes in the inner mitochondrial membrane, called the electron transport chain (ETC). Energy transport is achieved by the flow of electrons between complex I, complex II, coenzyme Q10, complex III, cytochrome c, and complex IV, with oxygen as the terminal electron acceptor (23). A methylation study has revealed a unique mechanism by which arginine and lysine methylation of *MRPS23* promote breast cancer metastasis by regulating OXPHOS (24). Bioinformatics analyses have revealed that *MRPS5* is closely related to the function of OXPHOS complex I and the acetylation status of *MRPS5* is directly regulated by the NAD^+-dependent deacetylase sirtuin-1 (*SIRT1*), indicating that the *SIRT1/MRPS5* axis is involved in metabolic reprogramming and tumor progression (25). *MRPL13* expression is reduced in OXPHOS-deficient hepatoma cells (SNU354 and SNU423 cell lines), and the specific inhibition of mitochondrial glycosomal translation by siRNA-mediated knockdown of *MRPL13* decreases expression of the OXPHOS complex IV subunit protein *COX2* (26).

Metabolic reprogramming in cancer cells confers the ability to adjust metabolic pathways to support heterogeneous biological processes. According to the Otto Warburg theory, glycolysis is upregulated in cancer cells compared to that in normal cells (7). However, this does not mean that oxidative phosphorylation is universally downregulated in cancer. A meta-analysis has suggested that the average contribution of OXPHOS to ATP production is 80% in normal cells and 83% in cancer cells (27), consistent with *in vivo* data from a study by Vaupel et al., who showed that the mitochondrial respiratory capacity is not always

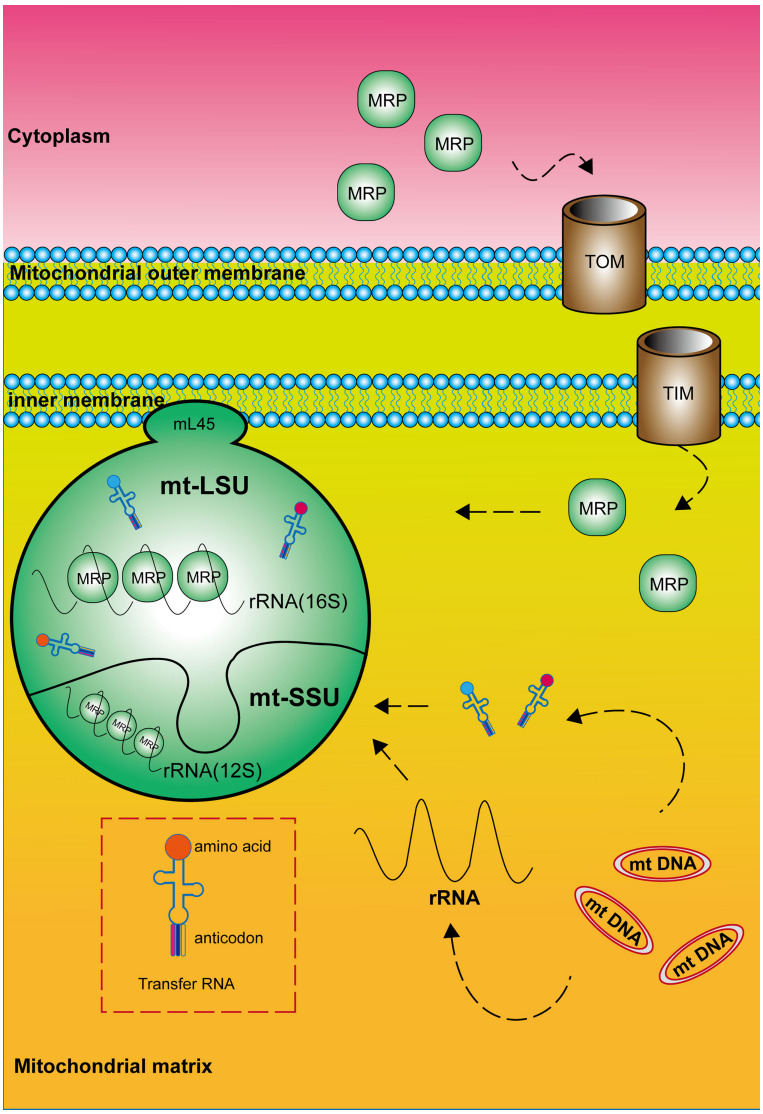

FIGURE 1 | Composition and structure of the mitochondrial ribosome. The mature mitochondrial ribosome, which consists of a large and a small subunit, is permanently anchored to the inner mitochondrial membrane by *MRPL45* (mL45) of the large subunit. Mitochondrial ribosomal proteins are synthesized within the cytosol and enter mitochondria mediated by the transmembrane transport complex including Translocase of the Outer mitochondrial Membrane (TOM) and Translocase of the Inner Membrane (TIM). RNA components are encoded by mitochondrial DNA.

functionally impaired (28). Variation in the contribution of OXPHOS among cancer types may be explained by differences in the mtDNA content. In particular, the mtDNA content is higher in many cancer tissues than in normal tissues, including tissues from patients with endometrial cancer, colorectal cancer, ovarian cancer, prostate cancer, head and neck squamous cell carcinoma, lung adenocarcinoma, esophageal squamous cell carcinoma, and thyroid cancer (20, 29). There is growing evidence that some cancers are critically dependent on OXPHOS, and inhibiting OXPHOS can effectively target specific cancer subtypes. For example, patients with diabetes receiving the anti-diabetic drug metformin have a lower incidence of cancer and a better prognosis than patients not receiving metformin (30, 31). *In vitro* studies suggest the effect of metformin is mediated by the inhibition of OXPHOS complex I, resulting in decreased ATP production by cancer cells (32).

Since the expression analyses of genes encoding OXPHOS related proteins in mtDNA may not fully reflect the function of OXPHOS, proteomic or metabolomic approaches are required to fully characterize OXPHOS activity. Furthermore, given that mitochondrial ribosomes are responsible for the synthesis of OXPHOS related proteins, relevant studies targeting the expression of genes encoding mitochondrial ribosomal proteins and the function of MRPs should not be overlooked.

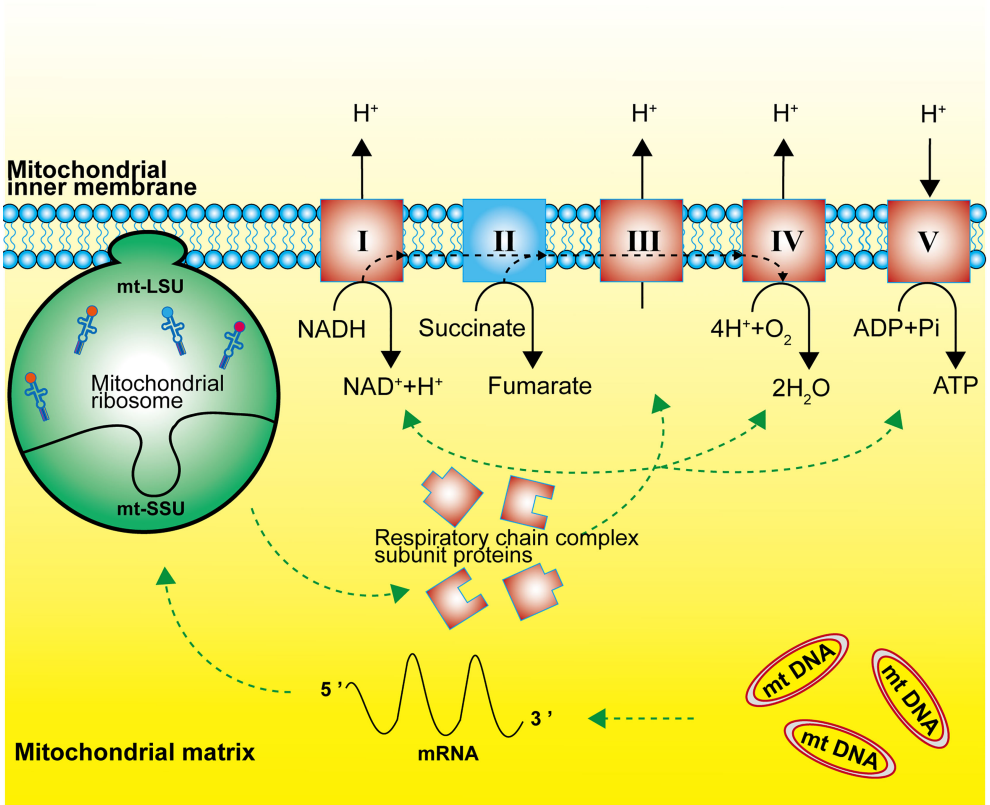

FIGURE 2 | Function of the mitochondrial ribosome. Mitochondrial ribosomes synthesize the subunit proteins of OXPHOS complex I, III, IV and V, which are encoded by the mitochondrial DNA. The dashed black line represents the flow of electrons.

2.3 MRPs and Apoptosis

One of the hallmarks of tumorigenesis and tumor progression is the evasion of apoptosis in cancer cells, and traditional chemoradiotherapy largely relies on the induction of cancer cell apoptosis. The mitochondrial pathway is an important apoptosis pathway and is regulated by pro-apoptotic factors (such as Bax and Bak) as opposed to anti-apoptotic factors (such as Bcl-2 and Bcl-xL) from the Bcl-2 (B-cell Lymphoma 2) protein family (33, 34). Subsequent mitochondrial outer membrane permeabilization (MOMP) and the release of mitochondrial pro-apoptotic proteins (cytochrome c, SMAC, and OMI) into the cytoplasm results in the activation of the caspase family of proteases, which promote apoptosis *via* a cascade of reactions, leading to cell death (35, 36). Among the mitochondrial ribosomal proteins, *MRPL41* (mL41), *MRPS29* (mS29), and *MRPS30* (mS30) have been implicated in the regulation of apoptosis.

In human cells, Bcl-2 blocks the apoptosis-inducing ability of *MRPL41* (mL41) *via* multiple mechanisms, and amino acid residues 13–17 of mL41 are essential for binding to Bcl-2; accordingly, mL41 has also been named BCL-2-interacting mitochondrial ribosomal protein (BMRP). *MRPS29* (mS29), originally also known as death-associated protein 3 (DAP3), is strongly associated with the Fas receptor-associated death-inducing signaling complex. *MRPS30* (mS30) is also known as programmed cell death protein 9 (PDCD9) (37). Although the roles of these three MRPs in the regulation of apoptosis are well-established, studies of their roles in cancer biology are limited. We utilized the visualization tool UALCAN (http://ualcan.path.uab.edu/index.html (38).) to analyze the gene expression data for these three genes from The Cancer Genome Atlas (**Figure 3**). These three representative genes are highly expressed in many malignancies, such as lung and breast cancer ($p < 0.01$) and can be intensively studied as potential tumor biomarkers. The expression of gene MRPS29 is higher in TCGA gastric adenocarcinoma samples than in controls (normal n = 34; primary tumor n = 415), consistent with the published conclusion of Jia y (40). Interestingly, they are not always highly expressed in cancer. For example, *MRPL41* and *MRPS30* are under expressed in renal clear cell carcinoma ($p < 0.01$), which may be associated with tumor heterogeneity, but requires further investigation.

3 BIOINFORMATICS, MITOCHONDRIAL RIBOSOMES, AND MALIGNANCY

In the early 1960s, bioinformatics was developed along with advances in molecular biology and computer science. In the

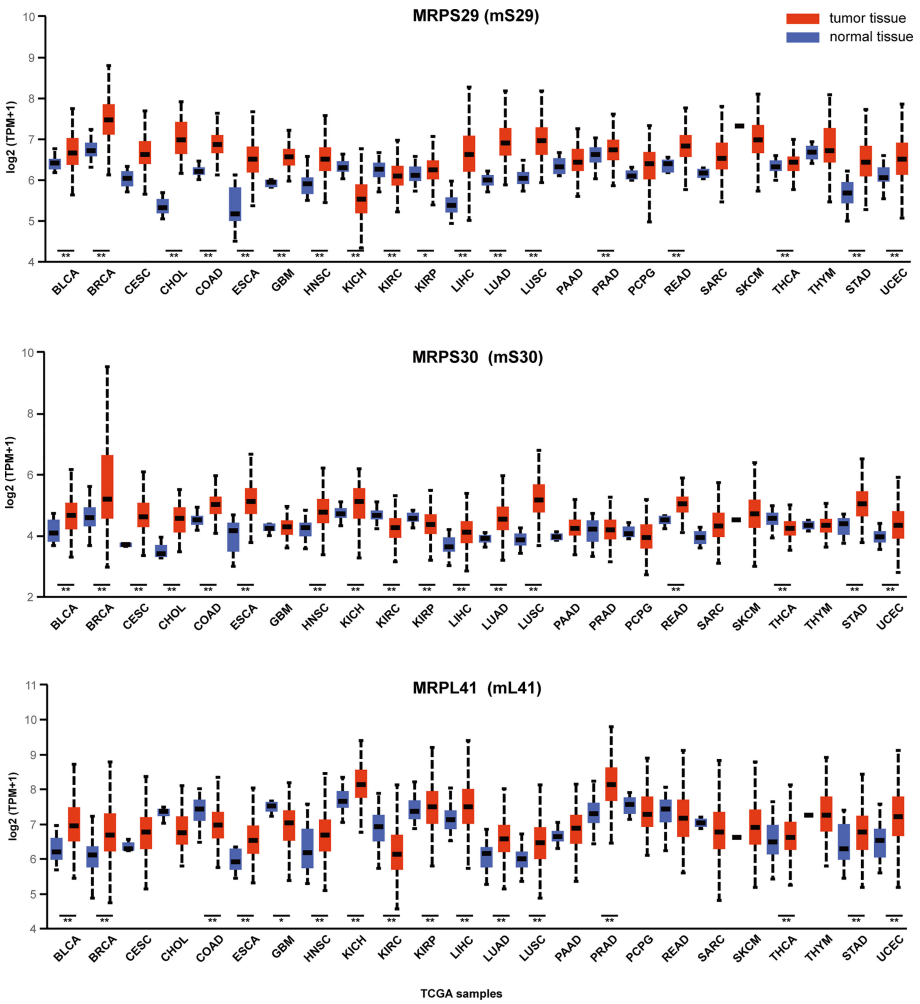

FIGURE 3 | Expression of MRPS29, MRPS30, MRPL41 across TCGA cancers. Three representative mitochondrial ribosomal genes are differentially expressed in cancer. TPM is the normalization of gene reads derived from high-throughput sequencing (39). (*p < 0.05; **p < 0.01).TPM, Transcripts Per Kilobase Million; BLCA, Bladder urothelial carcinoma; BRCA, Breast invasive carcinoma; CESC, Cervical squamous cell carcinoma; CHOL, Cholangiocarcinoma; COAD, Colon adenocarcinoma; ESCA, Esophageal carcinoma; GBM, Glioblastoma multiforme; HNSC, Head and Neck squamous cell carcinoma; KICH, Kidney Chromophobe; KIRC, Kidney renal clear cell carcinoma; KIRP, Kidney renal papillary cell carcinoma; LIHC, Liver hepatocellular carcinoma; LUAD, Lung adenocarcinoma; LUSC, Lung squamous cell carcinoma; PAAD, Pancreatic adenocarcinoma; PRAD, Prostate adenocarcinoma; PCPG, Pheochromocytoma and Paraganglioma; READ, Rectum adenocarcinoma; SARC, Sarcoma; SKCM, Skin Cutaneous Melanoma; THCA, Thyroid carcinoma; THYM, Thymoma; STAD, Stomach adenocarcinoma; UCEC, Uterine Corpus Endometrial Carcinoma.

2000s, major innovations in sequencing technology as well as decreasing costs led to the arrival of the "big data" era, with bioinformatics data mining and management forming a new area of expertise (41). Bioinformatics analytics based on next-generation sequencing aim to apply advanced computational tools and databases to convert sequencing signals into data with interpretable information. The whole analysis process can be simplified into three steps. The first step consists of processing the raw sequencing instrument signal into nucleotide bases and short-read data (42). The second step consists of alignment to the reference sequence or *de novo* assembly of nucleotide reads and subsequent variant detection, etc. (43). The third step relates sample-specific genomic profiles to disparate descriptive annotations, followed by statistical analysis and visualization. A comprehensive review (with classification and description) of major DNA, RNA, and protein related bioinformatics databases with publicly available tools was performed by Chen etc. (44–47).

With respect to bioinformatics and cancer, valuable databases have been established. For example, the Gene Expression Omnibus (GEO http://www.ncbi.nlm.nih.gov/geo/summary/) is a widely used database supported by the National Center for Biotechnology Information (NCBI), which primarily hosts global gene expression data for access by the research community (48). The Cancer Genome Atlas (TCGA http://cancergenome.nih.gov/abouttcga) is the landmark cancer genomics program initiated and funded by the National Institutes of Health to molecularly

characterize more than 20,000 primary cancers with the goal of improving cancer diagnosis, treatment, and prognosis prediction (49, 50). The massive genomic, epigenomic, transcriptomic, and proteomic data generated from sequencing are all available for subsequent bioinformatics analyses. TCGA data are based on microarrays (to test nucleic acids and proteins) and next-generation sequencing (for global analyses of nucleic acids), including but not limited to RNA sequencing, DNA sequencing, and reverse-phase protein arrays.

To meet the demand for multi-dimensional comprehensive analyses of massive genomic data, advanced visual analysis methods, such as weighted gene co-expression network analysis (WGCNA), have been developed. New advances in the field of mitochondrial ribosomes and malignancies using common high-throughput sequencing and bioinformatics techniques, coupled with *in vitro* and *in vivo* experimental validation, are described below. We have produced two Tables for readers' access based on the findings mentioned below (**Tables 1**, **2**).

3.1 RNA Sequencing

RNA sequencing (RNAseq) can be used to rapidly identify and quantify rare and common transcripts across a broad range of samples, providing information regarding gene expression, gene fusions, non-coding RNAs, exons, etc. (98).

3.1.1 Differential Gene Expression

Bioinformatic data analyses combined with *in vitro* and *in vivo* experimental results have revealed that *MRPL13* is highly expressed in non-small cell lung cancer tissues and cell lines and can promote cancer cell proliferation; the locus is, therefore, an independent tumor marker and candidate therapeutic target (51). Expression levels of *MRPS6*, *MRPS10*, *MRPS23*, and *MRPS31* are significantly elevated in breast cancer cells and tissues, and these findings have been corroborated by corresponding cell-based functional assay results (52, 53). In addition, *MRPS23* has been identified as a driver of proliferation in luminal breast cancer, as supported by a series of *in vitro* and *in vivo* studies (54, 55). The depletion of MRPS29 functions *via* the β-Catenin/Lgr5/Bcl-2 axis to induce drug resistance in gastric cancer cells (99). *MRPL54*, *EZH2*, *PPARGC1A*, and *EIF2AK4* were identified as hub genes in bioinformatics analysis of hepatocellular carcinoma (HCC). RNA sequence data extracted from TCGA, and the gene signatures based on these loci showed good predictive ability for HCC prognosis (57, 58). Using a similar data mining approach, 12 genes, including *MRPS23*, were identified as promising predictors with an important role in the pathogenesis of colorectal cancer (CRC) (56). *MRPS12* expression is significantly higher in ovarian cancer than in normal ovarian tissues and is positively correlated with the infiltration of macrophages and neutrophils (59). Another bioinformatics analysis using GEO data revealed seven differentially expressed genes related to osteosarcoma metastasis, including *MRPS7*, but further experimental studies are still needed to elucidate the biological functions and mechanisms of action of these genes (60).

3.1.2 Gene Fusions

Structural chromosomal rearrangements may result in the exchange of coding or regulatory DNA sequences between genes, and such gene fusions are strong driver mutations in the formation of malignant tumors, providing fundamental insights into mechanisms underlying tumorigenesis (100).

Fusion genes and epigenetic regulators (microRNAs, long non-coding RNAs, etc.) constitute an important part of the genomic landscape of tumors, including roles in CRC occurrence and progression. A tumor-specific gene fusion named *MRPS31-SUGT1*, generated by an intrachromosomal translocation on chromosome 13 and whose sequence was 100% identical to that of the lncRNA *MRPS31P5*, was discovered. *MRPS31P5* may be an

TABLE 1 | Association between mitochondrial ribosomal genes and cancer revealed by high-throughput sequencing.

Sequencing Categories	Molecular Event	*Molecular Signatures*	Cancer	Reference
RNA sequencing	Differential Gene Expression	*MRPL13*	Non-small cell lung cancer	(51)
		MRPS6 MRPS10 MRPS31	Breast cancer	(52, 53)
		MRPS23	Luminal breast cancer	(54, 55)
			Colorectal cancer	(56)
		MRPL54	Hepatocellular carcinoma	(57, 58)
		MRPS12	Ovarian cancer	(59)
		MRPS7	Osteosarcoma	(60)
		MRPL27	Lung adenocarcinoma	(61)
		MRPL9	Hepatocellular carcinoma	(40)
		MRPS18A	Cholangiocarcinoma	(62)
	Gene Fusions	*MRPS31-SUGT1*	Colorectal cancer	(63)
		MRPS30-ARID2	Intimal sarcoma	(64)
	LncRNAs	*MRPL23-AS1*	Bladder cancer	(65)
			Hepatocellular carcinoma	(66)
		LINC00152-USF1/MRPL52	Oral squamous cell carcinoma	(67)
		TRIM52-AS1-MRPS18A	Hepatocellular carcinoma	(68)
DNA sequencing	SNPs	*rs2839698-MRPL23-AS1*	Hepatoblastoma	(69)
		rs3024270 -MRPL23-AS1		
		rs4919510-MRPL43	Colorectal cancer	(70)
	Methylation	*lnc-MRPL3-2*	Neuroblastoma	(71)

TABLE 2 | Association between mitochondrial ribosomal genes and clinical features of cancer revealed by bioinformatics analyses.

Clinical Features	Cancer	Molecular Signatures	Reference
Prognosis	Head and neck squamous cell carcinoma	*MRPL47*	(72)
	Neuroblastoma	*MRPL11*	(73, 74)
	Non-small cell lung cancer	*MRPL15*	(75)
	Lung adenocarcinoma	*MRPL42*	(76)
	Breast cancer	*MRPL3*	(77)
		MRPL13	(78–81)
		MRPL12	(82)
		MRPL13	
	Gastric cancer	*MRPS5*	(83)
		MRPL35	(84)
		MRPS29	(85)
		MRPS17	(86)
	Hepatocellular carcinoma	*MRPL9*	(87)
		MRPS12	(88)
	Cholangiocarcinoma	*MRPL27*	(89)
	Colorectal cancer	*MRPL52*	(90)
		MRPL35	(91)
	Ovarian cancer	*MRPL15*	(92)
	Adrenocortical carcinoma	*MRPS23*	(93)
Metastasis	Breast cancer	*MRPL52*	(94)
		MRPL15	(95)
	Ovarian cancer	*MRPL38*	(96)
Drug responsiveness	Muscle invasive bladder cancer	*MRPL4*	(97)

important gene expression regulator and is a potential biomarker for detecting early CRC events (63). Intimal sarcoma is a rare, histologically heterogeneous tumor that usually originates from the pulmonary artery. Using data from the American Association for Cancer Research Project Genomics Evidence Neoplasia Information Exchange (AACRP GENIE) database, Roszik characterized genetic alterations in 13 patients with intimal sarcoma and their clinical value and identified genomic rearrangement events, especially the fusion of *MRPS30-ARID2* and *PDE4DIP-NOTCH2* (64).

3.1.3 Non-Coding RNAs

It is estimated that more than 90% of mammalian genomes are transcribed as non-coding RNAs. Long non-coding RNAs (lncRNAs) are broadly defined as non-coding RNA molecules longer than 200 nucleotides and lack the ability to encode proteins due to the lack of open reading frames (101, 102). LncRNAs located in nuclei regulate the expression of downstream target genes through epigenetic modification (103). The aberrant expression of lncRNAs leads to the development of many diseases such as cancer (104, 105).

lncRNAs have diverse functions in cancer immune responses and the tumor microenvironment. To investigate the immune-related lncRNA (IRlncRNA) signature for predicting bladder cancer (BLCA) prognosis and immunotherapy response, Wu extracted BLCA data from TCGA. Ultimately, eight IRlncRNAs with prognostic significance, including *MRPL23-AS1*, were identified as immunotherapy-related biomarkers (65). A recent study of oral squamous cell carcinoma has revealed a novel *LINC00152-USF1/MRPL52* signaling axis that promotes tumor growth. The long intergenic non-protein-coding RNA 152 (*LINC00152*) was identified as an oncogenic lncRNA in multiple cancers, which physically interacts with upstream transcription factor 1 (*USF1*) and can bind to the promoter region of *MRPL52* and activate its transcription (67). In another study, a risk score system based on five lncRNAs, including *MRPL23-AS1*, was used to predict the survival of patients with HCC with cirrhosis (66). Moreover, an *in-vitro* experimental study combined with a luciferase reporter assay revealed that the lncRNA *TRIM52-AS1* sponged *miR-514a-5p* to facilitate HCC progression through increasing *MRPS18A* expression (68).

3.1.4 CeRNAs

Competing endogenous RNAs (ceRNAs) are transcripts that regulate each other at the post-transcriptional level by competing for shared miRNAs. ceRNA networks, which link the function of protein-coding mRNAs and noncoding RNAs, contribute to the pathogenesis of cancers (106). Furthermore, host microbiota contributes to many diseases, including cancer. Therefore, Xiangzhou Tan constructed a ceRNA network using data from TCGA and GEO databases to identify the mechanisms underlying microbiota-mediated CRC development and progression, among which four gene signatures (*MRPL23-AS1*, *FRMD6-AS2*, and *LIFR-AS1*) were identified as independent prognostic factors for CRC (107).

3.2 DNA Sequencing

DNA sequencing (DNAseq) is used to detect nucleotide alterations, providing DNA-level information, such as insertions, deletions, single nucleotide polymorphisms (SNPs), as well as methylation *status* (108).

3.2.1 Single Nucleotide Polymorphisms

SNPs are single bases in the genome with variation in a population. SNP-based DNA microarray technology can measure allele-specific copy numbers at many different SNP sites in the genome and can be used to analyze genome-wide cancer-related structural variation (49, 109). *H19* is a 3.0 kb highly conserved lncRNA present on human chromosome 11; *H19* polymorphisms are associated with increased susceptibility to a variety of cancers. A study of three *H19* polymorphisms in 213 patients with hepatoblastoma demonstrated that the *rs2839698* and *rs3024270* polymorphisms are associated with decreased *MRPL23* antisense RNA 1 (*MRPL23-AS1*) expression, whereas the *rs217727* polymorphism is associated with increased *MRPL23-AS1* expression (69). Many studies have evaluated the association between the *miR-608 rs4919510* polymorphism and CRC susceptibility. The G allele of *rs4919510* located in *miR-608* is associated with increased expression of *MRPL43* in colon tissues (70). Functional experiments have shown that the knockdown of *MRPL43* could inhibit growth and promote apoptosis in the CRC HCT-116 cell line. In addition, SNP loci in *MRPS30* are associated with breast cancer (110–112).

3.2.2 Methylation

DNA methylation is a covalent modification in which methyl groups are added to the cytosine of CpG islands in the genome by *S*-adenosylmethionine. As an epigenetic modification,

methylation can regulate gene expression without altering the DNA sequence (113). DNA microarray-based high-throughput methylation sequencing provides information on epigenetic changes in the genome. In a study of neuroblastoma with the largest coverage to date, methylation-specific PCR assays for 78 differentially methylated regions revealed associations between event-free survival and five unique regions, including *lnc-MRPL3-2*; several novel prognostic biomarkers were identified and independently validated (71).

3.3 WGCNA

Weighted Gene Co-Expression Network Analysis (WGCNA) is a bioinformatics approach to determine intergenic associations in microarray samples, involving network construction, module detection, calculation of topological properties, and data simulation; this approach is useful for screening disease biomarkers or potential therapeutic targets (114). Co-expression is a commonly used strategy to analyze correlations. In the correlation network of genes, each node represents a gene, and lines between nodes are used to represent the correlation of the two genes. Traditional unweighted co-expression network calculates the correlation coefficient between two genes directly through a linear correlation function and judge whether there is a correlation between these two genes based on a given threshold of the correlation coefficient (115, 116). In fact, the correlation of two genes is a value that fluctuates from 0 to 1, and the traditional method ignores the originally changing trend, resulting in the unweighted co-expression network losing much information. Therefore, the development team of WGCNA optimized the algorithm. Pearson correlations are taken and then weighted by raising their absolute value to a power ("β" in adjacency function) (117). This operation guarantees the invariance of the correlation relationship and reinforces the level of variation of the correlation coefficient. Through this analysis, co-expressed gene modules can be identified, and furthermore, modules can be correlated with phenotypic data to mine potential mark genes through metrics such as connectivity, module membership (MM), and gene significance (GS) (117).

Using Dai's study as an example, WGCNA was used to identify central genes associated with the incidence and prognosis of KRAS-mutant lung adenocarcinoma (LUAD). A total of 2590 DEGs were found between 184 LUAD samples of different pathological stages and 59 normal lung tissue samples from TCGA database, and 10 gene modules were identified. Functional analysis of the key modules revealed enrichment of ribosome biogenesis related terms. Survival analysis revealed that the expression of 8 genes, including MRPL27, was positively correlated with poor survival in patients with KRAS-mutant LUAD (61). Tumor mutational burden (TMB) is associated with the efficacy of immunotherapy, but the prognostic role of TMB-related genes in HCC has not been clearly defined. A WGCNA identified *MRPL9* as a TMB-specific gene with good prognostic value. A cell-based functional study has shown that the knockdown of *MRPL9* could significantly inhibit cell proliferation and migration in HCC (40). Cholangiocarcinoma (CCA), a highly malignant tumor found in biliary epithelial cells, is the second most common primary tumor of the liver. A WGCNA based on mRNA sequencing data and clinical information for patients with CCA (from TCGA) revealed that *MRPS18A, CST1*, and *SCP2* are genes associated with clinical features, such as pathological stage, histological grade, and liver function, as well as overall survival (62).

3.4 Mitochondrial Ribosomes and Clinical Features

TCGA sample collection and processing involved multiple collaborating centers, including Tissue Source Sites (TSSs), Biospecimen Core Resource (BCR), and Data Coordinating Center (DCC) (http://cancergenome.nih.gov/abouttcga/overview). Biological samples (blood and tissue) are collected from eligible cancer patients, who have detailed clinical information. Potential biomarkers are screened by follow-up high-throughput sequencing and bioinformatics analyses related to clinical features, such as prognosis, lesion metastasis, and drug responsiveness.

3.4.1 Prognosis

Hu et al. identified 92 differentially expressed genes from TCGA and developed a gene signature and prognostic risk model based on *MRPL47, NCBP2, MKRN3, AZGP1, IGF2BP2*, and *EZH2*, providing a basis for personalized immunotherapy for patients with head and neck squamous cell carcinoma (72). *MRPL11* is highly expressed in stage 4 neuroblastoma and is associated with a poor prognosis. Tigecycline, an FDA-approved broad-spectrum antibiotic, may be an indirect therapeutic strategy for neuroblastoma *via* the dysregulation of *MRPL11 (*73, 74).

Another study has demonstrated that high *MRPL15* expression predicts a worse prognosis in non-small cell lung cancer; it revealed potential regulatory networks and demonstrated a negative correlation with immune infiltration (75). *MRPL42* is highly expressed in early-stage lung adenocarcinoma (LUAD) tissues and cell lines and is significantly associated with prognosis. The knockdown of *MRPL42* reduces cell proliferation, promotes cell cycle arrest at the G1/S phase, and attenuates the migration and invasion abilities of LUAD cells *in vitro (*76).

Breast cancer accounts for the largest number of datasets in TCGA. Yin et al. integrated several bioinformatics tools and RNA *in situ* detection to identify and validate breast cancer-related hub genes and found that the expression of four genes, including *MRPL3*, were upregulated in tumor tissues and correlated with cancer progression; these genes could serve as diagnostic and prognostic biomarkers (77). As a poor prognostic factor in breast cancer, *MRPL13* expression is significantly higher in cancer tissues than in normal tissues (78–80). This gene can promote tumor cell proliferation, migration, and EMT *via* the *PI3K-Akt-mTOR* pathway and is, therefore, a candidate therapeutic target and prognostic marker (81). In breast cancer, a three-gene prognostic model based on *MRPL12, MRPL13*, and *POP1* has significant predictive value for survival. Moreover, the downregulation of endogenous *MRPL12, MRPL13*, or *POP1* expression could significantly inhibit the viability and migration of breast cancer cells *in vitro (*82).

Gastric cancer (GC) is a digestive system disease with high morbidity and mortality; early clinical screening and diagnosis are difficult, and treatment efficacy at a later stage is unsatisfactory. Therefore, it is imperative to find new tumor markers and therapeutic targets for GC. Based on GC data in TCGA and Genotype Tissue Expression (GTEX), aberrantly expressed proteins between normal and cancer tissues were identified, and hub genes, such as *MRPS5*, were found to be associated with disease-specific survival (83). *MRPL35* expression is upregulated in GC and is associated with a poor prognosis. Cell functional studies have revealed that the knockdown of *MRPL35* inhibits cell proliferation in GC *via* related proteins, including PICK1, Bcl-xL, and AGR2 (84). High expression of *MRPS29* in GC is associated with a better prognosis, and the downregulation of *MRPS29* expression could increase resistance to chemotherapy by inhibiting apoptosis and promoting cell migration, consistent with the pro-apoptotic function of *MRPS29 (*85). In another study on gastric adenocarcinoma, a model based on seven genes, such as *MRPS17*, was identified as a reliable prognostic biomarker (86).

HCC is one of the most prevalent neoplasms and the leading cause of cancer-related deaths worldwide. An mRNA expression-based stemness index revealed a three-gene signature, including *PTDSS2, MRPL9*, and *SOCS*, as a potential prognostic biomarker for HCC (87). Based on the differentially expressed genes between HBV-related HCC and control specimens, screened by univariate analyses, a signature model based on 11 genes, including *MRPS12*, was finally developed. This gene signature showed high sensitivity and accuracy for the prediction of 1-, 3-, and 5-year overall survival, disease-free survival, and progression-free interval, with predictive power superior to those of other clinical parameters (88).

Cholangiocarcinoma, a highly malignant tumor found in biliary epithelial cells, is the second most common primary tumor of the liver. A study of 36 patients with cholangiocarcinoma demonstrated that *MRPL27* mRNA levels are significantly upregulated in tumor tissues, and patients with high *MRPL27* expression had a poorer overall survival and disease-free survival than those of patients with low *MRPL27* expression (89).

Additionally, 19 genes, including *MRPL52*, have been identified from microarray gene expression profiling data for 78 patients with CRC. Further validation using patient cohorts from Australia (n = 185), the United States (n = 114), Denmark (n = 37), and Norway (n = 95) revealed that this 19-gene signature has significantly better predictive value for survival in CRC than the traditional Dukes classification (90). Higher expression of *MRPL35* in CRC cells and tissues is associated with shorter overall survival in CRC, and *in vitro* studies have shown that the downregulation of *MRPL35* expression leads to increased production of reactive oxygen species (91).

Ovarian cancer (OC) is a leading cause of death among gynecological cancers, and unique tissue and genetic heterogeneity are huge obstacles to their diagnosis and treatment. Xu et al. screened six MRPs (uL10m, uL15m, bL36m, mL39, bS16m, and mS31) associated with OC, among which *MRPL15* (uL15m) was highly expressed and amplified in OC and associated with a poor prognosis. A mechanistic analysis revealed that *MRPL15* (uL15m) plays a role in OC *via* various pathways, including cell cycle, DNA repair, and *mTOR 1* signaling (92).

Adrenocortical carcinoma (ACC) is an extremely rare disease, and the current prognostic markers have limitations in identifying patients with poor prognosis. In a previous study, 45 formalin-fixed paraffin-embedded (FFPE) tissues of adrenal tumors were analyzed by liquid chromatography-tandem mass spectrometry (LC-MS/MS) to screen differentially expressed proteins by machine learning algorithms. *MRPS23* was found to be significantly associated with survival in ACC, and this finding was validated using the TCGA database; thus, *MRPS23* could be considered as a potential prognostic marker (93).

3.4.2 Metastasis

Xinyan Li identified differentially expressed mRNAs in breast tumors with and without metastasis by high-throughput RNA sequencing, revealing that the expression of *MRPL52* was upregulated in breast cancer and was significantly associated with aggressive clinicopathological features and a higher risk of metastasis (94). Sotgia combined four mitochondrial proteins (uL15m, *HSPD1*, *UQCRB*, and *COX17*) to generate a compact mitochondrial gene signature that successfully predicts distant metastasis in breast cancer, suggesting that mitochondrial biogenesis should be considered a novel therapeutic target to overcome tumor recurrence, distant metastasis, and treatment failure in breast cancer (95). Studies targeting human OC cell lines SKOV3 and SKOV3.ip1 with different metastatic potential revealed differential expression in 11 genes, such as *MRPL38*, suggesting that high *MRPL38* expression is associated with invasion and metastasis (96). Consistent with these findings, evaluation of data from the Human Protein Atlas revealed that the protein abundance of *MRPL38* (mL38) is highly elevated in most tumor types (1).

3.4.3 Drug Responsiveness

Cisplatin-based neoadjuvant chemotherapy (NAC) prior to radical cystectomy is recommended for patients with muscle invasive bladder cancer (MIBC). However, clinically approved biomarkers for predicting the response to NAC are lacking. A study involving 30 MIBC cases reported a new signature gene set, including *MRPL4*, and was able to select NAC responders with 100% prediction accuracy; this gene set could serve as a promising biomarker for predicting chemo-responsiveness in patients with MIBC (97).

CONCLUDING REMARKS

Mitochondrial ribosomes are involved in biological activities *via* the regulation of energy metabolism and apoptosis. Next-generation sequencing and novel bioinformatics analyses have revealed that mitochondrial ribosomal genes are closely related to malignancy. Given the potential of mitochondrial ribosomal genes as cancer biomarkers, the detection of abnormally expressed mitochondrial ribosomal coding genes and non-coding RNAs is expected to facilitate the early diagnosis of malignant tumors. In the future, therapies that specifically

target mitochondrial ribosomes may improve the prognosis of patients with cancers.

AUTHOR CONTRIBUTIONS

SB, XW, and ML: induction, analysis, writing, and financial support. ZG, DZ, and DS: literature search and curation. LL: guidance and modifications. All authors contributed to the article and approved the submitted version.

FUNDING

This work was supported by a grant from the National Natural Science Foundation of China (No. 81773523).

REFERENCES

1. Kim HJ, Maiti P, Barrientos A. Mitochondrial Ribosomes in Cancer. *Semin Cancer Biol* (2017) 47:67–81. doi: 10.1016/j.semcancer.2017.04.004
2. De Silva D, Tu YT, Amunts A, Fontanesi F, Barrientos A. Mitochondrial Ribosome Assembly in Health and Disease. *Cell Cycle* (2015) 14(14):2226–50. doi: 10.1080/15384101.2015.1053672
3. Bogenhagen DF, Ostermeyer-Fay AG, Haley JD, Garcia-Diaz M. Kinetics and Mechanism of Mammalian Mitochondrial Ribosome Assembly. *Cell Rep* (2018) 22(7):1935–44. doi: 10.1016/j.celrep.2018.01.066
4. Gopisetty G, Thangarajan R. Mammalian Mitochondrial Ribosomal Small Subunit (MRPS) Genes: A Putative Role in Human Disease. *Gene* (2016) 589 (1):27–35. doi: 10.1016/j.gene.2016.05.008
5. Wazir U, Orakzai MM, Khanzada ZS, Jiang WG, Sharma AK, Kasem A, et al. The Role of Death-Associated Protein 3 in Apoptosis, Anoikis and Human Cancer. *Cancer Cell Int* (2015) 15:39. doi: 10.1186/s12935-015-0187-z
6. Conde JA, Claunch CJ, Romo HE, Benito-Martin A, Ballestero RP, Gonzalez-Garcia M. Identification of a Motif in BMRP Required for Interaction With Bcl-2 by Site-Directed Mutagenesis Studies. *J Cell Biochem* (2012) 113(11):3498–508. doi: 10.1002/jcb.24226
7. Hanahan D, Weinberg RA. Hallmarks of Cancer: The Next Generation. *Cell* (2011) 144(5):646–74. doi: 10.1016/j.cell.2011.02.013
8. Masic I. The Most Influential Scientists in the Development of Medical Informatics (13): Margaret Belle Dayhoff. *Acta Inform Med* (2016) 24 (4):299. doi: 10.5455/aim.2016.24.299-299
9. Christian BE, Spremulli LL. Mechanism of Protein Biosynthesis in Mammalian Mitochondria. *Biochim Biophys Acta* (2012) 1819(9-10):1035–54. doi: 10.1016/j.bbagrm.2011.11.009
10. Amunts A, Brown A, Toots J, Scheres SHW, Ramakrishnan V. Ribosome. The Structure of the Human Mitochondrial Ribosome. *Science* (2015) 348 (6230):95–8. doi: 10.1126/science.aaa1193
11. Brown A, Amunts A, Bai XC, Sugimoto Y, Edwards PC, Murshudov G, et al. Structure of the Large Ribosomal Subunit From Human Mitochondria. *Science* (2014) 346(6210):718–22. doi: 10.1126/science.1258026
12. Greber BJ, Bieri P, Leibundgut M, Leitner A, Aebersold R, Boehringer D, et al. Ribosome. The Complete Structure of the 55S Mammalian Mitochondrial Ribosome. *Science* (2015) 348(6232):303–8. doi: 10.1126/science.aaa3872
13. Greber BJ, Boehringer D, Leibundgut M, Bieri P, Leitner A, Schmitz N, et al. The Complete Structure of the Large Subunit of the Mammalian Mitochondrial Ribosome. *Nature* (2014) 515(7526):283–6. doi: 10.1038/nature13895
14. Papa S, Martino PL, Capitanio G, Gaballo A, De Rasmo D, Signorile A, et al. The Oxidative Phosphorylation System in Mammalian Mitochondria. *Adv Exp Med Biol* (2012) 942:3–37. doi: 10.1007/978-94-007-2869-1_1
15. Horten P, Colina-Tenorio L, Rampelt H. Biogenesis of Mitochondrial Metabolite Carriers. *Biomolecules* (2020) 10(7):1008. doi: 10.3390/biom10071008
16. Chen J, Tsai A, O'Leary SE, Petrov A, Puglisi JD. Unraveling the Dynamics of Ribosome Translocation. *Curr Opin Struct Biol* (2012) 22(6):804–14. doi: 10.1016/j.sbi.2012.09.004
17. Greber BJ, Boehringer D, Leitner A, Bieri P, Voigts-Hoffmann F, Erzberger JP, et al. Architecture of the Large Subunit of the Mammalian Mitochondrial Ribosome. *Nature* (2014) 505(7484):515–9. doi: 10.1038/nature12890
18. Ban N, Beckmann R, Cate JH, Dinman JD, Dragon F, Ellis SR, et al. A New System for Naming Ribosomal Proteins. *Curr Opin Struct Biol* (2014) 24:165–9. doi: 10.1016/j.sbi.2014.01.002
19. Amunts A, Brown A, Bai XC, Llacer JL, Hussain T, Emsley P, et al. Structure of the Yeast Mitochondrial Large Ribosomal Subunit. *Science* (2014) 343 (6178):1485–9. doi: 10.1126/science.1249410
20. Yu M. Generation, Function and Diagnostic Value of Mitochondrial DNA Copy Number Alterations in Human Cancers. *Life Sci* (2011) 89(3-4):65–71. doi: 10.1016/j.lfs.2011.05.010
21. Yin P, Li Q, Yan C, Liu Y, Liu J, Yu F, et al. Structural Basis for the Modular Recognition of Single-Stranded RNA by PPR Proteins. *Nat* (2013) 504 (7478):168–71. doi: 10.1038/nature12651
22. Manavski N, Guyon V, Meurer J, Wienand U, Brettschneider R. An Essential Pentatricopeptide Repeat Protein Facilitates 5' Maturation and Translation Initiation of Rps3 mRNA in Maize Mitochondria. *Plant Cell* (2012) 24 (7):3087–105. doi: 10.1105/tpc.112.099051
23. Ashton TM, McKenna WG, Kunz-Schughart LA, Higgins GS. Oxidative Phosphorylation as an Emerging Target in Cancer Therapy. *Clin Cancer Res* (2018) 24(11):2482–90. doi: 10.1158/1078-0432.CCR-17-3070
24. Liu L, Zhang X, Ding H, Liu X, Cao D, Liu Y, et al. Arginine and Lysine Methylation of MRPS23 Promotes Breast Cancer Metastasis Through Regulating OXPHOS. *Oncogene* (2021) 40(20):3548–63. doi: 10.1038/s41388-021-01785-7
25. Wei Z, Jia J, Heng G, Xu H, Shan J, Wang G, et al. Sirtuin-1/Mitochondrial Ribosomal Protein S5 Axis Enhances the Metabolic Flexibility of Liver Cancer Stem Cells. *Hepatology* (2019) 70(4):1197–213. doi: 10.1002/hep.30622
26. Lee YK, Lim JJ, Jeoun UW, Min S, Lee EB, Kwon SM, et al. Lactate-mediated mitoribosomal defects impair mitochondrial oxidative phosphorylation and promote hepatoma cell invasiveness. *J Biol Chem*. (2017) 292(49):20208–17. doi: 10.1074/jbc.M117.809012
27. Zu XL, Guppy M. Cancer Metabolism: Facts, Fantasy, and Fiction. *Biochem Biophys Res Commun* (2004) 313(3):459–65. doi: 10.1016/j.bbrc.2003.11.136
28. Vaupel P, Mayer A. Availability, Not Respiratory Capacity Governs Oxygen Consumption of Solid Tumors. *Int J Biochem Cell Biol* (2012) 44(9):1477–81. doi: 10.1016/j.biocel.2012.05.019
29. Reznik E, Miller ML, Senbabaoglu Y, Riaz N, Sarungbam J, Tickoo SK, et al. Mitochondrial DNA Copy Number Variation Across Human Cancers. *Elife* (2016) 5:e10769. doi: 10.7554/eLife.10769
30. Koritzinsky M. Metformin: A Novel Biological Modifier of Tumor Response to Radiation Therapy. *Int J Radiat Oncol Biol Phys* (2015) 93(2):454–64. doi: 10.1016/j.ijrobp.2015.06.003
31. Pernicova I, Korbonits M. Metformin–mode of Action and Clinical Implications for Diabetes and Cancer. *Nat Rev Endocrinol* (2014) 10 (3):143–56. doi: 10.1038/nrendo.2013.256
32. Wheaton WW, Weinberg SE, Hamanaka RB, Soberanes S, Sullivan LB, Anso E, et al. Metformin Inhibits Mitochondrial Complex I of Cancer Cells to Reduce Tumorigenesis. *Elife* (2014) 3:e02242. doi: 10.7554/eLife.02242
33. Warren CFA, Wong-Brown MW, Bowden NA. BCL-2 Family Isoforms in Apoptosis and Cancer. *Cell Death Dis* (2019) 10(3):177. doi: 10.1038/s41419-019-1407-6
34. Edlich F. BCL-2 Proteins and Apoptosis: Recent Insights and Unknowns. *Biochem Biophys Res Commun* (2018) 500(1):26–34. doi: 10.1016/j.bbrc.2017.06.190

35. Dadsena S, King LE, Garcia-Saez AJ. Apoptosis Regulation at the Mitochondria Membrane Level. *Biochim Biophys Acta Biomembr* (2021) 1863(12):183716. doi: 10.1016/j.bbamem.2021.183716
36. Bock FJ, Tait SWG. Mitochondria as Multifaceted Regulators of Cell Death. *Nat Rev Mol Cell Biol* (2020) 21(2):85–100. doi: 10.1038/s41580-019-0173-8
37. Cavdar Koc E, Ranasinghe A, Burkhart W, Blackburn K, Koc H, Moseley A, et al. A New Face on Apoptosis: Death-Associated Protein 3 and PDCD9 are Mitochondrial Ribosomal Proteins. *FEBS Lett* (2001) 492(1-2):166–70. doi: 10.1016/S0014-5793(01)02250-5
38. Chandrashekar DS, Bashel B, Balasubramanya SAH, Creighton CJ, Ponce-Rodriguez I, Chakravarthi B, et al. UALCAN: A Portal for Facilitating Tumor Subgroup Gene Expression and Survival Analyses. *Neoplasia* (2017) 19(8):649–58. doi: 10.1016/j.neo.2017.05.002
39. Vera Alvarez R, Pongor LS, Marino-Ramirez L, Landsman D. TPMCalculator: One-Step Software to Quantify mRNA Abundance of Genomic Features. *Bioinformatics* (2019) 35(11):1960–2. doi: 10.1093/bioinformatics/bty896
40. Tang B, Zhu J, Zhao Z, Lu C, Liu S, Fang S, et al. Diagnosis and Prognosis Models for Hepatocellular Carcinoma Patient's Management Based on Tumor Mutation Burden. *J Adv Res* (2021) 33:153–65. doi: 10.1016/j.jare.2021.01.018
41. Gauthier J, Vincent AT, Charette SJ, Derome N. A Brief History of Bioinformatics. *Brief Bioinform* (2019) 20(6):1981–96. doi: 10.1093/bib/bby063
42. Moorthie S, Hall A, Wright CF. Informatics and Clinical Genome Sequencing: Opening the Black Box. *Genet Med* (2013) 15(3):165–71. doi: 10.1038/gim.2012.116
43. Horner DS, Pavesi G, Castrignano T, De Meo PD, Liuni S, Sammeth M, et al. Bioinformatics Approaches for Genomics and Post Genomics Applications of Next-Generation Sequencing. *Brief Bioinform* (2010) 11(2):181–97. doi: 10.1093/bib/bbp046
44. Hong M, Tao S, Zhang L, Diao LT, Huang X, Huang S, et al. RNA Sequencing: New Technologies and Applications in Cancer Research. *J Hematol Oncol* (2020) 13(1):166. doi: 10.1186/s13045-020-01005-x
45. Kukurba KR, Montgomery SB. RNA Sequencing and Analysis. *Cold Spring Harb Protoc* (2015) 2015(11):951–69. doi: 10.1101/pdb.top084970
46. Chen C, Huang H, Wu CH. Protein Bioinformatics Databases and Resources. *Methods Mol Biol* (2017) 1558:3–39. doi: 10.1007/978-1-4939-6783-4_1
47. Oliver GR, Hart SN, Klee EW. Bioinformatics for Clinical Next Generation Sequencing. *Clin Chem* (2015) 61(1):124–35. doi: 10.1373/clinchem.2014.224360
48. Clough E, Barrett T. The Gene Expression Omnibus Database. *Methods Mol Biol* (2016) 1418:93–110. doi: 10.1007/978-1-4939-3578-9_5
49. Tomczak K, Czerwinska P, Wiznerowicz M. The Cancer Genome Atlas (TCGA): An Immeasurable Source of Knowledge. *Contemp Oncol (Pozn)* (2015) 19(1A):A68–77. doi: 10.5114/wo.2014.47136
50. Chin L, Andersen JN, Futreal PA. Cancer Genomics: From Discovery Science to Personalized Medicine. *Nat Med* (2011) 17(3):297–303. doi: 10.1038/nm.2323
51. Jing C, Fu R, Wang C, Li X, Zhang W. MRPL13 Act as a Novel Therapeutic Target and Could Promote Cell Proliferation in Non-Small Cell Lung Cancer. *Cancer Manag Res* (2021) 13:5535–45. doi: 10.2147/CMAR.S316428
52. Revathi Paramasivam O, Gopisetty G, Subramani J, Thangarajan R. Expression and Affinity Purification of Recombinant Mammalian Mitochondrial Ribosomal Small Subunit (MRPS) Proteins and Protein-Protein Interaction Analysis Indicate Putative Role in Tumourigenic Cellular Processes. *J Biochem* (2021) 169(6):675–92. doi: 10.1093/jb/mvab004
53. Oviya RP, Gopal G, Shirley SS, Sridevi V, Jayavelu S, Rajkumar T. Mitochondrial Ribosomal Small Subunit Proteins (MRPS) MRPS6 and MRPS23 Show Dysregulation in Breast Cancer Affecting Tumorigenic Cellular Processes. *Gene* (2021) 790:145697. doi: 10.1016/j.gene.2021.145697
54. Klaestad E, Opdahl S, Engstrom MJ, Ytterhus B, Wik E, Bofin AM, et al. MRPS23 Amplification and Gene Expression in Breast Cancer; Association With Proliferation and the non-Basal Subtypes. *Breast Cancer Res Treat* (2020) 180(1):73–86. doi: 10.1007/s10549-020-05532-6
55. Gao Y, Li F, Zhou H, Yang Y, Wu R, Chen Y, et al. Down-Regulation of MRPS23 Inhibits Rat Breast Cancer Proliferation and Metastasis. *Oncotarget* (2017) 8(42):71772–81. doi: 10.18632/oncotarget.17888
56. Fan X, Liu L, Shi Y, Guo F, Wang H, Zhao X, et al. Integrated Analysis of RNA-Binding Proteins in Human Colorectal Cancer. *World J Surg Oncol* (2020) 18(1):222. doi: 10.1186/s12957-020-01995-5
57. Wang M, Jiang F, Wei K, Wang J, Zhou G, Wu C, et al. Development and Validation of a RNA Binding Protein-Associated Prognostic Model for Hepatocellular Carcinoma. *Technol Cancer Res Treat* (2021) 20:15330338211004936. doi: 10.1177/15330338211004936
58. Huang Y, Chen S, Qin W, Wang Y, Li L, Li Q, et al. A Novel RNA Binding Protein-Related Prognostic Signature for Hepatocellular Carcinoma. *Front Oncol* (2020) 10:580513. doi: 10.3389/fonc.2020.580513
59. Qiu X, Guo D, Du J, Bai Y, Wang F. A Novel Biomarker, MRPS12 Functions as a Potential Oncogene in Ovarian Cancer and is a Promising Prognostic Candidate. *Med (Baltimore)* (2021) 100(8):e24898. doi: 10.1097/MD.0000000000024898
60. Liu J, Wu S, Xie X, Wang Z, Lei Q. Identification of Potential Crucial Genes and Key Pathways in Osteosarcoma. *Hereditas* (2020) 157(1):29. doi: 10.1186/s41065-020-00142-0
61. Dai D, Shi R, Han S, Jin H, Wang X. Weighted Gene Coexpression Network Analysis Identifies Hub Genes Related to KRAS Mutant Lung Adenocarcinoma. *Med (Baltimore)* (2020) 99(32):e21478. doi: 10.1097/MD.0000000000021478
62. Tian A, Pu K, Li B, Li M, Liu X, Gao L, et al. Weighted Gene Coexpression Network Analysis Reveals Hub Genes Involved in Cholangiocarcinoma Progression and Prognosis. *Hepatol Res* (2019) 49(10):1195–206. doi: 10.1111/hepr.13386
63. Panza A, Castellana S, Biscaglia G, Piepoli A, Parca L, Gentile A, et al. Transcriptome and Gene Fusion Analysis of Synchronous Lesions Reveals Lncmrps31p5 as a Novel Transcript Involved in Colorectal Cancer. *Int J Mol Sci* (2020) 21(19):7120. doi: 10.3390/ijms21197120
64. Roszik J, Khan A, Conley AP, Livingston JA, Groisberg R, Ravi V, et al. Unique Aberrations in Intimal Sarcoma Identified by Next-Generation Sequencing as Potential Therapy Targets. *Cancers (Basel)* (2019) 11(9):1283. doi: 10.3390/cancers11091283
65. Wu Y, Zhang L, He S, Guan B, He A, Yang K, et al. Identification of Immune-Related LncRNA for Predicting Prognosis and Immunotherapeutic Response in Bladder Cancer. *Aging (Albany NY)* (2020) 12(22):23306–25. doi: 10.18632/aging.104115
66. Ye J, Li H, Wei J, Luo Y, Liu H, Zhang J, et al. Risk Scoring System Based on lncRNA Expression for Predicting Survival in Hepatocellular Carcinoma With Cirrhosis. *Asian Pac J Cancer Prev* (2020) 21(6):1787–95. doi: 10.31557/APJCP.2020.21.6.1787
67. Zou X, Hu X, He F, Zhang M, Kong X, Rui S, et al. LncRNA LINC00152 Promotes Oral Squamous Cell Carcinoma Growth via Enhancing Upstream Transcription Factor 1 Mediated Mitochondrial Ribosomal Protein L52 Transcription. *J Oral Pathol Med* (2021). doi: 10.1111/jop.13253
68. Zhou C, Chen Z, Peng C, Chen C, Li H. Long Noncoding RNA TRIM52-AS1 Sponges miR-514a-5p to Facilitate Hepatocellular Carcinoma Progression Through Increasing MRPS18A. *Cancer Biother Radiopharm* (2021) 36(2):211–9. doi: 10.1089/cbr.2019.3271
69. Tan T, Li J, Wen Y, Zou Y, Yang J, Pan J, et al. Association Between lncRNA-H19 Polymorphisms and Hepatoblastoma Risk in an Ethic Chinese Population. *J Cell Mol Med* (2021) 25(2):742–50. doi: 10.1111/jcmm.16124
70. Zhu X, Liu Y, Xu J, Cheng Z, Yu Y, Chu M, et al. miR-608 Rs4919510 Polymorphism May Affect Susceptibility to Colorectal Cancer by Upregulating MRPL43 Expression. *DNA Cell Biol* (2020) 39(11):2017–27. doi: 10.1089/dna.2020.5689
71. Decock A, Ongenaert M, Cannoodt R, Verniers K, De Wilde B, Laureys G, et al. Methyl-CpG-Binding Domain Sequencing Reveals a Prognostic Methylation Signature in Neuroblastoma. *Oncotarget* (2016) 7(2):1960–72. doi: 10.18632/oncotarget.6477
72. Hu G, Jiang Q, Liu L, Peng H, Wang Y, Li S, et al. Integrated Analysis of RNA-Binding Proteins Associated With the Prognosis and Immunosuppression in Squamous Cell Carcinoma of Head and Neck. *Front Genet* (2020) 11:571403. doi: 10.3389/fgene.2020.571403

73. Bell JL, Hagemann S, Holien JK, Liu T, Nagy Z, Schulte JH, et al. Identification of RNA-Binding Proteins as Targetable Putative Oncogenes in Neuroblastoma. *Int J Mol Sci* (2020) 21(14):5098. doi: 10.3390/ijms21145098
74. Hu B, Guo Y. Inhibition of Mitochondrial Translation as a Therapeutic Strategy for Human Ovarian Cancer to Overcome Chemoresistance. *Biochem Biophys Res Commun* (2019) 509(2):373–8. doi: 10.1016/j.bbrc.2018.12.127
75. Zeng Y, Shi Y, Xu L, Zeng Y, Cui X, Wang Y, et al. Prognostic Value and Related Regulatory Networks of MRPL15 in Non-Small-Cell Lung Cancer. *Front Oncol* (2021) 11:656172. doi: 10.3389/fonc.2021.656172
76. Jiang W, Zhang C, Kang Y, Yu X, Pang P, Li G, et al. MRPL42 is Activated by YY1 to Promote Lung Adenocarcinoma Progression. *J Cancer* (2021) 12 (8):2403–11. doi: 10.7150/jca.52277
77. Yin J, Lin C, Jiang M, Tang X, Xie D, Chen J, et al. CENPL, ISG20L2, LSM4, MRPL3 are Four Novel Hub Genes and may Serve as Diagnostic and Prognostic Markers in Breast Cancer. *Sci Rep* (2021) 11(1):15610. doi: 10.1038/s41598-021-95068-6
78. Tao Z, Suo H, Zhang L, Jin Z, Wang Z, Wang D, et al. MRPL13 is a Prognostic Cancer Biomarker and Correlates With Immune Infiltrates in Breast Cancer. *Onco Targets Ther* (2020) 13:12255–68. doi: 10.2147/OTT.S263998
79. Xu YH, Deng JL, Wang LP, Zhang HB, Tang L, Huang Y, et al. Identification of Candidate Genes Associated With Breast Cancer Prognosis. *DNA Cell Biol* (2020) 39(7):1205–27. doi: 10.1089/dna.2020.5482
80. Zhou X, Xiao C, Han T, Qiu S, Wang M, Chu J, et al. Prognostic Biomarkers Related to Breast Cancer Recurrence Identified Based on Logit Model Analysis. *World J Surg Oncol* (2020) 18(1):254. doi: 10.1186/s12957-020-02026-z
81. Cai M, Li H, Chen R, Zhou X. MRPL13 Promotes Tumor Cell Proliferation, Migration and EMT Process in Breast Cancer Through the PI3K-AKT-mTOR Pathway. *Cancer Manag Res* (2021) 13:2009–24. doi: 10.2147/CMAR.S296038
82. Liu Y, Sun H, Li X, Liu Q, Zhao Y, Li L, et al. Identification of a Three-RNA Binding Proteins (RBPs) Signature Predicting Prognosis for Breast Cancer. *Front Oncol* (2021) 11:663556. doi: 10.3389/fonc.2021.663556
83. Zhou L, Wu Y, Xin L, Zhou Q, Li S, Yuan Y, et al. Development of RNA Binding Proteins Expression Signature for Prognosis Prediction in Gastric Cancer Patients. *Am J Transl Res* (2020) 12(10):6775–92.
84. Yuan L, Li JX, Yang Y, Chen Y, Ma TT, Liang S, et al. Depletion of MRPL35 Inhibits Gastric Carcinoma Cell Proliferation by Regulating Downstream Signaling Proteins. *World J Gastroenterol* (2021) 27(16):1785–804. doi: 10.3748/wjg.v27.i16.1785
85. Jia Y, Ye L, Ji K, Zhang L, Hargest R, Ji J, et al. Death-Associated Protein-3, DAP-3, Correlates With Preoperative Chemotherapy Effectiveness and Prognosis of Gastric Cancer Patients Following Perioperative Chemotherapy and Radical Gastrectomy. *Br J Cancer* (2014) 110(2):421–9. doi: 10.1038/bjc.2013.712
86. Li J, Zhou W, Wei J, Xiao X, An T, Wu W, et al. Prognostic Value and Biological Functions of RNA Binding Proteins in Stomach Adenocarcinoma. *Onco Targets Ther* (2021) 14:1689–705. doi: 10.2147/OTT.S297973
87. Liu J, Lu J, Li W. A Comprehensive Prognostic and Immunological Analysis of a New Three-Gene Signature in Hepatocellular Carcinoma. *Stem Cells Int* (2021) 2021:5546032. doi: 10.1155/2021/5546032
88. Li M, Liu Z, Wang J, Liu H, Gong H, Li S, et al. Systematic Analysis Identifies a Specific RNA-Binding Protein-Related Gene Model for Prognostication and Risk-Adjustment in HBV-Related Hepatocellular Carcinoma. *Front Genet* (2021) 12:707305. doi: 10.3389/fgene.2021.707305
89. Zhuang L, Meng Z, Yang Z. MRPL27 Contributes to Unfavorable Overall Survival and Disease-Free Survival From Cholangiocarcinoma Patients. *Int J Med Sci* (2021) 18(4):936–43. doi: 10.7150/ijms.50782
90. Abdul Aziz NA, Mokhtar NM, Harun R, Mollah MM, Mohamed Rose I, Sagap I, et al. A 19-Gene Expression Signature as a Predictor of Survival in Colorectal Cancer. *BMC Med Genomics* (2016) 9(1):58. doi: 10.1186/s12920-016-0218-1
91. Zhang L, Lu P, Yan L, Yang L, Wang Y, Chen J, et al. MRPL35 Is Up-Regulated in Colorectal Cancer and Regulates Colorectal Cancer Cell Growth and Apoptosis. *Am J Pathol* (2019) 189(5):1105–20. doi: 10.1016/j.ajpath.2019.02.003
92. Xu H, Zou R, Li F, Liu J, Luan N, Wang S, et al. MRPL15 is a Novel Prognostic Biomarker and Therapeutic Target for Epithelial Ovarian Cancer. *Cancer Med* (2021) 10(11):3655–73. doi: 10.1002/cam4.3907
93. Jang HN, Moon SJ, Jung KC, Kim SW, Kim H, Han D, et al. Mass Spectrometry-Based Proteomic Discovery of Prognostic Biomarkers in Adrenal Cortical Carcinoma. *Cancers (Basel)* (2021) 13(15):3890. doi: 10.3390/cancers13153890
94. Li X, Wang M, Li S, Chen Y, Wang M, Wu Z, et al. HIF-1-Induced Mitochondrial Ribosome Protein L52: A Mechanism for Breast Cancer Cellular Adaptation and Metastatic Initiation in Response to Hypoxia. *Theranostics* (2021) 11(15):7337–59. doi: 10.7150/thno.57804
95. Sotgia F, Fiorillo M, Lisanti MP. Mitochondrial Markers Predict Recurrence, Metastasis and Tamoxifen-Resistance in Breast Cancer Patients: Early Detection of Treatment Failure With Companion Diagnostics. *Oncotarget* (2017) 8(40):68730–45. doi: 10.18632/oncotarget.19612
96. Wang Y, Dong L, Cui H, Shen DH, Wang Y, Chang XH, et al. Up-Regulation of Mitochondrial Antioxidation Signals in Ovarian Cancer Cells With Aggressive Biologic Behavior. *J Zhejiang Univ Sci B* (2011) 12(5):346–56. doi: 10.1631/jzus.B1000192
97. Hepburn AC, Lazzarini N, Veeratterapillay R, Wilson L, Bacardit J, Heer R. Identification of CNGB1 as a Predictor of Response to Neoadjuvant Chemotherapy in Muscle-Invasive Bladder Cancer. *Cancers (Basel)* (2021) 13(15):3903. doi: 10.3390/cancers13153903
98. Stark R, Grzelak M, Hadfield J. RNA Sequencing: The Teenage Years. *Nat Rev Genet* (2019) 20(11):631–56. doi: 10.1038/s41576-019-0150-2
99. Jia Y, Li Z, Cheng X, Wu X, Pang F, Shi J, et al. Depletion of Death-Associated Protein-3 Induces Chemoresistance in Gastric Cancer Cells Through the Beta-Catenin/LGR5/Bcl-2 Axis. *J Investig Med* (2019) 67 (5):856–61. doi: 10.1136/jim-2018-000934
100. Mertens F, Johansson B, Fioretos T, Mitelman F. The Emerging Complexity of Gene Fusions in Cancer. *Nat Rev Cancer* (2015) 15(6):371–81. doi: 10.1038/nrc3947
101. Spizzo R, Almeida MI, Colombatti A, Calin GA. Long Non-Coding RNAs and Cancer: A New Frontier of Translational Research? *Oncogene* (2012) 31 (43):4577–87. doi: 10.1038/onc.2011.621
102. Derrien T, Johnson R, Bussotti G, Tanzer A, Djebali S, Tilgner H, et al. The GENCODE V7 Catalog of Human Long Noncoding RNAs: Analysis of Their Gene Structure, Evolution, and Expression. *Genome Res* (2012) 22(9):1775–89. doi: 10.1101/gr.132159.111
103. Fatica A, Bozzoni I. Long non-Coding RNAs: New Players in Cell Differentiation and Development. *Nat Rev Genet* (2014) 15(1):7–21. doi: 10.1038/nrg3606
104. Xing C, Sun SG, Yue ZQ, Bai F. Role of lncRNA LUCAT1 in Cancer. *BioMed Pharmacother* (2021) 134:111158. doi: 10.1016/j.biopha.2020.111158
105. Wang J, Su Z, Lu S, Fu W, Liu Z, Jiang X, et al. LncRNA HOXA-AS2 and its Molecular Mechanisms in Human Cancer. *Clin Chim Acta* (2018) 485:229–33. doi: 10.1016/j.cca.2018.07.004
106. Qi X, Zhang DH, Wu N, Xiao JH, Wang X, Ma W. ceRNA in Cancer: Possible Functions and Clinical Implications. *J Med Genet* (2015) 52 (10):710–8. doi: 10.1136/jmedgenet-2015-103334
107. Tan X, Mao L, Huang C, Yang W, Guo J, Chen Z, et al. Comprehensive Analysis of lncRNA-miRNA-mRNA Regulatory Networks for Microbiota-Mediated Colorectal Cancer Associated With Immune Cell Infiltration. *Bioengineered* (2021) 12(1):3410–25. doi: 10.1080/21655979.2021.1940614
108. Shendure J, Balasubramanian S, Church GM, Gilbert W, Rogers J, Schloss JA, et al. DNA Sequencing at 40: Past, Present and Future. *Nat* (2017) 550 (7676):345–53. doi: 10.1038/nature24286
109. Van Loo P, Nilsen G, Nordgard SH, Vollan HK, Borresen-Dale AL, Kristensen VN, et al. Analyzing Cancer Samples With SNP Arrays. *Methods Mol Biol* (2012) 802:57–72. doi: 10.1007/978-1-61779-400-1_4
110. O'Brien KM, Cole SR, Poole C, Bensen JT, Herring AH, Engel LS, et al. Replication of Breast Cancer Susceptibility Loci in Whites and African Americans Using a Bayesian Approach. *Am J Epidemiol* (2014) 179 (3):382–94. doi: 10.1093/aje/kwt258

111. Quigley DA, Fiorito E, Nord S, Van Loo P, Alnaes GG, Fleischer T, et al. The 5p12 Breast Cancer Susceptibility Locus Affects MRPS30 Expression in Estrogen-Receptor Positive Tumors. *Mol Oncol* (2014) 8(2):273–84. doi: 10.1016/j.molonc.2013.11.008
112. Ellingjord-Dale M, Grotmol T, Lee E, Van Den Berg DJ, Hofvind S, Couto E, et al. Breast Cancer Susceptibility Variants and Mammographic Density Phenotypes in Norwegian Postmenopausal Women. *Cancer Epidemiol Biomarkers Prev* (2014) 23(9):1752–63. doi: 10.1158/1055-9965.EPI-13-1212
113. Li XQ, Guo YY, De W. DNA Methylation and microRNAs in Cancer. *World J Gastroenterol* (2012) 18(9):882–8. doi: 10.3748/wjg.v18.i9.882
114. Langfelder P, Horvath S. WGCNA: An R Package for Weighted Correlation Network Analysis. *BMC Bioinf* (2008) 9:559. doi: 10.1186/1471-2105-9-559
115. Zhang B, Horvath S. A General Framework for Weighted Gene Co-Expression Network Analysis. *Stat Appl Genet Mol Biol* (2005) 4:Article17. doi: 10.2202/1544-6115.1128
116. Horvath S, Dong J. Geometric Interpretation of Gene Coexpression Network Analysis. *PloS Comput Biol* (2008) 4(8):e1000117. doi: 10.1371/journal.pcbi.1000117
117. Miller JA, Horvath S, Geschwind DH. Divergence of Human and Mouse Brain Transcriptome Highlights Alzheimer Disease Pathways. *Proc Natl Acad Sci USA* (2010) 107(28):12698–703. doi: 10.1073/pnas.0914257107

Conflict of Interest: The authors declare that the research was conducted in the absence of any commercial or financial relationships that could be construed as a potential conflict of interest.

Publisher's Note: All claims expressed in this article are solely those of the authors and do not necessarily represent those of their affiliated organizations, or those of the publisher, the editors and the reviewers. Any product that may be evaluated in this article, or claim that may be made by its manufacturer, is not guaranteed or endorsed by the publisher.

frontiers | Frontiers in Oncology

ORIGINAL RESEARCH
published: 07 June 2022
doi: 10.3389/fonc.2022.904327

The Orexin-A/OX1R System Induces Cell Death in Pancreatic Cancer Cells Resistant to Gemcitabine and Nab-Paclitaxel Treatment

*Thierry Voisin[1], Pascal Nicole[1], Valérie Gratio[1], Anaïs Chassac[2], Dounia Mansour[2], Vinciane Rebours[1,3], Anne Couvelard[1,2] and Alain Couvineau[1]**

[1] INSERM UMR1149/Inflammation Research Center (CRI), Université Paris Cité, Team "From inflammation to cancer in digestive diseases" labeled by "la Ligue Nationale Contre le Cancer", DHU UNITY, Paris, France, [2] Department of Pathology, Bichat Hospital, Université Paris Cité, Paris, France, [3] Department of Pancreatology, Beaujon Hospital, Université Paris Cité, Clichy, France

OPEN ACCESS

Edited by:
Maen Abdelrahim,
Houston Methodist Research Institute, United States

Reviewed by:
Gang Yang,
Peking Union Medical College Hospital (CAMS), China
Yuichi Hori,
Kobe University, Japan

***Correspondence:**
Alain Couvineau
alain.couvineau@inserm.fr

Specialty section:
This article was submitted to Gastrointestinal Cancers: Hepato Pancreatic Biliary Cancers, a section of the journal Frontiers in Oncology

Received: 25 March 2022
Accepted: 13 May 2022
Published: 07 June 2022

Citation:
Voisin T, Nicole P, Gratio V, Chassac A, Mansour D, Rebours V, Couvelard A and Couvineau A (2022) The Orexin-A/OX1R System Induces Cell Death in Pancreatic Cancer Cells Resistant to Gemcitabine and Nab-Paclitaxel Treatment. Front. Oncol. 12:904327. doi: 10.3389/fonc.2022.904327

Pancreatic ductal adenocarcinoma (PDAC) represents the fourth cause of cancer-associated death in the West. This type of cancer has a very poor prognosis notably due to the development of chemoresistance when treatments including gemcitabine and Abraxane (Nab-paclitaxel) were prescribed. The identification of new treatment circumventing this chemoresistance represents a key challenge. Previous studies demonstrated that the activation of orexin receptor type 1 (OX1R), which was ectopically expressed in PDAC, by its natural ligand named orexin-A (OxA), led to anti-tumoral effect resulting in the activation of mitochondrial pro-apoptotic mechanism. Here, we demonstrated that OxA inhibited the pancreatic cancer cell (AsPC-1) growth and inhibited the tumor volume in preclinical models as effectively as gemcitabine and Nab-paclitaxel. Moreover, the combination therapy including OxA plus gemcitabine or OxA plus Nab-paclitaxel was additive on the inhibition of cancer cell growth and tumor development. More importantly, the treatment by OxA of chemoresistant tumors to gemcitabine or Nab-paclitaxel obtained by successive xenografts in mice revealed that OxA was able to induce a strong inhibition of tumor development, whereas no OxA resistance was identified in tumors. The OX1R/OxA system might be an innovative and powerful alternative treatment of chemoresistant PDAC.

Keywords: GPCR, pancreatic cancer, orexins, chemoresistance, apoptosis

INTRODUCTION

Pancreatic cancers widely represented (>90%) by pancreatic ductal adenocarcinoma (PDAC) are the most lethal human digestive cancer with a very poor 5-year-survival rate, which is <10% (1). To make matters worse, the statistical projection predicts that this cancer could become the second leading cause of cancer mortality in the next decade (2). Moreover, this sad description was mainly associated with the difficulty of early diagnosis of the disease, the risk of tumor recurrence after surgery, and the development of resistance to various therapies (3, 4). Currently, the major therapy

for unresectable advanced PDAC was regrouped into various combinatorial protocols used in first/second line of treatment and dependent on the countries that mostly based on Nab-paclitaxel/gemcitabine or FOLFIRINOX (folinic acid, 5-FU, irinotecan, and oxaliplatin) (5). In the last decade, gemcitabine (2′-desoxy-2′,2′-difluorocytidine), a deoxycytidine analog, which is a DNA synthesis inhibitor able to block cell cycle and cell proliferation, was mainly used in first-line treatment of PDAC (6). After intracellular phosphorylation, gemcitabine was transported and incorporated into DNA by various transporters and enzymes to induce their deleterious effects in cells by competition with deoxycytidine triphosphate (6). However, PDAC patients rapidly develop chemoresistance to gemcitabine, which strongly reduced the treatment effectiveness compared to other chemotherapeutic molecules (6). While the mechanism responsible for gemcitabine resistance remains broadly unclear, many studies have demonstrated that gemcitabine metabolism involved nucleoside transporters and enzymes (3, 7). Moreover, the role of epithelial–mesenchymal transition (EMT) that represents a phenotypic change in cancer cells leading to higher cell aggressiveness also play a role in gemcitabine-resistant mechanisms (3). Other mechanisms involving factors secreted in the tumor microenvironment by pancreatic stellate cells, fibroblasts, nerve cells, endothelial cells, exosomes, and inflammatory cells were reported (3, 6). Moreover, the inactivation of pro-apoptotic process, the alteration of the cell cycle, the cell stress modifications, the inhibition of DNA repair systems, the inactivation of important coding genes by genetic and/or epigenetic modifications, the amplification/deletion of miRNA genes associated or not to a dysregulation of miRNA transcription, and the overexpression of certain long non-coding RNAs (lncRNAs) were also identified as factors inducing drug resistance (8, 9). The combination of gemcitabine to Nab-paclitaxel (Trade name: Abraxane), which consisted of albumin nanoparticles (nab) associated to paclitaxel, in neoadjuvant treatment before surgery and in advanced metastatic PDAC has demonstrated a significant survival gain compared to gemcitabine monotherapy (10, 11). Paclitaxel belonging to the taxane family was an anti-mitotic drug blocking the microtubule depolarization leading to the inhibition of mitosis (12). Although lesser studied, the development of Nab-paclitaxel resistance seems to be related to drug metabolism involving oxidative reactions (13).

In this context, identification of new targets with antitumoral action on drug-resistant cancer cells represents an essential challenge. Since several years, our group demonstrated that orexin receptor type 1 (OX1R) but not orexin receptor type 2 (OX2R) was expressed in digestive cancer cells including pancreatic, colon, and liver cancers (14) where its activation by orexins induced a mitochondrial apoptosis leading to anti-tumoral impact of orexin/OX1R system (15). Orexins specifically activated two receptor subtypes belonging to the G-protein-coupled receptor (GPCR) family (16). Orexins, encompassing two isoforms named orexin-A (OxA) and orexin-B (OxB), are hypothalamic neuropeptides produced by the same precursor, the prepro-orexin (16). The main biological function of orexins was to control the wakefulness (17), and a dysregulation of this function led to human narcolepsy type I pathology (18). In 2018, it has been reported that OX1R was expressed in 96% of PDAC and also in pancreatic precancerous lesions (PanIN), whereas this receptor was not expressed in healthy pancreas exocrine tissue (19). Activation of OX1R by OxA in pancreatic cancer cells induced mitochondrial apoptosis (19). The orexin-inducted apoptosis was mediated by the phosphorylation of two immunoreceptor tyrosine-based inhibitory motifs (ITIMs) present in the OX1R sequence, the recruitment of the tyrosine-protein phosphatase non-receptor type 11 (SHP2), the activation of p38 mitogen-stress protein kinase leading to the translocation of proapoptotic Bax protein in mitochondria, releasing of cytochrome c, and activation of caspase 3 and 7 (20). In preclinical mouse models subcutaneously xenografted with the pancreatic cancer cell line, AsPC-1 or with isolated cells from PDAC patient named patient-derived xenografts (PDX), intraperitoneal injection of OxA induced a strong reduction in tumor volume (19). Based on these observations, the aim of the present study was to compare the anti-tumoral action on pancreatic cancer cell line, AsPC-1, of OxA to the action of gemcitabine and Nab-paclitaxel. Moreover, OxA is able to induce a strong inhibition of tumor growth in preclinical mouse models xenografted with pancreatic cancer cells made resistant to gemcitabine or Nab-paclitaxel treatment. These data demonstrate that the OxA/OX1R system represent a therapeutically innovative target in PDAC treatment notably in drug-resistant pancreatic cancers.

MATERIALS AND METHODS

Cell Culture

PDAC cell line, AsPC-1 (ATCC, CRL-1682), was cultured at 37°C in 5% CO_2/95% air in Roswell Park Memorial Institute (RPMI 1640) medium supplemented with 10% (v/v) fetal calf serum, 100 µg/ml streptomycin, 100 U/ml penicillin, and 1% (v/v) ZellShield (Minerva Biolabs, Berlin, Germany) to prevent mycoplasma contamination. AsPC-1 cells were incubated in the presence or in the absence of 0.1 µM orexin-A (OxA) (GL Biochemicals, Shangaï, China), 0.01 µM gemcitabine, 0.1 µM Nab-paclitaxel, 0.01 µM gemcitabine + 0.1 µM OxA, or 0.1 µM Nab-paclitaxel + 0.1 µM OxA. These doses of compounds corresponded to the dose that induced half of the effect on the cell growth inhibition. After 48 h of treatment, total cells were harvested and counted to determine the cell viability, as previously reported (19). To quantify apoptotic cells, the Guava Nexin Kit (Guava Technologies, Luminex, Austin, TX, USA) was used following the manufacturer's procedure. The dose–response curves of OxA, gemcitabine, Nab-paclitaxel, and their combination action were analyzed with SynergyFinder (v2.0) stand-alone-web application (21 and https://synergyfinder.fimm.fi/). In sequential treatment, AsPC-1 cells were incubated in the presence of 0.1 µM orexin-A or 0.01 µM gemcitabine or 0.1 µM Nab-paclitaxel for 48 h. After pretreatment, compounds were substituted for another 48 h by

0.01 μM gemcitabine or 0.1 μM Nab-paclitaxel for cells pretreated by OxA and 0.1 μM OxA for cells pretreated by 0.01 μM gemcitabine or 0.1 μM Nab-paclitaxel, respectively. Control corresponded to the absence of treatment for 96 h.

Immunohistochemical Procedure

Immunohistochemistry was performed on formalin-fixed paraffin-embedded 3-μm slices of spheroids or tumor tissue from xenografts with an automated immunohistochemical stainer according to the manufacturer's guidelines (automate BOND, Leica Microsystems). Slides were immunolabeled with antibodies against OX1R (Life Technology, PA5-33837, polyclonal rabbit, 1/250) or activated caspase-3 (Abgent, E87-77, polyclonal rabbit, 1/100).

Tumorigenicity Assays in Nude Mice Xenografts

A total of 2.10^6 AsPC-1 cells or 2.10^6 cancer cells isolated from pancreatic tumor patient were subcutaneously injected into the two flanks of five nude mice (to limit mouse number according to 3Rs rules) per arm corresponding to the development of 10 tumors per arm, as previously reported (19). At day 1 after cell injection, 100 μg OxA or 120 μg gemcitabine or 230 μg Nab-paclitaxel were intraperitoneally administered in 100 μl/injection three times per week until the endpoints defined in the protocol were reached. Control mice were intraperitoneally injected with phosphate-buffered saline (PBS). Tumor development was measured using a caliper according to a previous report (15). Briefly, the long and short axes (x,y) of tumors were determined three times per week, and tumor volumes were calculated according to the formula: $V = (^{x \cdot y^2 \cdot \pi}/_6)$. After necropsy, subcutaneous tumors were resected, weighted, and histologically analyzed. All experiments were performed in accordance with European ethical laws and in particular respecting the 3Rs rule according Apafis No. 17199-201810221522166v4. All along tumoral developments, the general condition and pain of animals were monitored, and endpoints were scored. At the end of the experiments, all animals were euthanized by cervical dislocation. The use of human materials was approved by the Institutional Review Board (CEERB GHU Paris Nord Nos. IRB12-059 and 12-033).

Establishment of Xenografted Resistant Tumors for Gemcitabine or Nab-Paclitaxel or OxA

To establish resistances to different compounds including PBS, gemcitabine, Nab-paclitaxel, or OxA, two successive runs of xenograft/treatment were planned. The first run (run01) consisted of subcutaneously inoculating AsPC-1 cells into nude mice followed by three intraperitoneal injections/week of PBS, 120 μg gemcitabine, 230 μg Nab-paclitaxel, or 100 μg OxA during 8 weeks before reaching the endpoints. Then, mice were euthanized, and tumors were resected. Tumors were sliced using scalpels and then incubated in dissociation medium containing culture medium added with collagenase IV (400 U/ml). The second run (run02) consisted of subcutaneously injecting dissociated cells corresponding to PBS-, gemcitabine-, Nab-paclitaxel-, or OxA-treated cells from run01 into a new batch of nude mice. Mice from run02 were again treated by three intraperitoneal 100-μl injections/week of PBS, 120 μg gemcitabine, 230 μg Nab-paclitaxel, or 100 μg OxA until endpoints defined in the protocol were reached. Tumor volumes were estimated as described above. At the end of the experiment, mice were euthanized and necropsied. Tumors were resected and weighted. Resected tumors were either formalin fixed or cell dissociated for RNA-seq and spheroid analyses.

Spheroids Analysis

Spheroid formation was obtained from AsPC-1 cells resistant to gemcitabine or Nab-paclitaxel or OxA isolated from xenografted tumors obtained in run02 experiments (see above). Briefly, xenografted tumors corresponding to control, gemcitabine treated, and Nab-paclitaxel treated were collected and dissociated, and tumoral cells were grown in 96-well plate (Corning, NY, USA) containing Dulbecco's modified Eagle's medium (DMEM) supplemented with 4.5 g/L of glucose, 10% (v/v) fetal calf serum, 100 μg/ml streptomycin, and 100 U/ml of 3,000 cells/well under agitation at 200 rpm, and were treated or not with 1 μM OxA, 0.01 μM gemcitabine, 0.1 μM Nab-paclitaxel, 1 μM OxA + 0.01μM gemcitabine, or 1 μM OxA + 0.1 μM Nab-paclitaxel up to 10–15 days. The volume of spheroids was determined using the plugin SpheroidSizer (21) under MathLab environment. Cell viability of spheroids was analyzed with ReadyProbes cell viability Imaging Kit (ThermoFisher Scientific, Illkirch, France) in which NucBlue live reagent stained alive cell nuclei and NucGreen death reagent stained only death cell nuclei.

RNA-seq Analysis

Transcriptomic analysis was performed on AsPC-1/gem^R or ASPC-1/pacli^R cells isolated from xenografted tumors acquired in run02 experiment (see above). After dissociation, tumor cells were cultivated in RPMI medium supplemented with 10% (v/v) fetal calf serum, 100 μg/ml streptomycin, 100 U/ml penicillin, and 1% (v/v) ZellShield in the presence of PBS (control), or 1 μM OxA for 24 h. Total RNA was extracted using Trizol reagent (Fisher Scientific, Illkirch, France) and then treated with DNAse I RNAse free (Fisher Scientific, Illkirch, France) to eliminate genomic DNA. The integrity of the total RNA was verified by agarose gel electrophoresis and quantified using NanoDrop One (Thermo Scientific, Les Ullis, France). RNA-seq was performed on genomic platform [Genomic Paris Centre (IBENS), Paris, France], and sequencing data were managed with the modular and scalable workflow engine, Eoulsan 2.5, which used DESeq 2 for normalization and differential analysis (IBENS, Paris, France). DESeq 2 files were analyzed with iDEP.94 (22), and the biological insight of mRNA significantly impacted by OxA was analyzed with WEB-based GEne SeT AnaLysis Toolkit (WebGeSTAT) packages using Kyoto Encyclopedia of Genes and Genomes (KEGG) database (https://www.genome.jp/kegg/). Heatmaps were generated with Morpheus (https://software.broadinstitute.org/morpheus).

Immunoblotting Assay

Semiconfluent AsPC-1, AsPC-1 gem^R, or AsPC-1 Nab-pacli^R cells were washed twice with phosphate-buffered saline and treated with 1 μM OxA in medium or with medium only at 37°C for 24 h. Cells were collected and lysed with RIPA buffer [10 mM Tris–HCl (pH 7.5), 150 mM NaCl, 1 mM EDTA, 1 mM EGTA, 2 mM Na_3VO_4, 0.1% sodium dodecyl sulfate (SDS), 1% Nonidet P-40, 1% sodium deoxycholate, 0.36 μg/ml phenylmethylsulfonyl fluoride, 0.01% soybean trypsin inhibitor, 0.01% leupeptin, and 0.01% aprotinin]. The mixture was gently agitated for 30 min at 4°C and centrifuged at 15,000×*g* for 15 min at 4°C, followed by collection of the supernatant. Solubilized proteins (100 μg) in Laemmli buffer (incubated for 5 min at 98°C) were loaded onto a 10% SDS-polyacrylamide gel, transferred to a nitrocellulose membrane, and immunoblotted with antibodies described below. Anti-SHP-2/SHPTP-2 (1:1,000) antibody was from Millipore (Guyancourt, France); anti-FoxM1 (D12D5) (1:1,000), anti-cleaved PARP (Asp214) (1:1,000), anti-PARP (46D11) (1:1,000), anti-elF2a (Ser51) (1:1,000 dilution), anti-ATF-3 (D2Y5W) (1:1,000 dilution), anti-ATF-4 (D4D8) (1:1,000 dilution), or anti b-actin (8H10D10) (1:1,000) antibodies were from Cell Signaling Technology (Dancers, USA); anti-DNA polymerase theta antibody (1C11) (1:1,000 dilution) was from Novus Biologicals (Centennial, USA); and anti-NrF2 (ab137550) (1:1,000 dilution) and anti-Bcl-2 (E17) (1:1,000 dilution) antibodies were from Abcam (Cambridge, UK). Immunoreactive proteins were secondary labeled with ECL™ anti-rabbit IgG antibody (1:10,000) (NA934) (Amersham, Little Chalfont, UK) or with anti-mouse IgG-peroxidase antibody (A9044) (1:8,000) (Sigma-Aldrich, Saint Quentin Fallavier, France), visualized by ECL immunodetection (Amersham, Little Chalfont, UK) and quantified by chemoluminescence analysis.

Statistical Analysis

Results were expressed as mean ± standard error of the mean (SEM). All data were analyzed with GraphPad Prism v8.4.3 software (GraphPad software, San Diego, CA, USA). The Student's t-test (two-tailed 95% confidence intervals) was used for comparison of two mean values. A normality test (Agostino–Pearson test) was applied to validate the use of an ANOVA with *post-hoc* Bonferroni's tests when groups of mean values were more than 2. In different figure legends, samples sizes were indicated, and statistical significance was defined as $p<0.05$.

RESULTS

Combined Effect of OxA and Gemcitabine on Cancer Cell Growth

As previously reported, OxA was able to induce a cell apoptosis through the recruitment of the tyrosine phosphatase SHP2 in pancreatic cancer cell line AsPC-1 (19). The pro-apoptotic action of OxA or gemcitabine, which represents a gold standard in the first-line treatment of metastatic PDAC (1), and their combinations were investigated. After 48 h of treatment with OxA or gemcitabine or their combination, AsPC-1 pancreatic cancer cells showed an inhibition of cell viability (**Figure 1A**). Gemcitabine (0.01 μM) or OxA (0.1 μM) reduced the cell growth of about 40%. Moreover, the addition of OxA (0.1 μM) to gemcitabine (0.01 μM) inhibited the cell viability of about 50% (**Figure 1A**). As expected, inhibition of cancer cell growth induced by OxA and gemcitabine resulted in apoptotic action of these compounds (**Figure 1B**). Gemcitabine (0.01 μM) induced a cell apoptosis of 12 ± 1%, 0.1 μM of OxA induced a cell apoptosis of 13 ± 1%, and the combination of these two compounds induced a cell apoptosis of 15 ± 1% (**Figure 1B**). It should be noted that the combination of both treatments was significantly different ($p<0.05$) from OxA or gemcitabine alone (**Figure 1B**). As shown in **Figure 1C**, the action of OxA or gemcitabine or the combination of OxA and gemcitabine decreased cell growth in a dose-dependent manner. To determine if the action of combined OxA and gemcitabine was additive or synergic, a Bliss synergy score was determined (**Figure 1D**). Currently, surface plot based on Bliss independence response is used to test anticancer synergic action of two independent drugs that targeted two different signaling pathways (23). The resulting Bliss synergy score can be interpreted as the average excess response due to drug interactions (23). In case of the additive action of two drugs, the Bliss synergy score was from −10 to 10 (23). In contrast, a Bliss synergy score >10 indicated that the interaction between these two drugs was synergic. Analysis of dose–response curves encompassing the cell viability action of OxA or gemcitabine and the combination of OxA plus gemcitabine revealed a Bliss synergy score of 5.099, suggesting that OxA and gemcitabine proceeded in an additive way to inhibit the cell growth of pancreatic cell line, AsPC-1 (**Figure 1D**). To investigate the influence of treatment sequence of OxA and gemcitabine on PDAC cell viability, AsPC-1 cells were incubated in the presence of (1) 0.01 μM of gemcitabine for 48 h followed by 0.1 μM of OxA treatment for 48 h (2), 0.1 μM of OxA for 48 h followed by 0.01 μM of gemcitabine treatment for 48 h, or (3) combination treatment for 96 h. As shown in **Figure 1E**, whatever was the treatment sequence, an inhibition of cancer cell viability of about 50% was observed, indicating that there is no influence of treatment sequence on the ability of these two molecules to inhibit cancer cell growth.

Combined Effect of OxA and NAB-Paclitaxel on Cancer Cell Growth

Currently, Nab-paclitaxel represents a molecule widely used in the treatment arsenal of metastatic PDAC, associated or not to gemcitabine (1). To compare the action of OxA and Nab-paclitaxel on AsPC-1 cell line growth, cells were incubated in the presence of 0.1 μM of OxA or 0.1 μM of Nab-paclitaxel or with a combination of 0.1 μM of each molecule. As shown in **Figure 2A**, the treatment of AsPC-1 by Nab-paclitaxel or OxA or their combinations inhibited cell viability of 57 ± 2%, 32 ± 4%, and 69 ± 2%, respectively. This cancer cell growth inhibition induced by OxA and Nab-paclitaxel resulted in an apoptotic action of these molecules (**Figure 2B**). Nab-paclitaxel

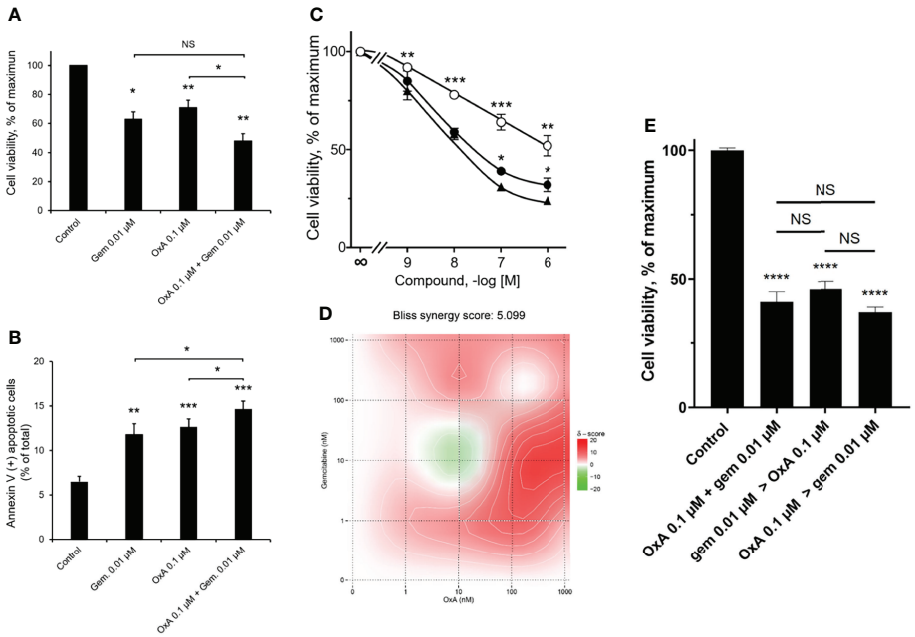

FIGURE 1 | Inhibition of AsPC-1 cell growth by OxA and/or gemcitabine. **(A)** Inhibition of AsPC-1 cell viability induced by 0.01 µM gemcitabine (gem), 0.1 µM OxA (OxA), or 0.01 µM gemcitabine plus 0.1 µM OxA. Results were expressed in the percentage of maximum obtained in the absence of treatment (control). **(B)** Effect of OxA or gemcitabine or their combination on apoptosis of ASPC-1 cells. Apoptosis was determined by annexin V/7-AAD binding, and results were expressed as the percentage of apoptotic cells. **(C)** Effect of the dose–response of OxA or gemcitabine or OxA plus gemcitabine on cell viability of AsPC-1 cells. **(D)** Bliss model diagram and estimation of Bliss synergy score. **(E)** OxA plus gemcitabine treatment and sequential treatment by OxA>gemcitabine or gemcitabine>OxA compared to control (absence of treatment). Results were expressed in the percentage of maximum obtained in the absence of treatment. Data were the means ± SEM of three separate experiments. (○) OxA, (●) gemcitabine, and (▲) OxA plus gemcitabine. NS, non-significant, *p<0.05, **p<0.01, ***p<0.001, and ****p<0.0001 corresponding to comparison with control.

(0.1 µM) induced 17.3 ± 1.2% of apoptosis, 0.1 µM of OxA induced 12.1 ± 1.0% of apoptosis, and the combination of these two molecules induced 25.1 ± 1% apoptosis (**Figure 2B**). As expected, the action of OxA or Nab-paclitaxel or their combination on cell viability was dose dependent (**Figure 2C**). The determination of Bliss synergy score of the cell viability dose–response curves of OxA or Nab-paclitaxel or OxA plus Nab-paclitaxel displayed a score of 4.044, indicating that OxA and Nab-paclitaxel were acting in an additive manner (**Figure 2D**). The treatment sequence influence of OxA and Nab-paclitaxel on cancer cell viability was tested as previously described above. As shown in **Figure 2E**, no significant differences were observed between the sequence of Nab-paclitaxel treatment followed by OxA treatment compared to the addition of OxA followed by Nab-paclitaxel treatment. In contrast, a significant difference was obtained between the sequence OxA treatment followed by Nab-paclitaxel treatment compared to addition of OxA and Nab-paclitaxel, indicating that the additive treatment was more favorable than the sequential treatment (**Figure 2E**).

Impact of OxA and Gemcitabine on Tumor Growth in Preclinical Models

One hundred micrograms of OxA (4 mg/kg) or 120 µg gemcitabine (5 mg/kg) or 100 µg OxA plus 120 µg gemcitabine was intraperitoneally injected three times/week in nude mice subcutaneously xenografted with 2.10^6 AsPC-1 cells at day 1 after implantation. As shown in **Figure 3A**, OxA and gemcitabine induced a significant and similar inhibition of tumor volume of 56% and 65%, respectively, as compared to untreated control mice. Treatment with the combination of OxA and gemcitabine revealed a significant inhibition of tumor volume of 74% as compared to untreated control mice. Moreover, the combination was significantly more effective than OxA treatment alone (**Figure 3A**). After animal sacrifice and tumor resections, histological analyses by anti-OX1R immunostaining revealed that the OX1R expression was not affected by OxA or gemcitabine or OxA plus gemcitabine treatments as compared to tumors resected from control mice (**Figure 3B**). However, an intense staining of activated cleaved caspase-3 revealing a cell apoptosis was observed in OxA, gemcitabine, and OxA plus gemcitabine treatment, whereas no immunostaining of activated caspase-3 was observed in control mice (**Figure 3B**).

Impact of OxA and Nab-Paclitaxel on Tumor Growth in Preclinical Models

After subcutaneous injection of 1.10^6 AsPC-1 cells in nude mice, intraperitoneal injection three times/week of 100 µg OxA (4 mg/kg) or 230 µg (9.2 mg/kg) Nab-paclitaxel and 100 µg OxA

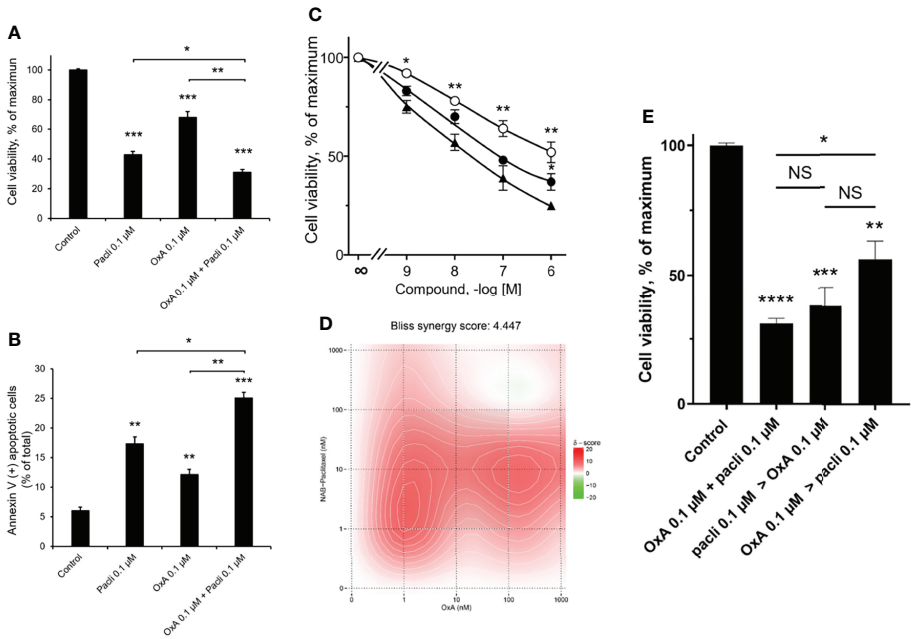

FIGURE 2 | Inhibition of AsPC-1 cell growth by OxA and/or Nab-paclitaxel. **(A)** Inhibition of AsPC-1 cell viability induced by 0.1 µM Nab-paclitaxel (pacli), 0.1 µM OxA (OxA), or 0.1 µM Nab-paclitaxel plus 0.1 µM OxA. Results were expressed in the percentage of maximum obtained in the absence of treatment (control). **(B)** Effect of OxA or Nab-paclitaxel or their addition on apoptosis of ASPC-1 cells. Apoptosis was determined by annexin V/7-AAD binding, and results were expressed as the percentage of apoptotic cells. **(C)** Effect of the dose–response of OxA or Nab-paclitaxel or OxA plus Nab-paclitaxel on cell viability of AsPC-1 cells. **(D)** Bliss model diagram and estimation of Bliss synergy score. **(E)** OxA plus Nab-paclitaxel treatment and Impact of sequential treatment by OxA>Nab-paclitaxel or Nab-paclitaxel>OxA compared to control (absence of treatment). Results were expressed in the percentage of maximum obtained in the absence of treatment. Data were the means ± SEM of three separate experiments. (○) OxA, (●) Nab-paclitaxel, and (▲) OxA plus Nab-paclitaxel. NS, non-significant, *p<0.05, **p<0.01, ***p<0.001, and ****p<0.0001 corresponding to comparison with control.

plus 230 µg Nab-paclitaxel on day 1 after implantation showed that OxA and Nab-paclitaxel were able to significantly reduce the tumor volume of 60% and 55%, respectively, as compared to control mice (**Figure 4A**). Moreover, intraperitoneal injection of OxA and Nab-paclitaxel reduced the tumor volume of 70% as compared to control mice. Although statistically insignificant, the addition of OxA to Nab-paclitaxel induced a higher trend of tumor volume reduction than the use of OxA or Nab-paclitaxel alone (**Figure 4A**). Histological analyses of resected tumors revealed that OX1R expression was not modified in Nab-paclitaxel and OxA plus Nab-paclitaxel treatments as compared to control tumors, indicating that different treatments did not have any impact on OX1R expression (**Figure 4B**). Furthermore, injection of OxA or Nab-paclitaxel and OxA plus Nab-paclitaxel induced an intense cell death by mitochondrial apoptosis in treated tumors but not in control tumors (**Figure 4B**).

Impact of OxA on Tumors Having Been Made Resistant to Gemcitabine or Nab-Paclitaxel

Tumors from mice xenografted with AsPC-1 cells, having been treated by gemcitabine or Nab-paclitaxel or OxA (run01) for 40 days (**Figure 5A**), were resected, dissociated with collagenase IV, and subcutaneously reinjected in nude mice to form new tumors (run02). As shown in **Figure 5B**, injection of gemcitabine did not inhibit run02 tumor growth as compared to control, suggesting that run02 tumors had acquired gemcitabine resistance. In contrast, OxA was always able to inhibit the tumor's growth obtained with the cell of run01 (**Figure 5B**), suggesting that OxA reduced the volume of gemcitabine-resistant tumors. Similarly, injection of Nab-paclitaxel had no effect on tumor growth of run02 as compared to control (**Figure 5C**), indicating that these tumors displayed resistance to Nab-paclitaxel. However, injection of OxA induced a reduction in tumor volume in Nab-paclitaxel-resistant tumors (**Figure 5C**). Moreover, no resistance to OxA treatment was observed in tumors. As shown in **Figure 5D**, tumors developed (run02) from previous OxA-treated tumors (run01) were fully sensitive to OxA. It should be noted that the OxA sensitivity of gemcitabine-resistant tumors was also observed for tumors developed from patient-derived xenograft (PDX) cells isolated from PDAC tumors. Indeed, cells from this PDX (PDAC15), which has been previously characterized as OX1R-expressing cells (22), were subcutaneously injected in nude mice followed by gemcitabine treatment (run01), and cells from resulting tumors were again injected to nude mice. As shown in **Figure 5E**, OxA was also able to reduce tumors volume of gemcitabine-resistant tumors from PDX.

Histological analyses show that OX1R was expressed in gemcitabine and Nab-paclitaxel tumors (**Figures 6A, B**). This

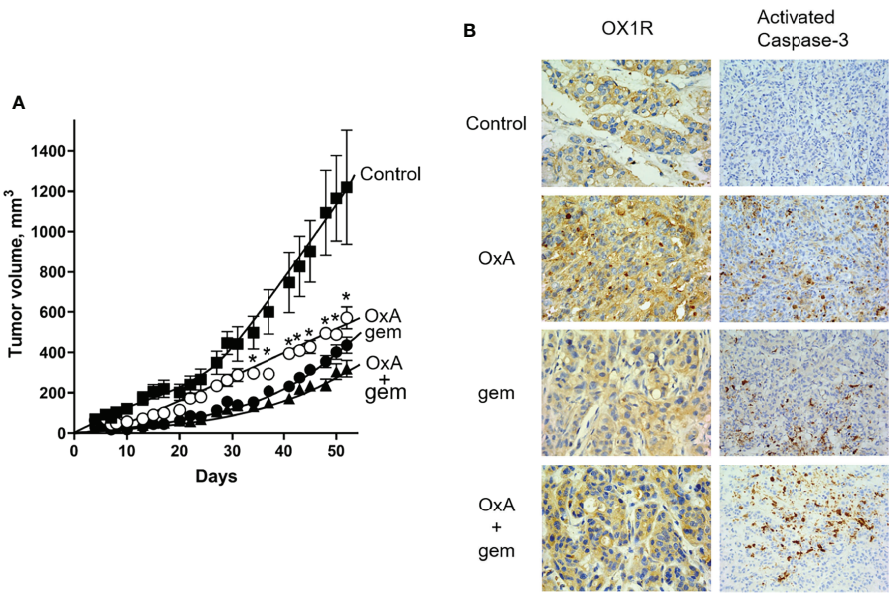

FIGURE 3 | Preclinical study and histological analysis of anti-tumoral effect of OxA and gemcitabine. **(A)** Impact of three injections/week of 100 µg OxA, 120 µg gemcitabine, or 100 µg OxA plus 120 µg gemcitabine on volume of tumors developed from subcutaneously xenografted ASPC-1 cells in nude mice. The tumor development was measured with a caliper. **(B)** Determination of OX1R expression and caspase-3 activation by histological immunostaining in xenografted AsPC-1 resected tumors from mice treated with PBS (control), OxA (OxA), gemcitabine (gem), or OxA plus gemcitabine (OxA + gem). Magnification was 40× (OX1R expression) and 20× (caspase-3 activation). Data were the means ± SEM of six tumors in each group. *p<0.05.

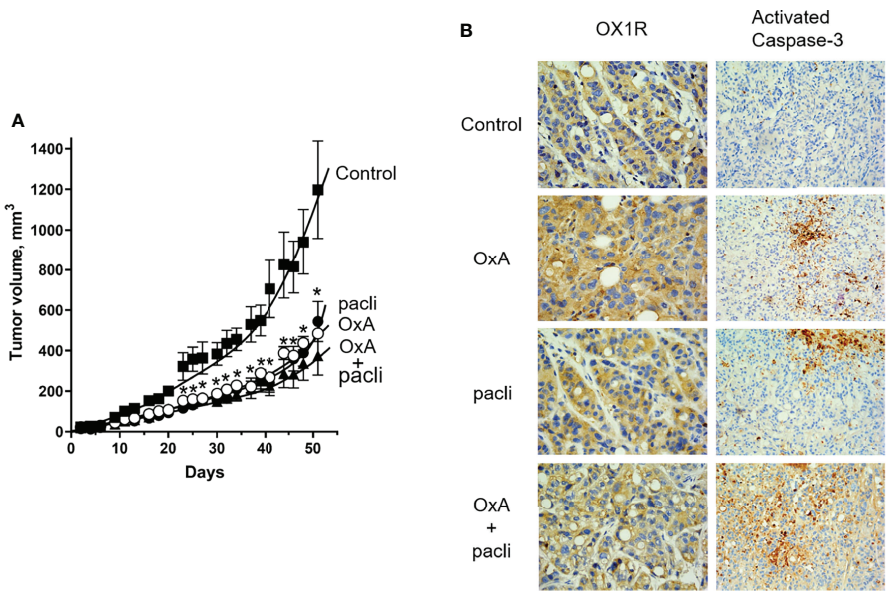

FIGURE 4 | Preclinical study and histological analysis of anti-tumoral effect of OxA and Nab-paclitaxel. **(A)** Impact of three injections/week of 100 µg OxA, 230 µg Nab-paclitaxel, or 100 µg OxA plus 230 µg Nab-paclitaxel on volume of tumors developed from subcutaneously xenografted ASPC-1 cells in nude mice. The tumor development was measured with a caliper. **(B)** Determination of OX1R expression and caspase-3 activation by histologic immunostaining in xenografted AsPC-1 resected tumors from mice treated with PBS (control), OxA (OxA), Nab-paclitaxel (pacli), or OxA plus Nab-paclitaxel (OxA + pacli). Magnification was 40× (OX1R expression) and 20× (caspase-3 activation). Data were the means ± SEM of six tumors in each group. *p<0.05.

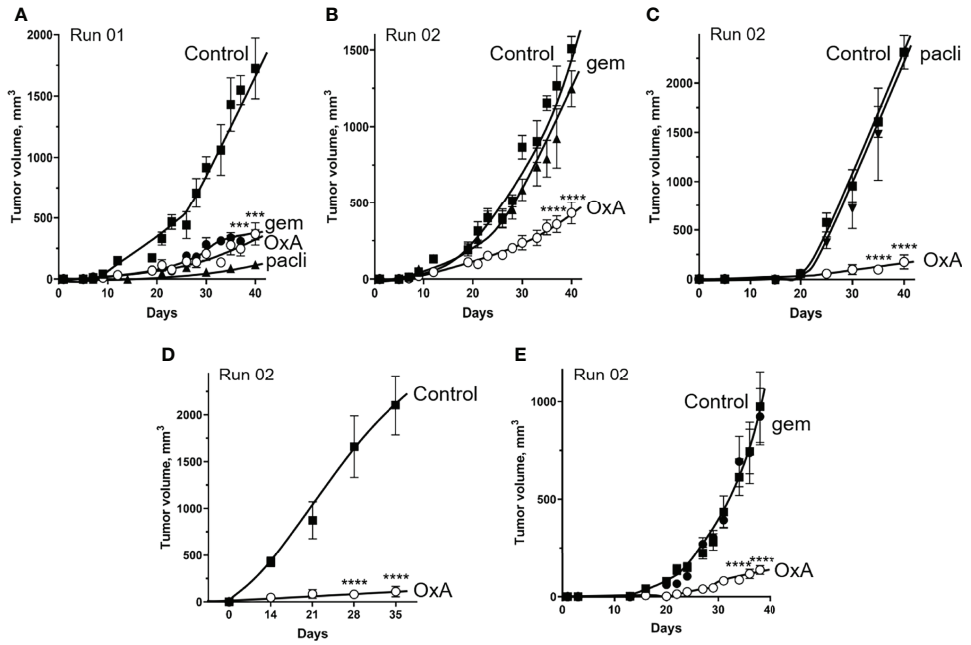

FIGURE 5 | Effect of OxA on tumor development of gemcitabine- and Nab-paclitaxel-chemoresistant tumors xenografted in nude mice. **(A)** A total of 2.10^6 AsPC-1 cells were subcutaneously injected in nude mice, which were treated by three injections/weeks of PBS (control), OxA (OxA), gemcitabine (gem), or Nab-paclitaxel (pacli). This first step of the experiment was noted as "Run 01." After 40 days, mice were sacrificed, and resected tumors were dissociated with collagenase and subcutaneously reinjected in nude mice. This step was named "Run 02" of experiments. **(B)** The impact of OxA and gemcitabine on tumor development of gemcitabine-treated tumors xenografted in nude mice (Run 02). **(C)** Impact of OxA and Nab-paclitaxel on tumor development of NAB-paclitaxel-treated tumors xenografted in nude mice (Run 02). **(D)** Impact of OxA on tumor development of OxA-treated tumors xenografted in nude mice (Run 02). **(E)** The impact of OxA and gemcitabine (Run 02) on tumor development of gemcitabine-treated tumors from Run 01 experiment in which tumors were obtained by xenografting of 2.10^6 PDAC15 (PDX) cells. Data were the means ± SEM of six tumors in each group. ***p<0.001 and ****p<0.0001.

expression was not modified by OxA and gemcitabine or Nab-paclitaxel treatment (**Figures 6A, B**). However, only OxA was able to induce the caspase-3 activation in tumor tissues as compared to control and gemcitabine or Nab-paclitaxel-treated tumors (**Figures 6A, B**). In addition, OX1R was expressed in tumors obtained with cells from tumors previously treated by OxA (**Figure 6C**). Moreover, the activation of caspase-3 was observed when the tumors were treated with OxA as compared to control tumors (**Figure 6C**). In the same way, OX1R was expressed in gemcitabine-resistant tumors from PDAC15, and OxA was able to activate caspase-3 in these tumors as compared to control tumors (**Figure 6D**). This set of results indicates that OxA was able to inhibit tumor growth of gemcitabine- or Nab-paclitaxel-resistant tumors involving a proapoptotic process, in preclinical models using PDAC cell lines or PDX.

To confirm these observations, spheroids were developed with AsPC-1 cells isolated from control, gemcitabine-resistant, or Nab-paclitaxel-resistant tumors (run02); then, they were treated with PBS, OxA, gemcitabine, or Nab-paclitaxel (**Figure 6E**). After 7 days of culture, the cell viability of spheroids was tested using ReadyProbes Cell Viability Imaging Kit in which live cells were associated to blue fluorescence and dead cells were associated with green fluorescence. As shown in **Figure 6E**, spheroids, in the absence of treatment (control), were mostly composed of living cells, whereas in the presence of OxA, gemcitabine, and Nab-paclitaxel, a lot of dead cells appeared. In contrast, spheroids obtained from gemcitabine-resistant tumor cells displayed a lack of dead cells when spheroids were untreated or treated with gemcitabine (**Figure 6E**), while dead cells appeared in the presence of OxA (**Figure 6E**). Under the same conditions, spheroids from Nab-paclitaxel-resistant tumor cells were insensitive to Nab-paclitaxel treatment as compared to untreated spheroids (**Figure 6E**). In contrast, OxA induced cell death in these spheroids (**Figure 6E**).

OxA Induced an Increase in ATF3 and Cleaved PARP in Gemcitabine- and Nab-Paclitaxel-Resistant Tumors

To determine whether OxA induced tumor growth inhibition *via* OX1R expression in gemcitabine- or Nab-paclitaxel-resistant tumors or/and modified the expression of proteins involved in the resistance processes, a transcriptomic analysis of expression of various proteins related to drug resistance in PDAC was carried out. Transcripts specifically regulated in gemcitabine- or Nab-paclitaxel-resistant tumors treated or not by OxA were identified by RNA-seq and analyzed by functional enrichment using GSEA software and WEB-based GEne SeT AnaLysis Toolkit (WebGeSTAT) (22). As shown in **Figure 7A**, few transcripts were impacted by OxA in gemcitabine- or Nab-paclitaxel-resistant tumors. These transcripts mainly represent pseudogene and long

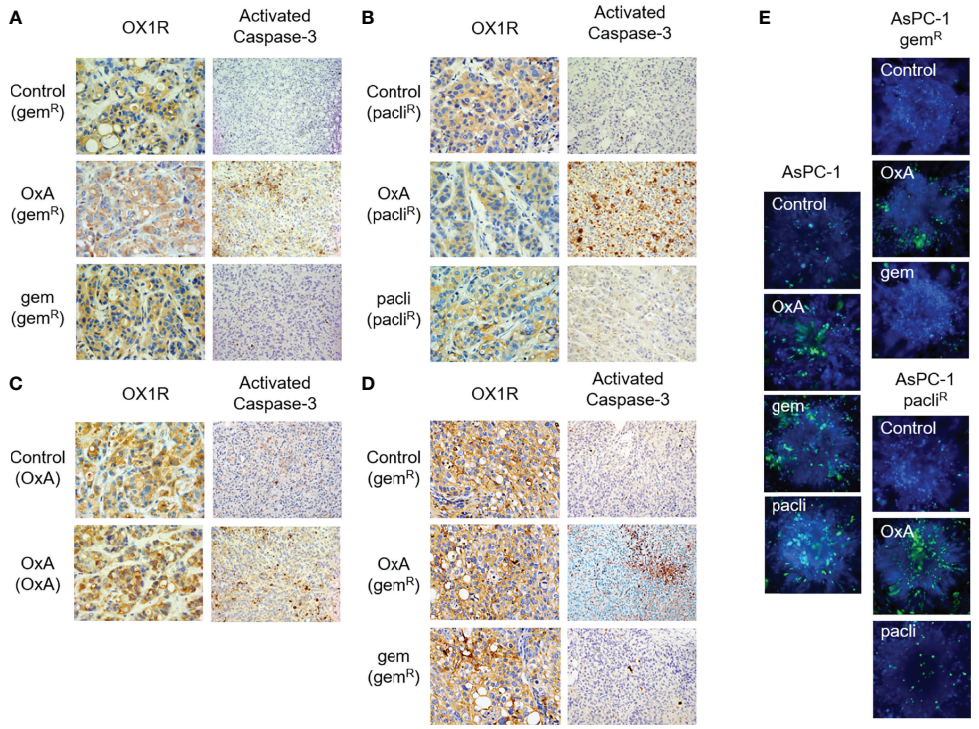

FIGURE 6 | Histological analysis of resected tumors from Run 02 experiments. **(A)** OX1R expression and caspase-3 activation in gemcitabine-chemoresistant AsPC-1 tumors (gem^R) treated with PBS (Control), OxA (OxA), and gemcitabine (gem). **(B)** OX1R expression and caspase-3 activation in Nab-paclitaxel-chemoresistant AsPC-1 tumors (pacli^R) treated with PBS (Control), OxA (OxA), and Nab-paclitaxel (pacli). **(C)** OX1R expression and caspase-3 activation in 50 days OxA-treated tumors (OxA) treated with PBS (control) and OxA (OxA). **(D)** OX1R expression and caspase-3 activation in gemcitabine-chemoresistant tumors obtained by xenografting of 50 days gemcitabine-treated PDAC15 cells (gem^R) treated with PBS (control), OxA (OxA), and gemcitabine (gem). **(E)** Cell viability determination of spheroids developed with parental AsPC-1, gemcitabine-resistant, and Nab-paclitaxel-resistant AsPC-1 cells isolated in Run 02 experiment. Magnification was 40× (OX1R expression) and 20× (caspase-3 activation).

non-coding RNA (lncRNA). Nevertheless, OxA was able to increase the expression of HRK coding for harakiri protein, which promoted apoptosis by interaction with Bcl-2 and Bcl-XL (24). Moreover, functional enrichment analysis using WikiPathway cancer database showed that differential expression of transcripts associated with OxA treatment in AsPC-1 cells resistant to gemcitabine or Nab-paclitaxel were related to apoptosis, Wnt signaling in cancer, olfactory transduction, and insulin or chemokine signaling pathways (**Figure 7B**). These results indicated that OxA treatment of gemcitabine- or Nab-paclitaxel-resistant tumors had very small impact on transcriptome excepted for HRK, which displayed pro-apoptotic properties. The expression of various proteins expressed in PDAC and participating in tumoral drug resistance including cell stress proteins (Nrf2, p-eIF2α, ATF3, and ATF4), DNA reparation proteins (PolQ and PARP), oncogenic protein (FoxM1), and anti-apoptotic protein (Bcl2) were analyzed in gemcitabine- or Nab-paclitaxel-resistant tumors treated or not by OxA. As shown in **Figure 7C**, the expression of Nrf2, Bcl2, peIF2α, PolQ, FoxM1, and ATF4 was not modified in the presence of OxA in gemcitabine- or Nab-paclitaxel-resistant tumors. It should be noted that the expression of SHP2, which played a key role in pro-apoptotic action of orexins in digestive cancers (15, 19), was not regulated by OxA (**Figure 7C**). In contrast, OxA was able to increase the expression of ATF3 in gemcitabine- or Nab-paclitaxel-resistant tumors. However, in non-resistant AsPC-1 cells, ATF3 was highly expressed, whereas in gemcitabine- or Nab-paclitaxel-resistant cells, ATF3 was much lower expressed (**Figure 7C**). Semi-quantitative analysis of Western blot showed that OxA also induced the expression of ATF3 in gemcitabine- or Nab-paclitaxel-resistant cells (**Figure 7D**, right panel). As PARP was involved in DNA reparation and cell survival of cancer cells (25), we determined the action of OxA on PARP cleavage leading to its inactivation, in gemcitabine- or Nab-paclitaxel-resistant tumors. As shown in **Figure 7C**, OxA induced an increase of PARP cleavage in gemcitabine- or Nab-paclitaxel-resistant tumors. Semi-quantitative analysis of Western blot confirmed these observations and revealed that OxA increased the cleavage of PARP in gemcitabine- or Nab-paclitaxel-resistant but not in non-resistant AsPC-1 cells (**Figure 7D**, left panel).

DISCUSSION

It is well known that GPCRs, identified as the largest cell surface receptor family that is the most common therapeutic target

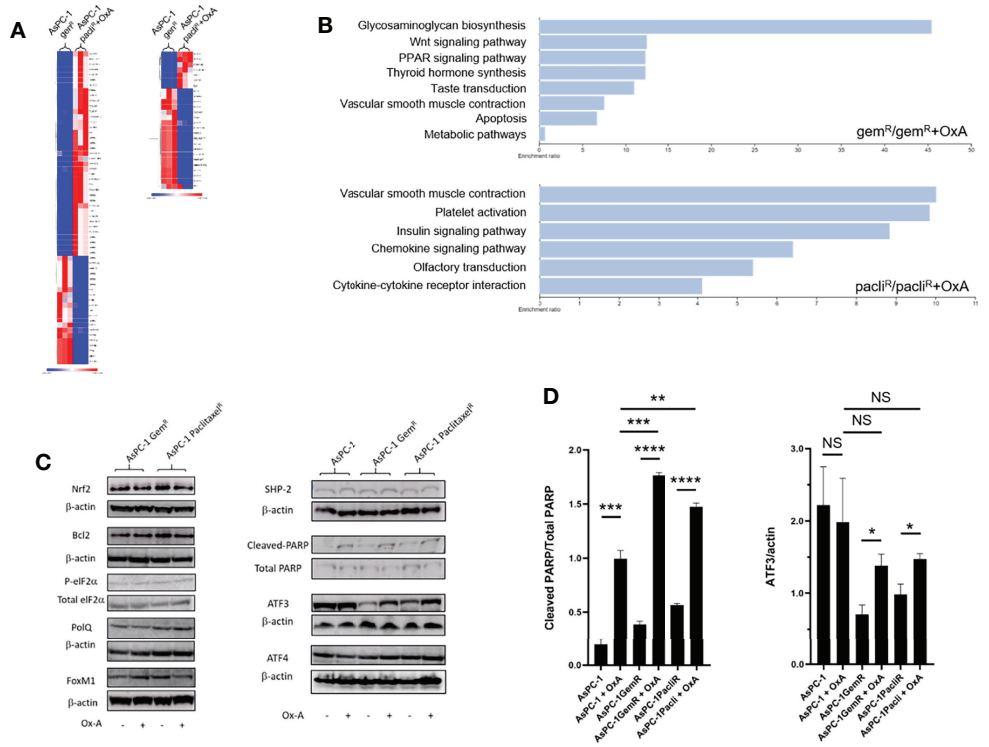

FIGURE 7 | RNA-seq and Western blot analysis of gemcitabine- and Nab-paclitaxel-chemoresistant tumors treated or not by OxA. **(A)** Heatmap of mRNA expression in gemcitabine- and Nab-paclitaxel-chemoresistant tumors treated or not by OxA. **(B)** Diagram of functional enrichment analysis of mRNA expression in gemcitabine- and Nab-paclitaxel-chemoresistant tumors treated or not by OxA. **(C)** NrF2, Bcl2, p-eIF2α, PolQ, FoxM1, SHP-2, cleaved-PARP, ATF3, and ATF4 factor expression in gemcitabine- and Nab-paclitaxel-chemoresistant tumors treated or not by OxA. **(D)** Semi-quantitative analysis of cleaved-PARP and ATF3 expression in gemcitabine- and Nab-paclitaxel-chemoresistant tumors treated or not by OxA, determined by Western blot.

encompassing about 40% of FDA-approved molecules, represent an innovative target in cancer (26). It is common that GPCRs emerged as key targets in tumor growth and/or metastasis associated to their overexpression/underexpression in cancer cells and also their abilities to stimulate/inhibit proliferation or inversely stimulate/inhibit apoptosis (27). Among this large family, we have demonstrated in 2011 that OX1R, but not OX2R, was ectopically expressed in colon cancer whatever its location and/or grade of development (15). The OX1R activation in colon cancer cells by exogenous orexins (OxA or OxB) induced the mitochondrial caspase-dependent apoptosis (28) The OxA/OX1R system was responsible for the anti-tumoral impact in preclinical models in which colon cancer cells were xenografted and also in preclinical models where pancreatic or liver cancer cells were xenografted (15, 19, 29). Usually, the first or second line of pancreatic cancer treatment, notably in metastatic pancreatic cancer, involved gemcitabine and Nab-paclitaxel (1). Here, the comparison between gemcitabine, Nab-paclitaxel, and OxA treatment on the OX1R-expressing pancreatic cancer cell line, AsPC-1, showed that OxA had a similar impact in terms of cancer cell growth as compared to gemcitabine and Nab-paclitaxel. Moreover, the addition of OxA to gemcitabine or Nab-paclitaxel improved the impact of those molecules. These potentiation effects were associated to an additive effect and not to a synergistic effect. The absence of synergic effect observed between OxA plus gemcitabine or OxA plus Nab-paclitaxel could be related to the different mechanisms of action of these three molecules. In fact, OxA/OX1R directly activates mitochondrial apoptosis in pancreatic cancer cells, whereas gemcitabine inhibited the DNA synthesis in pancreatic cancer cells, inducing cytotoxicity that leads to apoptosis (30), and Nab-paclitaxel inhibited microtubule dynamics inducing cytotoxicity that also leads to apoptosis (12). It should be noted that the sequences of first treatment by OxA followed by gemcitabine or inversely were not significantly different than the simultaneous addition of OxA and gemcitabine. In contrast, the sequence of first treatment by OxA followed by Nab-paclitaxel was significantly less effective than the simultaneous addition of OxA and Nab-paclitaxel, suggesting that the pro-apoptotic action of OxA in the first was not favorable to Nab-paclitaxel's following action. These observations reinforced the fact that the inhibition of AsPC-1 cell growth by OxA plus gemcitabine or OxA plus Nab-paclitaxel was fully additive and also indicated that the addition of OxA with gemcitabine or with Nab-paclitaxel was more effective than molecules alone. Our previous data

demonstrated that OxA reduced tumor volume of subcutaneously xenografted mice with AsPC-1 cells (19). In the present report, we confirmed that OxA strongly reduced the tumor volume of xenografted mice with AsPC-1 cells and show that this anti-tumoral effect was similar to gemcitabine or Nab-paclitaxel treatment. Although statistically not significant, it seems that the treatment by OxA plus gemcitabine or OxA plus Nab-paclitaxel was more effective than OxA alone, indicating that OxA, *in vivo*, also had an additive effect with the two drugs. It was well known that repetitive activation of GPCRs by agonist ligands led to a decrease in GPCR response associated to desensitization and cell internalization processes (31). However, histological analysis of xenografted tumors treated over the long term, with OxA, gemcitabine, Nab-paclitaxel, OxA plus gemcitabine, or OxA plus Nab-paclitaxel revealed that OX1R was always expressed in tumor cells after 50 days of these different treatments. These observations indicate that OX1R was not downregulated and/or the receptor turnover maintained OX1R expression at the cell surface in the presence of these three molecules. As expected, OxA-treated xenografted tumors revealed the presence of activated caspase-3, demonstrating that OxA-induced tumor volume reduction was associated to mitochondrial apoptosis (15, 19). Moreover, xenografted tumors treated with gemcitabine or Nab-paclitaxel displayed activated caspase-3, showing that these two drugs induced caspase-dependent apoptosis as previously reported in various models (12, 30).

The activation of OX1R by exogenous OxA induced a strong reduction in tumor volume in mice xenografted with AsPC-1 cells displaying a chemoresistance to gemcitabine or Nab-paclitaxel. In contrast, no resistance to OxA treatment has been identified to be probably associated to a permanent OX1R expression in xenografted tumors and the ability of this receptor to induce apoptosis after its activation by OxA. It should be noted that OX1R was also expressed in colon cancer cell line, HT29-FU, which presented resistance to 5-FU, established *in vitro*, and the activation of OX1R by OxA induced a pro-apoptotic effect in these cells (15). Histological analysis of gemcitabine- and Nab-paclitaxel-resistant xenografted tumors treated by OxA revealed a caspase-3 activation, demonstrating the induction of apoptosis by OxA in chemoresistant tumors. We have demonstrated that OX1R was expressed in PDX named PDAC15 isolated from a patient's tumor and that the activation of OX1R in PDAC15 led to a tumor growth inhibition in preclinical models (19). Here, we observed that OxA induced a tumor development inhibition in gemcitabine-resistant tumors xenografted with PDAC cells isolated from tumor patient (PDX). Taking these observations into account, we demonstrated that OX1R was already expressed in chemoresistant tumors and that its activation induced an anti-tumoral effect.

RNA sequence analysis of mRNA prepared from gemcitabine-resistant or Nab-paclitaxel-resistant PDAC cells isolated from tumors that developed in xenografted mice, treated or not by OxA, revealed that OxA had a poor effect on the transcriptome of these cells. The major impact was mainly focused on pseudogenes and lncRNA. This observation was confirmed by the functional enrichment analysis, which showed that the major impact was related to the markers of signaling pathways, such as Wnt, insulin, chemokine, and olfactory signaling pathways. However, in gemcitabine-resistant tumors treated with OxA, the apoptosis signaling pathway represented by an increase in HKR transcripts was revealed. HRK, also named harakiri, expressed in the pancreas, liver, lung, kidney, and prostate, was an activator of apoptosis through the inhibitory interaction with Bcl-2 and Bcl-X, which had anti-apoptosis properties (24). HRK gene seems to have an important role in the apoptosis regulation in tumor cells, and its inactivation by methylation could be related to tumorigenesis of prostate cancer (32). However, it cannot exclude that the overexpression/underexpression of lncRNA and/or pseudogenes in OxA-treated gemcitabine-resistant and Nab-paclitaxel-resistant PDAC cells could play a role in anti-tumoral action of OxA. Indeed, it was demonstrated that particular lncRNA or pseudogenes played a role in cancer by interacting with chromatin, proteins, and RNAs in cancer cells (33). The impact of OxA treatment on chemoresistant tumors, on the expression of various proteins such as Nrf2, p-eIF2α, ATF4, PolQ, FoxM1, and Bcl2, which are involved in cancer chemoresistance (34–38), is not shown. Interestingly, neither OX1R expression nor SHP2, which displayed a key role in cell apoptosis induced by orexins (14), was regulated by OxA. In contrast, OxA was able to increase the expression of ATF3 in gemcitabine- and Nab-paclitaxel-resistant tumors. Cyclic AMP-dependent transcription factor ATF-3 is also playing a role in modulating metabolism and stress in various tissues including the pancreas, liver, heart, hypothalamus, and adipose tissue (39). In stress condition, ATF3 was able to regulate the expression of Noxa and Bnip3, which are involved in pro-apoptotic process. In the colon, liver, and prostate cancers, ATF3 had tumor suppression impact by apoptosis activation (39). In PDAC, ATF3 increased the chemosensitivity of gemcitabine treatment (40). The overexpression of ATF3 induced by OxA on chemoresistant tumors could reinforce the anti-tumoral impact of orexins by increasing apoptosis. Moreover, OxA was able to increase the cleavage of PARP [poly (ADP-ribose) polymerase], which is a protein family involved in DNA repair and genomic stability, and was inactivated by caspase cleavage during the apoptotic pathway (41, 42). The PARP cleavage observed in gemcitabine- and Nab-paclitaxel-resistant tumors treated by OxA was likely a consequence of orexins caspase activation.

In conclusion, the activation by orexins of OX1R, which was expressed in non-resistant and resistant PDAC to gemcitabine or Nab-paclitaxel, induced important pro-apoptotic and anti-tumoral actions. It is of note that one current innovative therapeutical strategy is to reactivate mitochondrial apoptosis by action of new compounds as taxanes, BH3 mimetic, and metformin (32). In that respect, OxA or molecules derived from orexins represent emerging innovative therapeutical compounds with great potential interest in the treatment of PDAC and chemoresistant pancreatic cancers.

DATA AVAILABILITY STATEMENT

The raw data supporting the conclusions of this article will be made available by the authors, without undue reservation.

ETHICS STATEMENT

The studies involving human participants were reviewed and approved by the Institutional Review Board (CEERB GHU Paris Nord Nos. IRB12-059 and 12-033). The patients/participants provided their written informed consent to participate in this study. The animal study was reviewed and approved by Apafis No. 17199-201810221522166v4.

AUTHOR CONTRIBUTIONS

ACn, TV, and PN designed the experiments. ACn, TV, VG, and PN performed experiments. ACd, ACn, ACh, VR, TV, and DM have performed and analyzed histologic studies. ACn has written the manuscript. All authors have read, edited and approved the final version of manuscript.

FUNDING

Our work was supported by the "Institut National de la Santé et de la Recherche Medicale" (INSERM), the "Université de Paris," The "Institut National du Cancer (INCA)" (PAIR Pancreas, grant number PAN18-045), and the "Ligue Contre le Cancer" (grant numbers R16020HH and GB/MA/CD/EP-12062).

ACKNOWLEDGMENTS

Thanks to the genomic platform facilities IBENS (ENS, Paris, France).

REFERENCES

1. Mizrahi JD, Surana R, Valle JW, Shroff RT. Pancreatic Cancer. *Lancet* (2020) 395:2008–20. doi: 10.1016/S0140-6736(20)30974-0
2. Rahib L, Smith BD, Aizenberg R, Rosenzweig AB, Fleshman JM, Matrisian LM. Projecting Cancer Incidence and Deaths to 2030: The Unexpected Burden of Thyroid, Liver, and Pancreas Cancers in the United States. *Cancer Res* (2014) 74:2913–21. doi: 10.1158/0008-5472.CAN-14-0155
3. Yu S, Zhang C, Xie KP. Therapeutic Resistance of Pancreatic Cancer: Roadmap to its Reversal. *Biochim Biophys Acta Rev Cancer* (2021) 1875:188461–77. doi: 10.1016/j.bbcan.2020.188461
4. Singhi AD, Wood LD. Early Detection of Pancreatic Cancer Using DNA-Based Molecular Approaches. *Nat Rev Gastroenterol Hepatol* (2021) 18:457–68. doi: 10.1038/s41575-021-00470-0
5. Springfeld C, Jäger D, Büchler MW, Strobel O, Hackert T, Palmer DH, et al. Chemotherapy for Pancreatic Cancer. *Presse Med* (2019) 48:e159–74. doi: 10.1016/j.lpm.2019.02.025
6. Binenbaum Y, Na'ara S, Gil Z. Gemcitabine Resistance in Pancreatic Ductal Adenocarcinoma. *Drug Resist Updat* (2015) 23:55–68. doi: 10.1016/j.drup.2015.10.002
7. Grasso C, Jansen G, Giovannetti E. Drug Resistance in Pancreatic Cancer: Impact of Altered Energy Metabolism. *Crit Rev Oncol Hematol* (2017) 114:139–52. doi: 10.1016/j.critrevonc.2017.03.026
8. Si W, Shen J, Zheng H, Fan W. The Role and Mechanisms of Action of microRNAs in Cancer Drug Resistance. *Clin Epigenetics* (2019) 11:25–49. doi: 10.1186/s13148-018-0587-8
9. Lin Z, Lu S, Xie X, Yi X, Huang H. Noncoding RNAs in Drug-Resistant Pancreatic Cancer: A Review. *BioMed Pharmacother* (2020) 131:110768–80. doi: 10.1016/j.biopha.2020.110768
10. Abernero J, Chiorean EG, Infante JR, Hingorani SR, Ganju V, Weekes C, et al. Prognostic Factors of Survival in a Randomized Phase III Trial (MPACT) of Weekly Nab-Paclitaxel Plus Gemcitabine Versus Gemcitabine Alone in Patients With Metastatic Pancreatic Cancer. *Oncologist* (2015) 20:143–50. doi: 10.1634/theoncologist.2014-0394
11. Jain A, Bhardwaj V. Therapeutic Resistance in Pancreatic Ductal Adenocarcinoma: Current Challenges and Future Opportunities. *World J Gastroenterol* (2021) 27:6527–50. doi: 10.3748/wjg.v27.i39.6527
12. Wang TH, Wang HS, Soong YK. Paclitaxel-Induced Cell Death: Where the Cell Cycle and Apoptosis Come Together. *Cancer* (2000) 88:2619–28. doi: 10.1002/1097-0142(20000601)88:11<2619::AID-CNCR26>3.0.CO;2-J
13. Braun LM, Lagies S, Guenzle J, Fichtner-Feigl S, Wittel UA, Kammerer B. Metabolic Adaptation During Nab-Paclitaxel Resistance in Pancreatic Cancer Cell Lines. *Cells* (2020) 9:1251–64. doi: 10.3390/cells9051251
14. Couvineau A, Voisin T, Nicole P, Gratio V, Abad C, Tan YV. Orexins as Novel Therapeutic Targets in Inflammatory and Neurodegenerative Diseases. *Front Endocrinol (Lausanne)* (2019) 10:709–22. doi: 10.3389/fendo.2019.00709
15. Voisin T, El Firar A, Fasseu M, Rouyer-Fessard C, Descatoire V, Walker F, et al. Aberrant Expression of OX1 Receptors for Orexins in Colon Cancers and Liver Metastases: An Openable Gate to Apoptosis. *Cancer Res* (2011) 71:3341–51. doi: 10.1158/0008-5472.CAN-10-3473
16. Couvineau A, Voisin T, Nicole P, Gratio V, Blais A. Orexins: A Promising Target to Digestive Cancers, Inflammation, Obesity and Metabolism Dysfunctions. *World J Gastroenterol* (2021) 27:7582–96. doi: 10.3748/wjg.v27.i44.7582
17. Chemelli RM, Sinton CM. Yanagisawa M Polysomnographic Characterization of Orexin-2 Receptor Knockout Mice. *Sleep* (2000) 23:A296–7.
18. Li SB, de Lecea L. The Hypocretin (Orexin) System: From a Neural Circuitry Perspective. *Neuropharmacology* (2020) 167:107993–8004. doi: 10.1016/j.neuropharm.2020.107993
19. Dayot S, Speisky D, Couvelard A, Bourgoin P, Gratio V, Cros J, et al. *In Vitro*, *In Vivo* and *Ex Vivo* Demonstration of the Antitumoral Role of Hypocretin-1/Orexin-A and Almorexant in Pancreatic Ductal Adenocarcinoma. *Oncotarget* (2018) 9:6952–67. doi: 10.18632/oncotarget.24084
20. Voisin T, El Firar A, Rouyer-Fessard C, Gratio V, Laburthe M. A Hallmark of Immunoreceptor, the Tyrosine-Based Inhibitory Motif ITIM, is Present in the G Protein-Coupled Receptor OX1R for Orexins and Drives Apoptosis: A Novel Mechanism. *FASEB J* (2008) 22:1993–2002. doi: 10.1096/fj.07-098723
21. Chen W, Wong C, Vosburgh E, Levine AJ, Foran DJ, Xu EY. High-Throughput Image Analysis of Tumor Spheroids: A User-Friendly Software Application to Measure the Size of Spheroids Automatically and Accurately. *J Vis Exp* (2014) 89:51639–49. doi: 10.3791/51639
22. Ge X. iDEP Web Application for RNA-Seq Data Analysis. *Methods Mol Biol* (2021) 2284:417–43. doi: 10.1007/978-1-0716-1307-8_22
23. Ianevski A, Giri AK, Aittokallio T. SynergyFinder 2.0: Visual Analytics of Multi-Drug Combination Synergies. *Nucleic Acids Res* (2020) 48:W488–93. doi: 10-1093/nar/gkaa216
24. Nakamura M, Shimada K, Konishi N. The Role of HRK Gene in Human Cancer. *Oncogene* (2008) 27:S105–13. doi: 10.1038/onc.2009.48
25. Zhu H, Wei M, Xu J, Hua J, Liang C, Meng Q, et al. PARP Inhibitors in Pancreatic Cancer: Molecular Mechanisms and Clinical Applications. *Mol Cancer* (2020) 19:49–64. doi: 10.1186/s12943-020-01167-9
26. Cornwell AC, Feigin ME. Unintended Effects of GPCR-Targeted Drugs on the Cancer Phenotype. *Trends Pharmacol Sci* (2020) 41:1006–22. doi: 10.1016/j.tips.2020.10.001
27. Chaudhary PK, Kim S. An Insight Into GPCR and G-Proteins as Cancer Drivers. *Cells* (2021) 10:3288–330. doi: 10.3390/cells10123288

28. Alain C, Pascal N, Valérie G, Thierry V. Orexins/Hypocretins and Cancer: A Neuropeptide as Emerging Target. *Molecules* (2021) 26:4849–59. doi: 10.3390/molecules26164849
29. Couvineau A, Dayot S, Nicole P, Gratio V, Rebours V, Couvelard A, et al. The Anti-Tumoral Properties of Orexin/Hypocretin Hypothalamic Neuropeptides: An Unexpected Therapeutic Role. *Front Endocrinol (Lausanne)* (2018) 9:573–83. doi: 10.3389/fendo.2018.00573
30. Jiang PH, Motoo Y, Sawabu N, Minamoto T. Effect of Gemcitabine on the Expression of Apoptosis-Related Genes in Human Pancreatic Cancer Cells. *World J Gastroenterol* (2006) 12:1597–602. doi: 10.3748/wjg.v12.i10.1597
31. Soond SM, Zamyatnin AA Jr. Targeting G Protein-Coupled Receptors in Cancer Therapy. *Adv Cancer Res* (2020) 145:49–97. doi: 10.1016/bs.acr.2019.11.002
32. Higuchi T, Nakamura M, Shimada K, Ishida E, Hirao K, Konishi N. HRK Inactivation Associated With Promoter Methylation and LOH in Prostate Cancer. *Prostate* (2008) 68:105–13. doi: 10.1002/pros.20600
33. Chandra Gupta S, Nandan Tripathi Y. Potential of Long non-Coding RNAs in Cancer Patients: From Biomarkers to Therapeutic Targets. *Int J Cancer* (2017) 140:1955–67. doi: 10.1002/ijc.30546
34. Zheng H, Nong Z, Lu G. Correlation Between Nuclear Factor E2-Related Factor 2 Expression and Gastric Cancer Progression. *Med Sci Monit* (2015) 21:2893–9. doi: 10.12659/MSM.894467
35. Wang EM, Akasaka H, Zhao J, Varadhachary GR, Lee JE, Maitra A, et al. Expression and Clinical Significance of Protein Kinase RNA-Like Endoplasmic Reticulum Kinase and Phosphorylated Eukaryotic Initiation Factor 2α in Pancreatic Ductal Adenocarcinoma. *Pancreas* (2019) 48:323–8. doi: 10.1097/MPA.0000000000001248
36. Wang L, Zhang Y, Wang W, Zhu Y, Chen Y, Tian B. Gemcitabine Treatment Induces Endoplasmic Reticular (ER) Stress and Subsequently Upregulates Urokinase Plasminogen Activator (uPA) to Block Mitochondrial-Dependent Apoptosis in Panc-1 Cancer Stem-Like Cells (CSCs). *PloS One* (2017) 12:e0184110–e0184128. doi: 10.1371/journal.pone.0184110
37. Pan YR, Wu CE, Yeh CN. ATM Inhibitor Suppresses Gemcitabine-Resistant BTC Growth in a Polymerase θ Deficiency-Dependent Manner. *Biomolecules* (2020) 10:1529–46. doi: 10.3390/biom10111529
38. Song Z, Li J, Zhang L, Deng J, Fang Z, Xiang X, et al. UCHL3 Promotes Pancreatic Cancer Progression and Chemo-Resistance Through FOXM1 Stabilization. *Am J Cancer Res* (2019) 9:1970–81.
39. Ku HC, Cheng CF. Master Regulator Activating Transcription Factor 3 (ATF3) in Metabolic Homeostasis and Cancer. *Front Endocrinol (Lausanne)* (2020) 11:556–72. doi: 10.3389/fendo.2020.00556
40. Kha ML, Hesse L, Deisinger F, Sipos B, Röcken C, Arlt A, et al. The Antioxidant Transcription Factor Nrf2 Modulates the Stress Response and Phenotype of Malignant as Well as Premalignant Pancreatic Ductal Epithelial Cells by Inducing Expression of the ATF3 Splicing Variant Δzip2. *Oncogene* (2019) 38:1461–76. doi: 10.1038/s41388-018-0518-3
41. Soldani C, Scovassi AI. Poly(ADP-Ribose) Polymerase-1 Cleavage During Apoptosis: An Update. *Apoptosis* (2002) 7:321–8. doi: 10.1023/A:1016119328968
42. Rouet-Benzineb P, Rouyer-Fessard C, Jarry A, Avondo V, Pouzet C, Yanagisawa M, et al. Orexins Acting at Native OX(1) Receptor in Colon Cancer and Neuroblastoma Cells or at Recombinant OX(1) Receptor Suppress Cell Growth by Inducing Apoptosis. *J Biol Chem* (2004) 279:45875–86. doi: 10.1074/jbc.M404136200

Conflict of Interest: The authors declare that the research was conducted in the absence of any commercial or financial relationships that could be construed as a potential conflict of interest.

Publisher's Note: All claims expressed in this article are solely those of the authors and do not necessarily represent those of their affiliated organizations, or those of the publisher, the editors and the reviewers. Any product that may be evaluated in this article, or claim that may be made by its manufacturer, is not guaranteed or endorsed by the publisher.

frontiers | Frontiers in Oncology

ORIGINAL RESEARCH
published: 30 June 2022
doi: 10.3389/fonc.2022.925666

Glutor, a Glucose Transporter Inhibitor, Exerts Antineoplastic Action on Tumor Cells of Thymic Origin: Implication of Modulated Metabolism, Survival, Oxidative Stress, Mitochondrial Membrane Potential, pH Homeostasis, and Chemosensitivity

Mithlesh Kumar Temre[1], *Saveg Yadav*[1], *Yugal Goel*[1], *Shrish Kumar Pandey*[1], *Ajay Kumar*[2] *and Sukh Mahendra Singh*[1]*

[1] School of Biotechnology, Institute of Science, Banaras Hindu University, Varanasi, India, [2] Deparment of Zoology, Institute of Science, Banaras Hindu University, Varanasi, India

OPEN ACCESS

Edited by:
Matiullah Khan,
AIMST University, Malaysia

Reviewed by:
Stephen John Ralph,
Griffith University, Australia
Anita Bakrania,
University Health Network (UHN), Canada

***Correspondence:**
Sukh Mahendra Singh
smsinghbiotech@bhu.ac.in

Specialty section:
This article was submitted to Cancer Molecular Targets and Therapeutics, a section of the journal Frontiers in Oncology

Received: 21 April 2022
Accepted: 01 June 2022
Published: 30 June 2022

Citation:
Temre MK, Yadav S, Goel Y, Pandey SK, Kumar A and Singh SM (2022) Glutor, a Glucose Transporter Inhibitor, Exerts Antineoplastic Action on Tumor Cells of Thymic Origin: Implication of Modulated Metabolism, Survival, Oxidative Stress, Mitochondrial Membrane Potential, pH Homeostasis, and Chemosensitivity. Front. Oncol. 12:925666. doi: 10.3389/fonc.2022.925666

Neoplastic cells overexpress glucose transporters (GLUT), particularly GLUT1 and GLUT3, to support altered metabolism. Hence, novel strategies are being explored to effectively inhibit GLUTs for a daunting interference of glucose uptake. Glutor, a piperazine-2-one derivative, is a newly reported pan-GLUT inhibitor with a promising antineoplastic potential. However, several aspects of the underlying mechanisms remain obscure. To understand this better, tumor cells of thymic origin designated as Dalton's lymphoma (DL) were treated with glutor and analyzed for survival and metabolism regulatory molecular events. Treatment of tumor cells with glutor caused a decrease in cell survival with augmented induction of apoptosis. It also caused a decrease in glucose uptake associated with altered expression of GLUT1 and GLUT3. HIF-1α, HK-2, LDH-A, and MCT1 also decreased with diminished lactate production and deregulated pH homeostasis. Moreover, glutor treatment modulated the expression of cell survival regulatory molecules p53, Hsp70, IL-2 receptor CD25, and C-myc along with mitochondrial membrane depolarization, increased intracellular ROS expression, and altered Bcl-2/BAX ratio. Glutor also enhanced the chemosensitivity of tumor cells to cisplatin, accompanied by decreased MDR1 expression. Adding fructose to the culture medium containing glutor reversed the latter's inhibitory action on tumor cell survival. These results demonstrate that in addition to inhibited glucose uptake, modulated tumor growth regulatory molecular pathways are also implicated in the manifestation of the antineoplastic action of glutor. Thus, the novel findings of this study will have a long-lasting clinical significance in evaluating and optimizing the use of glutor in anticancer therapeutic strategies.

Keywords: glutor, GLUT, thymoma, metabolism, cell survival regulation, targeted therapeutics

INTRODUCTION

Neoplastic cells display dependence on glycolysis for their massive bioenergetic and biosynthetic requirements (1–3). Consequently, cancer cells display upregulated expression of various high-affinity glucose transporters (GLUT) to facilitate glucose uptake for accelerated glycolysis. Neoplastic cells overexpress GLUT1, GLUT3, GLUT4, and GLUT12, which vary depending on their etiology (4, 5). As glucose transporters are one of the crucial rate-limiting checkpoints of the reprogrammed carbohydrate metabolism of neoplastic cells, targeting GLUTs, particularly GLUT1 and GLUT3, has emerged as a promising antineoplastic approach (6). Thus, several inhibiting endeavors are being envisaged to imperil glucose uptake in neoplastic cells (7, 8). One of such strategies comprises GLUT inhibitors, being extensively explored for their antineoplastic potential (9). Natural products like genistein (10), quercetin (11), caffeine (12), phloretin (13), resveratrol (14), curcumin (15), and small synthetic inhibitors like cytochalasin B (16), fasentin (17), WZB117 (18), thiazolidinedione (19), STF31 (20), BAY876 (21), DRB18 (22), silybin (23, 24), and naringenin (25, 26) have been explored for their GLUT-inhibiting potential. They are also in various stages of preclinical and clinical trials (27). However, most of these inhibitors are isoform-specific and manifest antineoplastic action at higher concentrations, which can be potentially harmful to GLUT-expressing normal cells. Therefore, there is a necessity for developing GLUT inhibitors, which are expected to possess the ability for Pan-GLUT inhibition and manifest antineoplastic action at lower concentrations.

Recent reports have introduced a pan-GLUT inhibitory molecule named glutor, a piperazine-2-one derivative (**Supplementary Figure 1**), with a broad spectrum of anticancer potential, which is capable of exerting the antineoplastic action at nanomolar concentrations and is stable in an aqueous environment (22, 28–31). Moreover, glutor can synergistically interfere with tumor metabolism with glutaminase inhibitor CB-839 (29). Several aspects of the molecular mechanisms underlying its antimetabolic action remain unclear, which need to be deciphered for optimal utilization. To the best of our knowledge, no study has been conducted in this direction. It is well established that glucose metabolism can influence the chemosensitivity of neoplastic cells. However, it remains unclear if glutor can alter the tumoricidal action of chemotherapeutic agents. Furthermore, there is no report concerning the antineoplastic activity of glutor on neoplastic cells of thymic origin, which, though fatal, are rare in occurrence (32), and display elevated GLUT expression (33).

Considering the observations mentioned above, we used cells of a thymoma-derived tumor, designated as Dalton's lymphoma (DL), which is a spontaneously originated tumor of thymic origin (34) that has been widely used as an *in vivo* tumor model for testing the therapeutic efficacy of anticancer agents (35, 36) and host–tumor relationship (35, 37). The present study reports that glutor displays a potent antineoplastic action against DL cells *in vitro* by modulating glucose metabolism, pH homeostasis, cell survival, and metabolic machinery.

MATERIALS AND METHODS

Tumor, Mice, and Reagents

DL was used as a tumor model for understanding the effect of glutor. DL was discovered by Dr. A.J. Dalton (NCI, Bethesda, USA) as a thymoma of DBA mice with spontaneous origin (34). The DL cells were procured from the Department of Zoology, Banaras Hindu University. The DL's ascitic growth was established by Goldie and Felix (38). Mice handling and experimental procedures were carried out according to the Institutional Animal Ethical Committee (Approval No. BHU/DoZ/IAEC/2021-2022/016). All reagents, unless mentioned otherwise, were purchased from Sigma-Aldrich, USA. Fetal calf serum was purchased from the Hyclone USA and Annexin V/PI apoptosis detection kit from Invitrogen, USA. RPMI-1640 medium (Cat. No. 31800-022) was purchased from Thermofisher Scientific, with a final glucose concentration of 11.11 mM. Primary antibodies against GLUT1 (E-AB-31556), GLUT3 (E-AB-31557), HK-2 (E-AB-14706), and LDH-A (E-AB-19937) were purchased from Elabscience USA; HIF1-α (SC-31515), C-myc (SC-40), p53 (SC-126), β-actin (SC-47778), BAX (CST 2772S), Hsp70 (CST 4872S), and MDR1/ABCB1 (CST 13978) were purchased from Cell Signaling Technology (CST) USA; VEGF (IMG-80214), TGF-β (IMG-6667-E-100), Bcl-2 (IMG-3181), and MCT1 (IMG-4021) were purchased from Imagenex, USA; PE-CD25 (55386) was purchased from BD Biosciences, USA. Secondary antibodies anti-rabbit IgG (A9919) and anti-mouse IgG (A3562) were purchased from Sigma-Aldrich, USA. RT-PCR primers were purchased from Ambion International AG, Germany, Integrated DNA Technologies, USA, and Eurofins, USA.

Trypan Blue Dye Exclusion Test to Determine Cell Viability

The number of viable DL cells was enumerated by Trypan blue dye exclusion test following a method described earlier (35). The cell suspension was mixed with 0.4% (w/v) Trypan blue in PBS in equal volumes, and the viable cells (unstained cells) were enumerated using a hemocytometer under a light microscope (Leitz Wetzlar, Germany).

Examination of Apoptotic Cell Population

Wright–Giemsa and Annexin V/PI staining was used to identify the apoptotic cell population. Annexin V/PI staining was carried out following the manufacturer's instructions (Imagenex USA). Control and glutor-treated DL cells (1×10^6) were washed and incubated in a working solution of 1× annexin binding buffer, followed by the addition of 10 µl of annexin conjugate and 1 µl of PI working solution (100 µg/ml) and incubation for 15 min at room temperature in the dark. The cells were then washed by centrifugation with 1× annexin binding buffer. The stained cells were mounted on a slide and observed under a fluorescence microscope. Live cells were determined to be those with weak green fluorescence, whereas the deep green high fluorescence cells were marked as apoptotic cells. Apoptotic cells were also confirmed by simultaneous examination of apoptotic morphology under phase contrast optics. To examine

apoptotic cells by Wright–Giemsa staining, the cell suspension was smeared on a slide and air-dried. The cells were then fixed in methanol and stained with Wright–Giemsa staining solution. After mounting in glycerine, apoptotic cells were examined under a light microscope (Leitz Wetzlar, Germany). The apoptotic cells were identified based on the typical morphological features, including contracted cell bodies; densely stained, condensed, and uniformly circumscribed chromatin; and the presence of one or more membrane-bound apoptotic bodies containing nuclear fragments. The percentage of apoptotic cells was determined by counting more than 100 cells in at least three separate visions.

MTT Assay for Estimation of Cell Survival

The MTT assay was performed to assess cell survival as an indicator of cellular metabolic activity, proliferation, and cytotoxicity following the method described by Mosmann (39). MTT was dissolved in PBS, and 50 µl of this solution (final concentration, 0.5 mg/ml) was added to the tissue culture plate wells containing the final concentration of 0.5 mg/ml. Cultures were incubated for 4 h at 37°C in a CO_2 incubator to allow the formation of formazan crystals. The formazan crystals were solubilized using DMSO, and absorbance was measured at 540 nm using an ELISA plate reader (Labsystems, Finland).

Reverse Transcriptase-Polymerase Chain Reaction

The expression of GLUT1 and GLUT3 genes were examined using a previously described method (35). cDNA was prepared using a cell to cDNA kit (Ambion, USA). The primers' description is mentioned in **Table 1**. Thirty-five cycles of amplification were performed. Each cycle consisted of denaturation (2 min at 94°C), annealing (55–60°C) as per the genes' primers, and elongation (30 s at 72°C). The DNA was electrophoresed on an agarose gel (2%) containing ethidium bromide (0.25% w/v) and was visualized on a UV-transilluminator. The band intensity of each gene was analyzed by ImageJ software.

Western Blotting

Western blotting was carried out to detect the indicated proteins following the method described by Fido et al. (40) and Goel et al. (41) with slight modifications. Cells were lysed in lysis buffer [Tris-Cl 20 mM (pH 8.0), NaCl (137 mM), glycerol 10% (v/v), Triton X-100 1% (v/v), EDTA 2.0 mM, PMSF 1.0 mM, Leupeptin 20 mM, and aprotinin 0.15 U/ml] for 30 min on ice. Protein content was measured using the Bradford method (42). Samples for electrophoresis were mixed in loading buffer [Tris-Cl 0.5 M (pH 6.8), β-mercaptoethanol 100 mM, SDS 20% (w/v), bromophenol blue 0.1% (v/v), and glycerol 10% (v/v)] and were heated for 3 min in a water bath. A sample containing 30 µg of protein was subjected to electrophoresis by SDS-PAGE. Proteins were transferred to the nitrocellulose membrane (Sartorius, Germany) at 60 mA for 1 h. The membrane was then incubated with primary antibodies against the respective proteins and secondary antibodies conjugated to alkaline phosphatase. Bands were visualized using BCIP/NBT. The band density was examined by ImageJ software.

TABLE 1 | Primer sequences for RT-PCR analysis.

Genes	Primer sequences
GLUT1	F: 5'-CTTTGTGGCCTTCTTTGAAG-3 R: 5'-CCACACAGTTGCTCCACAT-3'
GLUT3	F: 5'-AACAGAAAGGAGGAAGACCA-3' R: 5'-CGCAGCCGAGGGGAAGAACA-3'
β-Actin	F: 5'-GGCACAGTGTGGGTGAC-3' R: 5'-CTGGCACCACACCTTCTAC-3'

Estimation of Intracellular Reactive Oxygen Species

A method described by Furuta et al. (43) was used to estimate ROS expression with slight modifications. Cells (1×10^5 cells/ml) were incubated with HBSS containing 0.1 mM dichlorodihydrofluorescein diacetate (DCFDA) at 37°C for 45 min. After washing with PBS, the stained cells were visualized under fluorescence optics (Nikon, Japan). The fluorescence intensity was analyzed by ImageJ software.

Quantification of Glucose

A commercial kit from Agappe Diagnostics Ltd. (Kerala, India) based on converting glucose to H_2O_2 by the action of glucose oxidase was used to measure glucose content in the culture supernatant. The generated H_2O_2 was estimated by converting it into a red quinine product by peroxidase action. Ten milliliters of the culture supernatant was added to 1 ml of working reagent [sodium phosphate buffer (pH 7.4), phenol, glucose-oxidase, peroxidase, and 4-amino antipyrine], followed by mixing and incubation at 37°C for 10 min. Absorbance was measured at 505 nm, and the glucose content was expressed in mM.

Estimation of Lactate

Lactate concentration in the culture supernatant was measured using an enzymatic colorimetric kit (Spinreact, Granada, Spain) based on a method described by Somoza et al. (44). Briefly, 1 ml of sample was diluted in 200 ml of PIPES (50 mM; pH 7.5) containing 4-chlorophenol (4 mM), lactate oxidase (800 U/L), peroxidase (2,000 U/L), and 4-aminophenazone (0.4 mM), followed by incubation for 10 min at room temperature, and measurement of absorbance at 505 nm. Lactate concentration was expressed in mg/dl.

Immunofluorescent Staining of Cell Surface Molecules

Cell surface expression of GLUT1, GLUT3, and CD25 was carried out using immunofluorescence staining following a previously described method (45). After washing with PBS, the stained cells were fixed in a mixture of acetic acid and ethanol (5:95) for 10 min at −10°C. Fluorescence was visualized on a fluorescence microscope (Nikon Instruments Inc.).

Estimation of Mitochondrial Membrane Potential by TMRE Staining

Mitochondrial membrane potential was determined following a method described by Crowley et al. by tetramethylrhodamine

ethyl ester (TMRE) perchlorate staining (46). Control and glutor-treated DL cells were incubated for 20 min in a medium containing TMRE (100 nM) at 37°C. Fluorescence was detected using a fluorescence microscope (Nikon Instruments Inc.). Data are presented as the percent of TMRE high cells.

Statistical Analysis

All experiments were conducted in triplicates. The Student's *t*-test analyzed the statistical significance of differences between test groups. The difference was considered significant when the *p*-value was less than 0.05.

RESULTS

Effect of Glutor Treatment on the Survival of DL Cells

DL cells (1×10^5) and thymocytes obtained from healthy mice were examined for expression of GLUT1 and GLUT3 by Western blotting as described in the *Materials and Methods* section. Results are shown in **Figure 1A**. DL cells displayed an upregulated expression of GLUT1 and GLUT3 compared to thymocytes. Therefore, in the subsequent experiments, the effect of glutor on the survival of DL cells was explored. DL cells (1×10^5) were incubated for 24 h in a medium alone or containing the indicated concentrations of glutor, followed by evaluation of cell viability by Trypan blue dye exclusion test (**Figure 1B**) and survival by MTT assay (**Figure 1C**). In another set of experiments, the DL cells (1×10^5) were incubated in a medium alone or containing glutor (0.01 μM) for the indicated time durations, followed by an evaluation of cell viability (**Figure 1D**) and survival (**Figure 1E**). As shown in the results (**Figures 1B–E**), exposure of DL cells to glutor *in vitro* caused a significant decrease in viable cell count and survival in a dose- and time-dependent manner compared to untreated control. The IC_{50} was determined to be 0.01 μM. Hence, in all subsequent experiments, DL cells were treated with 0.01 μM dose of glutor for 24 h, unless mentioned otherwise, a period determined to display optimal cytotoxic action of glutor for deciphering the molecular mechanisms underlying the antitumor action of glutor. Thymocytes (1×10^5) obtained from healthy mice without tumor transplantation were also incubated with various concentrations of glutor to estimate its effect on cell survival. Results indicated that glutor did not exert any cytotoxic action on thymocytes (data not shown). Given these observations that glutor can exert a tumor cell-specific cytotoxic action, the mode of observed cytostatic action of glutor was determined in the next set of experiments. DL cells (1×10^5) were incubated in a medium with or without glutor (0.01 μM) for 24 h, followed by an examination of the mode of cell death by Wright–Giemsa (**Figures 1F, G**) and Annexin V/PI (**Figures 1H, I**) staining. The cells displaying features of apoptotic morphology were enumerated. The results revealed that treatment of DL cells with glutor significantly increased the number of cells exhibiting typical characteristics of apoptotic morphology compared to untreated control.

Glutor Alters GLUT Expression in DL Cells, Accompanied by Decreased Glucose Uptake

To understand if the tumoricidal action of glutor was accompanied by alterations in GLUT expression and glucose uptake, DL cells (1×10^5) were incubated in a medium alone or containing glutor (0.01 μM) for 24 h followed by estimation of glucose level in culture supernatant and examination of GLUT1 and GLUT3 expression by RT-PCR, Western blot, and immunofluorescence microscopy as described in the *Materials and Methods* section. Results are shown in **Figure 2**. DL cells incubated with glutor displayed a decrease in the expression of GLUT1 and GLUT3 at the mRNA (**Figure 2A**) and protein levels (**Figures 2B–D**) compared to the untreated control. The glucose uptake of DL cells showed a significant decrease in the glutor-treated DL cells compared to the untreated control (**Figure 2E**). The culture medium containing glutor was supplemented with indicated amounts of glucose or fructose to understand if the anti-survival action of glutor could be reversed. Results are shown in **Figure 3**. The addition of glucose to the culture medium did not rescue the inhibition of DL cell survival by glutor, which was partially reversed by adding fructose.

Glutor-Induced Tumoricidal Action Is Associated With Modulated Expression of Cell Survival and Metabolism Regulatory Molecules

In the next set of experiments, DL cells (1×10^5) were incubated for 24 h in a medium alone or containing glutor (0.01 μM), followed by an examination of the expression pattern of indicated metabolism (**Figure 4A**) and cell survival regulatory molecules (**Figure 4B**) to understand the molecular mechanism (s) of the antineoplastic action of glutor. Treatment of DL cells with glutor inhibited the expression of hypoxia-inducible factor 1-α (HIF-1α), hexokinase 2 (HK-2), and lactate dehydrogenase A (LDH-A) compared to untreated control (**Figure 4A**). Furthermore, glutor treatment of DL cells also modulated the expression of cell survival regulatory molecules B-cell lymphoma 2 (Bcl-2), Bcl-2-associated X (BAX), and p53 (**Figure 4B**). The expression of Bcl-2, transforming growth factor-β (TGF-β), C-myc, and heat shock protein 70 (Hsp70) was decreased in DL cells treated with glutor, whereas the expression of BAX and p53 increased compared to the untreated control (**Figure 4B**). An immunofluorescence examination was carried out to investigate the effect of glutor on the expression of CD25. Glutor treatment of DL cells inhibited the expression of CD25 compared to the control (**Figure 4C**).

Glutor Treatment Alters the Expression of Intracellular Reactive Oxygen Species in DL Cells

Next, we checked the expression of intracellular ROS in glutor-treated DL cells. DL cells (1×10^5) were incubated in a medium alone or containing glutor (0.01 μM) for 2 h, followed by an estimation of ROS expression by dichlorodihydrofluorescein diacetate (DCFDA) staining as described in the *Materials and*

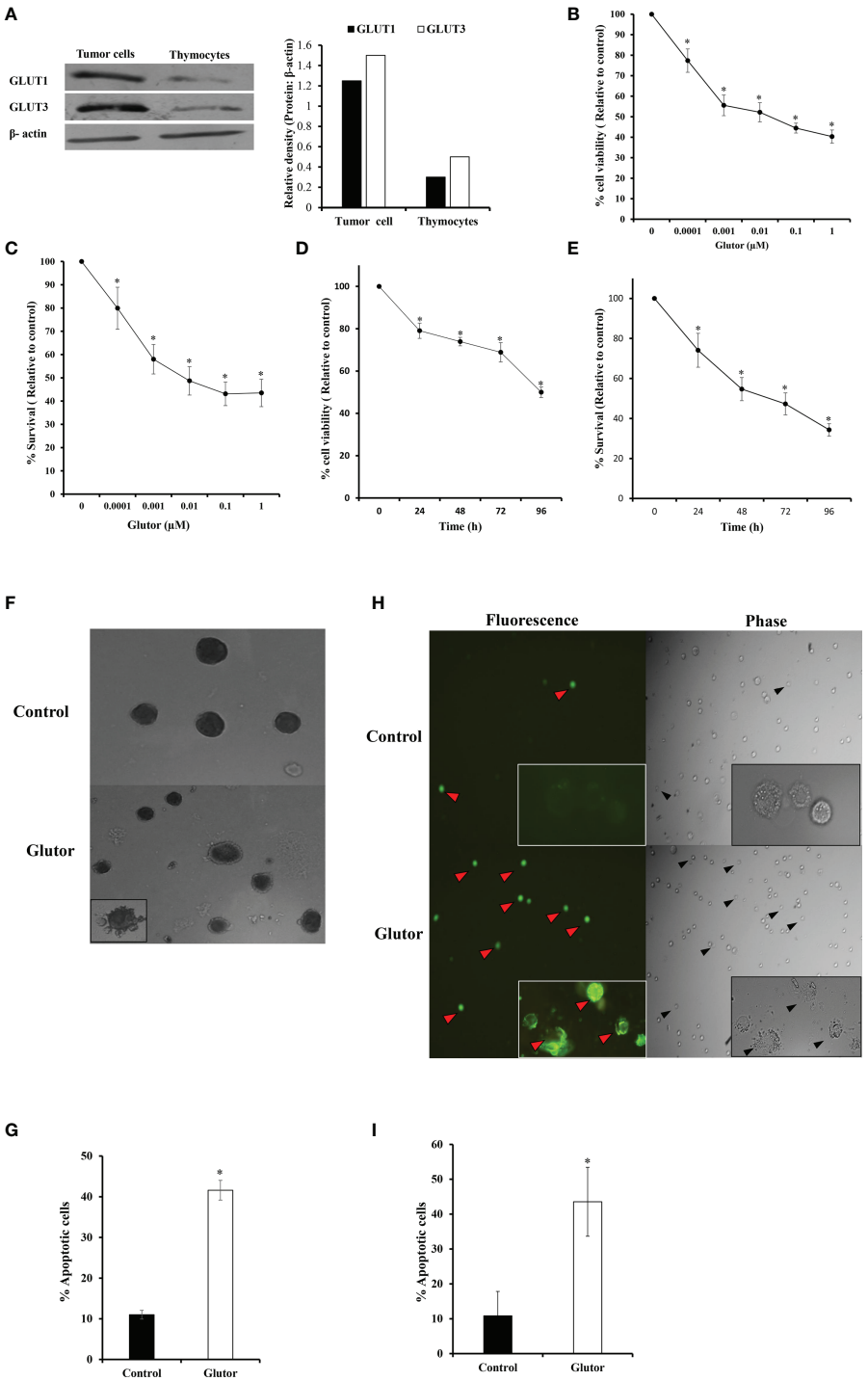

FIGURE 1 | Glutor exerts cytotoxic action on DL cells. DL cells or thymocytes (1×10^5) harvested from the thymi of healthy mice without tumor transplantation were processed for immunoblotting for GLUT1 and GLUT3 as described in the *Materials and Methods* section **(A)**. DL cells (1×10^5) were incubated in a medium alone or containing the indicated concentrations of glutor for 24 h **(B, C)** or with 0.01 μM of glutor for the various indicated time durations **(D, E)**, followed by estimation of cell viability by Trypan blue dye exclusion assay and cell survival by MTT assay as described in the *Materials and Methods* section. DL cells incubated in a medium alone or containing glutor (0.01 μM) for 24 h were examined for the mode of cell death by Annexin V/PI **(H, I)** and Wright–Giemsa **(F, G)** staining. Values shown in **(B–E)** and **(G, I)** are mean ± SD. The plates shown in **(A)**, **(F)**, and **(H)** are from a representative experiment out of at least two experiments with similar results. The bar diagram accompanying **(A)** is the densitometry of respective bands. *$p < 0.05$ vs. values of the respective control.

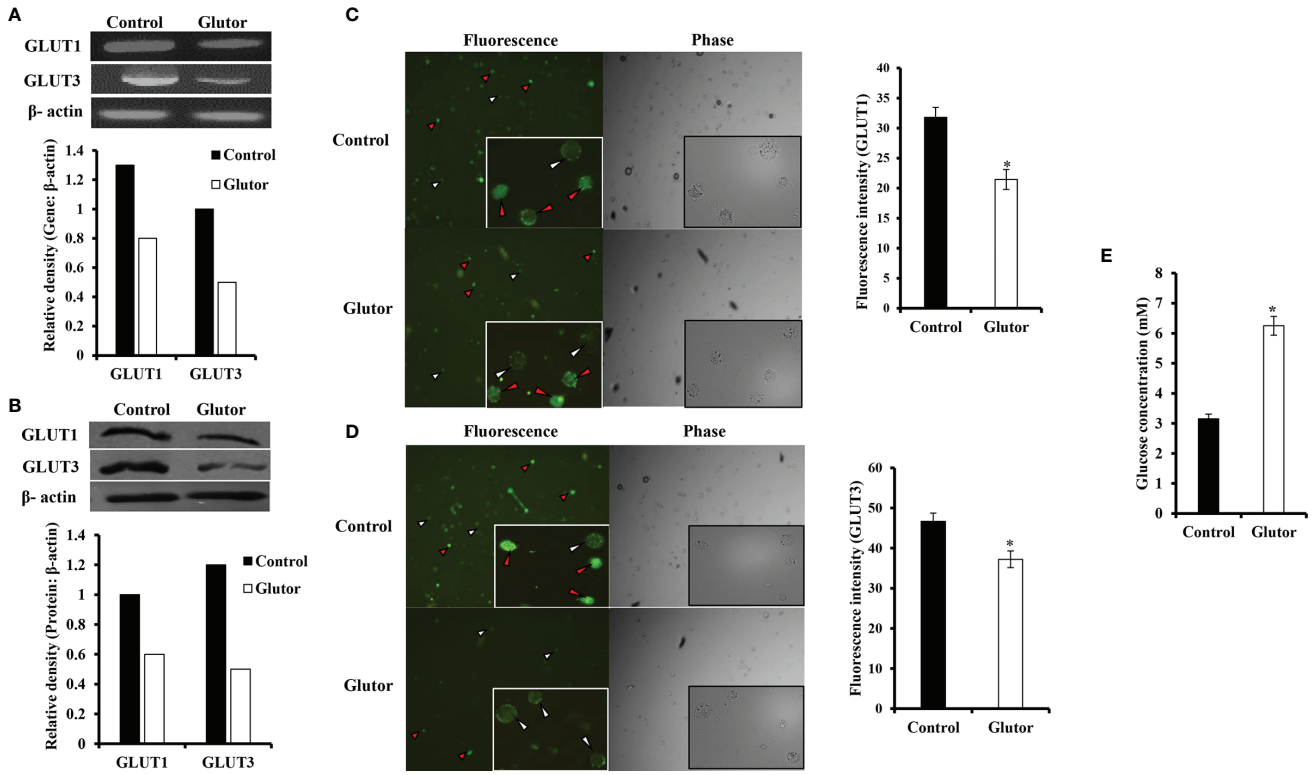

FIGURE 2 | Effect of glutor on the expression of GLUT1, GLUT3, and glucose uptake by DL cells. DL cells (1×10^5) were incubated in a medium alone or containing glutor (0.01 μM) for 24 h, followed by evaluation of GLUT1 and GLUT3 expression by RT-PCR **(A)** and Western blotting **(B)** as described in the *Materials and Methods* section. The expression of GLUT 1 and GLUT 3 was also examined by immunofluorescence **(C, D)**. The glucose level in the culture supernatant of control and glutor-treated DL cells was measured **(E)** as described in the *Materials and Methods* section. Values shown in **(E)** are mean ± SD. The plates shown in **(A–D)** are from a representative experiment out of at least two experiments with similar results. Accompanying bar diagrams are densitometric images of the respective bands. Bar diagrams accompanying the fluorescence images depict fluorescence intensity. *$p < 0.05$ vs. respective control.

Methods section. Results are shown in **Figure 5**. Glutor treatment of DL cells resulted in a significantly higher ROS expression than the untreated control.

Effect of Glutor on Mitochondrial Membrane Depolarization

We also examined the effect of glutor treatment of DL cells on mitochondrial membrane potential. DL cells (1×10^5) were incubated for 24 h in a medium alone or containing glutor (0.01 μM), followed by TMRE staining and observation of the stained cells under fluorescence optics. As shown in **Figure 6**, glutor treatment was found to trigger depolarization of the mitochondrial membrane as observed by inhibited fluorescence of TMRE compared to untreated control.

Glutor Interferes With pH Homeostasis of DL Cells

Considering that glucose metabolism influences the pH homeostasis of tumor cells, we investigated the impact of glutor treatment on the expression of pH regulator monocarboxylate transporter 1 (MCT1) along with the estimation of pH and lactate of the culture medium. Glutor (0.01 μM) treatment of DL cells inhibited the expression of MCT1 compared to untreated control (**Figure 7A**). The pH (**Figure 7B**) of the culture supernatant of glutor-treated DL cells was found to be remarkably increased whereas the level of lactate was significantly decreased (**Figure 7C**) compared to the respective untreated control.

Glutor Alters Chemosensitivity of DL Cells

As reprogrammed glucose metabolism of tumor cells is implicated in the modulation of the chemosensitivity of tumor cells, next, we examined the effect of glutor treatment on the susceptibility of DL cells to the anticancer drug cisplatin. DL cells (1×10^5) were incubated in a medium alone or containing glutor (0.01 μM) in the absence or presence of cisplatin for 24 h, followed by an examination of cell survival by MTT assay and expression of multidrug resistance protein 1 (MDR1) by Western blotting as described in the *Materials and Methods* section. The treatment of DL cells with glutor plus cisplatin resulted in a significantly higher inhibition of cell survival than the DL cells incubated in a medium alone or containing cisplatin or glutor (**Figure 8A**). The expression of MDR1 decreased in DL cells treated with glutor compared to the untreated control (**Figure 8B**).

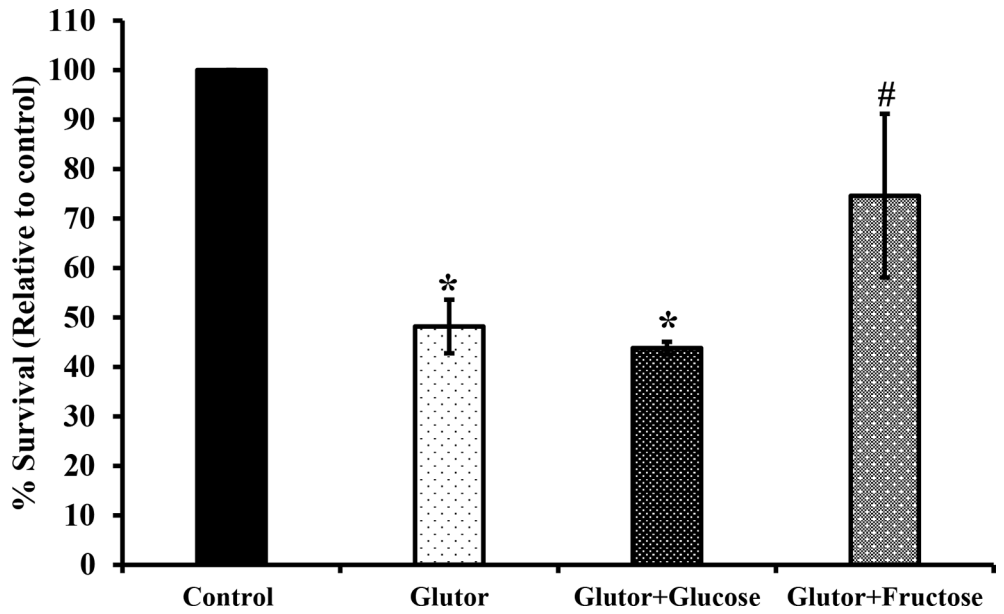

FIGURE 3 | Fructose antagonizes the inhibitory action of glutor on tumor cell survival .DL cells (1×10^5) were incubated in a medium alone or containing glutor in the presence or absence of glucose (1 mM) or fructose (1 mM) for 24 h, followed by an estimation of survival by MTT assay as described in the *Materials and Methods* section. Values are mean ± SD. $^*p < 0.05$ vs. DL cells incubated in a medium alone. $^{\#}p < 0.05$ vs. DL cells incubated in a medium containing glutor or glutor plus glucose.

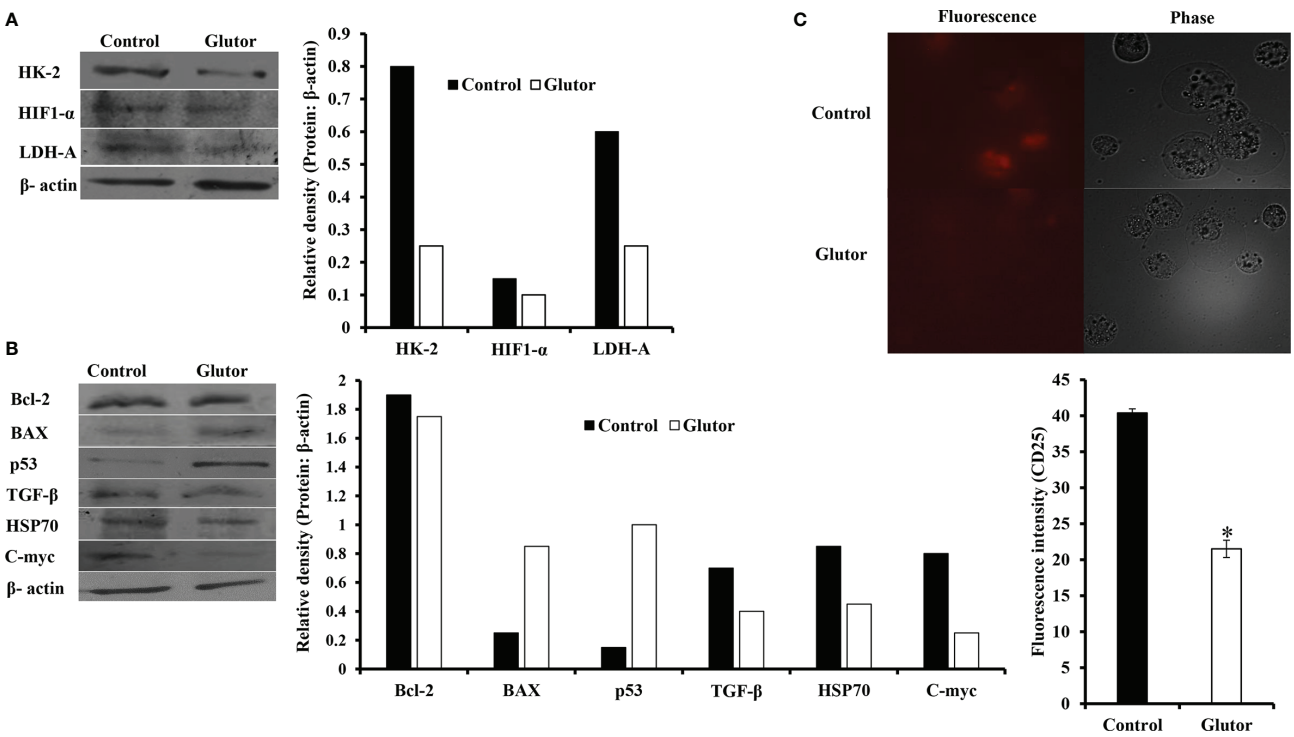

FIGURE 4 | Glutor modulates expression of metabolism and cell survival regulatory molecules in DL cells. DL cells (1×10^5) were incubated in a medium alone or containing glutor (0.01 μM) for 24 h, followed by Western blotting to study the expression of the indicated metabolism **(A)**, cell survival **(B)** regulatory molecules and CD25 **(C)** as described in the *Materials and Methods* section. The plates shown in **(A–C)** are from a representative experiment out of at least two experiments with similar results. The accompanying bar diagrams are densitometry of the respective bands.

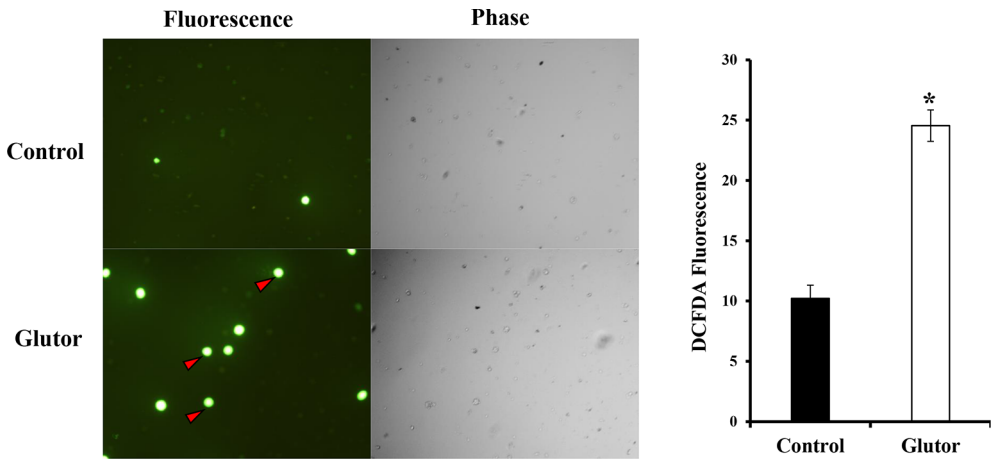

FIGURE 5 | Glutor treatment elevates intracellular ROS expression in DL cells. DL cells (1×10^5) were incubated for 2 h in a medium with or without glutor (0.01 μM), followed by staining with DCFDA and examination of the cells in fluorescence optics as described in the *Materials and Methods* section. The plates shown are from a representative experiment out of at least two experiments with similar results. The accompanying bar diagram depicts the fluorescence intensity of control and glutor-treated cells. Values are mean ± SD. *$p < 0.05$ vs. control.

DISCUSSION

The present investigation demonstrates the antineoplastic and chemosensitizing action of glutor against DL cells. To understand the underlying mechanisms, we considered various possibilities. The likelihood of impaired glucose uptake due to the inhibitory action of glutor was supported by the observation of diminished glucose consumption. This observation is validated further as glutor inhibits glucose uptake in neoplastic cells of other etiologies (29, 47). Although the mechanism(s) of the inhibition of GLUT by glutor is not precisely understood, observations from our *in silico* experiments indicate a direct binding of glutor to GLUTs, possibly causing transformational alterations, which may impair glucose transport (communicated). As we observed that glutor could efficiently inhibit DL cell survival and induce apoptosis at a low IC_{50} value of 10 nM, it strongly indicates that glutor may have a high-affinity binding to GLUTs.

The pioneering work of Reckzeh et al. (29) reported the upregulated expression of GLUT1 and GLUT3 in the colorectal cancer cell line DLD-1 cultured under hypoglycemic (1 mM), no glucose condition or following treatment with glutor (0.5 μM) in the presence of glucose (25 mM). The difference with our observations could be attributed to differences in the etiology and physiology of the target cells, glucose, and glutor concentrations used. Interestingly, cell-to-cell variations has been observed in many cancer cells for GLUT expression upon the treatment with GLUT inhibitors (22, 29, 48–51).

Interestingly, we also observed downregulation of HIF-1α in glutor-treated DL cells. Moreover, tumor cells display upregulation of GLUT1 and GLUT3 expression in response to HIF-1α (52). It is

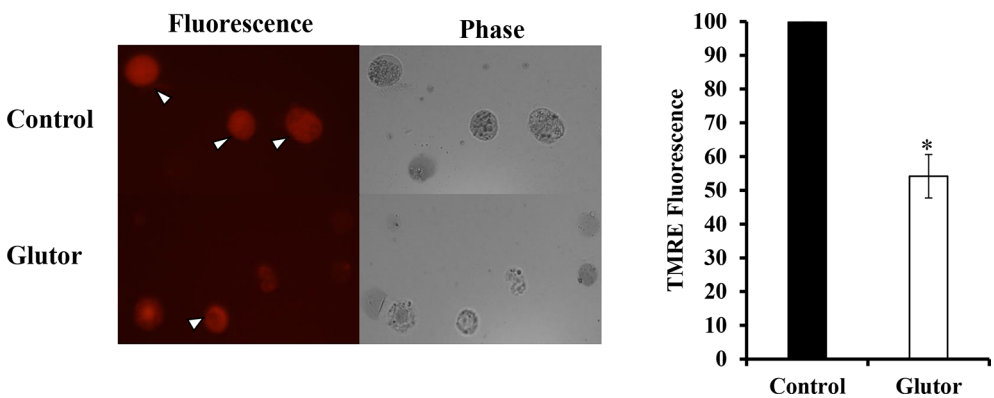

FIGURE 6 | Glutor alters mitochondrial membrane potential. DL cells (1×10^5) were incubated in a medium alone or containing glutor (0.01 μM) for 24 h, followed by TMRE staining as described in the *Materials and Methods* section. The plates shown are from a representative experiment out of at least two experiments with similar results. Values shown in the accompanying diagram are the mean ± SD of the fluorescence intensity. *$p < 0.05$ vs. control.

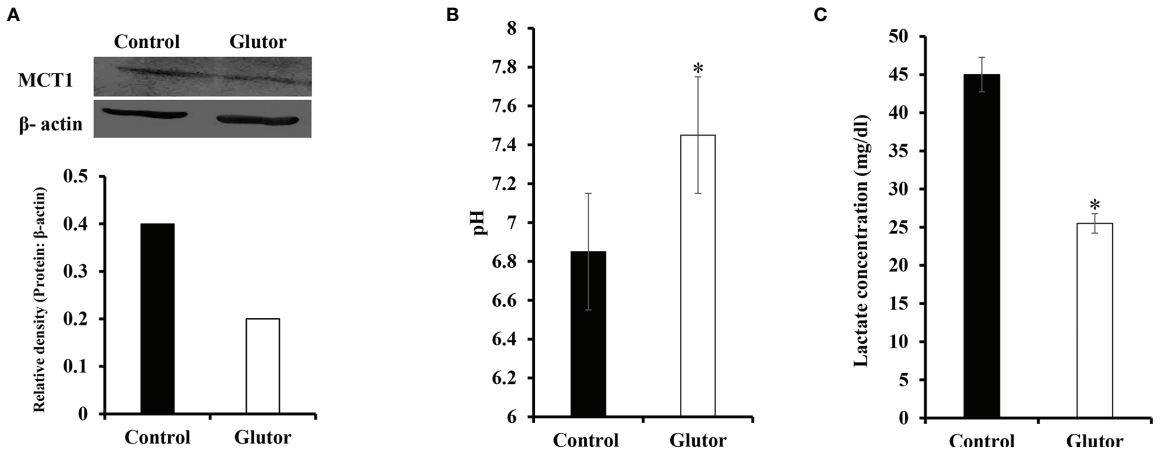

FIGURE 7 | Glutor interferes with pH homeostasis of DL cells. DL cells (1×10^5) were incubated for 24 h in a medium alone or containing glutor (0.01 μM), followed by an examination of MCT1 expression by Western blotting as described in the *Materials and Methods* section. The culture media of control and glutor-treated DL cells were also examined for pH and lactate levels. The plates shown in **(A)** are from a representative experiment out of at least two experiments with similar results. The accompanying bar diagram depicts the densitometry of the bands. Values in **(B)** and **(C)** are mean ± SD. *$p < 0.05$ vs. respective control.

noteworthy that GLUT expression is downstream of and regulated by HIF-1α (53–55). Moreover, high glucose concentrations have been reported to upregulate HIF-1α expression (56). As a result, the low glucose uptake caused by glutor-dependent-inhibition of GLUT would have triggered the observed downregulation in HIF-1α expression. Nevertheless, transcription of GLUT genes is also under the regulation of several HIF-1α independent factors, including the C-myc, K-Ras, PI3K/Akt/mTOR, cytokines, hormones, HOX transcript antisense RNA (HOTAIR), and miRNA (54, 57–64). Indeed, we also observed glutor-dependent inflection of C-myc. However, more studies will be required to interpret mechanisms underlying glutor-dependent inhibition of GLUT expression in hypoglycemic conditions.

The present observations also showed that glutor treatment of DL cells induced cell death, accompanying alterations in regulatory molecules and metabolic machinery. Indeed, our observations demonstrate mitochondrial membrane depolarization and increased ROS expression in glutor-treated DL cells. Moreover, hypoglycemia caused by impaired glucose uptake could be another trigger for induction of apoptosis. Hypoglycemia has been demonstrated to cause a decrease in ATP production associated with the induction of apoptosis (65, 66). Our experimental findings

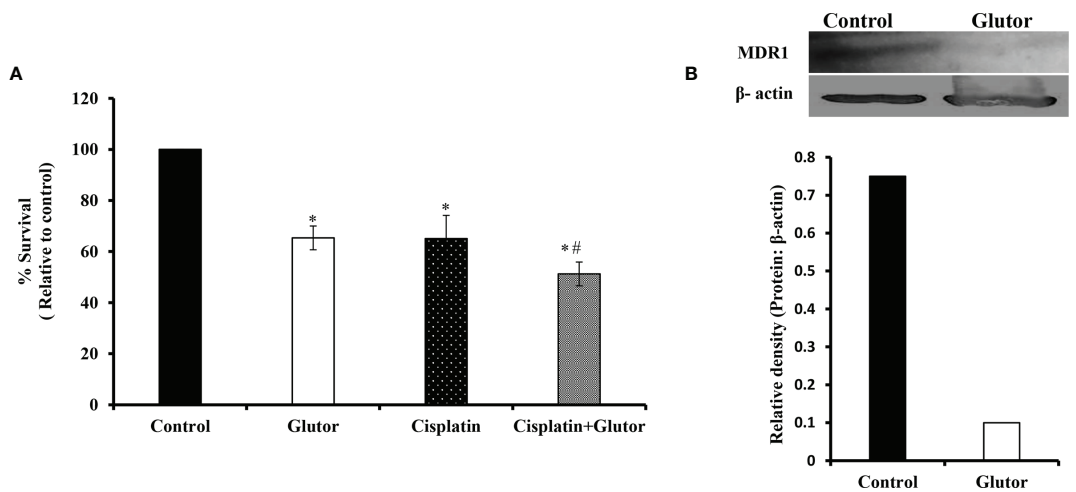

FIGURE 8 | Chemosensitizing action of glutor DL cells (1×10^5) were incubated in a medium alone or containing glutor (0.01 μM) for 24 h in the presence or absence of cisplatin, followed by estimation of cell survival **(A)** by MTT assay as described in the *Materials and Methods* section. Control and glutor-treated DL cells were also evaluated for MDR1 expression **(B)** by Western blotting. Values in **(A)** are the mean ± SD. The plates shown in **(B)** are from a representative experiment out of at least two experiments with similar results. The accompanying bar diagram depicts the densitometry of the bands. *$p < 0.05$ vs. respective control; $p < 0.05$ vs. DL cells treated with glutor or cisplatin alone.

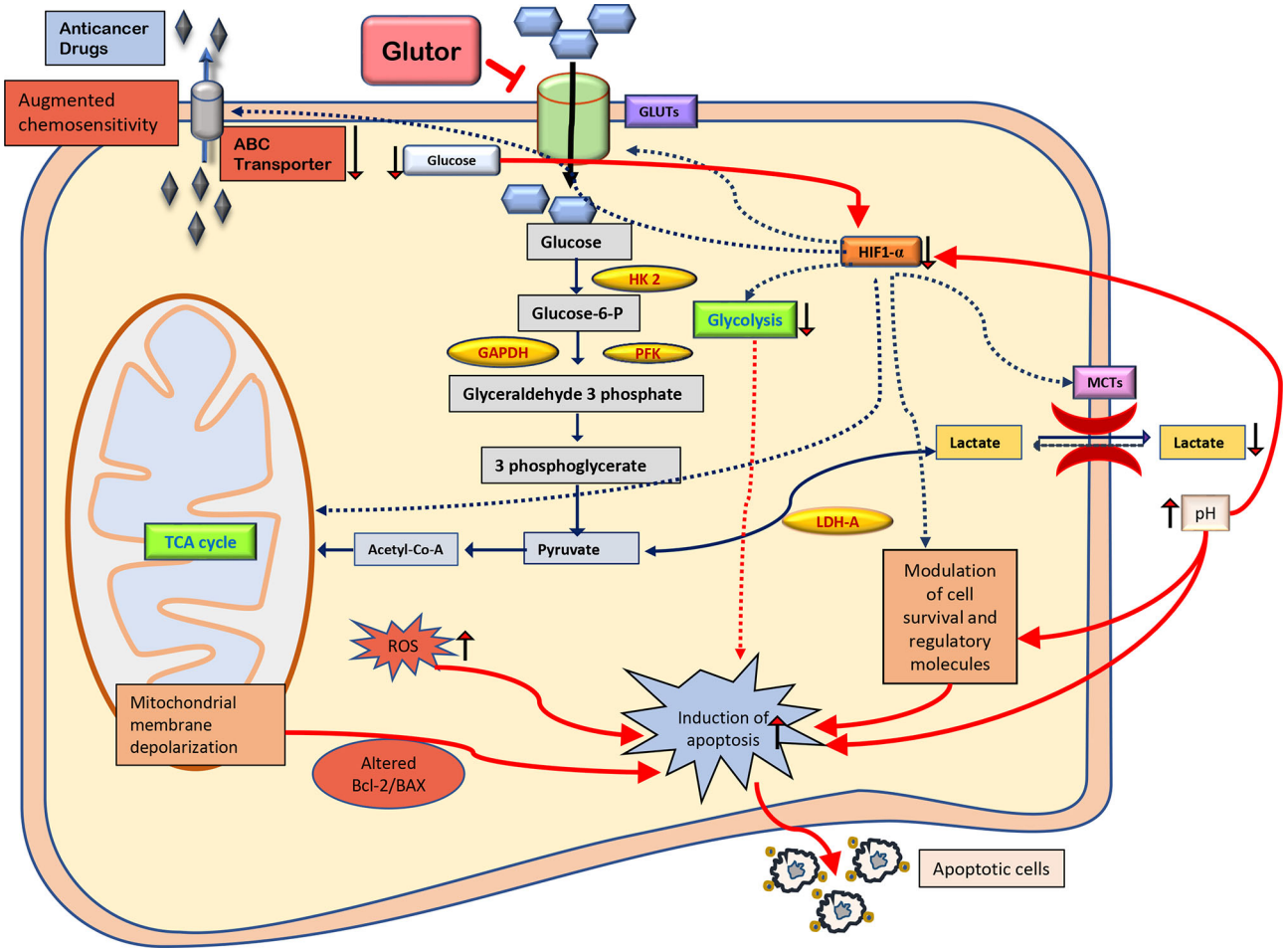

FIGURE 9 | Summary of the molecular mechanisms of the antineoplastic and chemosensitizing action of glutor. The antineoplastic action of glutor involves diminished uptake of glucose, modulated expression of metabolic and cell survival regulatory molecules, altered pH homeostasis, intracellular ROS production, and chemosensitivity.
Abbreviations: GLUT, glucose transporter; HK 2, hexokinase 2; GAPDH, glyceraldehyde 3-phosphate dehydrogenase; PFK, phosphofructokinase; HIF-1α, hypoxia-inducible factor 1-alpha; LDH-A, lactate dehydrogenase A; MCTs, monocarboxylate transporters; Bcl-2, B-cell lymphoma 2; BAX, Bcl-2 Associated X; ROS, reactive oxygen species; ABC transporter, ATP-binding cassette transporters.

do not indicate a direct implication of glutor in the modulation of mitochondrial functions such as mitochondrial membrane potential; however, our results suggest the role of glutor-modulated p53 expression in the implication of altered mitochondrial membrane polarization. Indeed, p53 is reported to maintain mitochondrial membrane integrity and oxidative phosphorylation (67). Moreover, elevated intracellular ROS is also observed in disrupting the mitochondrial membrane potential through the AMPK/p38 MAPK signaling pathway (G. T. 68). ROS also play a vital role in activating p53 (69). Besides ROS and p53, the altered levels of Bcl-2 and BAX have also been associated with the depolarization of the mitochondrial membrane and, consequently, mitochondrial-dependent apoptosis (70–72). Moreover, p53 upregulation is implicated in glycolytic inhibition and oxidative stress-induced apoptosis in DL cells (73). Together, the experimental evidence of the present study demonstrates that glutor alters mitochondrial membrane potential in DL cells, possibly *via* increasing the levels of p53 and ROS and altering Bcl-2 and BAX levels. Nevertheless, upregulation of BAX, along with inhibition of Bcl-2, is implicated in the induction of apoptosis in neoplastic cells (74–76). Moreover, the inhibited expression of HK-2 and LDH-A in glutor-treated DL cells could also impede glycolysis. Thus, the inhibited glycolysis-associated multiple alterations could be one of the likely reasons for the induction of apoptosis.

Interestingly, intracellular ROS has been shown to inhibit various enzymes of glycolysis such as GAPDH, PDK, and PFK, strongly suggesting its crucial role in the regulation of glycolysis (77, 78). Other studies have also reported that inhibition of GLUT1 leads to increased expression of ROS (79, 80). Moreover, intracellular ROS has been demonstrated to trigger apoptosis in neoplastic cells (81).

Nevertheless, glutor treatment also modulated the expression of Hsp70 and TGF-β, which are downstream of HIF-1α and play a crucial role in regulating cell survival (82, 83). As IL-2 plays an indispensable role in T-cell proliferation (84–88), we also checked if IL2 receptor expression is modulated in DL cells following the decrease of glucose assimilation. Interestingly, glutor treatment of DL cells caused a decrease in CD25 expression, which could be possibly another reason for the observed decrease in the proliferation of DL cells. Indeed, the expression of HIF-1α impacts CD25 expression (84).

Another exciting aspect of the present study was the deregulation of pH homeostasis in glutor-treated DL cells, associated with decreased lactate production and MCT1 expression. Additionally, lactate has been shown to exert a predisposing effect on HIF-1α expression in neoplastic cells displaying the Warburg phenomenon (89). Nevertheless, p53 can also regulate MCT1 expression and hence pH homeostasis of cancer cells (90; Monde 91, 92). Moreover, modulated ROS level has been demonstrated to alter the expression of MCT1 (78, 93, 94). Even glucose levels can modulate MCT1 expression (95). Moreover, HIF-1α also regulates the expression of both MCT1 and LDH-A in cancer cells (96, 97). As we observed a decrease in HIF-1α expression, it could be one of the crucial reasons for the observed decrease in the expression of MCT1 and LDH-A in glutor-treated DL cells.

Next, we examined if glutor can alter the vulnerability of cancer cells to the chemotherapeutic agent cisplatin, considering the role of glucose metabolism in regulating chemosensitivity and MDR expression in neoplastic cells (98). Treatment of DL cells with glutor resulted in augmented cytotoxicity of cisplatin, indicating that it enhances chemosensitivity. Thus, this observation reflects the potential of a new therapeutic modality of using glutor as an adjuvant to increase the chemosensitivity of DL cells. Our observations align with earlier studies showing that p-glycoprotein expression is modulated by glucose levels rendering neoplastic cells susceptible to anticancer drugs (99, 100). Indeed, accelerated glycolysis of cancer cells has been reported to elevate ABC transporter activity in neoplastic cells (101, 102). Moreover, GLUT inhibition has been associated with altered drug efflux in cancer cells. Nevertheless, the expression of MDR molecules is also downstream of HIF-1α, which was inhibited in glutor-treated DL cells. Moreover, modulated levels of lactate have also been implicated in altering MDR1 expression (103).

The present study's findings suggest that glutor exposure of thymic tumor cells can manifest hypoglycemic conditions leading to a catastrophic effect on the carbohydrate metabolism of neoplastic cells with multiple consequences. Moreover, the cytotoxic and chemosensitizing action of glutor could be facilitated by interdependent molecular events, implicating modulated expression of cell survival and metabolism regulatory molecules, pH regulation, intracellular ROS production, and MDR1 expression. It must also be noted that adding extra fructose but not glucose to the culture medium could partially reverse the inhibitory action of glutor on tumor cell survival. This observation indicates the extraordinary ability of neoplastic cells to utilize alternative fuels to compensate and revive their metabolism even if one pathway gets blocked by an inhibitor. Therefore, these observations must be considered while designing therapeutic regimens using glutor. A summary of the possible molecular mechanisms underlying glutor-dependent inhibition of tumor cell survival is depicted in **Figure 9**. This study also opens future possibilities to explore the translational value of these observations by testing the tumor growth-retarding action of glutor under *in vivo* preclinical models. Thus, these findings will have a long-lasting clinical significance in evaluating and optimizing the antineoplastic potential of glutor.

DATA AVAILABILITY STATEMENT

The raw data supporting the conclusions of this article will be made available by the authors, without undue reservation.

ETHICS STATEMENT

The animal study was reviewed and approved by the Institutional Animal Ethical Committee, Institute of Science, Banaras Hindu University, Varanasi 221005, UP, India (Approval No. BHU/DoZ/IAEC/2021-2022/016).

AUTHOR CONTRIBUTIONS

MT conceived the idea, performed experiments, contributed to data generation, interpreted data, and wrote the manuscript. SY interpreted data and wrote the manuscript. YG interpreted data and wrote the manuscript. SP interpreted data and wrote the manuscript. AK interpreted data and wrote the manuscript. SS conceived the idea, interpreted data, and wrote the manuscript. All authors contributed to the article and approved the submitted version.

ACKNOWLEDGMENTS

We acknowledge fellowship support to MT (Award No. DBT/JRF/BET-18/I/2018/AL/154) from DBT, New Delhi. Infrastructural support from DBT, New Delhi, ISLS, IOE, and UGC-UPE, Banaras Hindu University is acknowledged. The work contained in this manuscript is part of the Ph.D. dissertation of MT.

SUPPLEMENTARY MATERIAL

The Supplementary Material for this article can be found online at: https://www.frontiersin.org/articles/10.3389/fonc.2022.925666/full#supplementary-material

Supplementary Figure 1 | Molecular structure of glutor Glutor is a piperazine-2-one derivative with IUPAC Name- (S)-6-Methyl-5-(4-morpholinobenzyl)-4-oxo-2-phenyl-N-(pyridin-3-ylmethyl)-4,5,6,7-tetrahydropyrazolo[1,5-a]pyrazine-6-carboxamide.

REFERENCES

1. Bouillaud F, Hammad N, Schwartz L. Warburg Effect, Glutamine, Succinate, Alanine, When Oxygen Matters. *Biology* (2021) 10:1000. doi: 10.3390/biology10101000
2. Liberti MV, Locasale JW. The Warburg Effect: How Does It Benefit Cancer Cells? *Trends Biochem Sci* (2016) 41:211–8. doi: 10.1016/j.tibs.2015.12.001
3. Warburg O. On the Origin of Cancer Cells. *Science* (1956) 123:309–14. doi: 10.1126/science.123.3191.309
4. Barron C, Tsiani E, Tsakiridis T. Expression of the Glucose Transporters GLUT1, GLUT3, GLUT4 and GLUT12 in Human Cancer Cells. *BMC Proc* (2012) 6:P4. doi: 10.1186/1753-6561-6-S3-P4
5. Cervantes-Madrid D, Dueñas-González A. Antitumor Effects of a Drug Combination Targeting Glycolysis, Glutaminolysis and *De Novo* Synthesis of Fatty Acids. *Oncol Rep* (2015) 34:1533–42. doi: 10.3892/or.2015.4077
6. Dong Y, Tu R, Liu H, Qing G. Regulation of Cancer Cell Metabolism: Oncogenic MYC in the Driver's Seat. *Signal Transduction Targeting Ther* (2020) 5:124. doi: 10.1038/s41392-020-00235-2
7. Hay N. Reprogramming Glucose Metabolism in Cancer: Can it be Exploited for Cancer Therapy? *Nat Rev Cancer* (2016) 16:635–49. doi: 10.1038/nrc.2016.77
8. Tveit DM, Fjeld G, Drengstig T, Filipp FV, Ruoff P, Thorsen K. Exploring Mechanisms of Glucose Uptake Regulation and Dilution Resistance in Growing Cancer Cells. *bioRxiv* (2020), 2020.01.02.892729. doi: 10.1101/2020.01.02.892729
9. Stine ZE, Schug ZT, Salvino JM, Dang CV. Targeting Cancer Metabolism in the Era of Precision Oncology. *Nat Rev Drug Discov* (2022) 21:141–62. doi: 10.1038/s41573-021-00339-6
10. Tuli HS, Tuorkey MJ, Thakral F, Sak K, Kumar M, Sharma AK, et al. Molecular Mechanisms of Action of Genistein in Cancer: Recent Advances. *Front Pharmacol* (2019) 10. doi: 10.3389/fphar.2019.01336
11. Salehi B, Machin L, Monzote L, Sharifi-Rad J, Ezzat SM, Salem MA, et al. Therapeutic Potential of Quercetin: New Insights and Perspectives for Human Health. *ACS Omega* (2020) 5:11849–72. doi: 10.1021/acsomega.0c01818
12. Tabolacci C, Cordella M, Rossi S, Bonaccio M, Eramo A, Mischiati C, et al. Targeting Melanoma-Initiating Cells by Caffeine: *In Silico* and *In Vitro* Approaches. *Molecules* (2021) 26:3619. doi: 10.3390/molecules26123619
13. Wu K-H, Ho C-T, Chen Z-F, Chen L-C, Whang-Peng J, Lin T-N, et al. The Apple Polyphenol Phloretin Inhibits Breast Cancer Cell Migration and Proliferation *via* Inhibition of Signals by Type 2 Glucose Transporter. *J Food Drug Anal* (2018) 26:221–31. doi: 10.1016/j.jfda.2017.03.009
14. Poschner S, Maier-Salamon A, Zehl M, Wackerlig J, Dobusch D, Meshcheryakova A, et al. Resveratrol Inhibits Key Steps of Steroid Metabolism in a Human Estrogen-Receptor Positive Breast Cancer Model: Impact on Cellular Proliferation. *Front Pharmacol* (2018) 9:742. doi: 10.3389/fphar.2018.00742
15. Soni VK, Shukla D, Kumar A, Vishvakarma NK. Curcumin Circumvent Lactate-Induced Chemoresistance in Hepatic Cancer Cells Through Modulation of Hydroxycarboxylic Acid Receptor-1. *Int J Biochem Cell Biol* (2020) 123:105752. doi: 10.1016/j.biocel.2020.105752
16. Kapoor K, Finer-Moore JS, Pedersen BP, Caboni L, Waight A, Hillig RC, et al (2016). Mechanism of Inhibition of Human Glucose Transporter GLUT1 Is Conserved Between Cytochalasin B and Phenylalanine Amides. *Proc Natl Acad Sci* 113:4711. doi: 10.1073/pnas.1603735113
17. Ocaña MC, Martínez-Poveda B, Marí-Beffa M, Quesada AR, Medina M.Á. Fasentin Diminishes Endothelial Cell Proliferation, Differentiation and Invasion in a Glucose Metabolism-Independent Manner. *Sci Rep* (2020) 10:6132. doi: 10.1038/s41598-020-63232-z
18. Ojelabi O, DeZutter J, Lloyd K, Carruthers A. Novel Small Molecule, WZB117, Competitively Inhibit GLUT1-Mediated Glucose Transport to Halt Cancer Growth. *FASEB J* (2016) 30:1099.1–1. doi: 10.1096/fasebj.30.1_supplement.1099.1
19. Tilekar K, Upadhyay N, Hess JD, Macias LH, Mrowka P, Aguilera RJ, et al. Structure Guided Design and Synthesis of Furyl Thiazolidinedione Derivatives as Inhibitors of GLUT 1 and GLUT 4, and Evaluation of Their Anti-Leukemic Potential. *Eur J Med Chem* (2020) 202:112603. doi: 10.1016/j.ejmech.2020.112603
20. Meng Y, Xu X, Luan H, Li L, Dai W, Li Z, et al. The Progress and Development of GLUT1 Inhibitors Targeting Cancer Energy Metabolism. *Future Med Chem* (2019) 11:2333–52. doi: 10.4155/fmc-2019-0052
21. Siebeneicher H, Cleve A, Rehwinkel H, Neuhaus R, Heisler I, Müller T, et al. Identification and Optimization of the First Highly Selective GLUT1 Inhibitor BAY-876. *Chemmedchem* (2016) 11:2261–71. doi: 10.1002/cmdc.201600276
22. Shriwas P, Roberts D, Li Y, Wang L, Qian Y, Bergmeier S, et al. A Small-Molecule Pan-Class I Glucose Transporter Inhibitor Reduces Cancer Cell Proliferation *In Vitro* and Tumor Growth *In Vivo* by Targeting Glucose-Based Metabolism. *Cancer Metab* (2021) 9:1–14. doi: 10.1186/s40170-021-00248-7
23. Zhan T, Digel M, Küch E-M, Stremmel W, Füllekrug J. Silybin and Dehydrosilybin Decrease Glucose Uptake by Inhibiting GLUT Proteins. *J Cell Biochem* (2011) 112:849–59. doi: 10.1002/jcb.22984
24. Flaig TW, Gustafson DL, Su L-J, Zirrolli JA, Crighton F, Harrison GS, et al. A Phase I and Pharmacokinetic Study of Silybin-Phytosome in Prostate Cancer Patients. *Invest New Drugs* (2007) 25:139–46. doi: 10.1007/s10637-006-9019-2
25. Memariani Z, Abbas SQ, ul Hassan SS, Ahmadi A, Chabra A. Naringin and Naringenin as Anticancer Agents and Adjuvants in Cancer Combination Therapy: Efficacy and Molecular Mechanisms of Action, a Comprehensive Narrative Review. *Pharmacol Res* (2021) 171:105264. doi: 10.1016/j.phrs.2020.105264
26. Ghanbari-Movahed M, Jackson G, Farzaei MH, Bishayee A. A Systematic Review of the Preventive and Therapeutic Effects of Naringin Against Human Malignancies. *Front Pharmacol* (2021) 12. doi: 10.3389/fphar.2021.639840
27. Zambrano A, Molt M, Uribe E, Salas M. Glut 1 in Cancer Cells and the Inhibitory Action of Resveratrol as A Potential Therapeutic Strategy. *Int J Mol Sci* (2019) 20:3374. doi: 10.3390/ijms20133374
28. Davidson CD, Carr FE. Review of Pharmacological Inhibition of Thyroid Cancer Metabolism. *J Cancer Metastasis Treat* (2021) 7:45. doi: 10.20517/2394-4722.2021.77
29. Reckzeh ES, Karageorgis G, Schwalfenberg M, Ceballos J, Nowacki J, Stroet MCM, et al. Inhibition of Glucose Transporters and Glutaminase Synergistically Impairs Tumor Cell Growth. *Cell Chem Biol* (2019) 26:1214–1228.e25. doi: 10.1016/j.chembiol.2019.06.005
30. Reckzeh ES, Waldmann H. Development of Glucose Transporter (GLUT) Inhibitors. *Eur J Org Chem* (2020) 2020:2321–9. doi: 10.1002/ejoc.201901353
31. Schmidl S, Ursu O, Iancu CV, Oreb M, Oprea TI, Choe J. Identification of New GLUT2-Selective Inhibitors Through *in Silico* Ligand Screening and Validation in Eukaryotic Expression Systems. *Sci Rep* (2021) 11:13751. doi: 10.1038/s41598-021-93063-5
32. Tseng Y-L. Thymic Carcinoma: A Rare Cancer Requiring Special Attention. *Formos. J Surg* (2011) 44:136–40. doi: 10.1016/j.fjs.2011.08.007
33. Zeng H, Yang W, Xu B, Zou J, Su C, Zhong B, et al. Relationship of Possible Biomarkers With Malignancy of Thymic Tumors: A Meta-Analysis. *BMC Cancer* (2020) 20:928. doi: 10.1186/s12885-020-07332-z
34. Dunham LJ, Stewart HL. A Survey of Transplantable and Transmissible Animal Tumors. *J Natl Cancer Inst* (1953) 13:1299–377. doi: 10.1093/jnci/13.5.1299
35. Goel Y, Yadav S, Pandey SK, Temre MK, Maurya BN, Verma A, et al. Tumor Decelerating and Chemo-Potentiating Action of Methyl Jasmonate on a T Cell Lymphoma *In Vivo*: Role of Altered Regulation of Metabolism, Cell Survival, Drug Resistance, and Intratumoral Blood Flow. *Front Oncol* (2021) 11. doi: 10.3389/fonc.2021.619351
36. Yadav S, Pandey SK, Goel Y, Kujur PK, Maurya BN, Verma A, et al. Protective and Recuperative Effects of 3-Bromopyruvate on Immunological, Hepatic and Renal Homeostasis in a Murine Host Bearing Ascitic Lymphoma: Implication of Niche Dependent Differential Roles of Macrophages. *Biomed Pharmacother Biomedecine Pharmacother* (2018) 99:970–85. doi: 10.1016/j.biopha.2018.01.149
37. Bharti AC, Singh SM. Gangliosides Derived From a T Cell Lymphoma Inhibit Bone Marrow Cell Proliferation and Differentiation. *Int Immunopharmacol* (2001) 1:155–65. doi: 10.1016/S1567-5769(00)00004-7

38. Goldie H, Felix MD. Growth Characteristics of Free Tumor Cells Transferred Serially in the Peritoneal Fluid of the Mouse. *Cancer Res* (1951) 11:73–80.
39. Mosmann T. Rapid Colorimetric Assay for Cellular Growth and Survival: Application to Proliferation and Cytotoxicity Assays. *J Immunol Methods* (1983) 65:55–63. doi: 10.1016/0022-1759(83)90303-4
40. Fido RJ, Tatham AS, Shewry PR. Western Blotting Analysis. *Methods Mol Biol Clifton NJ* (1995) 49:423–37. doi: 10.1385/0-89603-321-X:423
41. Goel Y, Yadav S, Pandey SK, Temre MK, Singh VK, Kumar A, et al. Methyl Jasmonate Cytotoxicity and Chemosensitization of T Cell Lymphoma *In Vitro* Is Facilitated by HK 2, HIF-1α, and Hsp70: Implication of Altered Regulation of Cell Survival, pH Homeostasis, Mitochondrial Functions. *Front Pharmacol* (2021) 12:158. doi: 10.3389/fphar.2021.628329
42. Bradford MM. A Rapid and Sensitive Method for the Quantitation of Microgram Quantities of Protein Utilizing the Principle of Protein-Dye Binding. *Anal Biochem* (1976) 72:248–54. doi: 10.1006/abio.1976.9999
43. Furuta E, Pai SK, Zhan R, Bandyopadhyay S, Watabe M, Mo Y-Y, et al. Fatty Acid Synthase Gene is Up-Regulated by Hypoxia *via* Activation of Akt and Sterol Regulatory Element Binding Protein-1. *Cancer Res* (2008) 68:1003–11. doi: 10.1158/0008-5472.CAN-07-2489
44. Somoza B, Guzmán R, Cano V, Merino B, Ramos P, Díez-Fernández C, et al. Induction of Cardiac Uncoupling Protein-2 Expression and Adenosine 5'-Monophosphate-Activated Protein Kinase Phosphorylation During Early States of Diet-Induced Obesity in Mice. *Endocrinology* (2007) 148:924–31. doi: 10.1210/en.2006-0914
45. Yadav S, Pandey SK, Goel Y, Temre MK, Singh SM. Antimetabolic Agent 3-Bromopyruvate Exerts Myelopotentiating Action in a Murine Host Bearing a Progressively Growing Ascitic Thymoma. *Immunol Invest.* (2020) 49:425–42. doi: 10.1080/08820139.2019.1627368
46. Crowley LC, Christensen ME, Waterhouse NJ. Measuring Mitochondrial Transmembrane Potential by TMRE Staining. *Cold Spring Harb. Protoc* (2016). doi: 10.1101/pdb.prot087361
47. Reckzeh ES, Waldmann H. Small-Molecule Inhibition of Glucose Transporters GLUT-1–4. *ChemBioChem* (2020) 21:45–52. doi: 10.1002/cbic.201900544
48. Gonzalez-Menendez P, Hevia D, Alonso-Arias R, Alvarez-Artime A, Rodriguez-Garcia A, Kinet S, et al. GLUT1 Protects Prostate Cancer Cells From Glucose Deprivation-Induced Oxidative Stress. *Redox Biol* (2018) 17:112–27. doi: 10.1016/j.redox.2018.03.017
49. Liu Y, Cao Y, Zhang W, Bergmeier S, Qian Y, Akbar H, et al. A Small-Molecule Inhibitor of Glucose Transporter 1 Downregulates Glycolysis, Induces Cell-Cycle Arrest, and Inhibits Cancer Cell Growth *In Vitro* and *In Vivo*. Mol. *Cancer Ther* (2012) 11:1672–82. doi: 10.1158/1535-7163.MCT-12-0131
50. Ma Y, Wang W, Idowu MO, Oh U, Wang X-Y, Temkin SM, et al. Ovarian Cancer Relies on Glucose Transporter 1 to Fuel Glycolysis and Growth: Anti-Tumor Activity of BAY-876. *Cancers* (2018) 11:33. doi: 10.3390/cancers11010033
51. Zhao F, Ming J, Zhou Y, Fan L. Inhibition of Glut1 by WZB117 Sensitizes Radioresistant Breast Cancer Cells to Irradiation. *Cancer Chemother Pharmacol* (2016) 77:963–72. doi: 10.1007/s00280-016-3007-9
52. Masoud GN, Li W. HIF-1α Pathway: Role, Regulation and Intervention for Cancer Therapy. *Acta Pharm Sin B* (2015) 5:378–89. doi: 10.1016/j.apsb.2015.05.007
53. Hao L-S, Liu Q, Tian C, Zhang D-X, Wang B, Zhou D-X, et al. Correlation and Expression Analysis of Hypoxia–Inducible Factor 1α, Glucose Transporter 1 and Lactate Dehydrogenase 5 in Human Gastric Cancer. *Oncol Lett* (2019) 18:1431–41. doi: 10.3892/ol.2019.10457
54. Li Y, Sun X-X, Qian DZ, Dai M-S. Molecular Crosstalk Between MYC and HIF in Cancer. *Front Cell Dev Biol* (2020) 8. doi: 10.3389/fcell.2020.590576
55. Sadlecki P, Bodnar M, Grabiec M, Marszalek A, Walentowicz P, Sokup A, et al. The Role of Hypoxia-Inducible Factor-1α, Glucose Transporter-1, (GLUT-1) and Carbon Anhydrase IX in Endometrial Cancer Patients. *BioMed Res Int* (2014) 2014:e616850. doi: 10.1155/2014/616850
56. Li W, Liu H, Qian W, Cheng L, Yan B, Han L, et al. Hyperglycemia Aggravates Microenvironment Hypoxia and Promotes the Metastatic Ability of Pancreatic Cancer. *Comput Struct Biotechnol J* (2018) 16:479–87. doi: 10.1016/j.csbj.2018.10.006
57. Balihodzic A, Barth DA, Prinz F, Pichler M. Involvement of Long Non-Coding RNAs in Glucose Metabolism in Cancer. *Cancers* (2021) 13:977. doi: 10.3390/cancers13050977
58. Bishop EL, Gudgeon N, Dimeloe S. Control of T Cell Metabolism by Cytokines and Hormones. *Front Immunol* (2021) 12. doi: 10.3389/fimmu.2021.653605
59. Guo Y, Lv B, Liu R, Dai Z, Zhang F, Liang Y, et al. Role of LncRNAs in Regulating Cancer Amino Acid Metabolism. *Cancer Cell Int* (2021) 21:209. doi: 10.1186/s12935-021-01926-8
60. Hoxhaj G, Manning BD. The PI3K-AKT Network at the Interface of Oncogenic Signalling and Cancer Metabolism. *Nat Rev Cancer* (2020) 20:74–88. doi: 10.1038/s41568-019-0216-7
61. Lozano-Romero A, Astudillo-de la Vega H, Terrones-Gurrola MC, del R, Marchat LA, Hernández-Sotelo D, et al. HOX Transcript Antisense RNA HOTAIR Abrogates Vasculogenic Mimicry by Targeting the AngiomiR-204/FAK Axis in Triple Negative Breast Cancer Cells. *Non-Coding RNA* (2020) 6:19. doi: 10.3390/ncrna6020019
62. Evangelisti C, Chiarini F, Cappellini A, Paganelli F, Fini M, Santi S, et al. Targeting Wnt/β-Catenin and PI3K/Akt/mTOR Pathways in T-Cell Acute Lymphoblastic Leukemia. *J Cell Physiol* (2020) 235:5413–28. doi: 10.1002/jcp.29429
63. Li Y, Liu Y, Lu Y, Zhao B. Inhibitory Effects of 17β-Estradiol or a Resveratrol Dimer on Hypoxia-Inducible Factor-1α in Genioglossus Myoblasts: Involvement of Erα and its Downstream P38 MAPK Pathways. *Int J Mol Med* (2017) 40:1347–56. doi: 10.3892/ijmm.2017.3123
64. Cluff ER, Nolan J, Collins C, Varadaraj A, Rajasekaran N. Hypoxia-Inducible Factor-1α Is Upregulated in Natural Killer Cells by Interleukin-2 and Hypoxia *via* PI3K/mTOR Signaling Pathway. *J Immunol* (2019) 202:194.37–7. doi: 10.1007/s00262-021-03126-9
65. Elgendy M, Cirò M, Hosseini A, Weiszmann J, Mazzarella L, Ferrari E, et al. Combination of Hypoglycemia and Metformin Impairs Tumor Metabolic Plasticity and Growth by Modulating the PP2A-Gsk3β-MCL-1 Axis. *Cancer Cell* (2019) 35:798–815.e5. doi: 10.1016/j.ccell.2019.03.007
66. Olatunde A, Nigam M, Singh RK, Panwar AS, Lasisi A, Alhumaydhi FA, et al. Cancer and Diabetes: The Interlinking Metabolic Pathways and Repurposing Actions of Antidiabetic Drugs. *Cancer Cell Int* (2021) 21:499. doi: 10.1186/s12935-021-02202-5
67. Bergeaud M, Mathieu L, Guillaume A, Moll UM, Mignotte B, Le Floch N, et al. Mitochondrial P53 Mediates a Transcription-Independent Regulation of Cell Respiration and Interacts With the Mitochondrial F_1F0-ATP Synthase. *Cell Cycle Georget. Tex* (2013) 12:2781–93. doi: 10.4161/cc.25870
68. Kim GT, Lee SH, Kim YM. Torilis Japonica Extract-Generated Intracellular ROS Induces Apoptosis by Reducing the Mitochondrial Membrane Potential *via* Regulation of the AMPK-P38 MAPK Signaling Pathway in HCT116 Colon Cancer. *Int J Oncol* (2016) 49:1088–98. doi: 10.3892/ijo.2016.3578
69. Shi T, Dansen TB. Reactive Oxygen Species Induced P53 Activation: DNA Damage, Redox Signaling, or Both? *Antioxid Redox Signal* (2020) 33:839–59. doi: 10.1089/ars.2020.8074
70. Gyulkhandanyan AV, Allen DJ, Mykhaylov S, Lyubimov E, Ni H, Freedman J, et al. Mitochondrial Inner Membrane Depolarization as a Marker of Platelet Apoptosis: Disclosure of Nonapoptotic Membrane Depolarization. *Clin Appl Thromb* (2017) 23:139–47. doi: 10.1177/1076029616665924
71. Matsuyama S, Reed JC. Mitochondria-Dependent Apoptosis and Cellular pH Regulation. *Cell Death Differ* (2000) 7:1155–65. doi: 10.1038/sj.cdd.4400779
72. Wang C, Youle RJ. The Role of Mitochondria in Apoptosis*. *Annu Rev Genet* (2009) 43:95–118. doi: 10.1146/annurev-genet-102108-134850
73. Koiri RK, Trigun SK, Mishra L. Activation of P53 Mediated Glycolytic Inhibition-Oxidative Stress-Apoptosis Pathway in Dalton's Lymphoma by a Ruthenium (II)-Complex Containing 4-Carboxy N-Ethylbenzamide. *Biochimie* (2015) 110:52–61. doi: 10.1016/j.biochi.2014.12.021
74. Kapoor I, Bodo J, Hill BT, Hsi ED, Almasan A. Targeting BCL-2 in B-Cell Malignancies and Overcoming Therapeutic Resistance. *Cell Death Dis* (2020) 11:941. doi: 10.1038/s41419-020-03144-y
75. Lucantoni F, Düssmann H, Llorente-Folch I, Prehn JHM. BCL2 and BCL(X)L Selective Inhibitors Decrease Mitochondrial ATP Production in Breast

Cancer Cells and Are Synthetically Lethal When Combined With 2-Deoxy-D-Glucose. *Oncotarget* (2018) 9:26046–63. doi: 10.18632/oncotarget.25433
76. Sharma A, Boise LH, Shanmugam M. Cancer Metabolism and the Evasion of Apoptotic Cell Death. *Cancers* (2019) 11:1144. doi: 10.3390/cancers11081144
77. Ghanbari Movahed Z, Rastegari-Pouyani M, Mohammadi M, Mansouri K. Cancer Cells Change Their Glucose Metabolism to Overcome Increased ROS: One Step From Cancer Cell to Cancer Stem Cell? *Biomed Pharmacother.* (2019) 112:108690. doi: 10.1016/j.biopha.2019.108690
78. Rodic S, Vincent MD. Reactive Oxygen Species (ROS) Are a Key Determinant of Cancer's Metabolic Phenotype. *Int J Cancer* (2018) 142:440–8. doi: 10.1002/ijc.31069
79. Kim J, Kim J, Bae J-S. ROS Homeostasis and Metabolism: A Critical Liaison for Cancer Therapy. *Exp Mol Med* (2016) 48:e269–9. doi: 10.1038/emm.2016.119
80. Liemburg-Apers DC, Willems PHGM, Koopman WJH, Grefte S. Interactions Between Mitochondrial Reactive Oxygen Species and Cellular Glucose Metabolism. *Arch Toxicol* (2015) 89:1209–26. doi: 10.1007/s00204-015-1520-y
81. Perillo B, Di Donato M, Pezone A, Di Zazzo E, Giovannelli P, Galasso G, et al. ROS in Cancer Therapy: The Bright Side of the Moon. *Exp Mol Med* (2020) 52:192–203. doi: 10.1038/s12276-020-0384-2
82. Huang W-J, Xia L-M, Zhu F, Huang B, Zhou C, Zhu H-F, et al. Transcriptional Upregulation of HSP70-2 by HIF-1 in Cancer Cells in Response to Hypoxia. *Int J Cancer* (2009) 124:298–305. doi: 10.1002/ijc.23906
83. Huang Y, Chen Z, Lu T, Bi G, Li M, Liang J, et al. HIF-1α Switches the Functionality of TGF-β Signaling *via* Changing the Partners of Smads to Drive Glucose Metabolic Reprogramming in Non-Small Cell Lung Cancer. *J Exp Clin Cancer Res CR* (2021) 40:398. doi: 10.1186/s13046-021-02188-y
84. Jiang T, Zhou C, Ren S. Role of IL-2 in Cancer Immunotherapy. *Oncoimmunology* (2016) 5:e1163462. doi: 10.1080/2162402X.2016.1163462
85. Koiri RK, Mehrotra A, Trigun SK, Koiri RK, Mehrotra A, Trigun SK. Dalton's Lymphoma as a Murine Model for Understanding the Progression and Development of T-Cell Lymphoma and Its Role in Drug Discovery. *Int J Immunother. Cancer Res* (2017) 3:001–6. doi: 10.17352/2455-8591.000011
86. Ross SH, Cantrell DA. Signaling and Function of Interleukin-2 in T Lymphocytes. *Annu Rev Immunol* (2018) 36:411–33. doi: 10.1146/annurev-immunol-042617-053352
87. Serrate SA, Schulof RS, Leondaridis L, Goldstein AL, Sztein MB. Modulation of Human Natural Killer Cell Cytotoxic Activity, Lymphokine Production, and Interleukin 2 Receptor Expression by Thymic Hormones. *J Immunol Baltim. Md* (1987) 139:2338–43.
88. Shanker A, Singh SM, Sodhi A. Ascitic Growth of a Spontaneous Transplantable T Cell Lymphoma Induces Thymic Involution. *Tumor Biol* (2000) 21:288–98. doi: 10.1159/000030134
89. De Saedeleer CJ, Copetti T, Porporato PE, Verrax J, Feron O, Sonveaux P. Lactate Activates HIF-1 in Oxidative But Not in Warburg-Phenotype Human Tumor Cells. *PloS One* (2012) 7:e46571. doi: 10.1371/journal.pone.0046571
90. Liu J, Zhang C, Hu W, Feng Z. Tumor Suppressor P53 and Metabolism. *J Mol Cell Biol* (2019) 11:284–92. doi: 10.1093/jmcb/mjy070
91. Ntwasa M. Glucose Metabolism and Carcinogenesis: The Impact of the Tumor Suppressor. In: U Njende, HN Shahzad, editors. *Neoplasm*. Rijeka: IntechOpen (2018). p. p53. doi: 10.5772/intechopen.75976
92. Puzio-Kuter AM. The Role of P53 in Metabolic Regulation. *Genes Cancer* (2011) 2:385–91. doi: 10.1177/1947601911409738
93. De Saedeleer CJ, Porporato PE, Copetti T, Pérez-Escuredo J, Payen VL, Brisson L, et al. Glucose Deprivation Increases Monocarboxylate Transporter 1 (MCT1) Expression and MCT1-Dependent Tumor Cell Migration. *Oncogene* (2014) 33:4060–8. doi: 10.1038/onc.2013.454
94. Johnson JM, Cotzia P, Fratamico R, Mikkilineni L, Chen J, Colombo D, et al. MCT1 in Invasive Ductal Carcinoma: Monocarboxylate Metabolism and Aggressive Breast Cancer. *Front Cell Dev Biol* (2017) 5:27. doi: 10.3389/fcell.2017.00027
95. Zhang G, Zhang Y, Dong D, Wang F, Ma X, Guan F, et al. MCT1 Regulates Aggressive and Metabolic Phenotypes in Bladder Cancer. *J Cancer* (2018) 9:2492–501. doi: 10.7150/jca.25257
96. Cui X-G, Han Z-T, He S-H, Wu X, Chen T-R, Shao C-H, et al. Hif1/2α Mediates Hypoxia-Induced LDHA Expression in Human Pancreatic Cancer Cells. *Oncotarget* (2017) 8:24840–52. doi: 10.18632/oncotarget.15266
97. Lacher SE, Levings DC, Freeman S, Slattery M. Identification of a Functional Antioxidant Response Element at the HIF1A Locus. *Redox Biol* (2018) 19:401–11. doi: 10.1016/j.redox.2018.08.014
98. Qiu J, Zheng Q, Meng X. Hyperglycemia and Chemoresistance in Breast Cancer: From Cellular Mechanisms to Treatment Response. *Front Oncol* (2021) 11:628359. doi: 10.3389/fonc.2021.628359
99. Bukowski K, Kciuk M, Kontek R. Mechanisms of Multidrug Resistance in Cancer Chemotherapy. *Int J Mol Sci* (2020) 21:03233. doi: 10.3390/ijms21093233
100. Lee G, Joung J-Y, Cho J-H, Son C-G, Lee N. Overcoming P-Glycoprotein-Mediated Multidrug Resistance in Colorectal Cancer: Potential Reversal Agents Among Herbal Medicines. *Evid. Based Complement. Alternat. Med* (2018) 2018:3412074. doi: 10.1155/2018/3412074
101. Giddings EL, Champagne DP, Wu M-H, Laffin JM, Thornton TM, Valenca-Pereira F, et al. Mitochondrial ATP Fuels ABC Transporter-Mediated Drug Efflux in Cancer Chemoresistance. *Nat Commun* (2021) 12:2804. doi: 10.1038/s41467-021-23071-6
102. Nakano A, Tsuji D, Miki H, Cui Q, El Sayed SM, Ikegame A, et al. Glycolysis Inhibition Inactivates ABC Transporters to Restore Drug Sensitivity in Malignant Cells. *PloS One* (2011) 6:e27222. doi: 10.1371/journal.pone.0027222
103. Pérez-Tomás R, Pérez-Guillén I. Lactate in the Tumor Microenvironment: An Essential Molecule in Cancer Progression and Treatment. *Cancers* (2020) 12:3244. doi: 10.3390/cancers12113244

Conflict of Interest: The authors declare that the research was conducted in the absence of any commercial or financial relationships that could be construed as a potential conflict of interest.

Publisher's Note: All claims expressed in this article are solely those of the authors and do not necessarily represent those of their affiliated organizations, or those of the publisher, the editors and the reviewers. Any product that may be evaluated in this article, or claim that may be made by its manufacturer, is not guaranteed or endorsed by the publisher.

frontiers | Frontiers in Oncology

TYPE Original Research
PUBLISHED 12 October 2022
DOI 10.3389/fonc.2022.960109

OPEN ACCESS

EDITED BY
Dayanidhi Raman,
University of Toledo, United States

REVIEWED BY
Fatma Al-Awadhi,
Kuwait University, Kuwait
Anthony J. O'Donoghue,
University of California, San Diego, United States

*CORRESPONDENCE
Thomas Reinheckel
thomas.reinheckel@mol-med.uni-freiburg.de

SPECIALTY SECTION
This article was submitted to Breast Cancer, a section of the journal Frontiers in Oncology

RECEIVED 02 June 2022
ACCEPTED 20 September 2022
PUBLISHED 12 October 2022

CITATION
Hölzen L, Syré K, Mitschke J, Brummer T, Miething C and Reinheckel T (2022) Degradome-focused RNA interference screens to identify proteases important for breast cancer cell growth.
Front. Oncol. 12:960109.
doi: 10.3389/fonc.2022.960109

Degradome-focused RNA interference screens to identify proteases important for breast cancer cell growth

Lena Hölzen[1,2,3,4], Kerstin Syré[1], Jan Mitschke[5], Tilman Brummer[1,2,3,6,7], Cornelius Miething[2,3,5,7] and Thomas Reinheckel[1,2,3,6]*

[1]Institute of Molecular Medicine and Cell Research, Faculty of Medicine, University of Freiburg, Freiburg, Germany, [2]German Cancer Consortium (DKTK) Partner Site Freiburg, Freiburg, Germany, [3]German Cancer Research Center, Heidelberg, Germany, [4]Faculty of Biology, University of Freiburg, Freiburg, Germany, [5]Center for Translational Cell Research, Department of Internal Medicine I - Hematology, Oncology and Stem Cell Transplantation, Faculty of Medicine, University of Freiburg, Freiburg, Germany, [6]Center for Biological Signaling Studies BIOSS, University of Freiburg, Freiburg, Germany, [7]Comprehensive Cancer Center Freiburg (CCCF), University Medical Center, University of Freiburg, Freiburg, Germany

Proteases are known to promote or impair breast cancer progression and metastasis. However, while a small number of the 588 human and 672 murine protease genes have been extensively studied, others were neglected. For an unbiased functional analysis of all genome-encoded proteases, i.e., the degradome, in breast cancer cell growth, we applied an inducible RNA interference library for protease-focused genetic screens. Importantly, these functional screens were performed in two phenotypically different murine breast cancer cell lines, including one stem cell-like cell line that showed phenotypic plasticity under changed nutrient and oxygen availability. Our unbiased genetic screens identified 252 protease genes involved in breast cancer cell growth that were further restricted to 100 hits by a selection process. Many of those hits were supported by literature, but some proteases were novel in their functional link to breast cancer. Interestingly, we discovered that the environmental conditions influence the degree of breast cancer cell dependency on certain proteases. For example, breast cancer stem cell-like cells were less susceptible to depletion of several mitochondrial proteases in hypoxic conditions. From the 100 hits, nine proteases were functionally validated in murine breast cancer cell lines using individual knockdown constructs, highlighting the high reliability of our screens. Specifically, we focused on mitochondrial processing peptidase (MPP) subunits alpha (Pmpca) and beta (Pmpcb) and discovered that MPP depletion led to a disadvantage in cell growth, which was linked to mitochondrial dysfunction.

KEYWORDS

breast cancer, protease, degradome, genetic screen, RNA interference

1 Introduction

Short hairpin RNA (shRNA) library-based RNA interference (RNAi) is a widely used method for large-scale genetic loss of function screens, allowing for the unbiased discovery of cancer drivers, putative therapeutic targets, and genes with no previous links to cancer (1–3). shRNA libraries contain a heterogeneous mixture of different shRNA constructs targeting the whole genome (genome-wide screening) or a subset, i.e., all kinases, in so-called focused libraries. Although manifold genome-wide screens (4–6) and kinase-focused screens (7–9) were published in cancer cells in the last years, the study of an important class of enzymes, the proteases, was neglected so far.

Proteases are enzymes that irreversibly hydrolyze peptide bonds. Thereby, they (in)activate, degrade, or change the subcellular location of other proteins (10–12). Thus, they are essential for most physiological functions, and proteolytic activity is tightly controlled in cells, tissues, and body fluids. The complete set of proteases expressed in one organism or tissue is frequently defined as the degradome (13). According to the degradome database, 588 human and 672 murine protease and protease-like genes are currently known (13, 14). Degradome dysregulations are typical for cancers, facilitating or impairing tumor progression (10–12). Consequently, several proteases have been identified to be involved in all steps of cancer progression. Among the most studied groups of proteases are matrix metalloproteases (MMPs) that can promote tumor invasion by proteolysis of extracellular matrix and basement membrane components. In addition, they facilitate tumor growth by processing of bioactive molecules, e.g., growth factor receptors (15). Nevertheless, analysis of protease contribution to cancer has run into a bottleneck, with some proteases being extensively studied, e.g., MMPs or caspases (10–12), whereas the role of many degradome proteases remained understudied.

This paper presents a functional high-throughput degradome-focused RNAi screen to investigate the importance of all degradome-encoded proteases in murine breast cancer cell proliferation and/or survival. We chose to apply this screening method firstly to breast cancer cells because breast cancer is the most commonly diagnosed cancer in women and a global health burden with approximately 2.3 million new cases and 685,000 deaths in 2020 worldwide (16, 17). In 2022, 290,560 new cases and 43,780 deaths are estimated to occur in the United States alone (18). For our degradome-wide RNAi screens, we employed a customized shRNA library targeting the entire murine degradome (19). Specifically, we made use of a third-generation shRNA backbone, the enhanced microRNA (miR-E), generated by optimization of the native human miR-30a scaffold (20). Thus, miR-E constructs show increased pri-miRNA processing leading to higher mature shRNA levels that in turn boost potency and make miR-E constructs more useful for single-copy integration experiments (20, 21). Moreover, we employed an advanced RNAi vector system with inducible promoters for coexpression of the miR-E and a fluorescent reporter combined with a constitutive fluorescent marker to monitor vector integration. We have recently successfully applied this degradome-wide screening approach in a synthetic lethality setting (19). Now, we use it to define sets of proteases enabling or promoting breast cancer cell growth.

It is important to consider that tumors are complex tissues built from multiple cellular and genetically heterogenic cell subpopulations (22, 23). To reflect this, we chose to integrate the degradome-targeted library into two murine breast cancer cell lines with different properties, both previously generated by us from the transgenic MMTV-PyMT metastatic breast cancer model (24). The PyB6-313 cell line is an immortalized epithelial breast cancer cell line generated on a C57BL/6J mouse background (25). In contrast, PyMG-816 cells were immortalized from a primary CD24+CD90+CD45- tumor subpopulation from MMTV-PyMT mice with an FVB background and were shown to have cancer stem cell (CSC)-like properties (26). CSCs are a small tumor subpopulation that is of great importance for initiation, progression, and metastasis of cancer and is particularly problematic as the source of therapy-resisting cell populations (11, 27). It was previously shown that the PyMG-816 cells display a phenotypic and molecular plasticity when transferred from nutrient-deprived hypoxic (3% O_2) stem cell conditions to nutrient-rich normoxic (21% O_2) culture conditions (26). To prevent differentiation, the cells were normally kept in basement membrane extract (Cultrex^{TM})-supplemented culture with only 3% oxygen content. Cells transferred to normoxic conditions increased in cytoplasm content and became polynucleated and more spindle

Abbreviations: Adamts, a disintegrin and metalloproteinase with thrombospondin motifs; AML, acute myeloid leukemia; AvSSMD*, robust strictly standardized median difference; BGR, background; Clpp, caseinolytic mitochondrial matrix peptidase proteolytic subunit; Clpx, ATP-dependent Clp protease ATP-binding subunit clpX-like; CSC, cancer stem cell; Dox, doxycycline; DUB, deubiquitinase; Ctsf, cathepsin F; FGR, foreground; GEO, Gene Expression Omnibus; HCC, hepatocellular carcinoma; Lonp1, Lon protease 1; MAD, median absolute deviation; miR-E, enhanced microRNA; Metap1/Metap2, methionine aminopeptidase 1/2; MMP, matrix metalloprotease; MPP, mitochondrial processing peptidase; NGS, next-generation sequencing; NOR, number of reads; Psma/Psmb/Psmc, proteasomal α/β/γ subunit; Psmd13, 26S proteasome non-ATPase subunit 13; pTCEBAC, TRE-Cyan-miR-E-PGK-BSDr-2A-Cherry; pTREBAV, TRE-dsRed-miR-E-PGK-BSDr-2A-Venus; RNAi, RNA interference; ROS, reactive oxygen species; SD, standard deviation; shRNA, short hairpin RNA; STRING, Search Tool for the Retrieval of Interacting Genes/Proteins; TRE, tetracycline response element; rtTA3, reverse tetracycline transactivator 3; Tysnd1, peroxisomal matrix protein trypsin domain-containing 1; UPS, ubiquitin-proteasome system; Usp46/7, ubiquitin-carboxyl terminal hydrolase 46/7; Uspl1, ubiquitin-specific peptidase like 1.

shaped with close cell–cell contact (26). Functionally, normoxic culture conditions decreased anchorage-independent cell growth, impaired cell motility, and increased cell growth and metabolic activity *in vitro* as well as reduced lung metastasis formation in orthotopic transplantation models *in vivo*. Interestingly, transcriptome analysis revealed differently regulated protease messenger RNA (mRNA) expression upon changed environmental conditions (26).

By applying the miR-E library for our protease-focused genetic screening, we aim to investigate protease dependency in breast cancer cells and to discover proteases that have been overlooked in breast cancer so far. The use of two phenotypically different cell lines, one of them displaying CSC-like properties, reflects at least in part the tremendous cellular heterogeneity in tumors. In addition, the phenotypic plasticity of the PyMG-816 cells could be utilized to elucidate on the role for proteases under changed environmental conditions. We further employed inducible protease knockdown breast cancer cell lines to functionally validate our screens, whereby we, among other hits, identified and *in vitro* validated the mitochondrial processing peptidase (MPP) subunits alpha (Pmpca) and beta (Pmpcb) as important for breast cancer cell growth.

2 Results

2.1 Generation of murine degradome-targeted breast cancer cells for genetic screens

In our RNAi library, each protease transcript is targeted by 4–7 miR-Es (4,800 in total). The miR-Es are individually integrated into the doxycycline (Dox)-inducible double-fluorescence pTREBAV vector that enables time-controlled and traceable protease knockdown (Figure 1A). The pTREBAV vector constitutively expresses a Venus fluorescence reporter under control of the phosphoglycerate kinase (PGK) promoter. In addition, the vector carries an inducible dsRed reporter coupled to the miR-E sequence downstream of a tetracycline response element (TRE) that enables Dox-dependent gene silencing. The miR-E library was subdivided into 16 pools (300 miR-Es/pool) that were transduced into two self-generated breast cancer cell lines (PyB6-TA and PyMG-TA) expressing the reverse tetracycline transactivator 3 (rtTA3). Importantly, integration was performed under optimized conditions, ensuring single miR-E copy integration with 1,000× miR-E representation, i.e., 1,000 cells harboring the same miR-E construct. Library integration of the 16 miR-E pools was done in two independent biological replicates, leading to 32 degradome-targeted breast cancer cell pools for each cell line.

PyMG-TA and PyB6-TA cell lines were established from the parental PyMG-816 and PyB6-313 cells by integration of the rtTA3 as the second part of the Dox-inducible knockdown system, as well as the luciferase transgene (LNN; Figure 1B). The parental PyMG-816 and PyB6-313 cells have different properties and were both established in-house from the transgenic MMTV-PyMT metastatic breast cancer model (24). The CSC-like PyMG-TA cells were kept in basement membrane extract (Cultrex™)-supplemented culture with only 3% oxygen content to maintain their CSC properties, while changing to a normoxic growth medium induced a phenotypic switch (Figure 1B). Application of our degradome-targeted library to these biologically different cell lines allowed us to identify proteases generally important for breast cancer cell growth and proteases that are only important under certain environmental conditions.

2.2 Competitive growth screen performance is cell line-dependent

To investigate the protease dependencies of breast cancer cell proliferation and survival, we further applied our degradome-targeted cell pools to competitive growth screens (Figure 2A). Conceptually, in such screens, a loss of fitness due to impaired target gene expression leads to a dropout of the respective cells from the population, thereby identifying genes essential for cell survival or proliferation. Cells were cultured for 14 days in the absence or presence of Dox to induce protease silencing. At day 0 and day 14, DNA was extracted and used to PCR-amplify the miR-E cassettes followed by next-generation sequencing to compare the number of reads (NOR) for each miR-E insert between experimental conditions. Cells expressing miR-Es that downregulate proteases essential for cell growth become depleted in the Dox-treated cell population, leading to a lower NOR (cell depletion highlighted in red; Figure 2A). In contrast, targeting of proteases that negatively regulate cell growth results in overrepresentation of the respective cells upon protease knockdown (highlighted in blue; Figure 2A). However, targeting of most proteases was expected to have no effect (neutral; highlighted in orange; Figure 2A). Notably, the competitive growth screen in PyMG-TA cells was performed under two culture conditions, either under a nutrient-low 3% O_2 hypoxic condition (hypoxia) or after transfer to a nutrient-rich normoxic culture condition (21% O_2; normoxia). The two culture conditions were used to obtain insight into the role of proteases under different environmental settings and their involvement in the phenotypic plasticity of this cell line.

To assess data quality, the correlation of the normalized, bioinformatically trimmed, and log2-transformed NORs per miR-E was compared within replicates and between replicates (Figure 2B). The correlation of the NOR between day 0 and day 14 within each biological replicate was good (Pearson $R \geq 0.79$), indicating no severe loss of specific miR-E abundance due to

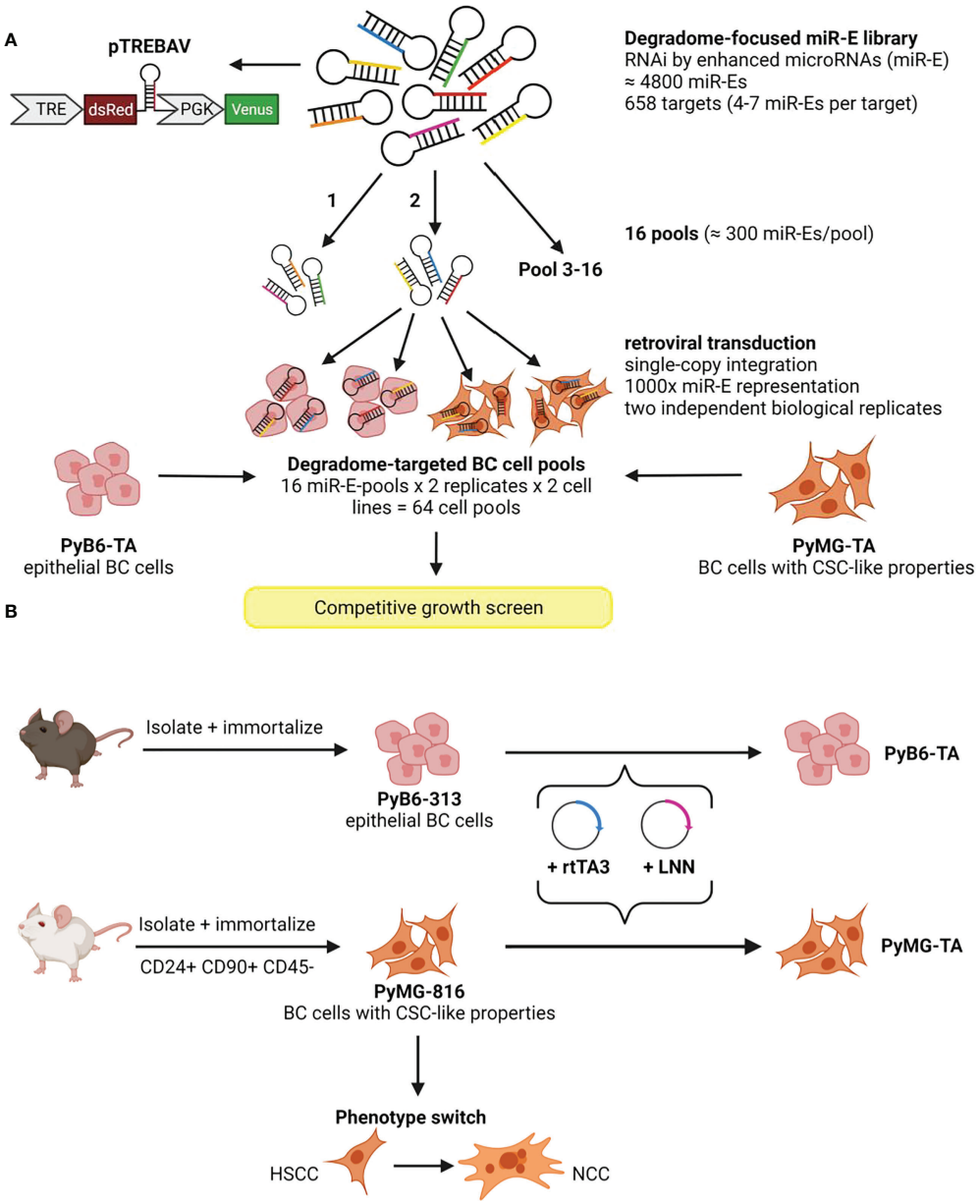

FIGURE 1
Generation of two degradome-targeted breast cancer cell lines. **(A)** Integration of a degradome-focused miR-E library into two MMTV-PyMT mouse model-derived breast cancer cell lines (PyB6-TA/PyMG-TA) leading to 64 cell pools for competitive growth screens. The miR-E library was inserted into the double-fluorescence Dox-inducible TRE-dsRed-miR-E-PGK-BSDr-2A-Venus (pTREBAV) vector; broad scheme; miR-E guide sequence in orange. TRE, tetracycline response element; PGK, phosphoglycerate kinase. **(B)** Establishment of MMTV-PyMT mouse model-derived breast cancer cell lines from different mouse backgrounds. BC, breast cancer; CSC, cancer stem cell-like; HSCC, hypoxic cancer stem cell conditions; LNN, luciferase; NCC, normoxic culture conditions; rtTA3, reverse tetracycline transactivator.

Dox-independent vector activation (leakiness) of the knockdown induction system. Correlation of the day 14 NORs between biological replicates was less (Pearson R = 0.56–0.79). However, because the biological replicates were generated via independent retroviral transductions with independently generated viral particles, this was not surprising.

To analyze the functionality and robustness of the screen, the NOR was further used to assess effect size by calculating the robust strictly standardized median difference [AvSSMD* (28)]. The AvSSMD* represented the difference in miR-E abundance between day 14 protease-targeted (Dox-treated) and day 14 untreated cells compared to the background effect between day

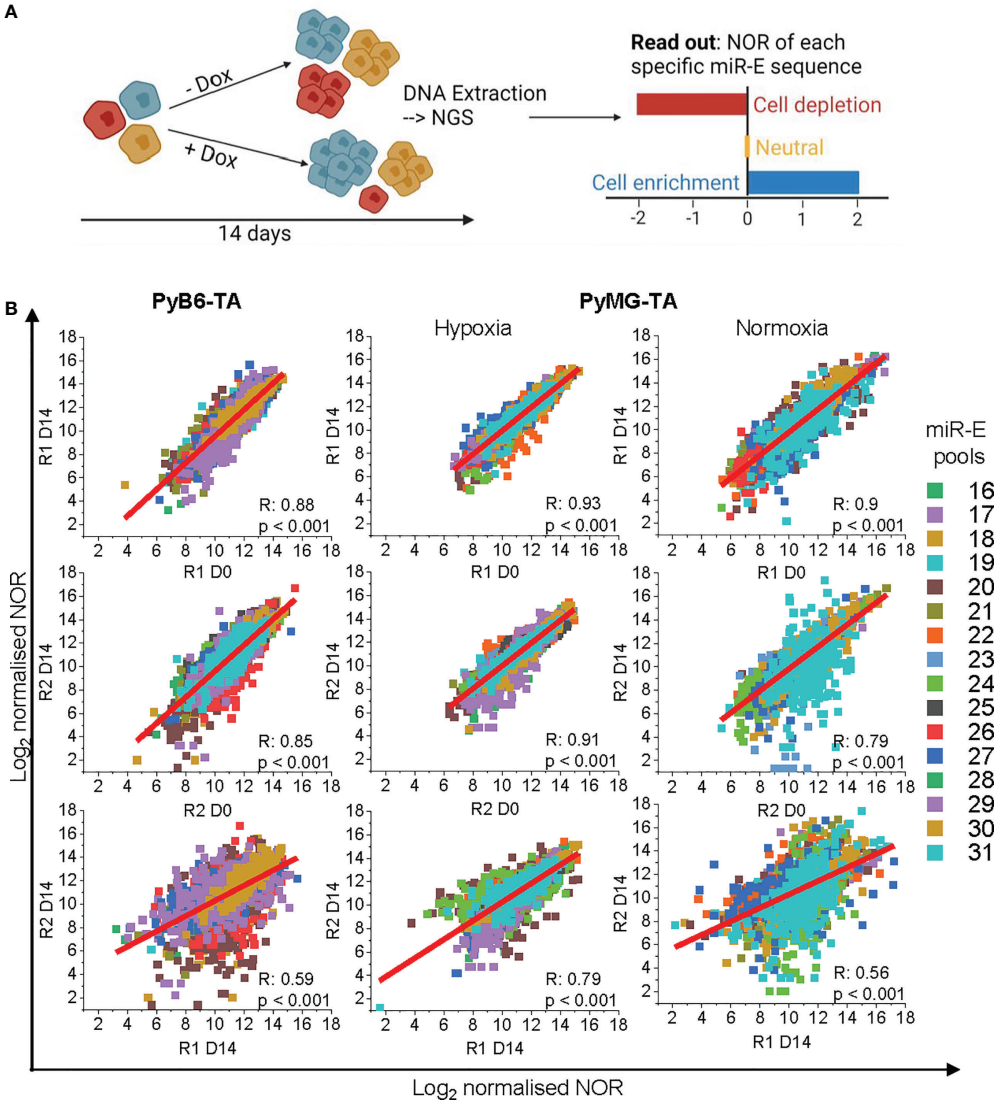

FIGURE 2
Competitive growth screen. **(A)** Schematic representation of the competitive growth screen setup. Cells carrying different miR-E constructs in different colors. NGS, next-generation sequencing; NOR, number of miR-E reads. **(B)** Correlation plots of Log_2-transformed normalized sequencing reads of Replicate 1 (R1) and Replicate 2 (R2) compared between day 14 and day 0 within the replicated and day 14 between the replicates. miR-Es corresponding to specific pools in color code. For technical reasons, the 16 miR-E pools were termed pools 16–31. R, Pearson R correlation coefficient; p, Pearson R corresponding significance. OriginPro function: linear fit.

14 untreated and day 0 samples. The validity of the screen was determined by controlling the distribution of the AvSSMD* scores for all miR-Es in the screen. As expected, the majority of miR-E constructs scored around zero because protease targeting did not significantly affect relative miR-E abundance and hence breast cancer cell growth (Figure 3A). One standard deviation (SD) from the AvSSMD* of all miR-E constructs in the screen (SD_AvSSMD*) was used to define the intrinsic variability of the screen, respectively, the effect region with no significant impact on breast cancer cell growth (SD_AvSSMD*: PyB6-TA ± 3.03 AvSSMD*; PyMG-TA hypoxia ± 4.7 AvSSMD*; PyMG-TA normoxia ± 5.7 AvSSMD*). Accordingly, miR-Es targeting proteases influencing breast cancer cell proliferation or survival would score as outliers outside ±1 SD_AvSSMD*. To assess the functionality of the screen, two shRNAs targeting Renilla luciferase (shRenilla) or firefly luciferase (shLuciferase) transcripts, not present in mammalian cells, were incorporated into the library pools during transduction to serve as internal stability controls in the screens. Furthermore, two shRNAs targeting Rpa3 (shRpa3-457/-Rpa3-218) were incorporated.

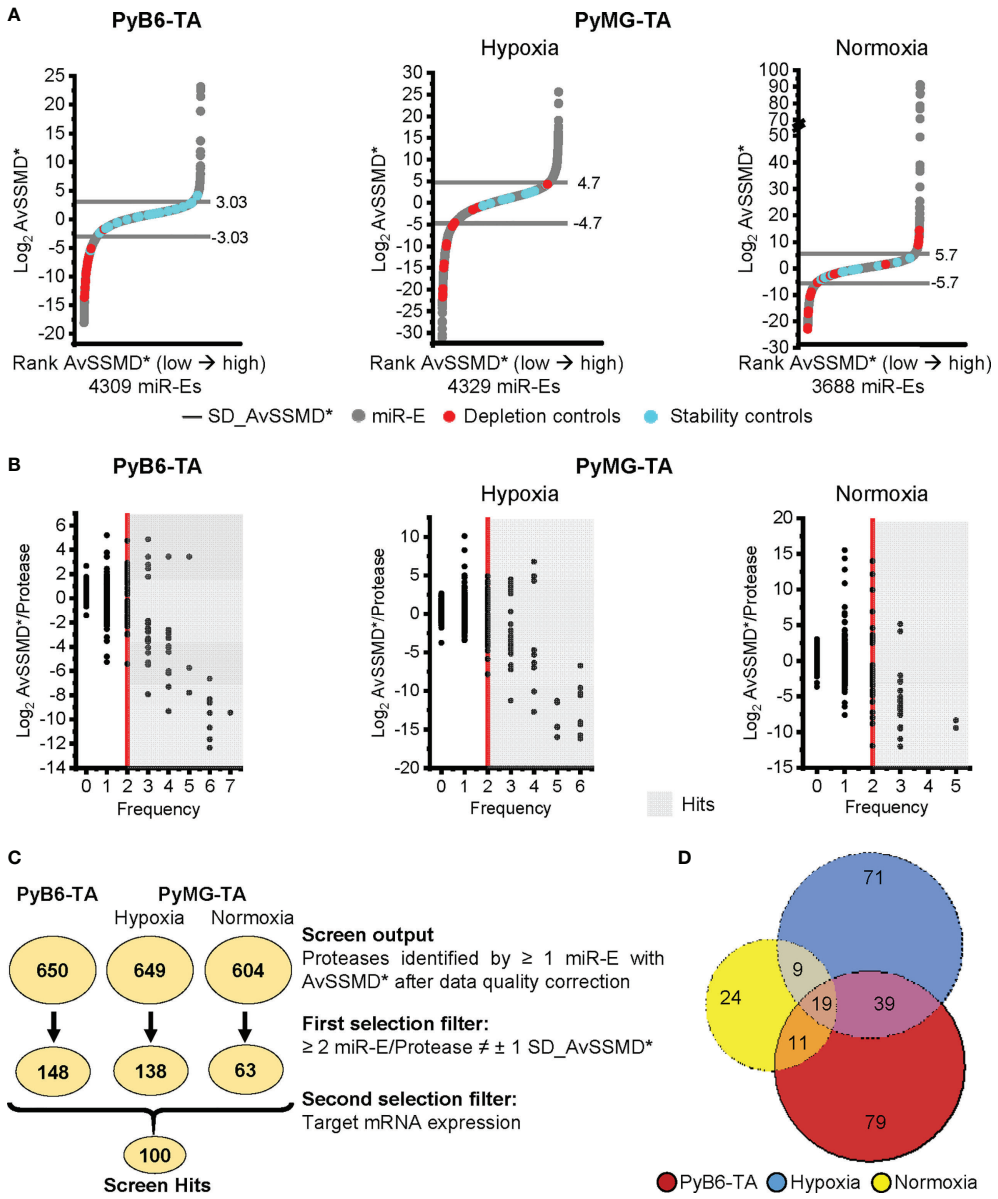

FIGURE 3
Competitive growth screen hit selection. **(A)** Distribution of Log_2 AvSSMD* effect scores for all miR-Es in the competitive growth screens. Cell lines and conditions as indicated. Rank AvSSMD*: values ranked by size. Gray: Log_2 AvSSMD* score of one miR-E. Blue: shRenilla/-Luciferase stability controls. Red: shRpa3-218/-Rpa3-457 depletion controls. Horizontal line: ± 1 SD_AvSSMD* of all miR-Es in the screen. **(B)** Dual flashlight plots. Black dot: Protease identified by minimum 1 corresponding miR-E with successfully calculated AvSSMD* after complete processing of sequencing reads. The term protease referred to all degradome-encoded proteins including proteases, protease-like proteins, and protease subunits. Hits highlighted in gray [≥2 miR-E/Protease outside ±1 SD_AvSSMD* (Frequency)]. **(C)** Summarized hit selection with number of identified proteases in circles according to the indicated criteria. ≠: outside. Searchable Excel file with the screen output and first selection filter hits in Supplementary Tables S1 and S2. **(D)** Venn diagram of the hits from the first selection filter (252 proteases in total). Searchable Excel file with the input of the Venn diagram in Supplementary Table S4.

Because Rpa3 is essential for cell replication and proliferation (29), knockdown diminishes the respective cell clones in the population, making those constructs useful as depletion controls. In a stable system with only moderate intrinsic background variability, the shRenilla/-Luciferase stability controls are expected to score within the ±1 SD_AvSSMD* intrinsic background variability. This expected distribution of the stability controls (blue dots; Figure 3A) was observed in all competitive growth screens in both cell lines. In contrast, the shRpa3-218/-Rpa3-457 depletion controls (red dots; Figure 3A)

should deplete stronger than the intrinsic variance, leading to negative effect scores below -1 SD_AvSSMD*. Indeed, strong depletion of Rpa3 cell clones was observed for 28 of 29 depletion controls in PyB6-TA cells. Screen performance in PyMG-TA cells was less strong, especially under normoxic culture conditions, as 12 of 28 depletion controls scored below -1 AvSSMD* and some Rpa3 knockdown cell clones were even enriched in the Dox-treated population leading to positive AvSSMD* effect scores. This observation was most likely due to some leakiness of the pTREBAV vector in combination with a higher sensitivity of the CSC-like PyMG-TA cells toward Rpa3 knockdown. This resulted in a loss of shRpa3 cell clones in the reference sample, i.e., day 14 without Dox treatment. Nevertheless, the distribution of the internal controls demonstrated sufficient quality of the data and overall functionality of the screens for both cell lines, with better screen performed in PyB6-TA cells.

2.3 Competitive growth screens reveal the importance of many proteases in breast cancer cells

For hit selection, the Log_2 AvSSMD* per protease was plotted against the number of miR-Es that scored outside ±1 SD_AvSSMD* (Frequency; Figure 3B). Subsequently, we employed a preselection procedure that was previously applied by others (4, 30, 31). We only considered proteases for which at least two of the corresponding 4–7 miR-Es targeting this protease scored outside our ±1 SD_AvSSMD* cutoff (Frequency ≥2; gray background; Figure 3B). In all three screens, most protease hits showed negative AvSSMD*/protease scores, indicating the importance of the particular protease for breast cancer cell growth. Notably, the competitive growth screen in PyMG-TA cells under normoxic conditions provided fewer hits with lower frequencies compared to the other screens.

For the 658 protease genes initially targeted by the degradome-wide library, miR-Es corresponding to 650 proteases were identified in the competitive growth screen sequencing output in PyB6-TA cells (Figure 3C). In PyMG-TA cells, 649 proteases were identified upon cultivation under hypoxic conditions and 604 under normoxic conditions. Notably, the term protease referred to all degradome-encoded proteins including proteases but also catalytically inactive protease subunits and protease-like proteins (pseudoproteases). Applying the ±1 SD_AvSSMD* cutoff that had to be reached by a minimum of two miR-Es targeting this protease as first selection filter, 148 hits were found in the PyB6-TA screen and 138 hits in the PyMG-TA screen in the hypoxic condition and 63 hits in the normoxic condition. In total, the hits from this first selection (Figure 3C) add up to 252 different proteases found in the three competitive growth screens (Figure 3D; Supplementary Table S4). Interestingly, 79 protease hits were only found in the screen in PyB6-TA cells and 71 in PyMG-TA cells cultivated under hypoxic conditions and 24 under normoxic conditions. Only 19 proteases were hits in all three cell lines. Search Tool for the Retrieval of Interacting Genes/Proteins (STRING)-based protein association network analysis of all 252 hits revealed a strong proteasome cluster in all screens composed of many proteasomal subunits (Figure 4). The proteasome cluster was accompanied by a cluster of deubiquitinases (DUBs). The importance of the ubiquitin-proteasome system (UPS) is well established in breast cancer cells (32–35). In PyB6-TA and PyMG-TA cells cultured under hypoxic conditions, an "a disintegrin and metalloproteinase with thrombospondin motifs" (Adamts) cluster was discovered that could not be found under normoxic conditions (Figures 4A–C). Furthermore, in PyMG-TA cells, an MMP cluster was found under hypoxic conditions and a cluster composed of different mitochondrial proteases was found under normoxic conditions (Figures 4B, C). These differences in overall protease clusters highlight the complex functions of proteases in different cell lines and culture conditions.

Because low target mRNA expression levels could increase the chance for false-positive findings, hits were further filtered for sufficient miR-E-target mRNA expression (Figure 3C, second selection filter). Specifically, we excluded all proteases with mRNA expression below certain threshold levels, i.e., threshold PyB6-TA: FPKM 0.5 [data previously published (25); Gene Expression Omnibus (GEO) accession code GSE133328] and threshold PyMG-TA: arbitrary log2 expression level <6.2 [data previously published (26); GEO accession code GSE113826]. The remaining 100 screen hits were further depicted in a heat map to compare their effect strength (AvSSMD*/protease) and number of miR-Es targeting this protease outside the ±1 SD_AvSSMD* (Figure 5). Notably, we excluded miR-Es showing positive AvSSMD*/protease scores (enrichment hits). Interestingly, 90 depleted protease hits (Figure 5; protease name indicated in red) were discovered with negative AvSSMD* scores per protease. Depletion hits represented proteases important for breast cancer cell proliferation or survival. As expected, many proteasomal α (Psma), β (Psmb), and γ (Psmc) subunits were among the top depletion hits. To address differences in protease dependencies between culture conditions or cell lines, we further searched for cell clones depleted in one cell line or environmental condition and enriched in the other. Those proteases, such as Usp46 and Usp50, were termed mixed hits (Figure 5; protease name indicated in blue).

In summary, the competitive growth screens performed in different cell lines and culture conditions yielded in a big data set of proteases involved in breast cancer cell growth. One hundred screen hits were identified by applying our strict selection criteria, thereby yielding the candidates for further analysis.

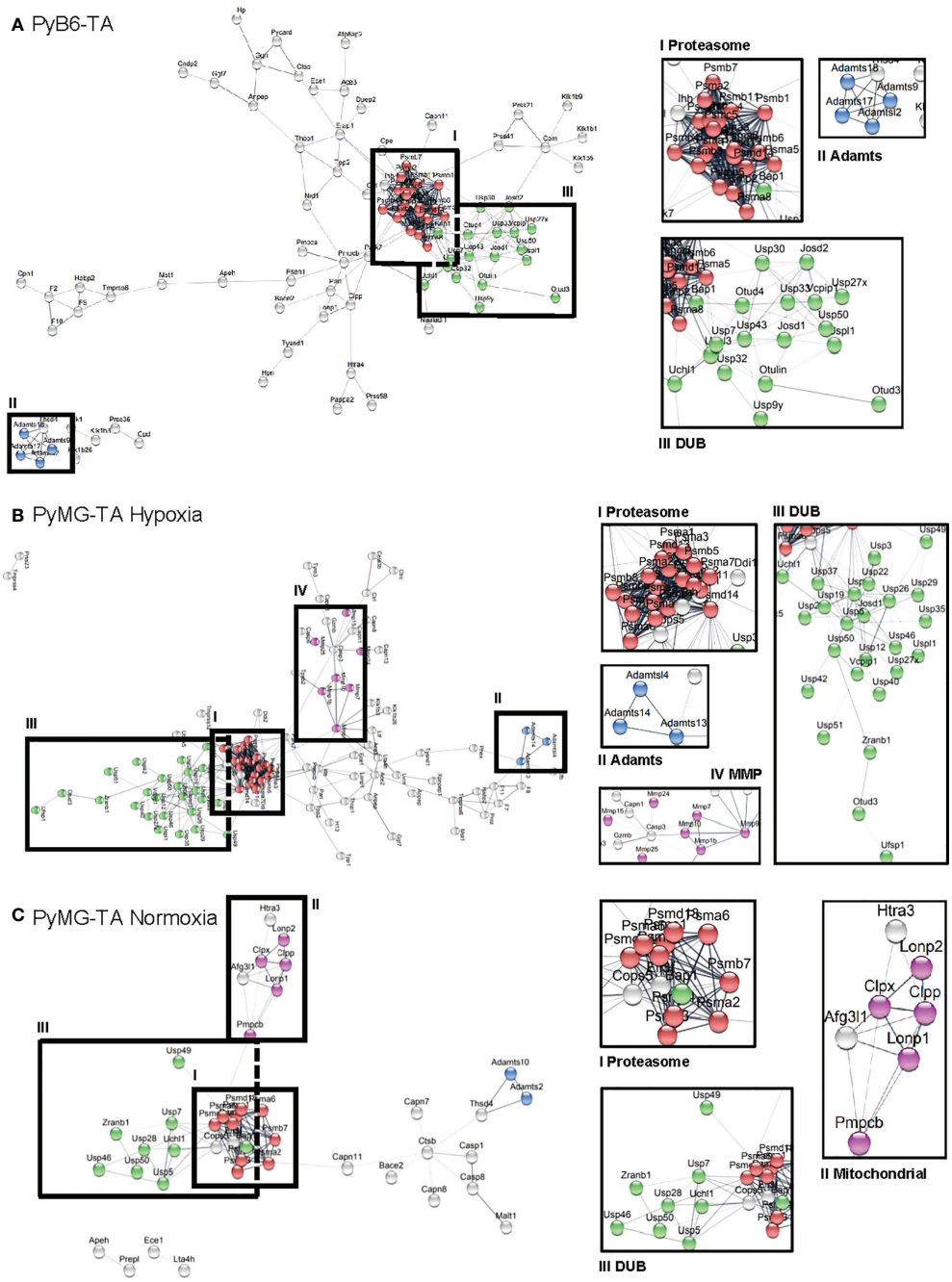

FIGURE 4
STRING-based cluster analysis. Analysis of hits from the competitive growth screens in PyB6-TA cells (**A**; 148 hits) and PyMG-TA cells cultured under hypoxic conditions (**B**; 138 hits) or normoxic conditions (**C**; 63 hits). Hits selected based on first selection criteria (≥2 miR-Es outside ±1 SD_AvSSMD*). Interesting clusters magnified on the right; associated proteins in color. Red: proteasomal subunits; Green: DUBs; Blue: Adamts; Pink: MMPs **(B)** or mitochondrial proteases **(C)**.

2.4 Functional validation of screen hits in breast cancer cells

To evaluate the hits from our competitive growth screens, we compared the 100 screen hits regarding their effect strength and robustness (number of miR-Es that showed the same effect) and subjected them to literature research. Nine hits were chosen as candidates, namely, cathepsin F (Ctsf), methionine aminopeptidases 1 and 2 (Metap1 and Metap2), matrix metalloprotease 17 (MMP17), MPP subunits alpha and beta (Pmpca/Pmpcb), 26S proteasome

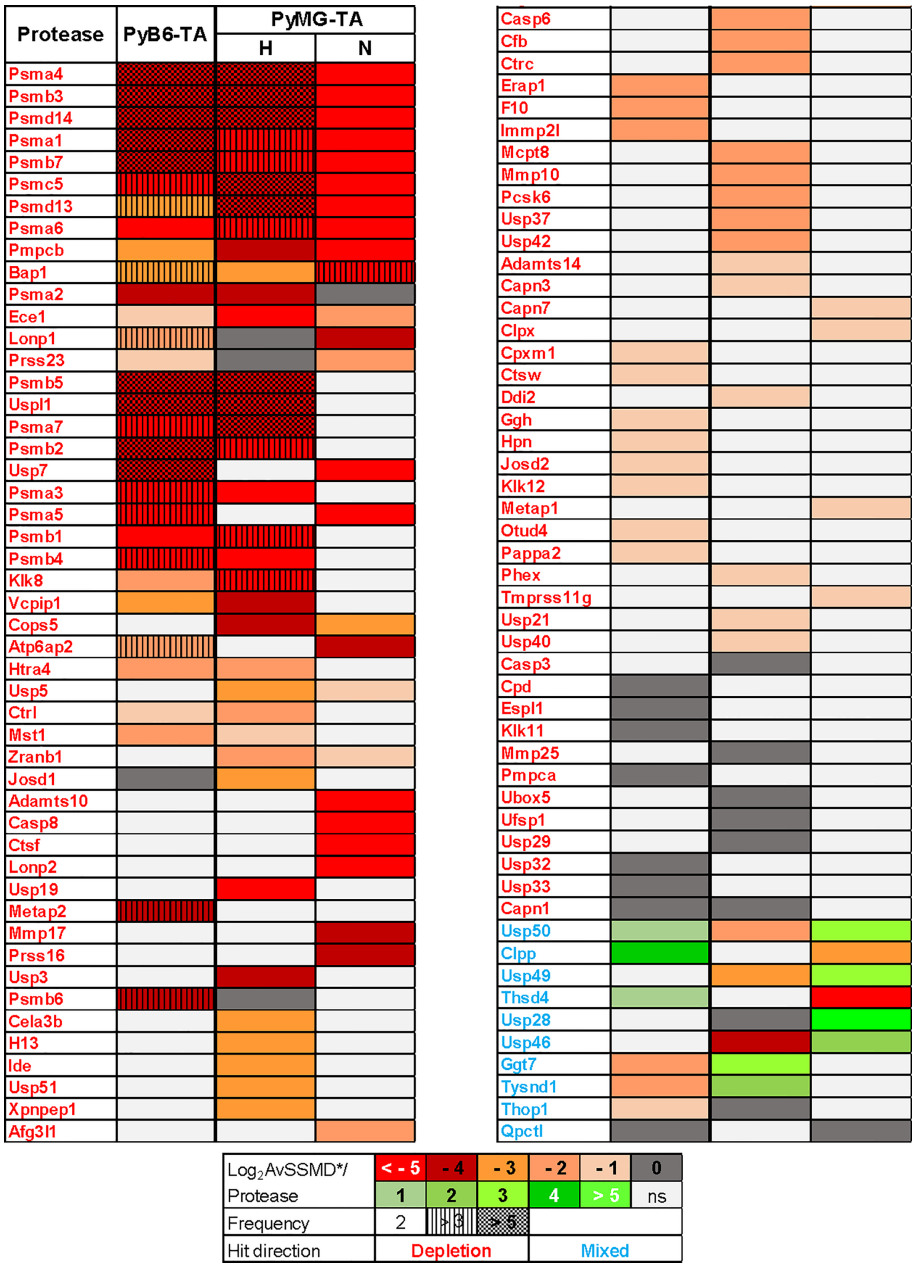

FIGURE 5
Competitive growth screen hits. Heat map of the competitive growth screen hits performed in miR-E library-transduced PyB6-TA or PyMG-TA cells cultured under 3% O_2 hypoxic (H) or 21% O_2 normoxic (N) culture conditions. Log_2 AvSSMD*/protease as color code. Light gray (ns): not significant due to preselection criteria 1 (≥2 miR-Es/protease outside ±1 SD_AvSSMD*, filtered for sufficient target mRNA expression in both cell lines). Hit direction: red names (depletion); blue names (mixed). Frequency: number of miR-Es/protease outside ±1 SD_AvSSMD*. The term protease referred to all degradome-encoded proteins including proteases, protease-like proteins, and protease subunits.

non-ATPase subunit 13 (Psmd13), and the ubiquitin-carboxyl terminal hydrolases 46 and 7 (Usp46 and Usp7). For those nine candidates, inducible single miR-E knockdown constructs were introduced into PyB6-TA and PyMG-TA breast cancer cells, each with two different miR-Es per protease. Those cells were then subjected to ***in vitro*** validation assays.

First, 3-(4,5-dimethylthiazol-2-yl)-2,5-diphenyltetrazolium bromide (MTT) assays were used to analyze the effect of short-term (5 days) protease targeting on cell viability. Targeting of all proteases impaired MTT viability to different extents, except for induction of shUsp46-1 in PyMG-TA cells (Figure 6A). Considering the two independent miR-Es for each target, the

strongest effects with more than 45% MTT reduction were measured upon targeting of Metap2 in PyMG-TA and Pmpcb in PyB6-TA (≥50% MTT reduction) and PyMG-TA (≥40% MTT reduction) cells. To validate the difference in enrichment or depletion of Usp46-targeted PyMG-TA cells upon changed culture conditions in the competitive growth assay, the MTT assay was repeated for miR-E-Usp46-transduced PyMG-TA cells under normoxic conditions (Figure 6B). In contrast to hypoxic conditions, targeting of Usp46 increased MTT viability under normoxic conditions. This effect was most prominent upon induction of miR-E-Usp46-2, leading to 58% increase of cell viability compared to uninduced cells.

As MTT assays are rather short-term experiments, a competitive growth assay was performed to address the long-term effects of protease knockdown. For this, we utilized the double-fluorescence miR-E vector constructs incorporated into the cells. miR-E-transduced cells were cultured together with pTCEBAC-shRenilla-transduced control cells for 14 days in the presence or absence of Dox (Figure 6C). Because both vectors express different constitutive (pTREBAV: Venus; pTCEBAC: Cherry) and inducible fluorescences (pTREBAV: dsRed; pTCEBAC: Cyan), changes in relative abundance of the miR-E-transduced cells could be analyzed by flow cytometry. Relative to day 14, protease knockdown induction of any candidate, with the exception of Psmd13 by shPsmd13-1 in PyMG-TA cells, reduced the percentage of $Venus^{+}dsRed^{+}$ double-positive cells in the cell population (Figure 6D). Targeting Pmpcb (shPmpcb-2) or Usp7 nearly completely depleted the cells from the population. To validate Usp46 as a mixed hit from the screens, the competitive growth assay was repeated for miR-E-Usp46-transduced PyMG-TA cells under normoxic conditions (Figure 6E). Indeed, under normoxic conditions, Usp46-targeted cells were enriched in the cell population, most drastically upon usage of the second miR-E construct.

In summary, targeting of all nine protease candidates showed impairments in MTT viability and in competitive cell growth, therefore validating the overall quality of our initial competitive growth screens. In addition, Usp46 could be confirmed as a mixed hit with differential responses to its targeting in hypoxic and normoxic growth conditions. Because knockdown of Pmpcb showed the strongest growth-impairing effects in our murine breast cancer cells and as mitochondria are core organelles for cellular oxygen metabolism (36–38), we decided to further investigate the MPP.

2.5 The mitochondrial processing peptidase is essential for murine breast cancer cells

Pmpca and Pmpcb are the two subunits of MPP, a protease complex essential for proteolytic removal of the mitochondrial import signal from the majority of mitochondrial proteins after their import into the mitochondrial matrix (36–38). First, the knockdown of Pmpca and Pmpcb in PyB6-TA cells was validated by Western blot (Figures 7A, B). A reduction of the Pmpca protein level by more than 50% was achieved by induction of the more potent miR-E-1 for 4 and 8 days. In the case of Pmpcb, between 20% and 40% reduction of protein levels was found after miR-E induction for 4 or 8 days. Although the protease knockdown efficiency was only moderate for both MPP subunits, cell growth was significantly impaired (Figures 7C, D). Pmpca knockdown in normoxic culture conditions significantly reduced colony growth by 47% and 75% for the two miR-E constructs, respectively. Targeting Pmpcb reduced colony growth even stronger, with 69% reduction upon induction of miR-E-Pmpcb-1 and 87% using miR-E-Pmpcb-2. In contrast, addition of Dox to shRenilla control cells did not significantly affect colony formation. Because MPP is known to be important for mitochondrial function (36–38), the colony formation assay was repeated under hypoxic conditions (3% O_2) in which oxidative phosphorylation is limited. Cultivation under hypoxic conditions impaired general cell growth as visible from the weaker crystal violet staining independent of cell line and Dox addition (Figure 7C). Compared to hypoxia, the knockdown of Pmpca and Pmpcb impaired colony growth more prominently under normoxic conditions (Figure 7D). Due to the importance of MPP in mitochondrial function, we next validated if Pmpca or Pmpcb knockdown would compromise mitochondrial activity utilizing the MitoTracker™ probe. This probe accumulates within active mitochondria and hence can be used to measure mitochondrial activity, in our case reflected by the median allophycocyanin (APC) fluorescence intensity (Figures 7E, F). As exemplary shown in Figure 7E, a left shift in APC intensity of the Dox-treated (blue peak) miR-E-Pmpca-1-transduced PyB6-TA cells compared to the untreated cells (red peak) indicated reduced mitochondrial activity upon Pmpca knockdown. Quantification of the MitoTracker™ assays showed slightly reduced (≥17%) mitochondrial activity (fluorescence intensity) relative to uninduced cells upon targeting of Pmpca by miR-E-1 (Figure 7F). In contrast, induction of miR-E-Pmpca-2 significantly increased mitochondrial activity by 56% after 4 days, which was reduced to 22% after 8 days. Knockdown of Pmpcb significantly decreased mitochondrial activity upon usage of miR-E-Pmpcb-2 after 4 days (-34%) and both miR-E constructs after 8 days (-24%/-57%).

Taken together, knockdown of either MPP subunit led to impaired cell viability, colony growth, and mitochondrial activity. Thereby, effects were more prominent upon knockdown of Pmpcb.

10.3389/fonc.2022.960109

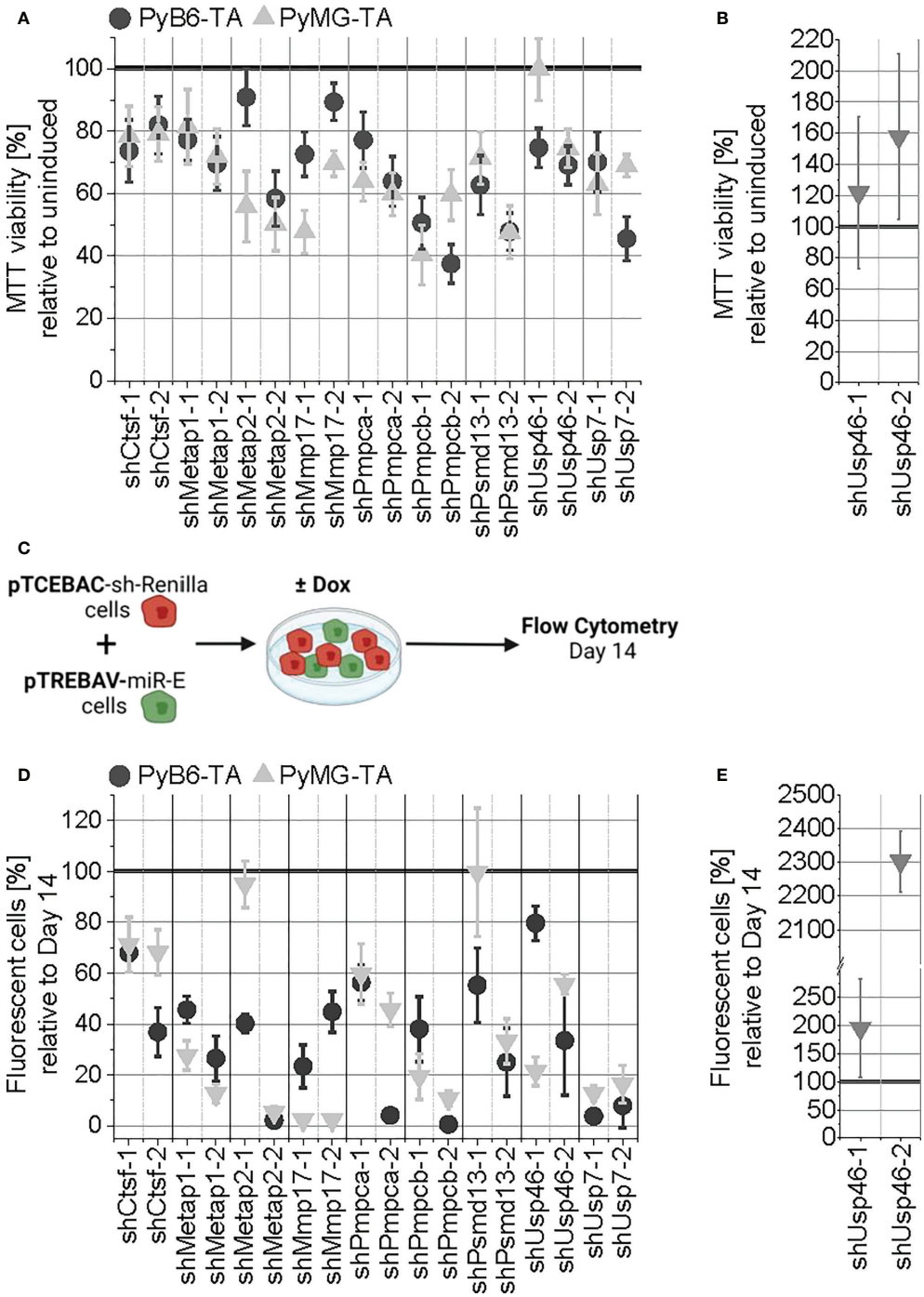

FIGURE 6
General validation of the competitive growth screen hits. **(A)** Short-term protease targeting in miR-E-transduced PyB6-TA and PyMG-TA cells. miR-E expression was induced for 5 days in total. Cell viability as mean ± SD ($n \geq 4$) relative to untreated, uninduced cells. **(B)** Repetition of A performed under normoxic conditions for the mixed hit Usp46 in PyMG-TA cells (n = 5). **(C–E)** Long-term protease targeting in PyB6-TA and PyMG-TA cells. **(C)** Schematic experimental setup. **(D)** Flow cytometry-based percentage of $Venus^{+}dsRed^{+}$ fluorescent pTREBAV protease knockdown cells from living single cells at day 14 relative to unindicted $Venus^{+}$ cells as average ± SD ($n \geq 3$). **(E)** Long-term protease targeting assay performed under normoxic conditions for the mixed hit Usp46 in PyMG-TA cells (n = 5). For simplification, miR-Es are indicated by sh.

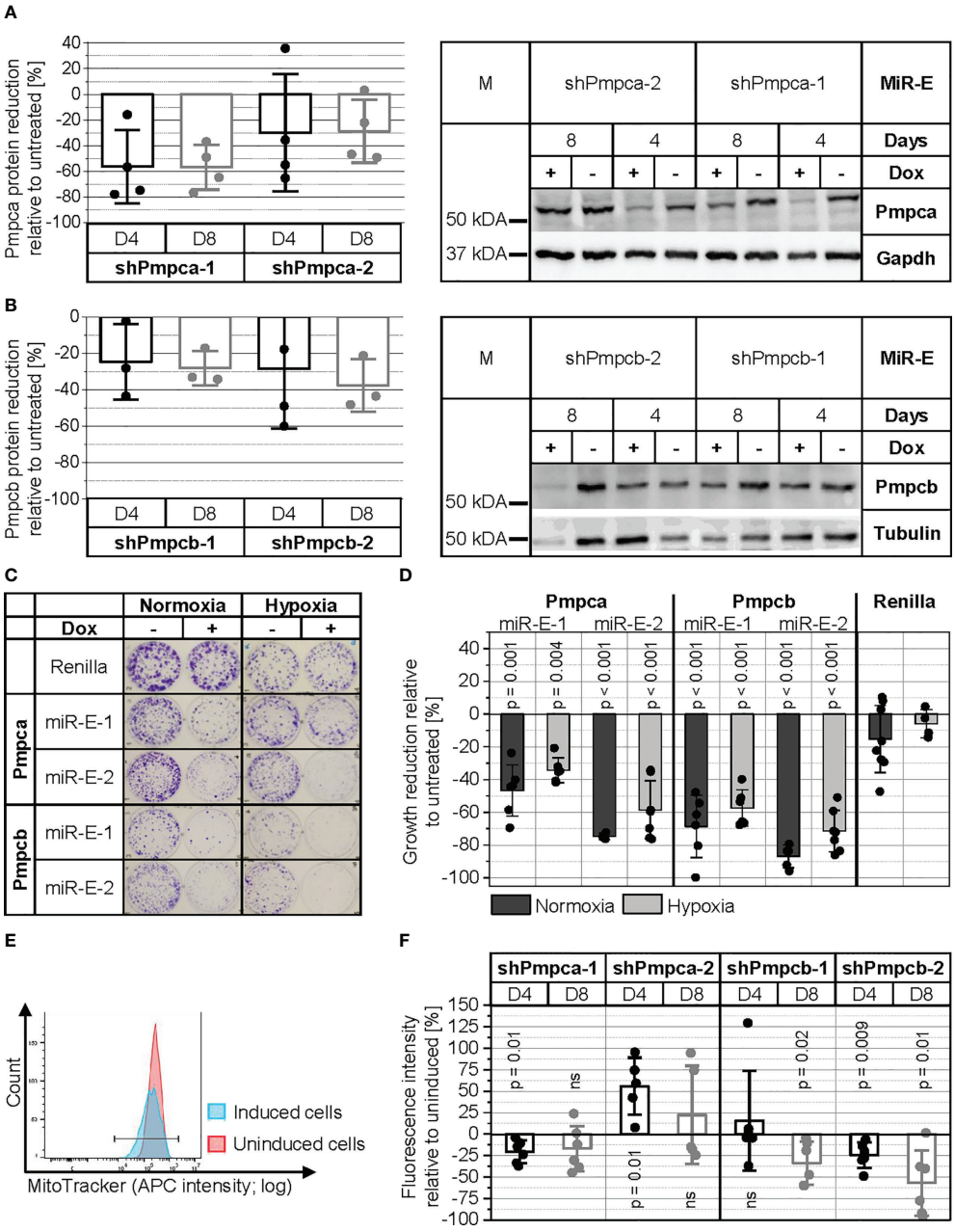

FIGURE 7
MPP is important for PyB6-TA cells. For simplification, miR-Es are indicated by sh. **(A, B)** Analysis of Pmpca **(A)** and Pmpcb **(B)** protein expression by Western blot in miR-E-transduced PyB6-TA cells cultured for 4 (D4) or 8 days (D8) ± Dox. Left: Quantification of Western blot data; mean reduction of protein level ± SD relative to uninduced cells normalized to tubulin or GAPDH. Right: Representative Western blots; tubulin or GAPDH as loading control; 25 µg protein loaded. M: marker. **(C, D)** Plate colony formation assay of miR-E-transduced PyB6-TA cells cultured ± Dox under normoxic conditions (21% O_2, 8–9 days) or hypoxic conditions (3% O_2, 12–14 days). ShRenilla-transduced cells as control. **(C)** Exemplary pictures. **(D)** Average cell growth reduction ± SD relative to untreated. Significance (p) one-sample t-test to 0 or two-sample t-test, equal variances assumed (n = 5–9). **(E, F)** Flow cytometry-based analysis of mitochondrial activity in miR-E-transduced PyB6-TA cells cultured for 4 or 8 days ± Dox by deep Red FM MitoTracker staining. **(E)** Exemplary median APC intensity. **(F)** Median APC fluorescence intensity ± SD relative to uninduced. Significance (p): one-sample t-test to 0 (n = 5–6). Ns, not significant.

3 Discussion

3.1 Degradome-focused RNA interference screens as a tool to investigate protease dependency of breast cancer cells

Although many proteases are linked to breast cancer (10–12), protease research has run into a bottleneck by only investigating already highly examined protease classes. Hence, the role of most of the 588 human and 672 murine protease and protease-like genes forming the degradome is still unknown (13, 14). In this work, we performed an RNAi-based genetic screen targeting the entire degradome in two murine breast cancer cell lines for an unbiased identification of proteases important for breast cancer cell proliferation and/or survival. Genetic screens are a widely used tool to efficiently discover cancer drivers, novel cancer-linked genes, and putative therapeutic targets (1, 2, 31), but genome-wide (4–6) or kinase-focused screens (7–9) missed out on proteases so far.

Our unbiased genetic competitive growth screens identified 252 protease genes involved in breast cancer cell survival/proliferation. STRING-based network analysis of first selection hits revealed that under all conditions, the biggest hit clusters comprised proteasomal subunits and DUBs (Figure 4), which are all components of the UPS (33, 34, 39). The UPS is central for protein turnover by proteasomal degradation of ubiquitin-tagged intracellular proteins controlling essential cellular functions such as cell death and proliferation. Because low expression of the miR-E target might increase the chance of off-target effects, we applied a second round of evaluations and filtered the hits obtained by the first selection filter for sufficient expression of the miR-E target mRNA, excluding all hits with low mRNA expression. By applying this multistep selection procedure, we detected 100 proteases important for breast cancer cell growth (Figure 5), of which many were supported by literature. Members of the UPS were among the strongest depletion hits. Indeed, the importance of a functioning UPS for cancer cells is well established (32–34), and proteasome inhibitors, which target the destructive part of the UPS, are useful anticancer drugs (40, 41). In all screens, the seven proteasomal α subunits (Psma) and at least six of the seven β subunits (Psmb) of the catalytic 20S core particle of the proteasome (42) were found as strong depletion hits (Figure 5), together with Psmc5, as well as Psmd13 and Psmd14 located in the 19S regulatory cap (42). In addition, many DUBs, such as Bap1 and Usp7, were found to be strong depletion hits in our screen (Figure 5). DUBs are part of the UPS and modify, trim, or remove ubiquitin chains on target proteins (43, 44). Thereby, DUBs change the "ubiquitin code" (number and position of attached ubiquitin molecules) that decides the fate of the tagged protein (45). Many DUBs are linked to cancer (34, 35, 46). For example, Usp7 is known to act as tumor-promoting in various cancer entities (47–50) including breast cancer (51–53). Together with the known cancer-promoting function of the UPS, the detection of many proteasomal components and DUBs as strong depletion hits proves the validity of our screening approach. In addition, many other depletion hits were supported by literature, e.g., Metap1 and Metap2. Metap2 is known to act as tumor-promoting in different cancers (54, 55) including breast cancer (19, 56). Metap1 is known to act as tumor-promoting in cervical cancer, fibrosarcoma, and lung cancer (57, 58), and we recently discovered a role for Metap1 in promoting the sensitivity of breast cancer cells to phosphoinositide 3-kinase (PI3K) inhibition (19). Also, MMP17 was already likened to breast cancer, promoting tumor growth (59). In line with our screen data, Usp7, Metap1, Metap2, and MMP17 could be validated as depletion hits *in vitro*, whereby targeting reduced MTT viability and competitive breast cancer cell growth (Figure 6).

Interestingly, although many of our depletion hits are known to promote cancer in general, our screen discovered that some of them were functionally connected to breast cancer. Among them was Lon protease 1 (Lonp1), being important in cervical cancer and colon cancer cells (60, 61), as discussed further below. Psmd14, one of our main depletion hits (Figure 5), stabilizes human epidermal growth factor receptor 2 (HER2) (62) and is upregulated in lung carcinoma associated with poor prognosis (63). Another protease was Uspl1 (ubiquitin-specific peptidase-like 1), a strong depletion hit in PyB6-TA cells and PyMG-TA cells cultured under hypoxia (Figure 5). In line with our data, Uspl1 mRNA expression was found to be upregulated in gastric cancer (64) and oral squamous cell carcinoma (65). In addition, genetic Uspl1 variants affecting its expression have been linked to breast cancer risk and cancer grade, indicating its importance in breast cancer (66). However, a functional link of those proteases to breast cancer biology has, until now, never been made. Other depletion hits, such as Psmd13 and the "peroxisomal matrix protein trypsin domain-containing 1" (Tysnd1), have to our knowledge not been postulated to be important for cancer growth. These proteases would be interesting to further investigate in the context of breast cancer. Here, we validated the role of Psmd13 for breast cancer cell growth *in vitro* by showing reduced MTT viability and colony growth upon targeting (Figure 6).

Because so many of our screen hits were supported by literature and all nine hits (Ctsf, Metap1, Metap2, MMP17, Pmpca, Pmpcb, Psmd13, Usp46, and Usp7) that we chose to validate individually showed impaired MTT viability and competitive growth in PyB6-TA and PyMG-TA breast cancer cells (Figure 6), we are confident that we established a robust and successful screen. More importantly, we were also able to detect proteases not linked to breast cancer before. Those could be interesting starting points for further investigation.

3.2 Breast cancer cells rely on mitocondrial processing peptidase for cell growth

Besides proteases corresponding to the UPS, the MPP subunit beta (Pmpcb) was one of the strongest depletion hits in both breast cancer cell lines (Figure 5). MPP consists of two subunits (α-MPP/Pmpca and β-MPP/Pmpcb), whereby Pmpcb has a catalytic function and Pmpca is involved in substrate binding and presenting and/or release of the cleaved peptide (36, 38, 67, 68). MPP is essential for the maturation of the majority of imported mitochondrial precursor proteins by proteolytic removal of their mitochondrial targeting sequence. Because mitochondrial activity is especially important in the energy-demanding brain, MPP dysfunction is associated with neurodegenerative diseases such as Friedreich ataxia (69), autosomal recessive cerebellar ataxia syndrome (70), neurodegeneration in early childhood, and cerebellar atrophy (71). The role of MPP in cancer, however, is rarely studied. In hepatocellular carcinoma (HCC) cells, Pmpcb knockdown led to apoptosis and tumor growth suppression by reactive oxygen species (ROS) formation and in turn suppressed Wnt/b-catenin signaling (4). Furthermore, Pmpcb silencing was shown to increase the susceptibility of murine and human HCC cell lines and HCC tumors to the multikinase inhibitor sorafenib (72). This combination decreased liver tumor burden and improved survival of the mice. In line with these HCC data, knockdown of Pmpca and especially Pmpcb in our PyB6-TA breast cancer cell line caused remarkable cell growth disadvantages (Figures 7C, D). Furthermore, knockdown of both protease subunits impaired MTT viability and competitive growth in PyB6-TA and PyMG-TA breast cancer cells (Figure 6). The antigrowth effect upon interference with MPP might be due to general impairment of mitochondrial function, as reduced mitochondrial activity was observed in PyB6-TA breast cancer cells upon knockdown of Pmpcb (Figure 7F). In general, mitochondrial function is known to support carcinogenesis *via* manifold processes, including oxidative phosphorylation to generate ATP, generation of ROS, and synthesis of precursors for biomass accumulation (38, 73). Furthermore, the association of MPP to mitophagy/apoptosis *via* the phosphatase and tensin homolog induced kinase (PINK)1-Parkin signaling pathway might contribute to the importance of Pmpca and Pmpcb for breast cancer growth, as already shown in human breast cancer MDA-MB-231 and MCF7 cells (74, 75). In those cells, inhibition of human Pmpcb led to accumulation of full-length PINK [in healthy mitochondria cleaved by MPP (76)] leading to PINK1-Parkin interaction-induced mitophagy (74) and apoptosis (75).

Interestingly, we observed that Pmpcb or Pmpca knockdown-dependent growth reduction was approximately 20% stronger under normoxic conditions as compared to that under hypoxia (Figures 7C, D). We hypothesize that cells under hypoxic conditions are less dependent on mitochondrial metabolism. Indeed, cancer cells have been shown to adapt their energy production to environmental changes by switching between glycolysis and oxidative phosphorylation as main energy source (77). Actually, most cancer cells prefer aerobic glycolysis over oxidative phosphorylation to produce ATP, a phenomenon termed "Warburg effect" (78). In line with the observed stronger growth reduction upon interference with MPP in normoxic conditions (Figures 7C, D), it was shown in yeast that growth arrest induced by MPP deficiency was attenuated in respiration-deficient mutants that do not rely on mitochondrial metabolism (79).

3.3 Environmental conditions influence breast cancer cell dependencies for specific mitochondrial proteases

Our STRING-based network analyses of all hits from the competitive growth screens also showed differences in protease dependencies upon changed environmental conditions (Figure 4). In PyMG-TA cells cultured under normoxic nutrient-rich conditions, a cluster composed of different mitochondrial proteases was discovered. This cluster was absent under nutrient-low hypoxic culture conditions. Although some of the cluster proteases, such as Pmpcb and Lonp1, were depletion hits in all conditions, only PyMG-TA cells in normoxic culture conditions were dependent on Lonp2, Clpp, and Clpx for proper survival and cell proliferation. As explained for Pmpcb and Pmpca above, we first hypothesized that cancer cells are less dependent on mitochondrial energy production under hypoxic conditions due to their preference for glycolysis (77). This could explain why the knockdown of certain proteases, such as Lonp2, Clpx and Clpp, only affects breast cancer growth under normoxic culture conditions strong enough to be detected as a screen deletion hit. In addition, we hypothesize that the condition-specific appearance of a protease as a depletion hit is based on its function. As already pointed out above, MPP has general relevance for mitochondrial function (36, 38, 67, 68), which explains why its catalytic subunit Pmpcb scored as a depletion hit in all screens (Figure 5). Another mitochondrial protease found to be important for cell growth under all tested conditions was Lonp1. Lonp1 is an ATP-dependent mitochondrial protease that degrades imported mitochondrial matrix proteins to maintain cellular homeostasis (80). Indeed, Lonp1 upregulation was found in several tumors, including lung, cervical, and oral cancer, associated with a worsened prognosis (38, 60, 81). In line with our data on breast cancer cells, Lonp1 downregulation suppressed cervical cancer cell proliferation and induced cell death in colon cancer cells (60, 61). In contrast to Pmpcb and

Lonp1, the "caseinolytic mitochondrial matrix peptidase proteolytic subunit" (Clpp) and the "ATP-dependent Clp protease ATP-binding subunit clpX-like" (Clpx) were only found to be depletion hits under normoxic conditions. Clpp and Clpx are both components of ClpXP, a protease that catalyzes degradation of misfolded and specifically tagged proteins in mitochondria, which is important to maintain oxidative phosphorylation (82, 83). The restricted function of ClpXP for oxidative phosphorylation might explain why its two components (Clpp and Clpx) were more important under oxygen-rich (normoxic) conditions. Clpp inhibition is known to result in respiratory chain dysfunction in acute myeloid leukemia (AML) cells (84). However, the impact of Clpp in cancer is complex. Clpp is overexpressed in AML, and Clpp inhibition decreases cell viability (84). Surprisingly, Clpp hyperactivation also induces cell death in leukemia and lymphoma cells (85). It appears that a well-balanced selective proteolysis of mitochondrial protein subsets is important for proper organelle function. Our data now propose a dependency of some breast cancer cell lines on Clpp and Clpx under certain environmental conditions (Figures 4, 5).

To sum up, our data reveal that breast cancer cells are dependent on MPP, and knockdown of its subunits, Pmpca or Pmpcb, led to reduced cell growth likely caused by mitochondrial dysfunction. Interestingly, we found that environmental conditions influence the degree of dependency on protease function, making breast cancer cells less susceptible to depletion of mitochondrial proteases under hypoxic conditions.

4 Conclusions

Based on internal controls and validation of many screen hits by experiment and literature, we prove degradome-focused RNAi-based pooled competitive growth screens as a suitable discovery pipeline to analyze the role of proteases in breast cancer cell proliferation/survival. The usability of our screening approach has previously been validated in context of synthetic lethality screens (19). Applying multistep selection criteria, our screens yielded 100 proteases that were identified to be important for breast cancer growth. Many of those hits were supported by literature, whereby some hits were so far overlooked in the context of breast cancer (e.g., Lonp1, Uspl1) or cancer in general (e.g., Psmd13, Tysnd1). Furthermore, our screen revealed cell line-specific and environmental condition-based dependencies of breast cancer cells to proteases, especially for mitochondrial proteases.

In conclusion, our data provide novel insights into the dependencies of different breast cancer cells onto protease function and discovered environmental condition-dependent protease importance.

5 Methods

5.1 Plasmids

Dox-inducible double-fluorescence retroviral pTREBAV (TRE-dsRed-miR-E-PGK-BSDr-2A-Venus) and pTCEBAC (TRE-Cyan-miR-E-PGK-BSDr-2A-Cherry) vectors, previously described (19), were designed based on the pTRMPV vector (86), which was kindly provided by Dr. Scott W. Lowe (Sloan Kettering Institute, Memorial Sloan Kettering Cancer Center, New York, USA). They allow for Dox-inducible TRE-driven dsRed (pTREBAV) or Cyan (pTCEBAC) fluorescent protein expression coupled to the miR-E expression. A constitutive PGK promoter drives Blasticidin resistance and Venus (pTREBAV) or Cherry (pTCEBAC) fluorescent reporter protein expression. The retroviral pMSCV-rtTA3-PGK-Puro and lentiviral pLNN plasmids [previously described (19)] were used to integrate the rtTA3 and LNN transgenes, respectively. Those vectors were kindly provided by Dr. Scott W. Lowe (Sloan Kettering Institute, Memorial Sloan Kettering Cancer Center, New York, USA) and Prof. Dr. Robert Zeiser (Department of Internal Medicine I, University Clinic, Freiburg, Germany), respectively. Single-target knockdown pTREBAV plasmids were generated as previously described (19) based on 97 nt oligonucleotides (97-mers) ordered from Sigma-Aldrich or Thermo (list in Supplementary Table S3) that encoded the specific shRNAs in a miR-E backbone.

5.2 Cell lines and cell culture

PyB6-TA and PyMG-TA cells (carrying the rtTA3 and LNN transgenes) were generated as previously described (19) *via* integration of the pMSCV-rtTA3-PGK-Puro and p-LNN vectors. PyB6-TA cells were cultured in Dulbecco's modified Eagle's medium (DMEM) high glucose, pyruvate supplemented with 10% fetal bovine serum, 1% penicillin/streptomycin, and 1% L-glutamine at 37°C with 5% CO_2 and 21% O_2. PyMG-TA stem cell-like murine breast cancer cells were cultivated in specific mammary stem cell medium under low-oxygen atmosphere [hypoxia (3% O_2, 5% CO_2, 92% N_2)] at 37°C, as previously described (26).

miR-E-transduced PyB6-TA or PyMG-TA single-knockdown cell lines were generated as previously described (19) by retroviral integration of single-knockdown pTREBAV plasmids. Cell lines were tested for *Mycoplasma* contaminations prior to transduction and freezing in-house.

5.3 Degradome-targeted cells

For the degradome-wide knockdown, a customized degradome-focused miR-E library was used that was

previously described (19). The miR-E library targeted 658 murine protease and protease-like transcripts with ≈4,800 miR-Es (4–7 miR-Es/target) incorporated into pTREBAV plasmids. The library was subdivided into 16 miR-E pools (≈300 miR-Es/pool).

Degradome-targeted PyB6-TA and PyMG-TA cells were generated as previously described (19) using specific protocols to ensure 1,000-fold miR-E representation and single-miR-E-copy integration. Briefly, PyB6-TA cells were cell cycle-synchronized prior to seeding by cultivation in starvation medium for 24 h [full DMEM 1% fetal calf serum (FCS)]. Infection of 13 plates per miR-E pool (0.75×10^6 cells/10-cm plate) with ectopically packed miR-E library pool plasmid retrovirus (1:6 diluted in medium) supplemented with Polybrene (8 µg/ml) was done 16 h after seeding to infect shortly before the M-phase. Degradome-targeted PyMG-TA cells were generated due to the same protocol, but infection of 10 plates per miRE pool (0.75×10^6 cells/10-cm plate) was done the next morning or 2 h after cell seeding. Blasticidin selection (10 µg/ml) started 48–72 h after infection, and transduction efficiency was controlled by flow cytometry. Blasticidin selection was continued until over 80% of fluorescent cells were obtained, repeating puromycin (4 µg/ml) and neomycin (500 µg/ml) selection to ensure the presence of the rtTA3 and LNN transgenes. Independently generated viral supernatant was used to perform two independent transductions per miR-E pool. Four miR30A backbone-based controls {stability controls: pTCEBAC-shRenilla (87); pTCEBAC-shLuciferase (88); depletion controls: pTREBAV-shRpa3-218 [termed Rpa3.276 in David et al. (87)]; pTREBAV-shRpa3-457 [termed Rpa3.455 in McJunkin et al. (88)]} served as internal quality controls and were incorporated during ecotropic virus production as one construct per miR-E pool (sequence information in Supplementary Table S3).

5.4 Virus production

Ecotropic virus was produced as previously described (19).

5.5 Competitive growth screen

Degradome-targeted PyB6-TA or PyMG-TA cell pools were cultured in their respective medium for 14 days ± Dox treatment (2 µg/ml). One miR-E pool was cultured per 15-cm plate (PyB6-TA) or 10-cm plate (PyMG-TA). Medium and Dox were changed every 2–3 days, cells were passaged regularly keeping 1.1×10^6 cells/plate to maintain miR-E representation. In PyMG-TA cells, the screen under hypoxic conditions was performed as described above. For the normoxia screen, PyMG-TA cells were transferred to normoxic culture conditions 10 days prior to the start of the screen as follows. Cells were detached, centrifuged, resuspended, and seeded in full DMEM. Cells were further cultivated at 37°C with 5% CO_2 and 21% O_2 in full DMEM, maintained throughout the screen.

At day 0 and after 14 days of cultivation, genomic DNA (2×10^6 cells/plate) was isolated using the Gentra Puregene Cell Kit (158767; Qiagen). Deep sequencing template libraries were generated by PCR amplification of the miR-E cassettes as previously described (19) resulting in PCR products (315 nt) that were tagged with standard Illumina P5/P7 adapters and a sample-specific 10-nt barcode sequence. PCR products were pooled to one sample for sequencing (theoretical sequencing depth of 1×10^6 bp per initial sample) according to their relative abundance in gels to archive equal sequencing reads. The sequencing sample was further column-purified [QIAquick PCR purification kit (28104; Qiagen)], and the concentration was adjusted to 0.832 nM for optimal cluster generation. Next-generation sequencing was performed on a HiSeq4000 [German Cancer Research Center (DKFZ)/Genomics & Proteomics Core Facilities/TP3/High-Throughput Sequencing Unit] using 150-bp paired-end sequencing and the Illumina sequencing primer (5′-TAGCCCCTTGAAGTCCGAGGCAGTA GGCA). Alternatively, sequencing was performed on a HiSeq2500 (MPI for Immunology and Epigenetics Freiburg/Deep Sequencing Facility) or Nextseq500 (Faculty of Medicine Freiburg/Department for Pediatrics/Pediatric Genetics) utilizing 75-bp single-end sequencing, the Illumina sequencing primer for miR-E cassette readout, and a custom index primer (5′-CGCTCACTGTCAACAG CAATATAC) for sequencing the 10-bp barcode as index reads.

5.6 Analysis and selection of screen hits

Sequence processing was performed as previously described (19) including cleaning, pool-based normalization, Log_2 transformation, and trimming [removal of extreme values or outliers; criteria see Hölzen et al. (19)] of the raw number of reads for each miR-E in the library per sample. R-scripts can be provided upon reasonable request to the first author. For calculation of effect strength, the robust strictly standardized median difference (AvSSMD*) calculated after a modified version of the method of moment estimate of the paired SSMD* by Zhang (28) was chosen, being suitable for screens with biological duplicates only. The AvSSMD was calculated as follows:

- FGR: NOR_Day14Dox/NOR_Day14
- BGR: NOR_Day0/NOR_Day14

Foreground (FGR): difference of a NOR of a specific miR-E between Dox-treated and untreated samples. Background (BGR): difference in NOR between day 0 and day 14 untreated samples. NOR: Number of reads of a specific miR-E in the respective sample. Day0: DNA isolated at day 0. Day14: DNA isolated at day 14 from untreated cells. Day14Dox: DNA isolated at day 14 from Dox-treated cells. If the corresponding Day14 sample was excluded due to bad quality during sample processing, the FGR was calculated as NOR_Day14Dox/NOR_Day0.

- SSMDR1* = (FGR_1-medianBGR)/MAD * √2
- SSMDR2* = (FGR_2-medianBGR)/MAD * √2
- **AvSSMD*** = Average (SSMDR1* + SSMDR2*)
- **AvSSMD*/Protease** = Average (AvSSMD*all miR-Es targeting the same transcript)

The SSMD* was calculated for each miR-E in both biological replicates independently [_1/_2 (Replicate 1 and 2)]. MedianBGR: Median of BGR from all miR-Es in both replicates. Median absolute deviation (MAD): 1.4826 * Median from the absolute values of BGRReplicate1-MedianBGR and BGRReplicate2-MedianBGR. AvSSMD* = Average of the SSMD* from both replicates, thereby allowing to keep the value of one replicate if the other is empty (use of only one is highlighting for score calculation).

Hits were defined as proteases with minimum two miR-Es per protease scoring outside of the ±1 SD from the AvSSMD*s of all constructs in the screen (SD_AvSSMD*). Following this, hits were filtered for miR-E target mRNA expression, selecting only hits with expression levels above defined thresholds {PyB6-TA: RNAseq FPKM >0.5; data previously published [GEO accession code GSE133328 (25);]; PyMG-TA: microarray arbitrary log2 expression level >6.2; data previously published [GEO accession code GSE113826 (26)]}.

5.7 MTT assay

Cells were cultured ± Dox (2 µg/ml) for 3 days prior to seeding onto 96-well plates [0.5×10^4 cells/well (PyB6-TA); 0.8×10^4 cells/well (PyMG-TA)] in triplicate. For the assay under normoxic culture conditions, miR-E-Usp46-transduced PyMG-TA cells were transferred to normoxic culture conditions 3–5 days prior to the start of the experiment, as described for the competitive growth screen, and were kept under these conditions throughput the assay. Cells were treated for 48 h ± Dox, following incubation for 1–6 h with indicator-free medium containing MTT (0.5 mg/ml). Plates were emptied, and Dimethyl sulfoxid (DMSO) was added to dissolve formazan crystals. The absorbance was measured at 570 nm (650 nm reference) using an EnSpire multimode plate reader. MTT viability was calculated by normalizing the 570-nm absorbance to reference readings at 650 nm. Following this, the MTT viability of Dox-treated samples was set relative to untreated cells averaged per triplicate. For calculation of means of biological replicates, values outside mean ±2 SD were excluded.

5.8 Long-term protease targeting flow cytometry assay

miR-E-transduced PyB6-TA or PyMG-TA cells were mixed with the respective pTCEBAC-shRenilla-transduced cells (≈70% to 30%), generating competitive growth conditions, and were seeded onto six-well plates [0.15×10^5 cells/well (PyB6-TA)] or 24-well plates [0.4×10^5 cells/well (PyMG-TA)]. Cells were cultured for 14 days ± Dox (2 µg/ml). For the assay under normoxic culture conditions, miR-E-Usp46-transduced PyMG-TA cells were transferred to normoxic culture conditions 3–5 days prior to the start of the experiment, as described for the competitive growth screen, and were kept under these conditions throughout the assay. Changes in relative abundance of pTREBAV-transduced cells were analyzed by flow cytometry comparing the constitutive and inducible fluorescence between Dox-treated and untreated samples at day 14. The percentage of $Venus^+dsRed^+$ double-positive cells from living single cells of Dox-treated day 14 samples was normalized to the percentage of $Venus^+$ cells in the untreated sample. Following this, the mean percentage of fluorescent knockdown cells to uninduced cells was calculated from all biological replicates, whereby values outside mean ±2 SD were excluded.

5.9 Plate colony formation assay

Cells were separated (70–100-µM cell strainer) and seeded at single-cell conditions onto six-well plates. Plates were either further cultivated under normal culture conditions (normoxia; 21% O_2) or were transferred to hypoxic culture conditions (3% O_2). After 24 h, Dox treatment was performed (2 µg/ml). Medium and treatment were changed every 2 days. After 8–9 days (normoxia) or 12–14 days (hypoxia), cells were stained with 1% crystal violet in 20% methanol (10 min). Pictures were taken in raw format using a light desk and the Canon Powershot G6 camera. After converting the raw files to 800-dpi tiff files using Adobe Photoshop CS2, the ImageJ plugin Colony Area by Guzmán et al. (89) was used to calculate colony intensity percentage (further referred to as cell/colony growth). Reduction in cell growth was calculated relative to uninduced cells for each biological replicate as follows: Growth reduction [%] = (Intensity percent Dox/Intensity percent no Dox) - 100. For calculation of the mean growth reduction of biological replicates, values outside mean ±2 SD were excluded.

5.10 MitoTracker assay

The MitoTracker™ Deep Red FM Special Packaging Assay (M22426; Thermo) was used according to the provided protocol. Briefly, cells were cultured ± Dox (2 µg/ml) for 8 days, whereby the MitoTracker assay was performed at days 4 and 8. The day before the assay, cells (2×10^5 cells/well) were seeded onto 24-well plates. The next day, medium was removed, cells were washed with Dulbecco's phosphate-buffered saline (DPBS), and 200 µl of the staining dilution [100 nM compound in DMSO diluted in FCS-free DMEM (1:5,000)] was added, following

incubation for 30 min at 37°C. For flow cytometry, cells were transferred into a 96-well round-bottom plate, spun down (3 min, 280 rcf), and washed with fresh DMEM. Single living cells from untreated samples were gated for $Venus^+/APC^+$. Dox-treated samples were gated for $Venus^+/dsRed^+/APC^+$. The change in median APC fluorescence intensities from Dox-treated $Venus^+/dsRed^+/APC^+$ cells were normalized to untreated $Venus^+/APC^+$ cells, and the change in fluorescence intensity was calculated as follows: Fluorescence intensity [%] = $(Venus^+/dsRed^+/APC^+_{Dox\ sample} * 100/Venus^+/APC^+_{no\ Dox\ sample}) - 100$.

5.11 Flow cytometry

Cells were harvested, pelleted (5 min, 280 rcf), and resuspended in fluorescence-activated cell scanning (FACS) buffer (DPBS, 2% FCS, 5 mM EDTA). Following this, samples were separated (70–100-µm cell strainer) and transferred to FACS tubes or plates. Analysis was performed using the Cytoflex SFlow (Beckmann Coulter) and the FlowJo 7.6.5/10.6.0 software (BD Bioscience). Gated viable cells [forward-scattered area (FSC-A) vs. side-scattered area (SSC-A)] were further restricted to singlets [forward-scattered width (FSC-W) vs. height (FSC-H)]. Living single cells were further gated individually for different fluorescences depending on the experiment. All biological replicates were gated with the same defined gates.

5.12 Protein isolation and immunoblotting (western blot)

Cells were harvested by scraping on ice in phospho-Radioimmunoprecipitation assay (RIPA) lysis buffer [Tris-HCl (50 mM, pH 7.5), NaCl (150 mM), Triton X100 (1%), sodium deoxycholate (0.5%), sodium dodecyl sulfate (SDS) (0.1%), ethylenediaminetetraacetic acid (EDTA) (1 mM, pH 7), Natriumpyrophosphate (2.5 mM), β-glycerophosphate (1 mM), Natriumvanadat (1 mM), PhosStop Phosphatase-inhibitor mix (04906845001; Roche), Complete Ultra tablets (5892970001; Sigma-Aldrich) in ddH_2O]. Cells were disrupted mechanically, and cell lysates (25 µg protein) were subjected to sodium dodecyl sulfate (SDS)-polyacrylamide gel electrophoresis (PAGE), following transfer to a nitrocellulose membrane (Hybond) by a wet blot system (BioRad). Membranes were blocked with 3% bovine serum albumin (BSA) in Tris-buffered saline (TBS)-Tween (0.1%, 1 h). Primary antibodies α-tubulin [T9026; Sigma (1:1,000)], Glyceraldehyde-3-phosphate dehydrogenase (GAPDH) [97166; Cell Signaling (1:1,000)], and Pmpca [sc-390471; Cell Signaling (1:5,000)] or Pmpcb [PA5-110185; Thermo Scientific (1:5,000)] were incubated overnight at room temperature. Membranes were washed with Tris-buffered saline with Tween20 (TBS-T) and incubated with the corresponding secondary goat-anti-mouse-horseradish peroxidase [A0168; Sigma (1:5,000)] or goat-anti-rabbit-horseradish peroxidase [111-035-003; Jackson Laboratories (1:5,000)] antibodies for 60–120 min at room temparature. Washing was repeated, and membranes were developed using the West Pico/Femto Chemiluminescent Substrate (34080/3 4095; Thermo Scientific). Chemiluminescent signal detection and analysis were done using the Fusion SL Detection System and FusionCapt Advance software (Vilber Lourmat). Protein quantification (volume under the signal peak) was done relative to α-tubulin or GAPDH (probed on the same membrane) employing the automatically set rolling ball function for background correction.

5.13 General statistical analysis and data presentation

Statistical analyses were carried out with OriginPro 2018/2020 (OriginLab). Quantitative data of independent biological replicates (n) were plotted as mean ± SD, if not stated differently. Technical replicates were corrected for SD ≥0.1. Values outside mean ±2 SD were excluded from calculating the mean of biological replicates. Statistical significance was determined by one-sample or two-sided two-sample t-test ($p \leq 0.05$ significance level). General graphical depiction was done with OriginPro 2018/2020 (OriginLab) or BioRender.com. The R package "eulerr" was utilized to generate Venn diagrams (90) prior to the final optimization using Microsoft Power Point.

5.14 String analysis

STRING (91) analysis was performed on the competitive growth screen hits of the first selection criteria (≥2 miR-Es outside ±1 SD_AvSSMD*). Default analysis parameters allowing textmining, experiments, and databases as active interaction sources only were used, choosing confidence as meaning of network edges. STRING-based networks were further processed in Cytoscape 3.8.2 (92), removing unconnected nodes, changing node color and label size.

Data availability statement

The original contributions presented in the study are included in the article/Supplementary Material. Further inquiries can be directed to the corresponding author.

Author contributions

LH and TR designed the study and wrote the manuscript. LH conducted experiments and analyzed data. CM and JM

designed the protease targeting miR-E shRNA library. CM developed the TREBAV vector, the shRNA library cloning protocol, the screening strategy and the protocol for miR-E deep sequencing. KS performed the experiments for Figure 7. JM performed sequencing library deconvolution and part of the bioinformatic sequencing data analysis. KS, JM, TB, and CM read and critically revised the manuscript. All authors approved the final version of the manuscript.

Funding

The work was supported by the German Cancer Consortium DKTK (projects L627 and FR01-371) to TB, CM, and TR. This work was further supported by the Deutsche Forschungsgemeinschaft (DFG), under Germany's Excellence Strategy (BIOSS-EXC-294), the Collaborative Research Centre 850 (projects B4 and B7), the Heisenberg-Professorship BR 3662/5 (to TB) and GRK 2606 (Project ID 423813989; to TR).

Acknowledgments

The authors sincerely thank Pia Veratti (Department of Internal Medicine I, University Clinic Freiburg, Germany) for her expert technical assistance and cloning of the protease targeting miR-E shRNA library. We further thank Dr. Stephanie Ketterer and Dr. Larissa Hillebrand (Institute of Molecular Medicine and Cell Research, Faculty of Medicine, University of Freiburg, Germany) for providing the PyB6-313 and PyMG-816 cells. In addition, we thank Prof. Dr. Robert Zeiser (Department of Internal Medicine I, University Clinic Freiburg, Germany) for providing the pLNN vector and Dr. Scott W. Lowe (Sloan Kettering Institute, Memorial Sloan Kettering Cancer Center, New York, USA) for the pMSCV-rtTA3-PGK-Puro and pTCEBAC vectors. We thank Dr. Sophia Ehrenfeld (Department of Internal Medicine I, University Clinic Freiburg, Germany) for help with deep DNA sequencing. Furthermore, we thank Dr. Anett Ketscher and Prof. Dr. Christoph Peters (Institute of Molecular Medicine and Cell Research, Faculty of Medicine, University of Freiburg, Germany) for their valuable discussions. Finally, we thank the Genomics and Proteomics Core Facility of the German Cancer Research Center (DKFZ) in Heidelberg for their DNA-sequencing service, the Department for Pediatric Genetics at the Medial Center Freiburg, especially Tanja Velten, for access to their Illumina Nextseq500 DNA sequencing platform and the Deep Sequencing Facility of the MPI for Immunology and Epigenetics in Freiburg for access to their Illumina HiSeq2500 platform.

Conflict of interest

The authors declare that the research was conducted in the absence of any commercial or financial relationships that could be construed as a potential conflict of interest.

Publisher's note

Supplementary material

The Supplementary Material for this article can be found online at: https://www.frontiersin.org/articles/10.3389/fonc.2022.960109/full#supplementary-material

References

1. Bernards R, Brummelkamp TR, Beijersbergen RL. shRNA libraries and their use in cancer genetics. *Nat Methods* (2006) 3:701–6. doi: 10.1038/nmeth921

2. Sundara Rajan S, Ludwig KR, Hall KL, Jones TL, Caplen NJ. Cancer biology functional genomics: From small RNAs to big dreams. *Mol Carcinog* (2020) 59:1343–61. doi: 10.1002/mc.23260

3. Setten RL, Rossi JJ, Han S. The current state and future directions of RNAi-based therapeutics. *Nat Rev Drug Discovery* (2019) 18:421–46. doi: 10.1038/s41573-019-0017-4

4. Takai A, Dang H, Oishi N, Khatib S, Martin SP, Dominguez DA, et al. Genome-wide RNAi screen identifies PMPCB as a therapeutic vulnerability in EpCAM+ hepatocellular carcinoma. *Cancer Res* (2019) 79:2379–92. doi: 10.1158/0008-5472.CAN-18-3015

5. Qiu Z, Fa P, Liu T, Prasad CB, Ma S, Hong Z, et al. A genome-wide pooled shRNA screen identifies PPP2R2A as a predictive biomarker for the response to ATR and CHK1 inhibitors. *Cancer Res* (2020) 80:3305–18. doi: 10.1158/0008-5472.CAN-20-0057

6. Kampmann M, Horlbeck MA, Chen Y, Tsai JC, Bassik MC, Gilbert LA, et al. Next-generation libraries for robust RNA interference-based genome-wide screens. *Proc Natl Acad Sci USA* (2015) 112:E3384–91. doi: 10.1073/pnas.1508821112

7. Aka Y, Karakas B, Acikbas U, Basaga H, Gul O, Kutuk O. Kinome-wide RNAi screening for mediators of ABT-199 resistance in breast cancer cells identifies Wee1 as a novel therapeutic target. *Int J Biochem Cell Biol* (2021) 137:106028. doi: 10.1016/j.biocel.2021.106028

8. Wang L, Adamski CJ, Bondar VV, Craigen E, Collette JR, Pang K, et al. A kinome-wide RNAi screen identifies ERK2 as a druggable regulator of Shank3 stability. *Mol Psychiatry* (2020) 25:2504–16. doi: 10.1038/s41380-018-0325-9

9. Silva-Evangelista C, Barret E, Ménez V, Merlevede J, Kergrohen T, Saccasyn A, et al. A kinome-wide shRNA screen uncovers vaccinia-related kinase 3 (VRK3) as an essential gene for diffuse intrinsic pontine glioma survival. *Oncogene* (2019) 38:6479–90. doi: 10.1038/s41388-019-0884-5

10. Song R, Qiao W, He J, Huang J, Luo Y, Yang T. Proteases and their modulators in cancer therapy: Challenges and opportunities. *J Med Chem* (2021) 64:2851–77. doi: 10.1021/acs.jmedchem.0c01640

11. Habič A, Novak M, Majc B, Lah Turnšek T, Breznik B. Proteases regulate cancer stem cell properties and remodel their microenvironment. *J Histochem Cytochem* (2021) 69:775–94. doi: 10.1369/00221554211035192

12. Vizovisek M, Ristanovic D, Menghini S, Christiansen MG, Schuerle S. The tumor proteolytic landscape: A challenging frontier in cancer diagnosis and therapy. *Int J Mol Sci* (2021) 22:1–30. doi: 10.3390/ijms22052514

13. Pérez-Silva JG, Español Y, Velasco G, Quesada V. The degradome database: expanding roles of mammalian proteases in life and disease. *Nucleic Acids Res* (2016) 44:D351–5. doi: 10.1093/nar/gkv1201

14. López-Otín C. *The mammalian degradome database*. Available at: http://degradome.uniovi.es/members.html (Accessed July 1, 2020).

15. Ali A, Khalid A, Priya D, Saad A, Anupam B, Appu R. Matrix metalloproteinases: A challenging paradigm of cancer management. *Semin Cancer Biol* (2019) 56:100–15. doi: 10.1016/j.semcancer.2017.11.008

16. Lei S, Zheng R, Zhang S, Wang S, Chen R, Sun K, et al. Global patterns of breast cancer incidence and mortality: A population-based cancer registry data analysis from 2000 to 2020. *Cancer Commun* (2021) 41:1183–94. doi: 10.1002/cac2.12207

17. Sung H, Ferlay J, Siegel RL, Laversanne M, Soerjomataram I, Jemal A, et al. Global cancer statistics 2020: GLOBOCAN estimates of incidence and mortality worldwide for 36 cancers in 185 countries. *CA Cancer J Clin* (2021) 71:209–49. doi: 10.3322/caac.21660

18. Siegel RL, Miller KD, Fuchs HE, Jemal A. Cancer statistics, 2022. *CA Cancer J Clin* (2022) 72:7–33. doi: 10.3322/caac.21708

19. Hölzen L, Mitschke J, Schönichen C, Hess ME, Ehrenfeld S, Boerries M, et al. RNA Interference screens discover proteases as synthetic lethal partners of PI3K inhibition in breast cancer cells. *Theranostics* (2022) 12:4348–73. doi: 10.7150/thno.68299

20. Fellmann C, Hoffmann T, Sridhar V, Hopfgartner B, Muhar M, Roth M, et al. An optimized microRNA backbone for effective single-copy RNAi. *Cell Rep* (2013) 5:1704–13. doi: 10.1016/j.celrep.2013.11.020

21. Schuster A, Erasimus H, Fritah S, Nazarov PV, Van DE, Niclou P, et al. RNAi/CRISPR screens: from a pool to a valid hit. *Trends Biotechnol* (2019) 37:38–55. doi: 10.1016/j.tibtech.2018.08.002

22. Hanahan D, Weinberg RA. Hallmarks of cancer: The next generation. *Cell* (2011) 144:646–74. doi: 10.1016/j.cell.2011.02.013

23. Kreso A, Dick JE. Evolution of the cancer stem cell model. *Cell Stem Cell* (2014) 14:275–91. doi: 10.1016/j.stem.2014.02.006

24. Guy CT, Cardiff RD, Muller WJ. Induction of mammary-tumors by expression of polyomavirus middle T-oncogene - a transgenic mouse model for metastatic disease. *Mol Cell Biol* (1992) 12:954–61. doi: 10.1128/mcb.12.3.954

25. Ketterer S, Mitschke J, Ketscher A, Schlimpert M, Reichardt W, Baeuerle N, et al. Cathepsin d deficiency in mammary epithelium transiently stalls breast cancer by interference with mTORC1 signaling. *Nat Commun* (2020) 11:5133. doi: 10.1038/s41467-020-18935-2

26. Hillebrand LE, Wickberg SM, Gomez-Auli A, Folio M, Maurer J, Busch H, et al. MMP14 empowers tumor-initiating breast cancer cells under hypoxic nutrient-depleted conditions. *FASEB J* (2019) 33:4124–40. doi: 10.1096/fj.201801127R

27. Zhou HM, Zhang JG, Zhang X, Li Q. Targeting cancer stem cells for reversing therapy resistance: mechanism, signaling, and prospective agents. *Signal Transduct Target Ther* (2021) 6:62. doi: 10.1038/s41392-020-00430-1

28. Zhang XD. Illustration of SSMD, z score, SSMD*, z* score, and t statistic for hit selection in RNAi high-throughput screens. *J Biomol Screen* (2011) 16:775–85. doi: 10.1177/1087057111405851

29. Wold MS. Replication protein a: A heterotrimeric, single-stranded DNA-binding protein required for eukaryotic DNA metabolism. *Annu Rev Biochem* (1997) 66:61–92. doi: 10.1146/annurev.biochem.66.1.61

30. Manchado E, Huang C-H, Tasdemir N, Tschaharganeh DF, WIlkinson JE, Lowe SW. A pipeline for drug target identification and validation. *Cold Spring Harb Symp Quant Biol* (2016) 81:257–67. doi: 10.1101/sqb.2016.81.031096

31. Togar T, Desai S, Mishra R, Terwadkar P, Ramteke M, Ranjan M, et al. Identifying cancer driver genes from functional genomics screens. *Swiss Med Wkly* (2020) 150:w20195. doi: 10.4414/smw.2020.20195

32. Sun T, Liu Z, Yang Q. The role of ubiquitination and deubiquitination in cancer metabolism. *Mol Cancer* (2020) 19:146. doi: 10.1186/s12943-020-01262-x

33. Wang X, Meul T, Meiners S. Exploring the proteasome system: A novel concept of proteasome inhibition and regulation. *Pharmacol Ther* (2020) 211:107526. doi: 10.1016/j.pharmthera.2020.107526

34. Lai KP, Chen J, Tse WKF. Role of deubiquitinases in human cancers: Potential targeted therapy. *Int J Mol Sci* (2020) 21:1–22. doi: 10.3390/ijms21072548

35. Aliabadi F, Sohrabi B, Mostafavi E, Pazoki-Toroudi H, Webster TJ. Ubiquitin-proteasome system and the role of its inhibitors in cancer therapy. *Open Biol* (2021) 11:200390. doi: 10.1098/rsob.200390

36. Witte C, Jensen RE, Yaffe P, Schatz G. MAS1, a gene essential for yeast mitochondrial assembly, encodes a subunit of the mitochondrial processing protease. *EMBO J* (1988) 7:1439–47. doi: 10.1002/j.1460-2075.1988.tb02961.x

37. Hawlitschek G, Schneider H, Schmidt B, Tropschug M, Hartl FU, Neupert W. Mitochondrial protein import: Identification of processing peptidase and of PEP, a processing enhancing protein. *Cell* (1988) 53:795–806. doi: 10.1016/0092-8674(88)90096-7

38. Gomez-Fabra Gala M, Vögtle FN. Mitochondrial proteases in human diseases. *FEBS Lett* (2021) 595:1205–22. doi: 10.1002/1873-3468.14039

39. Pohl C, Dikic I. Cellular quality control by the ubiquitin-proteasome system and autophagy. *Sci (80-)* (2019) 366:818–22. doi: 10.1126/science.aax3769

40. Chen D, Frezza M, Schmitt S, Kanwar J, P. Dou Q. Bortezomib as the first proteasome inhibitor anticancer drug: Current status and future perspectives. *Curr Cancer Drug Targets* (2011) 11:239–53. doi: 10.2174/156800911794519752

41. Manasanch EE, Orlowski RZ. Proteasome inhibitors in cancer therapy. *Nat Rev Clin Oncol* (2017) 14:417–33. doi: 10.1038/nrclinonc.2016.206

42. Tanaka K. The proteasome: Overview of structure and functions. *Proc Japan Acad Ser B Phys Biol Sci* (2009) 85:12–36. doi: 10.2183/pjab.85.12

43. Heideker J, Wertz IE. DUBs, the regulation of cell identity and disease. *Biochem J* (2015) 465:1–26. doi: 10.1042/BJ20140496

44. Harrigan JA, Jacq X, Martin NM, Jackson SP. Deubiquitylating enzymes and drug discovery: Emerging opportunities. *Nat Rev Drug Discovery* (2018) 17:57–77. doi: 10.1038/nrd.2017.152

45. Komander D, Rape M. The ubiquitin code. *Annu Rev Biochem* (2012) 81:203–29. doi: 10.1146/annurev-biochem-060310-170328

46. Cruz L, Soares P, Correia M. Ubiquitin-specific proteases: Players in cancer cellular processes. *Pharmaceuticals* (2021) 14:1–27. doi: 10.3390/ph14090848

47. Morotti A, Panuzzo C, Crivellaro S, Pergolizzi B, Familiari U, Berger AH, et al. BCR-ABL disrupts PTEN nuclear-cytoplasmic shuttling through phosphorylation-dependent activation of HAUSP. *Leukemia* (2014) 28:1326–33. doi: 10.1038/leu.2013.370

48. An T, Gong Y, Li X, Kong L, Ma P, Gong L, et al. USP7 inhibitor P5091 inhibits wnt signaling and colorectal tumor growth. *Biochem Pharmacol* (2017) 131:29–39. doi: 10.1016/j.bcp.2017.02.011

49. Carrà G, Panuzzo C, Torti D, Parvis G, Crivellaro S, Familiari U, et al. Therapeutic inhibition of USP7-PTEN network in chronic lymphocytic leukemia: A strategy to overcome TP53 mutated/ deleted clones. *Oncotarget* (2017) 8:35508–22. doi: 10.18632/oncotarget.16348

50. Dai X, Lu L, Deng S, Meng J, Wan C, Huang J, et al. USP7 targeting modulates anti-tumor immune response by reprogramming tumor-associated macrophages in lung cancer. *Theranostics* (2020) 10:9332–47. doi: 10.7150/thno.47137

51. Xia X, Liao Y, Huang C, Liu Y, He J, Shao Z, et al. Deubiquitination and stabilization of estrogen receptor α by ubiquitin-specific protease 7 promotes breast tumorigenesis. *Cancer Lett* (2019) 465:118–28. doi: 10.1016/j.canlet.2019.09.003

52. Hayal TB, Doğan A, Şişli HB, Kiratli B, Şahin F. Ubiquitin-specific protease 7 downregulation suppresses breast cancer. *vitro Turkish J Biol* (2020) 44:145–57. doi: 10.3906/biy-1912-83

53. Zhang Q, Cao C, Gong W, Bao K, Wang Q, Wang Y, et al. A feedforward circuit shaped by ECT2 and USP7 contributes to breast carcinogenesis. *Theranostics* (2020) 10:10769–90. doi: 10.7150/thno.46878

54. Goya A, Kallemeijn W, Tate E. Targeting methionine aminopeptidase 2 in cancer, obesity, and autoimmunity. *Trends Pharmacol Sci* (2021) 42:870–82. doi: 10.1016/j.tips.2021.07.004

55. Yin S-Q, Wang J-J, Zhang C-M, Liu Z-P. The development of MetAP-2 inhibitors in cancer treatment. *Curr Med Chem* (2012) 19:1021–35. doi: 10.2174/092986712799320709

56. Frottin F, Bienvenut WV, Bignon J, Jacquet E, Jacome ASV, Van Dorsselaer A, et al. MetAP1 and MetAP2 drive cell selectivity for a potent anti-cancer agent in synergy, by controlling glutathione redox state. *Oncotarget* (2016) 7:63306–23. doi: 10.18632/oncotarget.11216

57. Hu X, Addlagatta A, Lu J, Matthews BW, Liu JO. Elucidation of the function of type 1 human methionine aminopeptides during cell cycle progression. *Proc Natl Acad Sci USA* (2006) 103:18148–53. doi: 10.1073/pnas.0608389103

58. Bernier SG, Taghizadeh N, Thompson CD, Westlin WF, Hannig G. Methionine aminopeptidases type I and type II are essential to control cell proliferation. *J Cell Biochem* (2005) 95:1191–203. doi: 10.1002/jcb.20493

59. Chabottaux V, Sounni NE, Pennington CJ, English WR, Van Den Brûle F, Blacher S, et al. Membrane-type 4 matrix metalloproteinase promotes breast cancer

growth and metastases. *Cancer Res* (2006) 66:5165–72. doi: 10.1158/0008-5472.CAN-05-3012

60. Nie X, Li M, Lu B, Zhang Y, Lan L, Chen L, et al. Down-regulating overexpressed human lon in cervical cancer suppresses cell proliferation and bioenergetics. *PloS One* (2013) 8:1–9. doi: 10.1371/journal.pone.0081084

61. Gibellini L, Pinti M, Boraldi F, Giorgio V, Bernardi P, Bartolomeo R, et al. Silencing of mitochondrial lon protease deeply impairs mitochondrial proteome and function in colon cancer cells. *FASEB J* (2014) 28:5122–35. doi: 10.1096/fj.14-255869

62. Liu H, Buus R, Clague MJ, Urbe S. Regulation of ErbB2 receptor status by the proteasomal DUB POH1. *PloS One* (2009) 4:e5544–4. doi: 10.1371/Citation

63. Zhang L, Xu H, Ma C, Zhang J, Zhao Y, Yang X, et al. Upregulation of deubiquitinase PSMD14 in lung adenocarcinoma (LUAD) and its prognostic significance. *J Cancer* (2020) 11:2962–71. doi: 10.7150/jca.39539

64. Sun J, Shi X, Mamun M, Gao Y. The role of deubiquitinating enzymes in gastric cancer (Review). *Oncol Lett* (2019), 19:30–44. doi: 10.3892/ol.2019.11062

65. Meng Y, Li X. Expression and prognosis analysis of SUMOylation regulators in oral squamous cell carcinoma based on high-throughput sequencing. *Front Genet* (2021) 12:671392. doi: 10.3389/fgene.2021.671392

66. Bermejo JL, Kabisch M, Dünnebier T, Schnaidt S, Melchior F, Fischer HP, et al. Exploring the association between genetic variation in the SUMO isopeptidase gene USPL1 and breast cancer through integration of data from the population-based GENICA study and external genetic databases. *Int J Cancer* (2013) 133:362–72. doi: 10.1002/ijc.28040

67. Yang M, Jensen RE, Yaffe MP, Oppliger W, Schatz G. Import of proteins into yeast mitochondria: the purified matrix processing protease contains two subunits which are encoded by the nuclear MAS1 and MAS2 genes. *EMBO J* (1988) 7:3857–62. doi: 10.1002/j.1460-2075.1988.tb03271.x

68. Quirós PM, Langer T, López-Otín C. New roles for mitochondrial proteases in health, ageing and disease. *Nat Rev Mol Cell Biol* (2015) 16:345–59. doi: 10.1038/nrm3984

69. Branda SS, Cavadini P, Adamec J, Kalousek F, Taroni F, Isaya G. Yeast and human frataxin are processed to mature form in two sequential steps by the mitochondrial processing peptidase*. *J Biol Chem* (1999) 274:22763–9. doi: 10.1074/jbc.274.32.22763

70. Jobling RK, Assoum M, Gakh O, Blaser S, Raiman JA, Mignot C, et al. PMPCA mutations cause abnormal mitochondrial protein processing in patients with non-progressive cerebellar ataxia. *Brain* (2015) 138:1505–17. doi: 10.1093/brain/awv057

71. Muhle H, Friederich MW, White SM, Basinger A, Ku C, Keminer O, et al. Mutations in PMPCB encoding the catalytic subunit of the mitochondrial presequence protease cause neurodegeneration in early childhood. *Am J Hum Genet* (2018) 102:557–73. doi: 10.1016/j.ajhg.2018.02.014

72. Zheng J, He S, Zeng Z, Gu X, Cai L, Qi G. PMPCB silencing sensitizes HCC tumor cells to sorafenib therapy. *Mol Ther* (2019) 27:1784–95. doi: 10.1016/j.ymthe.2019.06.014

73. Thomas LW, Ashcroft M. The contextual essentiality of mitochondrial genes in cancer. *Front Cell Dev Biol* (2021) 9:695351. doi: 10.3389/fcell.2021.695351

74. Li GB, Fu RQ, Shen HM, Zhou J, Hu XY, Liu YX, et al. Polyphyllin I induces mitophagic and apoptotic cell death in human breast cancer cells by increasing mitochondrial PINK1 levels. *Oncotarget* (2017) 8:10359–74. doi: 10.18632/oncotarget.14413

75. Lee MS, Yuet-Wa JC, Kong SK, Yu B, Eng-Choon VO, Nai-Ching HW, et al. Effects of polyphyllin d, a steroidal saponin in Paris polyphylla, in growth inhibition of human breast cancer cells and in xenograft. *Cancer Biol Ther* (2005) 4:1248–54. doi: 10.4161/cbt.4.11.2136

76. Greene AW, Grenier K, Aguileta MA, Muise S, Farazifard R, Haque ME, et al. Mitochondrial processing peptidase regulates PINK1 processing, import and parkin recruitment. *EMBO Rep* (2012) 13:378–85. doi: 10.1038/embor.2012.14

77. Jose C, Bellance N, Rossignol R. Choosing between glycolysis and oxidative phosphorylation: A tumor's dilemma? *Biochim Biophys Acta - Bioenerg* (2011) 1807:552–61. doi: 10.1016/j.bbabio.2010.10.012

78. Heiden MGV, Cantley LC, Thompson CB. Understanding the warburg effect: The metabolic requirements of cell proliferation. *Sci (80-)* (2009) 324:1029–33. doi: 10.1126/science.1160809

79. Geli V, Yang M, Suda K, Lustig A, Schatz G. The MAS-encoded processing protease of yeast mitochondria. overproduction and characterization of its two nonidentical subunits. *J Biol Chem* (1990) 265:19216–22. doi: 10.1016/s0021-9258(17)30646-4

80. Su SC, Lin CC, Tai HC, Chang MY, Ho MR, Babu CS, et al. Structural basis for the magnesium-dependent activation and hexamerization of the lon AAA+ protease. *Structure* (2016) 24:676–86. doi: 10.1016/j.str.2016.03.003

81. Cheng CW, Kuo CY, Fan CC, Fang WC, Jiang SS, Lo YK, et al. Overexpression of lon contributes to survival and aggressive phenotype of cancer cells through mitochondrial complex I-mediated generation of reactive oxygen species. *Cell Death Dis* (2013) 4:1–13. doi: 10.1038/cddis.2013.204

82. Kang SG, Dimitrova MN, Ortega J, Ginsburg A, Maurizi MR. Human mitochondrial ClpP is a stable heptamer that assembles into a tetradecamer in the presence of ClpX. *J Biol Chem* (2005) 280:35424–32. doi: 10.1074/jbc.M507240200

83. Baker TA, Sauer RT. ClpXP, an ATP-powered unfolding and protein-degradation machine. *Biochim Biophys Acta - Mol Cell Res* (2012) 1823:15–28. doi: 10.1016/j.bbamcr.2011.06.007

84. Reinhardt P, Glatza M, Hemmer K, Tsytsyura Y, Thiel CS, Höing S, et al. Inhibition of the mitochondrial protease, ClpP, as a therapeutic strategy for human acute myeloid leuekmia. *Stem Cell Rep* (2017) 176:139–48. doi: 10.1016/j.ccell.2015.05.004.Inhibition

85. Reinhardt P, Glatza M, Hemmer K, Tsytsyura Y, Thiel CS, Höing S, et al. Mitochondrial ClpP-mediated proteolysis induces selective cancer cell lethality. *Stem Cell Rep* (2017) 176:139–48. doi: 10.1016/j.ccell.2019.03.014

86. Zuber J, McJunkin K, Fellmann C, Dow LE, Taylor MJ, Hannon GJ, et al. Toolkit for evaluating genes required for proliferation and survival using tetracycline-regulated RNAi. *Nat Biotechnol* (2011) 29:79–83. doi: 10.1038/nbt.1720

87. David CJ, Huang YH, Chen M, Su J, Zou Y, Bardeesy N, et al. TGF-β tumor suppression through a lethal EMT. *Cell* (2016) 164:1015–30. doi: 10.1016/j.cell.2016.01.009

88. McJunkin K, Mazurek A, Premsrirut PK, Zuber J, Dow LE, Simon J, et al. Reversible suppression of an essential gene in adult mice using transgenic RNA interference. *Proc Natl Acad Sci U S A* (2011) 108:7113–8. doi: 10.1073/pnas.1104097108

89. Guzmán C, Bagga M, Kaur A, Westermarck J, Abankwa D. ColonyArea: An ImageJ plugin to automatically quantify colony formation in clonogenic assays. *PLoS One* (2014) 9:14–7. doi: 10.1371/journal.pone.0092444

90. Larsson J. Eulerr: Area-proportional Euler and Venn diagrams with ellipses. In: *R package version 6.1.1* (2021). Available at: https://cran.r-project.org/package=eulerr.

91. Szklarczyk D, Gable AL, Lyon D, Junge A, Wyder S, Huerta-Cepas J, et al. STRING v11: Protein-protein association networks with increased coverage, supporting functional discovery in genome-wide experimental datasets. *Nucleic Acids Res* (2019) 47:D607–13. doi: 10.1093/nar/gky1131

92. Shannon P, Markiel A, Ozier O, Baliga, Wang, Ramage D, et al. Cytoscape: a software environment for integrated models of biomolecular interaction. *Genome Res* (2003) 13:2498–504. doi: 10.1101/gr.1239303

frontiers | Frontiers in Oncology

TYPE Original Research
PUBLISHED 25 October 2022
DOI 10.3389/fonc.2022.956190

OPEN ACCESS

EDITED BY
Jaroslav Truksa,
Institute of Biotechnology (ASCR), Czechia

REVIEWED BY
Paola Maycotte,
Instituto Mexicano del Seguro Social, Mexico
Che-Hung Shen,
National Health Research Institutes, Taiwan

*CORRESPONDENCE
Xiao-Jian Han
hanxiaojian@hotmail.com
Zhi-Ping Chen
zpchen5500@163.com

†These authors have contributed equally to this work

SPECIALTY SECTION
This article was submitted to Gastrointestinal Cancers: Gastric and Esophageal Cancers, a section of the journal Frontiers in Oncology

RECEIVED 30 May 2022
ACCEPTED 12 October 2022
PUBLISHED 25 October 2022

CITATION
Xiao Y-Y, Xiao J-X, Wang X-Y, Wang T, Qu X-H, Jiang L-P, Tou F-F, Chen Z-P and Han X-J (2022) Metformin-induced AMPK activation promotes cisplatin resistance through PINK1/Parkin dependent mitophagy in gastric cancer.
Front. Oncol. 12:956190.
doi: 10.3389/fonc.2022.956190

Metformin-induced AMPK activation promotes cisplatin resistance through PINK1/Parkin dependent mitophagy in gastric cancer

Yi-Yi Xiao[1,2†], Jin-Xing Xiao[2†], Xiao-Yu Wang[1], Tao Wang[1], Xin-Hui Qu[1,3], Li-Ping Jiang[2], Fang-Fang Tou[4], Zhi-Ping Chen[1,5*] and Xiao-Jian Han[1,2,3*]

[1]Institute of Geriatrics, Jiangxi Provincial People's Hospital, The First Affiliated Hospital of Nanchang Medical College, Nanchang, China, [2]Department of Pharmacology, School of Pharmaceutical Science, Nanchang University, Nanchang, China, [3]Department of Neurology, Jiangxi Provincial People's Hospital, The First Affiliated Hospital of Nanchang Medical College, Nanchang, China, [4]Department of Oncology, Jiangxi Provincial People's Hospital, The First Affiliated Hospital of Nanchang Medical College, Nanchang, China, [5]Department of Critical Care Medicine, Jiangxi Provincial People's Hospital, The First Affiliated Hospital of Nanchang Medical College, Nanchang, China

Gastric cancer (GC) is one of the most common tumors worldwide, and cisplatin is a standard chemotherapeutic reagent for GC treatment. However, chemoresistance is an inherent challenge which limits its application and effectiveness in clinic. This study aims to investigate the mechanism of metformin-induced cisplatin resistance in GC. Intriguingly, the upregulation of mitophagy markers, mitochondrial fission, autophagy and mitophagosome were observed in SGC-7901/DDP cells compared to those in the SGC-7901 cells. Treatment with metformin significantly increased mitochondrial fission and mitophagy in both AGS and SGC-7901 cells, resulting in decreased ATP production, which unexpectedly protected GC cells against the cytotoxicity of cisplatin. In contrast, application of Chloroquine and 3-methyladenine, two inhibitors of autophagy, significantly alleviated the protective effect of metformin on SGC-7901 and AGS cells against cytotoxicity of cisplatin. Moreover, metformin also stimulated the phosphorylation of AMPK (Thr172) and increased the expression of mitophagy markers including Parkin and PINK1 in the AMPK signaling-dependent manner. Consistently, the cell viability and cell apoptosis assay showed that metformin-induced cisplatin resistance was prevented by knockdown of AMPKα1. Taken together, all data in this study indicate that metformin induced AMPK activation and PINK1/Parkin dependent mitophagy, which may contribute to the progression of cisplatin resistance in GC.

KEYWORDS

cisplatin resistance, AMPK, mitophagy, gastric cancer, metformin

Introduction

Gastric cancer is a fatal disease with low survival rate worldwide. It is reported that there are over one million new cases every year, and gastric cancer is the fifth largest diagnosed malignant tumor in the world (1). Unfortunately, gastric cancers usually are not sensitive to immune checkpoint inhibitor monotherapies, which makes surgery and chemotherapy the principal approaches for treatment of GC. Cisplatin (DDP) is the first-line reagents for GC chemotherapy. However, cancer cells often develop resistance in the long-term use of cisplatin, which inevitably lead to primary or acquired drug resistance, an obstacle of successful cancer therapy (2). Therefore, re-sensitizing gastric cancer cells to chemotherapy and investigating the mechanism of drug resistance is of clinical significance.

Mitophagy controls mitochondrial quality by degrading superfluous and damaged mitochondria, which helps maintaining cellular homeostasis in response to stress (3). Mitochondrial fission is a prerequisite for mitophagy to remove damaged organelles, whereas mitochondrial fusion neutralizes mitophagy (4). In addition, mitochondrial oxidative stress, apoptotic factor and ATP generation are also related to the mitophagy (5). PTEN-induced putative kinase 1 (PINK1)/Parkin axis is a key regulator if mitophagy under cell stress (6). Normally, full-length PINK1 enters mitochondria, where it is cleaved by protease PARL for degradation. Under stressed and mitochondrial depolarization, PINK1 locates the mitochondrial outer membrane, and phosphorylates an E3 ubiquitin ligase Parkin. Activated Parkin induces ubiquitination of multiple mitochondrial outer membrane proteins, which are then degraded by autophagosomes. AMPK is recognized as a key sensor of cell nutrition and AMPK/ULK1 axis modulate Parkin, revealing close connections between AMPK and mitophagy (7). It is reported that mitophagy plays a central role in cancer progression and tumorigenesis (8, 9), but the role of mitophagy in cisplatin resistance of gastric cancer remains largely unknown.

Metformin (1,1-dimethylbiguanide hydrochloride), an effective hypoglycemic drug, is first reported as an antidiabetic drug in 1957 (10). Metformin is an antihyperglycemic drug for type 2 diabetes (T2D) due to its minimal side effects (11). Recent studies show that metformin has a promising role in cancer therapy. Metformin mediates anti-tumor effect may occur through several mechanisms, including inhibition of cancer cell proliferation (12), enhanced apoptosis (13), reduced angiogenesis (14), inhibition of EMT (15), regulating immune response (16) and targeting cancer stem cells (17). In contrast, it is also reported that metformin alleviates chemosensitivity to cisplatin in different cancer cells (18–20). However, the role of mitophagy in metformin-induced cisplatin-resistance in GC and its underlying mechanism remains to be elucidated.

Here, we showed that mitochondrial fission and mitophagy were enhanced in cisplatin-resistant GC cells. Intriguingly, metformin increased mitochondrial fission and mitophagy and protected GC cells against the cytotoxicity of cisplatin. In the term of mechanism, metformin activated AMPK signaling and upregulated the expression of mitophagy related proteins, including PINK, Parkin and LC3B. Further, application of mitophagy inhibitors alleviated metformin-induced cisplatin resistance. These results illustrate that metformin may facilitate cisplatin resistance of GC cells by promoting mitophagy *via* AMPK-PINK1/Parkin signaling axis. Our data also warrant caution over metformin treatment in diabetes patients with GC.

Materials and methods

Cell culture

Human gastric cancer AGS, SGC-7901 cells and cisplatin-resistant SGC-7901/DDP cells were purchased from the Cell Biology of Institute of Chinese Academy of Sciences (Shanghai, China). SGC-7901 and SGC-7901/DDP cells were cultured in RPMI 1640 (BI, Israel) and AGS cells were grown in DMEM/F12 medium (BI, Israel) supplemented with 1% penicillin/streptomycin (Solarbio, China) and 10% fetal bovine serum (FBS, BI, Israel) at 37° C with 5% CO_2 in a humidified atmosphere.

Reagents

Antibody against β-actin (#AC004,1:100000) was purchased from ABclonal Technology (Wuhan, China). Antibodies against PINK1 (#ab23707, 1:1000) and Parkin (#ab77924, 1:2000) were purchased from Abcam (Cambridge, UK). Antibodies against LC3B (#2775S, 1:1000), PINK1 (#6946S, 1:1000), AMPKα (#5832S,1:1000), Phospho-AMPKα (Thr172) (#2535S,1:1000) were purchased from Cell Signaling Technology (Danvers, MA, USA). Horseradish peroxidase (HRP)-conjugated goat anti-rabbit IgG secondary antibody (1:5000) was obtained from Proteintech (Wuhan, China). Enhanced chemiluminescence (ECL) detection kit (#KF005) was purchased from Affinity. Cisplatin and metformin were obtained from MCE (Shanghai, China). 3-Methyladenine (#S2767) was purchased from Selleck (Houston, TX, USA), and Chloroquine (#REVG1006) was obtained from Genechem (Shanghai, China).

Cell proliferation assay

SGC-7901 and AGS cells were seeded into 96-well plates and treated with metformin for indicated time. Subsequently, Cell proliferation was measured by CCK8 kit, following the

manufacturer's instructions. Absorbance at 450 nm was recorded using an optical density reader.

Measurement of mitochondrial DNA

Total DNA was isolated from SGC-7901 and SGC-7901DDP cells using the Universal Genomic DNA Purification Mini Spin Kit (#D0063, Beyotime, China) according to manufacturer's instructions. The amount of mitochondrial DNA was determined by quantitative real-time PCR using following primers : mtDNA-F 5'-CGCCTCACACTCATTCTCAACC-3' and mtDNA-R 5'-CAAGGAAGGGGTAGGCTATGTG-3', nDNA-F 5'- AGTCCCCCACAACACTGAGA-3' and nDNA-R 5'-AATGGCACACGACAAGGTGG-3'. Relative mitochondrial DNA levels were calculated based on the threshold cycle (Ct) as $2^{-\Delta(\Delta Ct)}$.

Mtphagy dye staining

SGC-7901 and SGC-7901/DDP cells were washed with serum-free medium twice and incubated with Mtphagy Dye working solution (#MDO1, Dojindo, Japan) at the final concentration of 100 nM for 30 min at 37°C. Cells were then washed with serum-free medium twice. Mitophagy in live cells was detected through tracking the fluorescence Mtphagy Dye under fluorescence microscope (Olympus, Tokyo, Japan).

Cell apoptosis assay

Cell apoptosis was detected with Annexin V-FITC/PI Apoptosis kit (#556547, BD Biosciences, San Jose, CA, USA) following manufacturer's instruction. Cells were washed with PBS and resuspended in 300 μl binding buffer. Next, cells were double-stained with 5 μl PI and 5 μl Annexin V-FITC at RT in the dark. Cells were analyzed using a flow cytometer equipped with a laser emitting at 488 nm and an optical filter FL1 (530/30 nm). Data was processed with the Follow JO software (BD Biosciences).

siRNA transfection

SGC-7901 cells were transfected with siRNA targeting PINK1 subunit (ChemShine Biotechnology Inc, Shanghai, China), AMPK-α1 subunit (GenePharma, Shanghai, China) or scrambled siRNA (GenePharma, Shanghai, China) as a control. The targeting sequences were as follows: PRKAA1-homo-825 5'-GGGAACAUGAAUGGUUUAATT-3'(sense) and 5'-UUAAACCAUUCAUGUUCCCTT-3' (antisense), PRKAA1-homo-477 5'-GCUUGAUGCACACAUGAAUTT-3' (sense) and 5'-AUUCAUGUGUGCAUCAAGCTT-3' (antisense), PRKAA1-homo-1132 5'-CCAUUCUUGGUUGCUGAAATT-3' (sense) and 5'-UUUCAGCAACCAAGAAUGGTT-3' (antisense). PINK1-si-1 5'-CGAAGCCAUCUUGAACACAAUdTdT-3'(sense) and 5'-AUUGUGUUCAAGAUGGCUUCGdTdT-3' (antisense), PINK1-si-2 5'-GCCGCAAAUGUGCUUCAUCUAdTdT-3' (sense) and 5'-UAGAUGAAGCACAUUUGCGGCdTdT-3' (antisense), PINK1-si-3 5'-GUUCCUCGUUAUGAAGAACUAdTdT-3' (sense) and 5'-UAGUUCUUCAUAACGAGGAACdTdT-3' (antisense). siRNAs were transfected intosiRNAs were transfected into SGC-7901 cells with ribo-FECT CP Transfection Kit (#C10511-05, ribo, Guangzhou, China) following the manufacturer's instructions.

Western blot analysis

Cells were lysed in RIPA buffer [20 mM Tris (pH 7.4), 10 mM sodium orthovanadate, 20 mM sodium fluoride, 150 mM NaCl, 1 mM dithiothreitol, 0.25 mM sucrose, 500 nM okadaic acid, and 0.5% Tween 20] and whole cell extracts were put to SDS-PAGE and transferred to PVDF membranes. The membranes were blocked with 5% skim milk and then incubated with primary antibodies anti-PINK1(Abcam, UK), anti-Parkin (Abcam, UK), anti-LC3B (CST, USA), anti-AMPKα (CST, USA), anti-phospho-AMPKα-Thr172 (CST, USA), anti-Tom20 (Santa Cruz Biotechnology, United States) or anti-β-actin (ABclonal Technology, China) for 1 h at room temperature. Next, the membranes were incubated with horseradish peroxidase (HRP)-conjugated anti-mouse or anti-rabbit secondary antibodies for 1 h at room temperature. Western blot bands were detected with a chemiluminescence kit. Densitometric analysis was carried out with ImageJ software (NIH, Bethesda, MD, United States). Protein levels were normalized to β-actin.

Measurement of intracellular ATP level

SGC-7901 and AGS cells were seeded into a 96-well plate. The ATP levels were detected with commercial ATP assay kit (Beyotime Biotechnology, China) following manufacturer's protocol. Each well was added with mixed reagent and incubated for 15 min. ATP levels were detected with Fluorescence/Multi-Detection Microplate Reader.

Transmission electron microscopy

SGC-7901/DDP and SGC-7901 cells were seeded at 5×10^5 cells/culture dish (35mm) and treated with indicated reagents. Then cells were collected and fixed by 3% glutaraldehyde at 4°C

followed by 1% osmium tetroxide. Next, cells were dehydrated in 30%~100% acetone, embedded with Epox 812 and cut to semithin sections. After stained with methylene bule, the ultrathin sections (60 nm~90 nm) were prepared by EM UC7 (Leica, Germany) and stained with lead citrate and uranyl acetate. The sections were detected by transmission electron microscope (JEM-1400FLASH, Electronics Co., Ltd, Japan).

Confocal microscopy

Cells were seeded in glass-bottom culture dishes at 50-60% confluence. To label mitochondria, SGC-7901 and AGS cells were transfected with pDsRed2-Mito with Lipofectamine 2000 (Invitrogen) following manufacturer's instructions. Then, cells were treated with 10mM metformin for 24h, Fluorescence images were acquired with confocal microscope (Olympus, FV3000D, Tokyo, Japan). Mitochondrial length was measured and analyzed in each group.

Statistical analysis

The results were analyzed by unpaired Student's *t*-test or one-way ANOVA. Statistical analysis was performed with GraphPad software. Data from three independent experiments are presented as mean ± SD. $p<0.05$ was considered to be statistically significant.

Results

Mitochondrial fission and mitophagy were increased in the cisplatin resistant SGC-7901/DDP cells

In this study, the cisplatin resistant SGC-7901/DDP and its parental SGC-7901 cells were used. First, the IC50 of two cell lines to cisplatin was determined by CCK8 assay. As shown in Figure S1, SGC-7901/DDP and SGC-7901 cells were treated with different concentrations of cisplatin and dose-response curves of cell viability were generated. IC50 values for cisplatin were calculated as 3.85 and 18.88 μg/ml in SGC-7901 and SGC-7901/DDP cells, respectively. Compared to SGC-7901 cells, the IC50 value for cisplatin against SGC-7901/DDP cells was increased 5-fold. To investigate whether mitochondrial dynamics was involved in cisplatin resistance, pDsRed2-Mito was transfected into SGC-7901 and SGC-7901/DDP cells for mitochondrial imaging. As shown in Figures 1A, B, mitochondria in SGC-7901 cells appeared as tubular, thread-like network, and the average mitochondrial length in SGC-7901 cells (4.9 ± 0.26 μm) was longer than that in SGC-7901/DDP cells (2.4 ± 0.09 μm). To explore the role of mitophagy in cisplatin resistance, expression of PINK, Parkin and LC3B were examined. As shown in Figures 1C, D, expression of PINK, Parkin and the ratio of LC3B-II/I was higher in SGC-7901/DDP cells than those in SGC-7901 cells in the presence or absence of chloroquine (CQ). Further results showed that the content of mitoDNA was decreased in SGC-7901/DDP cells compared with those in SGC-7901 cells (Figure 1E). The expression of TOM20, component of the TOM (translocase of outer membrane) receptor complex, was slightly down-regulated in SGC-7901/DDP cells, but it showed no significant difference between SGC-7901 and SGC-7901/DDP cells (Figures S2A, B). This result is consistent with previous finding that the change of mitoDNA proceeds that of mitochondrial mass (21). Then, cells were stained with Mtphagy Dye, and the fluorescence indicates the occurrence of mitophagy. As shown in Figure S2C, the fluorescent intensity of Mtphagy Dye is stronger in SGC-7901/DDP cells than that in the SGC-7901 cells. In accordance with western blot results, confocal imaging showed that LC3B puncta formation increased in SGC7901/DDP cells (Figure 1F). Finally, mitophagy in SGC-7901 and SGC-7901/DDP cells was detected by TE microscopy and the appearance of double membranes associated with mitochondria was observed in SGC-7901/DDP cells, but not in SGC-7901 cells (Figure 1G). These results indicate that mitochondrial fission and mitophagy are increased in the cisplatin resistant SGC-7901/DDP cells, also suggest that mitochondrial dynamics and mitophagy is involved in the cisplatin resistance in gastric cancer.

Metformin protects GC cells from cisplatin toxicity

The effect of metformin on sensitivity of SGC-7901 and AGS cells to cisplatin was examined. The proliferation of SGC-7901 and AGS cells was inhibited in dose-dependent manner at 24 h or 48 h after cisplatin (Figures 2A, B). To evaluate the effect of metformin on the sensitivity of GC cells to cisplatin, both SGC-7901 and AGS cells were pretreated with different concentrations of metformin. CCK-8 results showed that metformin significantly alleviated cisplatin-induced growth inhibition in SGC7901 and AGS cells (Figures 2C, D). Furthermore, cell apoptosis was examined in SGC-7901 and AGS cells treated with cisplatin and/or metformin. As shown in Figures 3A, B, 5 μg/mL cisplatin induced approximately 53% apoptosis in SGC7901 cells, and pretreatment with 10 mM metformin efficiently inhibited cisplatin-induced apoptosis in SGC7901 cells. The similar outcomes were obtained in AGS cells (Figures 3C, D). All these results indicate that metformin may promote the resistance of GC cells against cisplatin.

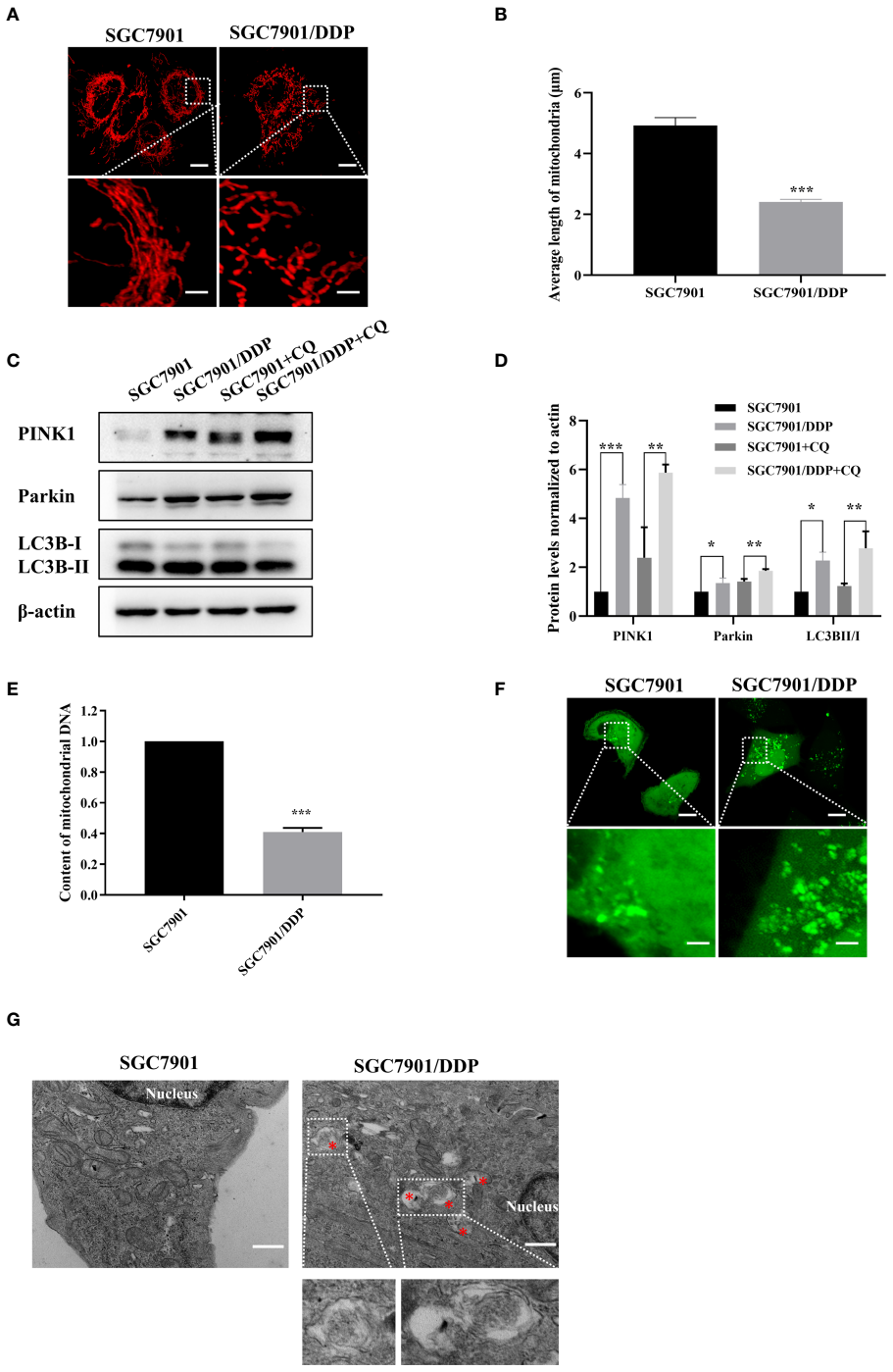

FIGURE 1
Mitochondrial fission and mitophagy were increased in the cisplatin resistant SGC-7901/DDP cells. **(A, B)** Mitochondrial morphology in SGC-7901 and SGC-7901/DDP cells. Cells were transfected with pDsRed2-Mito. Scale bar of top figures is 10 μm. Scale bar of bottom figures is 2 μm. Mitochondria length in each group was measured. **(C, D)** Expression of PINK1, Parkin and LC3B in SGC-7901 and SGC-7901/DDP cells. SGC-7901 and SGC-7901/DDP cells were treated with or without 10 μM CQ for 24 h. Whole cell lysates were collected for western blot assay. **(E)** Changes of mitochondrial DNA content. Total DNA were isolated from SGC-7901 and SGC-7901/DDP cells and the amount of mitochondrial DNA was determined by real-time PCR. **(F)** SGC7901 and SGC7901/DDP cells were transfected with pEGFP-LC3B for 24 h and then analyzed by confocal microscope. Scale bar=10 μm. Circled images at higher magnification are shown in the below panels. Scale bar= 2 μm. **(G)** SGC7901 and SGC7901/DDP cells were processed by transmission EM. Asterisk represents mitophagy vesicles. Circled images at higher magnification are shown in the below panels. Scale bar=0.5 μm. Data were presented as the means ± SD. The experiments were repeated three times independently. $^{**}p<0.01$, $^{***}p<0.001$.

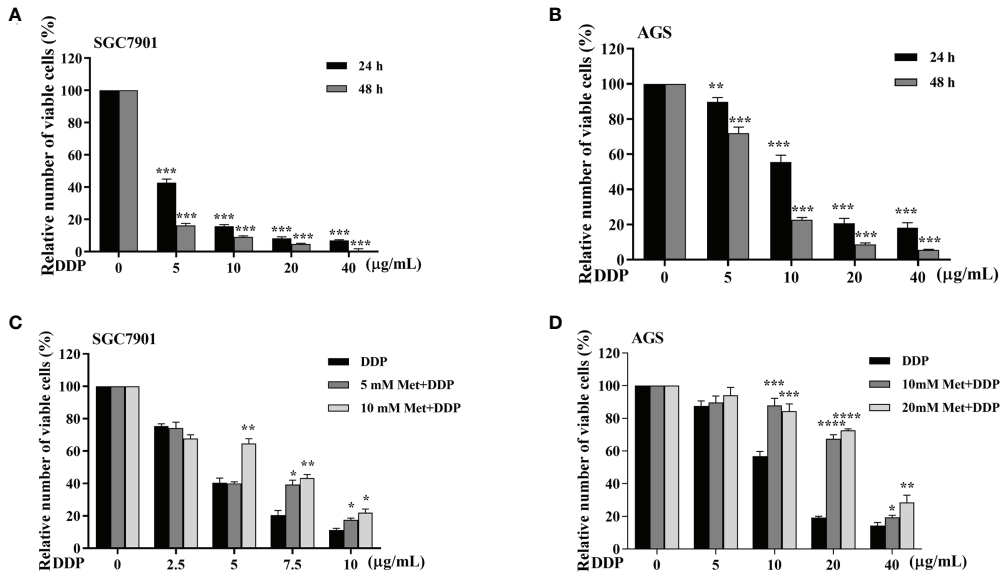

FIGURE 2
Metformin alleviates cisplatin-induced growth inhibition in GC cells. **(A, B)** SGC-7901 and AGS cells were treated with cisplatin for 24 or 48 h, followed by CCK8 assay. **(C, D)** SGC-7901 and AGS cells were pre-treated with metformin for 4 h followed with cisplatin treatment for 24 h. Cell viability was determined by CCK8 assay. Data were presented as the means ± SD. The experiments were repeated three times independently. *p<0.05, **p<0.01, ***p<0.001, ****p<0.0005.

Metformin promoted cisplatin resistance *via* PINK1/Parkin-dependent mitophagy in GC

As motioned in Figures 1C~F, PINK1/Parkin-dependent mitophagy was increased in cisplatin-resistant SGC7901/DDP cells. Thus, the mechanism of PINK1/Parkin-dependent mitophagy in metformin-induced cisplatin resistance was further explored. It was found that the expression of PINK1, Parkin and the ratio of LC3BII/I in both SGC7901 and AGS cells treated with cisplatin was decreased in dose-dependent manner (Figures 4A, B; Figures S3A, B). Furthermore, the effect of metformin on PINK1/Parkin signaling was examined in two GC cell lines. As shown in Figures 4C, D and Figures S3C, D, metformin significantly elevated the expression of Parkin, PINK1 and the ratio of LC3BII/I, indicating that metformin might activate PINK1/Parkin signaling. Then, SGC7901 cells were treated with cisplatin and/or metformin. Western blot results showed that metformin attenuated cisplatin-induced downregulation of PINK1, Parkin and the ratio of LC3B-II/I in the SGC-7901 cells (Figure 4E and Figure S3E). To examine whether the increased expression of PINK1 and ratio of LC3BII/I protect gastric cancer cells from cisplatin, SGC7901/DDP cells were transfected with PINK1 siRNAs to knockdown the expression of PINK1 or treated with PIK-III to down-regulate the ratio of LC3BII/I. PINK1 siRNA#1 showed best knockdown efficiency and was used in following experiments (Figure S4). As shown in Figures 4F, G, treatment with 5 μM PIK-III for 24 h or PINK1 knockdown alone had no effect on cell viability in SGC7901/DDP cells. However, combination of PIK-III or PINK1 knockdown with cisplatin showed more efficiency in inhibiting cell viability than cisplatin alone, although the inhibitory efficacy was weaker than AMPKα knockdown. These data suggest that cisplatin-resistance in gastric cancer cells is partially related to increased expression of PINK1 and up-regulated ratio of LC3BII/I, and AMPK might affect cisplatin resistance through other pathways.

To observe the autophagosome formation in live cells, SGC7901 cells were transfected with GFP-LC3B plasmid. The punctate aggregates of GFP-LC3B were decreased in SGC7901 cells treated with cisplatin, which could be reversed by metformin (Figure 5A). Moreover, the results of TEM also indicated that autophagic vacuoles were detected in SGC7901 cells treated with metformin (Figure 5B). These results suggested that mitophagy was involved in metformin-induced cisplatin resistance. To furthermore confirm our speculation, AGS and SGC-7901 cells were pretreated with 3-methyladenine (3-MA) or Chloroquine (CQ) prior to cisplatin. As shown in Figures 5C, D, CQ significantly alleviated the inhibitory effect of metformin on cisplatin-induced growth inhibition in SGC-7901 and AGS cells. Similar outcomes were obtained when SGC7901 cells were pretreated with 3-MA (Figure 5E). These data suggest that metformin may promote cisplatin resistance in GC cells *via* PINK1/Parkin dependent mitophagy.

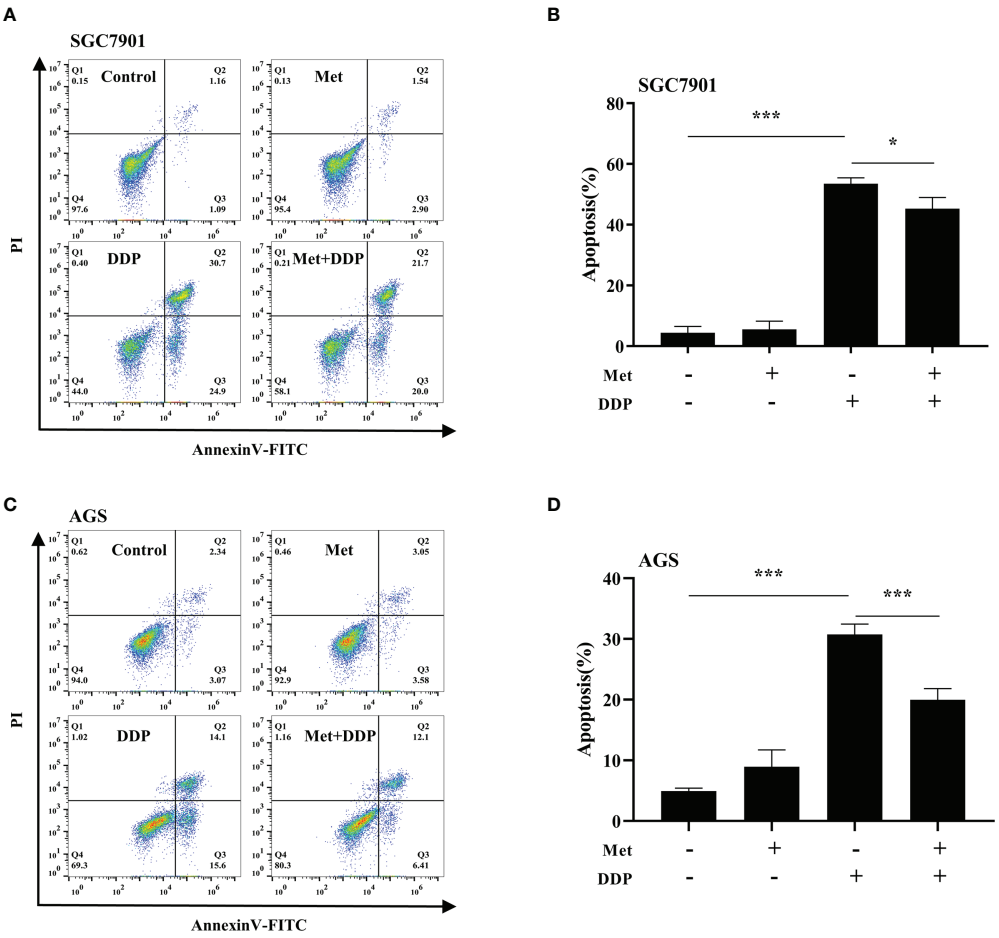

FIGURE 3
Metformin alleviates cisplatin-induced apoptosis in GC cells. **(A, B)** SGC-7901 cells were treated with metformin (10 mM), DDP (5 μg/mL), or the combination of metformin (10 mM) and DDP (5 μg/mL) for 24 h. **(C, D)** AGS cells were incubated with metformin (10 mM), DDP (10 μg/mL), or combination of metformin (10 mM) and DDP (10 μg/mL) for 24 h. Cell apoptosis was analyzed by Annexin V/PI staining. Bar diagram represents percentage of apoptotic cells. Data were presented as the means ± SD. The experiments were repeated three times. *p<0.05, ***p<0.001.

Metformin stimulated mitochondrial fission and decreased the intracellular ATP level in GC cells

As the increased mitochondrial fission was detected in SGC7901/DDP cells (Figures 1A, B), the influence of metformin on mitochondrial dynamics in GC cells was examined. To label mitochondria in live cells, two GC cell lines were transfected with transfected with pDsRed2-Mito plasmid. As shown in Figures 6A, B, mitochondria in GC cells appeared as the tubular networks or thread-like structures. In contrast, mitochondria were changed into punctate structures in GC cells treated with metformin, and metformin shortened the average length of mitochondria in GC cells (Figures S5A, B). Mitochondria are the major source for ATP production. Therefore, intracellular ATP level was detected in SGC-7901 and AGS cells. As expected, metformin significantly decreased the intracellular ATP levels in two GC cell lines (Figures 6C, D). All these results indicated that metformin regulated mitochondrial dynamics, which might contribute to mitophagy and prevent ATP generation.

Metformin induced mitophagy and cisplatin resistance through AMPK in GC cells

It is well-known AMPK acts as an upstream regulator of PINK1/Parkin dependent mitophagy and mitochondrial homeostasis. Hence, we examined if AMPK participated in metformin-induced cisplatin resistance *via* mitophagy. It was found that metformin up-regulated the expression of phos-

10.3389/fonc.2022.956190

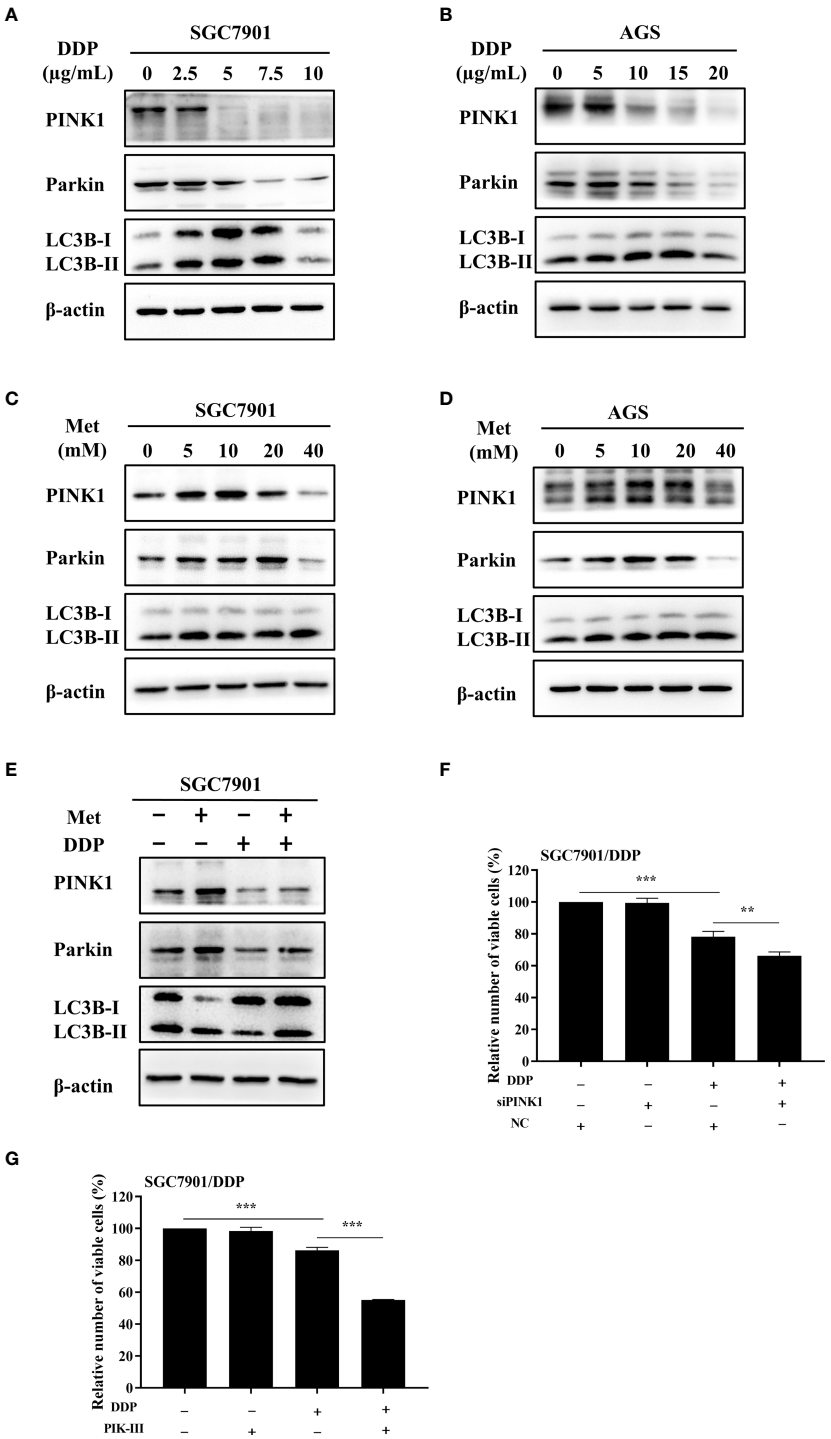

FIGURE 4
Metformin promoted cisplatin resistance *via* PINK1/Parkin axis in GC cells. **(A, B)** SGC7901 and AGS cells were treated with cisplatin and western blot was performed to determine the expression of PINK1, Parkin, LC3B. **(C, D)** SGC7901 and AGS cells were treated with indicated concentrations of metformin and western blot was performed to determine the expression of PINK1, Parkin, LC3B. **(E)** SGC7901 cells were pre-treated with 10 mM metformin for 4 h, followed by co-treating with 5 μg/mL cisplatin for 24h. The lysates were collected for western blot assay. **(F)** SGC7901/DDP cells were transfected with PINK1 siRNA or scramble siRNA (NC) for 24h and then treated with cisplatin. Cell proliferation was analyzed by CCK8 assay. **(G)** SGC7901/DDP cells were treated with cisplatin in the presence or absence of 5 μM PIK-III for 24 h. Cell proliferation was analyzed by CCK8 assay. Data were presented as the means ± SD. The experiments were repeated three times independently. $^{**}p<0.01$, $^{***}p<0.001$.

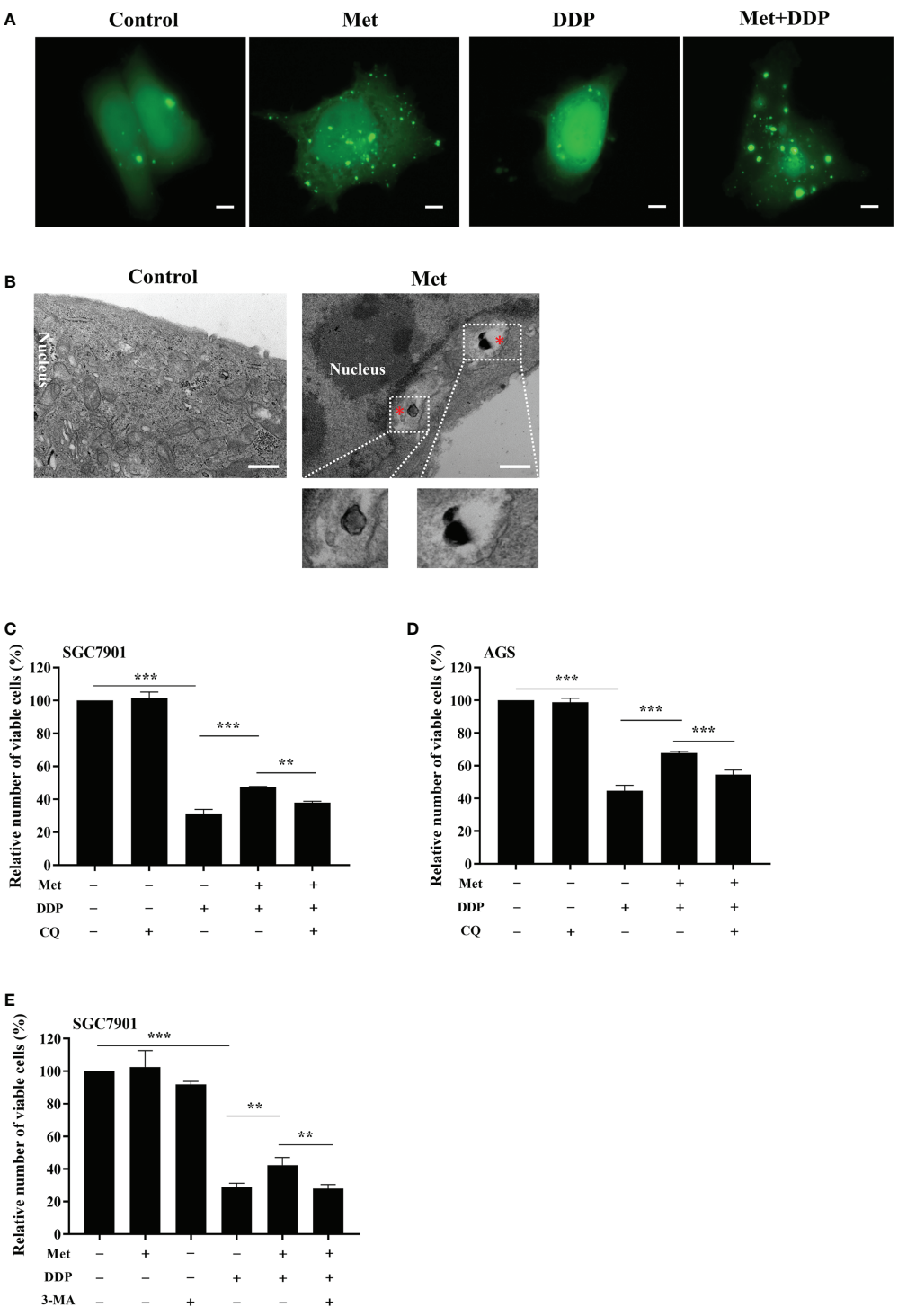

FIGURE 5
Metformin promoted cisplatin resistance *via* mitophagy in GC cells. **(A)** SGC7901 cells were transfected with pEGFP-LC3B for 24 h. Then cells were treated with indicated drug and analyzed by fluorescence microscopy. Scale bar=5 μm. **(B)** SGC7901 cells were treated with metformin and analyzed by transmission EM. Asterisk represents mitophagy vesicles. Circled images at higher magnification are shown in the below panels. Scale bar=0.5 μm. **(C, D)** SGC7901 and AGS cells were pre-treated with 10 mM metformin followed by co-treating with DDP in the absence or presence of 10 μM CQ for 24 **(h)** Cell viability was analyzed by CCK8 assay. **(E)** SGC7901 cells were pre-treated with 10 mM metformin followed by co-treating with cisplatin in the absence or presence of 5 mM 3-MA for 24 h. Cell proliferation was analyzed by CCK8 assay. Data were presented as the means ± SD. The experiments were repeated three times independently. $^{**}p<0.01$, $^{***}p<0.001$.

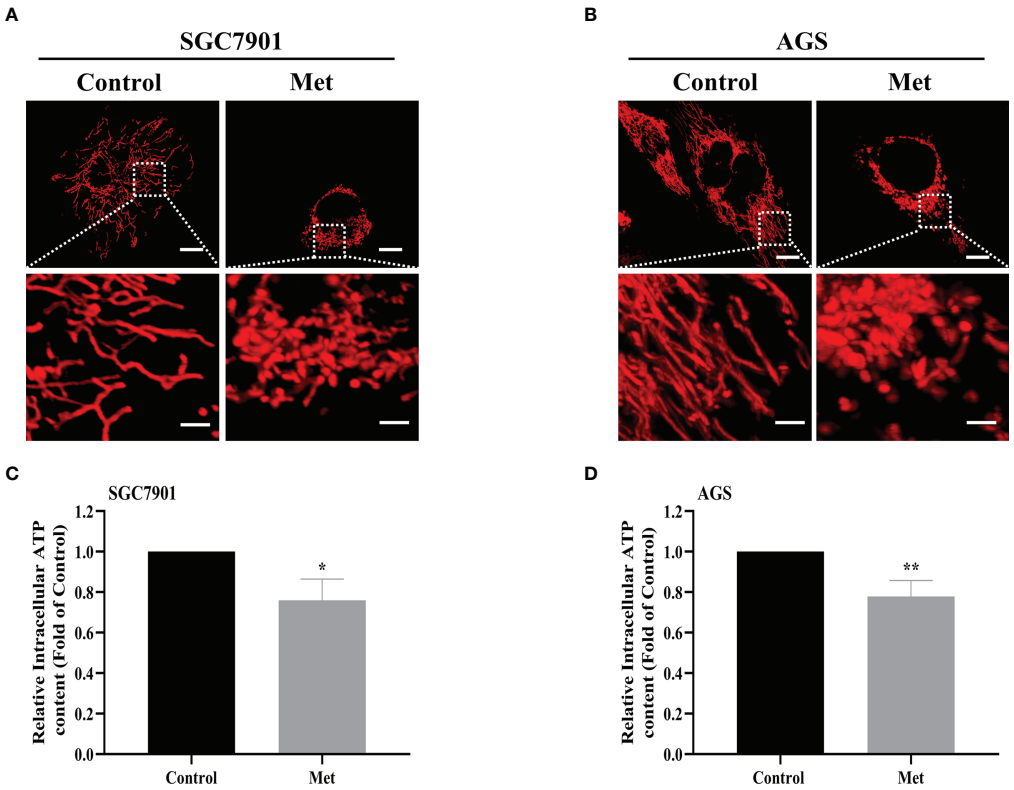

FIGURE 6
Metformin stimulated mitochondrial fission and decreased the intracellular ATP level in GC cells. **(A, B)** Mitochondrial morphology was shown. SGC7901 and AGS cells were transfected with pDsRed2-Mito and treated with or without 10 mM metformin for 24 h. Scale bar=10 μm. Circled images at higher magnification are shown in the below panels, scale bar=2 μm. **(C, D)** SGC7901 and AGS cells were incubated with 10 mM metformin for 24 h, then ATP levels were detected by ATP assay kit. Data were presented as the means ± SD. The experiments were repeated three times independently. *p<0.05; **p<0.01.

AMPKα (Thr172), but not total AMPK expression in SGC7901 cells (Figure 7A and Figure S6A). However, cisplatin down-regulated the expression of phos-AMPKα (Thr172), which was attenuated by pretreatment with metformin (Figure 7B and Figure S6B). To examine the role of AMPK in metformin-mediated mitophagy and cisplatin resistance, RNAi of AMPKα1 was conducted in SGC7901 cells using siRNAs. As shown in Figure 7C and Figure S6C, siRNA #2 showed the best knockdown efficiency on AMPKα1 expression. Thus, siRNA #2 was used for AMPKα1 silencing in the subsequent experiments. Intriguingly, knockdown of AMPKα1 by siRNA down-regulated the expression of PINK1, Parkin and LC3BII/I ratio in SGC7901 cells (Figure 7D and Figure S6D). In addition, AMPKα1 siRNA alleviated metformin-induced up-regulation of PINK1, Parkin and ratio of LC3BII/I in SGC7901 cells treated with cisplatin (Figure 7E and Figure S6E). Importantly, metformin mediated suppression on cisplatin-induced growth inhibition and apoptosis was also significantly prevented by AMPKα1 siRNA in SGC7901 cells (Figures 8A–C). In conclusion, all these data suggest that AMPK signaling may participate in the metformin-induced mitophagy, and metformin facilitates cisplatin resistance through AMPKα/PINK1/Parkin axis in gastric cancer cells.

Discussion

Gastric cancer is the third most common cause of cancer death globally. Primary or acquired drug resistance is the major challenge to GC therapy, which inevitably leads to recurrence and poor prognosis in clinic. Previous studies demonstrated that metformin exhibited anti-cancer properties, especially in patients with diabetes (22, 23). Mitophagy acts as a double-edged sword in the chemotherapy for gastric cancer (24, 25). However, the role of metformin-induced mitophagy in cisplatin resistance in GC remains unknown.

Combined application of metformin and cisplatin had shown controversial results in the treatment of various tumors. It has been reported that metformin could promote the anticancer effect of cisplatin in breast cancer (18), NSCLC

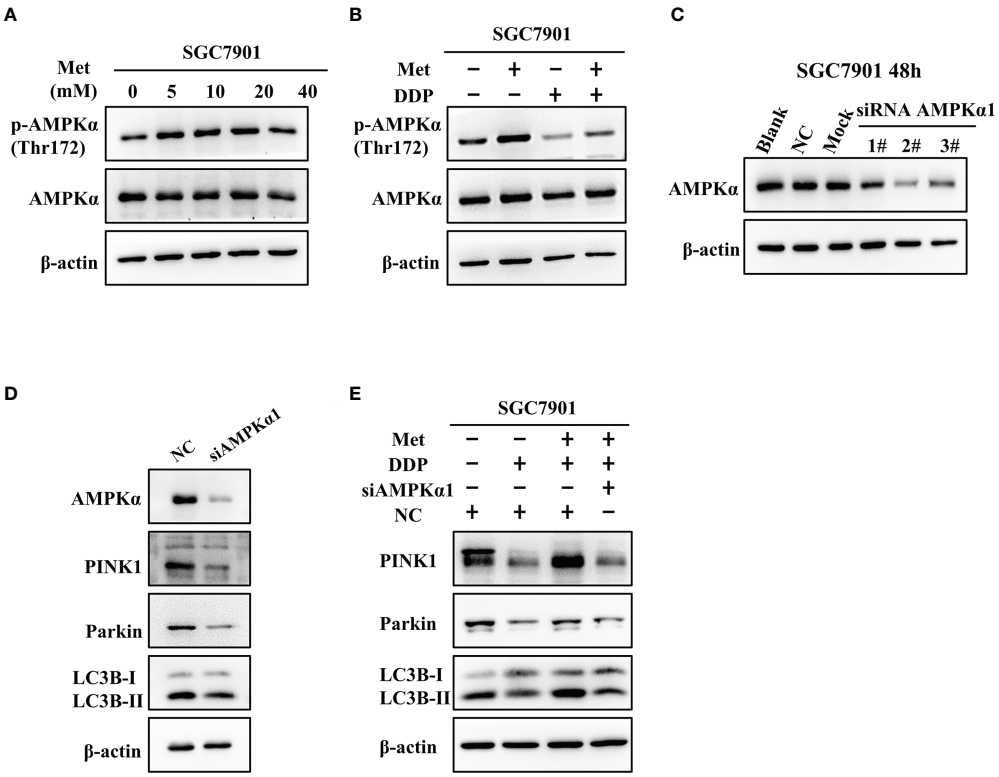

FIGURE 7
AMPK was involved in the metformin-induced up-regulation of mitophagy-related proteins in GC cells. **(A)** SGC7901 cells were treated with metformin for 24 h. The expression of AMPKα and phos-AMPKα (Thr172) was examined by western blot. **(B)** SGC7901 cells were pre-treated with 10 mM metformin followed by co-treating with 5 μg/mL cisplatin for 24 h. Then, cell lysates were collected for western blot using AMPKα- and phos-AMPKα (Thr172)-specific antibodies. **(C)** Expression of AMPK was determined by western blot in SGC-7901 cells transfected with siRNA-1~3 at 50nM or scramble siRNA (NC). **(D)** SGC7901 cells were transfected with control siRNA or AMPK siRNA#2 and the expression of PINK1, Parkin and LC3B was determined by western blot. **(E)** SGC7901 cells were transfected with scramble siRNA (NC) or AMPK siRNA#2 for 24 h. Then, cells were pre-treated with 10 mM metformin followed by co-treating with 5 μg/mL cisplatin for 24 h. The expression of PINK1, Parkin and LC3B was determined by western blot.

(26), nasopharyngeal carcinoma (20), liver cancer (27). On the contrary, metformin reduced the anti-proliferative effects of cisplatin through mTOR/AKT signaling pathways in the MKN-45 cells (28). Metformin could also protect OSCC cells from cisplatin toxicity by increasing glycolysis and intracellular NAD(P)H production (29). Additionally, metformin can reduce cisplatin sensitivity in cancer cells through the activation of Akt (30). In this study, we found that metformin alleviated cisplatin-induced growth inhibition in GC cells. Moreover, cisplatin-induced apoptosis was reversed by metformin. These data indicate that metformin promotes the development of cisplatin resistance in GC.

Mitophagy is a mitochondrial quality control system, which promotes tumorigenesis and cell survival by removing abnormal or damaged mitochondria (31). The PINK1/Parkin signaling is a canonical pathway that regulates mitophagy. Previous studies demonstrated that PINK1/Parkin dependent mitophagy can facilitate chemotherapy resistance in ovarian cancer (32), hepatic carcinoma (33, 34), breast adenocarcinoma (35) and lung cancer (36). The regulatory mechanism underlying metformin regulates PINK and Parkin expression and the ratio of LC3BII/I has been explored previously. It was reported that metformin protects against osteoarthritis through PINK1/Parkin-dependent mitophagy by up-regulating SIRT3 expression (37). Metformin alleviated renal oxidative stress and tubulointerstitial fibrosis *via* activating mitophagy through a p-AMPK-PINK1-Parkin pathway (38). In addition, metformin up-regulated the ratio of LC3BII/I and induced autophagy *via* AMPK/mTOR signaling pathway in hepatocellular carcinoma (39). Similar mechanism might also be involved in metformin-induced cisplatin resistance. Here, we showed that mitophagy was enhanced in cisplatin-resistant GC cells. Metformin activated PINK1/Parkin pathway, which resulted in mitophagy and cisplatin resistance in GC cells. Furthermore, pretreatment with mitophagy inhibitors, CQ and 3-MA, effectively attenuated metformin-induced cisplatin resistance in GC cells. AMPK is a

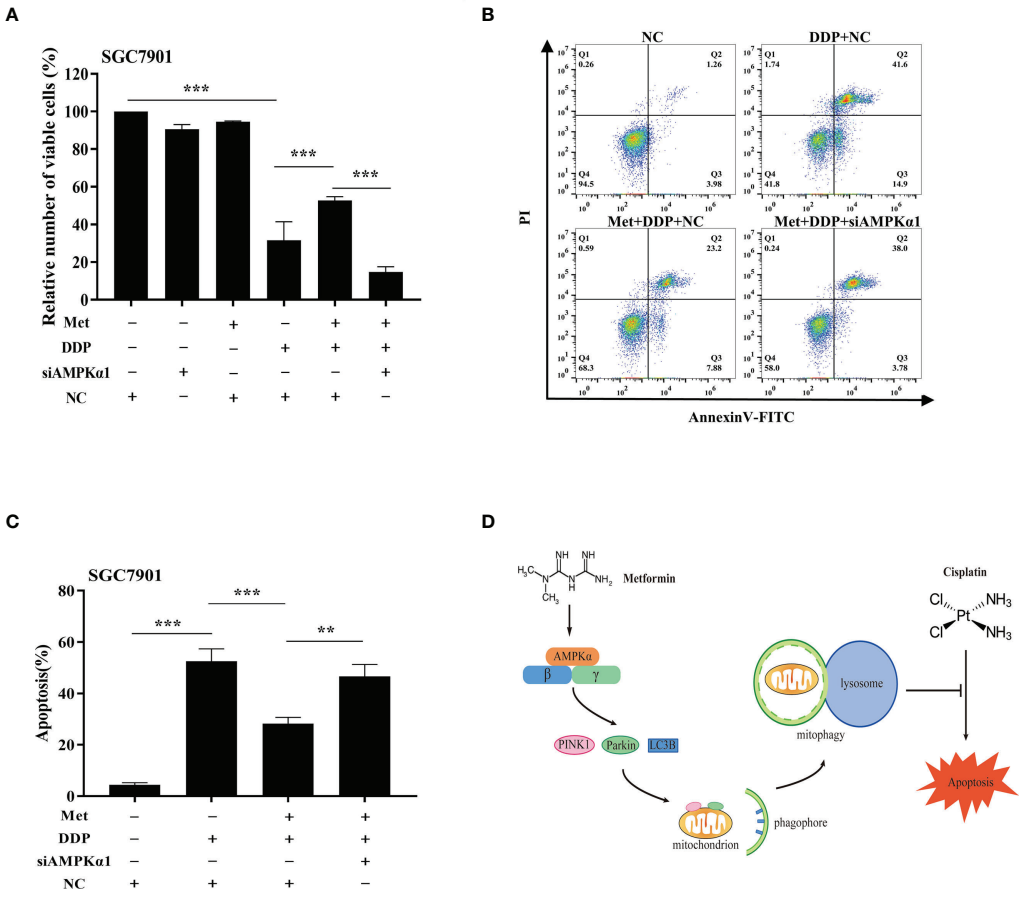

FIGURE 8
AMPK was involved in the metformin-induced mitophagy in GC cells. **(A)** SGC7901 cells were transfected with AMPK siRNA#2 or scramble siRNA (NC) for 24 h. Then, cells were pre-treated with 10 mM metformin followed by co-treating with 5 μg/mL cisplatin for 24 h. Cell viability was detected by CCK8 kit. **(B, C)** SGC7901 cells were transfected with scramble siRNA (NC) or AMPK siRNA#2 for 24 h. Then, cells were pre-treated with 10 mM metformin followed by co-treating with 5 μg/mL cisplatin for 24 h. Cell apoptosis was analyzed by Annexin V/PI staining. Bar diagram represents percentage of apoptotic cells. Data were presented as the means ± SD. The experiments were repeated three times independently. $^{**}p<0.01$, $^{***}p<0.001$. **(D)** A working model depicting the mechanism of metformin-induced cisplatin resistance in GC cells.

key regulator of PINK1/Parkin dependent mitophagy. Previous studies showed that metformin could activate AMPK by facilitating the phosphorylation at Thr172 on AMPK α (40, 41). Consistent with previous reports, up-regulation of phos-AMPKα (Thr172) was observed in GC cells following metformin treatment. Additionally, metformin-induced cisplatin resistance in GC cells could be counteracted by knockdown of AMPKα1 using siRNA. In conclusion, our results indicate that metformin may facilitate cisplatin resistance in GC cells by AMPK-PINK1/Parkin axis-mediated mitophagy.

On the other hand, mitochondrial dynamics is coordinated by balance between fusion and fission (42). Previous studies have suggested that mitochondrial dynamics could influence chemotherapy sensitivity in cancer cells. In our previous studies, it was found that mitochondrial dynamics participate in cisplatin resistance in ovarian cancer, and the level of mitochondrial fusion was higher in cisplatin resistant ovarian cancer cells (43). However, the contrary results were obtained in GC cells, as increased mitochondrial fission was observed in SGC-7901/DDP cells compared with that in SGC-7901 cells. Interestingly, increased mitochondrial fission and lower ATP level were detected in GC cells after metformin treatment. Since mitochondrial fission facilitates the occurrence of mitophagy, our results suggested that metformin-induced mitochondrial dynamics might also contribute to cisplatin resistance in GC cells.

In conclusion, we demonstrate metformin can promote resistance of GC cells to cisplatin through mitochondrial dynamics and AMPK-PINK/Parkin axis-mediated mitophagy (Figure 8D). It suggests mitochondrial dynamics as a promising target to overcome cisplatin resistance and improve the

chemotherapy efficacy in cancer treatment. Further, our findings warrant caution when considering metformin for treatment of diabetic patients with GC.

Data availability statement

The datasets presented in this study can be found in online repositories. The names of the repository/repositories and accession number(s) can be found in the article/ Supplementary Material.

Author contributions

Y-YX: investigation, methodology, and project administration. J-XX: investigation, methodology, and project administration. X-YW: formal analysis and writing-original draft preparation. TW: formal analysis and writing-original draft preparation. X-HQ: resources. L-PJ: formal analysis. F-FT: visualization. Z-PC: conceptualization and supervision. X-JH: conceptualization, supervision, writing- reviewing and editing, and funding acquisition. All authors contributed to the article and approved the submitted version.

Funding

This work was supported by National Natural Science Foundation of China (82060177), Major Discipline Academic and Technical Leaders Training Program of Jiangxi Province (20172BCB22028), the Research Fund for Jiangxi Geriatric Clinical Medical Research Centre (2020BCG74003), the Key Research and Development Program of Jiangxi Province (20192BBG70012) and the Key Projects from Department of Education of Jiangxi Province (GJJ218902).

Conflict of interest

The authors declare that the research was conducted in the absence of any commercial or financial relationships that could be construed as a potential conflict of interest.

Publisher's note

All claims expressed in this article are solely those of the authors and do not necessarily represent those of their affiliated organizations, or those of the publisher, the editors and the reviewers. Any product that may be evaluated in this article, or claim that may be made by its manufacturer, is not guaranteed or endorsed by the publisher.

Supplementary material

The Supplementary Material for this article can be found online at: https://www.frontiersin.org/articles/10.3389/fonc.2022.956190/full#supplementary-material

References

1. Smyth EC, Nilsson M, Grabsch HI, van Grieken NC, Lordick F. Gastric cancer. *Lancet (London England)* (2020) 396(10251):635–48. doi: 10.1016/s0140-6736(20)31288-5

2. Shen DW, Pouliot LM, Hall MD, Gottesman MM. Cisplatin resistance: A cellular self-defense mechanism resulting from multiple epigenetic and genetic changes. *Pharmacol Rev* (2012) 64(3):706–21. doi: 10.1124/pr.111.005637

3. Li X, He S, Ma B. Autophagy and autophagy-related proteins in cancer. *Mol Cancer* (2020) 19(1):12. doi: 10.1186/s12943-020-1138-4

4. Chen M, Chen Z, Wang Y, Tan Z, Zhu C, Li Y, et al. Mitophagy receptor Fundc1 regulates mitochondrial dynamics and mitophagy. *Autophagy* (2016) 12 (4):689–702. doi: 10.1080/15548627.2016.1151580

5. Shu L, Hu C, Xu M, Yu J, He H, Lin J, et al. Atad3b is a mitophagy receptor mediating clearance of oxidative stress-induced damaged mitochondrial DNA. *EMBO J* (2021) 40(8):e106283. doi: 10.15252/embj.2020106283

6. Eiyama A, Okamoto K. Pink1/Parkin-mediated mitophagy in mammalian cells. *Curr Opin Cell Biol* (2015) 33:95–101. doi: 10.1016/j.ceb.2015.01.002

7. Hung CM, Lombardo PS, Malik N, Brun SN, Hellberg K, Van Nostrand JL, et al. Ampk/Ulk1-mediated phosphorylation of parkin act domain mediates an early step in mitophagy. *Sci Adv* (2021) 7(15). doi: 10.1126/sciadv.abg4544

8. Yin K, Lee J, Liu Z, Kim H, Martin DR, Wu D, et al. Mitophagy protein Pink1 suppresses colon tumor growth by metabolic reprogramming *Via* P53 activation and reducing acetyl-coa production. *Cell Death Differ* (2021) 28(8):2421–35. doi: 10.1038/s41418-021-00760-9

9. Ziegler PK, Bollrath J, Pallangyo CK, Matsutani T, Canli O, De Oliveira T, et al. Mitophagy in intestinal epithelial cells triggers adaptive immunity during tumorigenesis. *Cell* (2018) 174(1):88–101 e16. doi: 10.1016/j.cell.2018.05.028

10. Bailey CJ. Metformin: Historical overview. *Diabetologia* (2017) 60(9):1566–76. doi: 10.1007/s00125-017-4318-z

11. Nathan DM, Buse JB, Davidson MB, Ferrannini E, Holman RR, Sherwin R, et al. Medical management of hyperglycemia in type 2 diabetes: A consensus algorithm for the initiation and adjustment of therapy: A consensus statement of the American diabetes association and the European association for the study of diabetes. *Diabetes Care* (2009) 32(1):193–203. doi: 10.2337/dc08-9025

12. Mogavero A, Maiorana MV, Zanutto S, Varinelli L, Bozzi F, Belfiore A, et al. Metformin transiently inhibits colorectal cancer cell proliferation as a result of either ampk activation or increased ros production. *Sci Rep* (2017) 7(1):15992. doi: 10.1038/s41598-017-16149-z

13. Al-Zaidan L, El Ruz RA, Malki AM. Screening novel molecular targets of metformin in breast cancer by proteomic approach. *Front Public Health* (2017) 5:277. doi: 10.3389/fpubh.2017.00277

14. Tadakawa M, Takeda T, Li B, Tsuiji K, Yaegashi N. The anti-diabetic drug metformin inhibits vascular endothelial growth factor expression *Via* the mammalian target of rapamycin complex 1/Hypoxia-inducible factor-1α signaling pathway in elt-3 cells. *Mol Cell Endocrinol* (2015) 399:1–8. doi: 10.1016/j.mce.2014.08.012

15. Tong D, Liu Q, Liu G, Xu J, Lan W, Jiang Y, et al. Metformin inhibits castration-induced emt in prostate cancer by repressing Cox2/Pge2/Stat3 axis. *Cancer Lett* (2017) 389:23–32. doi: 10.1016/j.canlet.2016.12.031

16. Pereira FV, Melo ACL, Low JS, de Castro ÍA, Braga TT, Almeida DC, et al. Metformin exerts antitumor activity *Via* induction of multiple death pathways in tumor cells and activation of a protective immune response. *Oncotarget* (2018) 9 (40):25808–25. doi: 10.18632/oncotarget.25380

17. Song Y, Chen Y, Li Y, Lyu X, Cui J, Cheng Y, et al. Metformin inhibits tgf-β1-Induced epithelial-to-Mesenchymal transition-like process and stem-like properties in gbm *Via* Akt/Mtor/Zeb1 pathway. *Oncotarget* (2018) 9(6):7023–35. doi: 10.18632/oncotarget.23317

18. Lee JO, Kang MJ, Byun WS, Kim SA, Seo IH, Han JA, et al. Metformin overcomes resistance to cisplatin in triple-negative breast cancer (Tnbc) cells by targeting Rad51. *Breast Cancer Res* (2019) 21(1):115. doi: 10.1186/s13058-019-1204-2

19. Fujita H, Hirose K, Sato M, Fujioka I, Fujita T, Aoki M, et al. Metformin attenuates hypoxia-induced resistance to cisplatin in the Hepg2 cell line. *Oncol Lett* (2019) 17(2):2431–40. doi: 10.3892/ol.2018.9869

20. Sun Y, Chen X, Zhou Y, Qiu S, Wu Y, Xie M, et al. Metformin reverses the drug resistance of cisplatin in irradiated cne-1 human nasopharyngeal carcinoma cells through pecam-1 mediated mrps down-regulation. *Int J Med Sci* (2020) 17 (16):2416–26. doi: 10.7150/ijms.48635

21. Cormio A, Guerra F, Cormio G, Pesce V, Fracasso F, Loizzi V, et al. Mitochondrial DNA content and mass increase in progression from normal to hyperplastic to cancer endometrium. *BMC Res Notes* (2012) 5:279. doi: 10.1186/1756-0500-5-279

22. Dulskas A, Patasius A, Kaceniene A, Linkeviciute-Ulinskiene D, Zabuliene L, Smailyte G. A cohort study of antihyperglycemic medication exposure and gastric cancer risk. *J Clin Med* (2020) 9(2). doi: 10.3390/jcm9020435

23. Shuai Y, Li C, Zhou X. The effect of metformin on gastric cancer in patients with type 2 diabetes: A systematic review and meta-analysis. *Clin Trans Oncol* (2020) 22(9):1580–90. doi: 10.1007/s12094-020-02304-y

24. Kim BR, Jeong YA, Kim DY, Kim JL, Jeong S, Na YJ, et al. Genipin increases oxaliplatin-induced cell death through autophagy in gastric cancer. *J Cancer* (2020) 11(2):460–7. doi: 10.7150/jca.34773

25. Russi S, Verma HK, Laurino S, Mazzone P, Storto G, Nardelli A, et al. Adapting and surviving: Intra and extra-cellular remodeling in drug-resistant gastric cancer cells. *Int J Mol Sci* (2019) 20(15). doi: 10.3390/ijms20153736

26. Moro M, Caiola E, Ganzinelli M, Zulato E, Rulli E, Marabese M, et al. Metformin enhances cisplatin-induced apoptosis and prevents resistance to cisplatin in Co-mutated Kras/Lkb1 nsclc. *J Thorac Oncol* (2018) 13(11):1692–704. doi: 10.1016/j.jtho.2018.07.102

27. Dong H, Huang J, Zheng K, Tan D, Chang Q, Gong G, et al. Metformin enhances the chemosensitivity of hepatocarcinoma cells to cisplatin through ampk pathway. *Oncol Lett* (2017) 14(6):7807–12. doi: 10.3892/ol.2017.7198

28. Lesan V, Ghaffari SH, Salaramoli J, Heidari M, Rostami M, Alimoghaddam K, et al. Evaluation of antagonistic effects of metformin with cisplatin in gastric cancer cells. *Int J hematology-oncology Stem Cell Res* (2014) 8(3):12–9.

29. Damelin LH, Jivan R, Veale RB, Rousseau AL, Mavri-Damelin D. Metformin induces an intracellular reductive state that protects oesophageal squamous cell carcinoma cells against cisplatin but not copper-Bis (Thiosemicarbazones). *BMC Cancer* (2014) 14:314. doi: 10.1186/1471-2407-14-314

30. Janjetovic K, Vucicevic L, Misirkic M, Vilimanovich U, Tovilovic G, Zogovic N, et al. Metformin reduces cisplatin-mediated apoptotic death of cancer cells through ampk-independent activation of akt. *Eur J Pharmacol* (2011) 651(1-3):41–50. doi: 10.1016/j.ejphar.2010.11.005

31. Yan C, Luo L, Guo CY, Goto S, Urata Y, Shao JH, et al. Doxorubicin-induced mitophagy contributes to drug resistance in cancer stem cells from Hct8 human colorectal cancer cells. *Cancer Lett* (2017) 388:34–42. doi: 10.1016/j.canlet.2016.11.018

32. Hu X, Wang J, Chai J, Yu X, Zhang Y, Feng Y, et al. Chaetomugilin J enhances apoptosis in human ovarian cancer A2780 cells induced by cisplatin through inhibiting Pink1/Parkin mediated mitophagy. *OncoTargets Ther* (2020) 13:9967–76. doi: 10.2147/ott.S273435

33. Yao N, Wang C, Hu N, Li Y, Liu M, Lei Y, et al. Inhibition of Pink1/Parkin-dependent mitophagy sensitizes multidrug-resistant cancer cells to B5g1, a new betulinic acid analog. *Cell Death Dis* (2019) 10(3):232. doi: 10.1038/s41419-019-1470-z

34. Wu H, Wang T, Liu Y, Li X, Xu S, Wu C, et al. Mitophagy promotes sorafenib resistance through hypoxia-inducible Atad3a dependent axis. *J Exp Clin Cancer Res* (2020) 39(1):274. doi: 10.1186/s13046-020-01768-8

35. Song L, Huang Y, Hou X, Yang Y, Kala S, Qiu Z, et al. Pink1/Parkin-mediated mitophagy promotes resistance to sonodynamic therapy. *Cell Physiol Biochem* (2018) 49(5):1825–39. doi: 10.1159/000493629

36. Dai K, Radin DP, Leonardi D. Pink1 depletion sensitizes non-small cell lung cancer to glycolytic inhibitor 3-bromopyruvate: Involvement of ros and mitophagy. *Pharmacol reports: PR* (2019) 71(6):1184–9. doi: 10.1016/j.pharep.2019.08.002

37. Han YC, Tang SQ, Liu YT, Li AM, Zhan M, Yang M, et al. Ampk agonist alleviate renal tubulointerstitial fibrosis *Via* activating mitophagy in high fat and streptozotocin induced diabetic mice. *Cell Death Dis* (2021) 12(10):925. doi: 10.1038/s41419-021-04184-8

38. Wang C, Yang Y, Zhang Y, Liu J, Yao Z, Zhang C. Protective effects of metformin against osteoarthritis through upregulation of Sirt3-mediated Pink1/Parkin-dependent mitophagy in primary chondrocytes. *Biosci Trends* (2019) 12 (6):605–12. doi: 10.5582/bst.2018.01263

39. Gao C, Fang L, Zhang H, Zhang WS, Li XO, Du SY. Metformin induces autophagy *Via* the ampk-mtor signaling pathway in human hepatocellular carcinoma cells. *Cancer Manag Res* (2020) 12:5803–11. doi: 10.2147/CMAR.S257966

40. Zhou G, Myers R, Li Y, Chen Y, Shen X, Fenyk-Melody J, et al. Role of amp-activated protein kinase in mechanism of metformin action. *J Clin Invest* (2001) 108(8):1167–74. doi: 10.1172/jci13505

41. Agius L, Ford BE, Chachra SS. The metformin mechanism on gluconeogenesis and ampk activation: The metabolite perspective. *Int J Mol Sci* (2020) 21(9). doi: 10.3390/ijms21093240

42. Wai T, Langer T. Mitochondrial dynamics and metabolic regulation. *Trends Endocrinol Metab* (2016) 27(2):105–17. doi: 10.1016/j.tem.2015.12.001

43. Zou GP, Yu CX, Shi SL, Li QG, Wang XH, Qu XH, et al. Mitochondrial dynamics mediated by Drp1 and Mfn2 contributes to cisplatin chemoresistance in human ovarian cancer Skov3 cells. *J Cancer* (2021) 12(24):7358–73. doi: 10.7150/jca.61379

frontiers | Frontiers in Oncology

TYPE Original Research
PUBLISHED 25 October 2022
DOI 10.3389/fonc.2022.981406

OPEN ACCESS

EDITED BY
Ying Liu,
Qingdao University, China

REVIEWED BY
Cuncun Lu,
China Academy of Chinese Medical Sciences, China
Manvendra Janmaijaya,
South Asian University, India

*CORRESPONDENCE
Nan Ji
jinan@mail.ccmu.edu.cn
Zhigang Zhao
1022zzg@sina.com

SPECIALTY SECTION
This article was submitted to Cancer Metabolism, a section of the journal Frontiers in Oncology

RECEIVED 29 June 2022
ACCEPTED 12 October 2022
PUBLISHED 25 October 2022

CITATION
Jiang R, Cao M, Mei S, Guo S, Zhang W, Ji N and Zhao Z (2022) Trends in metabolic signaling pathways of tumor drug resistance: A scientometric analysis.
Front. Oncol. 12:981406.
doi: 10.3389/fonc.2022.981406

Trends in metabolic signaling pathways of tumor drug resistance: A scientometric analysis

Ruiqi Jiang[1,2], Mingnan Cao[1], Shenghui Mei[1,2], Shanshan Guo[1], Wei Zhang[3], Nan Ji[4]* and Zhigang Zhao[1,2]*

[1]Department of Pharmacy, Beijing Tiantan Hospital, Capital Medical University, Beijing, China, [2]Department of Clinical Pharmacology, College of Pharmaceutical Sciences, Capital Medical University, Beijing, China, [3]Department of Neurology, Beijing Tiantan Hospital, Capital Medical University, Beijing, China, [4]Department of Neurosurgery, Beijing Tiantan Hospital, Capital Medical University, Beijing, China

Background: Cancer chemotherapy resistance is one of the most critical obstacles in cancer therapy. Since Warburg O first observed alterations in cancer metabolism in the 1950s, people gradually found tumor metabolism pathways play a fundamental role in regulating the response to chemotherapeutic drugs, and the attempts of targeting tumor energetics have shown promising preclinical outcomes in recent years. This study aimed to summarize the knowledge structure and identify emerging trends and potential hotspots in metabolic signaling pathways of tumor drug resistance research.

Methods: Publications related to metabolic signaling pathways of tumor drug resistance published from 1992 to 2022 were retrieved from the Web of Science Core Collection database. The document type was set to articles or reviews with language restriction to English. Two different scientometric software including Citespace and VOS viewer were used to conduct this scientometric analysis.

Results: A total of 2,537 publications including 1,704 articles and 833 reviews were retrieved in the final analysis. The USA made the most contributions to this field. The leading institution was the University of Texas MD Anderson Cancer Center. Avan A was the most productive author, and Hanahan D was the key researcher with the most co-citations, but there is no leader in this field yet. *Cancers* was the most influential academic journal, and Oncology was the most popular research field. Based on keywords occurrence analysis, these selected keywords could be roughly divided into five main topics: cluster 1 (study of cancer cell apoptosis pathway); cluster 2 (study of resistance mechanisms of different cancer types); cluster 3 (study of cancer stem cells); cluster 4 (study of tumor oxidative stress and inflammation signaling pathways); and cluster 5 (study of autophagy). The keywords burst detection identified several keywords as new research hotspots, including "tumor microenvironment," "invasion," and "target".

Conclusion: Tumor metabolic reprogramming of drug resistance research is advancing rapidly. This study serves as a starting point, providing a thorough overview, the development landscape, and future opportunities in this field.

KEYWORDS

scientometrics, tumor, metabolism, drug resistance, signaling pathways

Introduction

Drug resistance is prevalent in cancer treatment, and overcoming resistance is still one of the most pressing needs in cancer therapy (1). Drug resistance develops through a variety of mechanisms, including changes in drug transport and metabolism, mutation of the drug target, and activation of bypass survival pathways, which are frequently caused by tumor heterogeneity, allowing the escape and evolution of resistant cells (2). The intracellular physiology of drug-resistant cells is complex, with constant changes in energetic and oxidative-reductive metabolic signaling pathways (3).

The Warburg effect was first proposed by Warburg O in 1956 when he observed that many cancer cell lines relied on a high rate of glucose uptake and metabolism to maintain their viability despite being maintained in an oxygen-replete environment (4). It played an important role in tumor cell survival and proliferation, but the importance of metabolism in regulating drug resistance was only recently recognized (2). Scholars have now discovered some metabolic pathways of the Warburg effect and potential targets of these pathways that can improve drug resistance (5). In addition to glycolysis, other metabolic pathways of drug resistance have also been extensively studied in recent years, such as the pentose phosphate pathway (6), glutamine metabolism (7), and lipid metabolism (8).

In recent years, a significant number of researchers and academic journals have focused on reviewing relevant literature to summarize the current status of metabolic signaling pathways of tumor drug resistance. However, most of these papers have only centered on specific subfields of metabolic signaling pathways of tumor drug resistance (9, 10). For example, most reviews have paid attention to specific metabolic signaling pathways (11), autophagy (12), and targeted therapies (13). Little attention was paid to investigating the scientific output and current status systematically in this field from a global perspective, implying that there have been few reports focused on the scientometric perspective of this field. Therefore, it is critical to use an appropriate visualization method to reveal the global status, future research trends, and hotspots in this field.

Unlike systematic reviews, the scientometric analysis is a quantitative analysis of written scientific publications by analyzing data of these publications such as authors, countries, institutions, journals, and citations (14, 15). It may assist researchers in identifying core entities and development trends in a specific subject or research domain, as well as provide new insights and directions for future research (16).

At present, a variety of free tools have been developed for bibliometric mappings, such as Citespace and VOS viewer (15). CiteSpace V (Version 5.8 R3), a web-based Java application for data analysis and visualization, is an information visualization software tool created by Professor Chaomei Chen which visualizes the literature in the form of a co-citation network, which draws on article citations to reveal the structure of a field or fields (17). VOS viewer software is a scientometric visualization tool developed by Professor Eck and Waltman from Leiden University in the Netherlands using the Java language, which could visualize the knowledge structure, regularity, and distribution of scientific publications (18).

Rewiring of cell metabolism and bioenergetics is a characteristic feature of cancer development and has recently been recognized as a hallmark of cancer. However, the extent of the benefits these metabolic alterations provide to cancer cells is still not fully understood, particularly in terms of drug sensitivity and resistance. Even though current treatments can reduce tumor size and increase life expectancy, the main reason for the high mortality of cancer is the lack of effective treatments to overcome the natural acquisition of resistance (19). To the best of our knowledge, no previous study has specifically analyzed the knowledge structure and research frontiers in the field of metabolic signaling pathways of tumor drug resistance yet. As a result, this study is the first attempt to address this research gap. We use Citespace and VOS viewer to conduct a scientometric analysis of this field on the Web of Science Core Collection database from 1992 to 2022. This study aimed to (i) summarize the current research trends in this field, (ii) determine the knowledge structure, including the major academic groups and cooperation networks, (iii) identify the major participants and their collaboration networks, (iv) analyze

research status and hotspots, (v) summarize the main research themes and clusters, and (vi) offer a new line of thinking.

Materials and methods

Data source

Data from the Science Citation Index Expanded (SCI-Expanded) database of the Web of Science Core Collection (WOS) was used in this study. The reasons for choosing this database are as follows. First of all, when compared to other databases such as PubMed and Embase, WOS is the most widely used, comprehensive, and authoritative tool for scientometric analysis across scientific disciplines (20). Following that, WOS is a typical citation database including citation and research collaboration information, facilitating scientometric analysis (21). Last but not least, the reference files provided by WOS could meet the specific format requirements as dictated by VOS viewer, Citespace, and other scientometric software (20, 22). An additional process is required to convert file format if downloaded from other databases. Given that our objective was to conduct a high-quality scientometric analysis to identify research trends in the core of metabolic signaling pathways of tumor drug resistance, WOS may be the only appropriate choice.

Data collection

We performed online retrieval on 26 July 2022. Search terms used were chosen from the list of Medical Subject Headings (MeSH) and free text key terms were used as well. The following free terms were used: tumor, tumors, neoplasm, neoplasia, neoplasias, cancer, cancers, malignancy, malignancies, multidrug resistance, multiple drug resistance, metabolic pathways, metabolic pathway, metabolic networks, metabolic network, and metabolic signaling. The following MeSH terms were used: neoplasms, drug resistance, and metabolic networks and pathways. Therefore, the search terms and retrieval strategies were developed as follows: ((ALL= (neoplasias* OR tumor* OR cancer* OR malignanc*)) AND ALL= (drug resistance OR multidrug resistance OR multiple drug resistance)) AND ALL= (metabolic pathway* OR metabolic network* OR metabolic signaling). The MeSH term "Neoplasms" means new abnormal growth of tissue, malignant neoplasms show a greater degree of anaplasia and have the properties of invasion and metastasis, compared to benign neoplasms. Timespan: 1992 to 2022. The language type was limited to English. Original articles and reviews were included, while proceedings papers, early access, book chapters, editorial materials, meeting abstracts, and letters were excluded. The search retrieved a total of 2,537 records. Full records and cited references were downloaded in plain text format. Then the data files were imported into the software package CiteSpace (Version 5.8.R3) and VOS viewer (Version 1.6.18).

Data analysis

CiteSpace and VOS viewer software were used for visual analysis, then Excel 2019 was used for quantitative analysis of the included literature. Co-authorship analysis refers to the evaluation of the relationship among items based on the number of coauthored documents, which were considered one of the most tangible indicators to evaluate collaboration trends and identify leading countries, institutions, and scientists (23, 24). Co-citation refers to when two or more authors or references are simultaneously cited in one or more subsequent papers, which is called a co-cited relationship between these two or more authors or references (25, 26). Author co-citation analysis can discover highly influential scholars in a discipline area. When references were frequently cited at the same time, indicating these studies were highly correlated and had similar research topics. The relatedness of co-occurrence analysis is determined based on the number of documents in which they occur together (24). The burst detection of references and keywords was based on Kleinberg's algorithm, which can recognize sharp increases in scientific activity over a short time and capture the growing research interest in a specific research field (27).

Parameter Settings of CiteSpace: the period is from 1992 to 2022, the time zone is divided into one year, and the threshold (Top N) is set to 50, which means extracting the 50 nodes with the highest frequency every year. In the present study, this software was implemented for constructing network visualization of author co-authorship analysis, the co-occurring network of subject categories, as well as detecting the references and keywords with the strongest citation bursts.

Then, we use VOS viewer software to create co-authorship, co-citation, and co-occurrence networks in this field. Specifically, country co-authorship analysis, institution co-authorship analysis, author co-citation analysis, co-citation references analysis, and keyword co-occurrence analysis were performed and three visualization maps, including the network visualization map, the overlay visualization map, and the density visualization map were constructed in this study. Each node represents an individual country, and the node size is proportional to the number of publications. Line thickness between nodes indicates the link strength of a collaborative relationship and it is weighted by a quantitative evaluation indicator of total link strength (TLS). For a given item, the TLS attributes indicate the total strength of the links of an item with other items (28). For example, in the case of co-authorship links between researchers, the TLS attribute indicates the total strength of the co-authorship links of a given researcher with other researchers (29).

Apart from the above methods, an online visualization platform (https://www.datawrapper.de/) was also used to perform a geographical distribution map.

Results and discussion

Analysis of publications and citations

A total of 2,537 publications in WOS including 1,704 articles and 833 reviews were collected from 1992 to 2022 for further analysis (Figure 1). The cumulative total citations for all articles were 96,002 times, including 2,102 times of self-citations by 26 July 2022, and an average of approximately 37.8 per document. A total of 8,053 publications in PubMed were collected from 1992 to 2022. The changing trend of annual publications and citations of published papers of WOS and annual publications of published papers of PubMed databases from 1992 to 2022 are shown in Figures 2, S1. Although PubMed databases could provide a broader range of coverage, much of the "extra coverage" could be attributed to journals with potentially limited readers (22). Research on metabolic signaling pathways of tumor drug resistance could be divided into three stages: the initial stage from 1992 to 2003, the second stage from 2004 to 2011, and the third stage from 2012 to 2022. The initial stage lasted for 12 years, during which the number of annual publications was less than 10. In the second stage, the number of annual publications increased slightly, but none exceeded 60. Since 2012, the number of annual publications had grown rapidly, and in 2014, the number of papers exceeded 100 for the first time. In addition, the total number of papers published in this period accounted for 87.62% of the papers included in the entire period. Moreover, the total citations showed a trend similar to that of annual publications. According to the current data, metabolic signaling pathways of tumor drug resistance is an emerging field with significant progress, and the interest of researchers in this field has surged. It can be predicted that more research on metabolic signaling pathways of tumor drug resistance will be published in the future.

Country/region analysis

Of these 2,537 publications, 84 countries/regions have so far contributed to the publications on metabolic signaling pathways of tumor drug resistance research. Publications from Taiwan, Hong Kong, and Macau were assigned to China, and those from England, Northern Ireland, Scotland, and Wales were reclassified to the UK. As shown in Table 1, the top three countries with the most publications were the USA, China, Italy, and other countries that published <200 papers. A geographical distribution map based on the total publications of different countries is presented in Figure 3. In addition, considering that there were substantial differences in the number of populations among countries, which may have a direct impact on research achievements, another index of paper per million people was introduced for further analysis (24, 28). It can be used to compare author activity in different countries/

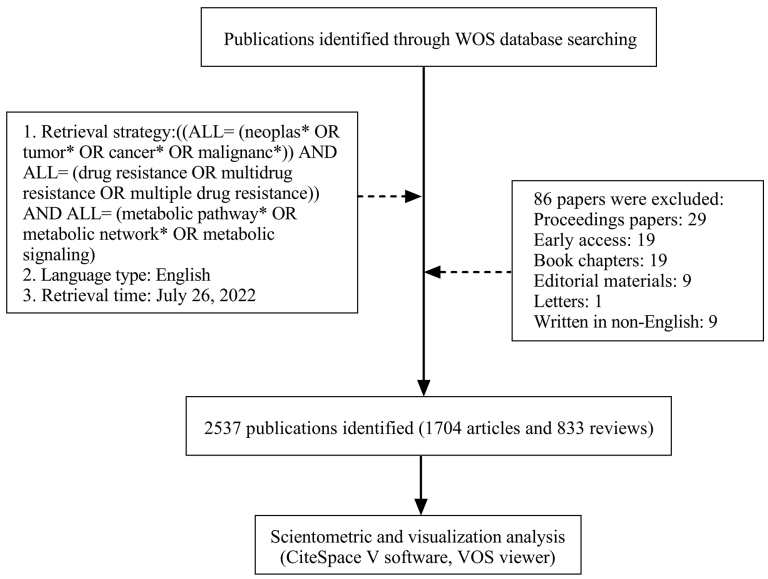

FIGURE 1
Flow chart of literature search and analysis.

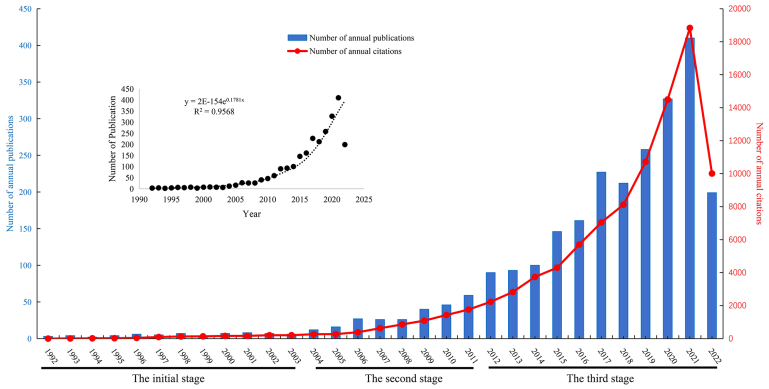

FIGURE 2
Distribution of the annual published documents and citations research related to metabolic signaling pathways of tumor drug resistance from 1992 to 2022.

regions. The latest demographic data (2021) were obtained from the World Bank official website (https://data.worldbank.org/indicator/SP.POP.TOTL) (30). After adjusting by population size, Sweden was on top with 4.80 papers per million people, followed by Italy (3.67) and the Netherlands (3.48), while the USA was only in the fifth position. Authors from North America, Eastern Asia, and Western Europe produced the majority of scientific publications in this field. The total amount of publications from these three regions were similar, and Western European authors were slightly more active than others.

In addition, Figure S2 illustrates the co-authorship among countries' visualization map. As we can see from the map, active collaboration was observed between prolific countries. For example, the USA collaborated closely with China and Spain. The top three with the largest TLS countries were the USA, the UK, and China.

Journal analysis

We have listed the top 10 most productive journals on metabolic signaling pathways of tumor drug resistance research in Table S1. These 10 prolific journals published 486 papers, constituting 19.16% of all 2,537 publications. Among the top 10 journals, the most noteworthy journal was *Cancers*,

TABLE 1 The top 15 productive countries contributed to publications on metabolic signaling pathways of tumor drug resistance research.

Ranking	Countries	Output [n (%)]	Population(in millions) (26)	Number of papers per million people	Optimized ranking	TLS	ACI
1	USA	894 (35.24%)	331.89	2.69	5	624	52.02
2	China	646 (25.46%)	1412.36	0.46	14	248	23.90
3	Italy	217 (8.55%)	59.07	3.67	2	194	37.65
4	UK	162 (6.39%)	67.33	2.41	7	248	47.09
5	Germany	157 (6.19%)	83.13	1.89	9	230	53.16
6	Spain	124 (4.89%)	47.33	2.62	6	129	40.63
7	Japan	123 (4.85%)	125.68	0.98	13	90	44.09
8	France	119 (4.69%)	67.50	1.76	10	154	33.93
9	India	94 (3.71%)	1393.41	0.07	15	62	21.21
10	Iran	85 (3.35%)	85.03	1.00	12	80	20.33
11	Canada	84 (3.31%)	38.25	2.20	8	97	40.95
12	Australia	79 (3.11%)	25.74	3.07	4	101	52.03
13	South Korea	73 (2.88%)	51.74	1.41	11	41	27.63
14	Netherlands	61 (2.40%)	17.53	3.48	3	85	42.44
15	Sweden	50 (1.97%)	10.42	4.80	1	102	42.10

TLS, Total link strength; ACI, Average citations per item.

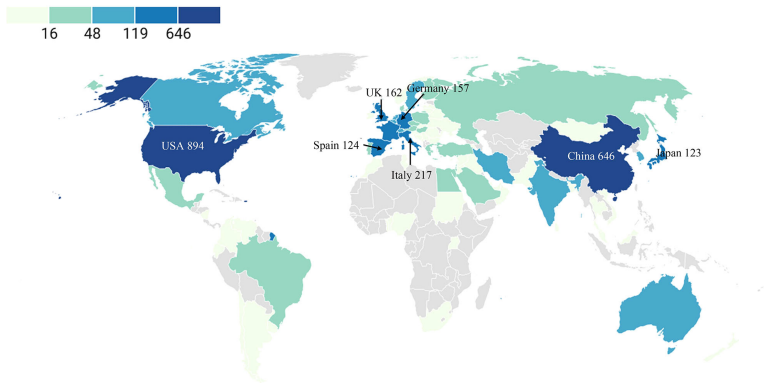

FIGURE 3
Geographic distribution map based on the total publications of different countries.

followed by *Frontiers in Oncology*, and *International Journal of Molecular Sciences*. It is not difficult to find that research outputs are mainly published in these journals focused on Oncology and Pharmacy. According to the 2021 Journal Citation Reports (JCR) reported, the impact factor (IF) of all the top 10 journals ranged from 3.752 (*Plos One*) to 13.312 (*Cancer Research*), and all journals were categorized in Q1 or Q2 except *Oncotarget*. Moreover, all the top 10 journals were hosted by North American (the USA) and Western European (England and Switzerland) countries, which might be one of the important factors for Euro-American countries to dominate this field.

Author analysis

Table S2 shows the top 20 authors according to the publication numbers in this field. Most of these authors came from the USA, Iran, and China. Avan A from Mashhad University Medical Science was the most productive author with 19 papers, followed by Mirzaei H from Kashan University of Medical Sciences with 14 papers. Most authors only contributed one or two papers, indicating that a few authors made sustained contributions to this field. The authors' co-authorship relationship network map is demonstrated in Figure S3A. The centrality index for each author was 0.0, and a quite small number of connection links were shown in the network map, which reflected that the collaboration between different research teams was not very common. Therefore, it's necessary to improve international communication between research groups to promote the development of this field.

What's more, collaborative maps of co-cited authors contributed to publications on metabolic signaling pathways of tumor drug resistance research by VOS viewer are shown in Figure S3B, and the top 20 co-cited authors are listed in Table S3. The color of the nodes and lines indicated different appearance clusters. The node size is proportional to citation frequency. A line between two nodes indicates that both were cited by one author. The association between items is created based on the number of times they are cited jointly by a third citing item, which is known as co-citation analysis (31). As can be seen from Figure S3B, co-cited authors could be roughly divided into four clusters. The authors in Cluster 1 (red nodes) focused on anticancer therapy targeting cancer cell metabolism, especially colorectal cancer (32); the authors in cluster 2 (green nodes) focused on the Warburg effect (33); the authors in cluster 3 (blue nodes) focused on autophagy dysfunction in cancer (34); the authors in cluster 4 (yellow nodes) focused on aging and cancer (35). The top 3 authors with the greatest TLS were as follows: Hanahan D, Warburg O, and Kim J. Compared with the top 20 productive authors, no author was included in the list of the top 20 co-cited authors, indicating that there is no leading figure in this field yet.

Table S4 illustrates the top 20 authors with the strongest citation bursts from 1992 to 2022. The top-ranked author by bursts was Jemal A and followed by Gatenby RA and Laplante M. Gottesman MM (36) was the first author who received special attention in this field in 2003. Bray F worked on cancer epidemiology (37), which was the most recent burst and has lasted for 2 years now.

Institution analysis

As for institutions analysis, the top 15 most prolific institutions and the number of publications in each institution are presented in Figure S4. The top 15 institutions, with 476 published articles, accounted for 20.13% of total publications. Among these six institutions originated from North America, seven from Asia, and two came from Western Europe. The most

prolific individual institution in terms of the number of publications was the University of Texas MD Anderson Cancer Center, followed by the National Cancer Institute and the Chinese Academy of Sciences. This may be one of the reasons for the high number of papers published in these regions.

Besides, the institution citation analysis was performed by VOS viewer (Figure S5). The top 3 institutions with the largest TLS were Sun Yat-sen University, the University of Texas MD Anderson Cancer Center, and the University of Florence. Surprisingly, Sun Yat-sen University and the University of Florence were not the top 3 productive institutions, but they still had such high impacts, indicating that they had performed a lot of high-quality research. In addition, the University of Texas MD Anderson Cancer Center was the most productive and influential institution.

Subject category analysis

Depending on the content classification of the Web of Science database, the study of metabolic signaling pathways of tumor drug resistance was distributed across 89 specific subject categories. The top 15 research areas covered by the leading journals are illustrated in Figure 4. The most represented categories based on the number of publications were Oncology, Biochemistry and Molecular Biology, and Pharmacology/Pharmacy. The co-occurring subject categories network of this field by using CiteSpace is mapped in Figure S6. A purple ring on the edge of the node represents that this node has a high betweenness centrality, in other words, indicates its critical role in bridging the nodes it links. The top five subject categories ranked by centrality were Biochemistry and Molecular Biology (0.46), Oncology (0.40), Pharmacology/Pharmacy (0.30), Cell Biology (0.19), and Biotechnology and Applied Microbiology (0.12). Taking the above results into consideration, it can be noted that intranasal delivery research involves multiple disciplines. Pharmacology/Pharmacy and Neurosciences/Neurology were the hottest research categories in this field. Research on metabolic signaling pathways of tumor drug resistance has covered multidisciplinary knowledge and interdisciplinary collaboration among different fields might help to improve scientific work and maximize the potential.

Research topics and clusters of global publications

Analysis of highly co-cited references

High-cited publications usually refer to high-quality studies with significant influence and innovation in a certain subject and have received greater attention in this field (38). The details of the top 10 co-citations of original articles related to metabolic signaling pathways of tumor drug resistance are shown in Table 2. Three of the top 10 references were published in 2013, and others were published before 2010. All of them were co-cited less than 50 times. Among them, the most highly cited reference was an article by Subramanian A (39) with 49 times. They described a powerful analytical method called Gene Set Enrichment Analysis (GSEA) for interpreting gene expression data. The common tumor signatures are closely associated with various tumor types. Tumor signatures identified through the gene set enrichment analysis based on gene expression profiling could help to establish and validate metabolism-related prognostic models, discovering drug resistance signaling pathways (40). Notably, the eighth article (41) provided another gene lists analysis protocol explaining how to use DAVID bioinformatics resources, which consisted of an integrated biological knowledge base and analytic tools aimed

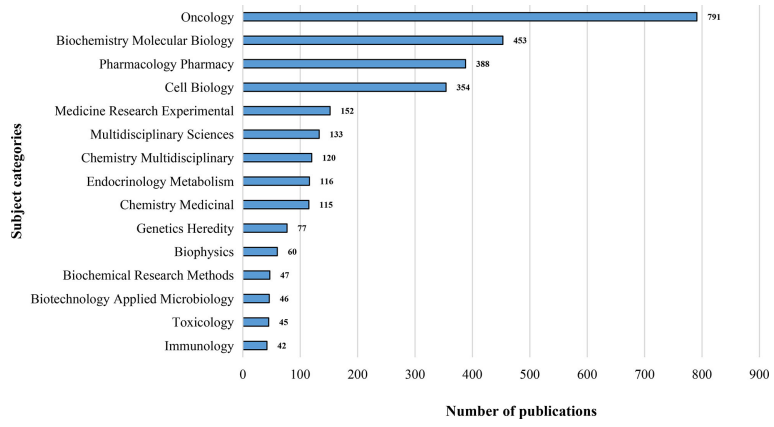

FIGURE 4
The top 15 subject categories related to metabolic signaling pathways of tumor drug resistance.

TABLE 2 The top 10 co-citation of original articles.

Ranking	Title	Total citations	Journal	First author	Year
1	Gene set enrichment analysis: a knowledge-based approach for interpreting genome-wide expression profiles	49	Proceedings of the National Academy of Sciences of The United States of America	Subramanian A	2005
2	HIF-1-mediated expression of pyruvate dehydrogenase kinase: a metabolic switch required for cellular adaptation to hypoxia	47	Cell Metabolism	Kim JW	2006
3	Oncogenic BRAF regulates oxidative metabolism via PGC1α and MITF	46	Cancer Cell	Haq R	2013
4	Glutamine supports pancreatic cancer growth through a KRAS-regulated metabolic pathway	41	Nature	Son J	2013
5	PGC1α expression defines a subset of human melanoma tumors with increased mitochondrial capacity and resistance to oxidative stress	41	Cancer Cell	Vazquez F	2013
6	The M2 splice isoform of pyruvate kinase is important for cancer metabolism and tumour growth	40	Nature	Christofk HR	2008
7	c-Myc suppression of miR-23a/b enhances mitochondrial glutaminase expression and glutamine metabolism	40	Nature	Gao P	2009
8	Systematic and integrative analysis of large gene lists using DAVID bioinformatics resources	40	Nature Protocols	Huang da W	2009
9	Myc regulates a transcriptional program that stimulates mitochondrial glutaminolysis and leads to glutamine addiction	40	Proceedings of the National Academy of Sciences of The United States of America	Wise DR	2008
10	Inhibition of glycolysis in cancer cells: a novel strategy to overcome drug resistance associated with mitochondrial respiratory defect and hypoxia	40	Cancer Research	Xu RH	2005

at systematically extracting biological meaning from large gene/protein lists.

Other papers (42–49) all focused on the Warburg effect, which referred to many cancer cell lines depending on a high rate of glucose uptake and metabolism to maintain their viability despite being maintained in an oxygen-replete environment (33). This metabolic phenotype had been termed aerobic glycolysis. Xu RH (49) proposed that depletion of ATP by glycolytic inhibition induced apoptosis in multidrug-resistant cells, therefore, deprivation of cellular energy supply might be an effective way to overcome multidrug resistance. Vazquez F (47) and Haq R (44) reported that the oncogenic melanocyte lineage-specification transcription factor MITF drove PGC1α overexpression in a subset of human melanomas and derived cell lines. In addition, Haq R (44) found that melanomas with activation of the BRAF/MAPK pathway had suppressed levels of MITF and PGC1α, and decreased oxidative metabolism. Gao P (43) and Wise DR (48) described that oncogenic levels of Myc induced a transcriptional program that promoted glutaminolysis and triggered cellular addiction to glutamine as a bioenergetic substrate.

Moreover, a co-citation network visualization map of references generated by the VOS viewer was shown in Figure S7. The color of the nodes and lines indicated different appearance clusters. The node size is proportional to citation frequency. A line between two nodes indicates that both were cited by one reference. The co-citation references could be roughly divided into five main topics: cluster 1 (red nodes) study of signaling pathways in the mutated gene in human cancer (41); cluster 2 (green nodes) study of the Warburg effect (50); cluster 3 (blue nodes) study of oxidative stress (51); cluster 4 (yellow nodes) study of cell metabolism regulator (52); cluster 5 (violet nodes) study of glutamine metabolism to cancer therapy (48). The reference of Hanahan D was located in central positions within the network. The review by Hanahan D published in 2011 (53) revisited, refined, and extended the concept of cancer hallmarks, and provided a useful conceptual framework for understanding the complex biology of cancer. They proposed that reprogramming energy metabolism was an emerging hallmark, and the role of aerobic glycolysis in malignant growth would be elucidated during the coming decade. The review by Vander Heiden MG published in 2009 (50) was another highly co-cited reference. They proposed that the metabolism of cancer cells, and indeed all proliferating cells, was adapted to facilitate the uptake and incorporation of nutrients into the biomass needed to produce a new cell.

Analysis of references with citation burst

References with citation bursts can be used to examine thematic trends due to bias between old and newly published literature. A citation burst shows that academia has paid extra attention to cited papers (54). Table S5 illustrates the top 25 references (44, 50, 53, 55–76) with the strongest citation bursts from 1992 to 2022 conducted through CiteSpace. The minimum duration of the burst was set for five years, and a red line segment represented the initial and final years of the burst duration. Reference with citation burst was first observed in 2011, which is due to a review by Vander Heiden MG in 2009 (50). This review related to Warburg Effect was also the second most highly cited reference which indicated that this article had

received special attention from associated academic circles in the past period. The most recent burst appeared in 2020 and has lasted for 1 year by now. The publication reviewed known cancer-associated metabolic changes into six hallmarks that have been identified as the strongest burst references since 2017 and the burst remains ongoing (55). Glycolysis and lipid metabolism were two metabolic pathways that attracted more attention, and researchers had discovered some drug resistance targets in these metabolic pathways, such as MYC and MCL1 cooperated in the maintenance of triple-negative breast cancer (56) and JAK/STAT3 regulated lipid metabolism and promoted breast cancer chemoresistance (57). In addition, cancer statistics were another topic of high interest (58–60). This reflects the importance and necessity of studying metabolic signaling pathways of tumor drug resistance and may be related to the major scientific progress made in this field in recent years.

Analysis of co-occurrence keywords

Analyzing the results of keywords co-occurrence can identify the research hotspots and frontiers of metabolic signaling pathways of tumor drug resistance. The keyword co-occurrence visualization map was constructed with VOS viewer. A density visualization map is shown in Figure S8, "drug resistance" was the most frequent keyword, followed by "cancer", "expression", "resistance", and "metabolism". This was consistent with our research theme. To further investigate the topic structure of metabolic signaling pathways of tumor drug resistance research, we also used CiteSpace to draw a keyword co-occurrence visualization map (Figure S9).

In addition, the overlay visualization map and network visualization map of keyword co-occurrence analysis are shown in Figures 5, S10, respectively. As can be seen from Figure S10, 192 keywords that occurred at least 20 times could be roughly divided into five main topics: cluster 1 (red nodes, upper right of the network); cluster 2 (green nodes, bottom side of the network); cluster 3 (blue nodes, bottom left of the network); cluster 4 (yellow nodes, bottom right of the network); cluster 5 (violet nodes, upper left of the network).

Cluster 1: Study of cancer cell apoptosis pathway

Cluster 1 was the largest cluster with 48 keywords, and the primary keywords were cancer, expression, resistance, apoptosis, pathway, inhibition, growth, cells, activation, and mechanism. Several researchers have investigated that intracellular apoptosis pathways in human cancers abnormally activated significantly promoted tumor progression, regulation of cell metabolism, and the development of drug resistance to chemotherapeutics (77). For example, Nuan-Aliman, S (78). reported that the alternative NF-κB pathway impacted diffuse large B-cell lymphoma cell energy homeostasis enhanced oxidative phosphorylation energy metabolism, and drove resistance of cells to apoptosis induced by mitochondrial metabolic stress upon treatment with two approved anti-metabolic drugs, or glutamine deprivation. Therefore, finding inhibitors that exerted a targeted therapeutic effect is an efficient method to relieve apoptosis inhibition and drug resistance, such as HSF1 inhibitor KRIBB11 (79), BCL-2 inhibitor Venetoclax (80), and ligustrazine-curcumin hybrids 10d (81).

Cluster 2: Study of resistance mechanisms of different cancer types

Cluster 2 was the second-largest cluster with 46 keywords. This cluster mainly focused on resistance mechanisms of different cancer types including the following keywords: *in-vitro*, multidrug resistance, hepatocellular carcinoma, colorectal cancer, tumor microenvironment, p-glycoprotein,

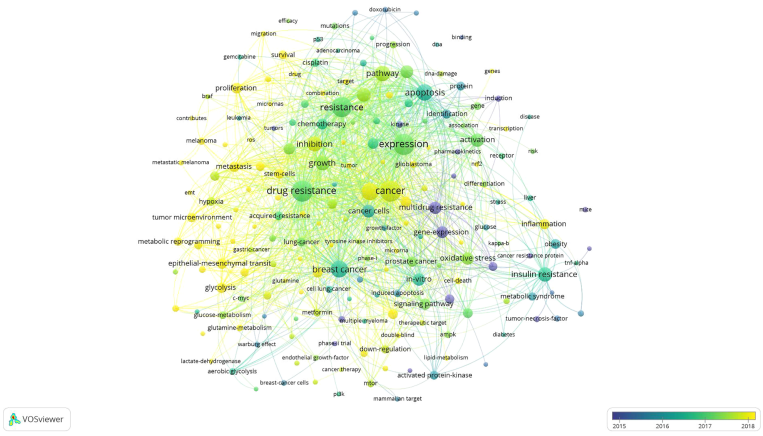

FIGURE 5
Overlay visualization map of keyword co-occurrence analysis. The node and label meanings in this map are the same as in the network visualization map. Furthermore, the color of a node indicates the APY of each keyword according to the color gradient shown in the lower right corner.

acquired resistance, down-regulation, acute myeloid leukemia, and cell lung cancer. The resistance mechanisms of cancer include changes in drug transport and metabolism and mutation of the drug target (61). Among mechanisms of resistance, multidrug resistance is a process independent of the chemical structures of drugs that reduce intracellular drug accumulation. It's often due to upregulation and/or amplification of the MDR1/ABCB1 gene that encodes p-glycoprotein (82). Some researchers developed a particular class of hybrid by conjugating anticancer agents with nitric oxide (NO) donors, the appropriate NO donors reversed drug resistance *via* nitration of ABC transporters, and by interfering with several metabolic enzymes and signaling pathways (83). Hepatocellular carcinoma is an aggressive human cancer with increasing incidence worldwide and its resistance becomes a research hotspot. Ren Y (84) proposed that CXCR3 induced metabolic alteration in SOR-resistance hepatocellular carcinoma cells through downregulating AMPK pathway activity and lipid peroxidation as well as upregulating levels of adipocytokines. In addition, some components (such as YAP/TAZ molecules and hypoxia-inducible factor-1) in the tumor microenvironment involved in mediating the altered metabolic pathways appear to be critical therapeutic targets that can be used to enhance current cancer treatment for metastatic and treatment-resistant cancers (85, 86).

Cluster 3: Study of cancer stem cells

Cluster 3 contained 45 keywords, mainly involved in metabolic of cancer drug resistance studies: drug resistance, breast cancer, epithelial-mesenchymal transition, metastasis, glycolysis, prostate cancer, stem cells, mitochondria, hypoxia, lung-cancer, chemoresistance, cancer metabolism, and metabolic reprogramming. In the presence of oxygen, cancer stem cells can switch between oxidative phosphorylation and glycolysis to maintain homeostasis (87). Due to their highly tumorigenic and drug-resistant properties, dual inhibition of metabolic pathways may be an effective therapeutic strategy for eradicating heterogeneous cancer stem cells rather than singularly targeting glycolysis or oxidative phosphorylation pathways (87, 88). In addition, cancer metastatic ability was closely associated with cancer stem cell phenotype, especially the process known as epithelial-mesenchymal transition, therefore, epithelial-mesenchymal transition plays a critical role in driving tumor metastatic dissemination and drug resistance (89). For example, a study (90) reported that podocalyxin-like protein 1 (PODXL) was induced during the epithelial-mesenchymal transition process, and it was a metabolic reprogramming inducer that enhanced glutamine metabolism and lipid metabolism, thereby increasing the proliferation of Raji Burkitt lymphoma cells. What's more, overexpression of PODXL in Raji Burkitt lymphoma cells decreases dexamethasone- and hydrogen peroxide-induced cell apoptosis (91). With a further understanding of cancer stem cells' metabolic pathways and principal players of metabolism, more potential therapeutic targets will be explored to improve cancer treatments.

Cluster 4: Study of tumor oxidative stress and inflammation signaling pathways

Cluster 4 contained 39 keywords, mainly focused on tumor oxidative stress and inflammation signaling pathways: metabolism, insulin resistance, oxidative stress, gene expression, signaling pathway, inflammation, NF-κB, obesity, *in-vivo*, and activated protein-kinase. Oxidative stress and inflammation damage lead to cancer initiation and progression (92). Overproduction of reactive oxygen species is linked to metabolic imbalance, and it has the potential to activate pro-oncogenic signaling pathways, change gene expression, and facilitate mutations, DNA damage, and genomic instability (93). In addition, reactive oxygen species and other overabundant radicals also lead to the activation of certain transcription factors and the hyperproduction of informative pro-inflammatory molecules (94). These processes can all switch healthy cells' regular metabolism to the creation of a tumor-like state. NF-κB is currently a research hotspot. NF-κB participates in the modulation of the inflammatory response and can be activated by the effects of oxidative stress (95). Its activation is closely related to the development and progression of malignant neoplasms, for example, NF-κB can change the metabolism of tumor cells from mitochondrial-dependent oxidative phosphorylation to anaerobic glycolysis, which leads to the emergence of the Warburg effect and the adaptation of cancer cells to hypoxia conditions (96). Sanchez-Lopez E (97) found that the activation of NF-κB dependent p62-NRF2 cascade contributed to the survival and therapy resistance of chronic lymphocytic leukemia cells that expressed high levels of ROR1. What's more, Zhang J (98) reported that TPH-1 facilitated cellular proliferation, migration, and chemoresistance in glioma through the serotonin/L1CAM/NF-κB pathway. Therefore, these targets may be effective strategies for the treatment of drug resistance.

Cluster 5: Study of autophagy

Cluster 5 was the smallest cluster with 14 keywords regarding autophagy. The main keywords in this cluster were: autophagy, proliferation, pancreatic cancer, progression, invasion, migration, overexpression, and gemcitabine. Autophagy is a double-edged sword: it suppresses tumorigenesis in the early stage and turns into an accomplice by controlling energy metabolism while cancer is established (99). Autophagy and mitochondrial metabolism collaborate in cancer cells to sustain their survival and proliferation in favor of tumor growth (100). Therefore, autophagy is of particular importance for cancers, such as pancreatic ductal adenocarcinoma. Reyes-Castellanos G (101) proposed that

high autophagic activity in pancreatic ductal adenocarcinoma is markedly related to resistance to current therapies. The inhibitions in the last stage of autophagy can overcome drug resistance, such as chloroquine and its derivative hydroxychloroquine (102).

The transition of research focus

As we can see from Figure 5, the nodes coded with dark violet represent the keywords that appeared relatively earlier in the time course before or around 2015, while keywords that appeared around 2018 were coded with yellow color. It can be seen by combining the specific position of five clusters from Figure 5 that early research around the year 2011, "study of tumor oxidative stress and inflammation signaling pathways and resistance mechanisms of different cancer types (cluster 4 and cluster 2)" had attracted a lot of attention in academia of this field. Afterward, "Study of cancer cell apoptosis pathway (cluster 1)" progressively gained importance around 2014, and some areas remain the hotpots until today, for example, "androgen receptor" (APY = 2018.82) (103), "glioblastoma" (APY= 2018.54) (79), and "transcription" (APY= 2018.15) (104). Notably, cluster 3 and cluster 5 ("study of cancer stem cells and autophagy") are the two clusters that had the smallest APY compared with other clusters, and "metabolic reprogramming" (APY= 2019.39) (105), "microRNAs" (APY= 2019.05) (106) were mainly found lately. This implies that these two clusters are emerging topics in recent years, and more related research may be published in the future. These results suggest that the research focus of this field has switched from "cluster 4 and cluster 2: the study of tumor oxidative stress and inflammation signaling pathways and resistance mechanisms of different cancer types" to "cluster 3 and cluster 5: the study of cancer stem cells and autophagy".

New hotspots and research frontiers

Burst detection was used to identify keywords that drew the attention of peer scholars over a specific period. It is also usually regarded as an important metric for determining research hotspots, developing trends, and research frontiers over time (107). We have analyzed the significant burst keywords between 1992 through 2022 by using CiteSpace, the top 25 keywords with the strongest citation bursts were shown in Table 3. As we can

TABLE 3 Top 25 keywords with the strongest citation bursts.

Keywords	Strength	Begin	End	1992-2021
gene expression	10.95	2007	2013	
tumor microenvironment	10.4	2020	2022	
in vivo	9.25	2004	2017	
tumor necrosis factor	9.1	1998	2013	
cancer resistance protein	7.89	2009	2016	
molecular mechanism	7.32	2018	2020	
multidrug resistance	6.84	2003	2013	
induction	5.81	2004	2010	
p glycoprotein	5.73	2006	2013	
activated protein kinase	5.7	2010	2014	
transcription factor	5.13	2014	2016	
induced apoptosis	4.78	2012	2016	
obesity	4.59	2016	2017	
pharmacokinetics	4.56	2011	2016	
invasion	4.54	2019	2022	
growth factor receptor	4.45	2011	2015	
phosphorylation	4.43	2014	2016	
poor prognosis	4.39	2018	2020	
adipose tissue	4.38	2008	2012	
metabolic syndrome	4.24	2008	2012	
skeletal muscle	4.16	2008	2014	
breast	4.13	2012	2016	
differentiation	4.07	2015	2017	
messenger rna	4.01	2010	2015	
target	3.96	2019	2022	

see from the overall change tendency of burst keywords, the research hotspot has experienced a transition to precision cancer medicine. Besides, it's interesting to note that three burst keywords including "tumor microenvironment" (2020–2022) (85), "invasion" (2019-2022) (108), and "target" (2019–2022) (109) are still ongoing. Metabolic signatures within the tumor microenvironment impact the immune function, therefore, overcoming individualized microenvironment-related resistance and identifying related novel targets and signatures will be research hotspots in the future (110). As a result, we can expect more research into these areas in the future, leading to even more exciting scientific discoveries.

Limitations

There are some limitations to this study. Firstly, our study is only based on the WOS database, it is possible to overlook some relevant publications from other databases. However, it can't combine data from different databases because the methods of calculating citations of different databases are various. PubMed does not provide references for an article as part of its metadata, the references cited by an article are not readily available from the dataset, which prevents researchers from conducting citation-based network analyses (29, 111). For example, data downloaded from PubMed cannot be used for identifying citation, bibliographic coupling, and co-citation links between items by VOS viewer and CiteSpace. When the literature is included and excluded, because the article type classification of PubMed is more complicated, it is difficult to directly include research articles and reviews like WOS. Therefore, the literature included in PubMed will have some deviations. Besides, most previous scientometric studies used only one database (21, 107). Secondly, our retrieval time is up to July 26th, since there are constantly new papers published, our research cannot include the recently published articles. Thirdly, our study only included English publications, which may be slightly biased for the research results, but non-English papers could not be included in scientometric studies due to the lack of references and other reasons (21).

Conclusion

For the first time, the total knowledge framework and current state of metabolic signaling pathways of tumor drug resistance research were visualized using a scientometric method in this study. The rapid development of this field was confirmed in publications between 1992 and 2022. Since 2012, the number of annual publications had grown rapidly, and in 2014, the number of papers exceeded 100 for the first time, indicating a surge of interest in this field over the previous decades. The USA made the most contributions to this field. The leading institution was the University of Texas MD Anderson Cancer Center. Avan A was the most productive author, and Hanahan D was the key researcher with the most co-citations, but there is no leader in this field yet. *Cancers* was the most influential academic journal, and Oncology was the most popular research field. The co-citation references could be roughly divided into five main topics: cluster 1 (signaling pathways in the mutated gene in human cancer); cluster 2 (the Warburg effect); cluster 3 (oxidative stress); cluster 4 (cell metabolism regulator); cluster 5 (glutamine metabolism to cancer therapy). Based on keywords occurrence analysis, these selected keywords could be roughly divided into five main topics: cluster 1 (study of cancer cell apoptosis pathway); cluster 2 (study of resistance mechanisms of different cancer types); cluster 3 (study of cancer stem cells); cluster 4 (study of tumor oxidative stress and inflammation signaling pathways); and cluster 5 (study of autophagy). Concerning the APY of the keywords, it can be concluded that precision cancer medicine may be the future frontier of this field. The keywords burst detection identified several keywords as new research hotspots, including "tumor microenvironment," "invasion," and "target". In a word, this study provides a comprehensive scientometric analysis of metabolic signaling pathways of tumor drug resistance research from a global perspective, and it can serve as a starting point for researchers and policymakers worldwide to identify and contribute to the growing scientific work in this field.

Data availability statement

The original contributions presented in the study are included in the article/Supplementary Material. Further inquiries can be directed to the corresponding authors.

Author contributions

RJ, MC, SM, SG, WZ, NJ, and ZZ designed the study. RJ collected the data. RJ and MC analyzed the data and drafted the manuscript. RJ, MC, SM, SG, WZ, NJ, and ZZ revised and approved the final version of the manuscript. All authors contributed to the article and approved the submitted version.

Funding

This study was supported by Capital Health Research and Development of Special Grant (2022-2-2047).

Conflict of interest

The authors declare that the research was conducted in the absence of any commercial or financial relationships that could be construed as a potential conflict of interest.

Publisher's note

All claims expressed in this article are solely those of the authors and do not necessarily represent those of their affiliated organizations, or those of the publisher, the editors and the reviewers. Any product that may be evaluated in this article, or claim that may be made by its manufacturer, is not guaranteed or endorsed by the publisher.

Supplementary material

The Supplementary Material for this article can be found online at: https://www.frontiersin.org/articles/10.3389/fonc.2022.981406/full#supplementary-material

References

1. Bahar E, Han SY, Kim JY, Yoon H. Chemotherapy resistance: Role of mitochondrial and autophagic components. *Cancers* (2022) 14(6):1462. doi: 10.3390/cancers14061462

2. Bhardwaj V, He J. Reactive oxygen species, metabolic plasticity, and drug resistance in cancer. *Int J Mol Sci* (2020) 21(10):3412. doi: 10.3390/ijms21103412

3. Alexa-Stratulat T, Pesic M, Gasparovic AC, Trougakos IP, Riganti C. What sustains the multidrug resistance phenotype beyond ABC efflux transporters? looking beyond the tip of the iceberg. *Drug Resist Update* (2019) 46:100643. doi: 10.1016/j.drup.2019.100643

4. Warburg O. On respiratory impairment in cancer cells. *Science* (1956) 124 (3215):269–70. doi: 10.1126/science.124.3215.269

5. Yang WY, Wang YC, Tao CH, Li YH, Cao S, Yang XQ. CRNDE silencing promotes apoptosis and enhances cisplatin sensitivity of colorectal carcinoma cells by inhibiting the Akt/mTORC1-mediated warburg effect. *Oncol Lett* (2022) 23 (2):70. doi: 10.3892/ol.2022.13190

6. Koomen DC, Meads MB, Magaletti DM, Guingab-Cagmat JD, Oliveira PS, Fang B, et al. Metabolic changes are associated with melphalan resistance in multiple myeloma. *J Proteome Res* (2021) 20(6):3134–49. doi: 10.1021/acs.jproteome.1c00022

7. Liu WJ, Pan PY, Sun Y, Wang JB, Zhou H, Xie X, et al. Deferoxamine counteracts cisplatin resistance in A549 lung adenocarcinoma cells by increasing vulnerability to glutamine deprivation-induced cell death. *Front Oncol* (2022) 11:794735. doi: 10.3389/fonc.2021.794735

8. Zhao YJ, Liu X, Si FS, Huang L, Gao AQ, Lin WL, et al. Citrate promotes excessive lipid biosynthesis and senescence in tumor cells for tumor therapy. *Adv Sci* (2022) 9(1):e2101553. doi: 10.1002/advs.202101553

9. Karaca C, Tokatli A, Tokatli A, Karadag A, Calibasi-Kocal G. Warburg and pasteur phenotypes modulate cancer behavior and therapy. *Anti-Cancer Drugs* (2022) 33(1):E69–75. doi: 10.1097/CAD.0000000000001236

10. Bernstock JD, Kang KD, Klinger NV, Olsen HE, Gary S, Totsch SK, et al. Targeting oncometabolism to maximize immunotherapy in malignant brain tumors. *Oncogene* (2022) 41(19):2663–71. doi: 10.1038/s41388-022-02312-y

11. Lee S, Rauch J, Kolch W. Targeting MAPK signaling in cancer: Mechanisms of drug resistance and sensitivity. *Int J Mol Sci* (2020) 21(3):1102. doi: 10.3390/ijms21031102

12. Chang H, Zou Z. Targeting autophagy to overcome drug resistance: further developments. *J Hematol Oncol* (2020) 13(1):159. doi: 10.1186/s13045-020-01000-2

13. Wood KC. Mapping the pathways of resistance to targeted therapies. *Cancer Res* (2015) 75(20):4247–51. doi: 10.1158/0008-5472.Can-15-1248

14. Liu SJ, Gao QH, Deng YJ, Zen Y, Zhao M, Guo J. Knowledge domain and emerging trends in chronic prostatitis/ chronic pelvic pain syndrome from 1970 to 2020: a scientometric analysis based on VOSviewer and CiteSpace. *Ann Palliat Med* (2022) 11(5):1714–24. doi: 10.21037/apm-21-3068

15. Long J, Zhang Y, Liu X, Pan M, Gao Q. Exosomes in the field of neuroscience: A scientometric study and visualization analysis. *Front Neurol* (2022) 13:871491. doi: 10.3389/fneur.2022.871491

16. Amin MN, Ahmad W, Khan K, Sayed MM. Mapping research knowledge on rice husk ash application in concrete: A scientometric review. *Materials (Basel Switzerland)* (2022) 15(10):3431. doi: 10.3390/ma15103431

17. Chen CM. Searching for intellectual turning points: Progressive knowledge domain visualization. *Proc Natl Acad Sci U S A* (2004) 101:5303–10. doi: 10.1073/pnas.0307513100

18. van Eck NJ, Waltman L. VOS: A new method for visualizing similarities between objects. In: Decker R, Lenz HJ, editors. *Advances in data analysis*. Berlin, Heidelberg: Springer Berlin Heidelberg (2007). p. 299–306.

19. Sung H, Ferlay J, Siegel RL, Laversanne M, Soerjomataram I, Jemal A, et al. Global cancer statistics 2020: GLOBOCAN estimates of incidence and mortality worldwide for 36 cancers in 185 countries. *CA Cancer J Clin* (2021) 71(3):209–49. doi: 10.3322/caac.21660

20. Ke L, Lu C, Shen R, Lu T, Ma B, Hua Y. Knowledge mapping of drug-induced liver injury: A scientometric investigation (2010-2019). *Front Pharmacol* (2020) 11:842. doi: 10.3389/fphar.2020.00842

21. Wu HY, Zhou Y, Xu LX, Tong LJ, Wang YL, Liu BL, et al. Mapping knowledge structure and research frontiers of ultrasound-induced blood-brain barrier opening: A scientometric study. *Front Neurosci* (2021) 15:706105. doi: 10.3389/fnins.2021.706105

22. Miao Y, Zhang Y, Yin L. Trends in hepatocellular carcinoma research from 2008 to 2017: a bibliometric analysis. *PeerJ* (2018) 6:e5477. doi: 10.7717/peerj.5477

23. Katz JS, Martin BR. What is research collaboration? res. *Policy* (1997) 26 (1):1–18. doi: 10.1016/S0048-7333(96)00917-1

24. Wu H, Li Y, Tong L, Wang Y, Sun Z. Worldwide research tendency and hotspots on hip fracture: a 20-year bibliometric analysis. *Arch Osteoporosis* (2021) 16(1):73. doi: 10.1007/s11657-021-00929-2

25. White HD, Griffith BC. Author cocitation: A literature measure of intellectual structure. *J Am Soc Inf Sci* (1981) 32(3):163–71. doi: 10.1002/asi.4630320302

26. Small H. Cocitation in scientific literature - new measure of relationship between 2 documents. *J Am Soc Inf Sci* (1973) 24(4):265–9. doi: 10.1002/asi.4630240406

27. Kleinberg. J. Bursty and hierarchical structure in streams. *Data Min. Knowl Discovery* (2003) 7(4):373–97. doi: 10.1023/A:1024940629314

28. Wu H, Zhou Y, Wang Y, Tong L, Wang F, Song S, et al. Current state and future directions of intranasal delivery route for central nervous system disorders: A scientometric and visualization analysis. *Front Pharmacol* (2021) 12:717192. doi: 10.3389/fphar.2021.717192

29. Eck NJV, Waltman L. *VOS viewer manual* (2020). Available at: https://www.vosviewer.com/documentation/Manual_VOSviewer_1.6.16.pdf.

30. World Bank. *Population, total* (2021). Available at: https://data.worldbank.org/indicator/SP.POP.TOTL.

31. Chen C, Hu Z, Liu S, Tseng H. Emerging trends in regenerative medicine: a scientometric analysis in CiteSpace. *Expert Opin Biol Ther* (2012) 12(5):593–608. doi: 10.1517/14712598.2012.674507

32. Liu Y, Wang Y, Song S, Zhang H. Cancer therapeutic strategies based on metal ions. *Chem Sci* (2021) 12(37):12234–47. doi: 10.1039/d1sc03516a

33. Warburg O. On the origin of cancer cells. *Science* (1956) 123(3191):309–14. doi: 10.1126/science.123.3191.309

34. Galluzzi L, Pietrocola F, Levine B, Kroemer G. Metabolic control of autophagy. *Cell* (2014) 159(6):1263–76. doi: 10.1016/j.cell.2014.11.006

35. Anisimov VN, Bartke A. The key role of growth hormone-insulin-IGF-1 signaling in aging and cancer. *Crit Rev oncology/hematol* (2013) 87(3):201–23. doi: 10.1016/j.critrevonc.2013.01.005

36. Gottesman MM. Mechanisms of cancer drug resistance. *Annu Rev Med* (2002) 53:615–27. doi: 10.1146/annurev.med.53.082901.103929

37. Arbyn M, Weiderpass E, Bruni L, de Sanjosé S, Saraiya M, Ferlay J, et al. Estimates of incidence and mortality of cervical cancer in 2018: a worldwide analysis. *Lancet Global Health* (2020) 8(2):e191–203. doi: 10.1016/s2214-109x(19)30482-6

38. Yang K, Qi H. Research on health disparities related to the COVID-19 pandemic: A bibliometric analysis. *Int J Environ Res Public Health* (2022) 19(3):1220. doi: 10.3390/ijerph19031220

39. Subramanian A, Tamayo P, Mootha VK, Mukherjee S, Ebert BL, Gillette MA, et al. Gene set enrichment analysis: a knowledge-based approach for interpreting genome-wide expression profiles. *Proc Natl Acad Sci U S A* (2005) 102(43):15545–50. doi: 10.1073/pnas.0506580102

40. Yu S, Li X, Ma M, Yang R, Zhang J, Wu S. The immunological contribution of a novel metabolism-related signature to the prognosis and anti-tumor immunity in cervical cancer. *Cancers* (2022) 14(10):2399. doi: 10.3390/cancers14102399

41. Huang da W, Sherman BT, Lempicki RA. Systematic and integrative analysis of large gene lists using DAVID bioinformatics resources. *Nat Protoc* (2009) 4(1):44–57. doi: 10.1038/nprot.2008.211

42. Christofk HR, Vander Heiden MG, Harris MH, Ramanathan A, Gerszten RE, Wei R, et al. The M2 splice isoform of pyruvate kinase is important for cancer metabolism and tumour growth. *Nature* (2008) 452(7184):230–3. doi: 10.1038/nature06734

43. Gao P, Tchernyshyov I, Chang TC, Lee YS, Kita K, Ochi T, et al. C-myc suppression of miR-23a/b enhances mitochondrial glutaminase expression and glutamine metabolism. *Nature* (2009) 458(7239):762–5. doi: 10.1038/nature07823

44. Haq R, Shoag J, Andreu-Perez P, Yokoyama S, Edelman H, Rowe GC, et al. Oncogenic BRAF regulates oxidative metabolism *via* PGC1alpha and MITF. *Cancer Cell* (2013) 23(3):302–15. doi: 10.1016/j.ccr.2013.02.003

45. Kim JW, Tchernyshyov I, Semenza GL, Dang CV. HIF-1-mediated expression of pyruvate dehydrogenase kinase: a metabolic switch required for cellular adaptation to hypoxia. *Cell Metab* (2006) 3(3):177–85. doi: 10.1016/j.cmet.2006.02.002

46. Son J, Lyssiotis CA, Ying H, Wang X, Hua S, Ligorio M, et al. Glutamine supports pancreatic cancer growth through a KRAS-regulated metabolic pathway. *Nature* (2013) 496(7443):101–5. doi: 10.1038/nature12040

47. Vazquez F, Lim JH, Chim H, Bhalla K, Girnun G, Pierce K, et al. PGC1alpha expression defines a subset of human melanoma tumors with increased mitochondrial capacity and resistance to oxidative stress. *Cancer Cell* (2013) 23(3):287–301. doi: 10.1016/j.ccr.2012.11.020

48. Wise DR, DeBerardinis RJ, Mancuso A, Sayed N, Zhang XY, Pfeiffer HK, et al. Myc regulates a transcriptional program that stimulates mitochondrial glutaminolysis and leads to glutamine addiction. *Proc Natl Acad Sci U S A* (2008) 105(48):18782–7. doi: 10.1073/pnas.0810199105

49. Xu RH, Pelicano H, Zhou Y, Carew JS, Feng L, Bhalla KN, et al. Inhibition of glycolysis in cancer cells: a novel strategy to overcome drug resistance associated with mitochondrial respiratory defect and hypoxia. *Cancer Res* (2005) 65(2):613–21. doi: 10.1158/0008-5472.613.65.2

50. Vander Heiden MG, Cantley LC, Thompson CB. Understanding the warburg effect: the metabolic requirements of cell proliferation. *Science* (2009) 324(5930):1029–33. doi: 10.1126/science.1160809

51. Haq R, Shoag J, Andreu-Perez P, Yokoyama S, Edelman H, Rowe GC, et al. Oncogenic BRAF regulates oxidative metabolism *via* PGC1α and MITF. *Cancer Cell* (2013) 23(3):302–15. doi: 10.1016/j.ccr.2013.02.003

52. Jeon SM, Chandel NS, Hay N. AMPK regulates NADPH homeostasis to promote tumour cell survival during energy stress. *Nature* (2012) 485(7400):661–5. doi: 10.1038/nature11066

53. Hanahan D, Weinberg RA. Hallmarks of cancer: the next generation. *Cell* (2011) 144(5):646–74. doi: 10.1016/j.cell.2011.02.013

54. Chen C, Dubin R, Kim MC. Orphan drugs and rare diseases: a scientometric review (2000-2014). *Expert Opin ON ORPHAN Drugs* (2014) 2(7):709–24. doi: 10.1517/21678707.2014.920251

55. Pavlova NN, Thompson CB. The emerging hallmarks of cancer metabolism. *Cell Metab* (2016) 23(1):27–47. doi: 10.1016/j.cmet.2015.12.006

56. Lee KM, Giltnane JM, Balko JM, Schwarz LJ, Guerrero-Zotano AL, Hutchinson KE, et al. MYC and MCL1 cooperatively promote chemotherapy-resistant breast cancer stem cells *via* regulation of mitochondrial oxidative phosphorylation. *Cell Metab* (2017) 26(4):633–47 e7. doi: 10.1016/j.cmet.2017.09.009

57. Wang T, Fahrmann JF, Lee H, Li YJ, Tripathi SC, Yue C, et al. JAK/STAT3-regulated fatty acid beta-oxidation is critical for breast cancer stem cell self-renewal and chemoresistance. *Cell Metab* (2018) 27(1):136–50 e5. doi: 10.1016/j.cmet.2017.11.001

58. Bray F, Ferlay J, Soerjomataram I, Siegel RL, Torre LA, Jemal A. Global cancer statistics 2018: GLOBOCAN estimates of incidence and mortality worldwide for 36 cancers in 185 countries. *CA Cancer J Clin* (2018) 68(6):394–424. doi: 10.3322/caac.21492

59. Siegel RL, Miller KD, Jemal A. Cancer statistics, 2019. *CA Cancer J Clin* (2019) 69(1):7–34. doi: 10.3322/caac.21551

60. Siegel RL, Fedewa SA, Miller KD, Goding-Sauer A, Pinheiro PS, Martinez-Tyson D, et al. Cancer statistics for Hispanics/Latinos, 2015. *CA Cancer J Clin* (2015) 65(6):457–80. doi: 10.3322/caac.21314

61. Holohan C, Van Schaeybroeck S, Longley DB, Johnston PG. Cancer drug resistance: an evolving paradigm. *Nat Rev Cancer* (2013) 13(10):714–26. doi: 10.1038/nrc3599

62. DeBerardinis RJ, Chandel NS. Fundamentals of cancer metabolism. *Sci Adv* (2016) 2(5):e1600200. doi: 10.1126/sciadv.1600200

63. Liberti MV, Locasale JW. The warburg effect: How does it benefit cancer cells? *Trends Biochem Sci* (2016) 41(3):211–8. doi: 10.1016/j.tibs.2015.12.001

64. Ward PS, Thompson CB. Metabolic reprogramming: a cancer hallmark even warburg did not anticipate. *Cancer Cell* (2012) 21(3):297–308. doi: 10.1016/j.ccr.2012.02.014

65. Zhao Y, Butler EB, Tan M. Targeting cellular metabolism to improve cancer therapeutics. *Cell Death Dis* (2013) 4:e532. doi: 10.1038/cddis.2013.60

66. Altman BJ, Stine ZE, Dang CV. From Krebs to clinic: glutamine metabolism to cancer therapy. *Nat Rev Cancer* (2016) 16(10):619–34. doi: 10.1038/nrc.2016.71

67. Vander Heiden MG, DeBerardinis RJ. Understanding the intersections between metabolism and cancer biology. *Cell* (2017) 168(4):657–69. doi: 10.1016/j.cell.2016.12.039

68. Saxton RA, Sabatini DM. mTOR signaling in growth, metabolism, and disease. *Cell* (2017) 168(6):960–76. doi: 10.1016/j.cell.2017.02.004

69. Cairns RA, Harris IS, Mak TW. Regulation of cancer cell metabolism. *Nat Rev Cancer* (2011) 11(2):85–95. doi: 10.1038/nrc2981

70. Kuntz EM, Baquero P, Michie AM, Dunn K, Tardito S, Holyoake TL, et al. Targeting mitochondrial oxidative phosphorylation eradicates therapy-resistant chronic myeloid leukemia stem cells. *Nat Med* (2017) 23(10):1234–40. doi: 10.1038/nm.4399

71. Sancho P, Burgos-Ramos E, Tavera A, Bou Kheir T, Jagust P, Schoenhals M, et al. MYC/PGC-1alpha balance determines the metabolic phenotype and plasticity of pancreatic cancer stem cells. *Cell Metab* (2015) 22(4):590–605. doi: 10.1016/j.cmet.2015.08.015

72. Pascual G, Avgustinova A, Mejetta S, Martin M, Castellanos A, Attolini CS, et al. Targeting metastasis-initiating cells through the fatty acid receptor CD36. *Nature* (2017) 541(7635):41–5. doi: 10.1038/nature20791

73. Siegel RL, Miller KD, Jemal A. Cancer statistics, 2017. *CA Cancer J Clin* (2017) 67(1):7–30. doi: 10.3322/caac.21387

74. Viale A, Pettazzoni P, Lyssiotis CA, Ying H, Sanchez N, Marchesini M, et al. Oncogene ablation-resistant pancreatic cancer cells depend on mitochondrial function. *Nature* (2014) 514(7524):628–32. doi: 10.1038/nature13611

75. Zhang G, Frederick DT, Wu L, Wei Z, Krepler C, Srinivasan S, et al. Targeting mitochondrial biogenesis to overcome drug resistance to MAPK inhibitors. *J Clin Invest* (2016) 126(5):1834–56. doi: 10.1172/JCI82661

76. Laplante M, Sabatini DM. mTOR signaling in growth control and disease. *Cell* (2012) 149(2):274–93. doi: 10.1016/j.cell.2012.03.017

77. Wu X, Xu Y, Liang Q, Yang X, Huang J, Wang J, et al. Recent advances in dual PI3K/mTOR inhibitors for tumour treatment. *Front Pharmacol* (2022) 13:875372. doi: 10.3389/fphar.2022.875372

78. Nuan-Aliman S, Bordereaux D, Thieblemont C, Baud V. The alternative RelB NF-kB subunit exerts a critical survival function upon metabolic stress in diffuse Large b-cell lymphoma-derived cells. *Biomedicines* (2022) 10(2):348. doi: 10.3390/biomedicines10020348

79. Yoo K, Yun HH, Jung SY, Lee JH. KRIBB11 induces apoptosis in A172 glioblastoma cells *via* MULE-dependent degradation of MCL-1. *Molecules* (2021) 26(14):4165. doi: 10.3390/molecules26144165

80. Xu Y, Ye H. Progress in understanding the mechanisms of resistance to BCL-2 inhibitors. *Exp Hematol Oncol* (2022) 11(1):31. doi: 10.1186/s40164-022-00283-0

81. Ai Y, Zhu B, Ren CP, Kang FH, Lo JL, Huang ZJ, et al. Discovery of new monocarbonyl ligustrazine-curcumin hybrids for intervention of drug-sensitive and drug-resistant lung cancer. *J Med Chem* (2016) 59(5):1747–60. doi: 10.1021/acs.jmedchem.5b01203

82. Endicott JA, Ling V. The biochemistry of p-glycoprotein-mediated multidrug resistance. *Annu Rev Biochem* (1989) 58:137–71. doi: 10.1146/annurev.bi.58.070189.001033

83. Dallavalle S, Dobricic V, Lazzarato L, Gazzano E, Machuqueiro M, Pajeva I, et al. Improvement of conventional anti-cancer drugs as new tools against multidrug resistant tumors. *Drug Resist Update* (2020) 50:100682. doi: 10.1016/j.drup.2020.100682

84. Ren Y, Gu YK, Li Z, Xu GZ, Zhang YM, Dong MX, et al. CXCR3 confers sorafenib resistance of HCC cells through regulating metabolic alteration and AMPK pathway. *Am J Transl Res* (2020) 12(3):825–36.

85. Ortega A, Vera I, Diaz MP, Navarro C, Rojas M, Torres W, et al. The YAP/TAZ signaling pathway in the tumor microenvironment and carcinogenesis: Current knowledge and therapeutic promises. *Int J Mol Sci* (2022) 23(1):430. doi: 10.3390/ijms23010430

86. Sharma A, Sinha S, Shrivastava N. Therapeutic targeting hypoxia-inducible factor (HIF-1) in cancer: Cutting Gordian knot of cancer cell metabolism. *Front Genet* (2022) 13:849040. doi: 10.3389/fgene.2022.849040

87. Snyder V, Reed-Newman TC, Arnold L, Thomas SM, Anant S. Cancer stem cell metabolism and potential therapeutic targets. *Front Oncol* (2018) 8:203. doi: 10.3389/fonc.2018.00203

88. Cheong JH, Park ES, Liang J, Dennison JB, Tsavachidou D, Nguyen-Charles C, et al. Dual inhibition of tumor energy pathway by 2-deoxyglucose and metformin is effective against a broad spectrum of preclinical cancer models. *Mol Cancer Ther* (2011) 10(12):2350–62. doi: 10.1158/1535-7163.MCT-11-0497

89. Frose J, Chen MB, Hebron KE, Reinhardt F, Hajal C, Zijlstra A, et al. Epithelial-mesenchymal transition induces podocalyxin to promote extravasation *via* ezrin signaling. *Cell Rep* (2018) 24(4):962–72. doi: 10.1016/j.celrep.2018.06.092

90. Tamayo-Orbegozo E, Amo L, Diez-Garcia J, Amutio E, Rinon M, Alonso M, et al. Emerging role of podocalyxin in the progression of mature b-cell non-Hodgkin lymphoma. *Cancers* (2020) 12(2):396. doi: 10.3390/cancers12020396

91. Tamayo-Orbegozo E, Amo L, Rinon M, Nieto N, Amutio E, Maruri N, et al. Podocalyxin promotes proliferation and survival in mature b-cell non-Hodgkin lymphoma cells. *Oncotarget* (2017) 8(59):99722–39. doi: 10.18632/oncotarget.21283

92. Neganova M, Liu JQ, Aleksandrova Y, Klochkov S, Fan RT. Therapeutic influence on important targets associated with chronic inflammation and oxidative stress in cancer treatment. *Cancers* (2021) 13(23):6062. doi: 10.3390/cancers13236062

93. Moloney JN, Cotter TG. ROS signalling in the biology of cancer. *Semin Cell Dev Biol* (2018) 80:50–64. doi: 10.1016/j.semcdb.2017.05.023

94. Marelli G, Sica A, Vannucci L, Allavena P. Inflammation as target in cancer therapy. *Curr Opin Pharmacol* (2017) 35:57–65. doi: 10.1016/j.coph.2017.05.007

95. Sen R, Baltimore D. Multiple nuclear factors interact with the immunoglobulin enhancer sequences. *Cell* (1986) 46(5):705–16. doi: 10.1016/0092-8674(86)90346-6

96. Capece D, Verzella D, Di Francesco B, Alesse E, Franzoso G, Zazzeroni F. NF-kappaB and mitochondria cross paths in cancer: mitochondrial metabolism and beyond. *Semin Cell Dev Biol* (2020) 98:118–28. doi: 10.1016/j.semcdb.2019.05.021

97. Sanchez-Lopez E, Ghia EM, Antonucci L, Sharma N, Rassenti LZ, Xu JY, et al. NF-kappa b-p62-NRF2 survival signaling is associated with high ROR1 expression in chronic lymphocytic leukemia. *Cell Death Differ* (2020) 27(7):2206–16. doi: 10.1038/s41418-020-0496-1

98. Zhang J, Guo ZC, Xie QL, Zhong CH, Gao XY, Yang QM. Tryptophan hydroxylase 1 drives glioma progression by modulating the serotonin/L1CAM/NF-kappa b signaling pathway. *BMC Cancer* (2022) 22(1):457. doi: 10.1186/s12885-022-09569-2

99. Kimmelman AC. The dynamic nature of autophagy in cancer. *Genes Dev* (2011) 25(19):1999–2010. doi: 10.1101/gad.17558811

100. Kimmelman AC, White E. Autophagy and tumor metabolism. *Cell Metab* (2017) 25(5):1037–43. doi: 10.1016/j.cmet.2017.04.004

101. Reyes-Castellanos G, Hadi NA, Carrier A. Autophagy contributes to metabolic reprogramming and therapeutic resistance in pancreatic tumors. *Cells* (2022) 11(3):426. doi: 10.3390/cells11030426

102. Zeh HJ, Bahary N, Boone BA, Singhi AD, Miller-Ocuin JL, Normolle DP, et al. A randomized phase II preoperative study of autophagy inhibition with high-dose hydroxychloroquine and Gemcitabine/Nab-paclitaxel in pancreatic cancer patients. *Clin Cancer Res* (2020) 26(13):3126–34. doi: 10.1158/1078-0432.CCR-19-4042

103. Wen YC, Liu CL, Yeh SL, Chen WH, Jiang KC, Tram VN, et al. PCK1 regulates neuroendocrine differentiation in a positive feedback loop of LIF/ZBTB46 signalling in castration-resistant prostate cancer. *Br J Cancer* (2022) 126(5):778–90. doi: 10.1038/s41416-021-01631-3

104. Lin JG, Xia LZ, Oyang LD, Liang JX, Tan SM, Wu NY, et al. The POU2F1-ALDOA axis promotes the proliferation and chemoresistance of colon cancer cells by enhancing glycolysis and the pentose phosphate pathway activity. *Oncogene* (2022) 41(7):1024–39. doi: 10.1038/s41388-021-02148-y

105. Tiersma JF, Evers B, Bakker BM, Jalving M, de Jong S. Pyruvate dehydrogenase kinase inhibition by dichloroacetate in melanoma cells unveils metabolic vulnerabilities. *Int J Mol Sci* (2022) 23(7):3745. doi: 10.3390/ijms23073745

106. Zhang CM, Liu N. Noncoding RNAs in the glycolysis of ovarian cancer. *Front Pharmacol* (2022) 13:855488. doi: 10.3389/fphar.2022.855488

107. Chen C, Dubin R, Kim MC. Emerging trends and new developments in regenerative medicine: a scientometric update (2000 - 2014). *Expert Opin Biol Ther* (2014) 14(9):1295–317. doi: 10.1517/14712598.2014.920813

108. Kielaite-Gulla A, Andriusaityte U, Zdanys GT, Babonaite E, Strupas K, Kelly H. The impact of epithelial-mesenchymal transition and metformin on pancreatic cancer chemoresistance: A pathway towards individualized therapy. *Med Lith* (2022) 58(4):467. doi: 10.3390/medicina58040467

109. Arjmand B, Hamidpour SK, Alavi-Moghadam S, Yavari H, Shahbazbadr A, Tavirani MR, et al. Molecular docking as a therapeutic approach for targeting cancer stem cell metabolic processes. *Front Pharmacol* (2022) 13:768556. doi: 10.3389/fphar.2022.768556

110. Benavente S, Sanchez-Garcia A, Naches S, Lleonart ME, Lorente J. Therapy-induced modulation of the tumor microenvironment: New opportunities for cancer therapies. *Front Oncol* (2020) 10:582884. doi: 10.3389/fonc.2020.582884

111. Chen C. A glimpse of the first eight months of the COVID-19 literature on Microsoft academic graph: Themes, citation contexts, and uncertainties. *Front Res metrics analytics* (2020) 5:607286. doi: 10.3389/frma.2020.607286

frontiers | Frontiers in Oncology

TYPE Original Research
PUBLISHED 09 November 2022
DOI 10.3389/fonc.2022.1046369

OPEN ACCESS

EDITED BY
Hifzur R. Siddique,
Aligarh Muslim University, India

REVIEWED BY
Viviane Aline Oliveira Silva,
Federal University of Bahia, Brazil
Ernesto Reverchon,
University of Salerno, Italy

*CORRESPONDENCE
Marta Gómez de Cedrón
marta.gomezdecedron@imdea.org
Ana Ramírez de Molina
ana.ramirez@imdea.org

†These authors have contributed equally to this work

SPECIALTY SECTION
This article was submitted to Cancer Metabolism, a section of the journal Frontiers in Oncology

RECEIVED 21 September 2022
ACCEPTED 17 October 2022
PUBLISHED 09 November 2022

CITATION
Bouzas A, Gómez de Cedrón M, Colmenarejo G, Laparra-Llopis JM, Moreno-Rubio J, Montoya JJ, Reglero G, Casado E, Tabares B, Sereno M and Ramírez de Molina A (2022) Phenolic diterpenes from Rosemary supercritical extract inhibit non-small cell lung cancer lipid metabolism and synergise with therapeutic drugs in the clinic. *Front. Oncol.* 12:1046369. doi: 10.3389/fonc.2022.1046369

Phenolic diterpenes from Rosemary supercritical extract inhibit non-small cell lung cancer lipid metabolism and synergise with therapeutic drugs in the clinic

Adrián Bouzas[1,2†], Marta Gómez de Cedrón[1*†], Gonzalo Colmenarejo[3], José Moisés Laparra-Llopis[4], Juan Moreno-Rubio[1,5], Juan José Montoya[2,6], Guillermo Reglero[1,7], Enrique Casado[5], Beatriz Tabares[5], María Sereno[5] and Ana Ramírez de Molina[1*]

[1]Precision Nutrition and Cancer Program, Molecular Oncology Group, IMDEA Food Institute, CEI UAM, CSIC, Madrid, Spain, [2]CANAAN Research & Investment Group, Madrid, Spain, [3]Biostatistics and Bioinformatics Unit, IMDEA Food Institute, CEI UAM, CSIC, Madrid, Spain, [4]Molecular Immuno-Nutrition Group, IMDEA-Food Institute, CEI UAM, CSIC, Madrid, Spain, [5]Medical Oncology Department, Infanta Sofía University Hospital, San Sebastián de los Reyes, Madrid, Spain, [6]Faculty of Medicine, Complutense University of Madrid, Madrid, Spain, [7]Department of Production and Characterization of Novel Foods, Institute of Food Science Research (CIAL) (CSIC.UAM), Madrid, Spain

Lung cancer is one of the most deadly and common cancers in the world. The molecular features of patient's tumours dictate the different therapeutic decisions, which combines targeted therapy, chemotherapy, and immunotherapy. Altered cellular metabolism is one of the hallmarks of cancer. Tumour cells reprogram their metabolism to adapt to their novel requirements of growth, proliferation, and survival. Together with the Warburg effect, the role of lipid metabolism alterations in cancer development and prognosis has been highlighted. Several lipid related genes have been shown to promote transformation and progression of cancer cells and have been proposed as biomarkers for prognosis. Nevertheless, the exact mechanisms of the regulation of lipid metabolism and the biological consequences in non-small cell lung cancer (NSCLC) have not been elucidated yet. There is an urgent necessity to develop multidisciplinary and complementary strategies to improve NSCLC patients´ well-being and treatment response. Nutrients can directly affect fundamental cellular processes and some diet-derived ingredients, bioactive natural compounds and natural extracts have been shown to inhibit the tumour growth in preclinical and clinical trials. Previously, we described a supercritical extract of rosemary (SFRE) (12 - 16% composition of phenolic diterpenes carnosic acid and carnosol) as a potential antitumoral agent in colon and breast cancer due to its effects on the inhibition of lipid metabolism and DNA synthesis, and in the

10.3389/fonc.2022.1046369

reduction of resistance to 5-FluoroUracil (5-FU). Herein, we demonstrate SFRE inhibits NSCLC cell bioenergetics identifying several lipid metabolism implicated targets. Moreover, SFRE synergises with standard therapeutic drugs used in the clinic, such as cisplatin, pemetrexed and pembrolizumab to inhibit of cell viability of NSCLC cells. Importantly, the clinical relevance of SFRE as a complement in the treatment of NSCLC patients is suggested based on the results of a pilot clinical trial where SFRE formulated with bioactive lipids (PCT/ES2017/070263) diminishes metabolic and inflammatory targets in peripheral-blood mononuclear cells (PBMC), such as *MAPK (p=0.04)*, *NLRP3 (p=0.044)*, and *SREBF1 (p=0.047)*, which may augment the immune antitumour function. Based on these results, SFRE merits further investigation as a co-adjuvant in the treatment of NSCLC.

Clinical trial registration: ClinicalTrials.gov Identifier NCT05080920

KEYWORDS

lipid metabolism, precision nutrition, NSCLC, rosemary extract, phenolic diterpenes

1 Introduction

Lung cancer is one of the most deadly and common types of cancer in the world (1). Based on cell origin, about 80–85% of lung cancers are of non-small-cell lung cancer (NSCLC). In the era of genomic medicine, precision oncology has improved the treatment and quality of life of patients (2). For example, in lung adenocarcinomas, the identification of targetable molecular pathways has improved the treatment and outcome of patients. Epidermal growth factor receptor (EGFR) is a key tumour driver and one of the main targets in the successful treatment of NSCLC (3, 4). In addition to EGFR inhibitors -first (erlotinib, gefitinib), second (afatrinib, dacomitinib) or third generation (Osimertinib) inhibitors-, other pathways like ALK or ROS-1 translocations, BRAF, K RAS, RET or NTRK/ROS1 are relevant in the NSCLC landscape (5). Nevertheless, majority of tumours develop drug resistance and a new generation of targeted therapeutic drugs, alone and/or in combination with different drugs, are being developed. Recently, immune checkpoint system inhibitors, such as the anti-PD-1/PD-L1 and anti-CTLA-4 antibodies, have shown additional clinical benefits in combination with chemotherapy (6). In this sense, numerous works indicate that activated EGFR signalling increases the expression of PD-L1, which is also associated to acquired resistance to EGFR-TKIs (7).

The altered cellular metabolism is one of the hallmarks of cancer (8). Tumour cells adapt their metabolism to to support cell growth, proliferation, and survival. In the past years, the relevance of lipid metabolism alterations in cancer has been highlighted (9). Several lipid-related genes in cancer promote transformation and progression and some of the have been proposed as biomarkers for prognosis in cancer (9–11). Lipids are structural components of cellular membranes, provide energy, and are key essential players in the control of the inflammation and oxidative stress (12, 13). Tumour cells present high avidity for fatty acids and cholesterol, which can be satisfied by the activation of *de novo* lipogenesis and cholesterogenesis and, alternatively, by augmenting the uptake of exogenous lipids and/or lipoproteins (14). Nevertheless, the exact mechanisms of regulation and the biological consequences of lipid metabolism in NSCLC have not been elucidated yet.

Nutrients affect fundamental metabolic cellular processes and some diet-derived ingredients, including bioactive natural compounds and natural extracts have been shown to inhibit the tumour growth in preclinical and clinical trials. The development of powerful "omics" technologies has opened new avenues towards nutritional sciences. In this way, genomic, transcriptomic, proteomic, metabolomic, lipidomic and metagenomic analysis have led to a new vision of the delivery of nutritional advice by mean of *Precision nutrition* (15). Previously, we have described a supercritical extract of rosemary SFRE (approved for human use by the European Food Safety Authority-EFSA) as a potential antitumoral agent in colon and breast cancer due to its effects on lipid metabolism, DNA synthesis, and in alleviating the appearance of resistance to 5-FluoroUracil (5-FU) (16–19).

Herein, we demonstrate the inhibitory effects of SFRE in NSCLC cells, alone and in combination with standard chemotherapeutic drugs such as cisplatin, pemetrexed and pembrolizumab. Importantly, we also demonstrate SFRE targets lipid metabolism which seems to be on the bases of the inhibition of NSCLC cell proliferation. In collaboration with the

Medical Oncology Department of Hospital Infanta Sofia (Madrid, Spain), we have conducted a pilot clinical trial with NSCLC patients where SFRE formulated with bioactive lipids (PCT/ES2017/070263) modulates metabolic and inflammatory targets in peripheral-blood mononuclear cells (PBMC) after sixteen weeks of treatment. Based on these results, SFRE merits further investigation as a co-adjuvant in the treatment of NSCLC.

2 Materials and methods

2.1 Reagents and cell culture

Human lung adenocarcinoma cell lines, NCI-H1299 (H1299) and NCI-H1975 (H1975) were obtained from the American Type Culture Collection (ATCC). Normal epithelial cells (CCD 841) were used to compare the effect of SFRE on tumour and normal cells. Roswell Park Memorial Institute (RPMI) 1640 Medium supplemented with 2 mM L-glutamine, fetal bovine serum (FBS) and 0.25% trypsin were purchased from Cultek. Cells were grown in RPMI 1640 supplemented with 10% FBS at 37°C in a humidified atmosphere with 5% CO_2. Dimethyl sulfoxide (DMSO), cisplatin and pemetrexed were purchased from Sigma (Oakville, ON, Canada).

Supercritical Rosemary Extract (Rosemary extract 25 Type No. 027.020) was purchased from Flavex Naturextrakte GmbH (Rehlingen-Siersburg, Germany). Composition of the extract was 12 - 16% composition of phenolic diterpenes carnosic acid and carnosol (calculated as carnosic acid) with > 10% of carnosic acid; total volatile flavour compounds < 4%, water < 1%, residual content of ethanol < 2%, cuticular waxes, as provided from Flavex.

For the analysis of effects of SFRE on cell bioenergetics, Glucosa XF 1 M (Ref: 103577-100) was purchased from Agilent; Oligomycin A (Ref: 75351), FCCP (Ref: C2920), Rotenone (Ref: R88757), Antimycin A (Ref: A8674), and 2-Deoxy-D-glucose (Ref: D8375) were purchased from Merck. Cisplatin (Ref: P4394) and Pemetrexed (Ref: PHR1596) were purchased from Merk. Pembrolizumab was kindly provided by the Medical Oncology Department of Hospital Infanta Sofia.

2.2 MTT proliferation assay

Cell proliferation after different treatments was determined using the 3-(4,5-Dimethylthiazol-2-yl)-2,5-Diphenyltetrazolium Bromide (MTT) method. Briefly, cells were seeded (4,000 cells per well) in 96-well plate in quadruplicates and kept in RPMI 1640 media o/n at 37°C in 5% CO_2. Then cells were treated with several concentrations of SFRE, cisplatin, pemetrexed or pembrolizumab. Cells treated with DMSO were used as controls. After 48 h, MTT solution was added (0.5 mg/mL final concentration) and cells were incubated for 3 h. 200 µL of DMSO were added to each well to dissolve the formazan crystals and absorbance was measured at 560 nm using a scanning spectrophotometer microplate reader (UVM 340 Biochrom). To determine the number of viable cells, the formazan produced by cells from the MTT (thiazolyl blue tetrazolium bromide) solution (50µL at 5 mg/mL in PBS) was solubilized by adding 200 µL DMSO. Then, the absorbance at 560 nm was measured using a scanning spectrophotometer microplate reader (UVM 340 Biochrom). The parameters IC50 (50% cell proliferation inhibition), GI50 (50% growth inhibition), TGI (total growth inhibition), and LC50 (50% cell death) were calculated according to the NIH definitions using a logistic regression (20, 21). The determination of cell proliferation at the beginning of the treatment (time zero) allows to calculate the parameters related to cell proliferation.

2.3 Evaluation of the combination indexes of SFRE with cisplatin, pemetrexed or pembrolizumab

To evaluate synergism between SFRE and therapeutic drugs -cisplatin, pemetrexed or pembrolizumab- NSCLC cells were pre-treated (for three hours in the case of pembrolizumab) and/or were concomitantly treated (in the case of cisplatin and pemetrexed), as indicated, with a fixed concentration of SFRE ($1/2xIC_{50}$) in the presence or not of increasing concentrations of the indicated drugs. The MTT assay was used to evaluate the percentage of the inhibition of cell proliferation relative to non-treated cells. The Combination Index was obtained using CalcuSyn software (Biosoft), which was developed based on the median-effects method by Chou and Talalay. Briefly, CI values significantly lower than 1.0 indicates a synergistic effect; CI values higher than 1.0 indicates antagonism; and additivity as CI values equal to 1.0 (22).

2.4 Quantitative real-time polymerase chain reaction in NSCLC cells

Both NCI-H1299 (H1299) and NCI-H1975 (H1975) cells were treated with SFRE for 48 hours at different doses based on the values obtained from cell proliferation ($1/2xIC_{50}$, $1xIC_{50}$, $2xIC_{50}$). Non-treated cells were kept as controls. Total RNA was extracted with Tri Reagent (Sigma). Then, 1 µg of RNA was reverse transcribed with High-Capacity RNA to cDNA Master Mix system (Life Technologies, Carlsbad, CA, USA). qPCR was performed in the 7900HT Real-Time PCR System (Life Technologies) using VeriQuest SYBR Green qPCR Master Mix (Affymetrix, Santa Clara, CA, USA). Supplementary Table 1 indicates the list of Taqman Probes and the sequences of the

oligos used in the study. The $2^{-\Delta\Delta Ct}$ method was applied to calculate the relative gene expression (23).

2.5 Extracellular flux analysis of the extracellular acidification rates and the oxygen consumption rates

Mitochondrial oxidative respiration (Cell MitoStress Test) and aerobic glycolysis (Cell GlycoStress Test) were monitored with the XFe96 Cell Bionalyzer (Seahorse Biosciences, XFe96). Optimal cell density and drugs titration were previously determined. The dependency of the cells on aerobic glycolysis and oxidative phosphorylation was monitored after the sequential addition of modulators of both bioenergetic pathways. Prior to the experiments, cells were pre-treated with different doses of SFRE for 48 h. Non-treated cells were kept as controls.

Before the experiments, same number of cells, previously pre-treated with SFRE, were seeded in XFe-plates and kept in the absence of any treatment to compare the bioenergetic metabolism of the very same number of cells.

For the *GlycoStress assay*, 10,000 cells were plated in an XFe-96 well-plate and kept 6 h in RPMI 1640 10% FBS to allow the cells to attach. Then, the culture medium was changed to 0.2 mM glutamine XFe-DMEM (5 mM Hepes pH 7.4) to starve the cells for 30 min. First, basal extracellular acidification rate (ECAR) was measured (1–3 measurements). Glucose (10 mM) was added to determine glycolysis; this is the increased ECAR from the basal situation, after the addition of glucose (4–6 measurements). This parameter indicates the capacity of the cells to use glucose. Next, maximal glycolytic capacity was monitored (7–9 measurements) after the addition of oligomycin (1.5 μM), which inhibits the ATP production from the oxidative mitochondrial respiration. Finally, 50 mM DG was added to specifically shut down aerobic glycolysis (10 to 12 measurements). *Glycolysis* was calculated as: (Maximal rate measurement before oligomycin injection: measurement 6) - (Last rate measurement before glucose injection, measurement 3). *Glycolytic capacity*: (Maximum rate measurement after oligomycin injection, measurement 8) - (Last rate measurement before glucose injection, measurement 3). *Glycolytic reserve* (*Glycolytic capacity*) - (*Glycolysis*). Non-glycolytic Acidification: Last rate measurement prior to glucose injection, measurement 3).

For the *MitoStress assay*, 10,000 cells were plated in an XFe-96 well-plate, and cells were kept for 6 h in RPMI 1640, 10% FBS to allow the cells to attach. Then, the medium was changed to 10 mM glucose, 2 mM glutamine, and 1 mM pyruvate XFe-DMEM (5 mM Hepes, pH7.4) and, then the cells were incubated for 30 min at 37°C without CO_2. Three different modulators of the mitochondrial respiratory chain were sequentially injected. After basal oxygen consumption rate (OCR) monitorization (1–3 measurements), oligomycin (1.5 μM), which inhibits ATPase, was added to determine the amount of oxygen dedicated to ATP production by mitochondria (3–6 measurements). To determine the maximal respiration rate or spare respiratory capacity, FCCP (carbonyl cyanide-4-(trifluoromethoxy) phenylhydrazone) was added (0.9 μM) to free the gradient of H^+ from the mitochondrial intermembrane space (7–9 measurements) and thus to activate maximal respiration. Finally, a mix of antimycin A and rotenone (0.5 μM) was added to completely inhibit the mitochondrial respiration (10–12 measurements).

Main parameters extracted from the bioenergetic profile were calculated as: Non-mitochondrial Oxygen Consumption: Minimum rate measurement after Rotenone/antimycin A injection (measurement 12); Basal Respiration Rate: (Last rate measurement before first injection-measurement 3)-(Non-mitochondrial Respiration Rate, measurement 12); Maximal Respiration Rate: (Maximum rate measurement after FCCP injection, measurement 8)-(Non-mitochondrial Respiration, measurement 12)); H^+Leak: (Minimum rate measurement after Oligomycin injection, measurement 6)-(Non-Mitochondrial Respiration, measurement 12); ATP production: (Last rate measurement before Oligomycin injection, measurement 3)-(Minimum rate measurement after Oligomycin injection, measurement 6).

2.6 Measurement of the intracellular ATP content

The relative cellular ATP content was measured by the ATP-based assay CellTiter-Glo Luminescent Cell Proliferation kit (Promega, Madison, WI, USA; Cat # G7571) with modifications from the manufacturer's protocol. Briefly, after 48h of treatment with SFRE at the indicated doses, 15,000 cells were plated in a 96-well clear bottom black polystyrene plates. Non-treated cells were plated in a similar way. Cells were then maintained for 6 h in complete media, without treatments, to allow attachment of the cells. Then, an equal volume of the single-one-step reagent provided by the kit was added to each well and rocked for 15 minutes at room temperature. Cellular ATP content was measured by a luminescent plate reader.

2.7 Flow cytometry analysis

H1299 and H1975 NSCLC cells pre-treated with SFRE were collected in RPMI 1640 media and centrifuged (1200 rpm, 5min). Cells were washed twice with PBS before adding an adequate volume to obtain a 2% (final concentration)

paraformaldehyde solution. According to the manufacturer's instructions, 1 µl of anti-human PDL1 (FITC Mouse Anti-Human CD274 antibody (Cat. No. 558065), and/or 1 µl of BV786 Rat Anti-Human CX3CR1 antibody (Cat. No. 744489) antibodies were added to cell suspensions. After gentle vortex, samples were incubated for 15 min in the dark. For the analysis of SREBP1, Mouse Anti-human SREBP1 was used as primary antibody (BD, 557036), and Goat anti-Mouse IgG (H+L) as secondary Antibody, Alexa Fluor™ Plus 488 (Cat # A-11001).

Cells were then analyzed using the FACS Diva software (BD Biosciences). At least 10,000 events were analysed for each independent sample. Mean values of arbitrary fluorescence unit for 10,000 cells were obtained and expressed as percentage of control.

2.8 Quantification of intracellular neutral lipid content and phospholipids

To analyse the effects of SFRE on intracellular neutral lipid content, we pre-treated H1299 and H1975 cells for 48 h at the indicated doses of SFRE. Non-treated cells were kept as controls. Then, viable cells were collected and 5,000 cells were plated in the absence of any treatment for 6 h to allow the cells to attach Intracellular neutral lipid content was measured using Oil Red O staining (24). Briefly, cells were gently washed with ice-cold PBS (pH 7.4) and then fixed with 10% formalin at room temperature (RT) for 1 h. After removal of the formalin, cells were washed with 60% isopropyl alcohol for 5 min and then washed twice with PBS. Wells were let to dry completely before the addition of filtered Oil Red O solution for 30 min at RT. Stained oil droplets were extracted with 100% isopropanol for 10 min, and absorbance was measured spectrophotometrically at 510 nm to quantify the neutral lipids (24).

For the quantification of phospholipids, only viable cells were collected and resuspended in a 20:80 (v/v) methanol: acetonitrile mixture (0.3 ml). Aliquots of the cells´ extracts were saved for protein quantification. The analysis was performed on an Agilent 1260 HPLC system (Agilent) equipped with a Photodiode array and an UV-VIS multivariate wavelength detector. The column used in these analyses was a C18 4.5 µm particle, 2.1 × 50mm (Poroshell, Agilent). The mobile phases consisted of deionised water, 18 MΩcm (A) and acetonitrile (B), both containing 0.1% (v/v) formic acid. Aliquots (5 µl) of the cell extracts were injected in each cycle and the analysis was performed with the following gradient (0.8 ml/min): 20% B for 2 min to 100% B in 16 min, held at 100% for 7 min. Three independent samples were analysed (three replicates). Identification of the different compounds was attained by matching retention times and co-injection of the standards.

2.9 Patient recruitment and gene expression analysis in PBMCs

The clinical trial was approved by the Ethics Committee for Clinical Investigation of La Paz University Hospital (Ref. HULP 5617), and it was carried out in accordance with The Code of Ethics of The World Medical Association (Declaration of Helsinki). Written informed consent was obtained by all subjects prior to starting the trial. The ClinicalTrials.gov Identifier: NCT05080920.

Eight NSCLC patients were recruited at the Medical Oncology Service of Infanta Sofia University Hospital (San Sebastian de los Reyes, Madrid, Spain) from November 27, 2020, to March 24, 2021. Clinical and pathological data were collected from medical reports (Supplementary Table 2). The set-up of the pilot clinical trial was a sixteen week, double-blind, randomised, and parallel pilot study with two study arms: SFRE formulated with alkylglycerols capsules (CR) (PCT/ES2017/070263), and control capsules (CC). Composition of CR and CC capsules were previously described (25).

The main objective of the study was to evaluate the effects of the intervention on the expression of a selected panel of genes related to lipid metabolism, inflammation, oxidative stress, immune system, and oncogenic pathways in PBMCs. A Taq-Man Low Density Array (Applied Biosystems, Madrid, Spain) was specifically designed for this experiment, including 46 selected genes (Supplementary Table 3) linked to immune system, inflammation, oxidative stress, lipid metabolism, and lipid related oncogenic genes.

Patients were instructed to fast overnight before each blood collection. Blood samples were collected in heparinized tubes (BD Vacutainer, Franklin Lakes, NJ, USA) at each visit between 08:00 and 10:00 to minimize circadian variations, and there were processed within 2 h of collection for the isolation of the PBMCs. Isolation was carried out under sterile conditions to avoid monocytes activation. Briefly, whole blood was diluted (1:1) with phosphate buffer solution (PBS) and centrifuged by density gradient with Histopaque-1077 (Sigma–Aldrich, Madrid, Spain), according to the manufacturer's instructions. After collection, PBMCs were washed twice with PBS.

It has been compared the evolution of gene expression in PBMCs from the initial visit (V1) to visit 4 (nine weeks of intervention) and to visit 6 (sixteen weeks of intervention). Intermediate visits V2, V3 and V5 were control visits.

Gene-expression assays were performed in a HT–7900 Fast Real-Time PCR. *B2M* and *18S* genes were used as endogenous controls. RT-StatMiner software (Integromics® Inc., Madison, WI, USA) was used to detect and determine the quality control and differential expression analyses. The Expression Suite Software (Life Technologies, Madrid, Spain) program was used to obtain the Ct data. The ΔCt (Ct gene-Ct endogenous gene) was calculated, and then the relative expression (RQ) between

visits was calculated (V4 *vs* V1, and V6 *vs* V1) following the $2^{-\Delta\Delta Ct}$ method (23).

2.10 Statistical analysis

Gene expression in NSCLC cells were analysed by non-parametric ANOVA with Bonferroni *post hoc* tests. Data were represented as mean ± S.E.M of at least three independent experiments. Statistical differences were defined as $p < 0.05$ (*); $p < 0.01$ (**); $p < 0.005$ (***); $p < 0.001$ (****). Statistical analysis was performed with Graph Pad Prism 8 software (Version 8.0.0, GraphPad Software, San Diego, CA, USA).

Gene expression in PBMCs from NSCLC patients was quantified with the ΔCt method as previously described (26). To ease interpretation of the results, data was sign-reversed so that lower ΔCt values corresponded to lower gene expression levels. A mixed linear model was used to test the differential evolution of gene expression through time (baseline V1, V4-nine weeks and V6-sixteen weeks) for the SFRE-treated patients *vs* the control-treated ones, adjusted for sex and age. Time and treatment were modelled as fixed interacting effects, and patient as random effect. P. values were corrected by the Bonferroni method to deal with multiple test type-I error inflation due to the multiple genes tested. Statistical significance was defined as P-value < 0.05 with bilateral tests, and 95% confidence intervals for estimated parameters were calculated.

The statistical analyses were performed using the R statistical software version 3.6.1 (www.r-project.org).

3 Results

3.1 SFRE inhibits cell proliferation of NSCLC cell lines

Previously, SFRE has been demonstrated to inhibit lipid metabolism in colorectal and breast cancer cell lines (17, 19, 27). Due to the relevance of the altered lipid metabolism in lung cancer (14, 28, 29), herein, we aimed to investigate the potential of SFRE on the inhibition of lipid metabolism in NSCLC.

Using the available data from the Cancer Cell Line Encyclopedia https://portals.broadinstitute.org/ccle/about) and COSMIC (https://cancer.sanger.ac.uk/cosmic) databases, we investigated the expression levels of *SREBF1, SCD* and *FASN* to select two NSCLC cell lines with intermediate gene expression levels for the three genes. As epidermal growth factor receptor (EGFR) is a key tumour driver and one of the main targets in the successful treatment of NSCLC (3, 4), and as T790M and L858R mutations have been related to the acquisition of resistance to EGFR tyrosine kinase inhibitors in the clinical setting (30), we decided to use H1299, which is *EGFR* wild type, and H1975, which presents the indicated mutations in EGFR, for the *in vitro* studies.

First, we analysed the effect of SFRE on the cell proliferation of the two NSCLC cell lines -H1299 and H1975- by mean of the MTT assay.

As shown in Figure 1, SFRE diminished the cell proliferation of both cell lines in a dose dependent manner. Concentrations corresponding to 50% of cell proliferation inhibition (IC_{50}), 50%

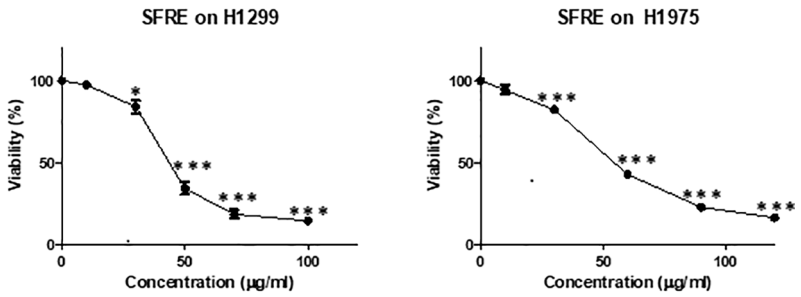

Cell line	IC_{50} (µg/mL)	GI_{50} (µg/mL)	TGI (µg/mL)	LC_{50} (µg/mL)
H1299	42,14 ± 0,926	33,84 ± 1,664	44,74 ± 1,301	60,16± 2,589
H1975	52,19 ± 0,614	28,66± 0,772	76,67± 0,997	105,2 ± 7,408

FIGURE 1
SFRE inhibits cell proliferation of NSCLC cell lines -H1299 and H1975. Dose–response curves of the cell proliferation assay after 48 h of treatment with increasing concentrations of SFRE. Data represent mean ± SEM of three independent experiments, each performed in triplicates. Values corresponding to IC_{50}, GI_{50}, TGI and LC_{50} after 48 h of SFRE treatment are indicated. Results are shown as the mean ± SEM of three independent experiments, with 4 replicates/experiment. Asterisks * and *** indicate *p* values < 0.05 and 0.005, respectively.

growth inhibition (GI_{50}), total growth inhibition (TGI), and 50% cell death (LC_{50}) are also shown.

H1299 was more sensitive to SFRE treatment as shown by the lower IC_{50} values obtained compared to H1975 which may be related to the different functional status of EGFR.

3.2 SFRE inhibits cell bioenergetics of NSCLC cell lines

It is well known that cancer cells adapt their metabolism to support cell proliferation, progression and/or resistance to chemotherapy. As SFRE inhibited the cell proliferation of NSCLC cells, we wanted to investigate if SFRE was able to diminish the main bioenergetic pathways, this is, mitochondrial oxidative phosphorylation and aerobic glycolysis of NSCLC cells. H1299 and H1975 NSCLC cells were pre-treated for 48 h with three different doses of SFRE, based on the previously determined values IC_{50} (Figure 1). Then, we quantified, by flux analysis of the extracellular media, the Extracellular Acidification Rate (ECAR) and the Oxygen Consumption Rate (OCR), as main readouts of aerobic glycolysis and mitochondrial oxidative phosphorylation, respectively.

3.3 SFRE diminishes aerobic glycolysis of NSCLC cells: GlycoStress assay

Highly proliferative cancer cells frequently upregulate aerobic glycolysis independently of oxygen availability (*Warburg effect*). For this reason, we first analysed the aerobic glycolysis performance of NSCLC cells after 48 h of treatment with SFRE, by the monitorization of the Extracellular Acidification Rate (ECAR), which is an indirect readout of the L-lactate production by the cells. We previously pre-treated H1299 and H1975 cells for 48 h with three different doses of SFRE corresponding to $1/2xIC_{50}$, $1xIC_{50}$ and $2xIC_{50}$. Non-treated cells were kept as controls. Importantly, after SFRE treatment, the very same number of cells (10,000 cells/well) were plated in a XFe-plate in the absence of SFRE extract. Cells were kept in the incubator for 6 h to allow the cells to attach to the plates. Then, the medium of the cells was changed to the non-buffered XFe Base media (pH 7.4), supplemented with 2 mM glutamine, in the absence of glucose, for 30 min at 37°C without CO_2. We first monitored the basal ECAR as an indirect readout of the basal L-lactate production by aerobic glycolysis. Interestingly, basal ECAR of NSCLC cells (three measurements before oligomycin injection) was diminished in SFRE treated cell compared to that of non-treated cells (Figure 2). Next, we injected glucose to the medium to monitor cells´ ability to upregulate aerobic glycolysis when glucose is available. After the injection of glucose, although NSCLC cells were able to respond to glucose, they showed diminished levels of ECAR compared to that of non-treated control cells. When oligomycin was added to block ATP production from mitochondria, maximal ECAR of NSCLC cells pre-treated with SFRE was clearly reduced compared to non-treated cells. Finally, 2-deoxyglucose, a glucokinase competitive inhibitor, was injected to quantify the ECAR specifically associated to aerobic glycolysis. Quantification of main parameters of glycolytic activity indicated that glycolysis, glycolytic capacity and glycolytic reserve were inhibited in the pre-treated H1299 and H1975 NSCLC cells, in line with the reduction of the gene expression levels of *GLUT4* in both cell lines and *LDHA* in H1299 (Supplementary Figure 1).

These results indicate that SFRE inhibits aerobic glycolysis of NSCLC cells.

3.4 SFRE diminishes mitochondrial oxidative phosphorylation: MitoStress assay

Due to the observed effects of SFRE in the inhibition of the aerobic glycolysis, we next investigated if SFRE had any effect on the mitochondrial oxidative phosphorylation. First, we monitored OCR in response to well defined modulators of mitochondrial function by mean of the MitoStress assay.

Before running the MitoStress assay, the very same number of non-treated cells and previously pre-treated cells were plated in a XFe Seahorse plate in complete media (RPMI, 10% FBS), and kept for 6 h to allow the cells to attach in the absence of any treatment, to compare the cell bioenergetic profile only of viable cells. Then, the media of the cells was changed to the non-buffered XFe Base media, pH 7.4, supplemented with 10 mM glucose, 2 mM glutamine, and 1 mM pyruvate, and cells were incubated for 30 min at 37°C without CO_2.

As it is shown in Figure 3A H1299 NSCLC cells pre-treated with SFRE displayed reduced basal respiration rates (BRR) compared to control non-treated cells (measurements 1 to 3) at all the doses tested. After the oligomycin injection, SFRE pre-treated cells showed reduced levels of ATP compared to control non-treated cells (measurements 4 to 6). The maximal respiration rate (MRR) (measurements 7 to 9), after the injection of FCCP, was also affected in SFRE pre-treated cells. Finally, rotenone and antimycin A, inhibitors of complexes I and III of the electron transport chain (ETC) respectively, were injected to shut down the OCR due to mitochondrial oxidative phosphorylation (measurements 10 to 12). These results indicate that SFRE compromises mitochondrial respiration. Similar results were obtained in H1975 cells (Figure 3B).

The effects of SFRE on the inhibition of the main bioenergetic pathways in NSCLC cells seemed to be on the bases of the observed effects on the inhibition of cell proliferation, as indicated by the quantification of the intracellular ATP content (Supplementary Figure 2A), and the

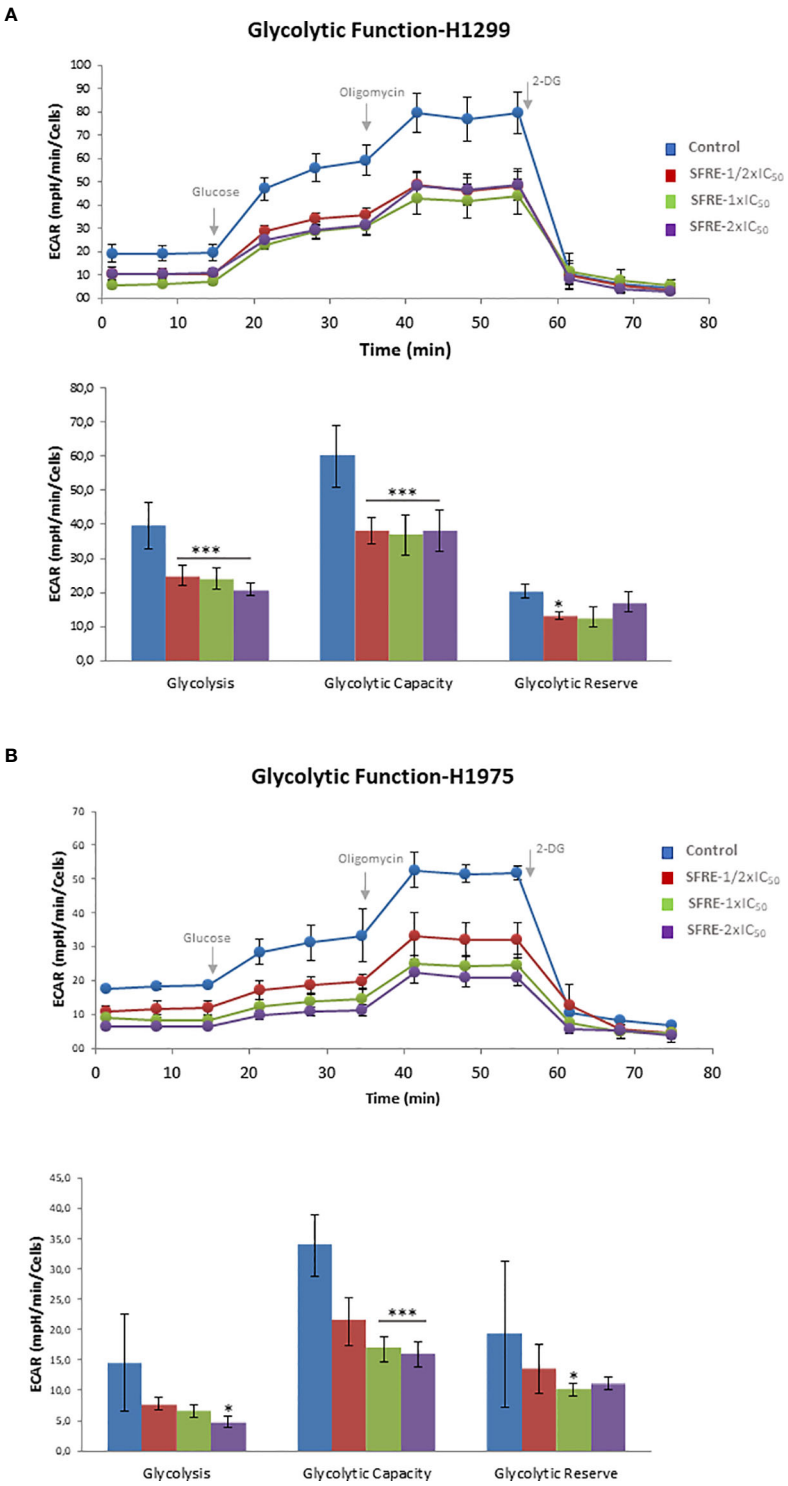

FIGURE 2
SFRE diminishes aerobic glycolysis. Aerobic glycolysis analysis by the flux analysis of the extracellular acidification rate (ECAR) of H1299 cells **(A)** and H1975 **(B)**, previously pre-treated with SFRE at three doses (1/2xIC$_{50}$, 1xIC$_{50}$ and 2xIC$_{50}$) for 48 h The basal ECAR, glycolysis and maximal ECAR of 10,000 cells per condition are compared. Data represent mean ± SEM of three independent experiments, each performed four to six replicates. Asterisks *, *** indicate p-values < 0.05, and 0.005, respectively.

upregulation of gene expression of apoptotic markers (*Caspase-9* and *DDIT3*) (Supplementary Figure 2B).

3.5 SFRE inhibits lipid metabolism related genes in NSCLC cell lines

Due to the observed effects of SFRE on cellular metabolism and, taking into consideration that SFRE diminished lipid metabolism in colorectal cancer (CRC), we wanted to evaluate if SFRE may affect lipid metabolism in NSCLC (25, 31).

With this objective we designed a panel of metabolic genes -including *de novo* lipogenesis and cholesterogenesis (*SREBF1, FASN, SCD and HMGCR*), fatty acid metabolism (*ACSL1, ACSL3, ACSL4, AGPAT1)*, exogenous uptake of lipids (*LDLR)* regulation of intracellular cholesterol levels (*ABCA1, ApoA1*), oncogenic pathways (*CHKA, EGFR*), inflammation and oxidative stress (*JAK1, NEF2L2*)-.

SFRE diminished the expression of the master regulator *SREBF1* implicated in the *de novo* lipogenesis and its downstream genes, *FASN* and *SCD*, as well as *HMGCR* implicated in the *de novo* cholesterogenesis, in H1299 cells (Figure 4). In addition, the expression of *LDLR*, implicated in the uptake of extracellular lipids, together with *ABCA1*, implicated in the reverse transport of cholesterol, were also downregulated. Targets related to the synthesis of phospholipids (*CHKA*), phospholipid remodelling at membranes (*AGPAT1*), oncogenic pathways (*EGFR)* and inflammation (*JAK1*) were also downregulated. Interestingly, SFRE upregulated the expression of *APOA1* which has been proposed to be a tumour suppressor in several cancers (32).

Similar results were obtained in H1975, although this cell line, EGFR mutated, seemed to be less sensitive to SFRE treatment (Figure 5).

3.6 Neutral lipids content and quantification of membrane phospholipids

Due to the observed effects of SFRE in the expression of lipid metabolism genes, we wanted to evaluate the biological relevance of these effects by quantifying the intracellular neutral lipid content and main membrane phospholipids. We previously pre-treated H1299 and H1975 cells for 48 h with three different doses of SFRE corresponding to 1/2xIC_{50}, 1xIC_{50} and 2xIC_{50}. Non-treated cells were kept as controls. Then, cells were kept in the incubator for 6 h to allow the cells to attach to the plates.

As shown in Figure 6A the total neutral lipid content was diminished in a dose dependent manner after SFRE treatment in H1299 and H1975 cell lines. In line with these results, SREBP1 levels, quantified by FACs analysis, were also found diminished (Supplementary Figure 3).

In addition, the quantification of main species of phospholipids indicated that SFRE reduced the levels of phosphatidyl-inositol (PI), phosphatidyl-ethanolamine (PE), phosphatidyl-choline (PC) and the lyso-forms (LPC) in both NSCLC cell lines (Figure 6B).

3.7 SFRE augments NSCLC sensitivity to chemotherapeutic drugs and immune checkpoint inhibitors used in the clinic

In almost all of stage I and stage II NSCLC patients, surgery remains the standard treatment in the clinic. Stage III cases involves a multidisciplinary therapy with a combination of chemo, radiation and, in PD-1 >1%, immunotherapy; Stage IV patients could be treated with immunotherapy or a chemo-immunotherapy according to PD-L1 expression of the tumor (33). Since dual therapy with platinum agents and other drugs, including taxanes or pemetrexed has been widely used as standard treatment for advanced NSCLC without specific mutations, attention has focused on combining these regimens with immunotherapy (34, 35).

An improvement in the understanding of the immunology of cancer and the tumour microenvironment has allowed the application of immunotherapy (36).

3.7.1 SFRE inhibits NSCLC cell proliferation synergistically in combination with cisplatin

As indicated, cisplatin is one of the most common standard first-line treatments, excluding targeted therapies. For this reason, we aimed to evaluate if SFRE could act synergistically with cisplatin in the inhibition of the cell proliferation of NSCLC cells. First, we calculated the IC_{50} values of cisplatin on NSCLC cell lines (Figure 7A, upper panel).

Importantly, the combination index (CI) after treatment NSCLC cell lines with SFRE for three hours at a fixed dose of 1/2 IC_{50} for H1299 and H1975, indicated a positive synergism between cisplatin and SFRE (Figure 7A).

In a previous work, we have demonstrated that SFRE inhibited thymidine kinase 1 (*TK1*) and thymidylate synthase (*TYMS*) synergising with 5- fluorouracil (5-FU) in the inhibition of colorectal cancer cell lines proliferation (19). The analysis of the expression of these genes in NSCLC cells after the treatment with SFRE indicated the downregulation of *TK1* and *TYMS* (Figure 7B) which may explain, at least partially, the observed synergism in the inhibition of cell proliferation between SFRE and cisplatin.

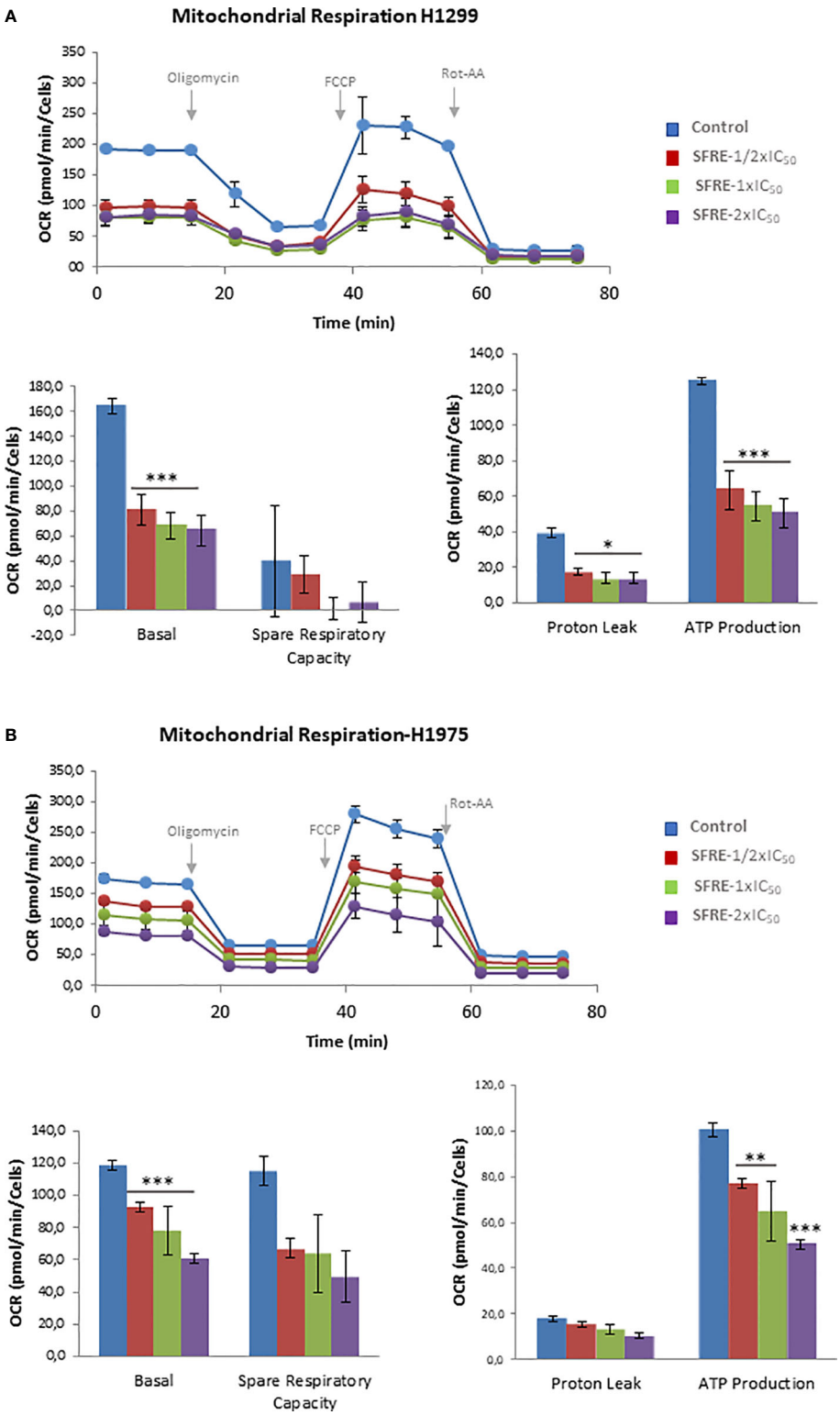

FIGURE 3
SFRE diminishes mitochondrial oxidative phosphorylation. Mitochondrial respiration analysis by flux analysis of the oxygen consumption rate (OCR) of H1299 cells **(A)** and H1975 **(B)** previously pre-treated with SFRE (1/2xIC_{50}, 1xIC_{50} and 2xIC_{50}) for 48 h The basal respiration rate, spare respiratory capacity, ATP production, and proton leak of 10,000 cells per condition are compared. Data represent mean ± SEM of three independent experiments, each performed with four to six replicates. Asterisks *, **, *** indicate *p* values < 0.05, 0.01 and 0.005, respectively.

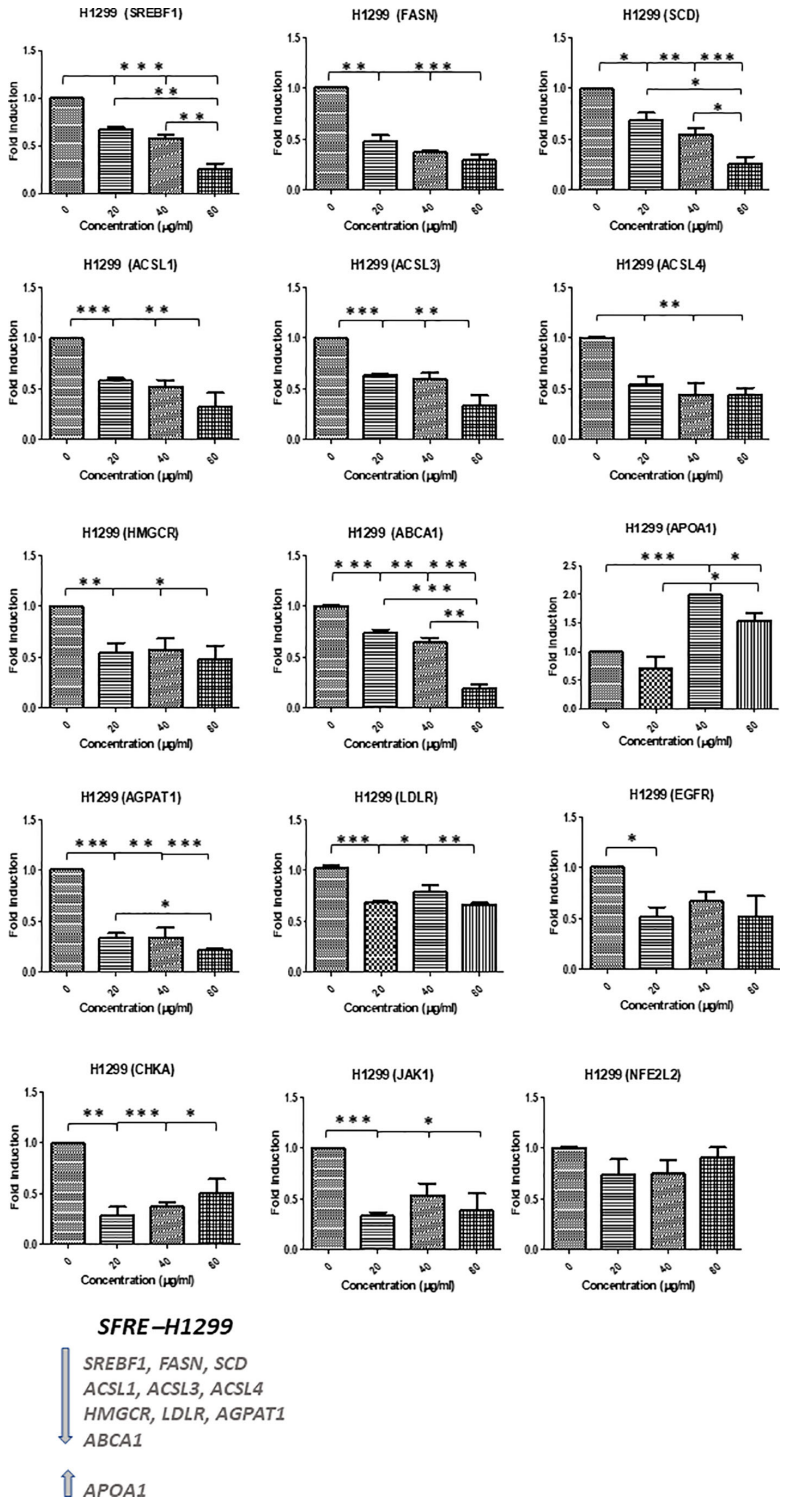

FIGURE 4
Effects of SFRE on lipid metabolism related genes after 48 h of treatment H1299 NSCLC cells. SFRE diminishes the expression of *SREBF1, FASN, SCD1, HMGCR* (*de novo* lipogenesis and cholesterogenesis); *ACSL1, ACSL3* and *ACSL4* (fatty acid activation); *ABCA1* (efflux of cholesterol and tumour microenvironment remodelling); *CHKA* and *AGPAT1* (biosynthesis of phospholipids and plasmatic membrane phospholipid remodelling) and oncogenic *EGFR*. On the contrary, SFRE upregulated the expression of *APOA1*. Results are shown in relation to non-treated cells and normalized to the endogenous control *B2M*. Results are expressed as the mean ± SEM of three independent experiments, each performed in triplicates. Asterisks *, **, *** indicate *p* values < 0.05, 0.01 and 0.005, respectively.

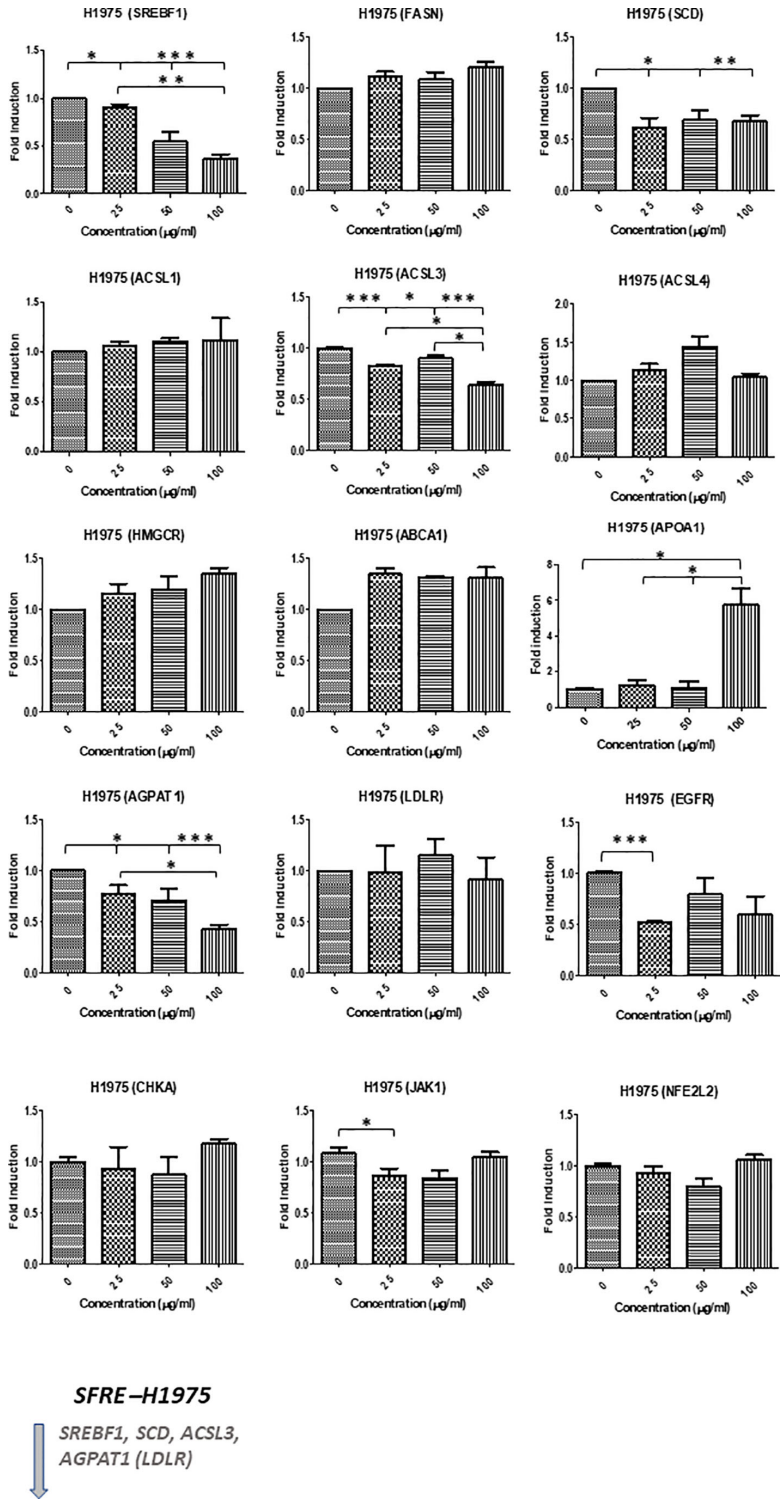

FIGURE 5
Effects of SFRE on lipid metabolism related genes after 48 h of treatment H1975 NSCLC cells. SFRE diminishes the expression of *SREBF1, FASN, SCD1, HMGCR* (*de novo* lipogenesis and cholesterogenesis); *ACSL1, ACSL3* and *ACSL4* (fatty acid activation); *ABCA1* (efflux of cholesterol and tumour microenvironment remodelling); *CHKA* and *AGPAT1* (biosynthesis of phospholipids and plasmatic membrane phospholipid remodelling) and oncogenic *EGFR*. On the contrary, SFRE upregulated the expression of *APOA1*. Results are shown in relation to non-treated cells and normalized to the endogenous control *B2M*. Results are expressed as the mean ± SEM of three independent experiments, each performed in triplicates. Asterisks *, **, *** indicate *p* values < 0.05, 0.01 and 0.005, respectively.

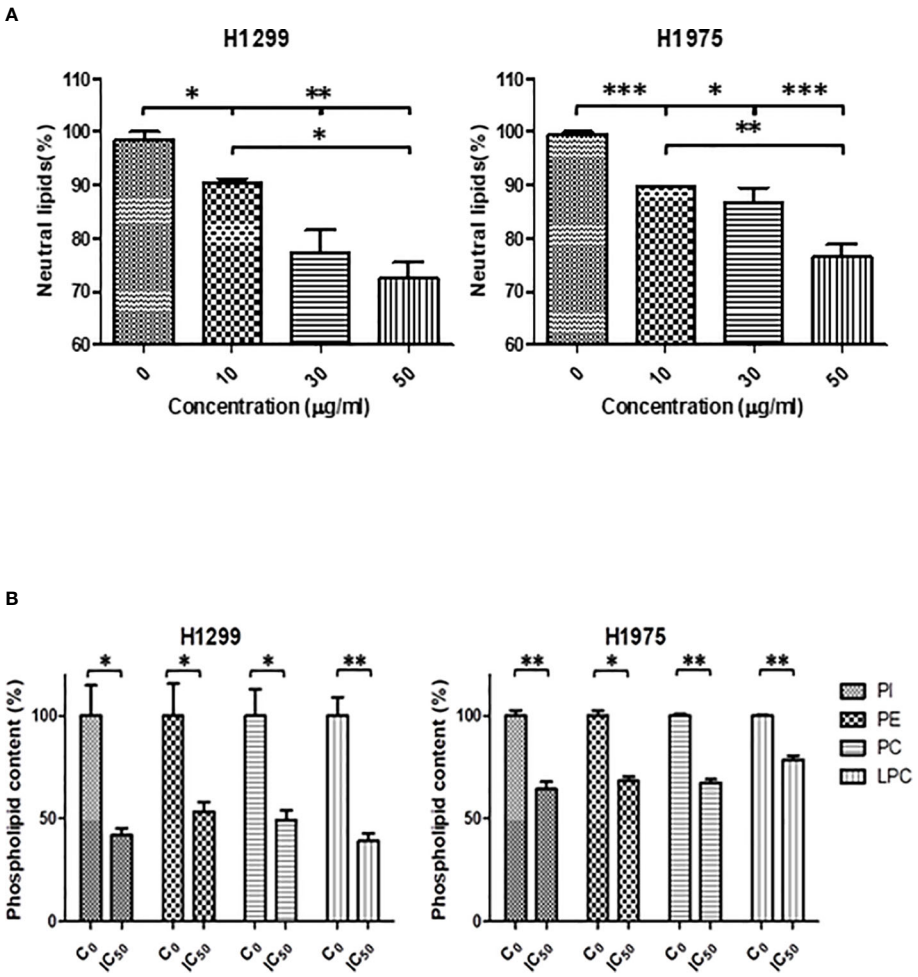

FIGURE 6
(A) SFRE reduced the intracellular neutral lipids content of H1299 and H1975 cells after 48 h of treatment at the indicated doses. Relative content of neutral lipids in cells pre-treated with SFRE after 48 h at different doses, compared with untreated control cells, normalized by the number of viable cells. Results are shown mean ± SEM of three independent experiments (three replicates). **(B)** SFRE reduced the total content of main phospholipids. Relative content of phospholipids in cells pre-treated with SFRE after 48 h at the fixed dose of IC_{50} for each cell line, compared with untreated control cells, normalized by protein content. Results are shown mean ± SEM of three independent experiments (three replicates). Asterisks *, **, *** indicate *p* values < 0.05, 0.01 and 0.005, respectively.

3.7.2 SFRE inhibits NSCLC cells proliferation synergistically in combination with pemetrexed

During the last decade, the place of pemetrexed for the treatment of non-squamous NSCLC became established. Pemetrexed belongs to the 'folate antimetabolites' class of chemotherapy agents, and it inhibits cell replication and tumor growth by inhibiting the activity of three enzymes involved in purine and pyrimidine synthesis: thymidylate synthase (*TYMS*), dihydrofolate reductase (*DHFR*) and glycinamide ribonucleotide formyl-transferase (*GARFT*) (37). For this reason, we aimed to evaluate if SFRE could act synergistically with pemetrexed in the inhibition of the cell proliferation of NSCLC cells. Taking into consideration the IC_{50} values described for pemetrexed in the inhibition of cell proliferation of H1299 [4.72 ± 1.9 µM (38) and 2.43 µM (39)] and the described IC_{50} values for H1975 (3.372 ± 0.082 µM (40) and 3.37 ± 0.14 µM (41), we pre-treated NSCLC cell lines with SFRE for three hours at a fixed dose of 1/2 IC_{50} for H1299 and H1975, and then a range of concentrations of pemetrexed from 2 to 8 ug/ml were used concomitantly with SFRE. Importantly, the combination index (CI) indicated a positive synergism between pemetrexed and SFRE (Figure 8A). The analysis of the expression of dihydrofolate reductase (*DHFR*) and glycinamide ribonucleotide formyl-transferase (*GARFT*) genes in NSCLC cells after the treatment with SFRE, indicated the downregulation of both genes (Figure 8B), which may explain, at least partially, the observed synergism between SFRE and pemetrexed.

10.3389/fonc.2022.1046369

A

Treatment	H1299	H1975
Cisplatin	11,89 ± 0,306 μg/ml	8,54 ± 0,19 μg/ml

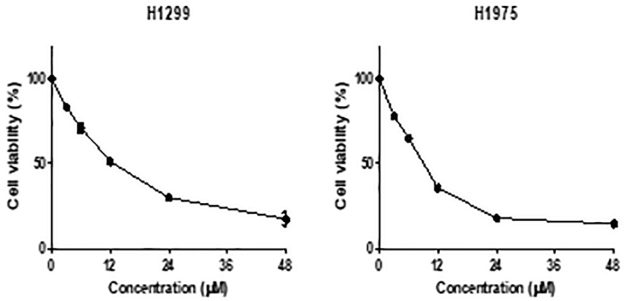

Cis-Pt (μM)	CI (H1299)	CI (H1975)
3	0,676	0,858
6	0,724	0,894
12	0,503	0,814
24	0,469	0,935

B

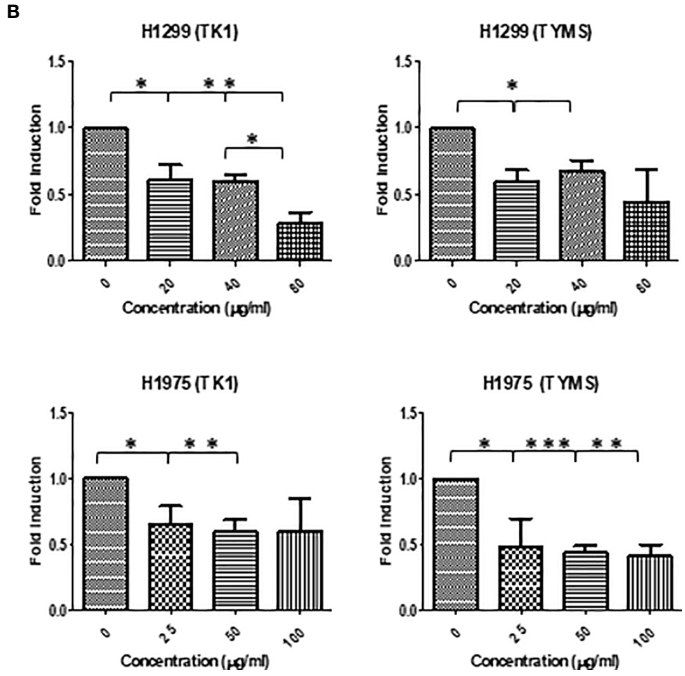

FIGURE 7
(A) Dose–response curves of the cell proliferation after 48 h of treatment with cisplatin in NSCLC H1299 and H1975. IC_{50} values after cisplatin treatment in the two different NSCLC cell lines (H1299 and H1975) after 48h of treatment are indicated (upper panel). SFRE synergised with cisplatin in the inhibition of NSCLC cell proliferation. NSCLC cells were pre-treated with the extract for 3h at a fixed dose of 1/2 IC_{50} for H1299 and H1975. Combinatory index (CI) according to Chou–Talalay method (lower panel). **(B)** SFRE diminished the expression of *TK1* and *TYMS*, in a dose dependent manner. Results are shown in relation to non-treated cells and normalized to the endogenous control *B2M*. Results are expressed as the mean ± SEM of three independent experiments, each performed in triplicates. Asterisks *, **, *** indicate p-values < 0.05, 0.01 and 0.005, respectively.

3.7.3 SFRE inhibits NSCLC cells proliferation synergistically in combination with pembrolizumab

Immunotherapy has made the breakthrough in cancer therapeutics, as it aims to modulate immune regulatory mechanisms to enhance the immune response against cancer cells. The introduction of the monoclonal antibodies anti-PD-1 and anti-PD-L1 has significantly changed the landscape of the treatments for advanced non-small-cell lung cancer (NSCLC). Clinical studies evaluating the response to immunotherapy in patients have demonstrated superior survival indexes as well as reduced toxicity profiles in comparison to standard chemotherapy regimens. Of note, anti-PD-1 therapy (pembrolizumab) has recently replaced chemotherapy in the first line treatment for NSCLC with high PD-L1 expression, and the addition of pembrolizumab to platinum chemotherapy resulted in a significant improvement in overall survival (OS) in patients with non-squamous NSCLC, regardless of PD-L1 expression. Although PD-1 is mainly expressed on the activated T cells, B cells, and monocytes, recent studies have shown that PD-1 is expressed in a subpopulation of various cancer cells, including melanoma, hepatocellular carcinoma (HCC) and NSCLC (42). In the absence of adaptive immune system, tumor cell-intrinsic PD-1/PD-L1 mediates the resistance to anti-PD-1/PD-L1 antibodies by activating AKT and ERK1/2. These findings provide an additional explanation for resistance to cancer immunotherapy. As pembrolizumab interacts with PD-1, we hypothesised that blocking the intracellular signalling could also affect the cell proliferation of NSCLC cells, as described by mean of the inhibition of the canonical signalling pathways, i.e. the AKT and ERK1/2 pathways (43).

For this reason, we evaluated if SFRE could act synergistically with pembrolizumab in the inhibition of the cell proliferation of NSCLC cells.

Considering a range of concentrations for pembrolizumab from 0.12 to 2μM, based on the described IC_{50} values of pembrolizumab in the inhibition of cell proliferation of the NSCLC A549 cell line (EGFR wt) (IC_{50} = 0.4 μM) (44), we treated NSCLC cell lines concomitantly with SFRE at a fixed dose of 1/2 IC_{50}. As shown in Figure 9A, the combination index (CI) indicated a positive synergism between pemetrexed and SFRE in the inhibition of NSCLC cell proliferation (Figure 9A).

To investigate the underlying mechanisms for the observed synergism and taking into consideration that the interaction of pembrolizumab with PD-1 occurs between 30 min and 3h of treatment, we analysed by flow cytometry the expression of PD-L1 after SFRE treatment for 3h and 24h. As shown in Figure 9B, SFRE diminished the expression of PD-L1, being this effect higher at the lowest doses (1/2 xIC_{50}) and at the shorter time of treatment (3h). As PD-L1 expression in tumours has been described to augment the expression of other immunosuppressive biomarkers such as CX3CR1 at the local tumour microenvironment (45), we also quantified the double expression of PD-L1 and CX3CR1 after SFRE treatment. SFRE diminished the expression of PD-L1 and CX3CR1 as shown in Figure 9C, which indicates the potential of SFRE ameliorating the expression of biomarkers that promote immune evasion of the lung cancer cells.

3.7.4 SFRE modulates the expression of lipid metabolism related targets in NSCLC patients

In a previous work, we conducted a nutritional trial in healthy volunteers with an SFRE extract formulated with alkylglycerols (AKG) to increase the bioavailability of the bioactive compounds from SFRE after gastrointestinal digestion (PCT/ES2017/070263). Importantly, it was demonstrated not only the tolerability and safety of the intervention, but also the potential therapeutic action of SFRE by mean of the activation of innate immunity and the modulation of the expression of genes related to immune system, inflammation, oxidative stress, and cancer (25).

Due to the observed effects of SFRE in NSCLC cells related to the inhibition of lipid metabolism together with its synergism with chemotherapeutic drugs used in the treatment of NSCLC patients, herein, we wanted to investigate the clinical relevance of SFRE as a putative co-adjuvant in the treatment of NSCLC patients.

In collaboration with the Medical Oncology Service of Infanta Sofia University Hospital, PBMCs were obtained from eight NSCLC patients.

To evaluate if genes related to inflammation, oxidative stress, and immune system as readouts of changes at the systemic level may be affected as readouts of changes at the systemic level, may be affected or not, we compared the evolution of gene expression from V1 to visit 4 (nine weeks of intervention) and to visit 6 (sixteen weeks of intervention), in the two groups of patients: SFRE-intervention group (CR) *vs* control (CC).

Supplementary Table 3 shows the panel of genes analysed and the metabolic pathways where they are implicated).

Thus, it was evaluated the differential time evolution of gene expression in PBMCs from the initial visit (V1) to visit 4 (nine weeks of intervention) and to visit 6 (sixteen weeks of intervention), in the two groups of patients: SFRE-treated (CR) vs control (CC).

The analysis of gene expression (ΔCt) through the different visits and treatments indicated a statistically significant visit x treatment interaction after multiple test correction for *MAPK (p=0.04)*, *NLRP3 (p=0.044)*, and *SREBF1 (p=0.047)* (Figure 10A and Supplementary Table 4).

The two treatments displayed very different time trends, with the CR group showing a strong decrease of gene expression with time in the three genes while the CC control showing an increase of *NLRP3* or slight decrease of *SREBF1* (Figure 10B). More specifically, the analysis in terms of the relative gene expression ($RQ = 2^{-\Delta\Delta Ct}$) of visits 4 and V6 relative to visit 1 indicated that *NLRP3, MAPK, SREBF1* displayed fold inductions below 1 in the CR group, corresponding to inhibition of gene

A

Pemetrexed (μM)	CI (H1299)	CI (H1975)
2	0,687	0,955
4	0,726	0,852
8	0,677	0,832
16	0,7	0,974

B

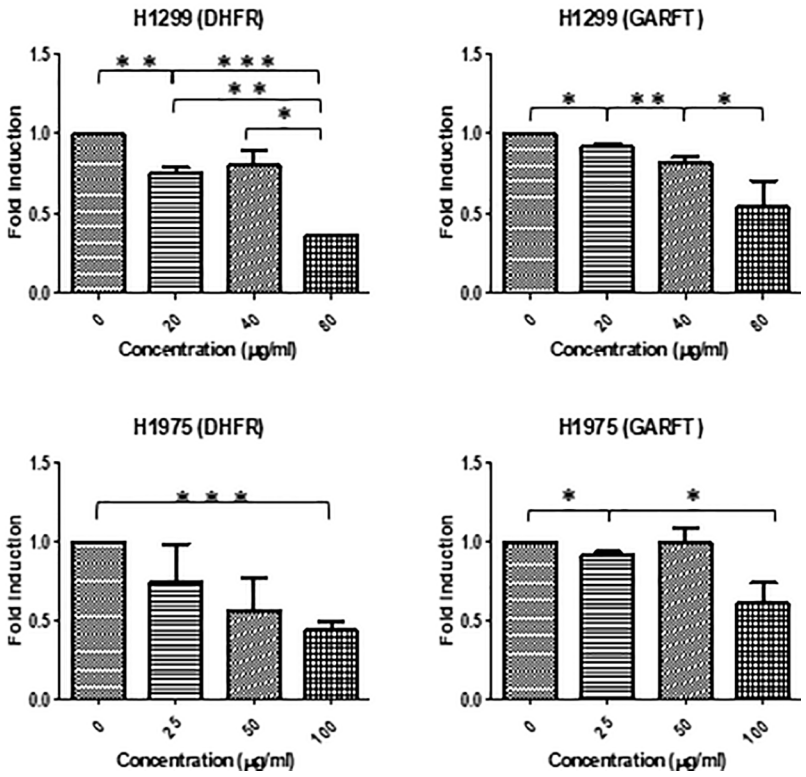

FIGURE 8
(A) SFRE synergised with pemetrexed in the inhibition of NSCLC cell proliferation. NSCLC cells were pre-treated with the extract for 3h at a fixed dose of 1/2 IC_{50} for H1299 and H1975. Combinatory index (CI) according to Chou–Talalay method. **(B)** SFRE diminished the expression of *DHFR* and *GARFT*, in a dose dependent manner. Results are shown in relation to non-treated cells and normalized to the endogenous control *B2M*. Results are expressed as the mean ± SEM of three independent experiments, each performed in triplicates. Asterisks *, **, *** indicate p-values < 0.05, 0.01 and 0.005, respectively.

expression, while in the case of the control CC group the fold induction was above 1, indicating an exacerbated gene expression Figure 10B).

Data suggest that CR group displayed a better control of lipid metabolism related inflammatory pathways at the systemic level, in accordance to the observed tendency, although not significant after multiple correction, towards the reduction of the expression of additional pro-inflammatory genes such as *JAK1 (p=0.018), PATFR (p=0.013), CXCR1 (p=0.01), GPD2*, and glycolytic genes *LDHA (p=0.003) and IRS1(p=0.026)*, which

A

Pembrolizumab (μM)	CI (H1299)	CI (H1975)
0,125	0,558	0,831
0,25	0,503	0,537
0,5	0,448	0,481
1	0,344	0,367
2	0,357	0,352

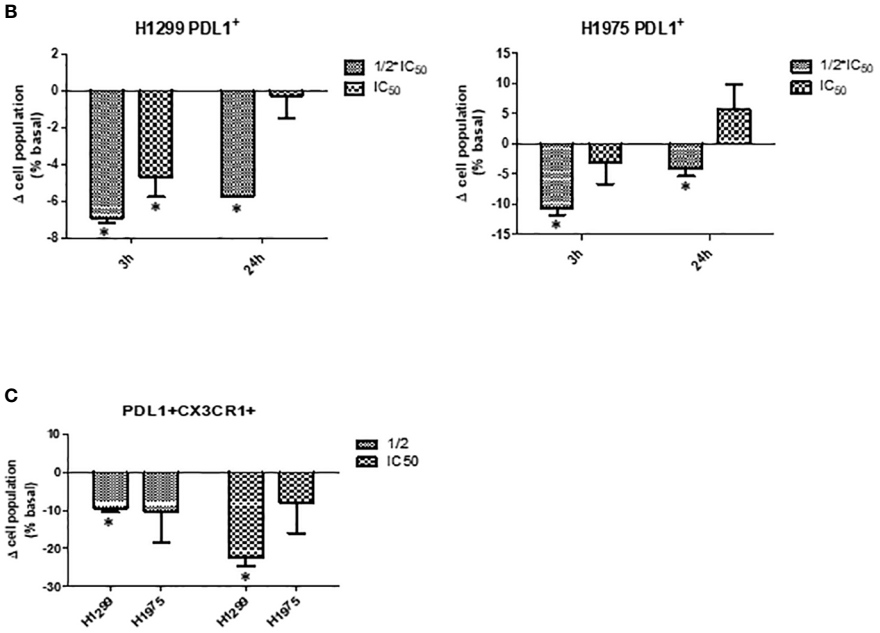

FIGURE 9
SFRE synergised with pembrolizumab in the inhibition of NSCLC cell proliferation. H1299 and H1975 NSCLC cells were treated concomitantly with SFRE at a fixed dose of 1/2xIC$_{50}$ and with pembrolizumab at the indicated doses. **(A)** The combinatory index (CI) according to Chou–Talay method indicated a positive synergism between SFRE and pembrolizumab in the inhibition of NSCLC proliferation. **(B)** FACs analysis of the expression of PD-L1 after 3h and 24h SFRE treatment of NSCLC cells at two different doses (1/2xIC$_{50}$, and 1xIC$_{50}$. **(C)** FACS analysis of the double expression of PD-L1 and CXCR1 after 3h and 24h SFRE treatment of NSCLC cells at two different doses (1/2 IC50, and 1xIC50. Data are expressed as fold induction respect to the expression levels of non-treated cells. Results are expressed as the mean ± SEM of three independent experiments, each performed in triplicates. Asterisks * indicates p-values < 0.05.

have been associated to immunosuppression in cancer (46–49) (Supplementary Table 4).

4 Discussion

Lung cancer is one of the most deadly and common types of cancer in the world (1). Although the identification of targetable molecular pathways such as EGFR inhibitors has improved the treatment and outcome of patients, majority of NSCLC tumours develop drug resistance and new generation of targeted therapeutic drugs, alone and/or in combination with different drugs, are being developed.

Nutrients can directly affect fundamental cellular processes and some diet derived ingredients, bioactive natural compounds and natural extracts have been shown to inhibit the tumour growth in preclinical and clinical trials (15).

We have previously described a supercritical extract of rosemary (*Rosmarinus Officinalis*) SFRE (EFSA approved for human use) as a potential antitumor agent in colon and breast cancers by mean of the inhibition of lipid metabolism related targets and DNA synthesis, synergising with 5-FluoroUracil (5-FU) in the inhibition of cell proliferation both *in vitro* and in preclinical models (16–19).

Herein, we aimed to investigate the potential antitumor effects of SFRE to be proposed as a co-adjuvant in the treatment of NSCLC.

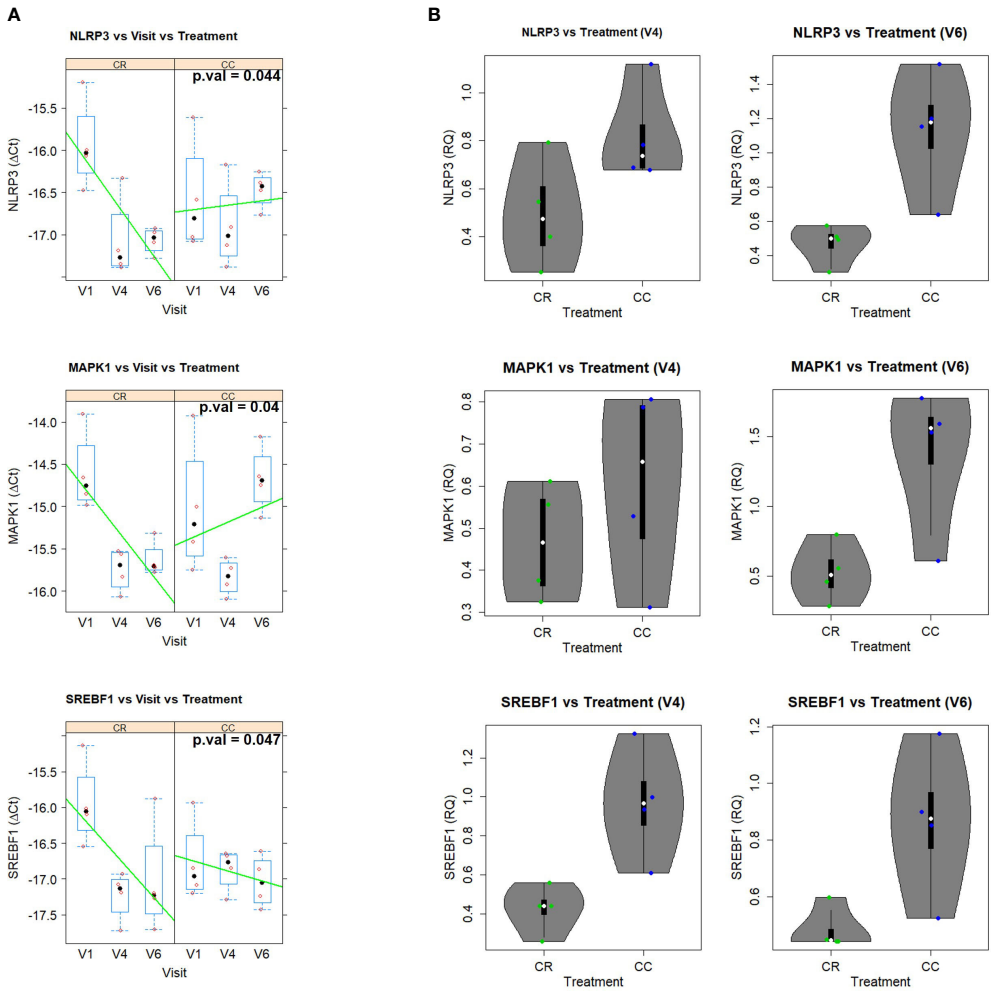

FIGURE 10
(A) Gene expression (DCt) patterns across time (V1 (baseline), V4 (nine weeks of intervention) and V6 (sixteen weeks of intervention), for the significant genes in the two groups: CR (SFRE treatment) and CC (control). Boxplots are displayed for each visit and group, together with the actual data points. Line trends are added in green to ease visualization of the trends. The corresponding p.values (after multiple test correction) are: 0.044, 0.04, and 0.047, for NLRP3, MAPK1, and SREBF1, respectively. **(B)** Violin plots showing the fold change (RQ = 2^-DDCt) of V4 and V6 in comparison to V1 of the statistically significant genes. Boxplots are also shown together with the actual data points.

In vitro treatment of NSCLC cells, H1299 and H1975, indicates that SFRE inhibits cell proliferation in a dose dependent manner (Figure 1). Importantly, SFRE diminishes the two main bioenergetic pathways, aerobic glycolysis (Figure 2) and mitochondrial oxidative phosphorylation (Figure 3), compromising the intracellular levels of ATP of tumour cells and activating apoptosis (Supplementary Figure 1).

Altered lipid metabolism has been found in many types of cancer and, consequently, lipid metabolism genes could constitute a prognostic and therapeutic tool in different tumours (31). Rosemary extracts has been described to inhibit relevant molecular pathways and transcription factors implicated in lipid metabolism (50, 51).

In a previous work, SFRE diminished lipid metabolism in CRC, and for this reason we hypothesized SFRE may affect lipid metabolism in NSCLC (25).

The analysis of lipid metabolism targets related to the *de novo* lipogenesis (*SREBF1, FASN, SCD*1) and cholesterogenesis (*HMGCR*), activation of fatty acids (*ACSLs*), homeostasis of cholesterol (*ABCA1, ApoA1*), biosynthesis and remodelling of membrane phospholipids (*CHKA, AGPAT*), as well as lipid related oncogenic pathways implicated in cell proliferation (*EGFR*) and inflammation (*JAK1*), indicated a relevant role of SFRE on the inhibition of lipid metabolism reprogramming in NSCLC cells. These effects are in line with the reduction of the intracellular neutral lipid content as well as main phospholipids,

indicating that the inhibition of lipid metabolism may be on the bases of the inhibition of the cell proliferation and/or cell survival pathways (Figures 4, 5).

Fatty acids (FAs) are indispensable components of cellular membranes, and they are essential for posttranslational protein modifications; moreover, they are energy generators and contribute to maintain redox homeostasis through β-oxidation. *De novo* lipogenesis is considered a new hallmark in many aggressive cancers. Overexpression of Fatty Acid Synthase (*FASN*) correlates with poor prognoses and treatment resistance in NSCLC (10), and stearoyl CoA desaturase 1 (*SCD1*) is highly expressed in lung adenocarcinomas promoting *in vitro* and *in vivo* tumorigenesis, cell migration and invasion (52). Acyl-coenzyme A synthetase long chain family members (ACSLs) are key components for the control of lipid synthesis and β-oxidation. ACSLs suppression is associated with depletion of cellular ATP causing the death of lung cancer cells (53–55). Other fundamental structural component of lipid membranes is cholesterol, that is also essential for cellular proliferation and tumour microenvironment remodelling (21). Tumour cells show a powerful fatty acid and cholesterol avidity which, together with the increased lipogenesis and cholesterogenesis (*HMGCR*), can be partially satisfied by increasing the uptake of exogenous lipids and/or lipoproteins (9). Increased serum cholesterol levels have also been associated with higher risk of cancer and poorer prognosis (22). ABCA1 contributes to maintain the cellular cholesterol homeostasis through the transfer of phospholipids and cholesterol to apolipoprotein A1 (*ApoA1*). In cancer cells, ABCA1 has been associated multidrug resistance as a drug efflux transporter and it is a key component of the tumour microenvironment remodelling. Related to ABCA1 come into sight the biosynthetic process of cholesterol. HMG-CoA reductase (*HMGCR*) is highly regulated and represents the rate-limiting step. Interestingly, HMGCR is the target for cholesterol lowering drugs known as statins (56, 57).

The successful application of bioactive compounds as co-adjuvants requires the demonstration of no interference and/or positive synergism with the therapeutic treatments in the clinic. For this reason, we next evaluated the effects of SFRE in combination with main standard drugs such as cisplatin, pemetrexed and pembrolizumab, used in the clinic in NSCLC patients.

Cisplatin is one of the most common first-line treatments in NSCLC, excluding targeted therapies. Importantly, the combination index (CI) after treatment NSCLC cell lines with SFRE for three hours at a fixed dose of 1/2 IC_{50} for H1299 and H1975, indicated a positive synergism between cisplatin and SFRE (Figure 7A). The analysis of the expression of these genes in NSCLC cells after the treatment with SFRE indicated the downregulation of *TK1* and *TYMS* (Figure 7B) which may explain, at least partially, the observed synergism between SFRE and cisplatin in the inhibition of cell proliferation.

During the last decade, the place of pemetrexed for the treatment of non-squamous NSCLC became established. Pemetrexed, an antifolate agent, is one of the recommended drugs combined with cisplatin or carboplatin for first-line treatment of these patients. Pemetrexed inhibits cell replication and growth by reducing the expression of three enzymes involved in purine and pyrimidine synthesis: thymidylate synthase (*TYMS*), dihydrofolate reductase (*DHFR*) and glycinamide ribonucleotide formyl-transferase (*GARFT*) (37). Importantly, the combination index (CI) after the treatment of H1299 and H1975 with SFRE for three hours at a fixed dose of 1/2 IC_{50} indicated a positive synergism between pemetrexed and SFRE (Figure 8A). The analysis of the expression of dihydrofolate reductase (*DHFR*) and glycinamide ribonucleotide formyl-transferase (*GARFT*) genes in NSCLC cells after the treatment with SFRE indicated the downregulation of both genes (Figure 8B), which may explain, at least partially, the observed synergism between SFRE and pemetrexed in the inhibition of cell proliferation.

Immunotherapy has made the breakthrough in cancer therapeutics by mean of immune regulatory mechanisms to enhance the immune response against cancer cells. Clinical studies evaluating the response to immunotherapy in lung cancer have demonstrated superior survival indices as well as reduced toxicity profiles in comparison to standard chemotherapy regimens. Of note, anti-PD-1 therapy (pembrolizumab) has recently replaced chemotherapy in the first line treatment for NSCLC with high PD-L1 expression, and the addition of pembrolizumab to platinum chemotherapy resulted in a significant improvement in overall survival (OS) in patients with non-squamous NSCLC, regardless of PD-L1 expression. For this reason, we aimed to evaluate if SFRE could act synergistically with pembrolizumab in the inhibition of the cell proliferation of NSCLC cells. A shown in Figure 9A, the combination index (CI) indicated a positive synergism between pemetrexed and SFRE in the inhibition of NSCLC cell proliferation. In addition, SFRE diminished the expression of PD-L1 and CX3CR1 which exert immunosuppressive effects at the tumour microenvironment (45), (Figure 9C) suggesting SFRE may contribute to diminish immune evasion of the lung cancer cells.

Due to the observed effects of SFRE in the inhibition of lipid metabolism targets in NSCLC cells together with its synergism with therapeutic drugs used in the treatment of NSCLC patients, next, we wanted to evaluate the relevance of SFRE in the clinic as a putative co-adjuvant in the treatment of NSCLC patients.

With this objective, and in collaboration with the Medical Oncology Service of Infanta Sofia University Hospital, we evaluated the effects of SFRE on the expression of a selected panel of genes related to lipid metabolism, inflammation, oxidative stress, immune system, and oncogenic pathways in PBMC from NSCLC patients.

The evolution of gene expression in PBMCs was compared from the initial visit (V1) to visit 4 (nine weeks of intervention) to

visit 6 (sixteen weeks of intervention) at the two treatment groups. The mixed model analysis of gene expression (ΔCt) for the evolution of gene expression across time for the two groups, treatment (CR) vs control (CC), showed statistically significant visit x treatment interactions after multiple test corrections for *NLRP3, MAPK, SREBF1*Other genes, such as *JAK1, LDHA, PATFR, CXCR1, GPD2* and *IRS1* showed statistically significant interactions, although significance was lost after multiple test correction (Supplementary Table 4).The differential time evolution observed for *NLRP3, MAPK, SREBF1* is of gene expression inhibition in the case of the CR group, and slight exacerbation in the case of the CC group (Figure 10).

These results suggest that the CR group displays a better control of lipid metabolism-related inflammatory pathways, in agreement also with the observed trend for reduction of expression in additional pro-inflammatory genes like *JAK1, PATRF, CXRC1, GPD2*, and glycolytic genes *LDHA* and *IRS1*, which are associated to immunosuppression in cancer (46–49).

The observed effects of SFRE on PBMCs lipid metabolism may be relevant in the management of NSCLC in the clinic. By one hand, increased lipid metabolism may lead to an exacerbated inflammation leading to the recruitment of immunosuppressive cells, such as bone marrow myeloid derived immunosuppressive cells and/or regulatory T cells (Treg) at the local tumour microenvironment. On the other hand, abnormal lipid accumulation in PBMCs subpopulations related to the innate immunity, such as dendritic cells (DC), have been shown to compromise the immune response at the local tumour microenvironment in patients with lung cancer (58) by reducing their antigen handling capacity, downregulating co-stimulating molecules such as CD86, and/or overexpressing tolerogenic cytokine IL-10 (59). Targeting FASN upregulation of the tumour-promoting pathway can enhance anti-tumour immunity (60, 61). In addition, lipid metabolism mediators such as inflammasome and prostaglandins are also associated to the production of lactate at the tumour microenvironment with immunosuppressive effects. Moreover, lactate has been proposed as a prognostic and predictive biomarker in several types of cancer (62).

In summary, SFRE exerts antitumour effects in NSCLC cells by diminishing lipid metabolism in cancer cells. In addition, *in vitro* experiments indicate that SFRE synergises with therapeutic drugs used in the clinic, such as cisplatin, pemetrexed and pembrolizumab. Finally, the clinical relevance of SFRE in NSCLC patients is suggested in a pilot intervention study where SFRE formulated with bioactive lipids (PCT/ES2017/070263) diminishes lipid metabolic and inflammatory targets in PBMC which have been shown to diminish the immune system antitumour functions. Based on these results, SFRE can be proposed as a co-adjuvant in the treatment of NSCLC that merits further investigation.

Main limitations of the study are the small number of patients analysed, heterogeneity in the clinical characteristics, including treatments and nutritional status, and the analysis of gene expression in PBMCs without the identification of the individual subpopulations responsible of the observed changes in gene expression.

Data availability statement

The original contributions presented in the study are included in the article/Supplementary Material. Further inquiries can be directed to the corresponding authors.

Ethics statement

The study was conducted according to the guidelines of the Declaration of Helsinki and approved by the Ethics Committee for Clinical Investigation of La Paz University Hospital (Ref. HULP 5617). The patients/participants provided their written informed consent to participate in this study.

Author contributions

Conceptualization, MGC, GR and ARM. Methodology, AB, MGC, JML-L.; formal analysis, AB, MGC, GC, BT and JML-L. Investigation, JM, JM-R, AB, MGC. and JML-L.; writing—original draft preparation, AB and MGC writing—review and editing, AB, MGC, GR and ARM. Clinical trial and data of patients: MS, EC and ARM supervision, MGC, GR and AM. Funding acquisition, GR and ARM. All authors contributed to the article and approved the submitted version

Funding

Funding: This research was funded by Regional Government of Community of Madrid (IND2017/BIO-7857; P2018/BAA-4343-ALIBIRD2020-CM), Ministerio de Ciencia e Innovación, Spain (PID2019-110183RB-C21); Ramon Areces Foundation (CIVP19A5937); EU Structural Funds and COST Action (CA17118); Synergistic Projects Community of Madrid (NUTRISION-CM/Y2020/BIO-6350) and REACT EU Program (Comunidad de Madrid and The European Regional Development Fund. ERDF. European Union- FACINGLCOVID-CM project). Adrián Bouzas has a predoctoral grant from the industrial predoctoral program of Community of Madrid (IND2017/BIO-7857).

Conflict of interest

The authors declare that the research was conducted in the absence of any commercial or financial relationships that could be construed as a potential conflict of interest.

Publisher's note

All claims expressed in this article are solely those of the authors and do not necessarily represent those of their affiliated organizations, or those of the publisher, the editors and the reviewers. Any product that may be evaluated in this article, or claim that may be made by its manufacturer, is not guaranteed or endorsed by the publisher.

Supplementary material

The Supplementary Material for this article can be found online at: https://www.frontiersin.org/articles/10.3389/fonc.2022.1046369/full#supplementary-material

References

1. Siegel RL, Miller KD, Jemal A. Cancer statistics, 2019. *CA Cancer J Clin* (2019) 69(1):7–34. doi: 10.3322/caac.21551

2. Herbst RS, Morgensztern D, Boshoff C. The biology and management of non-small cell lung cancer. *Nature* (2018) 553(7689):446–54. doi: 10.1038/nature25183

3. Maemondo M, Inoue A, Kobayashi K, Sugawara S, Oizumi S, Isobe H, et al. Gefitinib or chemotherapy for non-small-cell lung cancer with mutated EGFR. *N Engl J Med* (2010) 362(25):2380–8. doi: 10.1056/NEJMoa0909530

4. Rosell R, Karachaliou N. Brain metastases in patients with EGFR-mutant non-small-cell lung cancer. *Lancet Respir Med* (2017) 5(9):669–71. doi: 10.1016/S2213-2600(17)30265-5

5. Sos ML, Koker M, Weir BA, Heynck S, Rabinovsky R, Zander T, et al. PTEN loss contributes to erlotinib resistance in EGFR-mutant lung cancer by activation of akt and EGFR. *Cancer Res* (2009) 69(8):3256–61. doi: 10.1158/0008-5472.CAN-08-4055

6. Singh SS, Dahal A, Shrestha L, Jois SD. Genotype driven therapy for non-small cell lung cancer: Resistance, pan inhibitors and immunotherapy. *Curr Med Chem* (2020) 27(32):5274–316. doi: 10.2174/0929867326666190222183219

7. Han JJ, Kim DW, Koh J, Keam B, Kim TM, Jeon KY, et al. Change in PD-L1 expression after acquiring resistance to gefitinib in EGFR-mutant non-Small-Cell lung cancer. *Clin Lung Cancer* (2016) 17(4):263–270 e2. doi: 10.1016/j.cllc.2015.11.006

8. Hanahan D, Weinberg RA. Hallmarks of cancer: the next generation. *Cell* (2011) 144(5):646–74. doi: 10.1016/j.cell.2011.02.013

9. Fernandez LP, Ramos-Ruiz R, Herranz J, Martín-Hernández R, Vargas T, Mendiola M, et al. The transcriptional and mutational landscapes of lipid metabolism-related genes in colon cancer. *Oncotarget* (2018) 9(5):5919–30. doi: 10.18632/oncotarget.23592

10. Bueno MJ, Jimenez-Renard V, Samino S, Capellades J, Junza A, López-Rodríguez ML, et al. Essentiality of fatty acid synthase in the 2D to anchorage-independent growth transition in transforming cells. *Nat Commun* (2019) 10(1):5011. doi: 10.1038/s41467-019-13028-1

11. Carracedo A, Cantley LC, Pandolfi PP. Cancer metabolism: fatty acid oxidation in the limelight. *Nat Rev Cancer* (2013) 13(4):227–32. doi: 10.1038/nrc3483

12. Kamphorst JJ, Cross JR, Fan J, de Stanchina E, Mathew R, White EP, et al. Hypoxic and ras-transformed cells support growth by scavenging unsaturated fatty acids from lysophospholipids. *Proc Natl Acad Sci U.S.A.* (2013) 110(22):8882–7. doi: 10.1073/pnas.1307237110

13. Ruiz CF, Montal DE, Haley JA, Bott JA, Haley JD. SREBP1 regulates mitochondrial metabolism in oncogenic KRAS expressing NSCLC. *FASEB J* (2020) 34(8):10574–89. doi: 10.1096/fj.202000052R

14. Fernandez LP, Gomez de Cedron M, Ramirez de Molina A. Alterations of lipid metabolism in cancer: Implications in prognosis and treatment. *Front Oncol* (2020) 10:577420. doi: 10.3389/fonc.2020.577420

15. Aguirre-Portoles C, Fernandez LP, Ramirez de Molina A. Precision nutrition for targeting lipid metabolism in colorectal cancer. *Nutrients* (2017) 9(10):1076–96. doi: 10.3390/nu9101076

16. Gonzalez-Vallinas M, Molina S, Vicente G, Zarza V, Martín-Hernández R, García-Risco M, et al. Expression of microRNA-15b and the glycosyltransferase GCNT3 correlates with antitumor efficacy of rosemary diterpenes in colon and pancreatic cancer. *PloS One* (2014) 9(6):e98556. doi: 10.1371/journal.pone.0098556

17. González-Vallinas M, Molina S, Vicente G, Sánchez-Martínez R, Vargas T, García-Risco M, et al. Modulation of estrogen and epidermal growth factor receptors by rosemary extract in breast cancer cells. *Electrophoresis* (2014) 35(11):1719–27. doi: 10.1002/elps.201400011

18. Gonzalez-Vallinas M, González-Castejón M, Rodríguez-Casado A, Ramírez de Molina A. Dietary phytochemicals in cancer prevention and therapy: A complementary approach with promising perspectives. *Nutr Rev* (2013) 71(9):585–99. doi: 10.1111/nure.12051

19. Gonzalez-Vallinas M, Molina S, Vicente G, de la Cueva A, Vargas T, Santoyo S, et al. Antitumor effect of 5-fluorouracil is enhanced by rosemary extract in both drug sensitive and resistant colon cancer cells. *Pharmacol Res* (2013) 72:61–8. doi: 10.1016/j.phrs.2013.03.010

20. Boyd MR, Paull KD. Some practical considerations and applications of the national cancer institute *in vitro* anticancer drug discovery screen. *Drug Dev Res* (1995) 34:91–109. doi: 10.1002/ddr.430340203

21. Monks A, Scudiero D, Skehan P, Shoemaker R, Paull K, Vistica D, et al. Feasibility of a high-flux anticancer drug screen using a diverse panel of cultured human tumor cell lines. *J Natl Cancer Inst* (1991) 83(11):757–66. doi: 10.1093/jnci/83.11.757

22. Chou TC. Drug combination studies and their synergy quantification using the chou-talalay method. *Cancer Res* (2010) 70(2):440–6. doi: 10.1158/0008-5472.CAN-09-1947

23. Livak KJ, Schmittgen TD. Analysis of relative gene expression data using real-time quantitative PCR and the 2(-delta delta C(T)) method. *Methods* (2001) 25(4):402–8. doi: 10.1006/meth.2001.1262

24. Ramirez-Zacarias JL, Castro-Munozledo F, Kuri-Harcuch W. Quantitation of adipose conversion and triglycerides by staining intracytoplasmic lipids with oil red O. *Histochemistry* (1992) 97(6):493–7. doi: 10.1007/BF00316069

25. Gomez de Cedron M, Laparra-Llopis V, Loria-Kohen M, Molina S, Moreno-Rubio J, Montoya JJ, et al. Tolerability and safety of a nutritional supplement with potential as adjuvant in colorectal cancer therapy: A randomized trial in healthy volunteers. *Nutrients* (2019) 11(9). doi: 10.3390/nu11092001

26. Fernandez LP, Sánchez-Martínez R, Vargas T, Herranz J, Martín-Hernández R, Mendiola M, et al. The role of glycosyltransferase enzyme GCNT3 in colon and ovarian cancer prognosis and chemoresistance. *Sci Rep* (2018) 8(1):8485. doi: 10.1038/s41598-018-26468-4

27. Gonzalez-Vallinas M, Reglero G, Ramirez de Molina A. Rosemary (Rosmarinus officinalis l.) extract as a potential complementary agent in anticancer therapy. *Nutr Cancer* (2015) 67(8):1221–9. doi: 10.1080/01635581.2015.1082110

28. Merino Salvador M, Gómez de Cedrón M, Moreno Rubio J, Falagán Martínez S, Sánchez Martínez R, Casado E, et al. Lipid metabolism and lung cancer. *Crit Rev Oncol Hematol* (2017) 112:31–40. doi: 10.1016/j.critrevonc.2017.02.001

29. Fernandez LP, Merino M, Colmenarejo G, Moreno-Rubio J, Sánchez-Martínez R, Quijada-Freire A, et al. Metabolic enzyme ACSL3 is a prognostic biomarker and correlates with anticancer effectiveness of statins in non-small cell lung cancer. *Mol Oncol* (2020) 14(12):3135–52. doi: 10.1002/1878-0261.12816

30. Yuan M, Huang LL, Chen JH, Wu J, Xu Q. The emerging treatment landscape of targeted therapy in non-small-cell lung cancer. *Signal Transduct Target Ther* (2019) 4:61. doi: 10.1038/s41392-019-0099-9

31. Peck B, Schulze A. Lipid metabolism at the nexus of diet and tumor microenvironment. *Trends Cancer* (2019) 5(11):693–703. doi: 10.1016/j.trecan.2019.09.007

32. Aguirre-Portoles C, Feliu J, Reglero G, Ramírez de Molina A. ABCA1 overexpression worsens colorectal cancer prognosis by facilitating tumour growth and caveolin-1-dependent invasiveness, and these effects can be ameliorated using the BET inhibitor apabetalone. *Mol Oncol* (2018) 12(10):1735–52. doi: 10.1002/1878-0261.12367

33. Shah DR, Masters GA. Precision medicine in lung cancer treatment. *Surg Oncol Clin N Am* (2020) 29(1):15–21. doi: 10.1016/j.soc.2019.08.002

34. Nakagawa K, Hida T, Nokihara H, Morise M, Azuma K, Kim YH, et al. Final progression-free survival results from the J-ALEX study of alectinib versus crizotinib in ALK-positive non-small-cell lung cancer. *Lung Cancer* (2020) 139:195–9. doi: 10.1016/j.lungcan.2019.11.025

35. Doroshow DB, Sanmamed MF, Hastings K, Politi K, Rimm DL, Chen LB, et al. Immunotherapy in non-small cell lung cancer: Facts and hopes. *Clin Cancer Res* (2019) 25(15):4592–602. doi: 10.1158/1078-0432.CCR-18-1538

36. Bodor JN, Boumber Y, Borghaei H. Biomarkers for immune checkpoint inhibition in non-small cell lung cancer (NSCLC). *Cancer* (2020) 126(2):260–70. doi: 10.1002/cncr.32468

37. McLeod HL, Cassidy J, Powrie RH, Priest DG, Zorbas MA, Synold TW, et al. Pharmacokinetic and pharmacodynamic evaluation of the glycinamide ribonucleotide formyltransferase inhibitor AG2034. *Clin Cancer Res* (2000) 6 (7):2677–84.

38. Tang J, Guo F, Du Y, Liu X, Qin Q, Liu X, et al. Continuous exposure of non-small cell lung cancer cells with wild-type EGFR to an inhibitor of EGFR tyrosine kinase induces chemoresistance by activating STAT3. *Int J Oncol* (2015) 46 (5):2083–95. doi: 10.3892/ijo.2015.2898

39. Ku JM, Hong SH, Kim HI, Kim MJ, Kim SK, Kim M, et al. Synergistic anticancer effect of combined use of trichosanthes kirilowii with cisplatin and pemetrexed enhances apoptosis of H1299 non-small-cell lung cancer cells via modulation of ErbB3. *Phytomedicine* (2020) 66:153109. doi: 10.1016/j.phymed.2019.153109

40. Zhang Y, Feng X, Li T, Yi E, Li Y. Metformin synergistic pemetrexed suppresses non-small-cell lung cancer cell proliferation and invasion *in vitro*. *Cancer Med* (2017) 6(8):1965–75. doi: 10.1002/cam4.1133

41. Feng X, Zhang Y, Li T, Li Y. Sequentially administrated of pemetrexed with icotinib/erlotinib in lung adenocarcinoma cell lines *in vitro*. *Oncotarget* (2017) 8 (69):114292–9. doi: 10.18632/oncotarget.23224

42. Wang X, Yanga X, Zhang C, Wang Y, Cheng T, Duan L, et al. Tumor cell-intrinsic PD-1 receptor is a tumor suppressor and mediates resistance to PD-1 blockade therapy. *Proc Natl Acad Sci U.S.A.* (2020) 117(12):6640–50. doi: 10.1073/pnas.1921445117

43. Yao H, Wang H, Chushu LC, Fang JY, Xu J. Cancer cell-intrinsic PD-1 and implications in combinatorial immunotherapy. *Front Immunol* (2018) 9:1774. doi: 10.3389/fimmu.2018.01774

44. Ma L, Lv J, Dong Y, Zhang X, Li X, Zhang H, et al. PD-L1 expression and its regulation in lung adenocarcinoma with ALK translocation. *Interdiscip Sci* (2019) 11(2):266–72. doi: 10.1007/s12539-019-00331-0

45. He W, Liu Q, Wang L, Chen W, Li N, Cao X. TLR4 signaling promotes immune escape of human lung cancer cells by inducing immunosuppressive cytokines and apoptosis resistance. *Mol Immunol* (2007) 44(11):2850–9. doi: 10.1016/j.molimm.2007.01.022

46. Karki R, Man SM, Kanneganti TD. Inflammasomes and cancer. *Cancer Immunol Res* (2017) 5(2):94–9. doi: 10.1158/2326-6066.CIR-16-0269

47. Liang M, Chen X, Wang L, Qin L, Wang H, Sun Z, et al. Cancer-derived exosomal TRIM59 regulates macrophage NLRP3 inflammasome activation to promote lung cancer progression. *J Exp Clin Cancer Res* (2020) 39(1):176. doi: 10.1186/s13046-020-01688-7

48. Wang Y, Kong H, Zeng X, Liu W, Wang Z, Yan X, et al. Activation of NLRP3 inflammasome enhances the proliferation and migration of A549 lung cancer cells. *Oncol Rep* (2016) 35(4):2053–64. doi: 10.3892/or.2016.4569

49. Wang JB, Huang X, Li FR. Impaired dendritic cell functions in lung cancer: a review of recent advances and future perspectives. *Cancer Commun (Lond)* (2019) 39(1):43. doi: 10.1186/s40880-019-0387-3

50. Colson C, Batrow PL, Gautier N, Rochet N, Ailhaud G, Peiretti F, et al. The rosmarinus bioactive compound carnosic acid is a novel PPAR antagonist that inhibits the browning of white adipocytes. *Cells* (2020) 9(11):2433-48. doi: 10.3390/cells9112433

51. Tu Z, Moss-Pierce T, Ford P, Jiang TA. Rosemary (Rosmarinus officinalis l.) extract regulates glucose and lipid metabolism by activating AMPK and PPAR pathways in HepG2 cells. *J Agric Food Chem* (2013) 61(11):2803–10. doi: 10.1021/jf400298c

52. Pisanu ME, Noto A, De Vitis C, Morrone S, Scognamiglio G, Botti G, et al. Blockade of stearoyl-CoA-desaturase 1 activity reverts resistance to cisplatin in lung cancer stem cells. *Cancer Lett* (2017) 406:93–104. doi: 10.1016/j.canlet.2017.07.027

53. Padanad MS, Konstantinidou G, Venkateswaran N, Melegari M, Rindhe S, Mitsche M, et al. Fatty acid oxidation mediated by acyl-CoA synthetase long chain 3 is required for mutant KRAS lung tumorigenesis. *Cell Rep* (2016) 16(6):1614–28. doi: 10.1016/j.celrep.2016.07.009

54. Liu KT, Yeh IJ, Chou SK, Yen MC, Kuo PL. Regulatory mechanism of fatty acidCoA metabolic enzymes under endoplasmic reticulum stress in lung cancer. *Oncol Rep* (2018) 40(5):2674–82. doi: 10.3892/or.2018.6664

55. Chen WC, Wang CY, Hung YH, Weng TY, Yen MC, Lai MD. Systematic analysis of gene expression alterations and clinical outcomes for long-chain acyl-coenzyme a synthetase family in cancer. *PloS One* (2016) 11(5):e0155660. doi: 10.1371/journal.pone.0155660

56. Omori M, Okuma Y, Hakozaki T, Hosomi Y. Statins improve survival in patients previously treated with nivolumab for advanced non-small cell lung cancer: An observational study. *Mol Clin Oncol* (2019) 10(1):137–43. doi: 10.3892/mco.2018.1765

57. Park IH, Kim JY, Choi JY, Han JY. Simvastatin enhances irinotecan-induced apoptosis in human non-small cell lung cancer cells by inhibition of proteasome activity. *Invest New Drugs* (2011) 29(5):883–90. doi: 10.1007/s10637-010-9439-x

58. Arai R, Soda S, Okutomi T, Morita H, Ohmi F, Funakoshi T, et al. Lipid accumulation in peripheral blood dendritic cells and anticancer immunity in patients with lung cancer. *J Immunol Res* (2018) 2018:5708239. doi: 10.1155/2018/5708239

59. Gardner JK, Mamotte CDS, Patel P, Yeoh TL, Jackaman C, Nelson DJ, et al. Mesothelioma tumor cells modulate dendritic cell lipid content, phenotype and function. *PloS One* (2015) 10(4):e0123563. doi: 10.1371/journal.pone.0123563

60. Herber DL, Cao W, Nefedova Y, Novitskiy SV, Nagaraj S, Tyurin VA, et al. Lipid accumulation and dendritic cell dysfunction in cancer. *Nat Med* (2010) 16 (8):880–6. doi: 10.1038/nm.2172

61. Jiang L, Fang X, Wang H, Li D, Wang X. Ovarian cancer-intrinsic fatty acid synthase prevents anti-tumor immunity by disrupting tumor-infiltrating dendritic cells. *Front Immunol* (2018) 9:2927. doi: 10.3389/fimmu.2018.02927

62. Hayes C, Donohoe CL, Davern M, Donlon NE. The oncogenic and clinical implications of lactate induced immunosuppression in the tumour microenvironment. *Cancer Lett* (2021) 500:75–86. doi: 10.1016/j.canlet.2020.12.021

Frontiers in Oncology

Advances knowledge of carcinogenesis and tumor progression for better treatment and management

The third most-cited oncology journal, which highlights research in carcinogenesis and tumor progression, bridging the gap between basic research and applications to imrpove diagnosis, therapeutics and management strategies.

Discover the latest Research Topics

See more →

Frontiers

Avenue du Tribunal-Fédéral 34
1005 Lausanne, Switzerland
frontiersin.org

Contact us

+41 (0)21 510 17 00
frontiersin.org/about/contact